
**The Small Head Criterion in Hydropower and understanding the
Dimensions of Renewable Energy with Water Resources**

**A Synopsis
to Fulfill the Requirement for the
Award of Habilitation Degree at Karlsruhe Institute of Technology**

**By Dr.-Ing Punit Singh
July, 2015**

Contents

Personal Introduction.....	3
Abstract of the Synopsis	5
1. Foundation Phase for Habilitation (2005 – 2011).....	5
1.1 The Pump as Turbine (PAT) Journey	5
1.2 Propeller Turbine Journey	7
1.3 The Defining Field Survey	8
2. Habilitation Action Phase (2012 – 2014).....	8
3. Outcome	12
3.1 Research	12
3.2 Application chart	14
3.3 Teaching	15
3.4 Philosophy.....	16
4. Summary and Prospects.....	17
5. References.....	18
5.1 Ph.D Thesis	18
5.2 Journal Papers	18
5.3 Journal Papers: (under preparation).....	18
5.4 Conference Papers.....	19
5.5 Research Reports and Proposals	19
5.6 Project Reports	19
5.7 Refereed Papers.....	19
Nomenclature and Abbreviations	19
Appendix.....	19
A1 Flow Chart of the Habilitation Program	19

Personal Introduction

The grand arrival of renewable energy in modern world has happened despite the strong denial from centralized/conventional power suppliers who saw this as a liability. But, whether due to climate politics or legitimate concerns, renewable energy has become a vital component of the global energy mix notwithstanding its low intensity, variability and other unfavorable characteristics.

The great challenge to integrate renewable energy into the existing system (especially with solar energy having daily variation and wind having seasonal variation) and to ensure grid stability was by no means a trivial task. But, there is ample evidence that the innovative solution exists in a professionally managed grid by means of ramping up or down power plants when renewable energy leaves or joins the grid even at steep rates. Recently, the successful management of German grid during solar eclipse of 2015¹ is a leading and proved example of available solutions for a future scenario where the percentage of renewable energy would reach to 40% or 50% of total energy generation.

The underlining point is that renewable energy's integration to centralized grid happened due to operational advantages of 'Gegawatt' scale, political pressure and not to forget the skilled and innovative professionals involved. The critics of renewable energy have been left baffled that something unthinkable few decades back would ever be possible. And one should remember the renewable energy that is connected to the grid includes millions of solar rooftop power plants (less than 10 kW in capacity) accounting for 30%-40% of RE connected to grid in Germany.

The overcoming of the vexed grid issues with more and more Renewable Energy (RE) added by other countries will make centralized RE an acceptable solution to the user and this will also see a positive effect on climate warming rate. The subtle fact to remind ourselves is that the solutions for centralized RE have worked out well solely because of existence of a unified grid.

However, what will remain a challenge is in the decentralized world (with a size of few tens of kW) where a grid is non-existing and the setup of trained professionals is found wanting. The input or source level characteristics of decentralized RE as in their centralized counterparts don't change, i.e. having the same vulnerability of low intensity and variability, but in the output side, there is a contrast where communities' lifestyle and load spectrum adding more challenges to decentralized systems, which includes not only electricity but also other requirements.

One of the primary end-use requirement in remote areas relates to 'water', the lifeline of humanity, which has forced a decentralized RE to innovate much more than centralized counterparts. The source level innovation for decentralized RE has to cleverly manage end-uses like electricity as well as 'water resources' to make it a success to many isolated communities. Decentralized RE has remained largely on paper with only few successful examples to speak of, since active political pressure is missing and skilled personnel are not coming forward to participate. However, more importantly because decentralized systems are small in capacity or size, they have to deal with issue of 'economy of scale' (higher cost per unit due to significantly smaller size involved). One of the other reasons for their failure is to separate decentralized RE from 'water resources' management that have led to increased complexities and diminishing interests.

Based on the above conflicting background, the author has been debating and dabbling with the implementation of successful solutions of small capacity hydropower based RE technologies for both the centralized and decentralized environments. The author while having his heart for RE in general and decentralized systems in particular has spent roughly a decade, after his PhD, in 'small hydropower' as one of the chosen RE sources because of its qualification of being fully renewable unlike large hydro to come to a grasp of the problems facing mankind and possible solutions in one way or the other.

¹ On 20th March 2015, the German grid was put to a critical test when the moon partially blocked the solar radiation falling on PV panels between 12 noon and 3 pm. The power engineers worked out an excellent model of ramping up and down nearly 20 GW, gas fired and pumped storage power plants in addition to requesting some power guzzling cement plants to temporarily shut down, and hence ensuring no impact of the grid frequency. [source:<http://www.greentechmedia.com/articles/read/German-and-European-Power-Grids-Civilization-Intact-Following-Solar-Eclips#>]

Few of these issues concerning dimensions of renewable energy (centralized and decentralized), small hydropower along with the primary end-uses like electricity and water resources are highlighted in the flow chart in Fig. 1.

The following 'synopsis' discusses his justification on adding a further constraint to an already constrained topic of small hydropower, i.e. small head, which heralds 'two contrasting yet similar' field projects with ramifications not restricted to the scientific community alone but also to rationalists to define contours of small in the context of people and nature.

These two significant projects form the basis of author's philosophical understanding of the dimensions of renewable energy in both centralized and decentralized worlds with challenges to optimize the source and end-use technologies together, but uniquely for the two worlds. These projects also help him realize to keep 'water resource' technologies at the helm of his journey.

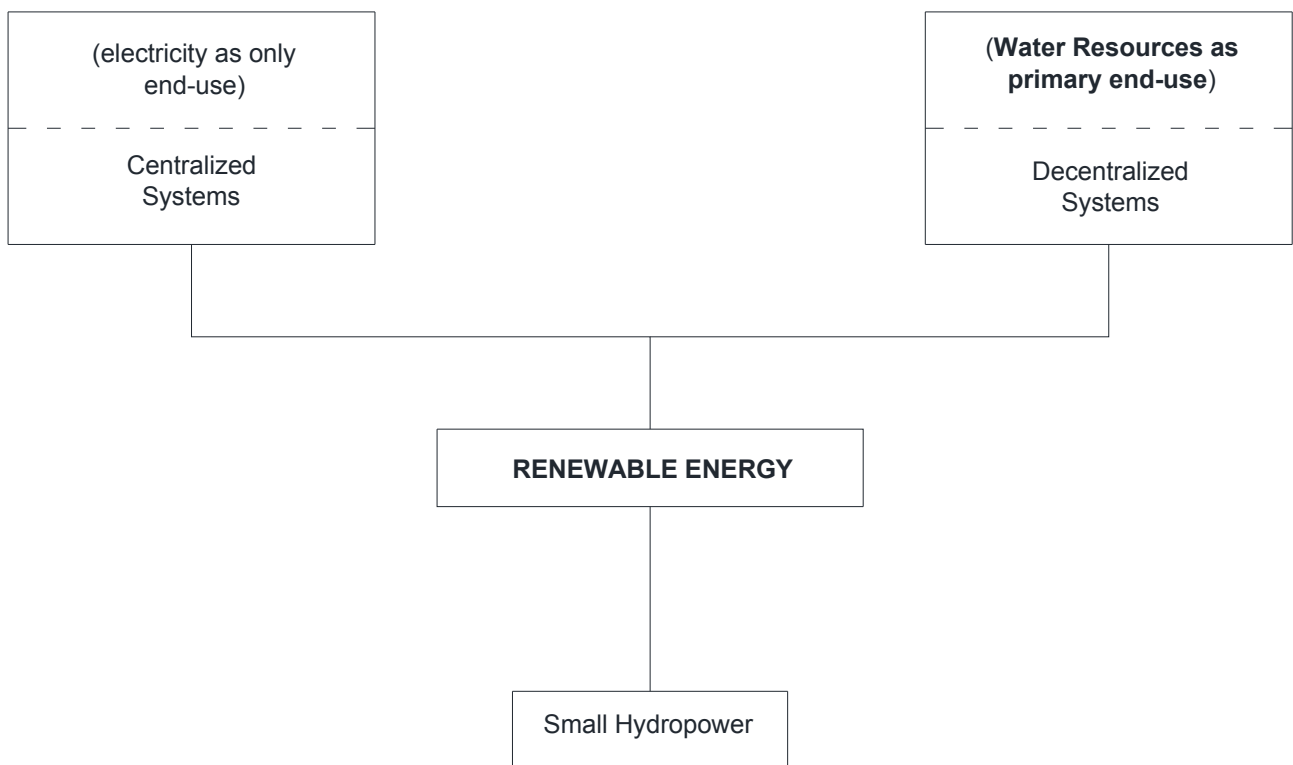


Fig. 1, Dimensions of Renewable Energy with small hydropower and water resources

Abstract of the Synopsis

The main script of the synopsis contains the author's journey of working on his chosen renewable energy source (i.e. small hydropower) through two phases with an aim to identify, assess and frame the problem correctly. After the first phase, which comprises of implementing projects in field and associated research at laboratory, he prescribes a turbine plan for medium heads in small hydro. However, the second phase leads him to two interesting projects through which he tries to unravel the diverse requirement for centralized and decentralized renewable energy systems, particularly pertaining to water resources management.

This takes him to the primary outcome phase related to research work in which he investigates different turbine technologies for electricity generation and pumping application for the two projects including a water pumping technology called the hydraulic ram pump. The research further encompasses special problems related to both fluid mechanics in turbomachinery at one side and to systems engineering at the other. In the second outcome he produces a head-flow-diameter (HQD) chart for small head hydropower that gives the real picture of the available turbine options and strategies to be devised.

The author highlights the importance of conceiving a teaching plan with an aim of adding value to the aforesaid topic. In the final outcome he introduces a philosophical debate on how to tackle the problem of size in small head hydropower in order to give a better meaning for the dimensions of renewable energy, with two end-uses under consideration namely, electricity and water resources.

1. Foundation Phase for Habilitation (2005 – 2011)

This phase saw the author working as an implementer of his PhD results in the field only to come back to the laboratory with more questions and once again return to the field for conceptualizing the 'small head hydro' problem. The foundation phase is categorized into 3 journeys as described below.

1.1 The Pump as Turbine (PAT) Journey

The PAT journey of the author, illustrated in Fig. 2, starts at the end of PhD defense [1] of the author during which he argued the enormous advantages of using PAT that included simplicity in design, robustness, widespread availability and economic value despite the fact that understanding of the exact turbine performance and operation of pumps was eluding scientists worldwide. In addition to this, PATs had an inherent disadvantage of 'narrow flow range' operation at optimum efficiency owing its fixed geometry design. The author's slogan of 'doing small things in a big way' by propelling the growth of decentralized renewable energy with meticulous implementation of PAT projects, was at the helm of this journey.

The author set out to the field with two goals in mind one, to validate the prediction model he proposed during the PhD thesis [1] and two, to deal with the imposing boundary conditions of varying flow rate (as in any renewable energy scenario).

As seen in the flow chart (Fig. 2), the author implemented the Darjeeling project in which the variable flow condition was solved by using mechanically synchronized PATs, while that at Karlapat the variable flow was solved using two PATs working independently instead of synchronization. The remaining 3 PAT projects at Bodamanjari, Sikkim and Tanzania involved a single PAT design since there was a guaranteed availability of a minimum flow throughout the year.

One of common features of all these projects was that the primary requirement was only electricity, with no other direct end-uses possible. Though the Darjeeling project was a hybrid one with availability of grid connection, its end-use was restricted only to electricity. The other projects were in remote areas and the priority was to give only electricity to the community.

In a sharp contrast to the above 5 PAT projects, the author participated in a 'defining' PAT project in Bribin, Indonesia [15], where the end-use was not electricity but a resource that defines the survival of humanity, i.e. water. This was done by directly connecting a PAT to a high pressure pump. Moreover, the civil engineering and geological challenges of building a system in karst regions underground made this project more unique. The variability in flow was solved by using multiple PAT-pump units.

After successful implementation of these projects, the hydraulic characteristics of the respective PATs were professionally tested in field conditions in order to validate the prediction model. It was only after getting

proof of field validation, the author found morale consciousness and authority to publish his work. The first publication [2] presented a prediction model, which was based on only his laboratory results of 9 pumps as turbines. This model was optimized in [3] following field validation and it involved 4 PAT shapes narrowing down the prediction errors ($<\pm 3\%$) even further. These publications obtained acceptance and attention in both academia worldwide as well as from praxis. The author in his subsequent publication [4] looked at a fundamental 'fluid mechanics' problem of impeller rounding and compared its value relative to a good prediction model.

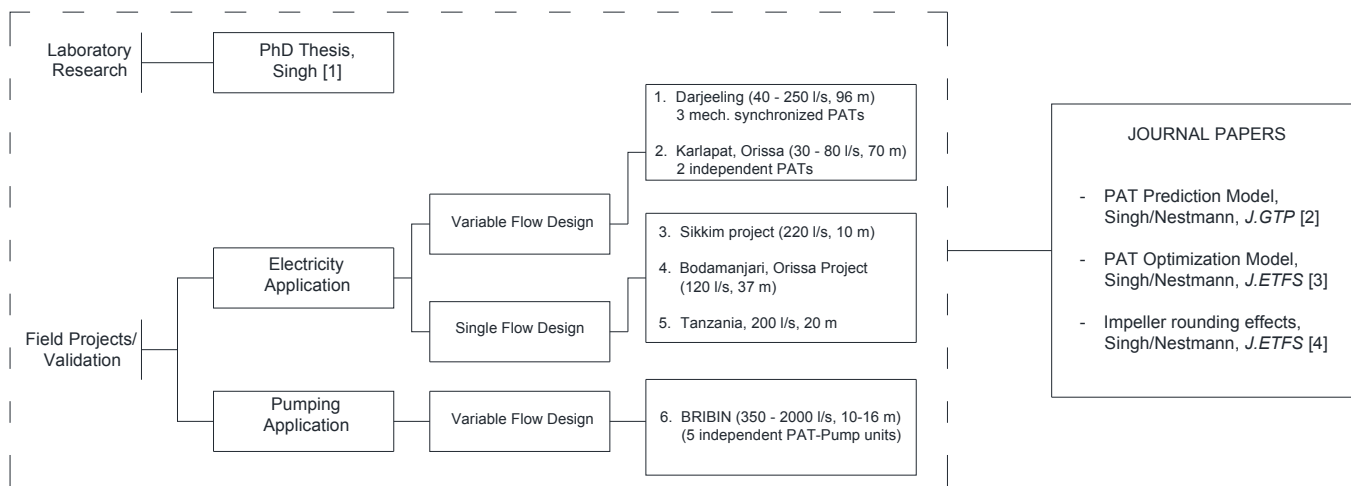


Fig. 2, Flow chart for the PAT Journey

Single Flow Design



Sikkim Project

Variable Flow Design



Darjeeling Project



Bodamanjari Orissa Project



Karlapat Orissa Project



Tanzania Project



Bribin, Indonesia Project



Fig. 3, Pictures of Implemented PAT projects

These projects and publications instilled a lot of confidence, but one of the greatest lessons that the author learnt (after Bribin [15]) was that water resource as an end-use to all PAT based remote hydro projects should be made fundamental in the design concept. Another outcome of this journey was to look for innovative turbine solutions at lower heads, since all the projects had a head between 10 and 100 meters, which took him to the next journey, the propeller turbine journey.

1.2 Propeller Turbine Journey

This research space was the most productive in terms of laboratory optimization stages and scientific publications. The journey began when the author was invited to design a challenging low head project in India, which has a head of only 1.5 meters, but with large fluctuations in flow from 25 l/s to 75 l/s. He returned to laboratory for a specific low head (1.5 to 2 meters) problem with an elaborate experiment comprising of 5 propeller geometries to study the effect of blade height, blade number, blade angles at hub and tip [4, 5, 6 and 7] as illustrated in Fig. 4 and Fig. 5.



Fig. 4, Propeller Turbine Journey (Field to Laboratory)

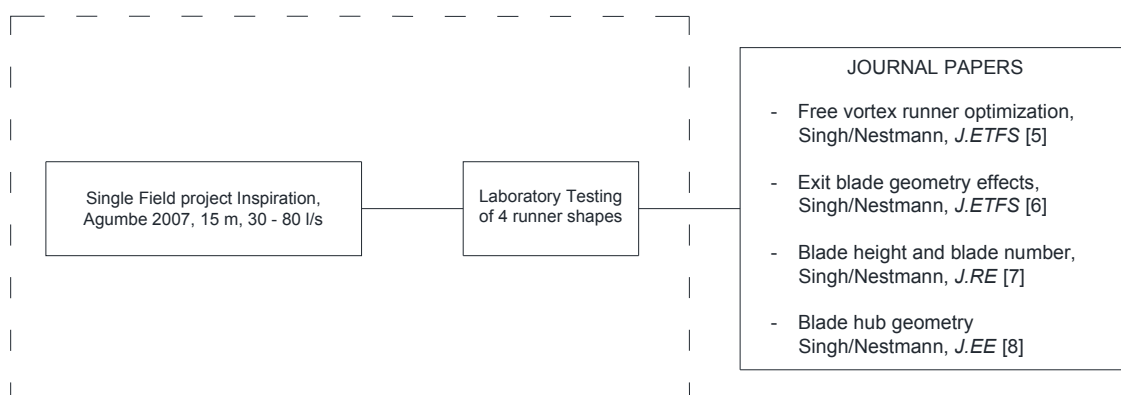


Fig. 5, Flow chart of the Propeller Research

This study could be classified as 'pre-scientific' that tried to bridge artisan blade manufacturing techniques (cold working of uniform thickness blades) with 'modest' performance indices. This interesting experiment on propeller runners was restricted to low flows (<100 l/s).

Through these publications, the author could investigate the effects of blade shape and recognize the value of camber line and blade twist propeller turbine design, which otherwise could be obtained only in cascade studies in water/wind tunnels. Even though there were not many field projects with propeller turbines after the laboratory investigation, it added a lot academic value.

1.3 The Defining Field Survey

In the third and final journey of this phase, the author travelled through country sites and some process industries in India to find questions time and again being asked about lower heads (less than 10 meters) and varying flows from very small ones of 50 l/s to larger capacities of 2000 l/s. As expected the process industries needed energy (electricity) recovery within a centralized connected grid, while the country sites required a decentralized solution of end-uses with both water resource and electricity.

The author realized that artisan techniques of blade manufacture could not hold the test of time, especially for larger flows. Hence, he went back to his PhD idea, scouting for mixed and axial flow pumps and working on their 'robust' adaption as turbines [9, 10, 16, 17, and 18].

He ended this phase by presenting a head-flow plan for hydro turbines (Fig. 6) with clearly defined laboratory and simulation tasks. This diagram also plots the laboratory and field projects involving both PAT and propeller turbines discussed in section 1.1 and 1.2. This 'turbine plan' became the basis of the Habilitation work for both remote hydro (open loop) and process applications (open and closed loop) in centralized grid network.

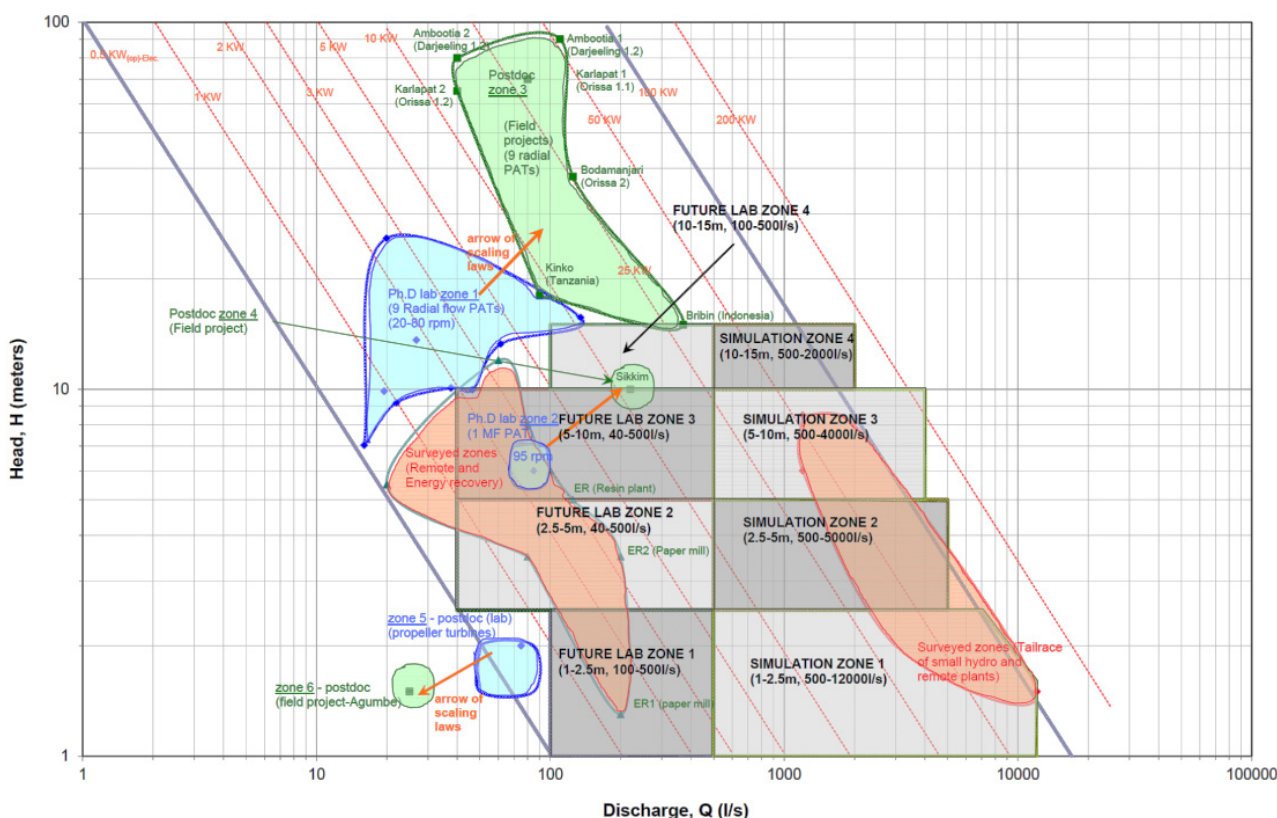


Fig. 6, The turbine plan

2. Habilitation Action Phase (2012 – 2014)

This phase comprised of planning two 'open loop' hydro power projects with strikingly identical input head conditions but contrasting end-use requirements. The selection of the two projects was carefully done to address the core philosophy of understanding the dimensions of renewable hydropower separately for

centralized and decentralized systems. The flow chart in Fig. 7 illustrates the two projects, their parameters, design and planning for the two projects.

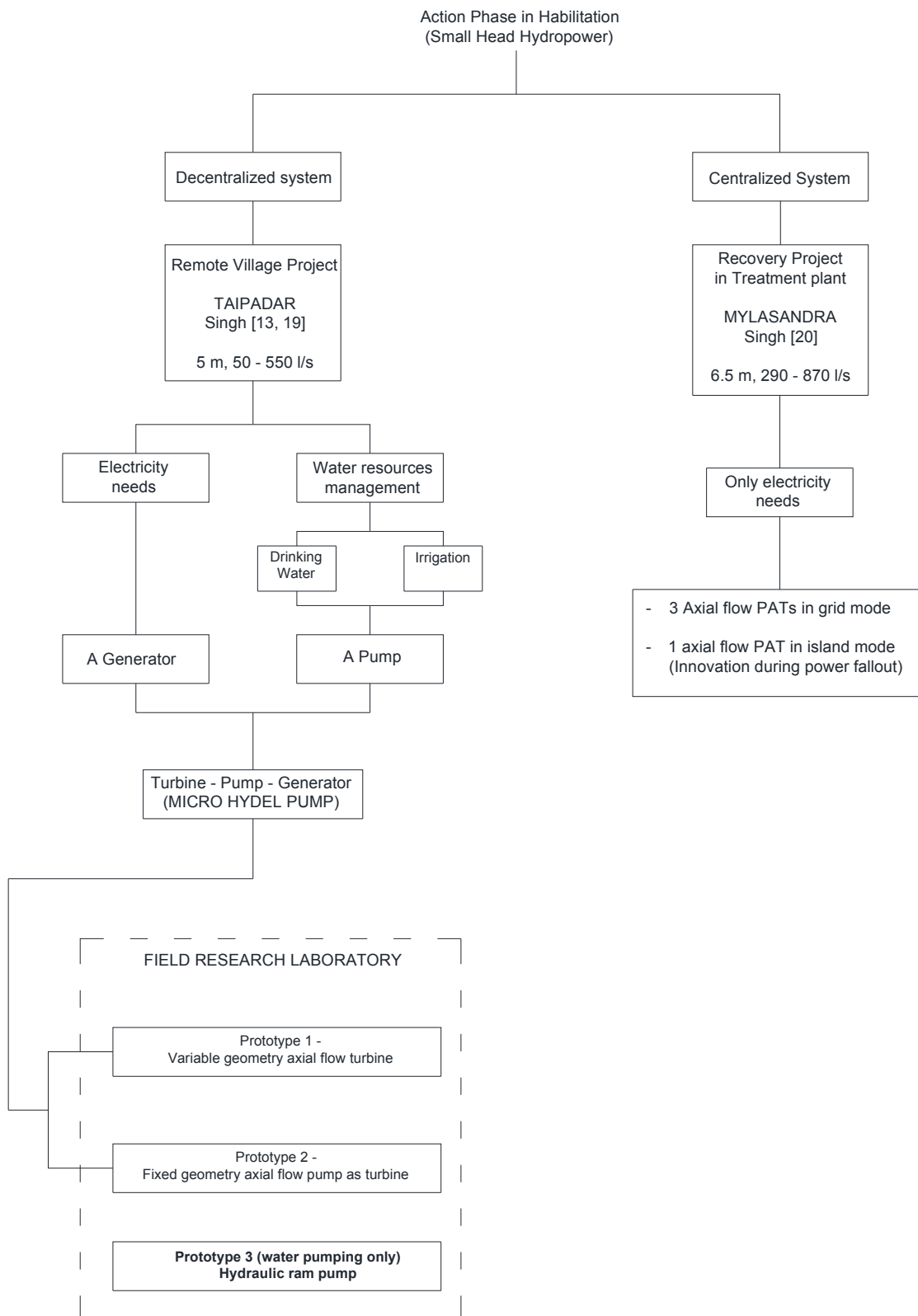
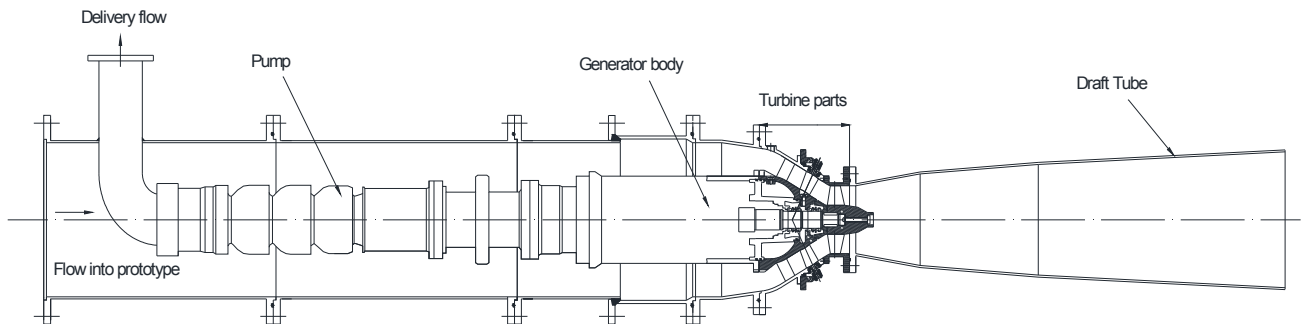


Fig. 7, Flow Chart of Habilitation Action Phase

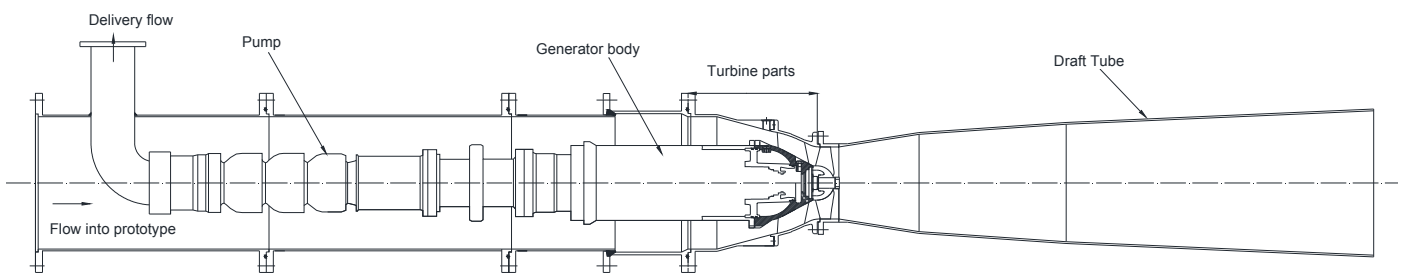
The first type [20] is a decentralized renewable energy project for an isolated village having gradually sloped perennial stream whose primary requirement pertains to water resources management, namely to supply pressurized water for irrigation and drinking purpose while electricity took the second preference.

The dual needs entailed an invention of a single turbine shaft system housing an electricity generator and multi-stage pump separated by a clutch, known as the 'micro hydel pump' (refer Fig. 8 and Fig. 9).

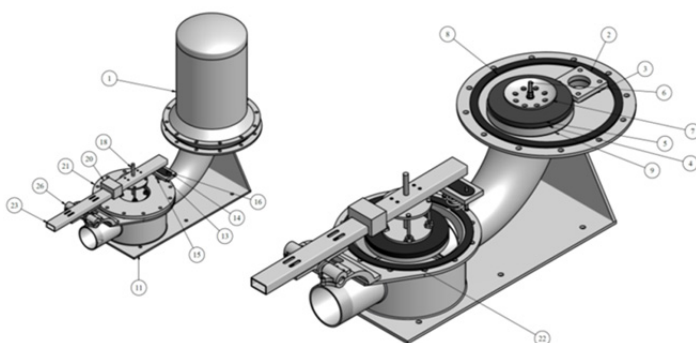
The most consequential feature of this project was the challenge and difficulty to design a turbine-pump for summer flows. The battle to find optimum turbine shape took the author to a completely different type of technology, couple of centuries old, which used hydraulic energy directly to pump water to higher levels with help of the 'water hammer' effect. This was the turning point of the planning phase of this project and author included a hydraulic ram pump in addition to the two types of turbine pumps.



Prototype 1: Adjustable geometry axial flow based micro hydel pump



Prototype 2: Fixed geometry axial flow PAT based micro hydel pump

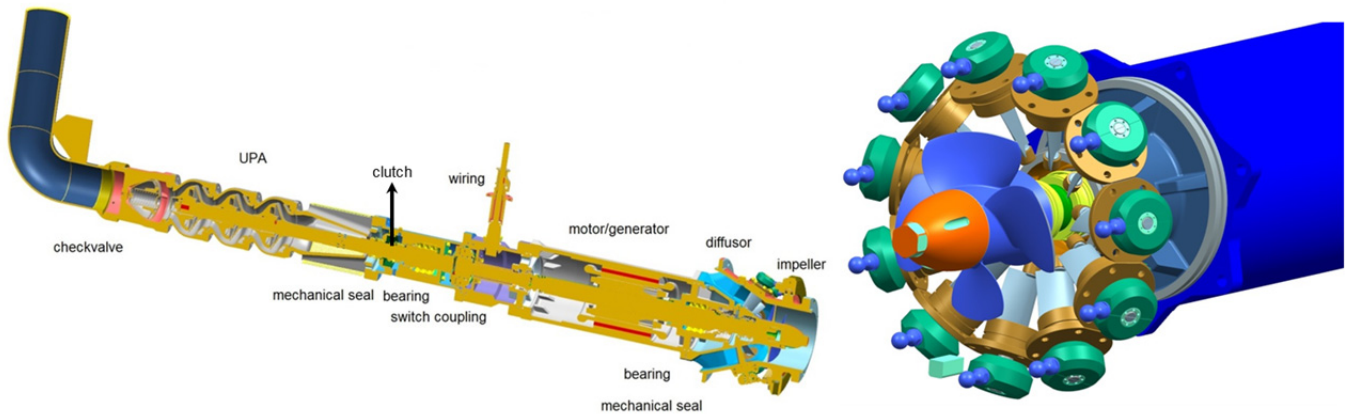


Prototype 3: Hydraulic Ram Pump (Summer operation)

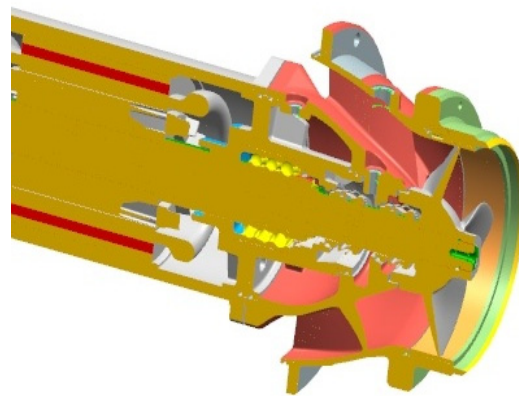
Fig. 8, The prototypes of the field research laboratory for low head hydropower pumping ([19, 20])

Figure 8 shows the contrasting designs of the three prototypes. Even within the two turbine prototypes (micro hydel pumps), the author is comparing the fixed geometry PAT idea with a variable geometry axial flow turbine. The difference in the prime mover design of these two micro hydel pumps is highlighted in

Fig. 9. A thorough laboratory test and an accurate field investigation will guide the turbine design for small head hydropower and pumping technologies (refer to section 3.1).



Prototype 1: Variable geometry axial flow turbine



Prototype 2: Fixed geometry axial flow PAT

Fig. 9, Inner details of prototype 1 and prototype 2²

The second type [21] of project (shown in flow chart, Fig. 7) comes under the category of centralized renewable energy, which envisages incorporation hydro generators in a sewage treatment plant to recover hydro energy and store it in the local electricity grid (as shown in Fig. 10). The innovation required was first to ensure self-regulation of the plant and second to provide ‘emergency’ power during a grid shutdown phase with help of the leftover water in the treatment circuit at the instant of grid disconnection. The second innovation in effect created an island or decentralized grid for a short duration of time.

Returning to the flow chart in Fig. 7, one can grasp the intensity of design involved with decentralized projects aimed for water resource as one of the end-uses to a centralized system involving only electricity as its end-use. The author had to garner all strength and resources to conceptualize a decentralized renewable hydropower with water resource as end-use application.

² A patent is planned to be filed on the concept of micro hydel pump after laboratory tests

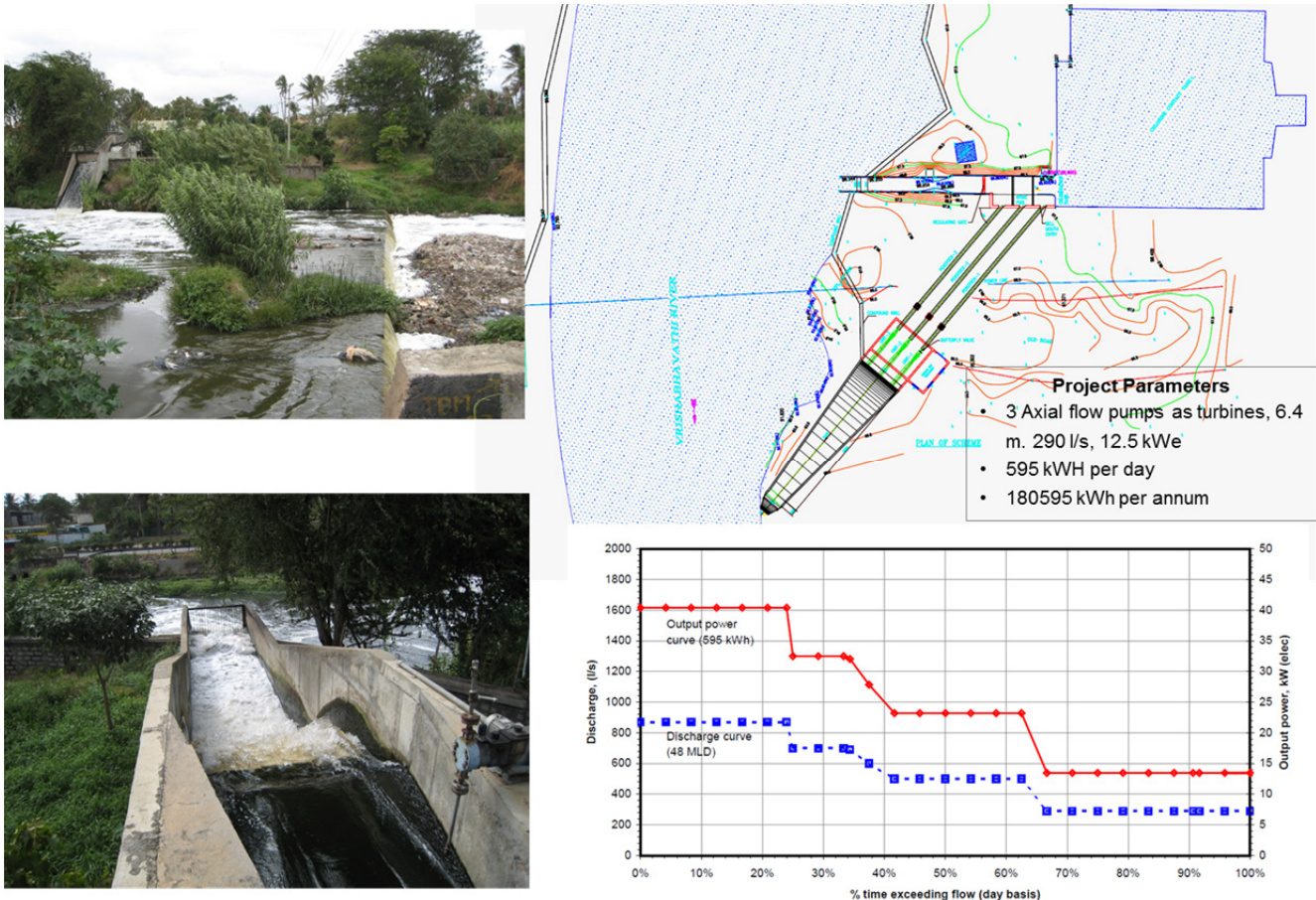


Fig. 10, Pictures and layout of a hydro recovery plant in centralized network ([21])

3. Outcome

The outcome of the working phase on two projects can be classified into direct outcomes envisaged for researchers and praxis, and indirect outcomes for the teacher/student community by developing 'diverse' subject material, which is not only interesting but also vital praxis-academia interaction.

3.1 Research

The research outcome of this program would encompass three facets namely modeling, laboratory and field investigation.

The primary investigation area covers the validation of the technology designed for the first project (decentralized RE) involving dual application (electricity and water pumping) from a small head hydropower source [19]. It includes a laboratory study of the two types of micro hydel pumps (one based on axial pump as turbine and the other based on conventional axial turbine) is scheduled later in 2015. The studies will also be at the system and operational level in pump and generator modes respectively.

The crucial field investigations (planned in 2016) will study the hydro energy utilization for pumping in two different ways, namely the direct way using ram pumps (water hammer based) and the indirect way of micro hydel pumps (turbine:-mechanical power-:pump). A field research station with the 3 prototypes as shown in Fig 11 is planned for executing this study.

A performance chart based on simulations [13, 19] in Fig. 12 reveals a superlative efficiency of 'direct' ram pumping compared to 'indirect' turbine pumping. If the simulations are found to be true, then 'hydraulic ram pumps' will become significant in addition to 'compact' rotating pumps for utilizing small heads. However, this result has to be validated in field tests before a final conclusion can be made.

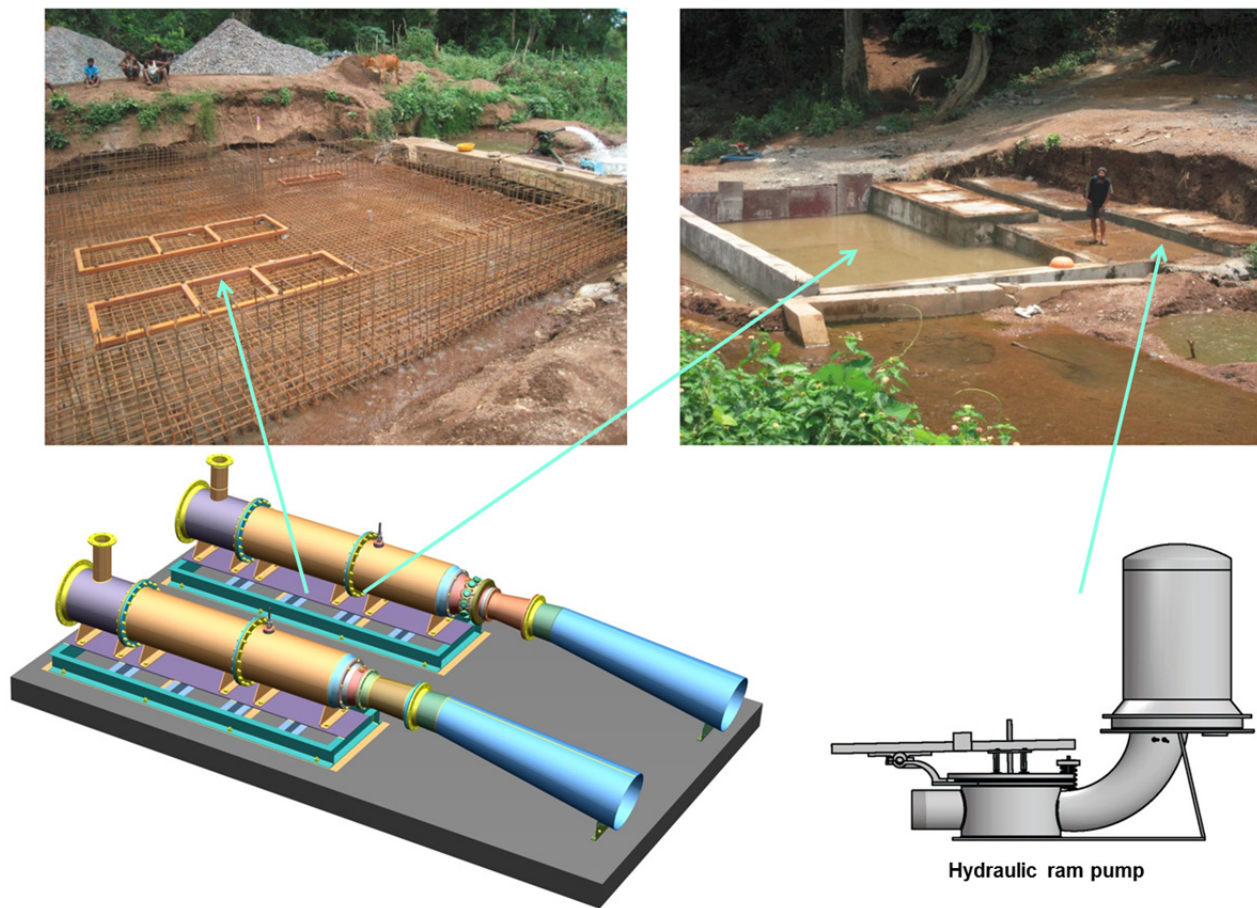


Fig. 11, The field research station for the prototypes based on concept of turbo pump and ram pump

Moving further into the research outcomes one of the themes under study, from the perspectives of fluid mechanics and turbomachinery, is the optimization of hydraulics in axial flow turbines especially within the stationary guide vanes [12]. The other research topic being readied for journals include a study of evaluates the recovery turbines (output mechanical power optimization) to variable speed pumps (input fluid power optimization) in process applications [11]. The author is also working on a new paper that considers a radical change of the impeller design for PAT application [14].

Further to the above laboratory and field studies, the author (after volunteering as a referee (section 5.7) in many journals) has gradually come to believe that the futuristic study of 'small head hydropower' will be done using computational tools because of the lower costs, continuously increasing experience and reasonably accurate results of validation.

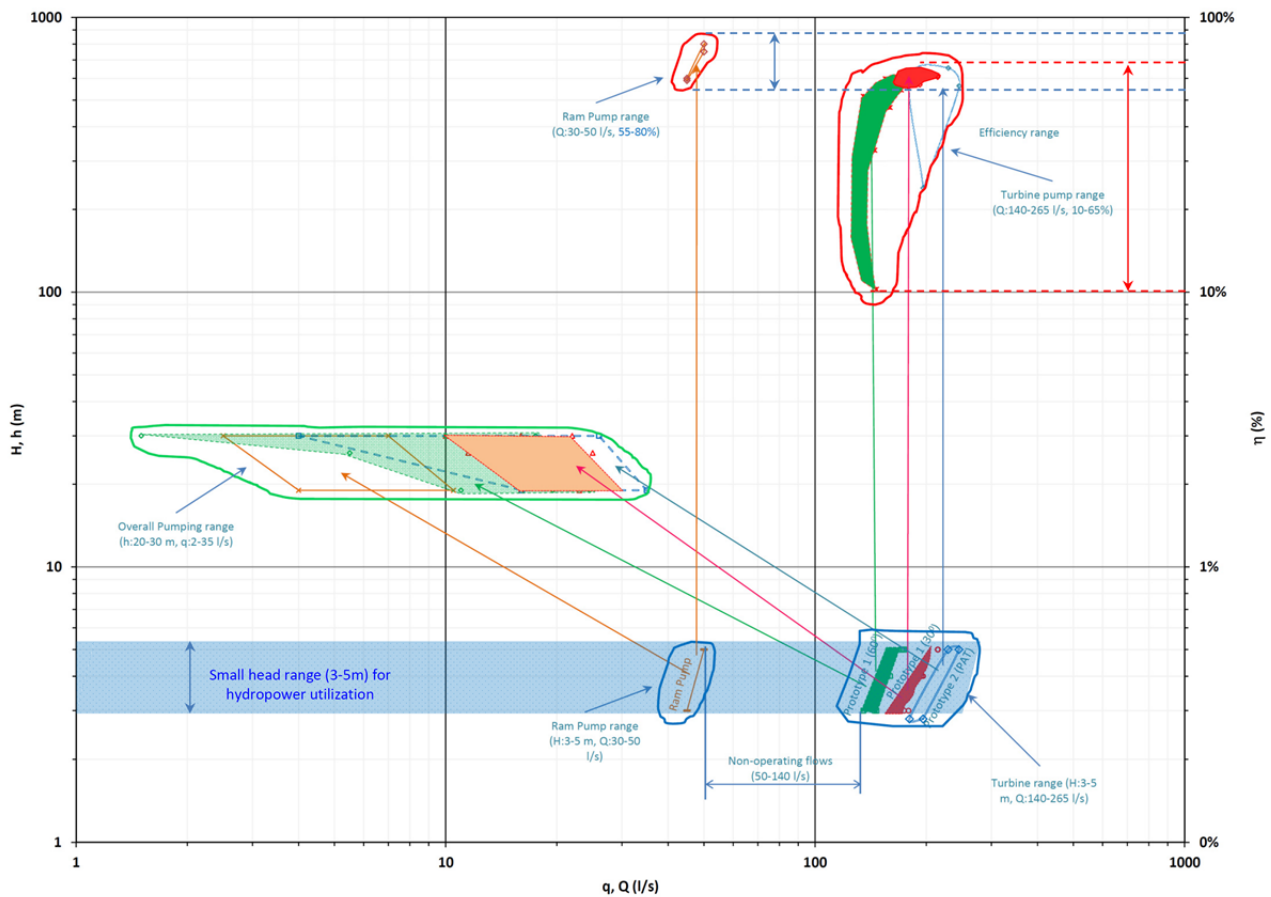


Fig. 12, An evaluation of pumping application of 'small head hydropower' devices³ ([19])

3.2 Application chart

The application chart is direct outcome of the Habilitation that enhances the scope HQ plan to include size parameter (D) and bring out HQD plan. In the special context of the 'small head' constraint, it becomes very important to relate H to the size D. The HQD plan developed (Fig. 13) clears some myths about how 'low' the parameter head can be reduced to.

It is found that stream flow turbines (operating on low flow velocities 1-3 m/s) have heads between 0.2 and 0.5 m only, but their diameters would have to be enhanced to ca 1.2 m in order to generate about 10 kW (mech). The scant availability of free flowing streams with large depths (which has to be 1.5 to 2 times the diameter) makes such turbine solutions ineffective in practice. The limiting small hydropower capacity of 10 kW specified above is based on the author's perspective on the favorable availability of flow less than 3000 l/s.

The above finding reinforces the fact that turbine solution for small heads should be based on creating pressure head artificially through elevation difference. The author finds an effective turbine solution possible only above 1.5 meter, which 'scientifically' sets the definition for the head parameter.

The turbine types in the HQD plan includes standard ones like axial flow turbines, axial flow pumps as turbines and other non-standard types like Archimedean screw turbines, water wheel family amongst a few. The authenticity of HQD plan is the goal of the Habilitation because it gives a clear cut understanding of the dimensions of a very important renewable energy source, i.e. small head hydropower.

While the application chart in Fig. 13 gives guidelines for planners, it will require enormous theoretical and computational modeling to establish the accurate HQD range for each type of turbine and further relate it to efficiency scale.

³ In Fig. 11, Prototype 1 is an adjustable gated axial flow turbine and prototype 2 is an axial flow pump as turbine of fixed geometry

system and will require exposure to systems engineering as well as electronic and mechanical controls for synchronization.

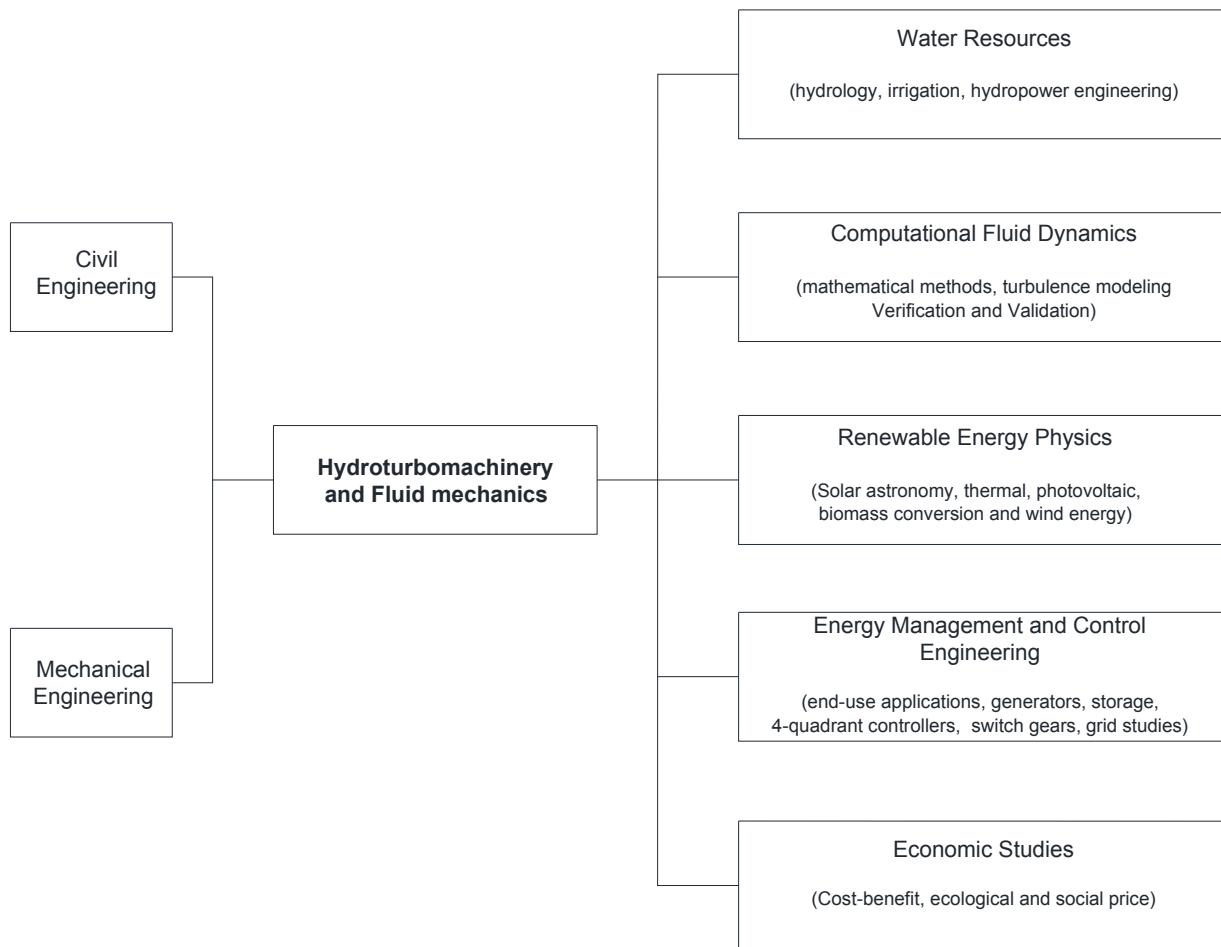


Fig. 14, Flow chart of the teaching program

Above all the above science and engineering subjects, the teaching plan will fail to address the larger question, if the subject of business and economics is excluded, because finally what matters is to make small head hydropower and RE affordable and sustainable.

3.4 Philosophy

To consider gaining intellects as one of the outcome of the 'Habilitation' program is not wrong because the objective of the Habilitation program is to intelligently and appropriately define small heads. Fluid sciences have signaled that head 'below' 1.5 meters would be difficult to conceive from perspective of size (turbine diameter and stream depth). However, the perspectives of other faculties and cultures should be taken into consideration to define the 'head' parameter.

While emphasis has been on defining magnitude for heads, another parameter whose smallness is equally important to address is the useful power. The author earlier specified 10 kW as the upper limit line based on his experience, but the lower limit line needs different consideration. What should be the lower power limit for human activity and dignity? It is definitely possible to design systems for few tens of watts, but what will this satisfy? Therefore author recommends 0.5 kW to be lower power limit line.

Further from the nature's context, the contours of small in heads and powers have different implications. While the small head is welcome causing minimum submergence, small power would imply a larger expense on the economy for the limited gains achieved.

The other philosophical (also technical) question is role of efficiency in 'small head hydropower' systems. Increase in efficiency is welcome but it needs to bring in intellectual expertise and necessarily results in

higher costs. Further to this, a query of the power gain in absolute terms by changing efficiency should also be made.

The debate of 'small heads in hydropower' is not restricted to only one dimension of hydropower, but can be applied to both centralized and decentralized systems, because size does not matter as seen from the outcome of these two projects. Further and eventually the 'philosophical' deliberation should move from small hydropower to other forms of renewable energy covering both centralized and decentralized dimensions because of the equanimity concerning the end-use challenges of electricity and water resources that hardly alter with change of source of renewable power.

4. Summary and Prospects

The decade long work of the author reveals that the function of hydro turbomachinery (whether a PAT or a regular turbine) is at the heart of renewable energy systems with electricity and water resource as their different end-uses. Without the hard laboratory research and field investigation on optimizing the hydro turbine (through peer reviewed references [2-10] and reports [19-21]) the scope of these RE projects would not have been realized.

On the PAT idea, the author's slogan 'to have self-propelled growth of decentralized RE' may have slowed down after implementing the first set of projects by 2008, much to his disappointment. However, over the last 12-18 months he is seeing a subtle but cognizable recognition of the PAT's growth in China where 9 small RE systems based on PAT have already been installed. He is also seeing academic interest being generated in India as well as in Europe. However, the industry (especially the pump industry) is still sceptic on the mass market success of PAT idea compared to the volume of pump sales. This is certainly a setback because industry is the backbone of business and not academia.

In this long and eventful journey, the author may have reached clarity on the relevance of small heads in small hydropower, but there are questions he battles because of the way the two identified field projects have been getting delayed. While outsiders may view this due lack of strategy and will, it is not easy to wish away the large inertia whether it comes from bureaucracy, industry or even scientific community when working on the concept of small.

The author believes that this topic is still a 'futuristic concept' that needs inputs from everyone, prioritizing the end users, then the government whose initial support is vital, a mature politics, a patient industry, a sensitive academia from various disciplines and not to forget the creativity and energy of the student community.

The author reflected in the 'personal introduction' to the quest of defining and realizing the contours of small head hydropower technologies and their efficacy. He will continue this stumbling journey with his two 'contrasting yet similar' projects reflecting both centralized and decentralized characteristics of small hydropower and the associated research, teaching and philosophical outcomes while he gradually promotes the cause of small heads in small hydro power for both end-use applications, electricity and water resource, in a unified way.

The author also recognizes that the scope of small head hydropower is restricted to small population living near flowing streams or few process industries and therefore there is need to look for other renewable energy sources like solar, wind and biomass. The only way to amicably solve and satisfy the ever growing and diverse requirements of society would be to combine two or more renewable energy sources. While integrating them with an available grid may be easy, hybridizing them in a decentralized setup will be challenging at the source level as well as contemplating the end-use strategy for both electricity and water resources application, similar to the small head hydropower case study.

In the future the author would like to focus on the hardware of hybrid renewable energy technologies, like thermal turbomachinery and interface systems. The author would have traversed a full circle only when a self-sustaining renewable energy hybrid systems in decentralized environment for 'electricity and water resources' kicks off in a big way and capturing the imagination of the world over.

5. References

5.1 Ph.D Thesis

- [1] Punit Singh, Optimization of internal hydraulics and of system design of pumps operating as turbines with field implementation and evaluation, Karlsruhe Institute of Technology, 2005

5.2 Journal Papers

- [2] Punit Singh, Franz Nestmann, *A consolidated model for the turbine operation of centrifugal pumps*, *Engineering for Gas Turbines and Power* (ASME), Vol. 133, Issue 6, 2011, pp 063002-1 to 9
- [3] Punit Singh, Franz Nestmann, *An optimization routine on a prediction and selection model of the turbine operation of centrifugal pumps*, *Experimental Thermal and Fluid Science* (Elsevier), Vol. 34, Issue 2, 2010, pp 152-164
- [4] Punit Singh, Franz Nestmann, *Internal hydraulic analysis of impeller rounding in centrifugal pumps as turbines*, *Experimental Thermal and Fluid Science* (Elsevier), Vol. 35, Issue 1, 2011, pp 121-134
- [5] Punit Singh, Franz Nestmann, *Experimental optimization of free vortex propeller runner for micro hydro application*, *Experimental Thermal and Fluid Science* (Elsevier), Vol. 33, Issue 6, 2009, pp 991-1002
- [6] Punit Singh, Franz Nestmann, *Exit blade geometry and part-load performance of small axial flow propeller turbines: An experimental investigation*, *Experimental Thermal and Fluid Science* (Elsevier), Vol. 34, Issue 6, 2011, pp 272-281
- [7] Punit Singh, Franz Nestmann, *Experimental investigation of the influence of blade height and blade number on the performance of low head axial flow turbines*, *Renewable Energy* (Elsevier), Vol. 36, Issue 1, 2011, pp 798-811
- [8] Punit Singh, Franz Nestmann, *Influence of the blade hub geometry on the performance of low head axial flow turbines*, *Energy Engineering* (ASCE), Vol. 33, No. 3, 2012, pp 36-39
- [9] Punit Singh, Franz Nestmann, *Axial flow impeller shapes: Part 1*, *World Pumps* (Elsevier), Vol. 2011, Issue 2, pp 1-4
- [10] Punit Singh, Franz Nestmann, *Axial flow impeller shapes: Part 2*, *World Pumps* (Elsevier), Vol. 2011, Issue 3, pp 109-118

5.3 Journal Papers: (under preparation)

- [11] *A case of energy recovery turbines and variable speed pumps in optimizing industrial process applications* (2011–2015)
- This paper attempts to bring clarity on the expectation of energy recovery turbines in process industries in comparison to variable speed pumps.
 - In both single and multiple process applications, variable speed pump technology is found to be more efficient when a particular process (s) is throttled.
 - However, for multiple processes, the study recommends to install recovery turbines across each individual process to increase the reliability and operation viability when more than half of the processes have to be run at part-load at the same time.
- [12] *A study of flow deviation in different guide vane shapes of an axial flow hydro turbine* (2015)
- This paper investigates the flow deviation (from the blade angle) at the exit of two different designs of guide vane shapes, namely, a circular camber and streamlined parabolic arc camber. The flow deviation has reduced from 15 to 25 deg in circular blades to only 2-3 deg by incorporating a parabolic camber and aerofoil shape.
 - The paper also tries to validate the conservation of momentum of fluid between the guide vane exit and runner inlet, from which a non-conformance of free-vortex theory is found calling for more optimum design of flow path upstream of the runner.
- [13] *A comparison of turbomachinery and ramming techniques for pumping application in small head hydropower systems* (2015)
- The utilization of small head in hydropower for high pressure water pumping is compared using two completely different techniques with startling results. The modern turbo-pump with overall pumping efficiency of 60-65% is found to have lower in comparison with hydraulic ram pump having an efficiency of 70%-80%.
 - The reason for this found to be due to the intermediate mechanical power stage of turbo pump, which does not exist in a ram pump.
 - However, the paper also highlights that the size of ram pump is large when compared with turbo-pumps for identical outputs

[14] *Internal fluid mechanics in pumps operating as turbines with forward and backward vane impellers* (2015)

- This paper studies the fluid mechanics within the two blade shapes of a pump impeller having the same volute in turbine operation. It is found that the losses have undergone a major transformation in forward shaped blades which is expected, but to find changes to rotational fluid or Euler momentum (Δc_u) is an interesting, which is introspected.
- The study is carried out using both experimental and CFD methods, which reveal an identical behavioral trend of the losses, but the relative changes to Euler momentum is different for the two methods. The experiment suggests improved torque for backward shaped blades, which is reverse to that obtained from CFD.
- The paper recommends the use of forward impellers in turbine operation for its superlative efficiency and also for a much improved overload performance.

5.4 Conference Papers

[15] Franz Nestmann, Peter Oberle, Mohammad Ikhwan, Punit Singh, *Bau eines Höhlenkraftwerks zur Trinkwassergewinnung auf, Betonbauwerke im Untergrund - Infrastruktur fuer die Zukunft*, 5. Symposium Baustoffe und Bauwerkserhaltung, University of Karlsruhe, pp 109 – 120, (2008)

5.5 Research Reports and Proposals

[16] Punit Singh, *Preliminary Development Stage of the Prediction Model for Mixed Flow Pumps as Turbines*, 2011

[17] Punit Singh, *A Proposal for a Preliminary Prediction Model for Axial Flow Pumps as Turbines*, 2011

[18] Punit Singh, *Critical Review of a Prediction Model for Axial Flow Pumps as Turbines and a Proposal to Optimize the Model*, 2011

[19] Punit Singh, *Field Research Laboratory for Low Head (Micro) Hydro Powered Water Pumping and Electricity Generation Technologies at Taipadar, Chhattisgarh*, 2014

5.6 Project Reports

[20] Punit Singh, *Taipadar Micro Hydro and Water Resources Management Project (Power, Irrigation and Drinking Water Supply Utilities)*, 2014

[21] Punit Singh, *Mylasandra Hydro Energy Recovery Project*, 2013

5.7 Refereed Papers

The author has volunteered to be referee for 9 papers from a mix of journal houses ranging from established ones like Fluids Engineering, Experimental Thermal and Fluid Sciences to upcoming ones like Engineering Applications in CFM, Energies, Applied Mathematical Modeling and couple of University journals. The topics cover pumps as turbines, pumps and low head turbines, with few being cited work of the author. There is an overwhelming use of computational tools compared to laboratory experiments being adopted in the papers. However, none of them cover case studies, on-field applications and experiences, a trend that should gradually change.

Nomenclature and Abbreviations

D	Turbine runner's outer diameter, m
H	Turbine head, m
h	Pump head, m
Q	Turbine discharge, l/s
q	Pump discharge, l/s
P	Output power (mech), kW
η	Efficiency, %

RE Renewable Energy

PAT Pumps as Turbines

CFD Computational Fluid Dynamics

Appendix

A1 Flow Chart of the Habilitation Program

SMALL HEADS IN SMALL HYDROPOWER

ACTUAL WORK

FOUNDATION PHASE (2005-11)

Journey 1 - Projects
 - Field implementation of PAT projects
 - 3 Journal papers on PATs [1, 2, 3]

Journey 2 - Lab
 - Experiments on 5 propeller runners with cold worked blades
 - 4 Journal papers in propeller turbines [4, 5, 6, 7]

Journey 3 - Field survey
 - Remote hydro and process Industries
 - The TURBINE PLAN (1-10 m, 50-2000 l/s)

ACTION PHASE (2012-14)

- 2 small head projects selected

- First Project [18]: Remote Hydro with dual application of water pumping and electricity

- Innovative design of 'micro hydel pump' (axial flow turbine with generator and multi stage centrifugal pump)
- Pumping method for low flows - selection of ram pump instead of turbine pump

- Second Project [19]: Hydro Energy Recovery in a water treatment plant with grid interface

OUTCOME

RESEARCH

MICRO HYDEL PUMP

- Laboratory study of adjustable geometry axial flow turbine and fixed geometry axial flow PAT

- Smooth switching operation from electricity to pump mode and vice versa

PUMPING APPLICATION

- Field investigation [12, 17] of,

- direct pumping (ram pump) and
- indirect pumping (turbine to mechanical power to pump)

FUNDAMENTAL

- Effect of guide vane shape on the fluid deviation in axial flow turbine [11]

- Forward and backward runner shapes in PATs [13]

APPLICATION CHARTS

- HQD chart
 . for a turbine mix with heads less than 5 meters

- Myths of stream flow turbines
 . with heads less than 0.5 m (ca 3 m/s) need large sizes (ca 1.2 m dia and 2 m stream depth) for 10 kW output.

- Lower head limit
 . above 1.5 meters.

- Recommended power limits
 . 0.5 to 10 kW.

TEACHING

CORE (FUNDAMENTAL)

FLUID MECHANICS

TURBO MACHINES

CFD

PHILOSOPHY

- How to define **small** for heads and power in small hydro In context of people and nature?

- Defining efficiency limits for small head technologies?

- Open up debate with rationalists

INTER-DISCIPLINE

WATER RESOURCES

IRRIGATION

BUSINESS

RENEWABLE ENERGY

PROSPECTS

- The decade of work has defined the relevance of small heads, but with many questions.

- Questions because of 'endlessly' delay in the two projects

- 'Small head small hydropower' Is a futuristic concept and the author will continue the stumbling journey of projects and its outcomes

**FULL PRINTS OF THE CITED REFERENCES IN THE
HABILITATION SYNOPSIS**

**‘THE SMALL HEAD CRITERION IN HYDROPOWER AND UNDERSTANDING THE
DIMENSIONS OF RENEWABLE ENERGY WITH WATER RESOURCES’**

Dr.-Ing. Punit Singh

July, 2015

5.2 JOURNAL PAPERS

- [2] Punit Singh, Franz Nestmann, *A consolidated model for the turbine operation of centrifugal pumps*, *Engineering for Gas Turbines and Power* (ASME), Vol. 133, Issue 6, 2011, pp 063002-1 to 9
 - [3] Punit Singh, Franz Nestmann, *An optimization routine on a prediction and selection model of the turbine operation of centrifugal pumps*, *Experimental Thermal and Fluid Science* (Elsevier), Vol. 34, Issue 2, 2010, pp 152-164
 - [4] Punit Singh, Franz Nestmann, *Internal hydraulic analysis of impeller rounding in centrifugal pumps as turbines*, *Experimental Thermal and Fluid Science* (Elsevier), Vol. 35, Issue 1, 2011, pp 121-134
 - [5] Punit Singh, Franz Nestmann, *Experimental optimization of free vortex propeller runner for micro hydro application*, *Experimental Thermal and Fluid Science* (Elsevier), Vol. 33, Issue 6, 2009, pp 991-1002
 - [6] Punit Singh, Franz Nestmann, *Exit blade geometry and part-load performance of small axial flow propeller turbines: An experimental investigation*, *Experimental Thermal and Fluid Science* (Elsevier), Vol. 34, Issue 6, 2011, pp 272-281
 - [7] Punit Singh, Franz Nestmann, *Experimental investigation of the influence of blade height and blade number on the performance of low head axial flow turbines*, *Renewable Energy* (Elsevier), Vol. 36, Issue 1, 2011, pp 798-811
 - [8] Punit Singh, Franz Nestmann, *Influence of the blade hub geometry on the performance of low head axial flow turbines*, *Energy Engineering* (ASCE), Vol. 33, No. 3, 2012, pp 36-39
 - [9] Punit Singh, Franz Nestmann, *Axial flow impeller shapes: Part 1*, *World Pumps* (Elsevier), Vol. 2011, Issue 2, pp 1-4
 - [10] Punit Singh, Franz Nestmann, *Axial flow impeller shapes: Part 2*, *World Pumps* (Elsevier), Vol. 2011, Issue 3, pp 109-118
-

A Consolidated Model for the Turbine Operation of Centrifugal Pumps

Punit Singh

e-mail: punit.singh@iwg.uka.de

Franz Nestmann

e-mail: nestmann@iwg.uka.de

Institute for Water and River Basin Management
(IWG),
Karlsruhe Institute of Technology,
Kaiser Strasse 12,
D 76128 Karlsruhe, Germany

A consolidated model for the turbine operation of centrifugal pumps comprising accurate prediction, optimum selection, and rigorous evaluation has been the primary need and the most challenging tasks for the industry to deal with. This paper introduces a consolidated model that is developed from experimental results of different pump shapes (20–80 rpm) and turbomachine fundamentals directly resulting in the parsimony feature of the model. The model also creates a new basis for dealing with uncertainties. The prediction model segment of the consolidated model requires only the pump shape and size as input parameters for bringing out the complete turbine characteristics. The selection model segment, on the other hand, requires the site head and flow as fixed input parameters and turbine speed as the control parameter to prescribe suitable pumps available in the market. The evaluation model segment compares the absolute turbine characteristics of the suitable pumps and recommends the most suitable pump for the given site. The model also includes an acceptance criterion that relates the deviation of the “pump as turbine” operating parameters with the site parameters, and it is very useful at the evaluation stage. The features of the consolidated model are illustrated with two case studies, which highlight the importance of evaluation in addition to the prediction and basic selection of pumps operating as turbines. In order to increase the accuracy and robustness of the model, the paper recommends an optimization routine stage on the existing model that comprises results of more pump shapes (obtained through field projects or extended laboratory work). The optimization procedure suggested would come a long way to provide a lasting solution for the search of a reliable pump as turbine model.

[DOI: 10.1115/1.4002270]

Keywords: pump as turbine, prediction, selection, evaluation, Cordier line, uncertainty analysis, acceptance criterion, optimization

1 Introduction

1.1 Background. The foremost aspect for the success of any application (energy recovery or microhydro) using pumps as turbines can be categorized into three major items that include an optimum selection of pump shapes, an accurate prediction of their turbine characteristics, and a true evaluation of their suitability for the given application. The importance of this threefold (selection, prediction, and evaluation) problem in modeling pumps as turbines is described by Singh [1]. The consequences of nonadherence to this process mainly relate to the pump as turbine (PAT) not being able to fully utilize the site condition (available flow and head) coupled to a fear of operating in the inefficient part-load condition.

The contemporary PAT researchers that include Williams [2], Cohrs [3], Amelio and Barbarelli [4], and Derakhshan and Nourbakhsh [5] have undoubtedly tried to develop a holistic model, but their attempt has still fallen short to address the comprehensive need for prediction, selection, and evaluation separately. While the focus of these scientists has been only on the prediction of turbine performance of pumps, the selection and evaluation components with respect to site conditions are not dealt with in more detail. Further, the basis of prediction of these models that relate the turbine mode and pump mode performances only to a single operating point at the best efficiency point (BEP) using complex formulations is questionable. The inaccuracies of these methods

pointed out by Singh [1] and Derakhshan and Nourbakhsh [5] are so large (between 20% and 60% at times) that the application of this technology becomes very difficult. Moreover, some of these models are difficult to apply since they require complex designs and geometric data, including some assumptions such as operating efficiency and hydraulic phenomena such as slip within the impeller. Above all this, they have not been rigorously tested on different pump shapes to get more insights about their features such as reliability, accuracy, and robustness.

The above situation reveals that there is a need for developing a comprehensive model that will predict the complete operating characteristics (including the no-load, part-load, and overload operating points) and not single-point predictions like most models do. Further, the model should be simple to apply and yet be accurate in performance. It should also bring about a new basis for defining the uncertainties in prediction. The model should clearly specify the shapes (or designs) of the pumps on which it could be used. Therefore, a new approach should be adopted that could comprise experimental results of different shapes of centrifugal pumps combined with principles of classical turbomachines. In addition to this, at the application level, the model should give a new dimension for selection and evaluation procedures for a given PAT by defining the criteria of acceptance under the specified operating conditions of head and flow. The prime focus should be on developing a permanent solution for modeling in pumps as turbines so that the model becomes valuable to the scientific and engineering world.

1.2 Objectives and Problem Outline

- (1) To experimentally characterize standard centrifugal pumps as turbines covering radial backward vane shapes.

Contributed by the Power Division of ASME for publication in the JOURNAL OF ENGINEERING FOR GAS TURBINES AND POWER. Manuscript received May 22, 2010; final manuscript received June 8, 2010; published online February 15, 2011. Editor: Dilip R. Ballal.

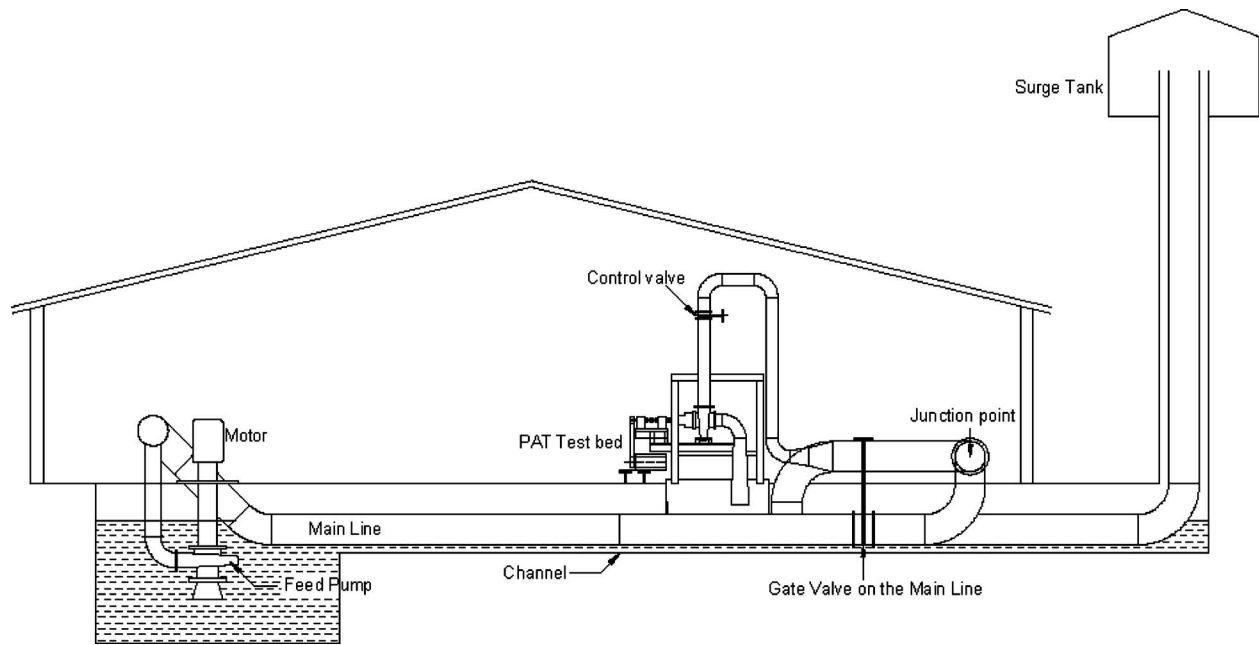


Fig. 1 Open loop hydraulic test rig for characterizing the pumps as turbines

- (2) To introduce the concept of consolidated model in PATs comprising prediction, selection, and evaluation procedures and to adopt a new basis of evaluating uncertainties.
- (3) To develop a prediction model that brings about the complete operating characteristics of a PAT with the help of the least number of input variables.
- (4) To develop a selection model that will choose suitable pumps from standard manufacturers for a given turbine application.
- (5) To introduce an evaluation procedure that will scrutinize the utilization potential of the selected PATs for the given site by defining a criterion of acceptance before recommending the most suitable pump.
- (6) To discuss the features of the consolidated model and recommend ways to improve its robustness and find a lasting solution.

The problem outline based on the defined objectives would first comprise the presentation of the detailed theory for modeling the prediction, selection, and evaluation segments. Next, the application of these model segments on two case studies having different head and flow conditions will have to be carried out in order to study its usefulness and make further refinements.

2 Means of Developing the Model

2.1 Experimental Means. A well-calibrated open loop hydraulic test rig (shown in Fig. 1) is constructed to characterize the turbine operation of the different centrifugal pumps, as described in Ref. [1]. The test arrangement also comprises state-of-the-art instrumentation such as inductive pressure transducers for measur-

ing pressure, a magnetic flow meter for discharge, a torque transducer for torque, and an optical transducer for speed. The centrifugal pumps are backward vane, single stage, end suction pumps in the range of 20–80 rpm, whose impellers of closed designs (with shrouds) are also illustrated in Ref. [1].

2.2 Theoretical Means. The optimum design and selection of any type of turbomachine has been revolutionized by the introduction of two dimensionless numbers defined at the BEP known as specific speed and specific diameter, which clearly relate to the shape (or design) and optimum size of the turbomachine. First, by Cordier [6] and then by Balje [7], the unique relationship between these two numbers has been very useful to designers to fix the dimensions of the turbomachines, be it a compressor, a pump, or a turbine. Hence, without doubt, the present problem of developing a robust model for PATs should also be based on these principles, and a unique relationship between specific speed and specific diameter for centrifugal pumps operating as turbines needs to be established.

3 Theory of the Models

3.1 Overview of the Consolidated PAT Model. The consolidated PAT model should comprise three separate segments, as highlighted in Sec. 1.1. The overview of all the model segments and their inter-relationship is shown in Fig. 2, which forms the basis of the consolidated model required for PAT application. The selection model should select the centrifugal pumps that would suit the given turbine application (head and flow). The prediction model, on the other hand, as seen should evaluate the turbine mode characteristics of the selected pump (of a given shape and

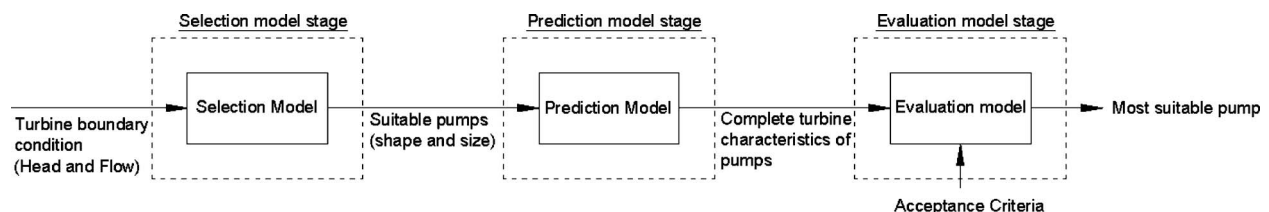


Fig. 2 Consolidated model for pumps as turbines

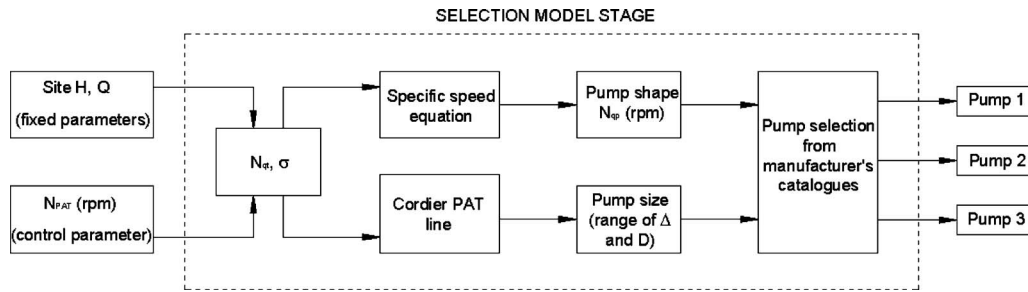


Fig. 3 Flow chart of the selection model

size). The final segment is the evaluation model that shall study the turbine mode characteristics of different pumps and select the best pump using an acceptance criterion.

3.2 Selection Model. The basic selection model of Fig. 2 is enhanced in Fig. 3 where other steps are described. The selection of the suitable pumps for a given site (with head and flow) is primarily guided by the experimentally determined mean Cordier PAT line (explained in Sec. 3.3.2). The fixed input parameters, namely, the head and flow, are used along with the turbine mode specific speed (N_{qt}) and σ (given by Eq. (A5)). The control parameter is the designer's choice and can take values to suit the best operating region along the Cordier line and also the available pump shapes with the manufacturer.

The turbine mode specific speed (N_{qt}) leads to the pump mode specific speed (N_{qp}) using the experimental relationship between them (whose philosophy is described in Sec. 3.3.1) and defines the shape of the required pump. The intersection of the constant σ line with the uncertainty bands of the mean Cordier line (represented by Eq. (6) and explained in Sec. 3.3.4) gives a range of specific diameters, which can be translated to absolute diameters using relations in Appendix B.

The final output parameters of the selection model are the pump mode specific speed, which represents the pump shape, and the range of impeller diameters, which represents the pump size. The choice of pumps will be solely guided by these two parameters. A manufacturer's catalog should be referred to at this stage, and it has to be emphasized that there could be a possibility that more than one pump could be suitable for the same site, but with a different shape.

3.3 Prediction Model. The prediction model as introduced in Fig. 2 is completed in five different steps described in the following sections.

3.3.1 Turbine Mode and Pump Mode Specific Speeds. To initiate the application of the prediction model, it is important to establish a relation between the shapes (or the specific speed) of the two operating modes of a centrifugal pump. This is done by creating a plot between the experimental specific speeds of the tested pumps (Table 7) in both pump and turbine modes, as shown in Fig. 4, which brings out an approximate straight-line relationship. It can be interpreted from the available data that any given centrifugal pump has a marginal lower specific speed in the turbine mode due to the larger impact of the head number compared with the discharge number (Eq. (A3)). The turbine specific speed given by Eq. (1) would obviously have errors given the varied design methods employed by manufacturers and shall be treated separately in Sec. 3.3.4,

$$N_{qt} = 0.942 \cdot N_{qp} - 3.2 \quad (1)$$

3.3.2 The Cordier PAT Line. The best efficiency points of all the tested PATs (using data in Table 7 and relations in Appendix B) are plotted on the Cordier diagram format [6], as shown in Fig.

5. This figure also plots the constant efficiency lines (that signify the part-load condition) along with constant head number lines. The mean Cordier PAT line that forms a relationship between specific speed and specific diameter is given by Eq. (2). As mentioned in Sec. 2.2, the Cordier line has a major significance in turbomachinery design, and hence it is quite natural that a unique line developed exclusively for PATs would also play a significant role in PAT modeling. There are two more bands plotted along with the mean Cordier line, which shall be discussed in Sec. 3.3.4,

$$\sigma = 1.225\Delta^{-1.288} \quad (2)$$

Equation (2) can be converted to the respective head number and discharge number values at the BEP at any given point on the mean Cordier PAT line, which corresponds to a PAT shape under consideration. The magnitude of the BEP of this PAT (or prototype) is determined using the standard efficiency scaling law (Eq. (3)) proposed by Moody and Zowski in Ref. [8] with the test data (summarized in Table 7) used as model values. Equation (3) signifies that the loss coefficients within a turbine of same shape do

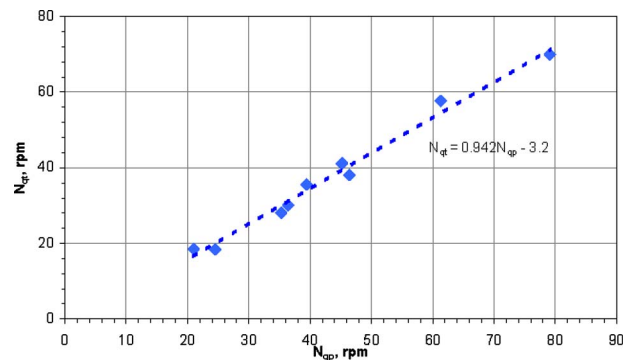


Fig. 4 A plot showing the relationship between the pump and turbine mode specific speeds

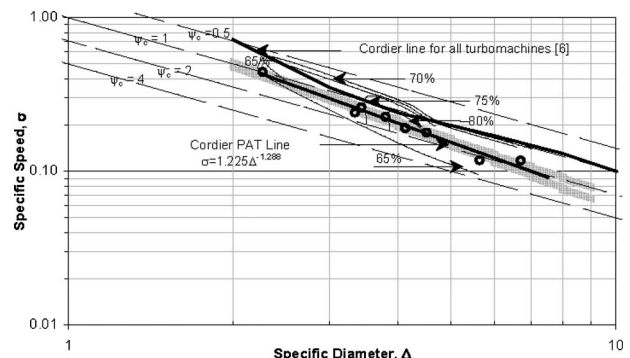


Fig. 5 The Cordier PAT line

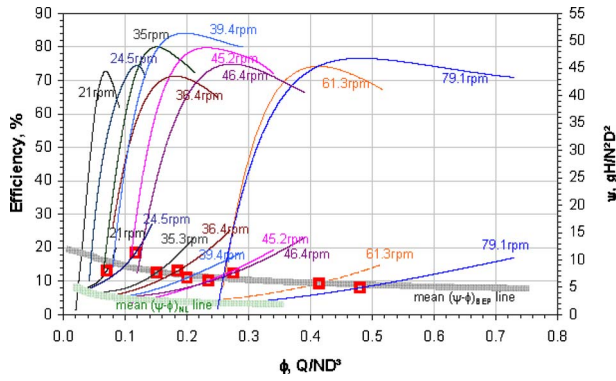


Fig. 6 Overall ψ - ϕ and η - ϕ characteristics of nine PATs

not scale with size, and necessary corrections would have to be adopted,

$$\frac{1 - \eta_{pt}}{1 - \eta_{mo}} = \left(\frac{D_{mo}}{D_{pt}} \right)^n \quad \text{where } n = 0.2 - 0.25 \quad (3)$$

3.3.3 Predictions at No-Load Condition. It is prerequisite to make predictions of the no-load condition of the respective PAT in order to evaluate its complete turbine characteristics. For this purpose, the dimensionless head number and efficiency characteristics of all the nine experimentally PATs are plotted on the same abscissa and ordinates, as shown in Fig. 6, and the no-load points (ϕ, ψ) are related by Eq. (4). The equation signifies that within the space formed by ϕ and ψ , the dependent number ψ at the no-load condition has a unique relation with control number ϕ ,

$$\psi_{nl} = 1.354 \cdot \phi_{nl}^{-0.341} \quad (4)$$

Equation (4) will be useful only if there is a relationship between the turbine shape (specific speed) and the no-load discharge number. This is done with the help of Eq. (5). Both Eqs. (4) and (5) are developed from experimental data of the nine PATs in Appendix A. It is to be pointed out that the methodology of no-load predictions is broadly similar to the Cordier analysis (Sec. 3.3.2), carried out at the no-load condition instead of BEP,

$$\phi_{nl} = 1.190 \cdot \sigma^{1.734} \quad (5)$$

3.3.4 Uncertainty Analysis in the Prediction Model. There are two sources of error in the model, namely, the experimental and external errors. Experimental errors are associated with the measured variables on the test rig and can be determined in a straightforward manner using techniques proposed by Moffat [9] and Kline [10]. However, the external variables are associated with the unknown specimen pump, which are more complex in nature. These errors deal with the accuracy of determining the pump mode BEP, pump design (or specific speed as pointed out in Sec. 3.3.1), and manufacturing tolerances adopted that vary from manufacturer to manufacturer.

A creative methodology is proposed to include both the experimental and external errors for the mean Cordier PAT line (given Eq. (2)) by proposing some kind of tolerance bands. The experimental errors for the parameters ϕ and ψ at BEP for all the tested PATs (in Appendix A) are summarized in Fig. 7, which shows that ϕ errors are significant at lower specific speeds, while the ψ errors are of smaller magnitude and consistent over all specific speeds. It would hence make more sense to proceed with ϕ errors as the reference for developing uncertainty analysis. On the other hand, external errors are very difficult to quantify. Nevertheless, it is assumed to have errors in the range of about $\pm 5\%$ for lower specific speeds and $\pm 2\%$ to $\pm 3\%$ for higher speeds on the ϕ scale. The combined errors of ϕ_{bep} (experimental and external) are plotted in Fig. 8. The tolerance bands for Δ are selected such that

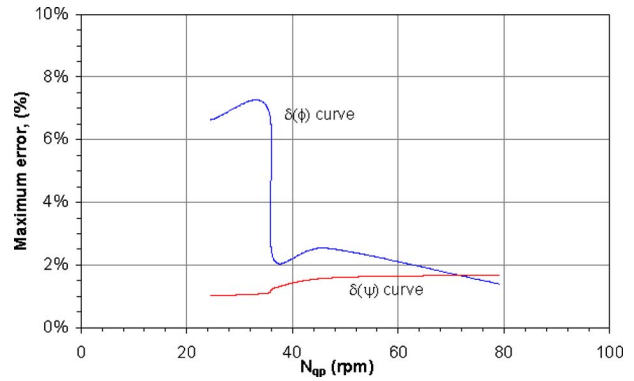


Fig. 7 Experimental uncertainty at BEP versus N_{qp}

an introduction of parameter R_Δ in Eq. (2) gives the identical error pattern for ϕ , as shown in Fig. 8. The modified mean Cordier line with error bands is represented in Eq. (6). The physical significance of error bands for Δ is the lateral shifting of the ψ - ϕ and η - ϕ characteristics, as will be seen in the case studies dealt in Sec. 4,

$$\sigma = (1.225 \pm R_\Delta) \cdot \Delta^{-1.288} \quad (6)$$

The analysis in Fig. 8 provides for the uncertainties only at the BEP, but it becomes imperative to specify the uncertainty limits for the no-load points as well. To simplify the approach, the uncertainty levels obtained for the discharge number at BEP ($\delta\phi_{bep}$) are retained for the discharge number at the no-load point ($\delta\phi_{nl}$) as well. Once the range of no-load discharge numbers is obtained, the corresponding range for the head numbers is calculated from the modified form of Eq. (4), given by Eq. (7). The significance of Eq. (7) is similar to that of Eq. (4) except that it gives head number limits for the upper and lower discharge numbers,

$$\psi_{nl} = (1.354 \pm 0.1) \cdot \phi_{nl}^{-0.341} \quad (7)$$

This range of head number and discharge number points at the no-load and the BEP essentially specify the upper and lower bands of the mean ψ - ϕ characteristics (as illustrated in Sec. 4). The final task is to join the no-load points and BEPs of the respective bands with the help of a best-fit curve to obtain the desired predicted characteristics of the PAT.

3.3.5 Interpolation Using the Hermite Spline Approach. The construction of the head number (ψ - ϕ) and efficiency (η - ϕ) curves is the hallmark of the prediction model stage. This is achieved using a widely used curve fitting methodology, documented by Holman [11] and Boor [12]. It can be seen from Fig. 6 (the experimental plot) that both the head number and efficiency parameters are functions of both specific speed and discharge number. The ψ - ϕ and η - ϕ curves show a characteristic pattern

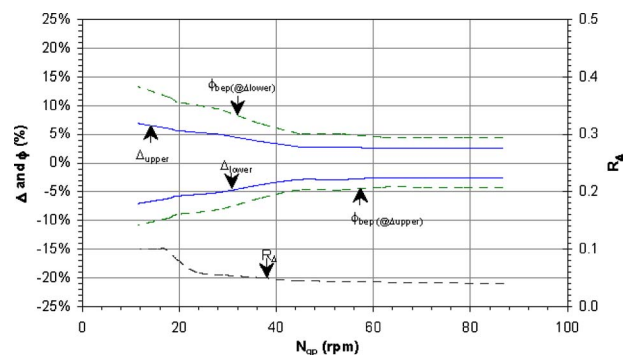


Fig. 8 Uncertainty bands for Δ and ϕ

of slopes and range along the abscissa, where the lower specific speed PATs are closer to the origin compared with higher specific speeds.

In order to construct the head number and efficiency characteristics of a new PAT (with a given N_{qp}), the Hermite spline interpolation technique is used [12]. This technique consists in using two fixed points on the characteristics (i.e., BEP and no-load point, which have already been determined) and the slopes at these points to generate a three-degree polynomial for the respective characteristics, i.e., head number and efficiency.

The slopes of both ψ and η with respect to ϕ can be readily determined from the experimental results illustrated in Fig. 6. Using separate polynomials for the efficiency and head number characteristics, the mean as well as the uncertainty bands for turbine operation can be plotted for any given pump specific speed. The resultant polynomials have shown excellent fitting for all the nine experimentally tested PATs. It has to be remembered that the interpolation holds good for the curve between the no-load point and BEP. However, some extrapolation is carried out to evaluate the characteristics in the overload region.

3.4 Evaluation Model and Criterion of Acceptance. The selection of the pumps in Fig. 3 does not mean that they would be the automatic and final choice for the site. The selected pump needs to pass the test of acceptance where the actual operating point of the PAT (after the prediction of the characteristics) is compared with that of the site. The evaluation stage (Fig. 2) consists in using the predicted mean $\psi-\phi$ and $\eta-\phi$ curves to develop the absolute characteristics of the PAT. These characteristics (also known as Muschel curves) will also combine the constant speed, the constant efficiency lines, and the no-load line of the given PAT along with the field point, from which the PAT's ability to utilize the complete head and discharge can be investigated. If there is a situation of nonutilization of either head or flow, which

may often be the case, these deviations will be compared with the criterion of acceptance, and a decision of the pump's applicability for the site can be taken.

The criterion of acceptance for the selected pumps is an important aspect of the evaluation model, as seen in Fig. 2. This parameter is mainly user or customer defined. For an initial evaluation, the percentage of nonutilization of either of the site parameters (either head or flow) keeping the other constant in comparison with the turbine operating point should not exceed $\pm 4\%$. This interval can be reduced further to make the final choice of PAT to exactly conform to site conditions.

4 Results

As mentioned in Sec. 1.2, the application of the consolidated PAT model will be carried on two separate sites. The various aspects of the model such as selection (Sec. 3.2), prediction (Sec. 3.3), and evaluation (Sec. 3.4) will be illustrated. The first site has a flow of 45 l/s and a head of 60 m, while the second site has a flow of 80 l/s and a head remaining at 60 m.

4.1 Case Study: 1–45 l/s and 60 m

4.1.1 Application of the Selection Model. The selection of pumps for this site condition is summarized in Table 1 at two trial speeds (1500 rpm and 3000 rpm) using steps described in the selection model stage of Fig. 3. The table provides the required pump mode specific speeds and the range of impeller diameters for both the low-speed and high-speed operations, respectively. These specifications lead to the selection of two pumps (18.2 rpm and 35.1 rpm) from the catalogs [13], whose BEP points are also summarized in Table 1. The 18.2 rpm PAT is slightly outside the diameter range specified by the model, but this does not matter since this is only an initial selection, and a detailed evaluation will determine its final suitability and applicability.

Table 1 Selection table for site 1 with 45 l/s and 60 m

Speed option	Pump requirements				Selected pump from Ref. [13]	
	Pump shape		Pump size			
Option 1, speed –1500 rpm	N_t	1500 rpm	Range of Δ and D required		Impeller diameter, D	329 mm
	N_{qt}	14.8 rpm	$\Delta_1=6.912$	$D_1=282$ mm	Pump mode	H_p 32.5 m
	σ	0.094	$\Delta_m=7.364$	$D_m=301$ mm	BEP	Q_p 29.2 l/s
	N_{qp} (reqd)	19.1 rpm	$\Delta_u=7.809$	$D_u=319$ mm		N_p 1450 rpm
						N_{qp} 18.2 rpm
Option 2, speed –3000 rpm	N_t	3000 rpm	Range of Δ and D required		Impeller diameter, D	174 mm
	N_{qt}	29.5 rpm	$\Delta_1=4.127$	$D_1=169$ mm	Pump mode	H_p 33.5 m
	σ	0.187	$\Delta_m=4.300$	$D_m=176$ mm	BEP	Q_p 28.3 l/s
	N_{qp} (reqd)	34.7 rpm	$\Delta_u=4.471$	$D_u=183$ mm		N_p 2900 rpm
						N_{qp} 35.1 rpm

Table 2 Consolidated prediction table for 18.2 rpm PAT

Pump data		Cordier PAT data				No-load points			PAT operating points		
$H=32.5$ m $Q=29.2$ l/s	Cordier line intersection	Coefficients at different Δ $\Delta_m=7.696$ $\Delta_1=7.224$ $\Delta_u=8.161$				$\psi-\phi$ line Mean	ϕ_{nl} 0.019 (+11.5%, -9.5%)	ψ_{nl} 5.25	$\psi-\phi$ line Mean	$(\phi, \psi)_{nl}$ (0.019, 5.25)	$(\phi, \psi)_{BEP}$ (0.061, 10.66)
$N=1450$ rpm	$N_{qt}=13.9$ rpm	σ_m	0.088	0.096	0.082	Upper	0.017	5.83	Upper	(0.017, 5.83)	(0.055, 11.03)
$D=0.329$ m	$\sigma=0.088$	ϕ_{mt}	0.061 (+11.5%, -9.5%)	0.068	0.055	Lower	0.021	4.68	Lower	(0.021, 4.68)	(0.068, 10.28)
$N_{qp}=18.2$ rpm	$\Delta_m=7.696$ (+6.0%, -6.1%)	ψ_{mt}	10.66	10.28	11.03				η value	0%	74%
$\psi_p=5.043$	$\Delta_1=7.224$	ϕ_{mt}/ϕ_p	1.81	2.01	1.63						
$\phi_p=0.034$	$\Delta_u=8.161$	ψ_{mt}/ψ_p	2.11	2.04	2.19						

Table 3 Consolidated prediction table for 35.1 rpm PAT

Pump data		Cordier PAT data				No-load points			PAT operating points		
H=33.5 m Q=28.3 l/s	Cordier line intersection	Coefficients at different Δ $\Delta_m=4.264$ $\Delta_l=4.093$ $\Delta_u=4.434$				$\psi-\phi$ line Mean	ϕ_{nl} 0.066 (+7.3%, -6.4%)	ψ_{nl} 3.41	$\psi-\phi$ line Mean	$(\phi, \psi)_{nl}$ (0.066, 3.41)	$(\phi, \psi)_{BEP}$ (0.168, 7.59)
N=2900 rpm	$N_{qt}=29.8$ rpm	σ_m	0.189	0.199	0.180	Upper	0.062	3.75	Upper	(0.062, 3.75)	(0.157, 7.76)
D=0.174 m	$\sigma=0.189$	ϕ_{mt}	0.168 (+7.3%, -6.4%)	0.180	0.157	Lower	0.071	3.08	Lower	(0.071, 3.08)	(0.180, 7.41)
$N_{qp}=35.1$ rpm	$\Delta_m=4.264$ (+4.0%, -4.0%)	ψ_{mt}	7.59	7.41	7.76			η value	0%	76%	
$\psi_p=4.646$ $\phi_p=0.11$	$\Delta_l=4.093$ $\Delta_u=4.434$	ϕ_{mt}/ϕ_p	1.51	1.62	1.41						
		ψ_{mt}/ψ_p	1.63	1.59	1.67						

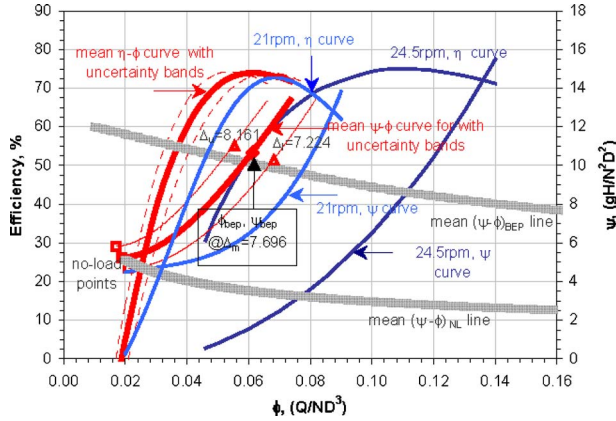


Fig. 9 $\psi-\phi$ and $\eta-\phi$ curves for 18.2 rpm PAT

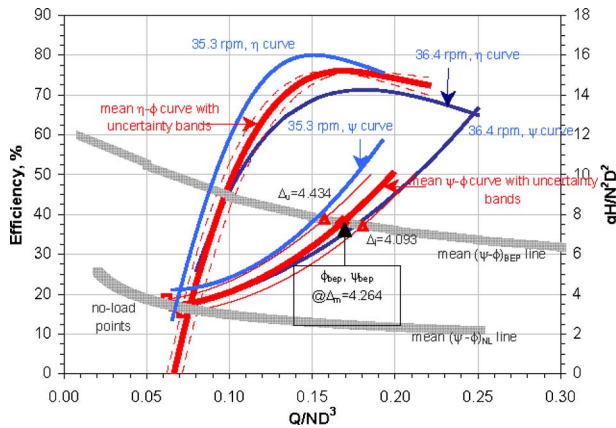


Fig. 10 $\psi-\phi$ and $\eta-\phi$ curves for 35.1 rpm PAT

4.1.2 Application of the Prediction Model. The next step involves the prediction of the turbine characteristics for these two pumps using the prediction model described in Sec. 3.3. The results of the prediction model are summarized in the form of a table (Table 2 for 18.2 rpm PAT and Table 3 for the 35.1 rpm PAT), illustrating the predictions of the BEP and the no-load condition for the mean, lower, and upper uncertainty limits. Subsequently, the dimensionless characteristics are constructed using Hermite splines (Sec. 3.3.5) for the two PATs (Fig. 9 for 18.2 rpm PAT and Fig. 10 for the 35.1 rpm). The lateral shifting of the $\psi-\phi$ and $\eta-\phi$ curves of these PATs is a direct consequence of the error bands on Δ (as discussed in Sec. 3.3.4). Finally, the Muschel characteristics are constructed, as shown in Fig. 11 for the 18.2 rpm PAT and in Fig. 12 for the 35.1 rpm PAT.

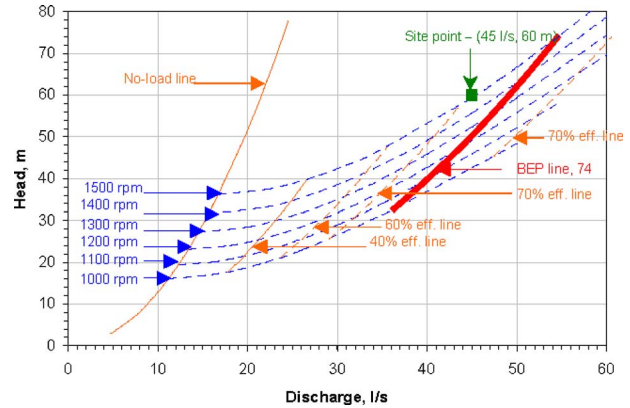


Fig. 11 Muschel curves for 18.2 rpm PAT

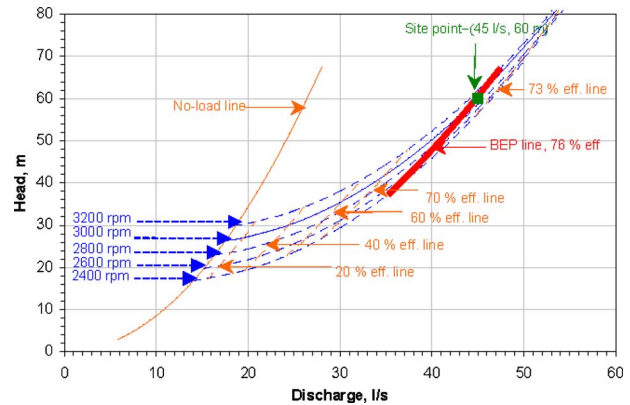


Fig. 12 Muschel curves for 35.1 rpm PAT

4.1.3 Application of Evaluation Model. The field point (45 l/s and 60 m) is integrated into these characteristics, and the evaluation is carried out in Table 4. For the given boundary conditions, the 18.2 rpm PAT is seen to operate in the part-load region at a speed of 1500 rpm and to generate 18.7 kW of shaft power. However, it utilizes a head of 59.4 m (with a deviation of $\pm 1\%$) at 45 l/s and hence passes the acceptance test ($\pm 4\%$). On the other hand, the 35.1 rpm PAT realizes the complete utilization of available head and flow, but at a higher speed of 3000 rpm. In addition, this PAT operates on the BEP line and generates 1.5 kW more shaft power compared with the 18.2 rpm PAT. For a designer, the obvious choice would be to go in for a higher speed PAT for this site. But other factors such as mechanical design and system design issues, like the critical speed and the availability of high-speed generators, should be considered before making the final decision.

Table 4 Evaluation of the merits of the two PATs for site 1 with 45 l/s and 60 m

PAT (rpm)	H (m)	δH (%)	Q (l/s)	δQ (%)	N_{optimum} (rpm)	Predicted shaft power	Operating region
18.2	59.4	-1.0	45	0	1500	18.7 kW @ $\eta=71.4\%$	Part-load (near BEP)
35.1	60	0	45	0	3000	20.2 kW @ $\eta=76.0\%$	On the BEP line

4.2 Case Study 2: 80 l/s and 60 m

4.2.1 *Application of the Selection Model.* For the second site, the selection procedure is carried out at two trial speeds (1150 rpm and 1500 rpm) with the help of the Cordier PAT diagram, and the results are summarized in Table 5. Two pumps of 19.7 rpm and

25.4 rpm that meet the requirement of the site are chosen from the manufacturer’s catalog [13].

4.2.2 *Application of the Prediction Model.* The prediction model as in the case of the previous site is implemented, and the Muschel curves for the 19.7 rpm and 25.4 rpm PATs are developed in Figs. 13 and 14, respectively.

4.2.3 *Application of Evaluation Model.* The evaluation of the selected PATs (19.7 rpm and 25.4 rpm) with respect to the site specifications is carried out in Table 6. For the 25.4 rpm PAT, it can be seen from Fig. 14 that the field point (80 l/s, 60 m) does not fall within the range of constant speed characteristics plotted. To meet the site flow condition of 80 l/s, this PAT would have to eventually operate at a reduced head of 49.9 m, losing nearly 17% of the head and generating a much lower output shaft power. The 19.7 rpm PAT, on the other hand, operating at an optimum speed of 1200 rpm, as seen from Fig. 13, would utilize 57 m at a flow of 80 l/s representing a 5% underutilization of head and further would operate in the part-load region. It will nevertheless generate 2.7 kW of shaft power more than that of the 25.4 rpm PAT, and since there is no other pump available from the catalog, the 19.7 rpm PAT may have to be selected for this site with some compromise in the performance.

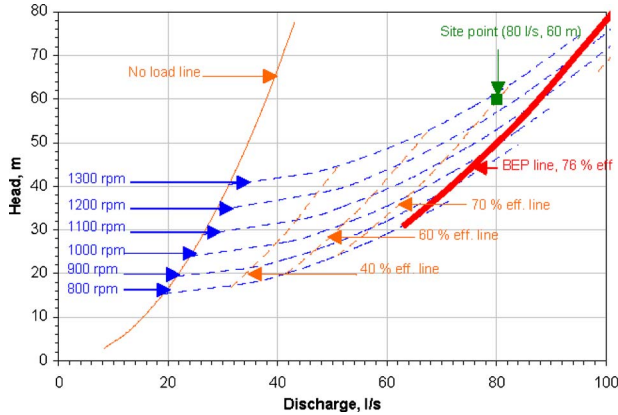


Fig. 13 Muschel curves of the 19.7 rpm PAT with field point

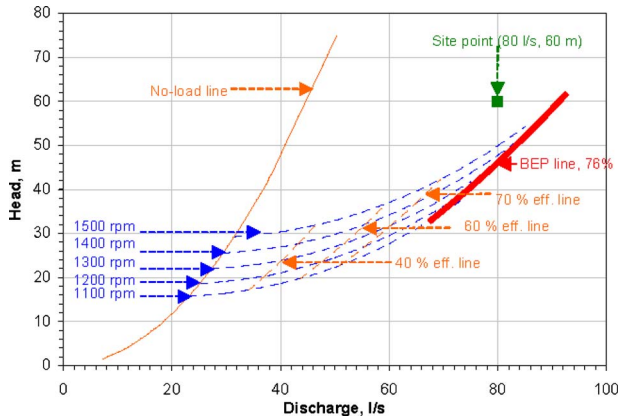


Fig. 14 Muschel curves of 25.4 rpm PAT with field point

5 Discussion of the Model

As seen in Secs. 3 and 4, the primary components of the consolidated model, namely, the selection and prediction model segments depend on the experimentally determined Cordier PAT line (Eq. (2)). Further, it can be seen from the PAT database (in Appendix A) that between 46 rpm and 79 rpm, the data of only one PAT (61 rpm) are available. Therefore, the predictions of the turbine performance in this zone could be inaccurate. Hence, the Cordier PAT line is naturally a subject of improvement or optimization. One method of improving this line is to incorporate more specific speeds in addition to the nine already available. It is, therefore, proposed to incorporate a small input program (optimization routine) to the consolidated PAT model, as illustrated in Fig. 15, which would lead to a new equation for the Cordier PAT line (following similar steps in Sec. 3.3.2) that would help in improving the accuracy of prediction over the complete range of 20–80 rpm. The routine would also improve the accuracy of pre-

Table 5 Selection table for site 2 with 80 l/s and 60 m

Speed option	Pump requirements				Selected pump from Ref. [13]	
	Pump shape	Pump size				
Option 1, speed, -1150 rpm	N_t	1150 rpm	Range of Δ and D required		Impeller diameter, D	409 mm
	N_{qt}	15.1 rpm	$\Delta_1=6.823$	$D_1=372$ mm	Pump mode	H_p 52 m
	σ	0.096	$\Delta_m=7.240$	$D_m=394$ mm	BEP	Q_p 68.9 l/s
	N_{qp} (reqd)	19.4 rpm	$\Delta_u=7.649$	$D_u=417$ mm		N_p 1450 rpm
Option 2, speed, -1500 rpm	N_t	1500 rpm	Range of Δ and D required		Impeller diameter, D	329 mm
	N_{qt}	19.7 rpm	$\Delta_1=5.576$	$D_1=304$ mm	Pump mode	H_p 32 m
	σ	0.125	$\Delta_m=5.890$	$D_m=321$ mm	BEP	Q_p 55.6 l/s
	N_{qp} (reqd)	24.3 rpm	$\Delta_u=6.200$	$D_u=338$ mm		N_p 1450 rpm
					N_{qp}	25.4 rpm

Table 6 Evaluation of the merits of the two PATs for site with 80 l/s and 60 m

PAT (rpm)	H (m)	δH (%)	Q (l/s)	δQ (%)	N_{optimum} (rpm)	Operating region	Predicted shaft power
19.7	57.0	-5.0	80	0	ca 1200	Part-load	32.2 kW @ $\eta=71.9\%$
25.4	49.9	-16.8	80	0	ca 1500	Near the BEP line	29.5 kW @ $\eta=75.2\%$

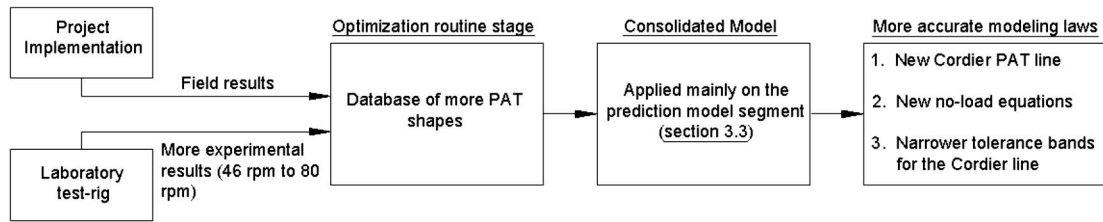


Fig. 15 Optimization routine on the consolidated model for pumps as turbines

diction in the no-load zone (as in Sec. 3.3.3) and would further decrease the error bands (by reducing the Δ interval of Fig. 8 compared with the one adopted in this paper), as the external errors (described in Sec. 3.3.4) would be significantly lower. This routine step, as shown in Fig. 15, could comprise results of either implemented PAT projects or laboratory specimen whose shapes are well defined. The optimization routine could also incorporate experimental results of PATs from other researchers, provided that the data that normalized in the format presented here and there are a reasonable amount of confidence in the accuracy of the results.

6 Conclusions and Recommendations

The conclusions of this current research work on the consolidated model on the turbine performance of centrifugal pumps can be summarized in three major points.

1. Salient features of the model: The origin of consolidated model is from the classical theory of turbomachines (specific speed-specific diameter or Cordier charts), which has brought about the parsimony features of the model that requires least variables to make predictions of the complete turbine characteristics. The other feature of the model is to give special reference to uncertainties (arising from experimental and external sources) as a function of the pump shape. More importantly, this model specifies the range on PAT shapes (20–80 rpm) on which it can be applied.
2. Application of the consolidated model: From the application point of view, within the selection model segment, the importance of speed as a control variable was evident. The prediction model segment was easy to apply, while the evaluation model segment and acceptance criteria helped in giving prior information that available PATs may or may not utilize the site conditions. The case studies clearly underlined the value of having a consolidated model (selection, prediction, and evaluation) for the application of centrifugal pumps as turbines.
3. Future of the model: One of the objectives of the research was to find a lasting solution for modeling in pumps as turbines. For achieving this objective, it is strongly recommended to have an additional database of PAT results, particularly those that are not available in the original database, and build new model equations for the Cordier PAT line (at BEP) and no-load points. This step defined, as optimization routine should aim to reduce the errors of prediction within $\pm 1\%$ bands, which can be achieved through planned testing and continuous validation. At a future step, it would also be

beneficial to have range specific modeling equations unlike one common model for a wide range of 20–80 rpm that has been considered in the present study.

Acknowledgment

The authors would like to thank the entire staff at the Theodore-Rehbock-Laboratory, Institute for Water and River Basin Management for all the support during the development of the test rig and subsequent testing. Sincere acknowledgments also go to Martin Gabi, Saban Caglar, Arthur Williams, and Shakun Paudel for the fruitful collaboration. The authors are very grateful to Kirloskar Brothers in India and KSB AG in Germany for providing the pumps that were used in the experiments reported here.

Nomenclature

Full Scripts

D = impeller outer diameter, m
H = head, m
g = gravitational acceleration, m/s^2
Q = discharge, m^3/s
N = speed, rps
 N_q = specific speed, $NQ^{1/2}/H^{3/4}$ (N in rpm, H in m, and Q in m^3/s)
u = tangential blade velocity, m/s
R = random error

Greek Symbols

Δ = turbine specific diameter, Eq. (A4)
 ϕ = discharge number, Q/ND^3 (Q in m^3/s , N in rps, and D in m)
 η = efficiency, %
 σ = turbine specific speed, Eq. (A3)
 ψ = head number, gH/N^2D^2 (gH in m^2/s^2 , N in rps, and D in m)

Superscripts

N = scaling index

Subscripts

c = Cordier definition
l = lower limit
m = mean
mo = model
nl = no-load
p = pump mode
pt = prototype
t = turbine mode

Table 7 Summary of the BEP parameters of the nine PATs both in pump and turbine mode

Sl. No.	Pump mode BEP (absolute and dimensionless)							Turbine mode BEP (dimensionless)				Comparisons		
	H _p (m)	Q _p (l/s)	N _p (rpm)	D (mm)	N _{qp} (rpm)	φ _p	ψ _p	η _p (%)	N _{qt} (rpm)	φ _t	ψ _t	η _t (%)	φ _t /φ _p	ψ _t /ψ _p
1	14.5	10.8	1500	225	21.0	0.038	4.496	77.0	18.5	0.070	8.000	72.5	1.85	1.78
2	21.5	26.5	1500	258	24.5	0.062	5.070	78.0	18.6	0.117	11.170	76.5	1.90	2.20
3	12.8	25.4	1500	206	35.3	0.116	4.734	78.5	28.1	0.151	7.640	81.0	1.30	1.61
4	8.38	15.3	1450	174	36.4	0.120	4.650	74.4	30.1	0.185	8.000	71.5	1.54	1.72
5	19.8	65.9	1450	264	39.7	0.148	4.772	85.0	35.7	0.200	6.700	83.5	1.35	1.40
6	10.5	33.0	1450	200	45.2	0.171	4.409	80.0	41.1	0.235	6.180	79.5	1.38	1.40
7	5.6	13.5	1450	139	46.4	0.208	4.850	76.0	38.1	0.275	7.600	76.0	1.32	1.57
8	6.4	28.9	1450	165	61.3	0.266	3.949	72.0	57.6	0.414	5.748	74.3	1.56	1.46
9	10.6	103.0	1450	224	79.1	0.379	3.555	84.0	70.0	0.480	4.900	75.5	1.27	1.38

u = upper limit

Abbreviations

PAT = pump as turbine

BEP = best efficiency point

Naming code for all ‘pumps as turbines’ is based on the pump mode specific speed in rpm

$$\sigma = \frac{2^{1/4} \pi^{1/2} N Q^{1/2}}{g^{3/4} 60 H^{3/4}} = 6.3383 \times 10^{-3} N_{qt} \quad (A5)$$

Appendix A: Experimental Results of Pumps as Turbines

See Table 7.

Appendix B: Inter-Relationship Between Dimensionless Numbers

Head number:

$$\psi_c = \frac{2gH}{u^2} = \frac{2}{\pi^2} \frac{gH}{N^2 D^2} = \frac{2}{\pi^2} \psi \quad (A1)$$

Discharge number:

$$\phi_c = \frac{4Q}{\pi D^2 u} = \frac{4}{\pi^2} \frac{Q}{N D^3} = \frac{4}{\pi^2} \phi \quad (A2)$$

Turbine specific speed:

$$\sigma = \frac{\phi_c^{1/2}}{\psi_c^{3/4}} = 2^{1/4} \pi^{1/2} \frac{\phi_t^{1/2}}{\psi_t^{3/4}} \quad (A3)$$

Turbine specific diameter:

$$\Delta = \frac{\psi_c^{1/4}}{\phi_c^{1/2}} = \frac{\pi^{1/2} \psi_t^{1/4}}{2^{3/4} \phi_t^{1/2}} \quad (A4)$$

The relationship between the Cordier σ and N_{qt} is given by

References

- [1] Singh, P., 2005, "Optimization of the Internal Hydraulic and of System Design in Pumps as Turbines With Field Implementation and Evaluation," Ph.D. thesis, University of Karlsruhe, Germany, pp. 50–59, 95–121, and 284–292.
- [2] Williams, A. A., 1992, "Pumps as Turbines Used With Induction Generators for Stand-Alone Micro-Hydroelectric Power Plants," Ph.D. thesis, Nottingham Trent University, pp 51–80, 88–91, 149–153.
- [3] Cohrs, D., 1997, "Untersuchungen an einer mehrstufigen rückwärtslaufenden Kreiselpumpe im Turbinenbetrieb," Sulzbach Verlag und Bildarciv, Faragallah, W. H., pp. 8–41.
- [4] Amelio, M., and Barbarelli, S., 2004, "A One-Dimensional Numerical Model for Calculating the Efficiency of Pumps as Turbines for Implementation in Micro Hydro Power Plants," ASME Seventh Biennial Conference on Engineering System Design and Analysis, pp 65–77.
- [5] Derakhshan, S., and Nourbakhsh, A., 2008, "Experimental Study of Characteristic Curves of Centrifugal Pumps Working as Turbines in Different Specific Speeds," *Exp. Therm. Fluid Sci.*, **32**, pp. 800–807.
- [6] Cordier, O., 1953, "Aehnlichkeitsbedingungen für Strömungsmaschinen," *Brennst.-Waerme-Kraft*, **5**(10), pp. 337–340.
- [7] Balje, O. E., 1981, *Turbomachines—A Guide to Design, Selection and Theory*, Wiley, New York, Chap. 3.
- [8] Dixon, S. L., 2005, *Fluid Mechanics and Thermodynamics of Turbomachinery*, 5th ed., Elsevier, New York, Chap. 9.
- [9] Moffat, R. J., 1982, "Contributions to the Theory of Single-Sample Uncertainty Analysis," *ASME J. Fluids Eng.*, **104**, pp. 250–258.
- [10] Kline, S. J., 1985, "The Purposes of Uncertainty Analysis," *ASME J. Fluids Eng.*, **107**, pp. 153–160.
- [11] Holman, J. P., 2001, *Experimental Methods for Engineers*, 7th ed., Tata McGraw-Hill Publishing Company Limited, New Delhi, Chap. 3.
- [12] Boor, C. D., 2001, "Practical Guide to Splines," *Applied Mathematical Sciences*, Springer, New York, Vol. 27, p. 40.
- [13] Kirloskar Brothers Limited, 2005, *Catalogues Specifying the Duty Points for DB and KPD Pumps*, Corporate Research and Engineering Division, Pune, India.



Contents lists available at ScienceDirect

Experimental Thermal and Fluid Science

journal homepage: www.elsevier.com/locate/etfs

An optimization routine on a prediction and selection model for the turbine operation of centrifugal pumps

Punit Singh*, Franz Nestmann

Institute for Water and River Basin Management (IWG), University of Karlsruhe, Kaiser Str. 12, D 76128 Karlsruhe, Germany

ARTICLE INFO

Article history:

Received 18 June 2009

Received in revised form 8 October 2009

Accepted 9 October 2009

Keywords:

Pumps as turbines

Optimization

Prediction

Specific diameter

Cordier diagram

Hermite splines

ABSTRACT

The paper presents an experimentally validated optimization routine for the turbine-mode operation of radial flow centrifugal pumps. The optimization routine outlined here is designed to be used with prediction (predicting turbine mode characteristics of a pump) and selection (selecting the most appropriate pump for turbine-mode operation) models. The optimization routine improves upon previous uncertainties in prediction, especially in the low specific speed range.

The optimization routine is evaluated experimentally for three pumps with specific speeds of 18.2 rpm, 19.7 rpm and 44.7 rpm, and a significant improvement in the accuracy of the turbine predictions with the errors for all the three pumps falling within the $\pm 4\%$ acceptance bands in the full load operating region is found.

It is also shown how the optimization routine validates an approach to selection and prediction based on model experiments and classical principles of applied turbomachinery (specific speed-specific diameter or the Cordier/Balje plots). Such an approach is shown to be the most economic in terms of pump mode input variables.

The paper recommends the extensive use of the optimization routine in micro hydro and other energy recovery projects involving pumps as turbines and the creation of a database of accurate field results that can be used to improve the routine further.

© 2009 Elsevier Inc. All rights reserved.

1. Introduction

1.1. Background

The main objective of all PAT researchers all over the world has been to build a model that would make accurate predictions of the turbine operation of pumps, be it for micro hydro or energy recovery schemes. There have been more than a dozen of prediction techniques published so far, as reported by Williams [3], Singh [1] and Derakshan and Nourbakhsh [2]. While researchers have tested their models on few pumps and recorded deviations that are in the order of $\pm 10\text{--}20\%$, they have not been able to report the repeatability of their prediction accuracies with pumps of different designs and different manufacturers. This has prevented a continuous optimization of their respective models.

The common methodology employed by these researchers is to compare the performance of the pump and turbine operation at the BEP and bring out the so-called head and discharge ratios. The uncertainties associated with these ratios are enormous as re-

ported by both Singh [1] and Derakshan and Nourbakhsh [2], with deviations exceeding over 40% for some specific speeds.

Subsequently, few other researchers like Cohrs [4] and Amelio and Barbarelli [5] have tried to use detailed theoretical models that are based on the pump design, its geometry and assumptions of some complex hydraulic phenomena like losses and slip effects in an effort to bring out more accurate turbine characteristic predictions. These methods are definitely comprehensive, but they are difficult to implement and simply beyond the reach of planners, since these models need very detailed information, which is sometimes patented or available only with the manufacturers.

In order to overcome the challenges of prediction in PATs, a new and simpler prediction model has been proposed by the authors (as illustrated in Section 2.2), which is based purely on experimental results of 9 model PATs (from $N_{qp}20\text{--}80$ rpm) and the fundamentals of applied turbomachinery like the specific speed-specific diameter plots. This approach of the model leads to a economic feature, which refers to the fewer input variables required to accomplish predictions. However, the authors have reported a deviation in the order of $\pm 5\text{--}7\%$ for the low specific speed pumps and in the range of less than $\pm 2\%$ for the medium specific speed range. They also reported substantial deviations in the no-load operating region and have recommended for the development of a more refined and robust prediction model. They have also proposed a

* Corresponding author. Tel.: +49 721 608 2194; fax: +49 721 606 046.

E-mail addresses: punit.singh@iwg.uka.de (P. Singh), nestmann@iwg.uka.de (F. Nestmann).

Nomenclature*Full scripts*

D	impeller outer diameter, m
g	gravitational acceleration, m/s^2
h	Hermite basis function
H	head, m
n	speed, rps
N_q	specific speed, $NQ^{1/2}/H^{3/4}$ (N in rpm, H in m, Q in m^3/s)
Q	discharge, m^3/s
R	random error
S	slope between head and discharge number
t	relative position parameter
u	tangential blade velocity, m/s
x	range of discharge number
PAT	pump as turbine
BEP	best efficiency point
CFD	computational fluid dynamics

Naming code for all 'pumps as turbines' is based on the pump mode specific speed in rpm.

Greek symbols

Δ	turbine specific diameter, (in A3, Eq. (A4))
ϕ	discharge number, Q/nD^3 (Q in ' m^3/s ', n in 'rps', D in 'm')
η	efficiency, %
σ	turbine specific speed, (in A3, Eq. (A3))
ψ	head number, gH/n^2D^2 (gH in m^2/s^2 , n in 'rps', D in 'm')

Subscripts

c	Cordier definition
l	lower limit
m	mean
mo	model
nl	no-load
p	pump mode
t	turbine mode
u	upper limit

selection model (Section 2.2) that would enable the selection of the most optimum pump for a given turbine application following a detailed evaluation methodology.

1.2. Objectives

- To introduce an optimization routine that will improve the accuracy and reliability of prediction and selection models for pumps as turbines, and yet to keep the model simple to apply for project planners and small pump manufacturers.
- To make the criterion of acceptance that is more stringent by decreasing the tolerance bands of the prediction errors.
- To realize an accurate, useful and robust model for centrifugal pumps as turbines.

1.3. Problem outline

The problem of developing the new 'optimization routine' would comprise of using additional experimental data of pumps as turbines and incorporating them within the basic prediction model (Section 2.2), without changing the governing philosophy of the basic model. The problem would further encompass one to one comparisons of the results of both the basic model and the optimization routine, and to evaluate if the new routine has succeeded in achieving the objective of decreasing the prediction errors. The problem would also include appropriate conclusions of the comparative study and spell out recommendations for the future scope of work.

2. Theory of the basic model

2.1. Experimental and theoretical means

The key for developing any model that is close to reality is without doubt linked to accurate and rigorous experimentation. Hence for the purpose of building a PAT model, a well-calibrated open loop hydraulic test rig as shown in Fig. A1 is constructed and used to characterize all the pumps as turbines (also called model PATs). The instrumentation and details of the experimental uncertainty are discussed in Singh [1]. The pumps used are radial flow end-suction pumps with standard backward vane designs for the impellers (closed) as shown in Fig. A2 and in the specific speed range from 20 rpm to 80 rpm.

The classical design approach used in turbomachines is known as the 'specific speed-specific diameter' plots, which was first introduced by Cordier [6] and then pursued intensively by Balje [7]. The 'specific speed-specific diameter' plots have revolutionized the design and selection of turbomachines. Balje [7] plotted these plots for all kinds of turbomachines (steam and gas turbines, hydro turbines, compressors and pumps) and also included effects like loss mechanisms, design constants and even cavitation limits within them. He also argued the 'specific speed-specific diameter' plots could be used as a powerful tool to analyze and optimize the flow paths in a turbomachine.

Given the worldwide acceptance of the 'specific speed-specific diameter' plots, the basic PAT model (in Section 2.2) is developed based on this approach and further it is retained for the development of the optimization routine as well.

2.2. The basic PAT model

The basic PAT model comprises of the prediction model and selection model, whose functions are briefly illustrated in Fig. 1. The prediction model performs the complete synthesis of the turbine characteristics of a given pump of known shape and size by evaluating the BEP as well as the no-load points using the governing equations summarized in Appendix A.5. On the other hand the selection model first selects a few appropriate pumps from manufacturer's catalogues that satisfy the given turbine operating conditions (head and flow) as shown in Fig. 1. And further, in combination with prediction model, the selection model is able to evaluate the most optimum pump from the given choices by precisely comparing the degree of utilization of the boundary parameters (head and flow) and shaft output power generated. The selection model is also based on the Cordier PAT line and the individual steps of this model are illustrated in Appendix A.4.

3. Theory of the optimization routine

3.1. Introduction to the optimization routine

As mentioned the purpose of 'optimization routine' is to improve the reliability of the basic model without changing the philosophy of the methodology used in the basic PAT model. Hence, it cannot be called a new model and instead called a routine, which is

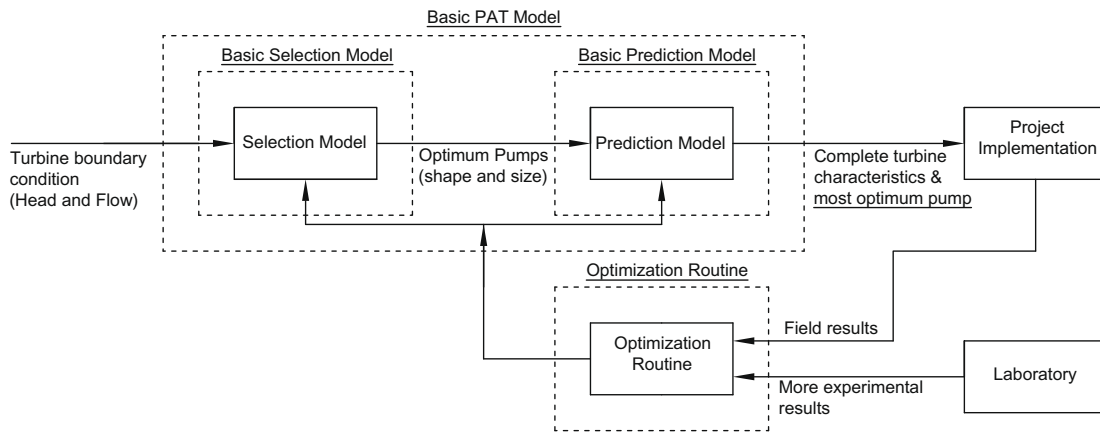


Fig. 1. Block diagram of the consolidated model for pumps as turbines with optimization routine.

analogous to a small computer program that forms a loop with the basic model.

As illustrated in the block diagram of Fig. 1, the optimization routine forms an important component in the consolidated model being conceived for the turbine operation of centrifugal pumps. With respect to the prediction model, the optimization routine should reduce the prediction errors to the limits of $\pm 4\%$. While from the perspective of the selection model, it should be able to make a better choice of a pump for given turbine-mode operating conditions. The optimization routine will essentially contain an increased database of more pump shapes (sourced from field and experimental results).

3.2. Additional experimental data

The optimization PAT routine is developed by using additional data from Derakshan and Nourbakhsh's [2] experimental work of 4 PATs having pump specific speeds of 14.6 rpm, 23.0 rpm, 37.6 rpm and 55.6 rpm, respectively. It is to be noted that lowest specific tested by the authors (Appendix A.1) is 21 rpm. With the inclusion of test results of 14.6 rpm and 23 rpm PATs into the Cordier diagram, the scope of the model with respect to accuracy and reliability, especially in the lower specific speed range needs to be tested.

The consolidated data of the 13 model PATs used in the optimization routine is summarized in Appendix A.1. In short, the basic PAT model comprises of a databank of 9 PATs, while the 'optimization routine' uses additional data of 4 PATs taking the total number of PATs to 13.

3.3. Cordier diagram for the optimization routine

The consolidated head number–discharge number ($\psi-\phi$) and efficiency–discharge number ($\eta-\phi$) characteristics of these 13 PATs are plotted in Fig. 2. The Cordier diagram showing the BEP line is sketched in Fig. 3 along with the constant efficiency and constant head number lines. The purpose of incorporating the constant head number lines is to give an indication of how the head number changes along the mean Cordier PAT line. The original Cordier line (proposed by Cordier [6] himself for all turbomachines) is also plotted, and is seen to deviate from the mean Cordier PAT line.

The uncertainty bands are also plotted across the mean Cordier PAT line, which are seen to have a broader span in the lower specific speed (larger specific diameter) region and a smaller span in the higher specific speed region. The reason for doing this goes back to the higher experimental uncertainty (as described in Section 3.4.1) and other influences in the lower specific speed pumps.

3.4. Governing equations for the optimization routine

3.4.1. Optimized mean Cordier PAT line

The mean Cordier line of the optimization routine along with the corresponding uncertainty bands is given by Eq. (1). The uncertainty bands are defined by introducing a consolidated random error term R_A , which combines both experimental and external uncertainties. The experimental uncertainties are straightforward to deal with and determined using the single sample techniques

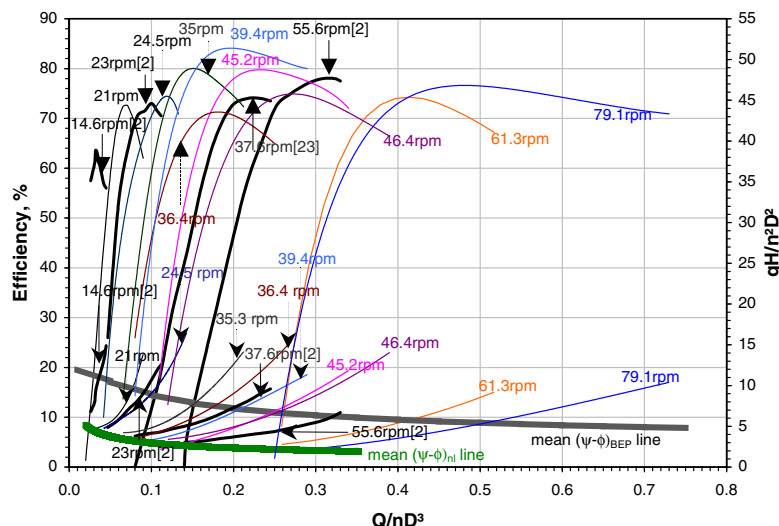


Fig. 2. The $\eta-\phi$ and $\psi-\phi$ characteristics of 13 PATs.

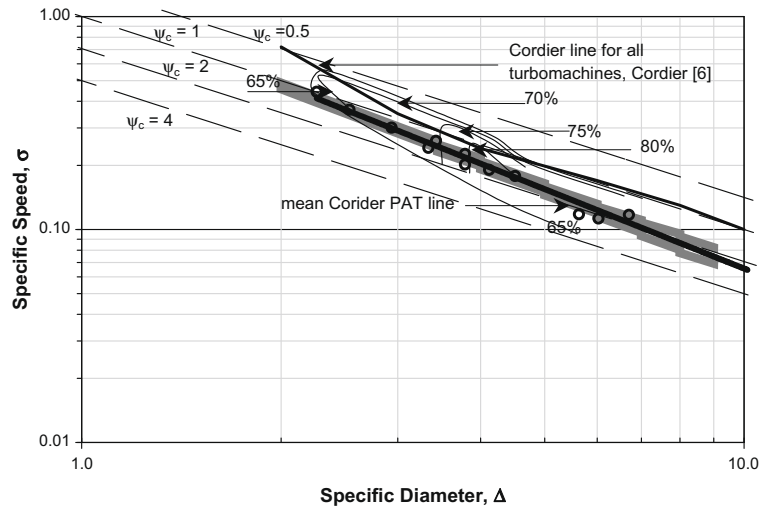


Fig. 3. The mean Cordier line for the optimization routine.

proposed by Moffat [9] and Kline [10]. The external errors on the other hand are associated with the unknown specimen pump and are more complex in nature. These errors deal with accuracy of determining the pump mode BEP, the geometry and manufacturing tolerances that vary from manufacturer to manufacturer. Hence, it is recommended to use pumps of reliable manufacturers following standard protocols for design as well as for testing the pumps

$$\sigma = (1.136 \pm R_A) \cdot \Delta^{-1.239} \quad (1)$$

The experimental uncertainty of the model PATs at BEP is summarized in Fig. 4 (and in Appendix A.8), which gives evidence of greater errors for discharge numbers in the lower specific speed range. With this in mind, a creative methodology is proposed by treating the random error component, R_A , as a variable and defined as a function of pump specific speed. The corresponding error bands for specific diameter (Δ) as function of pump specific speed (N_{qp}) plotted in Fig. 5, which also plots the respective error bands for the discharge number at BEP.

3.4.2. Relation between pump mode and turbine mode specific speed

The experimental relationship between the pump mode and turbine mode specific speeds is developed using the BEP data from all 13 PATs and is given by Eq. (2). This is an important relation and will be required in the application of the optimization routine

$$N_{qt} = 0.94 \cdot N_{qp} - 3.12 \quad (2)$$

Fig. 6 plots the pump mode and the turbine mode specific speed points for the 13 PATs used in the optimization routine stage. There seems

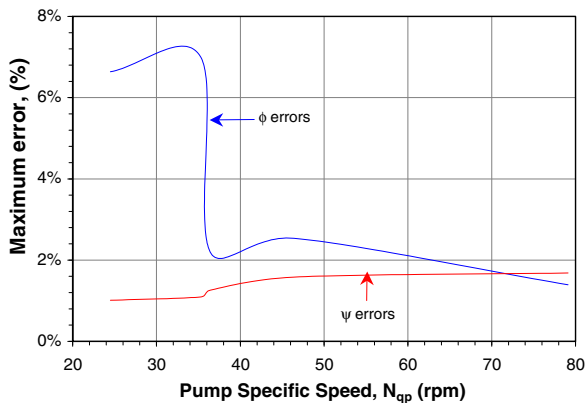


Fig. 4. Summary of the experimental uncertainty.

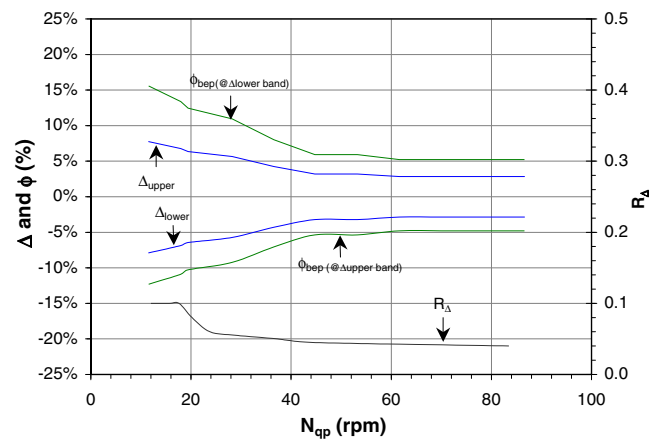


Fig. 5. Uncertainty bands for Δ and ϕ .

to be some scatter of the points, which could lead to uncertainties in predictions. The uncertainty due to this conversion of specific speed is accounted as a component of the external errors within the R_A term of Eq. (1), which automatically gets accommodated in the range of specific diameters for a given specific speed illustrated in Fig. 5.

3.4.3. BEP with uncertainty limits

The BEP defined by the ϕ and ψ coordinates need to be evaluated from the Δ_m (defined by mean PAT line Eq. (1)) and for the uncertainty limits (Δ_l and Δ_u) illustrated in Fig. 5 at a given pump specific speed (and hence, σ). The conversion of constants used in the Cordier diagram (σ and Δ) and the coefficients used in the paper (ϕ and ψ) are summarized in Appendix A.3. For each of the specific diameters (Δ_m , Δ_l and Δ_u) only the mean specific speed (σ_m) is used to bring about the respective ϕ and ψ . This exercise results in three pairs of points that define the boundaries for the ψ - ϕ characteristics of given PAT passing through their respective BEPs (an example is illustrated in Appendix A.10).

The magnitude of efficiency at the BEP of given specific speed pump is function of both its shape (N_q) and size (D). This can be obtained by first reading out the magnitude of efficiency for a similar pump shape from Appendix A.1 and then using the scaling law for hydraulic turbines given by Moody in Eq. (3) and confirmed by Dixon [8]

$$\frac{1 - \eta_{pt}}{1 - \eta_{mo}} = \left(\frac{D_{mo}}{D_{pt}} \right)^n, \quad \text{where } n = 0.2-0.25 \quad (3)$$

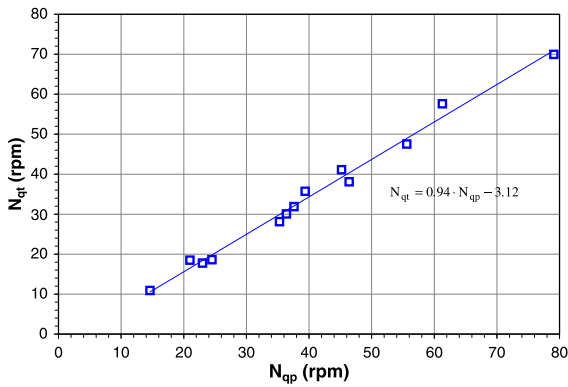


Fig. 6. The specific speed relationship between for the 13 PATs.

3.4.4. No-load points with uncertainty limits

The no-load discharge number is first determined from Eq. (4) from the turbine specific speed (σ) and the corresponding head number from Eq. (5) that relates both the discharge number and the head number. These equations are developed from the overall ψ - ϕ characteristics shown in Fig. 2. The uncertainty limits for ϕ_{nl} are assumed to be identical to that for the ϕ_{BEP} and are read directly from the Fig. 5 for the given pump specific speed.

$$\phi_{nl} = 0.83 \cdot \sigma^{1.51} \quad (4)$$

$$\psi_{nl} = 1.39 \cdot \phi_{nl}^{-0.344} \quad (5)$$

3.4.5. Optimized curve fitting for the ψ - ϕ and the η - ϕ curves

The construction of the head number and efficiency curves with uncertainty bands is the hallmark of the optimization routine. This is achieved using a widely used curve fitting methodology, documented by Holman [11] and Boor [12].

It can be seen from Fig. 2 that both the head number and efficiency are functions of both specific speed and discharge number. In order to construct the head number and efficiency characteristics of a new PAT (with a given N_{qp}), the Hermite spline interpolation technique is used [12]. This technique comprises of using two fixed points on the characteristics (i.e. BEP and no-load point, which have already been determined) and the slopes at these points to generate a three degree polynomial for the respective characteristics, i.e. head number and efficiency. The slopes of both ψ and η with respect to ϕ can be readily determined from the experimental results illustrated in Fig. 2.

Using separate polynomials for the efficiency and the head number characteristics, the mean as well as the uncertainty bands for turbine operation can be plotted for any given pump specific speed. The resultant polynomials have shown excellent fitting for all the 13 experimentally tested PATs. It has to be remembered that the interpolation holds good for the curve between no-load point and BEP. However, some extrapolation is carried out to evaluate the characteristics in the overload region.

Appendix A.6 provides a brief insight into the use of Hermite spline interpolation for the head number characteristics of the PATs used for evaluating both the optimization routine and basic prediction model.

4. Testing the optimization routine

The evaluation of the optimization routine is carried out on 3 PATs that have been tested in field conditions. A brief discussion of the field test setup for turbine mode testing is carried out in Appendix A.9 along with the summary of the measurement uncertainties. The test PATs have pump mode specific speeds of 18.2 rpm,

19.7 rpm and 44.7 rpm, respectively. This data has been supplied by the manufacturer [13] following in-house pump mode tests.

The investigation of the optimization routine is restricted to only the head number characteristics (ψ - ϕ) and not the efficiency characteristics (η - ϕ) since the shaft power on the turbine could not be accurately measured in field conditions.

5. Results and discussion

5.1. Prediction model control

5.1.1. Results for the 18.2 rpm PAT

The detailed workout for both the basic prediction model and the optimization routine comprising of the consolidated table that summarizes the range of specific diameters, BEP and no-load points, along with the synthesis of the dimensionless performance characteristics is carried out in Appendix A.10. Based on these results, the comparisons with the actual field curve are illustrated in Figs. 7 and 8, respectively.

In Fig. 7, the predicted ψ - ϕ curves pertaining to the basic model and the routine are compared with the actual ψ - ϕ curve obtained from the field measurements (Appendices A.7 and A.9). It is clearly evident that the head number curve from the optimization routine has moved closer to the actual head number curve. There also seems to be a very good coincidence at the maximum load point of the tested PAT. In Fig. 8, the percentage deviations of the head number from the actual values are plotted at the different discharge numbers. At the maximum load point (at $\phi = 0.052$) of the tested PAT, the deviation of the head number with basic prediction model corresponds to -6.2% , which has improved to -2.6% with the optimization routine. This deviation falls within the $\pm 4\%$ acceptance criterion and it clearly indicates improvement in prediction. However, the deviations in the no-load region are in the order of 10–15%, which is still a considerable error.

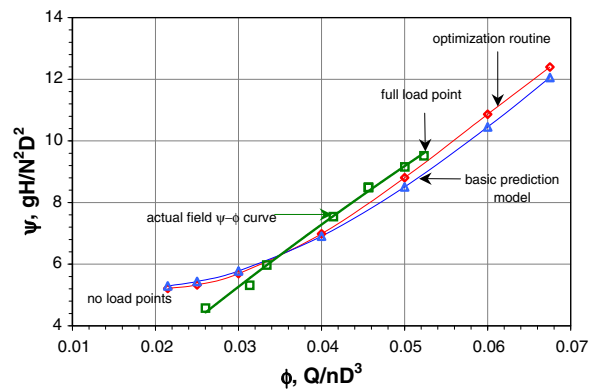


Fig. 7. Model and actual ψ - ϕ curves for the 18.2 rpm PAT.

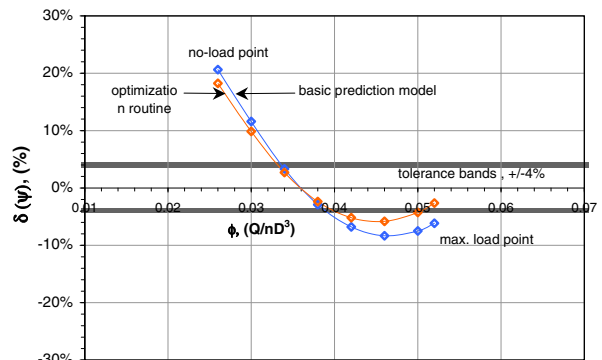


Fig. 8. Deviation of head numbers for the 18.2 rpm PAT.

5.1.2. Results for the 19.7 rpm PAT

Similar to the workout in the 18.2 rpm PAT, the basic model and the routine are independently implemented for the 19.7 rpm PAT and the comparative studies are carried out Figs. 9 and 10, respectively. Once again the predictions from the optimization routine have shown an improvement over the basic model's predictions. It can be seen from both Figs. 9 and 10 that the predictions in the part-load region have improved considerably. At the full load point the percentage deviation of head number has reduced from -4.2% for the basic model to -3.0% for the routine, which can be seen as positive result of the optimization routine.

5.1.3. Results for the 44.7 rpm PAT

Again the model and the routine are implemented separately and the overall comparisons for the 44.7 rpm PAT are presented in Figs. 11 and 12. It can be seen from the comparison of the ψ - ϕ curves in Fig. 11 that towards the full load region, the optimization routine curve gets closer and merges with the actual field curve. However, in the no-load and part-load region the deviations of the optimization routine are higher compared to the deviations of basic prediction model. Nevertheless, at the full load point (at $\phi = 0.203$) the deviation with the basic model is +1.7% compared to +1.5% with the routine, which is a small improvement. This result reflects on the goodness and completeness of the basic prediction model, at least in the medium specific speed range.

5.1.4. Discussion on the prediction model control

It has been seen for the lower specific speed PATs (18.2 rpm and 19.7 rpm) that the predictions of optimization routine are more accurate and closer to reality compared to that of the basic PAT model. As for the medium specific speed PAT (44.7 rpm), the errors using the basic model were already below $\pm 2\%$ and hence a major improvement with the routine could not be expected.

On the whole, the errors of head number at the maximum load point for all the PATs fall within the acceptance criterion of $\pm 4\%$.

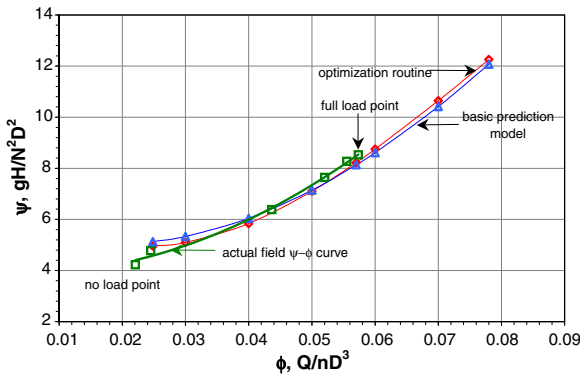


Fig. 9. Model and actual ψ - ϕ curves for the 19.7 rpm PAT.

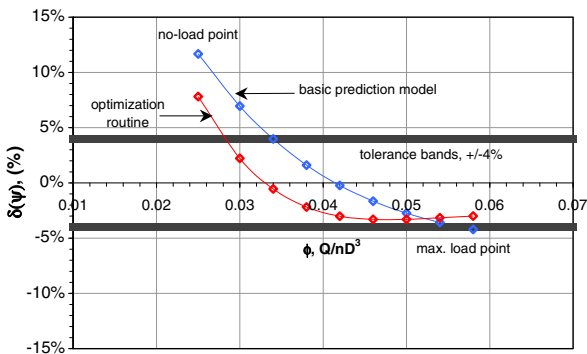


Fig. 10. Deviation of head numbers for the 19.7 rpm PAT.

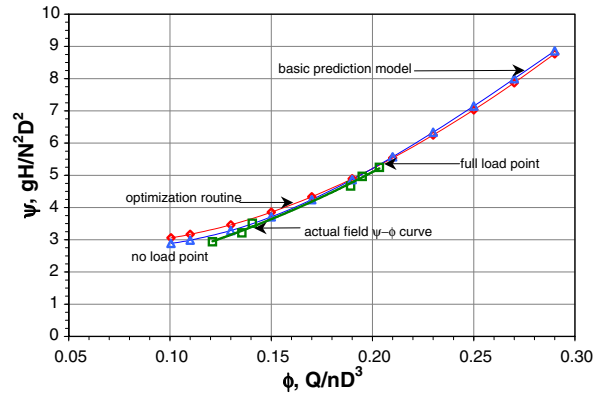


Fig. 11. Model and actual ψ - ϕ curves for the 44.7 rpm PAT.

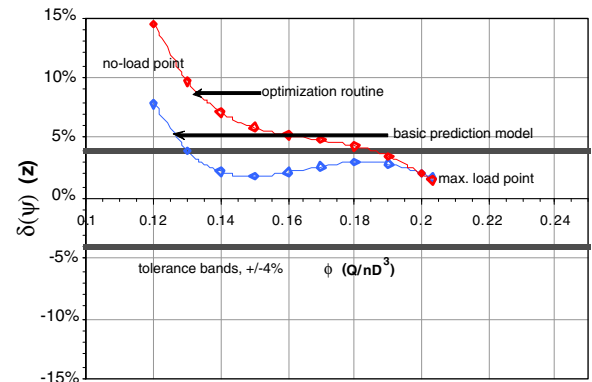


Fig. 12. Deviation of head numbers for the 44.7 rpm PAT.

These results have clearly indicated that by including the test data of more PAT shapes within the Cordier diagram, the accuracy of prediction eventually improves and thus validates the purpose of optimization routine.

However, the no-load point predictions are outside the acceptance criteria ($\pm 4\%$) using both the basic model and the optimization routine. This is definitely a limitation, especially when the assessment of the runaway condition has to be carried out during the system design phase of the PAT.

5.2. Selection model control

The comparison of the results of the selection model for a given input condition, using both the basic model and optimization routine, is summarized in Table 1. The results are obtained by following the steps illustrated in Appendix A.4 and equations in Appendix A.5.

It is clearly evident that the proposed pump shape and size (range of diameters) using the basic model and the routine is not very different and will essentially lead to identical pump selection from the manufacturer's catalogue. However, for the evaluation of the given pump's ability to meet the utilization criterion of the input conditions of head and flow, the prediction model would have to be used (as articulated in the detailed flow chart of the selection model in Appendix A.4).

In addition, the prediction model comes into use when the selection model gives multiple pumps options. In these circumstances, the optimization routine is recommended because of the improved results of prediction as seen in Section 5.1.

6. Conclusions and recommendations

The foremost conclusion drawn from the results of the optimization routine for turbine operation of centrifugal pumps is that the

Table 1
Comparison of the results of the basic selection model and the optimization routine.

Input conditions	Model type	Pump shape			Pump size					
		N_{qt} (rpm)	σ	N_{qp} (rpm)	Δ_l	Δ_m	Δ_u	D_l (m)	D_m (m)	D_u (m)
$H = 60$ m, $Q = 45$ l/s, $N = 3000$ rpm	Basic PAT model (9 PATs)	29.5	0.187	34.7	4.127	4.300	4.471	0.169	0.176	0.183
	Optimization routine (13 PATs)	29.5	0.187	34.8	4.118	4.289	4.459	0.168	0.175	0.182

approach of incorporating performance data of more pump shapes within the basic model is reasonably fulfilling the goal of improving the reliability and accuracy of prediction. Further, these results validate the core philosophy of the model developed around experimental findings and the principles of applied turbomachinery, i.e. the specific speed–specific diameter or Cordier charts.

The prediction errors of the head number at the maximum load point using the optimization routine concept for the 3 tested PATs have considerably reduced, especially for the lower specific speed PATs. While for the 18.2 rpm PAT the errors have fallen from 6.2% to 2.6%, it has dropped from 4.2% to about 2.7% for the 19.7 rpm PAT. For the 44.7 rpm PAT, the extent of errors lies within $\pm 2\%$ bands. Based on these results, it could be proposed that the acceptance criteria be reduced further to $\pm 2\%$ in order to make the model more stringent.

However, the errors in the no-load region are still substantial (in the range of ± 10 – 20%) even though they have improved for the lower specific speed pumps, which could still be viewed as an inadequacy.

The experimental means along with established theory of applied turbomachinery (comprising of plots of specific speed and specific diameter) has been a success. This approach also has resulted in the economic feature of the optimization routine, in which the only required input parameters for predicting the complete turbine characteristics are the pump specific speed and outer impeller diameter, and for the selecting a pump, the required parameters are the turbine head and flow conditions.

Further, the ‘Hermite spline’ curve fitting approach of plotting the complete ψ – ϕ and η – ϕ characteristics of the PAT has proved to be relatively simple to apply and very effective as well. In short, the optimization routine has reasonably succeeded in achieving the set objectives of improving the reliability, robustness and accuracy of the previous prediction and selection models for centrifugal pumps as turbines.

The above conclusions lead to some important recommendations. Firstly, in pursuit of greater accuracy, it is advised that a methodological approach be employed for using the optimization

routine in field projects and collecting accurate operational data. Special emphasis needs to be given to the accurate predictions in the no-load operating region of the PATs.

Secondly, it has to be pointed out that the validation studies of this paper have been restricted to the comparison of only the ψ – ϕ characteristics and not the η – ϕ characteristics, since the tested PATs were in field conditions where the shaft power and the turbine efficiency could not be accurately measured. Hence, it is recommended to validate the efficiency characteristics on a calibrated test rig, for realizing the complete value of the optimization routine.

Whether it is field or laboratory data, the inclusion of ‘accurate’ turbine characteristics of different pumps shapes into the basic model will continually improve the model’s performance. This continual alleviation is the essence of the philosophy behind the initiative of making PAT technology a resounding success at the application level. Hence, it has to be duly stressed that the proposed optimization routine may not be the final version and there should always be a pursuit of excellence.

Acknowledgements

The authors would like to deeply acknowledge the wholehearted support provided by the engineers, mechanics, and technicians at the Theodore-Rehbock-Laboratory of the Institute of Water and River Basin Management, University of Karlsruhe for the construction of the test rig and for its maintenance for over 4 years during the period of research. They would like to thank Shakun Paudel for excellent research assistance. Sincere acknowledgements also go to Martin Gabi and Saban Caglar of the Department of Fluid Machinery, University of Karlsruhe for their support in the PAT program. They would also like to mention Dr. Arthur Williams and his team at the Nottingham Trent University for the fruitful collaboration. The authors are very grateful to Kirloskar Brothers, India and KSB, Germany for providing the pumps that were used in the experiments reported here.

Appendix A

A.1. Experimental data for 13 model PATs

Sr. no.	Pump mode BEP (absolute and dimensionless)								Turbine mode BEP (dimensionless)				Comparisons	
	H_p (m)	Q_p (l/s)	N_p (rpm)	D_l (mm)	N_{qp} (rpm)	ϕ_p	ψ_p	η_p (%)	N_{qt} (rpm)	ϕ_t	ψ_t	η_t (%)	ϕ_t/ϕ_p	ψ_t/ψ_p
<i>Data of 9 PATs from author used in the basic prediction model</i>														
1	14.5	10.8	1500	225	21.0	0.038	4.496	77.0	18.5	0.070	8.000	72.5	1.85	1.78
2	21.5	26.5	1500	258	24.5	0.062	5.070	78.0	18.6	0.117	11.170	76.5	1.90	2.20
3	12.8	25.4	1500	206	35.3	0.116	4.734	78.5	28.1	0.151	7.640	81.0	1.30	1.61
4	8.38	15.3	1450	174	36.4	0.120	4.650	74.4	30.1	0.185	8.000	71.5	1.54	1.72
5	19.8	65.9	1450	264	39.7	0.148	4.772	85.0	35.7	0.200	6.700	83.5	1.35	1.40
6	10.5	33.0	1450	200	45.2	0.171	4.409	80.0	41.1	0.235	6.180	79.5	1.38	1.40
7	5.6	13.5	1450	139	46.4	0.208	4.850	76.0	38.1	0.275	7.600	76.0	1.32	1.57
8	6.4	28.9	1450	165	61.3	0.266	3.949	72.0	57.6	0.414	5.748	74.3	1.56	1.46
9	10.6	103.0	1450	224	79.1	0.379	3.555	84.0	70.0	0.480	4.900	75.5	1.27	1.38
<i>Additional data from Derakshan and Nourbakhsh [2] used in the optimization routine</i>														
1 [2]	17.8	8.0	1450	250	14.6	0.021	4.780	65.0	10.9	0.033	9.800	64.0	1.56	2.05
2 [2]	20.4	23.7	1450	250	23.0	0.063	5.487	76.0	17.8	0.100	10.700	73.0	1.59	1.95
3 [2]	18.1	57.2	1450	250	37.6	0.151	4.855	86.5	31.9	0.224	8.400	74.0	1.48	1.73
4 [2]	17.5	107.0	1450	250	55.6	0.283	4.701	87.0	47.5	0.323	6.300	78.0	1.14	1.34

A.2. Experimental test facility

See Figs. A1 and A2.

A.3. Conversion equations

$$\text{Head number, } \psi_c = \frac{2gH}{u^2} = \frac{2}{\pi^2} \frac{gH}{n^2 D^2} = \frac{2}{\pi^2} \psi \quad (\text{A1})$$

$$\text{Discharge number, } \phi_c = \frac{4Q}{\pi D^2 u} = \frac{4}{\pi^2} \frac{Q}{n D^3} = \frac{4}{\pi^2} \phi \quad (\text{A2})$$

$$\text{Turbine specific speed, } \sigma = \frac{\phi_c^{1/2}}{\psi_c^{3/4}} = 2^{1/4} \pi^{1/2} \frac{\phi_t^{1/2}}{\psi_t^{3/4}} \quad (\text{A3})$$

$$\text{Specific diameter, } \Delta = \frac{\psi_c^{1/4}}{\phi_c^{1/2}} = \frac{\pi^{1/2}}{2^{3/4}} \frac{\psi_t^{1/4}}{\phi_t^{1/2}} \quad (\text{A4})$$

The relationship between the Cordier σ and $N_q(\text{SI})$ is given by, σ

$$= \frac{2^{1/4} \pi^{1/2}}{g^{3/460}} \frac{NQ^{1/2}}{H^{3/4}} = 6.3383 \times 10^{-3} N_{qt} \quad (\text{A5})$$

A.4. Flow chart of the selection model

Fig. A3 describes the finer aspects of selection model stage of the comprehensive PAT model introduced in Fig. 1 (Section 2.2). Similar to the prediction model, the selection of an optimum pump for a given site (with head and flow) is also guided by the mean Cordier PAT line (in Fig. 3). The fixed input parameters namely the head and flow are used along with the turbine speed, which is the control parameter, to determine the turbine mode specific speed (N_{qt}) and σ (given by Eq. (A5)). The control parameter is the designer choice and can take values to suit the best operating region along the Cordier line and also the available pump shapes with the manufacturer.

The turbine mode specific speed (N_{qt}) leads to the pump mode specific speed (N_{qp}) using the experimental relationship between them, given by equations in Appendix A.5 and defines the shape of required pump. The intersection of the constant σ line with the Cordier lines gives a range of specific diameters, which can be translated to absolute diameters using relations in Appendix A.3. The final output parameters of the selection model are the pump mode specific speed, which represents the pump shape and the range of impeller diameters, which represents the pump size. The choice of pumps will be solely guided by these two parameters. Manufacturer's catalogue are referred at this stage

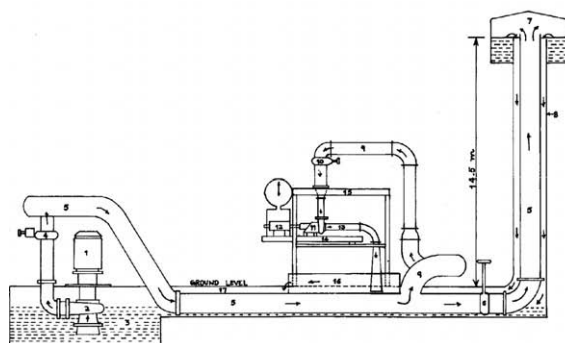


Fig. A1. The open loop hydraulic test rig for studying pumps as turbines.

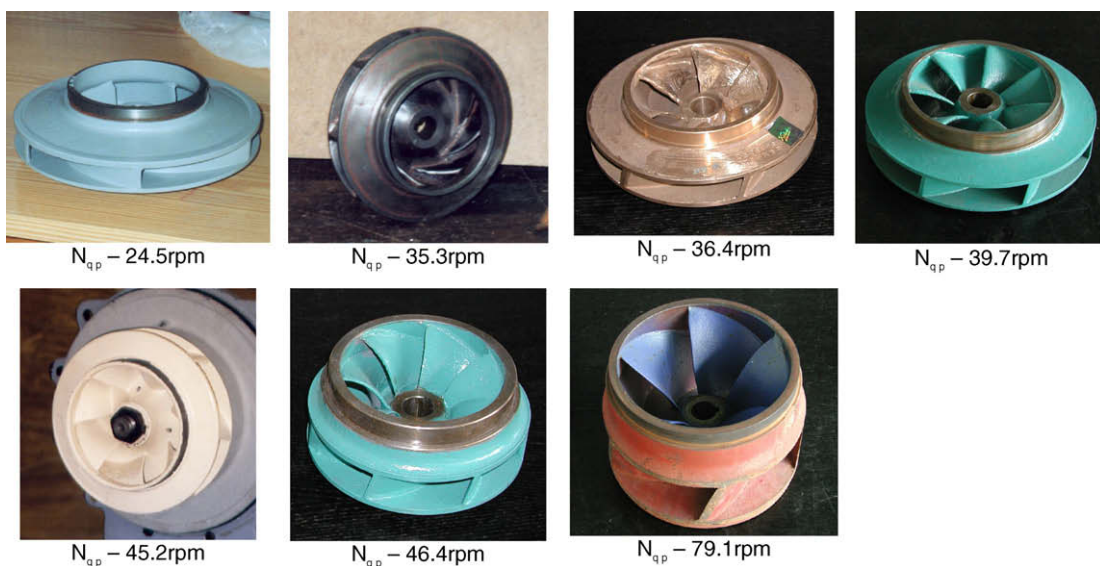


Fig. A2. Hydraulics of the tested radial pump impellers.

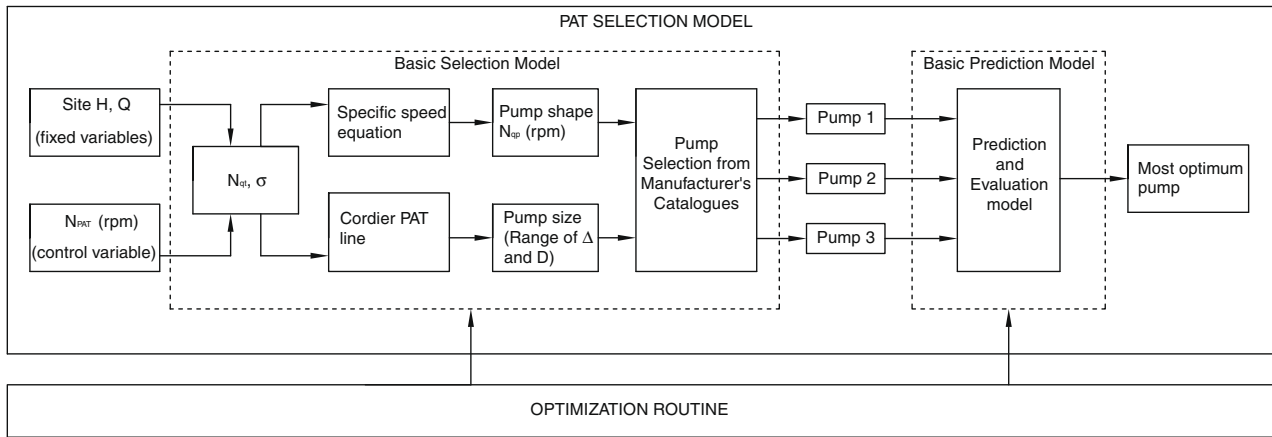


Fig. A3. Flow chart for the PAT selection model.

and it has to be emphasized that there could be a possibility, that more than one pump could be suitable for the same site, but with a different shape.

The selection of these pumps does not mean that they would be the automatic and the final choice for the site. The selected pump has to pass the test of acceptance where the actual operating point (obtained after using the prediction model) is compared to the field point. When there is more than one pump involved, a similar evaluation needs to be done and other factors like mechanical characteristics need to be counterweighed before the final choice of the pump is made.

A.4.1. Application of selection model using optimization routine

The selection model is implemented on the example sited in Section 5.2 for a site with a net head of 60 m and discharge of 45 l/s. The turbine speed proposed for these site conditions is 3000 rpm.

N_{qt} : From definition, $N_{qt} = \frac{N \cdot \sqrt{Q}}{H^{3/4}} = \frac{3000 \cdot \sqrt{0.045}}{60^{3/4}} = 29.5$ rpm
 N_{qp} : From Eq. (2), $N_{qp} = (N_{qt} + 3.12)/0.94 = (29.5 + 3.12)/0.94 = 34.8$ rpm
 σ : From Eq. (A5), $\sigma = 6.3383 \times 10^{-3} \cdot N_{qt} = 6.3383 \times 10^{-3} \cdot (29.5) = 0.187$
 Δ_m : From Eq. (1), $\sigma = (1.136) \cdot \Delta^{-1.239}$, $\Delta_m = (0.187 / 1.136)^{-1/(1.239)} = 4.289$
 D_m : Simplifying Eq. (A4), $D_m = (2^{3/4} / (\pi^{1/2} \cdot g^{1/4})) \cdot \frac{\Delta Q^{1/2}}{H^{1/4}} = (0.536) \cdot \frac{4.289 \cdot 0.045^{1/2}}{60^{1/4}} = 0.175$ m

From Fig. 5 (Section 3.4.1), the R_A is found to be ± 0.056 and using Eq. (1), $\Delta_l = 4.118$ and $\Delta_u = 4.459$. These specific diameters are converted to absolute diameters for the same head and flow using the Eq. (A4), which specifies D_l as 0.168 m and D_u as 0.182 m. The range of diameter (0.168–0.183 m) and the approximate pump specific speed (34.8 rpm) are used to select a pump from the manufacturers catalogues.

Table A1 Summary of the governing equations for simulation.

Sr. no.	Governing equation	Optimization routine (13 PATs)	Basic prediction model (9 PATs)
1	Specific speed equation	$N_{qt} = 0.94 \cdot N_{qp} - 3.12$	$N_{qt} = 0.94 \cdot N_{qp} - 3.2$
2	Mean Cordier PAT Line	$\sigma = 1.136 \Delta^{-1.239}$	$\sigma = 1.225 \Delta^{-1.288}$
3	No-load discharge number	$\phi_{nl} = 0.83 \cdot \sigma^{1.51}$	$\phi_{nl} = 1.19 \cdot \sigma^{1.73}$
4	No-load head number	$\psi_{nl} = 1.39 \cdot \phi_{nl}^{-0.344}$	$\psi_{nl} = 1.35 \cdot \phi_{nl}^{-0.341}$

A.5. Comparison of model equations for basic prediction model and optimization routine

The governing equations for simulation are summarized in Table A1, whose origin comes from experimental tests on corresponding PATs. The detailed methodology of developing the specific speed equation, mean Cordier PAT line and the no-load points has been discussed in Section 3.4 for the optimization routine, which uses data of 13 PATs. In the similar way, the governing equations for the basic prediction model based on 9 PAT data are also developed.

A.6. Hermite spline interpolation

The Hermite spline interpolation is a technique that fits a three degree polynomial for a function or curve that already has two fixed points and slopes at these two points. The theory of this interpolation technique has been dealt in detail in Boor [12]. This section briefly summarizes the methodology and also presents the complete set of equations for the 3 field tested PATs for both the basic prediction model and the optimization routine.

This interpolation technique introduces a parameter 'h' that defines the range between no-load and BEP on the discharge number scale (Eq. (A6)) and a parameter 'x' that signifies the incremental value on the abscissa scale (Eq. (A7)). A dimensionless parameter 't' given by Eq. (A8) defines the relative position of the discharge number on the abscissa scale. It can take a value between 0 and 1. For conditions beyond the BEP, the parameters 't' takes a value beyond 1

$h = \phi_{BEP} - \phi_{nl}$ (A6)

$x = \phi_{nl} + \text{incremental value still BEP}$ (A7)

$t = (x - \phi_{nl})/h$ (A8)

The interpolation technique further defines four Hermite basis functions or polynomials in terms of the position parameter 't', which are given by

$$h_{00} = 2 \cdot t^3 - 3 \cdot t^2 + 1 \quad (A9)$$

$$h_{10} = t^3 - 2 \cdot t^2 + t \quad (A10)$$

$$h_{01} = -2 \cdot t^3 + 3 \cdot t^2 \quad (A11)$$

$$h_{11} = t^3 - t^2 \quad (A12)$$

The required polynomial for the head number is represented by Eq. (A13), which is function of the parameter 't'. Since, the parameter 't' is essentially a function of discharge number (as seen in Eq. (A8)), the polynomial can be represented in terms of discharge number

$$\psi = \psi_{nl} \cdot h_{00} + S_{nl} \cdot h_{10} \cdot h + \psi_{BEP} \cdot h_{01} + S_{BEP} \cdot h_{11} \cdot h \quad (A13)$$

The head number–discharge number equation for any PAT can be formed from Eq. (A13) provided the no-load point, the BEP and respective slopes at these points are known with the help of any calculation program.

Table A2
Summary of Hermite spline data for the optimization routine.

Sr. no.	PAT (rpm)	$\ln(S_{BEP}/N_{qp}^2) = \beta$	$(\delta\psi/\delta\phi)_{BEP} = S_{BEP}$	$(\delta\psi/\delta\phi)_{nl} = S_{nl}$	ϕ_{nl}	ϕ_{BEP}	ψ_{nl}	ψ_{BEP}
1	18.2	-0.46	208.5	10	0.021	0.057	5.21	10.24
2	19.7	-0.70	192.1	10	0.025	0.066	4.96	9.87
3	44.7	-3.88	41.1	10	0.100	0.246	3.06	6.90

Table A3
Summary of Hermite spline data for the basic prediction model.

Sr. no.	PAT (rpm)	$\ln(S_{BEP}/N_{qp}^2) = \beta$	$(\delta\psi/\delta\phi)_{BEP} = S_{BEP}$	$(\delta\psi/\delta\phi)_{nl} = S_{nl}$	ϕ_{nl}	ϕ_{BEP}	ψ_{nl}	ψ_{BEP}
1	18.2	-0.46	209.0	10	0.019	0.061	5.25	10.66
2	19.7	-0.70	192.5	10	0.021	0.069	5.06	10.22
3	44.7	-3.89	40.8	10	0.105	0.240	2.92	6.73

A.7. Dimensionless numbers used in Figs. 7–12

18.2 rpm PAT (Figs. 7 and 8)						19.7 rpm PAT (Figs. 9 and 10)						44.7 rpm PAT (Figs. 11 and 12)					
Field		Basic model (Table A3)		Optimization routine (Table A2)		Field		Basic model (Table A3)		Optimization routine (Table A2)		Field		Basic model (Table A3)		Optimization routine (Table A2)	
ϕ	ψ	ϕ	ψ	ϕ	ψ	ϕ	ψ	ϕ	ψ	ϕ	ψ	ϕ	ψ	ϕ	ψ	ϕ	ψ
0.026	4.57	0.0215	5.295	0.0215	5.215	0.0221	4.23	0.025	5.13	0.02	4.96	0.121	2.94	0.100	2.890	0.100	3.06
0.031	5.31	0.0250	5.438	0.0250	5.330	0.0245	4.78	0.030	5.33	0.03	5.10	0.136	3.21	0.110	2.986	0.110	3.17
0.033	5.97	0.0300	5.782	0.0300	5.693	0.0437	6.39	0.040	6.04	0.04	5.84	0.141	3.51	0.130	3.287	0.130	3.46
0.041	7.54	0.0400	6.909	0.0400	6.988	0.0520	7.64	0.050	7.14	0.05	7.10	0.189	4.67	0.150	3.711	0.150	3.85
0.046	8.49	0.0500	8.509	0.0500	8.806	0.0555	8.27	0.057	8.14	0.06	8.22	0.195	4.97	0.170	4.243	0.170	4.33
0.046	8.49	0.0600	10.452	0.0600	10.865	0.0574	8.53	0.060	8.61	0.06	8.75	0.203	5.25	0.190	4.868	0.190	4.89
0.050	9.16	0.0675	12.055	0.0675	12.398			0.070	10.41	0.07	10.65			0.210	5.571	0.210	5.54
0.052	9.52							0.078	12.07	0.08	12.26			0.230	6.336	0.230	6.25
														0.250	7.150	0.250	7.03
														0.270	7.996	0.270	7.87
														0.290	8.861	0.290	8.77

A.8. Experimental uncertainty in the basic model and the optimization routine

Sr. no.	N_{qp} (rpm)	ϕ_t	ψ_t	$\delta\phi/\phi$ (%)	$\delta\psi/\psi$ (%)
<i>Data of 9 PATs used in the basic prediction model</i>					
1	21.0	0.033	9.80	±7.8	±1.8
2	24.5	0.117	11.17	±6.6	±1.0
3	35.3	0.151	7.64	±7.0	±1.1
4	36.4	0.185	8.00	±2.2	±1.3
5	39.7	0.200	6.70	±1.5	±1.1
6	45.2	0.235	6.18	±4.6	±1.2
7	46.4	0.275	7.60	±2.5	±1.6
8	61.3	0.414	5.75	±2.2	±1.5
9	79.1	0.480	4.90	±1.4	±1.7
<i>Additional data from Derakshan and Nourbakhsh [2]</i>					
1 [2]	14.6	0.033	9.80	NA	NA
2 [2]	23.0	0.070	8.00	NA	NA
3 [2]	37.6	0.100	10.70	NA	NA
4 [2]	55.6	0.117	11.17	NA	NA

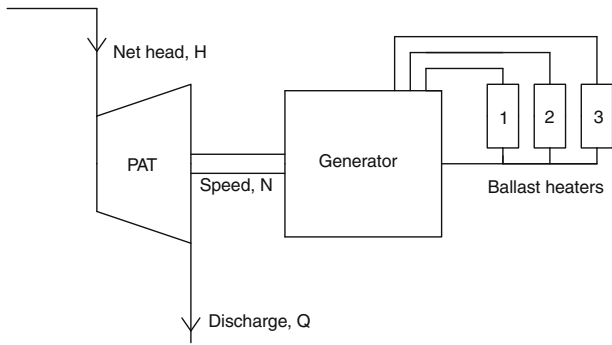


Fig. A4. The field experimental setup.

Table A4
Summary of uncertainty at BEP field tested PATs.

Sr. no.	N_{qp} (rpm)	ϕ_t	ψ_t	$\delta\phi/\phi$ (%)	$\delta\psi/\psi$ (%)
1	18.2	0.052	9.517	± 6.5	± 1.0
2	19.7	0.057	8.525	± 5.2	± 1.2
3	44.7	0.203	5.246	± 4.6	± 3.0

A.9. Field setup

The field setup used to characterize the 3 PATs is illustrated in Fig. A4. This setup measures only the total head, discharge and electrical output power along with turbine speed. The uncertainties of the discharge number and head number values are presented in Table A4 at the respective BEP of the PATs.

A.10. Application of the model for the 18.2 rpm PAT

The application of the model begins from the Cordier line intersection and establishment of mean specific diameter with its uncertainty limits. The BEP comprising of the discharge number and head number at these 3 specific diameters are then evaluated. Similarly, the no-load points with its uncertainty limits are also determined. Sample calculations for the optimization routine is carried on Sections A.10.1–A.10.3.

A.10.4. Summary of the predictions with the optimization routine for 18.2 rpm PAT

Pump data	Cordier PAT data					No-load points			PAT operating points		
	$H = 32.5$ m	Cordier line intersection	Coefficients at different D			ψ - ϕ line	ϕ_{nl}	ψ_{nl}	ψ - ϕ line	$(\phi, \psi)_{nl}$	$(\phi, \psi)_{BEP}$
$Q = 29.2$ l/s			$\Delta_m = 7.868$	$\Delta_l = 7.332$	$\Delta_u = 8.395$	Mean	0.021	5.21	Mean	(0.021, 5.21)	(0.057, 10.24) _{BEP}
$N = 1450$ rpm	$N_{qt} = 13.92$ rpm	σ_m	0.0882	0.0963	0.0814	Upper	0.019	5.81	Upper	(0.019, 5.81)	(0.051, 10.56) _{BEP}
$D = 0.329$	$\sigma = 0.0882$	ϕ_{mt}	0.057	0.065	0.051	Lower	0.024	4.63	Lower	(0.024, 4.63)	(0.065, 9.90) _{BEP}
$N_{qp} = 18.2$ rpm	$\Delta_m = 7.868$ (+6.8%, -6.7%)	ψ_{mt}	10.24	9.90	10.56				η value	0%	74%
$\psi_p = 5.043$	$\Delta_l = 7.332$	ϕ_{mt}/ϕ_p	1.69	1.92	1.51						
$\phi_p = 0.034$	$\Delta_u = 8.395$	ψ_{mt}/ψ_p	2.03	1.96	2.09						

The BEP and no-load predictions for the 18.2 rpm PAT are summarized in Section A.10.4 for the optimization routine and in Section A.10.5 for the basic prediction model. These points are plotted on the consolidated PAT characteristics (Fig. 2) and curve fitting is carried out using the Hermite spline interpolation (as described in Section A.6) separately for the basic prediction model and the optimization routine. The resulting curves are illustrated in Figs. A5 and A6, and the ψ - ϕ characteristics obtained from the basic model and routine are compared with the field ψ - ϕ curves.

A.10.1. Cordier line intersection for optimization routine

$$N_{qt}: \text{From Eq. (2), } N_{qt} = 0.94 \cdot (18.2) - 3.12 = 13.92 \text{ rpm}$$

$$\sigma: \text{From Eq. (A5), } \sigma = 6.3383 \times 10^{-3} N_{qt} = 0.0882$$

$$\Delta_m: \text{From Eq. (1), } \sigma = (1.136) \cdot \Delta^{-1.239}, \Delta_m = (0.0882/1.136)^{-1/(1.239)} = 7.868$$

$$\Delta_l: \text{From Eq. (1) and Fig. 5, } R_{\Delta} = +0.095, \Delta_l = (0.0882/(1.136 - 0.095))^{-1/(1.239)} = 7.332$$

$$\Delta_u: \text{From Eq. (1) and Fig. 5, } R_{\Delta} = -0.095, \Delta_u = (0.0882/(1.136 + 0.095))^{-1/(1.239)} = 8.395$$

A.10.2. BEP discharge and head number at $\Delta_m = 7.868$

$$\psi_{mt}: \text{Combining } \Delta_m \text{ (Eq. (A4)) and } \sigma_m \text{ (Eq. (A3)), } \psi_{mt} = \left(\frac{\pi}{(2^{0.5} \cdot \Delta_m \cdot \sigma)} \right)^2 = \left(\frac{\pi}{(2^{0.5} \cdot 7.868 \cdot 0.0882)} \right)^2 = 10.24$$

$$\phi_{mt}: \text{Combining } \Delta_m \text{ (Eq. (A4)) and } \psi_{mt}, \phi_{mt} = \left(\frac{\pi^{0.5} \cdot \psi_{mt}^{0.25}}{2^{0.75} \cdot \Delta_m} \right)^2 = \left(\frac{\pi^{0.5} \cdot 10.24^{0.25}}{2^{0.75} \cdot 7.868} \right)^2 = 0.057$$

The same methodology is employed to get the discharge numbers and head numbers at the lower and upper specific diameter, respectively at the same Cordier specific speed. The uncertainty band for the discharge number obtained is the same that is presented in Fig. 5 (+13.2%, -10.8%).

A.10.3. Evaluation of no-load points

$$\phi_{nl-m}: \text{Using Eq. (4), } \phi_{nl-m} = 0.83 \cdot \sigma^{1.51} = 0.83 \cdot 0.0882^{1.51} \approx 0.021$$

$$\psi_{nl-m}: \text{Using Eq. (5), } \psi_{nl-m} = 1.39 \cdot \phi_{nl-m}^{-0.344} = 1.39 \cdot 0.021^{-0.344} \approx 5.21$$

Similarly, the lower and upper limits of the no-load points (ϕ and ψ) are determined by considering the identical range of discharge number as for the BEP discharge number (+13.2%, -10.8%).

A.10.5. Summary of predictions with the basic prediction model for 18.2 rpm PAT

Pump data	Cordier PAT data					No-load points			PAT operating points		
	Cordier line intersection	Coefficients at different Δ				ψ - ϕ line	ϕ_{nl}	ψ_{nl}	ψ - ϕ line	$(\phi, \psi)_{nl}$	$(\phi, \psi)_{BEP}$
$Q = 29.2$ l/s		$\Delta_m = 7.696$	$\Delta_l = 7.224$	$\Delta_u = 8.161$		Mean	0.019 (+11.5%, -9.5%)	5.25	Mean	(0.019, 5.25)	(0.061, 10.66)
$N = 1450$ rpm	$N_{qt} = 13.94$ rpm	σ_m	0.0884	0.0959	0.0820	Upper	0.017	5.83	Upper	(0.017, 5.83)	(0.055, 11.03)
$D = 0.329$ m	$\sigma = 0.0884$	ϕ_{mt}	0.061 (+11.5%, -9.5%)	0.068	0.055	Lower	0.021	4.68	Lower	(0.021, 4.68)	(0.068, 10.28)
$N_{qp} = 18.2$ rpm	$\Delta_m = 7.696$ (+6.0%, -6.1%)	ψ_{mt}	10.66	10.28	11.03				η value	0%	74%
$\psi_p = 5.043$	$\Delta_l = 7.224$	ϕ_{mt}/ϕ_p	1.81	2.01	1.63						
$\phi_p = 0.034$	$\Delta_u = 8.161$	ψ_{mt}/ψ_p	2.11	2.04	2.19						

A.10.6. Construction of the dimensionless curves for 18.2 rpm PAT

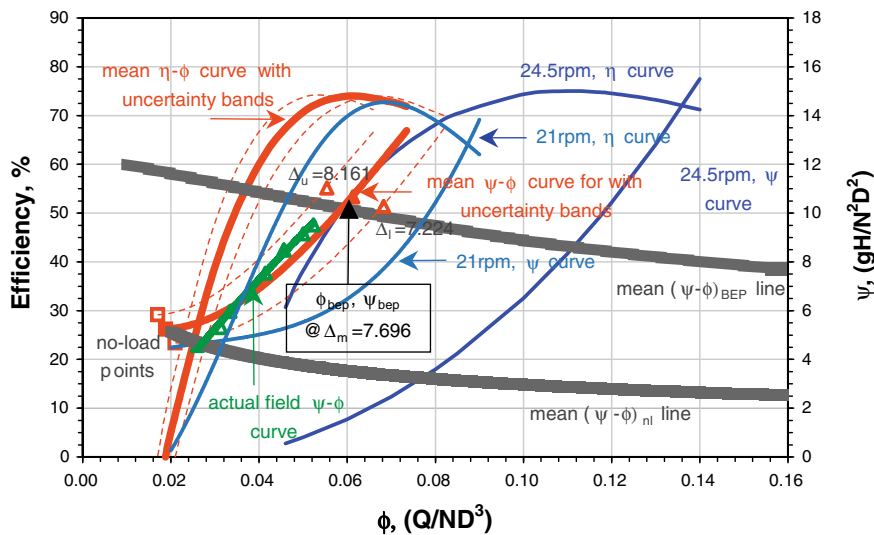


Fig. A5. ψ - ϕ and η - ϕ curves using the basic prediction model for the 18.2 rpm PAT.

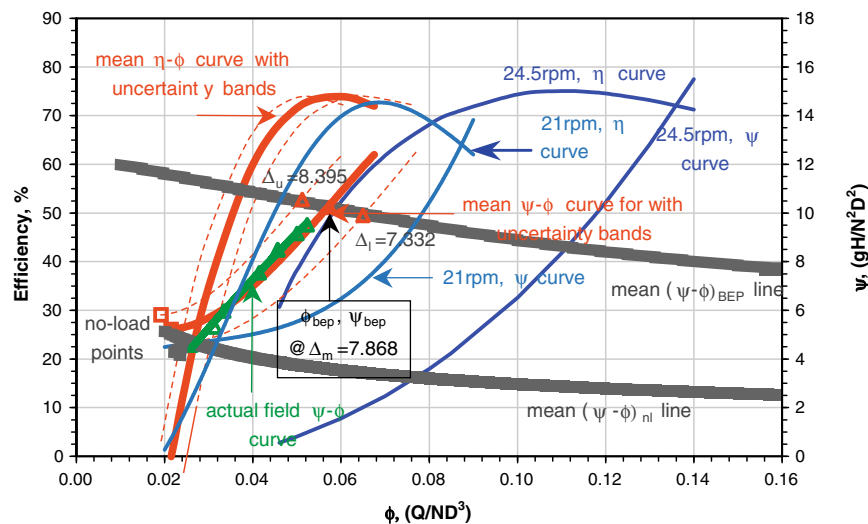


Fig. A6. ψ - ϕ and η - ϕ curves using the optimization routine for the 18.2 rpm PAT.

References

- [1] P. Singh, Optimization of the Internal Hydraulic and of System Design in Pumps as Turbines with Field Implementation and Evaluation, Ph.D. Thesis, University of Karlsruhe, Germany, 2005.
- [2] S. Derakhshan, A. Nourbakhsh, Experimental study of characteristic curves of centrifugal pumps working as turbines in different specific speeds, *Elsevier Journal of Experimental Thermal and Fluid Science* 32 (2008) 800–807.
- [3] A.A. Williams, Pumps as Turbines Used with Induction Generators for Stand-alone Micro-Hydroelectric Power Plants, PhD Thesis, Nottingham Trent University, 1992, pp. 51–80, 88–91, 149–153.
- [4] D. Cohrs, Investigations of a multistage pump operated as a turbine, Untersuchungen an einer mehrstufigen rückwärtslaufenden Kreiselpumpe im Turbinenbetrieb, Verlag und Bildarchiv, W.H. Faragallah, German, 1997, pp. 8–41.
- [5] M. Amelio, S. Barbarelli, A one-dimensional numerical model for calculating the efficiency of pumps and turbines for implementation in micro hydro power plants, in: ASME 7th Biennial Conference on Engineering System Design and Analysis, 2004, pp. 65–77.
- [6] O. Cordier, Similarity conditions in turbomachines, Aehnlichkeitsbedingungen für Strömungsmaschinen, *BWK (Brennstoff-Wärme-Kraft)*, German, 1953, pp. 337–340 (Bd. 5, Nr. 10, October).
- [7] O.E. Balje, *Turbomachines – A Guide to Design, Selection and Theory*, John Wiley and Sons, 1981 (Chapter 3).
- [8] S.L. Dixon, *Fluid Mechanics and Thermodynamics of Turbomachinery*, fifth ed., Elsevier, 2005 (Chapter 9).
- [9] R.J. Moffat, Contributions to the theory of single-sample uncertainty analysis, *ASME Journal of Fluids Engineering* (1982) 250–260.
- [10] S.J. Kline, The purposes of uncertainty analysis, *ASME Journal Fluids Engineering* (1985) 153–160.
- [11] J.P. Holman, *Experimental Methods for Engineers*, seventh ed., McGraw-Hill, 2001 (Chapter 3).
- [12] C.D. Boor, Practical guide to splines, *Applied Mathematical Sciences*, vol. 27, Springer, 2001, p. 40 (Chapter 4).
- [13] Kirloskar Brothers Limited, Catalogues Specifying the Duty Points for DB and KPD pumps, Corporate Research and Engineering Division, Pune, India, 2005.



Contents lists available at ScienceDirect

Experimental Thermal and Fluid Science

journal homepage: www.elsevier.com/locate/etfs

Internal hydraulic analysis of impeller rounding in centrifugal pumps as turbines

Punit Singh*, Franz Nestmann

Institute of Water and River Basin Management (IWG), Karlsruhe Institute of Technology, Kaiser Str. 12, D 76131 Karlsruhe, Germany

ARTICLE INFO

Article history:

Received 22 May 2010

Received in revised form 3 August 2010

Accepted 22 August 2010

Keywords:

Impeller rounding

Pump as turbine

Free vortex theory

Loss coefficient

Exit relative flow angle

Prediction model

ABSTRACT

The use of pumps as turbines in different applications has been gaining importance in the recent years, but the subject of hydraulic optimization still remains an open research problem. One of these optimization techniques that include rounding of the sharp edges at the impeller periphery (or turbine inlet) has shown tendencies of performance enhancement.

In order to understand the effect of this hydraulic optimization, the paper introduces an analytical model in the pump as turbine control volume and brings out the functionalities of the internal variables classified under control variables consisting of the system loss coefficient and exit relative flow direction and under dependent variables consisting of net tangential flow velocity, net head and efficiency.

The paper studies the effects of impeller rounding on a combination of radial flow and mixed flow pumps as turbines using experimental data. The impeller rounding is seen to have positive impact on the overall efficiency in different operating regions with an improvement in the range of 1–3%. The behaviour of the two control variables have been elaborately studied in which it is found that the system loss coefficient has reduced drastically due to rounding effects, while the extent of changes to the exit relative flow direction seems to be limited in comparison. The reasons for changes to these control variables have been physically interpreted and attributed to the behaviour of the wake zone at the turbine inlet and circulation within the impeller control volume.

The larger picture of impeller rounding has been discussed in comparison with performance prediction models in pumps as turbines. The possible limitations of the analytical model as well as the test setup are also presented. The paper concludes that the impeller rounding technique is very important for performance optimization and recommends its application on all pump as turbine projects. It also recommends the standardization of the rounding effects over wide range of pump shapes including axial pumps.

© 2010 Elsevier Inc. All rights reserved.

1. Introduction

1.1. Background

Pumps as turbines have come a long way since its accidental discovery by Thoma [1] for both energy recovery and decentralized power generation. The focus of the pump companies as well as the scientists has been to develop accurate prediction models for the turbine operation of different designs of centrifugal pumps. Despite there being considerable work by various scientists as reported by Williams [2], Amelio et al. [3] and Derakhshan and Nourbakhsh [4], the accuracy of these models has remained a question mark. Recently, Singh and Nestmann in [5] presented an optimization model with accuracies within $\pm 3\%$ for pump specific

speeds 20–80 rpm. However, even this model requires continuous verification and optimization.

While the prediction model for pumps as turbines will undergo further development, there are other important issues that have to be dealt with. Singh [6] demonstrated various possibilities of modifying the pump geometry to improve the performance of a given pump in turbine mode. The topic of hydraulic optimization is the next stage of research activity in PATs and should be treated on par with the topic of prediction model. The issue of hydraulic performance optimization comes only after a convincing pump selection has been made for a given turbine application. Singh [6] showed that off the different geometric modifications attempted, the modification at the periphery of the impeller blades known as impeller rounding was the most beneficial. This type of modification was first carried out by Lueneberg and Nelson [7] and Cohrs [8] on individual pumps and both reported an efficiency improvement in the range of 1.5–2%. Singh [6] carried out inlet rounding on eight different centrifugal pumps and presented a qualitative understanding of impeller rounding effects with respect to the

Abbreviations: PAT, pump as turbine; BEP, best efficiency point.

* Corresponding author.

E-mail addresses: punit.singh@iwg.uka.de (P. Singh), nestmann@iwg.uka.de (F. Nestmann).

Nomenclature*Full scripts*

A	flow area, m^2
c	absolute velocity, m/s
D	outer impeller diameter, m
g	acceleration due to gravity, m/s^2
H	head parameter, m
k	loss coefficient, $1/m^4$
\dot{m}	mass flow rate, kg/s
N	speed, rpm
N_q	specific speed, $NQ^{1/2}/H^{3/4}$ (N in rpm , H in m , Q in m^3/s)
P	power, kW
Q	discharge, m^3/s
r	radius vector, m
T	torque, $N\ m$
u	tangential blade velocity, m/s
w	relative velocity, m/s

Greek symbols

η	efficiency, %
α	absolute flow angle, $^\circ$
β	relative flow angle, $^\circ$

Superscripts

*	blade condition
---	-----------------

Subscripts

1	impeller inlet (turbine mode)
2	impeller exit (turbine mode)
L	losses
p	pump mode
r	radial direction
u	tangential component

internal hydraulics. Derakhshan et al. [9] used a computer model to study the effects of impeller rounding on a low specific speed pump, but did not discuss the internal hydraulic effects.

The internal flow phenomena resulting from impeller rounding is not clear despite the fact that it is pretty evident that this modification improves performance in the turbine mode. Further, accurate understanding of these phenomena in a wide range of pump shapes remains a bigger challenge, which involves the characterization of turbomachinery parameters like the Euler momentum, impeller losses and different velocity vectors involved in the energy transfer. In addition, the relevance of inlet rounding should also be studied in comparison with prediction errors of the PAT operating line to give a holistic perspective to this modification technique. The contemporary study of impeller rounding only reports the change in performance in few pumps but falls short of bringing out the accurate internal hydraulic behaviour and its relevance to system issues like pump selection and performance prediction.

1.2. Objectives and problem outline

The background of the stated problem leads to the following objectives of the study.

- To develop a theoretical model based on turbomachine fundamentals with help of a zonal approach in a PAT control volume and to identify the internal variables and their behaviour.
- To experimentally study impeller rounding effects in a wide range of PAT shapes and to accurately characterize these effects with respect to internal hydraulic variables over the complete operating region of the PAT (part-load, BEP and overload).
- To study the relevance of impeller rounding compared to system issues in pumps as turbines like selection and performance prediction.

2. The pump as turbine control volume

In order to develop a meaningful model for understanding the internal hydraulic behaviour, the pump as turbine system can be treated as control volume. Beginning from the spiral volute to the draft tube entry, it is divided into five different zones as represented in Figs. 1 and 2. The hydraulics within these zones (both

stationary and rotary) is function of fluid flow condition, geometry and frictional effects at the solid boundaries. But, there are more complex mechanisms involved in these zones.

The hydraulics of the zones that could be subjected to change due to impeller rounding are zone iii, zone iv and zone v. While zone iii and zone v are transition zones, zone iv is the rotary zone within the impeller. Hydraulic changes can take place with respect to flow lines at zone iii and zone iv, particularly in the inlet flow space of the zone iv. The changes in the transition zone iii and zone v are associated with relative flow direction. The flow conditions in these three zones due to impeller rounding would have to be investigated using experimental studies.

3. Theoretical model for optimization studies

The theoretical model (mentioned in Section 1.2) involves the development of a link between the external operating variables on the PAT and the internal variables using fundamental hydraulic and turbomachine laws. The model will be objected to identify the internal variables that control the entire performance and how

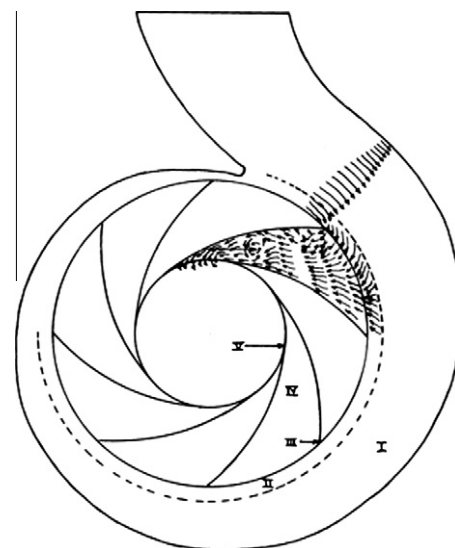


Fig. 1. Flow zones in a radial flow PAT control volume-view 1.

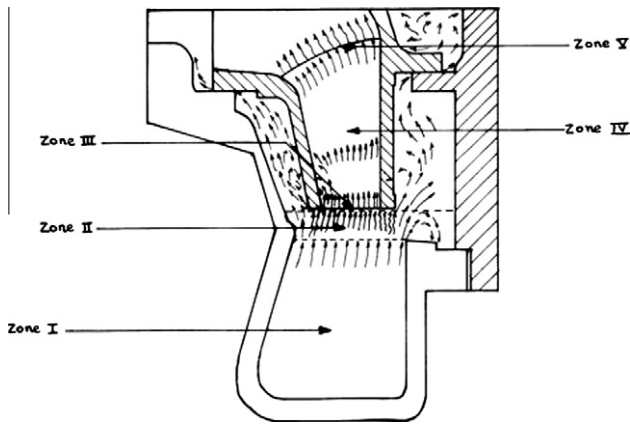


Fig. 2. Flow zones in a radial flow PAT control volume-view 2.

they influence the other variables, especially under circumstances of geometric modification.

3.1. External variables in a PAT control volume

Analysis of turbomachinery performance is generally carried out either on the basis of constant speed or on the basis of constant head. Constant speed methodology will be used in this study to understand the inter-relationships between the external variables and the internal variables. The general functional relationship for the external variables is represented in Eq. (1), where speed and flow rate are the control variables while head, shaft power and efficiency are the dependent variables.

$$H, P, \eta = f(N, Q) \quad (1)$$

3.2. Internal variables in a PAT control volume and their behaviour

3.2.1. Functionality for all internal variables

3.2.1.1. Control variables. The two external control variables in Eq. (1) are expanded to obtain the corresponding internal variables. The discharge can be represented by the radial flow velocity component at either the inlet or exit impeller area as shown in Eq. (2). Focusing on the inlet impeller, which is undergoing change due to impeller rounding, the internal variable of interest is the inlet radial velocity, c_{r1} . It will be seen from Fig. 6 that the impeller rounding creates an increase in area, which implies that at constant discharge condition, c_{r1} has to proportionally decrease.

$$Q = c_{r1} \cdot A_1 \text{ or } c_{r2} \cdot A_2 \quad (2)$$

The other control variable of Eq. (1) is speed, which can be related to the peripheral impeller speed at the inlet or exit and respective diameter. The expansion of discharge and speed variables lead to two internal control variables namely, the radial flow velocity and peripheral impeller velocity.

3.2.1.2. Dependent variables.

3.2.1.2.1. Shaft power. Shaft power is an external dependent variable and can be represented by Euler momentum and the mass flow rate considering negligible effects of disc friction and leakage as reasoned out in [10] and shown in Eq. (3). The internal variables obtained from shaft power variable are the net tangential flow velocity and radial flow velocity is seen in Eq. (3).

$$P_{shaft} = \dot{m} \cdot (\Delta c_u \cdot u) = (\rho \cdot A \cdot c_r) \cdot (\Delta c_u \cdot u) \quad (3)$$

Further, the expansion of the internal variable Δc_u , as illustrated in Eqs. (4) and (5), shows that it is a function of radial flow velocity (inlet or exit from Eq. (2)), inlet vortex angle, relative flow angle at

exit and peripheral velocity. This expansion in Eq. (4) can be obtained from the velocity triangles at the inlet and exit of a PAT control volume shown in Fig. 3.

$$\Delta c_u = c_{u1} - c_{u2} = c_{r1} \cdot \tan \alpha_1 + c_{r2} \cdot \tan \beta_2 - u_2 \quad (4)$$

$$\Delta c_u = f(c_{r1}, \alpha_1, \beta_2, u) \quad (5)$$

It can be shown that c_{r1} and α_1 are related and it is enough to use one of these variables. This follows from the free vortex theory (as discussed in Section 3.2.2.1), where c_{u1} (represented by c_{r1} and α_1 as seen in Eq. (4)) is a function of radius only and hence it would be constant for both stages of optimization. After incorporating these relations, the final functionality of Δc_u (initially given by Eq. (5)) reduces to the dependency on only one variable, i.e. the relative exit flow angle, at constant speed conditions, as shown in Eq. (6).

$$\Delta c_u = f(\beta_2) \text{ at constant peripheral velocity, } u \quad (6)$$

3.2.1.2.2. Net head (gH). The next dependent variable according to functionality in Eq. (1) to be analyzed is the net head, which can be represented as the sum of Euler momentum and the losses within all the five zones of the PAT control volume illustrated in Eq. (7). It is convenient to represent the hydraulic losses as function of a system loss coefficient (k_{system}) based on discharge. The system loss coefficient includes loss mechanisms in the complete PAT control volume (zone i to zone v as defined in Figs. 1 and 2). As seen in Eq. (6), the net tangential flow velocity is a function of exit relative flow angle, which results in the overall functionality of the net head to be a function of exit relative flow angle and the system loss coefficient (Eq. (8)).

$$gH = \Delta c_u \cdot u + g \cdot H_L = \Delta c_u \cdot u + k_{system} \cdot Q^2 \quad (7)$$

$$gH = f(\beta_2, k_{system}) \quad (8)$$

The above analysis brings about two internal dependent variables comprising on Δc_u and gH and four internal control variables that include c_r , k_{system} , u and β_2 . These internal variables need to be studied in more detail because they form the basis of analyzing the effects of optimization.

3.2.2. Internal control variables

3.2.2.1. Radial flow velocity (or inlet vortex angle). As seen from Eq. (2), radial flow velocity depends on the discharge and the flow area under consideration. Since, the inlet area (in PAT mode) is undergoing modification due to impeller rounding, the inlet radial velocity will be analyzed as an internal control variable. The change to the radial flow velocity component causes a change to the inlet vortex angle as well. However, this change to both radial flow velocity and inlet vortex angle will not have any impact on the tangential flow velocity component (c_{u1}) at the inlet, which is related to only radius as seen from the free vortex condition in Eq. (9) and will remain a constant for both stages of optimization. Hence, there would be no influence of either of these parameters (c_r or α_1) on the net tangential flow velocity and also on the net head (already discussed in Eq. (6)).

$$c_{u1} \cdot r = \text{constant for both stages of optimization} \quad (9)$$

However, as seen from the velocity triangles in Fig. 3, the change to radial flow velocity could affect the relative flow entry (β_1) at the inlet, which could in turn have an influence on the hydraulics in zone iii and zone iv.

3.2.2.2. System loss coefficient. This is an important variable that will undergo transformation due to impeller rounding and would take into consideration affects in zone iii, zone iv and probably

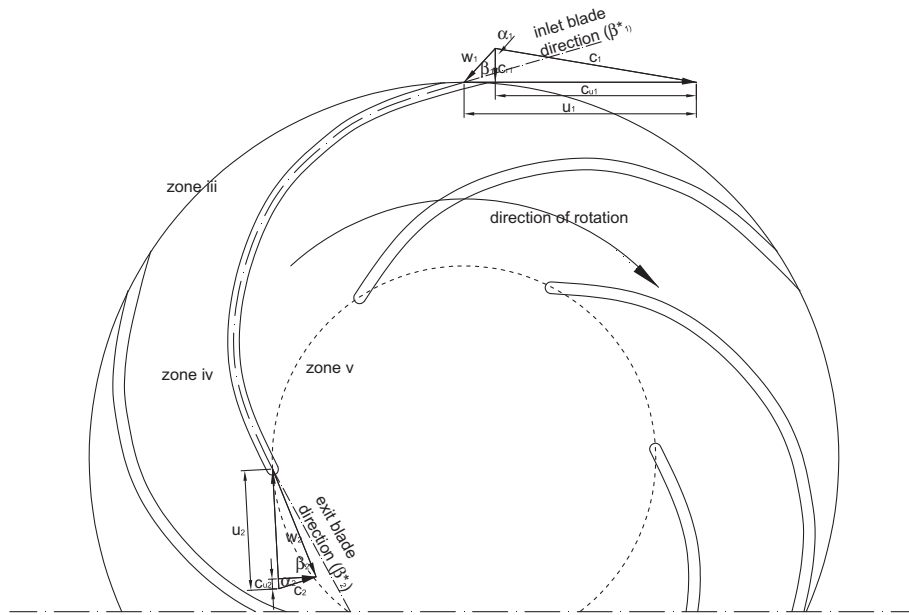


Fig. 3. Typical velocity triangles in a radial flow PAT.

even in zone v. While the zone iv (impeller control volume) would be the most significant region accounting for the transformation of loss coefficient due to changes within the wake zone at turbine inlet, the orientation of the relative flow direction (β_1 and β_2) could change hydraulics in zone iii and zone v respectively, and also transform k_{system} . It has to be pointed out that k_{system} is affecting only the net head (gH) and not the Euler momentum factor (Δc_u) as seen from Eqs. (6) and (8).

3.2.2.3. *Exit relative flow angle.* This variable can be influenced only by the flow within the blade passages. Since, the inlet tangential velocity (c_{u1}) is held constant, any change to the shaft power (from Eq. (4)) will be effected by a change to the exit relative flow angle. Moreover, this variable influences both the net head (gH) and the net tangential flow velocity (Δc_u).

Amongst the three control variables, it will be useful to neglect the radial flow velocity and to focus only on the system loss coefficient and exit relative flow angle. Both these variables (k_{system} and β_2) can be treated as mutually exclusive although there could be a small influence of exit relative flow direction on the hydraulics in zone v and hence, the system loss coefficient.

3.2.3. *Internal dependent variables*

Once, the behaviour of the internal control variables (k_{system} and β_2) due to the impeller rounding technique are characterized for a given PAT shape, the relative influences of each of these variables on both the dependent variables, net head and net tangential flow velocity, can be studied. Another dependent variable of interest is the efficiency, which will also be a function of both k_{system} and β_2 .

3.3. *Summary of the theoretical model*

The theoretical model (which is pre-requisite for understanding hydraulic optimization) consists of developing functionalities for the internal hydraulic variables based on the behaviour of external variables. The model identifies two control variables (k_{system} and β_2) and three dependent variables ($gH, \Delta c_u, \eta$) for the PAT control volume in order to understand the effects of impeller rounding.

4. Means of solution

4.1. *Experimental test-rig*

The experimental setup for characterizing both the non-modified and impeller rounding stages of the PAT consists of an open loop hydraulic circuit with major components like feed pump, surge tank, test bed, control valves and piping arrangement as shown in Fig. 4. The instrumentation used for the external variables is summarized in Table 1 along with the principle of measurement, range and accuracy. Further, the experimental uncertainty of the tested PAT stages at the BEP is discussed in Appendix A.3.

4.2. *Test pumps*

There are two categories of pumps analyzed for impeller rounding effects. The first category includes seven pumps studied by the authors in [6] from which six pumps are radial backward vane shapes covering a specific speed range of 20–80 rpm and one pump is of mixed flow design (94.4 rpm). The shapes of the impellers of these pumps are illustrated in Fig. 5. The second category includes two pumps of low specific speed (radial flow designs) investigated by Derakhshan et al. [9] of 23 rpm and Cohrs [8] of 24 rpm respectively.

4.3. *Extent of impeller rounding*

The extent of rounding of the peripheral edges of the impeller is shown in Fig. 6, which comprises of ‘bullet shaped’ rounding of the blade edges in the front view and the shrouds in the side view. The radii of rounding used is a function of the blade thickness and shroud thickness respectively and is maintained constant for all pumps tested by the authors. However, the exact degree of rounding of the two external impellers (Cohrs [8] and Derakhshan et al. [9]) is not known.

4.4. *Interpretation of data*

The interpretation of the data consists of analyzing the change in performance (both external and internal variables) at three

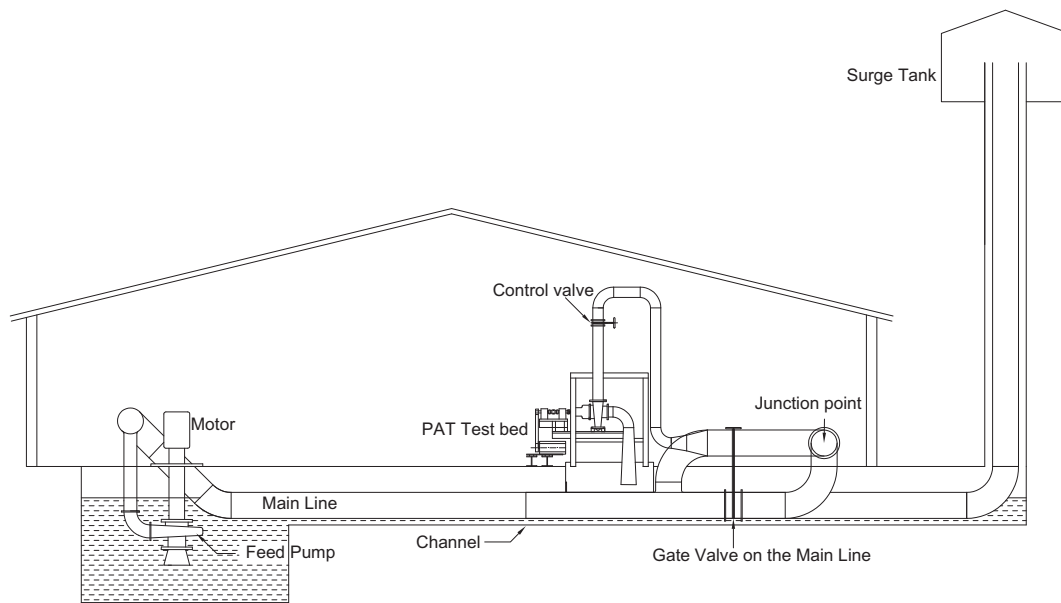


Fig. 4. Experimental test-rig for PAT optimization.

Table 1
Instrumentation used in the test-rig and measurement uncertainties at full scale.

Variable	Device	Measurement principle	Range	Accuracy
Inlet head (positive)	Pressure transducer	Inductive + wheatstone bridge	0–2 bar	±0.5% of full scale
Exit head (negative)	Pressure transducer	Inductive + wheatstone bridge	0–1 bar	±1% of full scale
Discharge	Magnetic flow meter	Faradays magnetic law	0–200 l/s	±0.1% of full scale
Torque	Torque sensor	Wheatstone bridge	±100 N m	±0.1% of full scale
Speed	Speed sensor	Optical counts		±1 rpm

operating points covering the entire range of characteristics including part-load, BEP and overload zones. The changes to the following parameters will be investigated.

(a) $\delta(\Delta c_u)$: The change of net tangential flow velocity can also be represented by the change of Euler momentum $\delta(\Delta c_u \cdot u)$, since peripheral velocity u is constant for both the stages. For the experimental stages, $\delta(\Delta c_u \cdot u)$ is obtained from Eq. (10). As seen from Eq. (6) for a given point of analysis, Δc_u is function of the relative exit flow angle only, which means that any change to $(\Delta c_u \cdot u)$ (or Δc_u) confirms that the effective direction of the exit relative flow velocity has been altered.

$$\delta(\Delta c_u \cdot u) = |P/\dot{m}|_{imp-rounding} - |P/\dot{m}|_{non-modified} \quad (10)$$

(b) $\delta(gH)$: The change in net head is directly recorded from the experimental head-flow characteristics for the two stages. It has been pointed that the net head is function of both the loss coefficient and the relative flow angle at the exit as seen in Eq. (8). Sensitivity analysis of Eq. (7) gives an indication on how the two control variables (k_{system} and β_2) are affecting the net head.



Fig. 5. Experimental impellers under investigation.

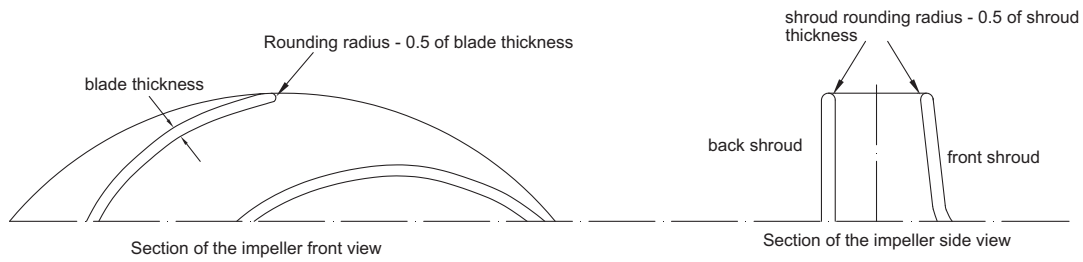


Fig. 6. Design of impeller rounding.

(c) $\delta(k_{system})$: The change in system loss coefficient can be obtained from Eq. (11), which is a modified form of Eq. (7)

$$\delta(k_{system}) = |(gH - \Delta c_u \cdot u) / g \cdot Q^2|_{imp\text{-}rounding} - |(gH - \Delta c_u \cdot u) / g \cdot Q^2|_{non\text{-}modified} \quad (11)$$

(d) $\delta(\beta_2)$: The change in relative flow angle can either be obtained from a graphical construction of velocity triangles or more accurately from the Eq. (12).

$$\delta(\beta_2) = |\tan^{-1}((\Delta c_u - c_{u1} + u_2) / c_{r2})|_{imp\text{-}rounding} - |\tan^{-1}((\Delta c_u - c_{u1} + u_2) / c_{r2})|_{non\text{-}modified} \quad (12)$$

5. Results and discussion

5.1. Overall impact of impeller rounding

The impact of impeller rounding at the three operating points for all the pump shapes show a positive change in efficiency as seen from the data provided in Appendix A.1 and efficiency rise curves in Fig. 7. The efficiency pattern in the BEP region lies between +1% and +2% for specific speeds below 45 rpm. However, for the higher specific speeds the efficiency rise seems to have reduced. In the part-load region the efficiency rise for few PATs crosses the +2% mark, while most of the other PATs are within +2%. In the overload region, the magnitude of efficiency rise is about +2% for low specific speed PATs, while there is a decrease (less than +1%) in the higher specific speed range.

5.2. Internal hydraulic analysis

5.2.1. Behaviour of internal variables in the BEP region

Fig. 8 shows the behaviour of all internal variables under the influence of impeller rounding in the BEP region. It can be seen that the drop in head (gH), an internal dependent variable is significant (0% to -3%) in the pump specific speeds till 80 rpm indicating the net head has decreased for all the impeller rounding stages. The other dependent variable, Euler momentum $\delta(\Delta c_u \cdot u)$ is marginally positive in the same range. However, for two PATs (39.7 rpm and 46.4 rpm) the Euler momentum has slightly decreased for the impeller rounding stage. The control variable, system loss coefficient (k_{system}) has demonstrated large reductions (-5% to -17%) over the entire range of specific speeds, while the other control variable relative flow angle (β_2) has marginally increased for all PATs except for 39.7 rpm and 46.4 rpm PATs. The resulting efficiency rise is positive for all the specific speeds and the magnitude lies between +1% and +2%.

5.2.2. Behaviour of internal variables in the part-load region

Within the part-load region, it can be seen from charts in Fig. 9 that the dependent variable quantity $\delta(gH)$ is negative with a magnitude maintained nearly constant at -2% for all the pump shapes.

The other dependent variable $\delta(\Delta c_u \cdot u)$ shows a significant improvement in the lower specific speed and again in higher specific speed PATs. But, within the medium specific speed range the increase of $\delta(\Delta c_u \cdot u)$ is not very significant. The peaks of $\delta(\Delta c_u \cdot u)$ are related to three pump specific speeds (24 rpm, 36.4 rpm and 94.1 rpm). This efficiency pattern is a resultant of the behaviour of these two variables, gH and $\Delta c_u \cdot u$. As far as the control variables are concerned, it can be seen that k_{system} has decreased by a significant margin (-5% to -20%), while β_2 has shown marginal increase for the low and high specific speed pumps.

5.2.3. Behaviour of internal variables in the overload region

The overload region similar to the part-load and BEP region shows significant reductions of head over the entire specific speed range barring the 79 rpm PAT as seen in Fig. 10. The dependent parameter $\delta(\Delta c_u \cdot u)$ on the other hand does not follow a pattern with reductions (negative value) reported in the two

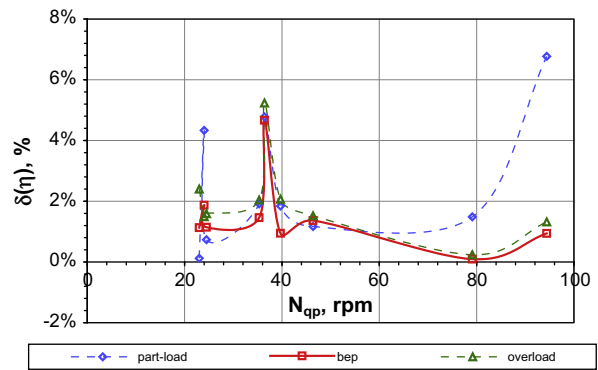


Fig. 7. Efficiency rise for all the operating points.

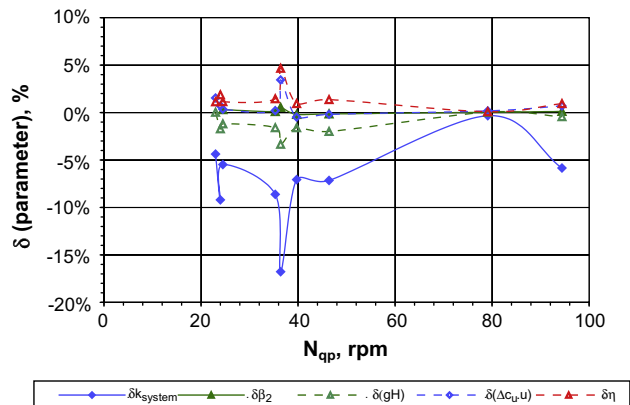


Fig. 8. Behaviour of internal variables in the BEP region.

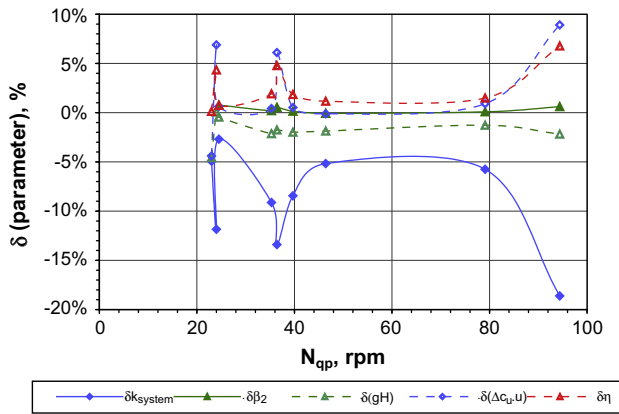


Fig. 9. Behaviour of internal variables in the part-load region.

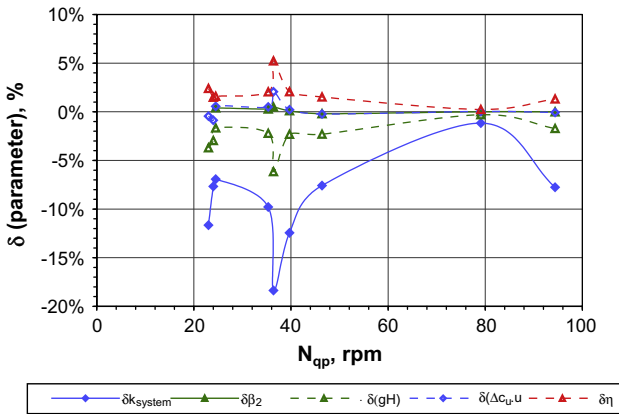


Fig. 10. Behaviour of internal variables in the overload region.

external PATs (23 rpm and 24 rpm). However, for the same specific speeds in the BEP region, the change in Euler momentum is positive (Fig. 8). This behaviour is not normal and needs to be investigated. There is marginal drop of Euler momentum in the overload region for the 46.4 rpm PAT, which is also seen in the part-load and BEP regions. The control variable k_{system} has effectively decreased (–5% to –20%) for the impeller rounding stage, while the other control variable β_2 is following the identical trend of the Euler momentum variable.

5.3. Discussion of control variables

It is important to understand two aspects regarding the control variables, k_{system} and β_2 . The first aspect is to see how the two control variables are controlling the other dependent variables, discussed in Section 5.3.1 and the second aspect is to find out reasons for the respective changes to these control variables, covered in Section 5.3.2.

5.3.1. Sensitivity analysis of the control variables

This section presents an understanding on how the changes to the control variables k_{system} and β_2 are relatively affecting the behaviour of net head, Euler momentum and hence efficiency. From the sensitivity analysis section of BEP region (Appendix A.1.2) and Fig. 11, it can be seen that the decrease of k_{system} is causing a decrease to the net head significantly while small increase to β_2 is resulting in an increase of the net head for all the tested PATs. It has to be noted that even a small increase to β_2 is sufficient to increase gH considerably. Only for one PAT with specific speed of 39.7 rpm, there is a decrease in β_2 that causes net head to decrease further. Since, the other dependent variable $\Delta c_u \cdot u$ depends only on β_2 , all changes to it come from β_2 and not from k_{system} . Hence, sensitivity analysis is not carried out for this parameter. The efficiency is function of net head and Euler momentum, and hence it also affected by k_{system} and β_2 (Section 3.2.3). In broad terms, the decrease of k_{system} and the increase of β_2 is causing an increase in η . It can also be seen from Fig. 11 and Appendix A.1.2 that the influence of k_{system} on efficiency is more than that of β_2 .

The relative influences of k_{system} and β_2 on net head and efficiency for the part-load and overload regions are shown in Figs. 12 and 13 (with the help of data points listed in Appendices A.1.1 and A.1.3) respectively. These results show the stronger influence of k_{system} in decreasing gH and increasing efficiency compared to β_2 .

5.3.2. Changes to the control variables

The next important issue to be discussed is about the reasons for changes to k_{system} and β_2 . To understand changes to k_{system} , the front view and side view of the two impellers is shown in Fig. 14.1, which analyzes the hydraulic situation at the inlet and the exit for both the non-modified and impeller rounding stages based on the actual results for the 35.3 rpm PAT. It can be seen that the rounding of the blades results in a much smaller wake and a reduction of losses in zone iv. Further, it can also be seen from Fig. 14.2 that the rounding of shrouds further reduces wake region and the corresponding (flow separation) losses as well. The influence of rounding of the outside shroud would decrease the exter-

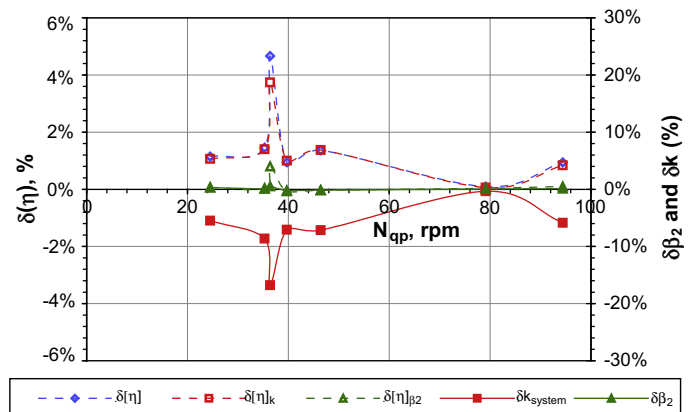
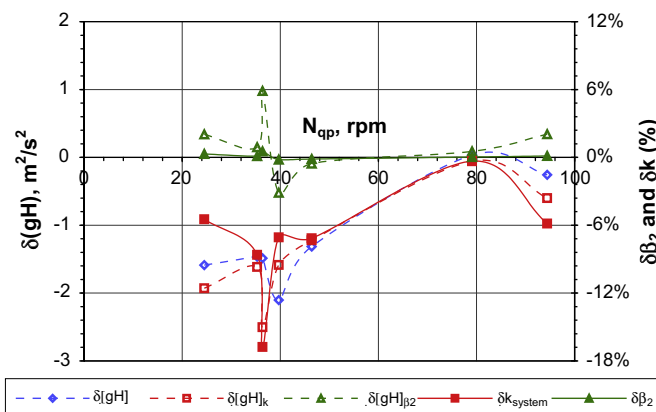


Fig. 11. Sensitivity analysis for gH and η at BEP.

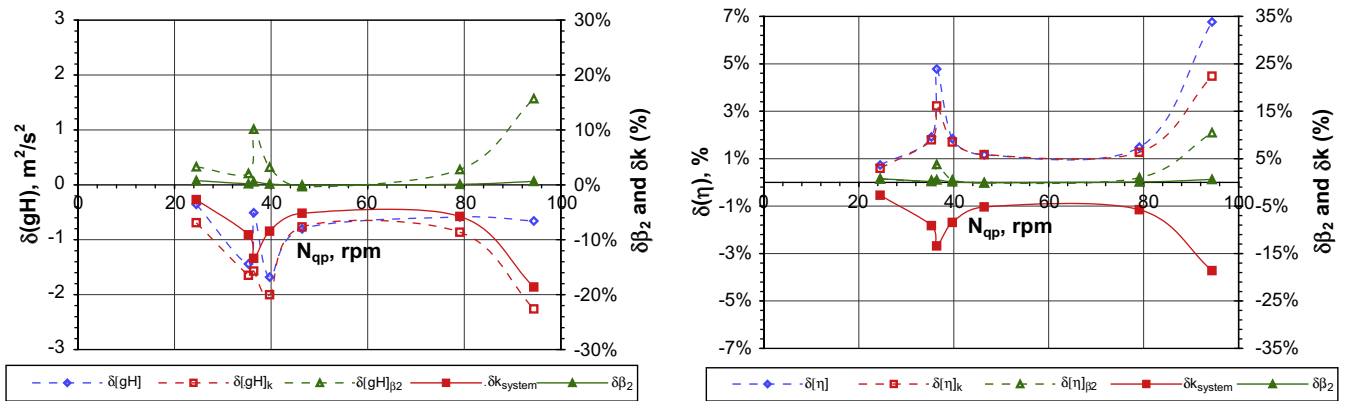


Fig. 12. Sensitivity analysis for gH and η in the part-load region.

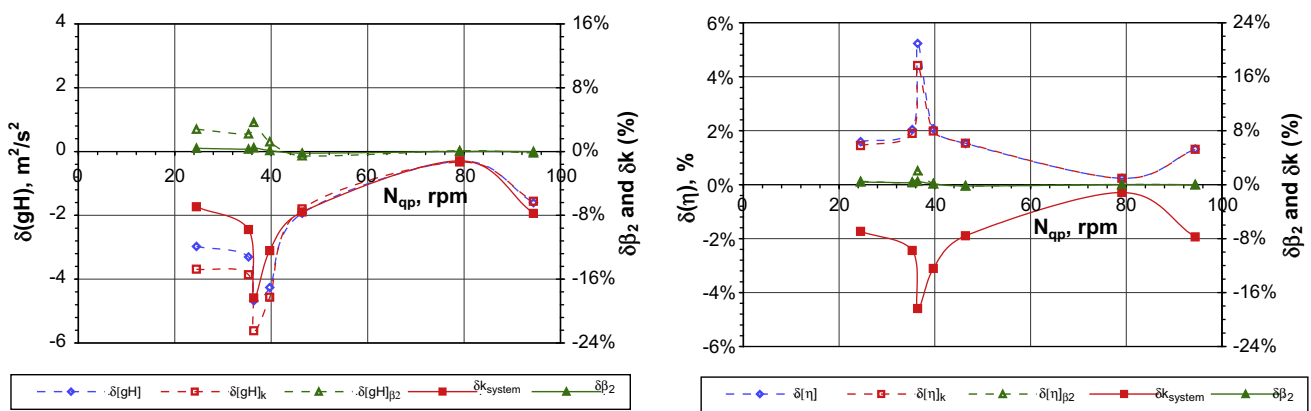


Fig. 13. Sensitivity analysis for gH and η in the overload region.

nal losses, which can be bracketed as the disc friction losses and reflects in the shaft power. The small change to the inlet flow direction (due to the theory in Section 3.2.2.1) could influence the losses in the transition zone iii. All these changes to losses would result in substantial changes to k_{system} at a given flow rate. In total, it can be concluded the decrease of k_{system} is mainly due to decrease in losses in zone iv with small influences from zone iii and zone v.

From Fig. 14.2, it can be seen that change in the direction of exit relative flow angle (β_2) can be related to the new situation of hydraulics within the blade passages (under impeller rounding modification) resulting from circulation effects. This increased circulation is facilitating the increase of β_2 , which is causing the de-

crease in exit swirl velocity (c_{i2}) in all the PATs showing increased power generation. It has to be pointed out that the changes at the exit condition due to impeller rounding at the turbine inlet is a significant hydraulic phenomenon. However, the change in the exit relative flow direction can also influence the losses in transition zone v, but this influence would be marginal.

5.4. Abnormal behaviour of 23 rpm and 24 rpm PAT curves

Closer inspection of the test results of the 23 rpm PAT [9] (from Figs. 8–10 and Appendix A.1) show that within the part-load region there is decrease in Euler momentum, but as the BEP condition is

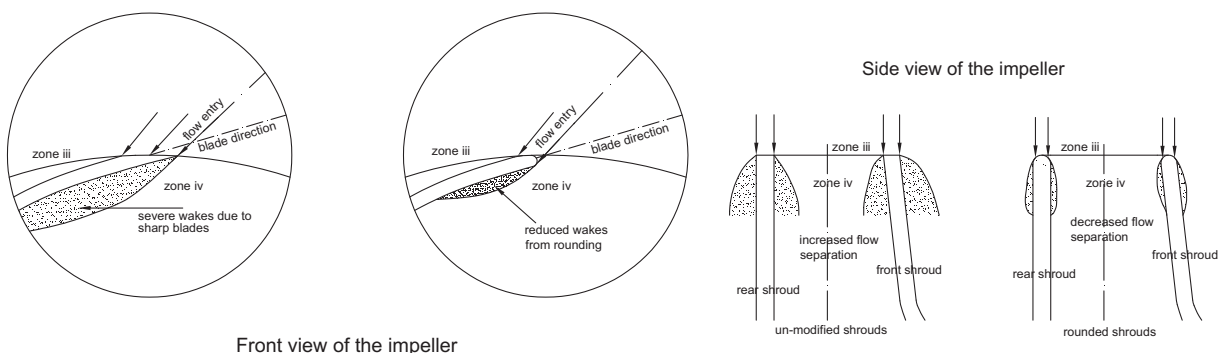


Fig. 14.1. Physical understanding of impeller rounding effects at the inlet.

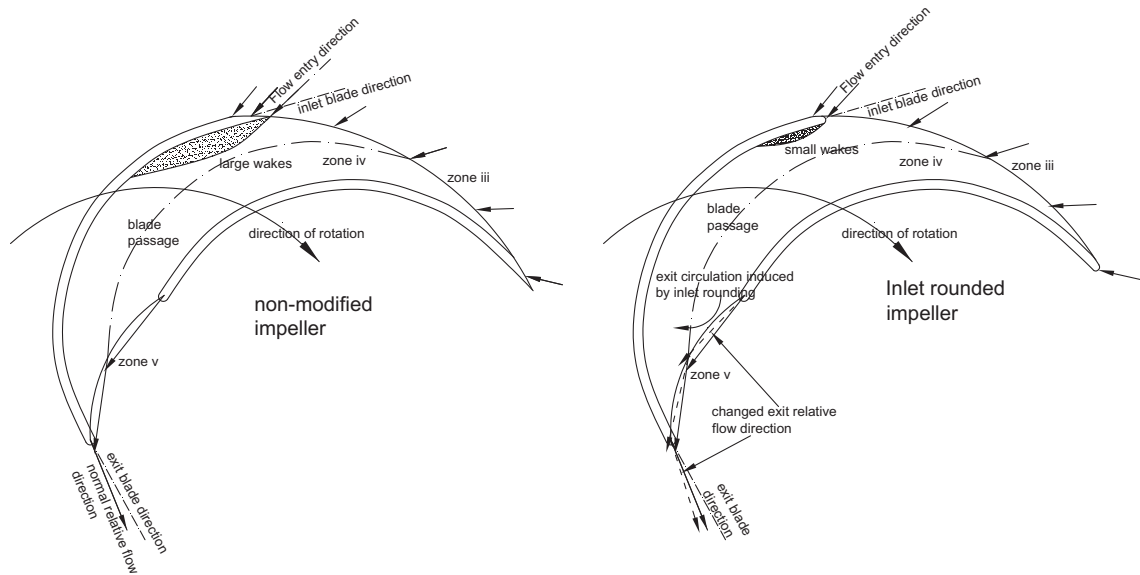


Fig. 14.2. Physical understanding of impeller rounding effects at the exit.

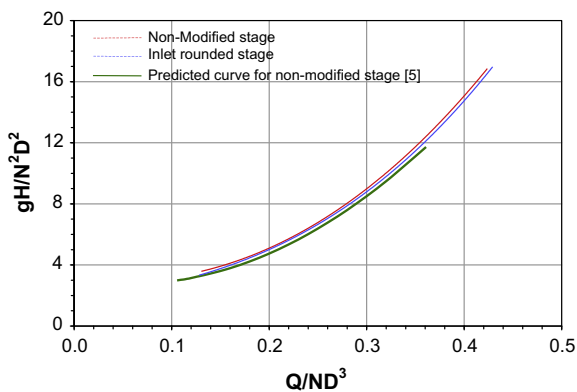


Fig. 15. Physical understanding of the importance of impeller rounding and accurate prediction.

reached the net momentum increases considerably and becomes positive. Further, quite strangely this parameter again becomes negative in the overload region. This behaviour of the Euler momentum for the impeller rounding stage is certainly abnormal given the seesaw changes. The behaviour of net head parameter on the other hand shows decrease in the part-load region, no change in the BEP region and a very significant drop in the overload region. This complex trend of net head and Euler momentum curves has not been seen in any of the other PATs tested by the authors. This phenomenon cannot be interpreted from a hydraulic perspective and in all probability could be associated with measurement uncertainties.

The 24 rpm PAT [8], another external PAT, has also shown discrepancy in the behaviour of the Euler momentum variable in the BEP and overload region, but the trend of the net head variable is largely similar to that of the tested PATs by the authors.

5.5. Larger picture of impeller rounding

To understand the larger picture of impeller rounding effects, Fig. 15 is plotted that includes the PAT characteristics under non-modified and impeller rounded condition along with the predicted

curves (based on model in [5]). It can be seen that non-modified and impeller rounded characteristics are very close to each other and the predicted curve is offset by a margin of over 3–4%. The predicted curve could have been more displaced from the actual curves for some pump shapes (as discussed by Singh and Nestmann in [5]) depending on the prediction model selected. This discussion point leads to the interpretation that while inlet impeller rounding for PAT operation is important from the perspectives of hydraulic optimization, it is still significant to build accurate prediction models for different pump shapes. It makes more sense to have an accurate non-modified curve rather than a predicted impeller rounded curve that is deviating from the real characteristics.

5.6. Limitations of the theoretical model

It would be important to discuss the limitation of the analytical model developed for this study, because many important conclusions have been made based on it. Firstly, the free vortex condition assumed in the spiral volute (zone i in Figs. 1 and 2) may not be seen in reality. This could lead to an error in the direction of inlet swirl and also the distribution of radial flow velocity could vary along the inlet impeller width. The inlet swirl angle would then become another control variable. Further, the assumption that all changes to net Euler momentum are taking place at the exit only could also be incorrect. This would then change the behaviour of the control variables like exit relative flow angle and result in new functionalities. However, since the impeller rounding study is carried out mostly on radial turbomachines, the constancy of angular momentum at the inlet is a reasonable assumption to be made compared to that for axial flow turbomachines.

5.7. Limitations of the test-rig

5.7.1. Planning the experiment

As seen in Section 4.1, the instrumentation on the test-rig is planned on the complete 'PAT control volume', which includes the entire spiral volute and a section of the draft tube entrance. It would make it a wiser analysis if the instrumentation were to be planned only across the impeller control volume (zone iv) with sensors mounted at the impeller inlet (zone iii) and impeller exit

Table 2
Comparison of efficiency improvements and maximum uncertainty.

Sr. No.	PAT (rpm)	$\delta(\eta)$ (nm ir) (%)	$\Delta(\eta)$ (%)
1	24.5	+1.1	± 0.6
2	35.3	+1.5	± 1.0
3	36.4	+4.7	± 2.4
4	39.7	+0.9	± 0.6
5	46.4	+1.4	± 1.1
6	79.1	+0.1	± 0.8
7	94.4	+0.9	± 1.2

(zone v) respectively. The data to be measured should include the flow direction as well as the magnitude of velocity across the respective flow areas. This setup would help in estimating the accurate value of both the inlet vortex and exit swirl angle distribution. The exit swirl angle would further help in accurately quantifying the relative flow angle at exit and validate the experimental findings about its influence on the performance.

5.7.2. Measurement accuracy

In order to compare the improvements obtained from impeller rounding with the overall uncertainty of the measurements made in the test-rig, Table 2 that summarizes the BEP information of the PATs tested by the authors is presented. The maximum uncertainty of the efficiency parameter is obtained from the analysis carried out in Appendix A.3. It can be seen that the efficiency improvement due to impeller rounding is larger than the maximum uncertainty for most of the PATs. However, the uncertainty is in fact more than the improvement in efficiency for the 79.1 rpm and 94.4 rpm PATs. It can also be seen from Table A4 that the variable net head contributes to the maximum uncertainty of the efficiency parameter compared to other variables. It is, hence, recommended to increase the sophistication and accuracy of measuring the head variable especially in the low ranges (less than 10 m).

6. Conclusions and recommendations

The theoretical model developed specifically for the PAT optimization study under the background of some assumptions was very useful in isolating the important internal hydraulic variables. Under constant speed and free vortex condition, the model indicated that the impeller loss coefficient and exit relative flow angle as the primary control variables. The model also gave a common basis to study the performance changes due to any geometric modification on a PAT of any shape.

The effects of impeller rounding were experimentally determined on radial flow and mixed flow PATs. The application of the model on the experimental results indicated that the system loss coefficient that happens to be the chief control variable has consistently decreased for all the impeller rounded PATs in all the three operating regions (part-load, BEP and overload) and this effect was primarily attributed to the improved hydraulics within zone iv (of the impeller control volume) coming from reduced wakes at the turbine inlet. This decrease contributed to drop of the net head for the impeller rounding stage, but did not affect the net Euler momentum or shaft power. On the other hand, the exit relative flow angle (the second control variable) increased marginally for most of the PATs, which could be directly linked to the changed hydraulics (circulation effects) within the flow passages in the impeller rounding stage. The increase of exit relative flow angle caused an increase to the net Euler momentum and also increase to the net head across the PAT. On the whole, the behaviour of the two control variables due to impeller rounding modification improved the efficiency for all PATs (within +2% band) in the

part-load, BEP and overload regions. Amongst the two, the system loss coefficient was found to have a dominating influence compared to that of the exit relative flow angle.

In a sharp contrast to the above behaviour, the results of the two external PATs showed an abnormal behaviour of the Euler momentum variable in different operating regions. This effect cannot be explained through the theoretical model and could be attributed to measurement uncertainties.

The impeller rounding optimization on the PATs is no doubt a beneficial and important step recommended for all PAT applications, but it should also be seen from the perspectives of other important topics of PAT research like performance prediction, which also needs continuous optimization. The true benefits of impeller rounding will be realized only with an accurate performance prediction model.

The results of the impeller rounding study further helped in evaluating the limitations of the model, which were directly linked to the planning of the test-rig. This leads to the recommendation of more sophisticated level of experimentation in determining the inlet and exit flow characteristics. Further, improvements in the accuracies of the instruments, especially for the determination of net head parameter are desirable. Finally, it would be beneficial to standardize (or create a benchmark) the internal hydraulic effects due to impeller rounding with respect to pump shapes using more experimental data as well as computational models with a focus on mixed flow and axial flow pumps as turbines that could not be covered in the present study.

The objective of the present study pertained only to the turbine operation of pumps, but there are some applications that involve dual operation of same pump, like in pump storage plants. It is highly recommended to extend the study of impeller rounding on the pump performance following the same model approach introduced in this paper.

Acknowledgements

The authors are deeply grateful to the workshop and technical staff at the Institute of Water and River Basin Management (IWG) for the erection of the test-rig and patient modification on the different pump impellers.

Appendix A. Appendix

A.1. Consolidated experimental data of impeller rounding

The consolidated data is presented separately for the part-load, BEP and overload points. For each PAT, the changes (both absolute and percentage scales) to the variables (gH , P , η , $\Delta c_{ii} \cdot u$, β_2 and k_{system}) from non-modified impeller stage to impeller rounding stage are illustrated using the methodology discussed in Section 4.4. The results of sensitivity analysis for the dependent variables gH and efficiency with respect to control variables (k_{system} and β_2) are also presented.

A.1.1. Part-load comparisons

See Table A1.

A.1.2. BEP comparisons

See Table A2.

A.1.3. Overload comparisons

See Table A3.

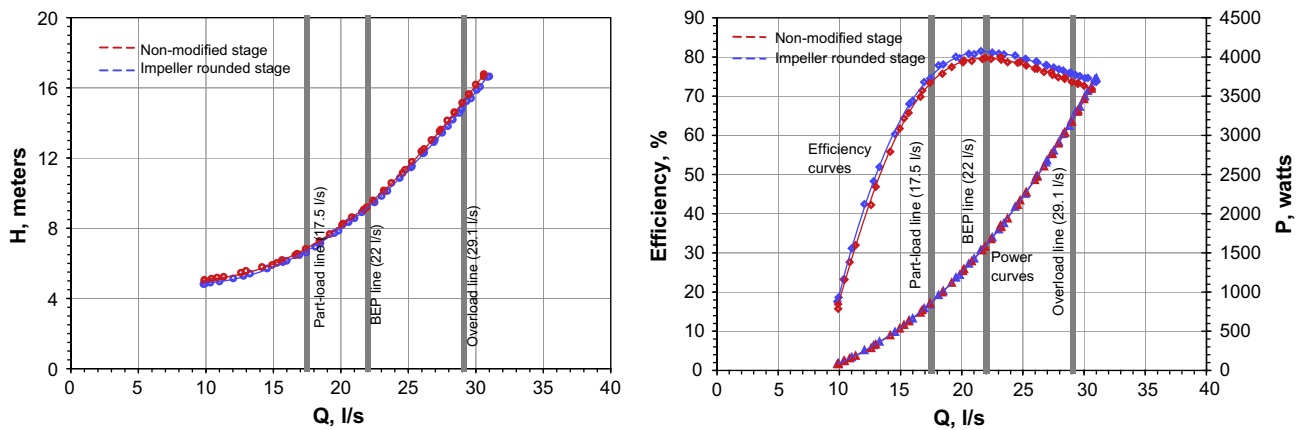


Fig. A1. Impeller rounding optimization for 35.3 rpm PAT at 1000 rpm.

Table A4

Experimental uncertainty at the BEP for all the tested PATs.

PAT (rpm) (nm ir)	Independent or control parameters						Dependent parameters (change from non-modified to inlet rounded)							
	Speed			Discharge			Head			Torque			Efficiency	
	N (rpm)	ΔN (rpm)	$\Delta N/N$ (%)	Q (l/s)	ΔQ (l/s)	$\Delta Q/Q$ (%)	H (m)	ΔH (m)	$\Delta H/H$ (%)	T (N m)	ΔT (N m)	$\Delta T/T$ (%)	η (%)	$\Delta \eta/\eta$ (%)
24.5	800	± 1	± 0.1	26.8	± 0.2	0.7	13.6	± 0.1	± 0.7	31.5	± 0.1	± 0.3	73.7	± 0.8
							13.5	± 0.1	± 0.7	31.6	± 0.1	± 0.3	74.8	± 0.8
35.3	1000	± 1	± 0.1	22.0	± 0.2	0.9	9.3	± 0.1	± 1.1	15.3	± 0.1	± 0.7	79.5	± 1.2
							9.2	± 0.1	± 1.1	15.3	± 0.1	± 0.7	81.0	± 1.3
36.4	1000	± 1	± 0.1	8.3	± 0.2	2.4	4.5	± 0.1	± 2.2	2.3	± 0.1	± 4.3	66.4	± 3.6
							4.4	± 0.1	± 2.3	2.4	± 0.1	± 4.1	71.1	± 3.8
39.7	1000	± 1	± 0.1	61.3	± 0.2	0.3	13.4	± 0.1	± 0.7	64.1	± 0.1	± 0.2	83.0	± 0.7
							13.2	± 0.1	± 0.8	63.8	± 0.1	± 0.2	83.9	± 0.7
46.4	1000	± 1	± 0.1	24.1	± 0.2	0.8	6.7	± 0.1	± 1.5	11.2	± 0.1	± 0.9	74.0	± 1.4
							6.6	± 0.1	± 1.5	11.2	± 0.1	± 0.9	75.4	± 1.5
79.1	1000	± 1	± 0.1	89.9	± 0.2	0.2	6.9	± 0.1	± 1.4	44.1	± 0.1	± 0.2	75.5	± 1.1
							6.9	± 0.1	± 1.4	44.2	± 0.1	± 0.2	75.6	± 1.1
94.4	1000	± 1	± 0.1	87.6	± 0.2	0.2	6.0	± 0.1	± 1.7	40.9	± 0.1	± 0.2	82.7	± 1.4
							6.0	± 0.1	± 1.7	41.2	± 0.1	± 0.2	83.6	± 1.4

A.2. Typical plot of impeller rounding optimization

A typical plot showing the effects of impeller rounding optimization covering the complete operating characteristics is presented in Fig. A1 for a 35.3 rpm PAT at constant operating speed of 1000 rpm. The data for the part-load, BEP and overload points correspond to that presented in Appendix A.1. The efficiency curve for the impeller rounded PAT is much improved compared to the non-modified impeller over the complete range. The head curves for impeller rounded condition are seen to be significantly lower compared to that of the non-modified PAT, while the power curves for the two stages are nearly coinciding.

A.3. Experimental uncertainty

The overall uncertainty analysis is carried out using the single sample study proposed by Moffat [11] and Kline [12] at the BEP points of the different PAT stages and is summarized in Table A4.

References

[1] D. Thoma, Vorgaenge beim Ausfallen des Antriebes von Kreiselpumpen, vol. 4, Mitt. Hyd. Inst. Tech. Hochschule, Muenchen, Germany, 1931. pp. 102–104.

[2] A.A. Williams, Pumps as Turbines used with Induction Generators for Stand-alone Micro-hydroelectric Power Plants, PhD Thesis, Nottingham Trent University, 1992, pp. 51–80, 88–91, 149–153.

[3] M. Amelio, S. Barbarelli, A one-dimensional numerical model for calculating the efficiency of pumps as turbines for implementation in micro hydro power plants, In: ASME 7th Biennial Conference on Engineering System Design and Analysis, 2004, pp. 65–77.

[4] S. Derakhshan, A. Nourbakhsh, Experimental study of characteristic curves of centrifugal pumps working as turbines in different specific speeds, Elsevier J. Exp. Therm. Fluid Sci. 32 (2008) 800–807.

[5] P. Singh, F. Nestmann, An optimization routine on a prediction and selection model for the turbine operation of centrifugal pumps, J. Exp. Therm. Fluid Sci. 34 (2010) 152–164.

[6] P. Singh, Optimization of the Internal Hydraulic and of System Design in Pumps as Turbines with Field Implementation and Evaluation, PhD Thesis, University of Karlsruhe, Germany, 2005.

[7] R. Lueneburg, R.M. Nelson, Hydraulic power recovery turbines, in: V.S. Lobanoff et al. (Eds.), Centrifugal Pumps – Design and Application, second ed., Gulf Publishing Company, 1992, pp. 246–282 (Chapter 14).

[8] D. Cohrs, Untersuchungen an einer mehrstufigen rückwärtslaufenden Kreiselpumpe im Turbinenbetrieb, Verlag und Bildarchiv, Faragallah, W.H., 1997, pp. 8–41.

[9] S. Derakhshan, B. Mohammadi, A. Nourbakhsh, Efficiency improvement of centrifugal reverse pumps, J. Fluids Eng. 131 (2009).

[10] P. Singh, F. Nestmann, Experimental optimization of a free vortex propeller runner for micro hydro application, J. Exp. Therm. Fluid Sci. 33 (2009) 991–1002.

[11] R.J. Moffat, Contributions to the theory of single-sample uncertainty analysis, J. Fluids Eng. (1982) 250–260.

[12] S.J. Kline, The purposes of uncertainty analysis, J. Fluids Eng. (1985) 53–160.



Contents lists available at ScienceDirect

Experimental Thermal and Fluid Science

journal homepage: www.elsevier.com/locate/etfs

Experimental optimization of a free vortex propeller runner for micro hydro application

Punit Singh *, Franz Nestmann

Institute for Water and River Basin Management (IWG), University of Karlsruhe, Kaiser Str. 12, D 76128 Karlsruhe, Germany

ARTICLE INFO

Article history:

Received 22 February 2009

Received in revised form 29 April 2009

Accepted 30 April 2009

Keywords:

Micro hydro

Free vortex

Propeller runner

Geometric optimization

Exit tip angle

Inlet tip angle

ABSTRACT

The turbine technology for low head application in the micro hydro range has been vastly neglected despite niche available in scattered regions of valley flows as well as in wastewater canals and other energy recovery schemes, where the available head does not exceed 2 meters. The goal of this study is to develop hydraulically optimized propeller turbines for the micro hydro range with a particular focus on ease of manufacture.

This paper presents a wide range of geometrical optimization steps carried out on a propeller runner, whose blades have been designed using the free vortex theory, and operating with a gross head from 1.5 to 2 m and discharge of approximately 75 l/s. It further illustrates 3 stages of geometrical modifications carried out on the runner with an objective of optimizing the runner performance. These modifications comprised of changes to the tip angles (both at the runner inlet and exit) as well as the hub angles (at the runner inlet) of the runner blades.

The paper also presents an interesting theoretical methodology to analyze the effects of each optimization stage. This method looks at the relative changes to shaft power and discharge at constant head and speed and gives wonderful insight as to how the internal parameters like Euler shaft work and runner hydraulic losses are behaving with respect to each optimization stage.

It was found that the performance of the runner was very sensitive to changes to exit tip angle. At two levels of modification, the discharge increased in the range of 15–30%, while shaft power increased in the range of 12–45%, thus influencing the efficiency characteristics.

The results of the runner inlet tip modification were very interesting in that a very significant rise of turbine efficiency was recorded from 55% to 74% at the best efficiency point, which was caused by a reduced discharge consumption as well as a higher power generation.

It was also found that the optimization study on a propeller runner has reasonably validated the estimates of the free vortex theory despite small deviations. The final runner configuration demonstrated a maximum efficiency of 74% ($\pm 1.8\%$), which is very encouraging from the perspectives of micro hydro application.

The paper concludes with recommendations of a series of optimization steps to increase the efficiency of the runner. It also recommends the attempt of Computational Fluid Dynamics both as a validation and optimization tool for future research on propeller runners.

© 2009 Elsevier Inc. All rights reserved.

1. Introduction

1.1. Background

Axial flow hydro turbines for low head application have come a long way since Viktor Kaplan (as mentioned by Dixon [1]) obtained a patent for it in 1912. Subsequently, the optimization of these turbines both from the perspectives of performance and cavitation

was then taken over by host of other engineers, which has enabled the modern axial flow hydro turbines to reach operating efficiencies of over 92–94%. However, their capacities range from few tens to few hundreds of MWs.

In the recent years, axial flow turbines for small hydro in the range of 500 KWs to few MWs has also attracted the interests of industry and developers. However, for micro hydro in the range of 150 W to few tens of KWs, the mainstream industry has been insensitive, thus making it an open and exciting area of study. The design and development of micro axial or propeller turbines cannot be based on the methodology of exactly scaling down large axial turbines due to both the economic and manufacturing constraints, which gives a scope for a creative design work under

Abbreviation: BEP, best efficiency point; PMG, permanent magnet generator.

* Corresponding author. Tel.: +49 721 608 2194; fax: +49 721 606 046.

E-mail addresses: punit.singh@iwg.uka.de (P. Singh), nestmann@iwg.uka.de (F. Nestmann).

Nomenclature*Full Scripts*

<i>c</i>	absolute velocity, m/s
<i>d</i>	hub diameter, m
<i>D</i>	tip diameter, m
<i>g</i>	acceleration due to gravity, m/s ²
<i>h</i>	specific energy, kJ/kg
<i>H</i>	head parameter, m
<i>k</i>	loss coefficient, 1/m ⁴
<i>m</i>	mass flow rate, kg/s
<i>N</i>	speed, rpm
<i>P</i>	power, kW
<i>Q</i>	discharge, l/s or m ³ /s
<i>r</i>	radius vector, m
<i>T</i>	torque, Nm
<i>u</i>	tangential blade velocity, m/s
<i>V</i>	voltage, volts
<i>w</i>	relative velocity, m/s

Greek symbols

η	efficiency, %
--------	---------------

ρ	density, kg/m ³
α	absolute flow angle, degrees
β	relative flow or blade angle, degrees

Subscripts

0	stagnation condition
1	guide vane exit
2	runner inlet
3	runner exit
<i>dt</i>	draft tube
<i>gv</i>	guide vane
<i>h</i>	hub region
<i>L</i>	losses
<i>r</i>	radial direction
<i>sv</i>	spiral volute
<i>t</i>	tip region
<i>u</i>	tangential component
<i>x</i>	axial direction

challenging boundary conditions. Research work in micro propellers has been scanty and carried out by few concerned individuals and mainly focused for application in developing countries.

APRL [12], a group in Vietnam has marketed propeller turbines between 200 W and 1000 W, but these have low operating efficiencies between 35% and 50%. The other contributors include Rao et al. [7] who developed a 5 KW propeller with a maximum efficiency 67% and Soundranayagam [8] who designed a 40 KW propeller runner for a canal drop application. More recently Demetriades [6] developed a simpler propeller design for applications below 1 KW and later on his work was carried forward by Upadhyay [9], who used numerical techniques to validate the experimental findings of Demetriades and then proposed design optimization on the guide vanes and the runner. Further to this Simpson and Williams [10] used computational tools to design and implement a 5 KW propeller turbine project with a head range of 3–4 m in Peru and reported a field efficiency of 65%. Very recently Alexander et al. [11] from New Zealand has attempted to standardize 4 propeller runner models working in the head range of 3–9 m and generating power in the range of 1.5–3 KW on an experimental test rig and has recorded peak efficiencies in the range of 68–74%.

As seen most the work in micro propeller turbines has been isolated, which underlines a greater need for a concrete and holistic effort to optimize them using both experimental and computational tools. Hence, the greater objective of the paper is to initiate and inspire the development of hydraulically optimized propeller runners for micro hydro application that can be easily manufactured and installed in regions where the head drop is not more than 2 m and population living in the vicinity is either deprived or having unreliable grid power. Energy recovery could be another area of application for propeller units across wastewater canals and drinking water projects.

1.2. Technical objectives

1. To develop an optimum runner with peak efficiencies between 75% and 80%, operating with a gross head of 1.5–2 m and flow rate of 60–75 l/s using the well-known free vortex theory.
2. To check the validity of the free-vortex theory on different sections of the blade using experimental techniques.
3. To experimentally study the internal hydraulic effects due to geometrical changes at the inlet and exit blade profile of the

runner, enabling the optimization the overall performance of the runner.

4. To recommend that particular runner design for future application, which gives the highest efficiency and which is also easy and economical to manufacture.

*1.3. Problem statement**1.3.1. Problem 1: development of the runner*

The above problem comprises of a full-fledged design procedure to determine the shape of the runner blade profile starting from the available boundary condition of head and flow (1.75 m and 75 l/s), which clearly point towards an axial flow turbine design. Since the most popular design procedure for axial flow turbo-machines (whether a compressor or a turbine) is undoubtedly the free vortex design, it should be considered for the runner development. In order to determine the blade shape it is important to fix the operating speed and the tip diameter of the runner, in addition to the head and flow data. The blade shape comprises of determining the chord length, inlet and exit blade angles at all the radial sections beginning from the hub to the tip. The number of blades is another parameter that will need to be fixed.

1.3.2. Problem 2: validation of the free vortex theory

For validating the free vortex theory a basic runner design can be manufactured which is deviating from the specifications of the free vortex design. The runner design can then be altered in calculated steps (i.e. change the inlet and exit blades at the tip and the hub) towards the free vortex design specifications. The runner is characterized on a experimental test-rig at every step of geometric modification and the change in performance is recorded, which is subsequently analyzed to check if the actual runner performance is matching with that of the free vortex theory. The above problem further comprises of investigating the limitations in the free vortex design.

1.3.3. Problem 3: optimization of the internal hydraulics of the runner

This problem is a further refinement of Problem 2, where the performance of the runner needs to be thoroughly studied under these calculated geometric modifications (also referred to as optimization stage). The objective of this study is to understand the internal hydraulics with respect to three parameters namely, the

Euler shaft work, the flow rate and the hydraulic losses within the runner at given gross head and operating speed. A theoretical analysis model based on fundamental Euler turbine theory will be required for this. This study should be aimed on understanding how geometry of the blade affects the individual performance parameters and it should lead to the most optimum runner for the given design condition.

2. Theory

2.1. Free vortex theory

Dixon [1], Saravanamuttoo et al. [2] and Hothersall [3] have provided a consolidated overview of the free vortex theory used in axial flow turbomachinery. Dixon [1] has discussed the practical application and merits of this theory in the design of axial flow compressors, gas turbines, steam turbines and traditional hydraulic turbines (Kaplan turbines). Since, the propeller turbine also classifies in the category of incompressible axial flow turbines, it makes more sense to use this popular theory. Even Alexander [11] has used the free vortex theory for the design his propeller runners.

The origins of free vortex law come essentially from the law of conservation of angular momentum. The primary conditions like irrotational flow and constant axial velocity need to be satisfied for this law. Eq. (1) represents the final form of the free vortex law.

$$c_u \cdot r = \text{constant} \tag{1}$$

The free vortex law calls for maintaining the product of tangential flow velocity and the radius vector constant all along the inlet region and the exit region of the blade as given by Eq. (2).

$$[c_u \cdot r]_{\text{inlet}} = K_{\text{inlet}} \quad \text{and} \quad [c_u \cdot r]_{\text{exit}} = K_{\text{exit}} \tag{2}$$

The constants of Eq. (2) are not same in magnitude. In general for an axial flow turbine the constant (K_{inlet}) at the inlet depends on the hydraulic (Euler) head to be realized on the shaft. In order to maximize the energy transfer, the exit tangential velocity is taken as zero (i.e. $c_{u,\text{exit}} = 0$) all along the exit blade profile and hence $K_{\text{exit}} = 0$. Further, the radius vector of the axial flow turbine increases continuously from the hub to the tip, which causes the c_u component to decrease (Figs. 1.1 and 1.2). This causes fluid to enter each radial section with a different swirl angle, α . Moreover, since every radial section has a different the tangential blade velocity (u), the blade angle (or relative flow angle, β) should also change from the hub to tip (refer to velocity triangles in Figs. 1.1 and 1.2 and Table 1). The same holds true for the exit blade section despite $c_{u,\text{exit}} = 0$.

2.2. Runner design based on free vortex

The primary governing design or efficiency equation for a turbine given by Eq. (3).

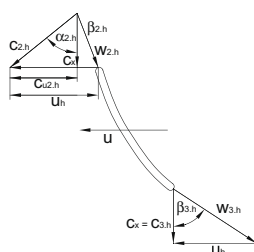


Fig. 1.1. Inlet and exit velocity triangles at the runner hub.

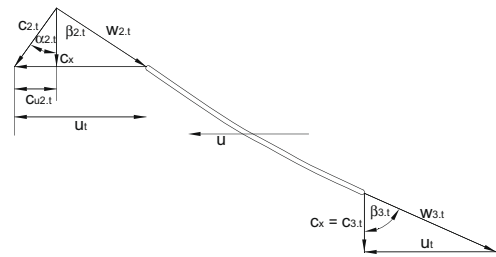


Fig. 1.2. Inlet and exit velocity triangles at the runner tip.

$$\eta_{\text{hyd}} = \frac{\text{Euler head (hyd shaft head)}}{\text{Gross head}} = \frac{\Delta c_u \cdot u}{g \cdot H_{\text{gross}}} \tag{3}$$

The runner design is developed for a gross head of 1.75 m and a flow of 75 l/s. A moderate working hydraulic efficiency of 75% is assumed and from Eq. (3) the Euler shaft head of 1.3 m is obtained, which is used to determine the blade shape beginning from the hub to the tip. Further, the runner tip diameter is taken as 200 mm and operating speed of 1000 rpm is fixed. Table 1 summarizes inlet flow angles and blade angles (or relative flow angle) at the inlet and exit of the blade from the hub ($d/D = 0.3$) to tip ($d/D = 1$). The ratio of the hub diameter to the tip diameter (d_h/D) is taken to be 0.3. This is in contrast to Alexander [11], who has designed his propellers with d_h/D greater than 0.6. The runner is designed with 5 blades and with a blade pitch to chord ratio between 0.8 and 1.2 at different radial sections. The plan of the runner is illustrated in Fig. 2.

The choice of the hub to tip ratio and the number of blades needs some explanation. Technically, both these parameters depend on the specific speed of the turbine. However, a designer's freedom can also be exercised in choosing the values. The hub to tip ratio was restricted to 0.3 as it was believed that this would increase the flow area and reduces the flow velocity (axial compo-

Table 1
Relative and absolute flow angle along the blade.

Diameter ratio d/D	Absolute inlet flow angle α_2 (°)	Inlet blade angle, β_2 (°)	Exit blade angle β_3 (°)
0.3	59	-25	50
0.4	51	19	58
0.5	45	45	62
0.6	40	57	67
0.7	35	64	70
0.8	32	69	73
0.9	29	72	74
1.0	27	74	76

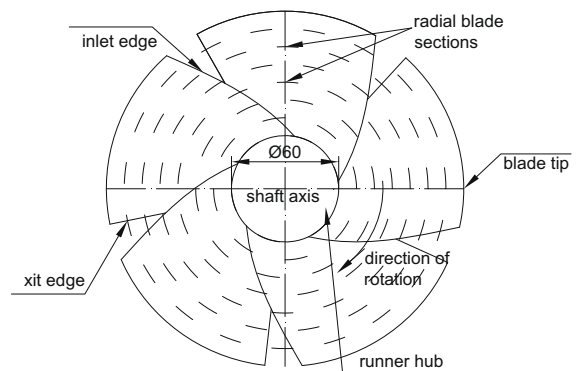


Fig. 2. Plan of the runner.

ment) and thereby the hydraulic losses to some extent. The choice of number of blades largely depended on optimizing the blade chord length and blade pitch. It was preferred to have larger number of shorter blades than fewer blades with longer chord length for given runner outer diameter of 200 mm.

The influence of hub to tip ratio and number blades on the runner performance is very important topic for future research of low head micro hydro propellers. While large hydro have established optimum relationship for them, micro hydro research also needs to be developed on these standardizing methods.

2.3. Other turbine components

The other components include the open spiral volute and the guide vane apparatus. The spiral volute creates a free vortex flow combined with radial sink flow. This combination results in a uniform spiral shape with an approximate angle of 11° (or 79° in the radial reference) as shown in Fig. 3 is selected, which is largely based on the design of APRL [12]. For the given gross head of 1.75 m, the turbine is envisaged to work under a suction head of 1.3–1.4 m and an inlet head with 0.3–0.4 m, which eliminates the need of a closed spiral volute inlet. The volutes of other propeller researchers ([6,9,10], and [11]) are closed type since their runners operate at a higher inlet head.

A radial guide vane ring with 11 fixed vanes is used as seen in Fig. 4. The chosen guide vane angle at the entry is 47° , while at the exit it is 45° . However, it has to be investigated whether the absolute flow angles generated by the present guide vane design satisfies the free vortex requirement at the runner inlet (as described in Table 1).

3. Means of solution

3.1. Experimental test-rig and procedure

The complete turbine assembly is illustrated in Fig. 5. The experimental test-rig as shown in Figs. 6 and 7, is kept as simple

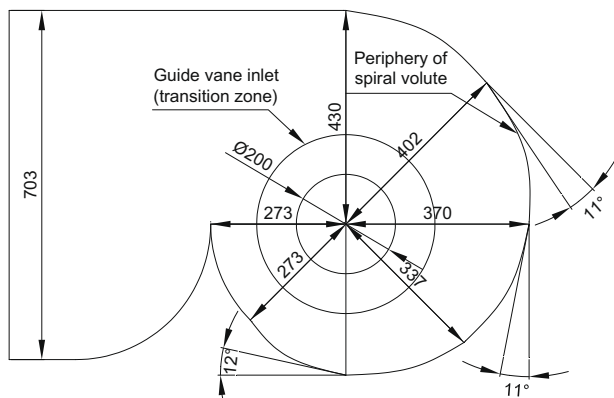


Fig. 3. Open spiral volute (dimensions in mm).

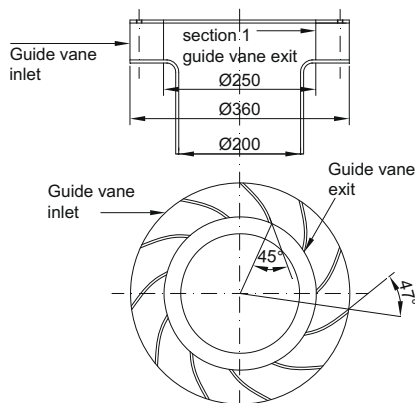


Fig. 4. Radial guide vane.

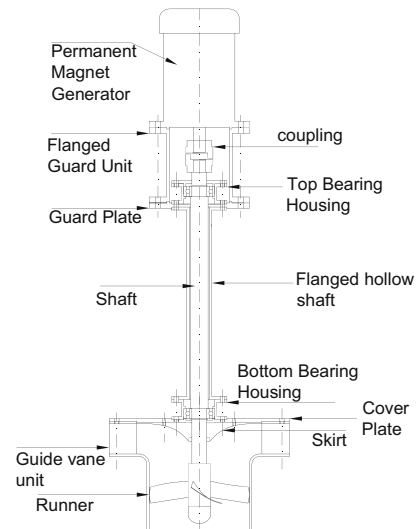


Fig. 5. Assembly of the propeller turbine.

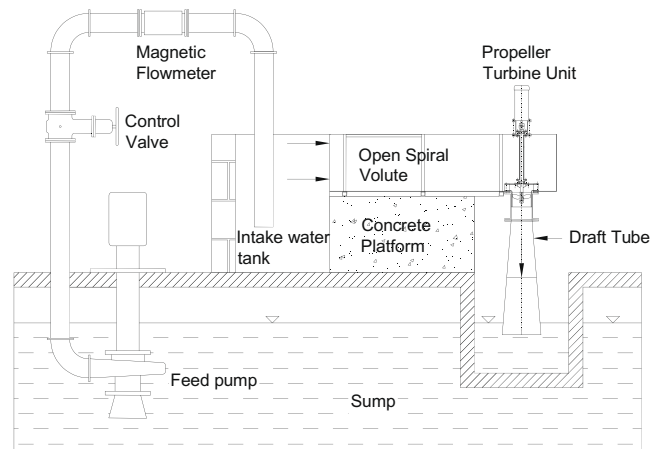


Fig. 6. Layout of the hydraulic test-rig.



Fig. 7. View of the spiral volute and propeller turbine unit.

and as close as possible to the actual operating conditions in the field. The hydraulic test-rig (Figs. 6 and 7) is designed to measure only the hydraulic input power and the electrical output power accurately. Since, the mechanical output shaft power at every load point is required to evaluate the turbine efficiency, another test setup as illustrated in Fig. 8 was constructed to accurately determine the generator performance (i.e. efficiency at different speeds and load currents in Fig. 9). The variables, instrumentation and associated uncertainties for both the setups are summarized in Table 2.

Due to the fixed excitation of the permanent magnet generator, it becomes very difficult to keep the operating speed constant at all load points. Hence, the turbine is operated at constant gross head



Fig. 8. Electrical test-rig with driving motor, torque transducer and PMG.

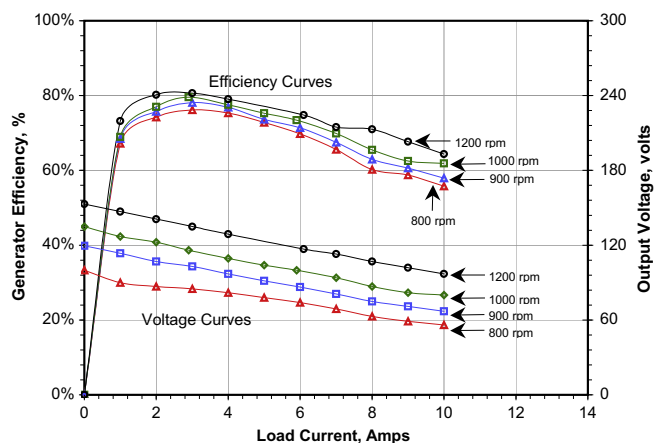


Fig. 9. Characteristics of the permanent magnet generator.

Table 2
Summary of the instrumentation.

Sr. No.	Variable	Instrument	Accuracy/uncertainty
<i>Hydraulic test rig</i>			
1	Gross head	Meter scale	5 mm
2	Discharge	Magnetic flow meter	0.1 l/s
3	Speed	Mechanical tachometer	1 rpm
4	Load voltage	Voltmeter	0.5 V
5	Load current	Ammeter	0.1 A
<i>Electrical test rig</i>			
1	Speed	Speed transducer	1 rpm
2	Torque	Torque transducer	0.1 Nm
3	Load voltage	Voltmeter	0.1 V
4	Load current	Current meter	0.1A

at all load points (no-load to full load) and other parameters (speed, flow, voltage and current) are measured. The mechanical characteristics of the turbine is subsequently determined using the electrical characteristics of the generator shown in Fig. 9, where the generator efficiency is recorded at identical operating points (speed and load current) as that obtained in the hydraulic test-rig. Subsequently, the turbine shaft power is computed from Eq. (13) using the respective generator efficiency and electrical output power.

Graphical plots: it is well known from dimensional analyses that for constant head characteristics, speed is used as the independent control variable, while discharge, output power and turbine efficiency is used as the dependent variables. To analyze the results between any two optimization stages, the graphs of discharge vs speed, output shaft power vs speed, and turbine efficiency vs. speed are plotted from no-load to maximum load at a constant gross head of 1.75 m.

3.2. Theory of analysis

As mentioned in Section 1 (Problem 3), one of the main objectives of the propeller turbine research is to understand the complicated internal hydraulics taking place within the runner as a result of geometric modification. Singh [4] presented an interesting methodology of analyzing the internal hydraulics in pumps operated as turbines that were subjected to geometric modifications on the impeller and the stationary parts. This methodology was based on constant speed analysis of turbine characteristics and comprised of using the macroscopic parameters like net head, flow, speed and power to ascertain the internal hydraulic loss phenomenon and the behaviour of the Euler shaft work, $\Delta c_u \cdot u$.

The case of propeller turbines is not different from 'pumps as turbines'. However, since the analysis of propellers has been carried out at constant head, a new methodology will have to be developed. This is done with respect to the behaviour of three parameters namely shaft power, discharge and hydraulic efficiency in the following sections.

3.2.1. Behaviour of output shaft power

From the fundamentals of energy transfer in turbines (steady state flow equation and Euler turbine equation), the output mechanical shaft power can be represented by Eq. (4).

$$P_{\text{mesh}} = m(\Delta c_u \cdot u) - P_{L-\text{mesh}} - m_{\text{leak}} \cdot \Delta h_0 \quad (4)$$

Pfleiderer and Petermann [5] have shown that the measured turbine shaft power comprises of the Euler momentum change (given by the velocity triangles at the inlet and exit) as well as the mechanical losses comprising of disk, gland and bearing friction. Pfleiderer and Petermann [5] further clarified that the Euler shaft work ($\Delta c_u \cdot u$) would not account for any hydraulic losses within the runner. This concept presented was further reinforced by Dixon [1] and other turbine designers. Hence, it can be concluded that the Euler shaft work (also called ideal hydraulic shaft work) would solely represent the mechanical work quantity.

The change in mechanical power at constant speed between two optimization stages will become a useful measure to obtain clarity about the runner hydraulics. As seen from Eq. (4), the change of shaft power can be grossly represented by two important parameters,

- (a) Euler's specific shaft work, $\Delta c_u \cdot u$ and,
- (b) Mass flow rate, m (or discharge).

Under constant speed and assuming no effects of leakage and mechanical losses, the change in shaft power can be represented as in Eq. (5).

$$dP_{\text{mech}} = d[m \cdot (\Delta c_u \cdot u)] = dm \cdot (\Delta c_u \cdot u) + m \cdot u \cdot d\Delta c_u + m\Delta c_u \cdot du$$

Further for constant speed $du = 0$, $dP_{\text{mech}} = (\Delta c_u \cdot u) \cdot dm + m \cdot u \cdot d\Delta c_u$ (5)

Condition: increase in shaft power at constant gross head and speed
From Eq. (5), we can conclude the following conditions.

- (i) Increase of mass flow rate at constant Δc_u (or $\Delta c_u \cdot u$).
- (ii) Increase in Δc_u (or $\Delta c_u \cdot u$) at constant mass flow rate.
- (iii) Small increase to both mass flow rate and Δc_u .

The behaviour of mass flow rate (or discharge) can be separately obtained from the 'Discharge vs. Speed' plots.

3.2.2. Behaviour of discharge and hydraulic losses

The gross head comprises of the Euler shaft work and the total system losses comprising of the spiral volute, guide vane ring, runner and draft tube zones and is given by Eq. (6), where 'k' is the respective loss coefficient in different zones.

$$gH_{\text{gross}} = \Delta c_u \cdot u + H_{L\text{-total}} = \Delta c_u \cdot u + (k_{\text{total}}) \cdot Q^2$$

$$= \Delta c_u \cdot u + (k_{sv} + k_{gv} + k_{\text{runner}} + k_{dt}) \cdot Q^2$$
 (6)

For constant gross head operating between any two optimization stages and further with no hydraulic changes taking place within the spiral volute, guide vane and draft tube (or constant k_{sv} , k_{gv} and k_{dt}), the differential form of Eq. (6) is reduced to Eq. (7).

$$d(gH_{\text{gross}}) - d(k_{\text{runner}}) \cdot Q^2 + d(\Delta c_u \cdot u) = 0,$$

hence $d(k_{\text{runner}} \cdot Q^2) = -u \cdot d\Delta c_u$ (7)

Condition: characteristics of runner losses at constant gross head and speed

From Eq. (7), if Δc_u was to increase, then the hydraulic losses should have to decrease, which can happen under the following conditions.

- (i) Decrease in runner loss coefficient at constant Q.
- (ii) Decrease in Q at constant runner loss coefficient.
- (iii) Decrease in both Q and runner loss coefficient.
- (iv) Larger decrease in Q but a small increase in k_{runner} .

The above analysis proves that there is deeper connection between the hydraulic losses and change in the Euler work for a constant value of gross head and speed. With a known change of the discharge variable, the behaviour of runner loss coefficient can be estimated.

3.2.3. Behaviour of hydraulic efficiency

The hydraulic efficiency illustrated in Eq. (3) can be further represented by Eq. (8).

$$\eta_{\text{hyd}} = \frac{\Delta c_u \cdot u}{\Delta c_u \cdot u + H_L} = \frac{\Delta c_u \cdot u}{\Delta c_u \cdot u + k_{\text{total}} \cdot Q^2}$$
 (8)

The hydraulic efficiency can be further related to the turbine efficiency directly by Eq. (9)

$$\eta_{\text{hyd}} = (\eta_{\text{turbine}}) / (\eta_{\text{leakage}} \cdot \eta_{\text{mech}})$$
 (9)

For a constant value of leakage and mechanical losses, the pattern of the behaviour of hydraulic efficiency and turbine efficiency (determined using Eq. (15) after determining shaft power from Eq. (13)) is identical or proportional. This can be represented by Eq. (10).

$$\frac{\Delta c_u \cdot u}{\Delta c_u \cdot u + k_{\text{total}} \cdot Q^2} \approx \frac{P_{\text{mech}}}{\rho \cdot Q \cdot gH_{\text{gross}}}$$
 (10)

Therefore, a change in the turbine efficiency at constant gross head depends on the relative changes to the shaft power and the discharge, which in turn depends on the Euler shaft work and the hydraulic losses.

3.2.4. Summarizing the analytical model

The change in the magnitudes of shaft power and discharge at constant head and speed will be analyzed in the vicinity of the best efficiency point between the two stages of optimization. A percentage analysis will be carried out at this point for changes to the shaft power, discharge and efficiency, which will be used to study the behaviour of the Euler shaft work (in Section 3.2.1) and hydraulic losses (in Section 3.2.2) respectively to get greater insights into the hydraulic phenomena within the runner.

4. Results and discussion

4.1. Effect of exit tip angle

The effect of exit tip angle of the runner is studied at two different stages. In the first stage the exit tip angle is changed from 85° to 77°, while in the second stage the angle is further reduced to 74°. The hydraulic phenomena for these two stages of optimization stages are independently studied. It is to be noted that the free vortex design requirement specifies the exit tip angle to be 76° (Table 1).

4.1.1. Change of exit tip angle from 85° to 77°

Fig. 10 illustrates this modification on the runner. The conditions at the runner inlet remain unchanged. The runner inlet tip angle is 38°.

The performance characteristics have been compared in Figs. 11.1 and 11.2. It can be seen that the discharge curves (Fig. 11.1) for modified exit tip have been completely transformed. At corresponding speeds, the discharge consumption has increased substantially (20–30%), while the power curves show a remarkable improvement (40–50%) for the modified stage. The comparison of the efficiency curves (Fig. 11.2) clearly show that the efficiency for the modified exit has increased in the range of 8–10% between operating speeds of 850 rpm and 950 rpm.

Though the best efficiency point has not been reached for the modified runner, the hydraulic analysis is carried out at a load point defined at speed of 900 rpm in Table 3. It is clearly visible

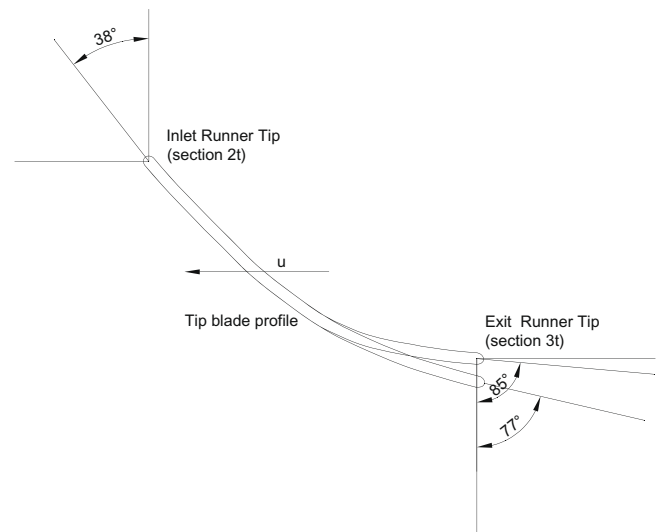


Fig. 10. Exit tip modification (β_{3t} –85–77°).

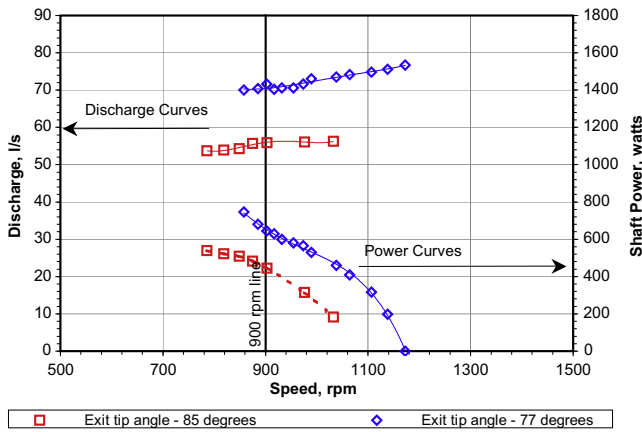


Fig. 11.1. Comparison of discharge and power curves (β_{3t} -85–77°).

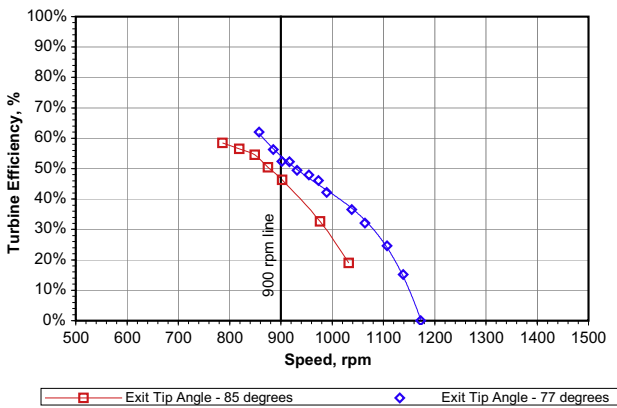


Fig. 11.2. Comparison of efficiency curves (β_{3t} -85–77°).

Table 3

Percentage analysis due to exit tip modification (85–77°) at 900 rpm.

Optimization stage	Shaft power		Discharge		Efficiency	
	(watts)	% change	(l/s)	% change	(%)	% change
Exit tip angle –85°	452	+45.6%	56.0	+26.1%	47.0	+7.3%
Exit tip angle –77°	658		70.6		54.3	

that there is a 45% increase in shaft power and a 26% increase in discharge, while efficiency has increased by over 7%.

From the methodology presented in Section 3.2.1 and Eq. (5), increase in power would either mean an increase to the mass flow rate (discharge) or the Euler shaft work $\Delta c_u \cdot u$. As the discharge is seen to increase, it would definitely assist in generating more shaft power. From the percentage analysis, it can be seen that the discharge has increased by 26%, but the shaft power has gone up by 45%, which means that in addition to the mass flow rate effects, the Euler shaft work has also increased, which internally refers to change in the velocity triangles (increase in the c_u and c_x components).

It is now important to understand the behaviour of the runner losses. It can be interpreted from the methodology in Section 3.2.2 and Eq. (7) that the increase in the Euler shaft work (at constant gross head) would mean a decrease in runner losses given by $k_{runner} \cdot Q^2$. However, for the net runner losses to decrease despite an increase in discharge of 26%, the runner loss coefficient should de-

crease by an even greater margin. It can hence be concluded that the exit tip modification from 84° to 77° has caused both the Euler shaft work and mass flow rate to increase on one hand, while it has caused the substantial decrease of runner loss coefficient on the other.

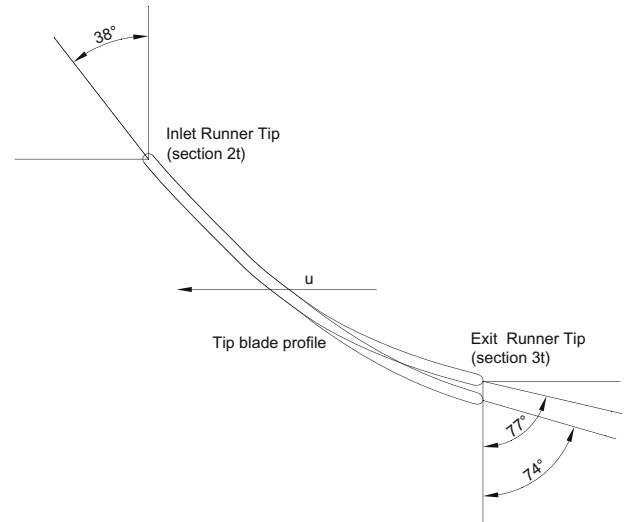


Fig. 12. Exit tip modification (β_{3t} -77–74°).

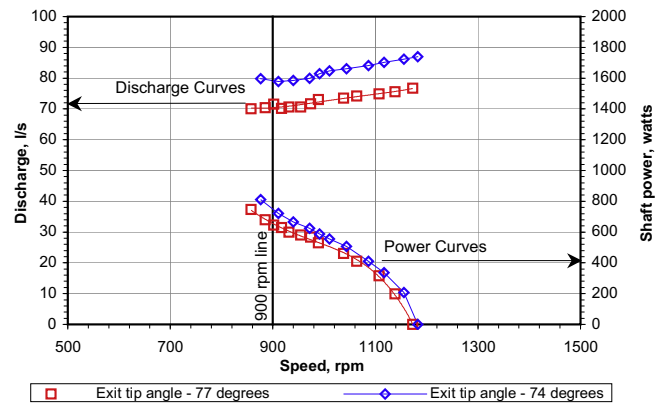


Fig. 13.1. Comparison of discharge and power curves (β_{3t} -77–74°).

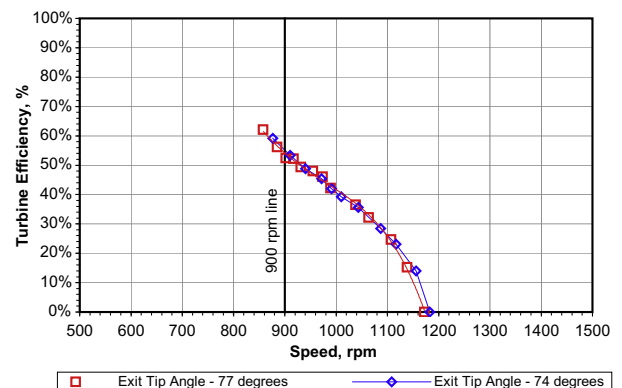


Fig. 13.2. Comparison of efficiency curves (β_{3t} -77–74°).

Table 4
Percentage analysis due to exit tip modification (77–74°) at 900 rpm.

Optimization stage	Shaft power		Discharge		Efficiency	
	(watts)	% change	(l/s)	% change	(%)	% change
Exit tip angle –77°	658	+13.7%	70.6	+12.2%	54.3%	+0.7%
Exit tip angle –74°	748		79.2		55.0%	

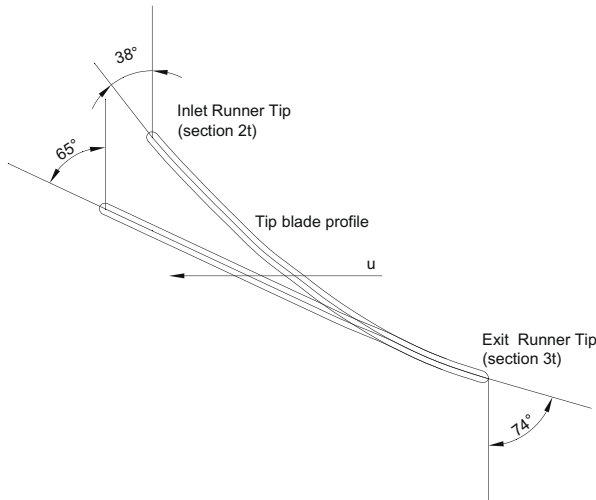


Fig. 14.1. Inlet tip modification (β_{2t} -38–65°).



Fig. 14.2. Picture of the runner with inlet edge modified.

4.1.2. Change of exit tip angle from 77° to 74°

This is the second level of understanding the effects of the exit tip angle and is as illustrated in Fig. 12. The performance characteristics are compared in Figs. 13.1 and 13.2, respectively. Similar to the previous stage it can be seen that the shaft power as well as the discharge curves for the 74° exit tip angle stage have risen above their counterparts.

However, comparison of efficiency characteristics reveals that the curves collapse into each other, which means that there is no improvement in efficiency.

The percentage analysis in Table 4 shows that the shaft power has increased by 13.7%, while the discharge has increased by 12.2% with no marked change in the efficiency. Analyzing from the methodology presented in Section 3.2.1, the increase in shaft power could come only from the rise in discharge (because the percentage rise of both shaft power and discharge is almost comparable), which means that changes to the Euler shaft work $\Delta C_{u,u}$ is negligible. This would further imply that the runner losses ($k_{runner} \cdot Q^2$) have remained unchanged (from conditions in Section 3.2.2). But, since the discharge has increased for the modified exit,

the runner loss coefficient should decrease to maintain the constancy of the runner loss (from Eq. (7)).

Therefore, one can conclude from the above analysis that the change of the exit tip angle from 77° to 74° has increased the discharge and shaft power, but in absolute terms there is no increase in efficiency. Further, the absolute hydraulic losses within the runner and the Euler shaft work have remained grossly unchanged.

4.2. Effect of inlet tip and hub angle

This modification is illustrated in Figs. 14.1 and 14.2, which comprises of a major alteration to the inlet tip angle (from 38° to 65°) and a minor change to the inlet hub angle from 30° to 55°.

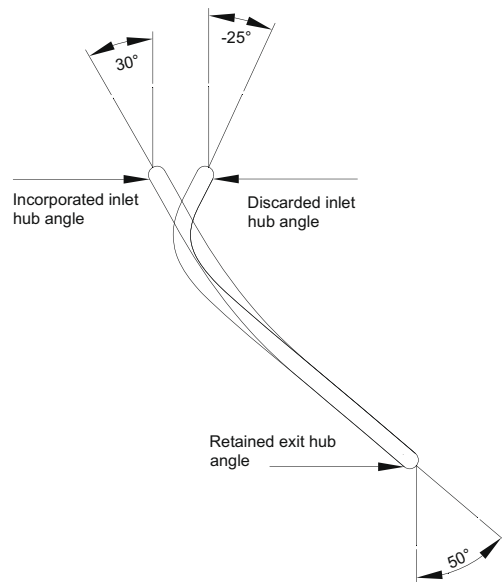


Fig. 15. Discarded and incorporated inlet hub before inlet modification.

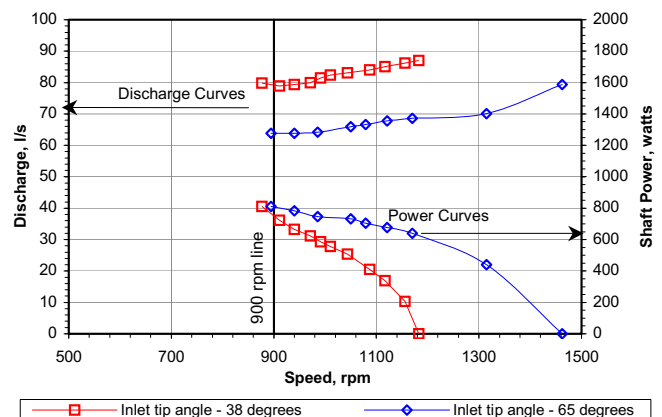


Fig. 16.1. Comparison of discharge and power curves (β_{2t} -38–65°).

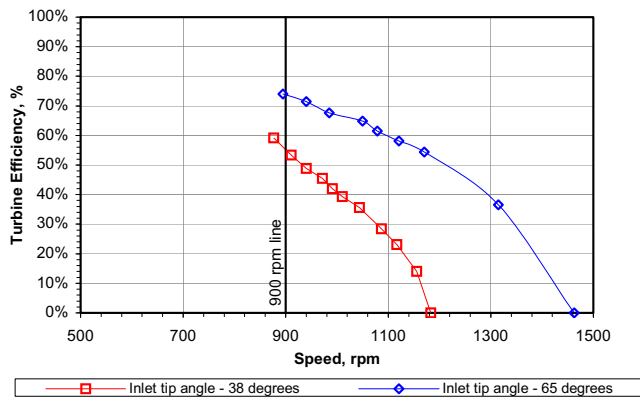


Fig. 16.2. Comparison of efficiency curves (β_{2t} -38–65°).

Table 5
Percentage analysis due to inlet blade modification at 900 rpm.

Optimization stage	Shaft power		Discharge		Efficiency	
	(watts)	% change	(l/s)	% change	(%)	% change
Inlet tip angle –38°	748	+8.3%	79.2	–19.3%	55.0	+18.9%
Inlet tip angle –65°	810		63.9		73.9	

Table 6
Comparison of the design and experimental runner at BEP.

Runner	N (rpm)	H_{gross} (m)	Q (l/s)	η_{hyd} (%)
Free vortex design runner	900	1.42	67.5	75.0
Optimized experimental runner	900	1.75	63.9	73.9

The free vortex design condition for the inlet tip is 74°, while for the inlet hub it specifies an angle of –25° (as seen in Table 1), which has been discarded and 30° was incorporated as the inlet hub angle prior to this modification. A relative flow angle at the inlet hub takes peculiar orientation of –25°, which is obtained by solving the free vortex design equations with constant axial velocity and swirl free exit as explained in Section 2.1 and 2.2. The manufacture a blade profile at the hub with –25° having a large curvature was very complex and hence an inlet hub angle of 30° was chosen that would result in a smoother profile between the inlet and the exit hub. The situation of the inlet hub is explained in Fig. 15.

The comparison of the characteristics in Fig. 16.1 shows a sharp drop in the discharge consumption for the modified inlet stage while the power has increased over the complete range of operating characteristics. Owing to both the increase in power and decrease in discharge the efficiency has increased by a very large margin of 15–20% in the best efficiency region (Fig. 16.2).

The percentage analysis presented in Table 5 clearly demonstrates increase in power (by 8.3%) despite the fact that discharge has decreased over 19%. From the conditions understood in Section 3.2.1, the only way for power to increase despite a drop in the discharge (or mass flow rate) is by having a very large increase in the Euler shaft work.

On the other hand a greater increase in Euler shaft work directly means a correspondingly large drop in the runner losses (Eq. (7)). The runner losses, given by $k_{runner} \cdot Q^2$, depend both on the square of discharge and the loss coefficient (k_{runner}). Since, the discharge has fallen by 19%, its square would decrease the losses by even a greater margin. Hence, it is very difficult to comment on the behaviour of the runner loss coefficient (k_{runner}) for the modified runner. Nevertheless, it can be concluded that the inlet modification has decreased the discharge consumption and greatly increased the Euler shaft work (rearranging the velocity triangles) and reduced the runner losses.

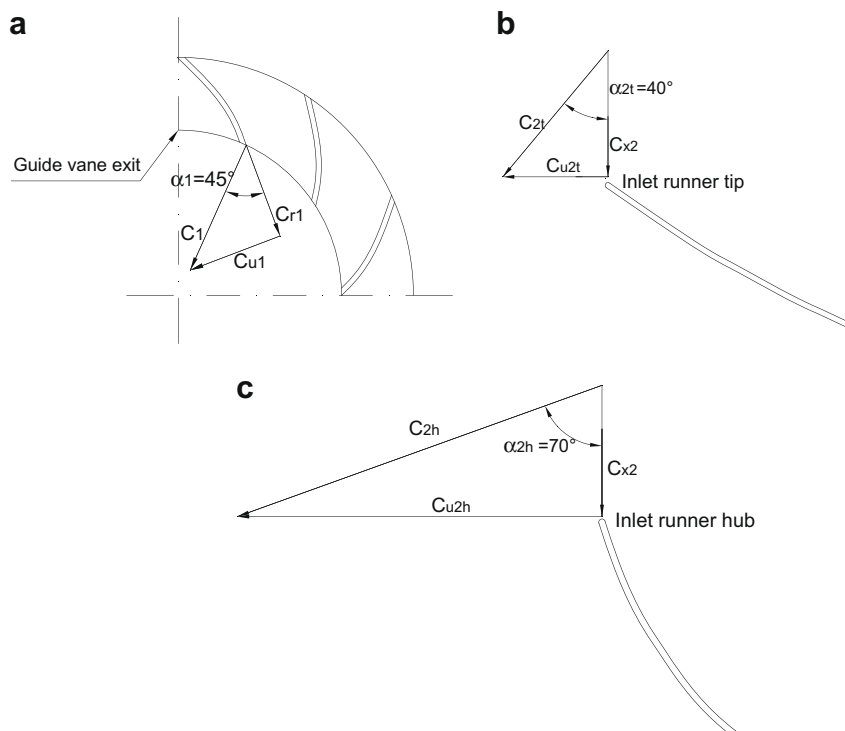


Fig. 17. Comparison of velocity triangles at (a) the guide vane exit, (b) inlet runner tip and (c) inlet runner hub.

4.3. Realizing the optimized free vortex runner

4.3.1. Comparison at BEP

The free vortex (or design) runner conceptualized to operate with a gross head of 1.75 m and flow of 75 l/s (Section 2.2) at 1000 rpm needs to be compared with the results of the ultimate optimization stage of the experimental runner. As studied in Section 4.2, this optimization stage comprises of the modified inlet with inlet tip angle of 65° and exit tip angle of 74°.

The operating point at BEP for the design and the experimental runner is compared in Table 6. From the characteristics (Fig. 16.2) of the optimized runner it is clear that the BEP point could not be reached under experimental conditions. Hence, the comparison is carried out at 900 rpm for both the design and the experimental runner. It can be seen that the design runner would operate under a lower gross head and at a higher discharge compared to that of the experimental runner. While the design runner is at the BEP, the experimental runner is nearing the BEP. If the experimental runner were to reach its BEP the speed would fall below 900 rpm, but the deviations would still persist.

These deviations could be attributed to either the change in the absolute flow conditions at the runner inlet (stationary frame) or changes to the runner design (relative or rotary frame). Both these aspects need to be considered separately.

4.3.2. Examining the flow conditions at runner inlet

Firstly, the flow conditions at the runner inlet need to be examined. Using principles of conservation of angular momentum and continuity equation, it can be shown that for the given guide vane exit angle of 45°, the swirl angle just ahead of the runner tip will be 40°. Further, from the free vortex law, swirl angle ahead of the runner hub is 70°. Fig. 17 analyzes the velocity triangle at these 3 locations.

Table 7 summarizes the extent of deviation between the free vortex and the optimized experimental runner. It can be seen that the deviations at the tip is of the order of 13° and at the hub it is about 11°, which will definitely cause changes to the inlet velocity triangle and hence affect the generated Euler shaft work. In that, it would result in an increase of c_{u2} and also the Euler shaft work ($\Delta c_{u,u}$) and H_{gross} (from Eq. (6)), which is evident from the comparisons in Table 6, where the gross head for the experimental runner is greater than that for the design runner.

4.3.3. Examining the runner geometry

Secondly, the runner design itself is an issue here. The geometrical angles at the tip and hub for the two runners are presented in Table 8. It can be seen that the tip conditions of the experimental

Table 7
Comparison of the absolute flow conditions at the runner inlet.

Runner	Absolute swirl angle (α) at runner inlet	
	Tip (°)	Hub (°)
Free vortex design runner	27	59
Optimized runner (with 45° guide vane angle)	40	70

Table 8
Comparison of the geometric conditions of the runners.

Runner	Inlet blade profile		Exit blade profile	
	Hub (°)	Tip (°)	Hub (°)	Tip (°)
Free vortex design runner	–25	74	50	76
Optimized experimental runner	50	65	55	74

runner seems to reasonably match with the free vortex design runner. However, the inlet hub has been completely transformed for the experimental runner, as the free vortex specification was not practical to manufacture. These deviations in the runner geometry could also be the cause of the mismatch of the operating points in addition to the absolute flow deviations.

But, as far as the peak performance is concerned, the maximum efficiency of 74% for the experimental runner is a very positive result and this particular runner can be treated both as a 'near free vortex' and 'optimized' runner for micro hydro application.

5. Conclusion and recommendations

The test results of the optimization stages have demonstrated considerable success in developing an optimum free vortex runner under the given boundary conditions. The optimized experimental runner delivered 810 watts of shaft power at 1.75 m and 900 rpm consuming 64 l/s of water with a healthy operating efficiency of 73.9%. This performance is acceptable by any standards and this runner is recommended for micro hydro application.

It was also found that operating point of final experimentally optimized runner deviated slightly from the specifications of the free vortex design, which could be attributed to a probable variation of the absolute flow angle at the entry to the runner (caused by the selected exit guide vane angle of 45°) and a small variation with respect to the runner geometry itself. However, the runner design near the tip region closely resembled the free vortex design runner. Despite the above deviations, the peak performances of the both the free vortex and experimental runners were still comparable, which in a way validates the free vortex design approach as a starting point in the design of micro hydro propellers. Nevertheless, the results also open up an opportunity to contemplate other design methodologies.

The most interesting conclusions of the experimental study were with respect to the internal optimization of runner hydraulics. The experimental study along with an innovative theoretical methodology helped in understanding the internal hydraulic phenomenon within the runner subjected to geometric modifications, which comprised of studying the behaviour of the Euler shaft work, discharge and runner hydraulic loss coefficient at constant values of gross head and turbine speed.

The first stage of optimization comprised of the decreasing the exit angle at the runner tip from a near flat (tangential) design condition. This optimization was carried out at two levels. The first level was from 85° to 77° and the second level was from 77° to 74°. It could be concluded that the exit tip angle modification brought about an increase in the Euler shaft work (which means a rearrangement of the velocity triangles) and also an increase in the discharge at constant operating gross head and speed. Further, this optimization also gave a proof of an improvement in the runner hydraulics with a decrease in the runner loss coefficient and increase in the hydraulic efficiency.

The second stage optimization was with respect to the inlet tip of the runner. This modification (change of inlet tip angle from 38° to 65°) resulted in amazing hydraulic effects within the runner with an efficiency rise of nearly 20%. It was concluded that this optimization increased the Euler shaft work, decreased the runner losses and also reduced the discharge consumption of the runner. This modification gave the best runner performance with a maximum operating efficiency of 74%.

In addition to the above conclusions, this experimental optimization study leads to several interesting questions and hence, recommendations for further study.

Firstly, an optimized runner with a maximum efficiency of 74% was nearly realized through a well-sketched experimental pro-

gramme. However, this efficiency could still be improved to about 80% with more optimization steps. The present experimental runner was largely based on the free vortex design with some deviations. However, there still remain interesting questions regarding the energy transfer of experimental runner that need to be investigated further in order to evolve an alternate and a more optimum design. In addition, it would be worthwhile to study the feasibility of other design approaches like constant blade reaction and zero power blading designs.

Secondly, it is recommended to manufacture the runner accurately as per the free vortex design specifications at least at the tip (74° at inlet tip and 76° at inlet hub) and investigate if the discharge of 75 l/s and efficiency of 75% can be realized at 1000 rpm and gross head of 1.75 m. Another recommendation in this regard is to build a turbine without the incorporation of guide vanes and allow unhindered free vortex flows.

The influence of the number of blades and hub to tip ratio on the runner performance is another very important aspect of future experimental work with an objective to develop optimum design standards for micro hydro application.

The effects of radial guide vane angle on the performance of runner would be very interesting especially to evaluate the guide vane angle that would generate inlet swirl flow as per free vortex specification. This can be done by incorporating adjustable guide vanes.

Finally, in the world of computational fluid dynamics it would be very important to validate all the experimental results using numerical tools. These tools could throw more light on the hydraulic behaviour, which can be compared with the behaviour predicted by analytical model developed in this paper. Once, the numerical tools are successful in validating all the experimental findings, it could then be used more as optimization tool.

6. Uncertainty analysis

To get an overall picture of the experimental uncertainty, the analysis is carried out at 3 levels for the maximum efficiency point obtained after the inlet tip modification (Table 6). The first level is that of the generator efficiency followed by the mechanical shaft power and finally leading to the turbine efficiency. The uncertainty of each variable comprises of both random and bias (fixed) errors.

6.1. Uncertainty in generator efficiency

The maximum uncertainties of the electrical parameters were PRESENTED in Table 3. Given $\Delta V = 0.1$ V, $\Delta I = 0.1$ A, $\Delta T = 0.1$ nm and $\Delta N = 1$ rpm, and the BEP defined at 900 rpm and $T = 8.6$ nm, with $V = 80$ V and $I = 6.9$ A, a generator efficiency of 68% is obtained using Eq. (11).

$$\eta_{\text{gen}} = V \cdot I / (2 \cdot \pi \cdot N \cdot T) / 60 \quad (11)$$

The uncertainty in the generator efficiency is determined from Eq. (12).

$$\Delta \eta_{\text{gen}} / \eta_{\text{gen}} = [(\Delta V / V)^2 + (\Delta I / I)^2 + (\Delta N / N)^2 + (\Delta T / T)^2]^{1/2} = \pm 1.9\% \quad (12)$$

6.2. Uncertainty in mechanical power

The mechanical shaft power on the turbine is determined from the generator characteristics using Eq. (13) and is found to be 810 watts.

$$P_{\text{mech}} = V \cdot I / \eta_{\text{gen}} \quad (13)$$

The relative uncertainty in mechanical power for the identical point is given by Eq. (14), where the relative uncertainty of the generator efficiency is $\pm 1.9\%$ (Eq. (12))

$$\Delta P_{\text{mech}} / P_{\text{mech}} = [(\Delta V / V)^2 + (\Delta I / I)^2 + (\Delta \eta_{\text{gen}} / \eta_{\text{gen}})^2]^{1/2} = \pm 2.4\% \quad (14)$$

6.3. Uncertainty in turbine efficiency

The relative uncertainty of turbine efficiency is finally determined from the Eq. (15).

$$\eta_{\text{turbine}} = P_{\text{mech}} / (\rho \cdot Q \cdot gH) \quad (15)$$

For the turbine operating point as illustrated in Table 6 ($H = 1.75$ m, $Q = 63.9$ l/s, $N = 900$ rpm and $P_{\text{mech}} = 810$ watts and $\eta_{\text{turbine}} = 73.9\%$), the relative uncertainty in turbine efficiency is $\pm 2.4\%$, given by Eq. (16). The corresponding absolute uncertainty will be $\pm 1.8\%$

$$\Delta \eta_{\text{tur}} / \eta_{\text{tur}} = [(\Delta P_{\text{mech}} / P_{\text{mech}})^2 + (\Delta Q / Q)^2 + (\Delta H / H)^2]^{1/2} = \pm 2.4\% \\ \Delta \eta_{\text{tur}} = 0.739 \cdot 2.4\% = \pm 1.8\% \quad (16)$$

Acknowledgements

The authors would like to acknowledge of the honest contribution of Mr. Ravichandran and his team who took up the task of manufacture of the propeller turbine in Bangalore, India. The efforts of the German team at Institute of Water and River Basin Management also needs to be acknowledged. The authors would like to thank the Department Heads, Dr.-Ing Boris Lehmann and Dr.-Ing Peter Oberle, and Foreman Mr. Werner Helm for the erection of the test-rig. Special thanks is reserved for Mr. Günther Kühn who carried out all the modifications to the runner with great care and precision. The contributions Mr. Marcus Plate, Mr. Michael Ritzmann, Mr. Manfred Lösche and the other personnel of the Institute were also very useful. At the end the authors would like to thank Prof. Dr.-Ing Martin Gabi and Dr.-Ing Saban Caglar of the Department of Fluid Machinery, University of Karlsruhe for their support during testing as well as Dr.-Ing Gerhard Clos and his colleagues of the Department of Electrical Engineering and Information Technology, University of Karlsruhe for carrying out detailed tests on the permanent magnet generator in their laboratory.

References

- [1] S.L. Dixon, Fluid Mechanics and Thermodynamics of Turbomachinery, Elsevier, Oxford, UK, 2005. Chapters 2, 6 and 9.
- [2] H.I.H. Saravanamuttoo, G.F.C. Rogers, H. Cohen, Gas Turbine Theory, Pearson Education, Singapore, 2005. Chapters 5 and 7.
- [3] R. Hothersall, Hydrodynamic Design Guide for Small Francis and Propeller Turbines, United Nations Industrial Development Organization, Vienna, Austria, 2004. Chapters 2, 3 and 10.
- [4] P. Singh, Optimization of the Internal Hydraulic and of System Design in Pumps as Turbines with Field Implementation and Evaluation, Ph.D. Thesis. University of Karlsruhe, Germany, 2005.
- [5] C. Pfeleiderer, H. Petermann, Strömungsmaschinen, Springer-Verlag, 1964. Chapter 1.
- [6] G.M. Demetriades, Design of Low-Cost Propeller Turbines for Standalone Micro-hydroelectric Generation Units, Ph.D. Thesis. University of Nottingham, United Kingdom, 1997.
- [7] G.J. Rao, R. Prasad, J.K.S. Rao, Investigation of an Axial Flow Runner for Micro Hydro Power Development, in: Proceedings of 8th Fluid Machinery Conference, Budapest, Hungary, 1988, pp. 616–23.
- [8] S. Soundranayagam, A. Suryanarayanan, Ultra Low-Head Propeller Turbines for Small Canal Drops, Turbomachines Laboratory Report, Indian Institute of Science, Bangalore, India, 1988.

- [9] D. Upadhyay, Low Head Turbine Development using Computational Fluid Dynamics, Ph.D. Thesis. University of Nottingham, United Kingdom, 2004.
- [10] R.G. Simpson, A.A. Williams, Application of Computational Fluid Dynamics to the Design of Pico Propeller Turbines, in: Proceedings of the International Conference on Renewable Energy for Developing Countries, 2006.
- [11] K.V. Alexander, E.P. Giddens, A.M. Fuller, Axial-flow turbines for microhydro systems, Elsevier Journal of Renewable Energy 34 (2009) 35–47.
- [12] Asian Pheonix Resources Ltd. (APRL), Powerpal Brochure, 2001, <<http://www.powerpal.com>>, (accessed February 2009).



Contents lists available at ScienceDirect

Experimental Thermal and Fluid Science

journal homepage: www.elsevier.com/locate/etfs

Exit blade geometry and part-load performance of small axial flow propeller turbines: An experimental investigation

Punit Singh*, Franz Nestmann

Institute for Water and River Basin Management (IWG), University of Karlsruhe, Kaiser Str. 12, D 76128 Karlsruhe, Germany

ARTICLE INFO

Article history:

Received 17 July 2009

Received in revised form 15 January 2010

Accepted 18 January 2010

Keywords:

Exit tip angle
 Runner loss coefficient
 Relative flow angle
 Free vortex
 Slip phenomena
 Part-load

ABSTRACT

A detailed experimental investigation of the effects of exit blade geometry on the part-load performance of low-head, axial flow propeller turbines is presented. Even as these turbines find important applications in small-scale energy generation using micro-hydro, the relationship between the layout of blade profile, geometry and turbine performance continues to be poorly characterized.

The experimental results presented here help understand the relationship between exit tip angle, discharge through the turbine, shaft power, and efficiency. The modification was implemented on two different propeller runners and it was found that the power and efficiency gains from decreasing the exit tip angle could be explained by a theoretical model presented here based on classical theory of turbomachines. In particular, the focus is on the behaviour of internal parameters like the runner loss coefficient, relative flow angle at exit, mean axial flow velocity and net tangential flow velocity.

The study concluded that the effects of exit tip modification were significant. The introspective discussion on the theoretical model's limitation and test facility suggests wider and continued experimentation pertaining to the internal parameters like inlet vortex profile and exit swirl profile. It also recommends thorough validation of the model and its improvement so that it can be made capable for accurate characterization of blade geometric effects.

© 2010 Elsevier Inc. All rights reserved.

1. Introduction

1.1. Background

Research interests in axial flow or propeller turbines for power outputs ranging from few hundred watts to few tens of KW has been slowly picking pace especially in developing countries for micro-hydro and energy recovery application. The activities have been restricted mostly to the design and performance evaluation.

APRL [15], Rao et al. [1] and Soundranayagam and Suryanarayanan [2] were amongst the early contributors. More recently, Demetriades [3] and Upadhyay [4] worked on the design for a 1 KW unit and carried out the experimental and numerical studies on it. Upadhyay [4] further suggested modifications to the blade profiles and guide vanes for improved performance using computational results, but did not carryout experimental validation for these modifications. Alexander et al. [6] brought out the designs

of four different propeller units and attempted to standardize designs, however did not report any model specific optimization to these runners.

Simpson and Williams [5] attempted a field level optimization that comprised of redesigning a runner with the same guide vane design and mechanical setup in order to match the system boundary conditions more accurately. He reported a considerable improvement in performance, but did not analyze the hydraulic phenomena with respect to the geometric changes. Further, he did not specify the exact geometric changes carried out on the blades.

Singh and Nestmann [7] carried out a series of optimization on a particular runner, that included modifications to inlet and exit tip of the blade profiles. They also developed a simple theoretical model to analyze the hydraulic phenomena due to these geometric modifications, which gave a qualitative study to the internal hydraulic phenomena. But, their study falls short of quantifying these internal hydraulic effects.

The need for detailed hydraulic analysis of internal parameters with respect to the blade geometry is very important to understand how each region (tip, hub, inlet or exit) of the blade's geometry influences the performance. This understanding will help in optimizing the performance and will serve as a useful design tool

Abbreviations: BEP, best efficiency point; CFD, computational fluid dynamics; PAT, pump as turbine.

* Corresponding author. Tel.: +49 721 608 2194; fax: +49 721 606 046.

E-mail addresses: punit.singh@iwg.uka.de (P. Singh), nestmann@iwg.uka.de (F. Nestmann).

Nomenclature

<i>c</i>	absolute velocity, m/s	ρ	density, kg/m ³
<i>d</i>	local diameter, m	α	absolute flow angle, °
<i>D</i>	tip diameter, m	β	relative flow angle, °
<i>g</i>	acceleration due to gravity, m/s ²	ζ	pressure loss coefficient
<i>H</i>	head parameter, m		
<i>i</i>	angle of incidence, °	<i>Superscript</i>	
<i>I</i>	current, A	*	blade condition
<i>k</i>	loss coefficient, 1/m ⁴		
<i>m</i>	mass flow rate, kg/s	<i>Subscripts</i>	
<i>N</i>	speed, rpm	1	guide vane exit
<i>P</i>	power, kW	2	runner inlet
<i>Q</i>	discharge, l/s or m ³ /s	3	runner exit
<i>T</i>	torque, Nm	4	draft tube exit
<i>u</i>	tangential blade velocity, m/s	<i>g</i>	generator
<i>V</i>	voltage, V	<i>h</i>	hub region
<i>w</i>	relative velocity, m/s	<i>m</i>	mechanical
<i>z</i>	number of blades	<i>t</i>	tip region
		<i>u</i>	tangential direction
		<i>x</i>	axial direction
<i>Greek symbols</i>			
η	efficiency, %		

for accurate system design, instead of relying on correlations. In the larger picture, this should enable the realization of optimum runners for different boundary conditions.

1.2. Objectives and problem outline

- (1) To develop a general theoretical model, which determines the functional relationships between different internal variables that govern loss mechanisms, momentum transfer, incidence, deflection and other effects, using classical theory of axial flow turbomachines.
- (2) To fabricate runners with different exit blade designs and to study the performance of these runners on an experimental test-rig and use the theoretical model to comprehensively understand the effects of different exit blade designs.
- (3) To compare the performance of experimental runners with that of the free vortex runner with respect to the exit tip design.
- (4) To recommend the standardization of the optimum design of the exit blade geometry for different boundary conditions.

2. The theoretical model

2.1. Free vortex runner

The summary of the design of a free vortex propeller runner that has been discussed in [7] for a gross head of 1.75 m and discharge of 75 l/s, with a diameter of 200 mm is presented in Table 1. It can be seen that the relative flow angle at the inlet tip is 74° and at the exit tip is 76°. The vortex flow angle at the inlet tip required is around 26.6°.

Table 1
Free vortex specifications of an axial flow turbine blade.

<i>d/D</i>	0.3	0.4	0.5	0.6	0.65	0.7	0.8	0.9	1
α_2	59.1°	51.4°	45.0°	39.9°	37.6°	35.6°	32.0°	29.1°	26.6°
β_2	-25.3°	19.0°	44.8°	57.3°	61.3°	64.3°	68.7°	71.8°	74.0°
α_3	0°	0°	0°	0°	0°	0°	0°	0°	0°
β_3	50.1°	57.9°	62.4°	67.3°	68.9°	70.3°	72.6°	74.4°	75.9°

2.2. Main variables and their functional relationship

The main working variables for any hydro turbine are classified as input variables, which include available head and discharge, and output variables comprising of shaft power and speed. Using the standard dimensional analysis, the control (or independent) variables for this system are taken as the head and speed, while discharge and shaft power are considered as dependent variables. Another performance parameter is efficiency, which is again a dependent variable. The overall dimensional functional equation is represented by

$$Q, P_{\text{shaft}}, \eta = f(N, gH) \tag{1}$$

Singh and Nestmann [7] attempted to give a greater physical meaning to the behaviour of these dependent variables (discharge, power and efficiency) individually with respect to two important internal variables – the Euler shaft work or net rotational momentum and the runner loss coefficient, and related it to the geometric modifications carried out on the runner.

2.3. Internal variables and their functional relationships

The classification of internal variables and determination of their behaviour is done by defining and the expanding the main variables without changing the original functional relationship in Eq. (1). The velocity triangle approach along with the cascade approach is then utilized to develop a deeper understanding of the physical significance of internal variables in the context of propeller geometry. A typical inlet and velocity triangle for a low-pressure axial stage at the blade tip is shown in Fig. 1 without any incidence or deviation effects.

2.3.1. Identifying the internal variables

2.3.1.1. Expanding the dependent variables.

- (1) *Discharge (Q)*: The discharge is a dependent variable as from Eq. (1) and is given by the mean axial flow velocity and flow area in Eq. (2). If diameter (*D*) is taken as an independent geometric variable and *d_h/D* taken as a design variable, then the mean axial flow velocity (*c_x*) directly corresponds to *Q* and becomes an internal dependent variable.

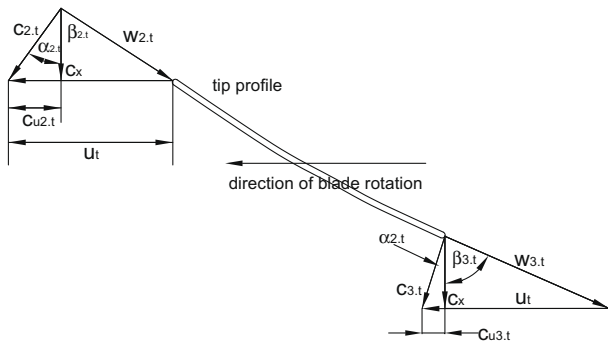


Fig. 1. Typical velocity triangles of a low-pressure axial turbine at the blade hub and tip.

$$Q = c_x \cdot (\pi \cdot D^2/4) \cdot (1 - (d_h/D)^2) \quad (2)$$

$$c_x \approx Q$$

(2) Shaft power, P_{shaft} : As shown in [7] (based on Euler turbine fundamentals discussed by Pfleiderer and Petermann [9] and Dixon [8]), it is appropriate to represent shaft power by Euler shaft work ($\Delta c_u \cdot u$ or change of rotational momentum) and leakage losses.

$$P_{\text{shaft}} = m \cdot (\Delta c_u \cdot u) - \text{leakage losses} \quad (3)$$

If leakage effects are neglected especially while comparing two optimization stages, the shaft power's proportionality is given by Eq. (4). It can be easily shown that the net tangential flow velocity Δc_u is another internal dependent variable that represents an important parameter of energy transfer or rotational momentum and hence, shaft work.

$$P_{\text{shaft}} \approx (\rho \cdot A \cdot c_x) \cdot (\Delta c_u \cdot u) = (\rho \cdot Q) \cdot (\Delta c_u \cdot u) \quad (4)$$

Using velocity triangles in Fig. 1, the net tangential flow velocity Δc_u is represented as in Eq. (5). For constant blade velocity (u) and inlet vortex angle (α_2), a functional relationship for Δc_u in terms of mean axial velocity (c_x) and relative flow angle at exit (β_3) can be established. It is to be noted that for the fixed guide vane design, α_2 is always constant for a particular blade height and is a function of d_h/D and local diameter (as discussed in Section 3.3).

$$\Delta c_u = c_{u2} - c_{u3}$$

$$\Delta c_u = (c_x \cdot \tan \alpha_2) - (u - c_x \cdot \tan \beta_3) = c_x \cdot (\tan \alpha_2 + \tan \beta_3) - u$$

$$\Delta c_u = f(c_x, \beta_3) \text{ for constant } u \text{ and } \alpha_2 \quad (5)$$

2.3.1.2. Expanding the independent variables.

(1) Head, gH : The available head is an independent variable of the turbine control volume and can be represented by Euler shaft work and total system losses, of which runner losses is an important component. The system loss coefficient, k_{system} , in Eq. (6) is another internal variable of the propeller system.

$$gH = \Delta c_u \cdot u + h_{\text{losses}} = \Delta c_u \cdot u + k_{\text{system}} \cdot Q^2$$

$$= \Delta c_u \cdot u + k_{\text{system}} \cdot A^2 \cdot c_x^2 \quad (6)$$

(2) Speed, N : This independent variable can be studied with respect to the blade velocity (u), which finds a place in Eq. (5) as well as in Eq. (6).

2.3.1.3. Summary of the internal variables. The above methodology of expanding the three main variables (discharge, shaft power and head) identifies the internal variables as the mean axial flow velocity, net tangential flow velocity, relative exit flow angle, inlet vortex angle and system loss coefficient. The mean axial flow velocity and net tangential velocity classify as the internal dependent variables.

The next step would be to develop functional relationships for them and to identify independent or control variables that are mutually exclusive.

2.3.2. Functional relationship for the internal dependent variables

2.3.2.1. Mean axial flow velocity. Combining Eqs. (5) and (6), a second-degree polynomial for c_x can be developed and is represented by Eq. (7). If the tangential blade speed, available head and inlet swirl angle are kept constant, then c_x would depend only on k_{system} and β_3 . This is very important functional relation for analyzing the results of geometric changes to blades. The relative influences of k_{system} and β_3 can be obtained by performing sensitivity analysis on

$$k_{\text{system}} \cdot A^2 \cdot (c_x^2) + u \cdot (\tan \alpha_2 + \tan \beta_3) \cdot (c_x) - (gH + u^2) = 0 \quad (7)$$

$$c_x = f(k_{\text{system}}, \beta_3) \text{ given that } gH, u \text{ and } \alpha_2 \text{ are kept constant}$$

2.3.2.2. Net tangential flow velocity. Eliminating c_x from Eqs. (5) and (7), a relationship between Δc_u and the other variables can be determined as illustrated in Eq. (8). It can be seen that Δc_u will again remain a function of the two control variables of k_{system} and β_3 . The individual influences of these two control variables can be studied by carrying out a sensitivity analysis on Eq. (8).

$$\Delta c_u^2 \cdot (k_{\text{system}} \cdot A^2) + \Delta c_u \cdot u \cdot (2 \cdot k_{\text{system}} \cdot A^2 + (\tan \alpha_2 + \tan \beta_3)^2)$$

$$+ k_{\text{system}} \cdot A^2 \cdot u^2 - gH \cdot (\tan \alpha_2 + \tan \beta_3)^2 = 0$$

$$\Delta c_u = f(k_{\text{system}}, \beta_3) \text{ for constant } u, gH \text{ and } \alpha_2 \quad (8)$$

2.3.2.3. Overall functional relationship for the internal variables. Combining functional relationships for c_x and Δc_u , the internal functional relationship can be specified with k_{system} and β_3 as control variables, and c_x and Δc_u as dependent variables in Eq. (9). This relationship will be the basis of analyzing the hydraulic phenomenon within the runner.

$$c_x, \Delta c_u = f(k_{\text{system}}, \beta_3) \text{ for constant } u, gH \text{ and } \alpha_2 \quad (9)$$

2.3.3. Internal control variables

The internal functional equation given by Eq. (9) naturally calls for a better understanding of the two control variables namely, system loss coefficient and exit relative flow angle. It is important to show that these two variables are mutually exclusive. The inlet vortex angle is also a control variable, but it is considered as fixed variable in the present scenario and its effects will be discussed in Section 3.3.

2.3.3.1. System loss coefficient (k_{system}). The overall loss coefficient (k_{system}) as defined in the gross head parameter (in Eq. (6)) comprises of coefficients within different components of the turbine control volume like spiral volute, guide vane ring, zone between the guide vane exit and runner, runner and draft tube. To simplify the understanding of the system loss coefficient, a zonal approach is adopted.

The first zone is represented as upstream stationary zone comprising of the spiral volute, guide vanes and the space between guide vanes and the runner that transforms flow from radial to axial direction. The second zone is the runner while the stationary draft tube is treated as the third zone. The system loss coefficient can then be written as the sum of the loss coefficients in these three individual zones as shown in

$$k_{\text{system}} = k_{\text{upstream}} + k_{\text{runner}} + k_{\text{draft tube}}$$

$$k_{\text{system}} = k_{\text{turbine}} + k_{\text{draft tube}} \text{ where}$$

$$(k_{\text{upstream}} + k_{\text{runner}}) = k_{\text{turbine}} \quad (10)$$

2.3.3.1.1. Upstream stationary loss coefficient (k_{upstream}). This coefficient depends on the surface friction of the solid elements and also

on the flow interaction of different flow lines. These losses are represented by Eq. (11). Unfortunately, the present experimental test facility does not permit the determination of this loss component.

$$H_{\text{loss-upstream}} = k_{\text{upstream}} \cdot Q^2 \quad (11)$$

2.3.3.1.2. *Runner loss coefficient (k_{runner})*. The runner loss coefficient can be related to the pressure loss coefficient ζ as shown in Eq. (12). Physically, there is no difference between ζ and k_{runner} .

$$k_{\text{runner}} \cdot Q^2 = \zeta / 2 \cdot c_x^2 \quad (12)$$

The runner loss coefficient for axial blade profiles is generally evaluated using the cascade and wind tunnel approach as discussed in [8,10], where this coefficient is treated as a function of angle of incidence and flow separation effects. However, k_{runner} also depends on local boundary layers, which is influenced by geometry of blade passage, blade height (or d_h/D), blade number (or blade pitch to chord length ratio), blade chord length at different radial sections and other factors. The behaviour of the k_{runner} is quite complex and a detailed experimental analysis can reveal more information about the relative dependence of k_{runner} on the different parameters.

$$k_{\text{runner}} = f(\text{angle of incidence, flow passage geometry, blade height, blade number and others}) \quad (13)$$

2.3.3.1.3. *Draft tube coefficient ($k_{\text{draft tube}}$)*. The loss coefficient within the draft tube for a given diffuser design depends on swirl profiles of the absolute flow at runner exit (or draft tube entrance) and the local Reynolds number. The swirl flow has been studied by few scientists and has been shown in [14] that it mainly depends on the load condition (linked to the velocity triangle formation) for a given blade design. The blade angle at the exit could influence swirl flow behaviour and hence, the draft tube coefficient.

The draft tube losses can be determined from the exit swirl velocity and diffuser specification as shown in Eq. (14), which in turn helps in quantifying the overall draft tube coefficient.

$$\text{Draft tube losses} = k_{\text{draft tube}} \cdot Q^2 = c_{u3}^2 / 2g + \zeta_{\text{diffuser}} \cdot (1 - (d_3/d_4)^2)^2 \cdot c_{x3}^2 / 2g \quad (14)$$

2.3.3.2. *Relative flow angle at runner exit (β_3)*. The relative flow angle at runner exit depends solely on the energy mechanism within the runner and is very closely associated with the exit velocity triangle for any load (no-load, part-load, BEP and overload). The relative flow may be guided by the exit blade direction, but without any doubt the load condition decides the ultimate direction of the relative flow vector.

In addition, there is a complex slip mechanism (as reported by Cohrs [11] at the exit of pumps operating as turbines) taking place within the runner control volume. This slip (or deviation of the relative flow vector away from the exit blade direction) is governed by circulation within the blade passages and is dependent on the space between two consecutive blades, which is associated with blade number. The functional relationship of the relative flow angle can be grossly represented as,

$$\beta_3 = f(\text{load condition, slip effects, blade geometry}) \quad (15)$$

The relative flow angle in turn influences the absolute flow angle or swirl angle at exit and hence, the draft tube coefficient as discussed in Section 2.3.3.1.3. However, the influence of relative flow angle on the runner coefficient is very small since the governing physics of these two parameters are different, even though the same geometric modification influences both variables. Moreover, it is very difficult to determine how the relative flow angle can influence the runner loss coefficient.

From the above analysis, it is safe to consider the two control variables, runner loss coefficient (or system loss coefficient consid-

ering a relatively smaller influence of draft tube effects) and relative flow angle as separate and mutually exclusive.

2.4. Construction of velocity triangles

The construction of inlet and exit velocity triangles for actual operating conditions helps in establishing two important parameters namely, the angle of incidence (i) and the relative flow angle at the exit (β_3). As seen from Eqs. (13) and (9), both these angles are controlling the internal performance parameters. The velocity triangles are constructed only at the tip blade profile since the geometric conditions at the tip are known.

2.4.1. Inlet velocity triangle

The inlet velocity triangle can be constructed with the known inlet vortex angle, α_2 (refer Fig. 5), mean axial velocity c_x (obtained from the Eq. (2)) and tangential blade velocity, u (given the speed and tip diameter).

2.4.2. Exit velocity triangle

The important parameter to be determined for the construction of exit velocity triangle is the exit tangential flow velocity c_{u3} , which is obtained from Eq. (5) provided Δc_u and c_{u2} are known. Δc_u is obtained from Eq. (4) for a measured shaft power and mean axial velocity. The exit velocity triangle gives both the relative (β_3) and absolute flow (α_3) directions. It is important to note that the exit blade angle (β'_3) is not used for the construction of the exit triangle.

3. Means of solution

3.1. Experimental test-rig

The experimental test-rig for characterizing the propeller stages is shown in Fig. 2 and discussed in detail in [7]. The complete propeller unit comprising of runner, mechanical assembly and generator is shown in Fig. 3.

The test-rig facilitates the measurement of only main variables like gross head, discharge, output mechanical power and speed. However, internal parameters like swirl profiles at inlet and exit are not measured. Further, the dynamic head across the turbine stage is not determined. Instead, gross head comprising the difference of upstream and downstream elevations is used in the calculations.

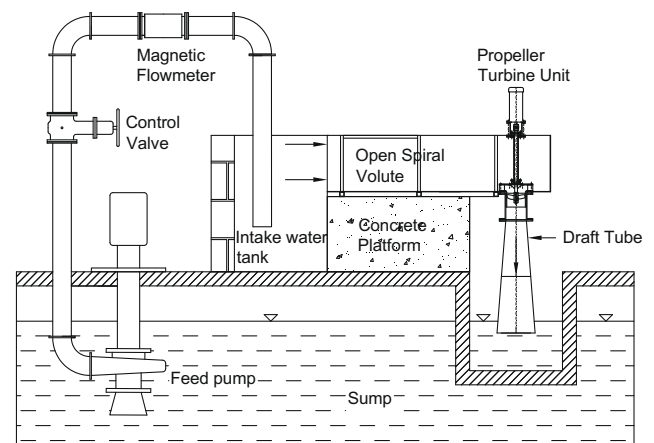


Fig. 2. The hydraulic test-rig for the propeller turbine.

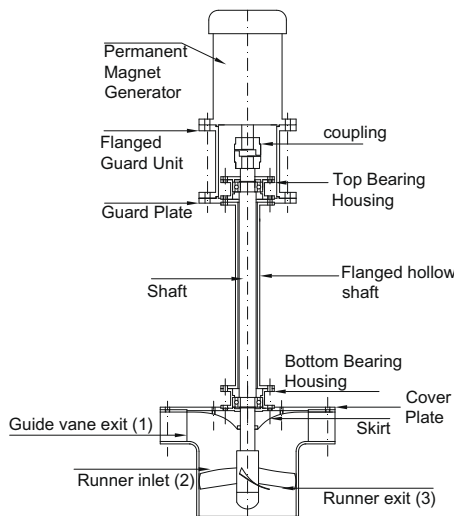


Fig. 3. Assembly of the propeller turbine unit.

3.2. Experimental runners

There are two experimental runners used in the study, whose hub to tip ratio, inlet vortex angle at the hub and tip along with blade number are summarized in Table 2. The details of modification to the blade exit are discussed in Sections 4.1–4.3 for the three runner stages. The pictures of runner A and runner B are illustrated in Figs. 6 and 13 respectively.

The extent of modification to runner exit tip for all the runner stages has been illustrated in Fig. 4. It can be seen that about 40% of the blade length along the exit edge has been altered while the remaining section of the blade length till the hub remains unchanged.

3.3. Absolute flow conditions between guide vane exit and runner inlet

Fig. 5 describes the absolute flow triangles at the guide vane exit, at the tip inlet and hub inlet of the experimental runner B,

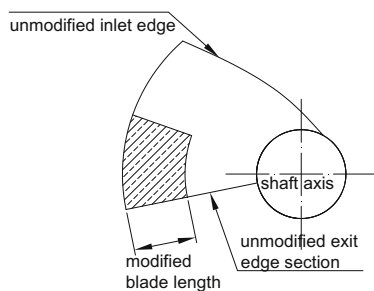


Fig. 4. The extent of exit tip modification along the blade length.

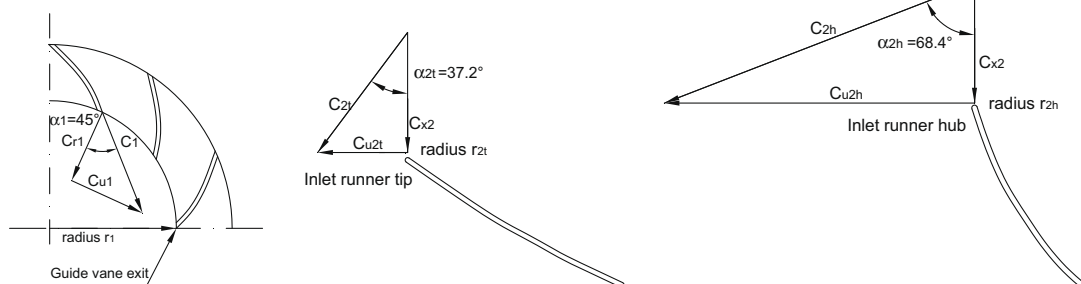


Fig. 5. Velocity triangles at the guide vane exit, inlet runner hub and inlet runner tip.

Table 2
Summary of the specifications of the experimental runners.

Parameters	d_h/D	α_{2h} (°)	α_{2t} (°)	z
Runner A	0.25	71.8	38.0	5
Runner B	0.3	68.4	37.2	5

developed using the continuity and the free vortex equation. This model assumes negligible deviation at the guide vane exit.

It can be seen that the absolute flow angle at guide vane exit is 45° and transforms to 37° at blade tip and 68.4° at blade hub respectively. The axial velocity has slightly increased from guide vane exit to runner inlet. It should be remembered that in reality there would a small radial component and secondary flows as well, which may actually disturb the axial flow pattern. But, in the current analysis, c_x is assumed to be constant from hub to tip. This is a reasonable assumption considering the pre-requisite of the free vortex theory is to have constant axial flow velocity. The inlet vortex angle, which is a fixed control variable in the present propeller runner analysis, can easily shown to be a function of the local diameter, the hub to tip ratio for a given guide vane design.

$$\alpha_2 = f(d, d_h/D) \text{ for a given guide vane design} \quad (16)$$

3.4. Analysis of the internal variables

The performance analysis between two optimization stages is carried out at a gross head of 1.75 m and a constant speed of 900 rpm, which includes the study of the behaviour of both the main and the internal variables using the theory in Section 2. This point is known as the ‘point of comparison’ and it may not be necessarily at the BEP. The percentage deviations of main variables are graphically read out from the constant head characteristics, which are related to the internal variables by the analytical equations (Eqs. (17)–(19)).

3.4.1. Internal dependent variables

- (a) Change in axial velocity, $\delta(c_x)$: from Eq. (2), it is seen that c_x is proportional to Q , hence, $\delta(c_x)$ is also proportional to $\delta(Q)$

$$\delta(c_x) \approx \delta(Q) \quad (17)$$

Physically, the change in axial velocity implies some change due to either k_{system} or β_3 or both as seen Eq. (7). The exact pattern of behaviour can be determined only by solving the quadratic polynomial in Eq. (7). However, sensitivity analysis can be performed on Eq. (7) between any two stages of optimization and the relative influences of k_{system} and β_3 can be obtained from the individual slopes $\partial(c_x)/\partial(k)$ and $\partial(c_x)/\partial(\beta_3)$ for fixed changes of k_{system} and β_3 .

(b) Change in net tangential flow velocity, $\delta(\Delta c_u)$: this component can be evolved from Eq. (4) and evaluated using experimental results of two stages, which is combined with the differential form of Δc_u (given by Eq. (8)) to determine the relative influences of k_{system} and β_3 , using individual slopes $\partial(\Delta c_u)/\partial(k)$ and $\partial(\Delta c_u)/\partial(\beta_3)$ for fixed changes of k_{system} and β_3 .

$$\delta(\Delta c_u) \approx |P_{shaft}/(\rho \cdot Q) \cdot u|_A - |P_{shaft}/(\rho \cdot Q) \cdot u|_B \quad (18)$$

3.4.2. Internal control variables

The change within the internal control variables at the 'point of comparison' can be evaluated from simple equations and velocity triangles.

(c) Change in system loss coefficient, $\delta(k_{system})$: this can be determined using the differential form of Eq. (6) as shown in Eq. (19). For the present scenario, the change in system loss coefficient is analyzed with respect to runner loss coefficient only without considering the effects in the draft tube and upstream stationary zones.

$$\delta(k_{system}) = |(gH - \Delta c_u \cdot u)/Q^2|_A - |(gH \Delta c_u \cdot u)/Q^2|_B \quad (19)$$

(d) Change in exit relative flow angle ($\delta\beta_3$) and angle of incidence at inlet (i_2) are determined from velocity triangles.

4. Results and discussion

4.1. Runner A: exit tip angle changed from 85° to 77°

This modification is illustrated in Figs. 6 and 7. It can be clearly seen that the decrease of exit blade angle opens up the exit flow area creating a decreased contraction effect from inlet to exit. The performance characteristics of the two stages are summarized in Fig. 8a and b, respectively. It can be observed that both power and discharge capacity of the modified exit stage has remarkably increased, while efficiency has consistently improved in the complete operating range.

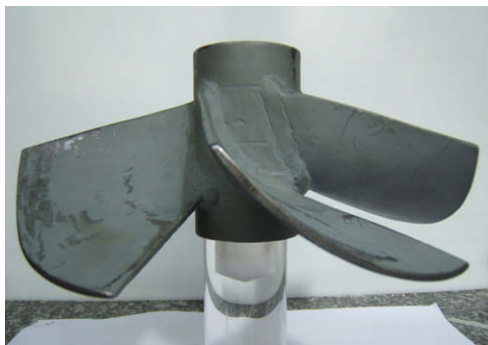


Fig. 6. Runner A with $\beta_{3t} = 85^\circ$

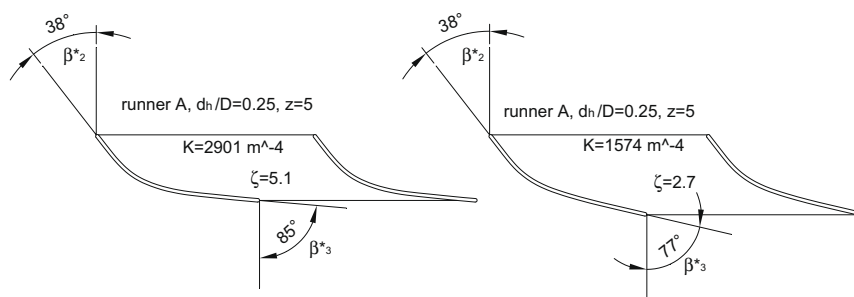


Fig. 7. Cascade for the exit tip modification stages of runner A ($\beta_{3t} = 85^\circ$ to 77°).

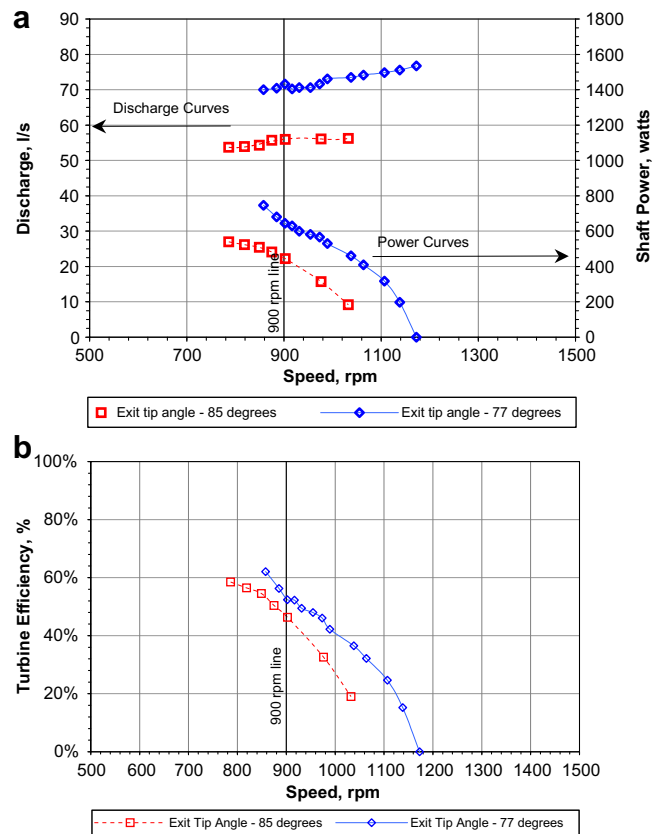


Fig. 8. (a) Discharge and power curves of runner A ($\beta_{3t} = 85^\circ$ to 77°). (b) Efficiency curves of runner A ($\beta_{3t} = 85^\circ$ to 77°).

The comparisons of main variables and the internal variables are carried out in Table 3. The output shaft power has increased by 45%, while discharge increased by 26% resulting in a 7.5% rise in efficiency. The velocity triangles are also plotted for both the stages in Fig. 9, and internal parameters like β_3 , Δc_u , c_x and α_3 along with their respective deviations are also illustrated in Table 3. The internal control parameter k_{system} has decreased by nearly 46%, while the other control parameter β_3 , has decreased by nearly 4° (4.5%) causing a decrease in c_x by 26% and an increase in Δc_u by 15.5%. The overall runner losses have also reduced by nearly 13%.

4.1.1. Discussion on the behaviour of internal control variables

4.1.1.1. Decrease of k_{system} . As discussed in Section 3.4.2, the change to the system loss coefficient will be analyzed from the perspectives of runner loss coefficient only. It is seen from Eq. (13) that the k_{runner} depends on the incidence, flow passage geometry and other effects. The incidence angle has changed only from -38° to -34° ,

Table 3
Percentage analysis of the major and minor variables of runner A ($\beta_{3t} - 85^\circ$ to 77°).

Modification stage	Summary of main variables								Summary of the internal variables											
	Control variables				Dependent variables				Independent variables					Dependent variables						
	H (m)	N (rpm)	Q (l/s)	δQ (%)	P (w)	δP (%)	η (%)	$\delta \eta$ (%)	k_{system} (1/m ⁴)	δk (%)	β_3 (°)	$\delta \beta_3$ (%)	c_x (m/s)	δc_x (%)	Δc_u (m/s)	$\delta \Delta c_u$ (%)	α_3 (°)	$\delta \alpha_3$ (%)	kQ^2 (m)	$\delta(kQ^2)$ (m)
$\beta_{3t} - 85^\circ$	1.75	900	56.0	+26.1	452	+45.6	47.0	+7.3	2901	-45.7	77.8	-4.5	1.90	+26.1	0.86	+15.5	18.3	+10.6	0.93	-13%
$\beta_{3t} - 77^\circ$	1.75	900	70.6		658		54.3		1574		74.3		2.40		0.99		20.2		0.80	

Table 4
Sensitivity analysis for changes to c_x and Δc_u on runner A ($\beta_{3t} - 85^\circ$ to 77°).

Overall change in δc_x (m/s)	δc_x due to k_{system}				δc_x due to β_3			
	$\partial(c_x)/\partial(k)$	δk (m ⁻⁴)	$[\delta c_x]_k$ (m/s)	% Contribution	$\partial(c_x)/\partial(\beta_3)$	$\delta \beta_3$ (Rads)	$[\delta c_x]_{\beta_3}$ (m/s)	% Contribution
+0.50	-5.4E-05	-1326	+0.07	15%	-6.97	-0.061	+0.42	85%
Overall change in $\delta \Delta c_u$ (m/s)	$\delta \Delta c_u$ due to k_{system}				$\delta \Delta c_u$ due to β_3			
	$\partial(\Delta c_u)/\partial(k)$	δk (m ⁻⁴)	$[\delta \Delta c_u]_k$ (m/s)	% Contribution	$\partial(\Delta c_u)/\partial(\beta_3)$	$\delta \beta_3$ (Rads)	$[\delta \Delta c_u]_{\beta_3}$ (m/s)	% Contribution
+0.13	-2.8E-04	-1326	+0.37	280%	+3.93	-0.061	-0.24	-180%

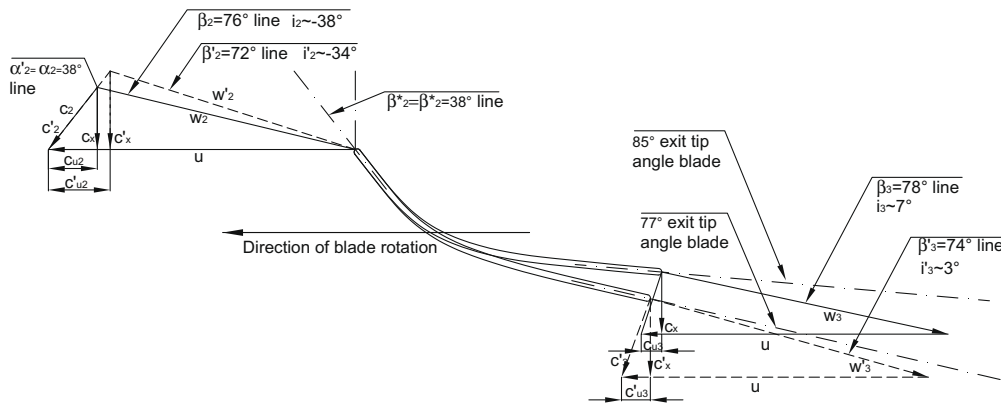


Fig. 9. Consolidated velocity triangles for the 85° and 77° exit tip angle stages of runner A.

which is definitely a positive effect on k_{runner} . But, the decrease of k_{runner} cannot be just due to this change of incidence. The passage between two blades has changed completely due to the decrease in blade angle. As seen from Fig. 7, the excessive blockade in the 85° exit tip stage has been reduced, which would definitely alter boundary layer formations decreasing the overall runner loss coefficient. It can be concluded from this brief discussion that the flow passage geometry has played a greater role in reducing k_{runner} compared to effects of incidence.

4.1.1.2. Decrease of β_3 . It has been seen from the analysis in Section 2.3.3.2 that β_3 is function of circulation within the passage and blade geometry for a given load. Further, it can be observed from Fig. 9 that the relative flow direction for the modified exit is coming closer to the exit blade angle and it is moving in a direction opposite to blade rotation (relative to the non-modified exit), which clarifies the influence of both slip and the new blade angle.

4.1.2. Discussion on the behaviour of internal dependent variables

4.1.2.1. Increase of c_x . The increase of axial velocity is a very interesting effect and can be attributed to independent influences from both the control variables. The sensitivity analysis in Table 4 reveals that increase in c_x is mainly coming from the 3.5° decrease in the β_3 . It is quite surprising that a large decrease in k_{runner} (by

over 46%) has contributed only to a 15% rise in c_x . The slope ($\partial \Delta c_u / \partial k$) is negative with a small magnitude, while slope ($\partial \Delta c_u / \partial \beta_3$) is also negative, but with a larger magnitude.

4.1.2.2. Increase of Δc_u . The sensitivity analysis carried out on Δc_u in Table 4, shows that the slope ($\partial \Delta c_u / \partial k$) is negative. Therefore, decrease in k_{system} (by 46%) has increased the Δc_u by 0.37 m/s. On the other hand the slope ($\partial \Delta c_u / \partial \beta_3$) is positive, which means that decrease in β_3 by 3.5° is causing the Δc_u to drop by 0.24 m/s. The net effect is that there is an overall rise in Δc_u by 0.13 m/s. This is a very important result on how the two control parameters (k_{system} and β_3) are affecting the net tangential flow velocity.

4.2. Runner A: exit tip angle changed from 77° to 74°

The cascade sections of the two stages are illustrated in Fig. 10. The performance comparisons in Fig. 11a and b reveal that the exit tip modification has enhanced both discharge and power in the complete operating range, but no change in efficiency curves. The main variables and internal variables have been compared in Table 5. It can be seen that the power has increased by 14% and discharge by 12% causing a marginal increase of efficiency. The internal control variable k_{system} has decreased by 22%, while the β_3 has fallen

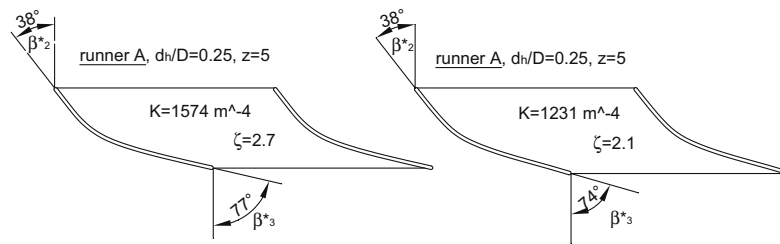


Fig. 10. Cascade for the exit tip modification stages in runner A ($\beta_{3t} - 77^\circ$ to 74°).

from 74.3° to 72° causing the c_x to increase by nearly 12% and Δc_u to increase by only 1.2%.

4.2.1. Discussion on the behaviour of internal control variables

4.2.1.1. Decrease of k_{system} or k_{runner} . It can be seen from Fig. 12, that the angle of incidence has changed only marginally from 34° to 32° . Hence, the 22% decrease of runner loss coefficient can be attributed to only the improved geometry of the flow passage.

4.2.1.2. Decrease of β_3 . The change of the relative flow angle from 74.3° to 72° , is moving closer to the modified blade angle and also in a direction opposite (relative to the non-modified exit) to the blade rotation. This effect can be attributed to both slip phenomena and the new exit blade angle.

4.2.2. Discussion on the behaviour of internal dependent variables

4.2.2.1. Increase of c_x . It is found from Table 6 that increase in c_x by 0.29 m/s is primarily arising from the changes to the β_3 rather than the changes to k_{system} . The decrease in β_3 is increasing c_x by 0.26 m/s (88% contribution), while the decrease of k_{system} is contributing only to the remaining 12% rise of c_x .

4.2.2.2. Increase of Δc_u . The Δc_u has only marginally increased. The sensitivity analysis in Table 6 reveals that change in k_{system} is increasing Δc_u by 0.15 m/s, while change in β_3 brings it down by 0.14 m/s and resulting in the rise of Δc_u by only 0.01 m/s. This again proves the contrasting influences of the control variables on Δc_u .

4.3. Runner B: exit tip angle changed from 75° to 70°

The exit tip modification is illustrated in Figs. 13 and 14. The comparison of the performance in Fig. 15a and b reveals an overall improvement in the efficiency characteristics, with increased power generation and greater flow capacities for the modified runner. In terms of relative performance as illustrated in Table 7, the power has gone up by 22%, while the discharge has increased by 20% resulting in a 2% rise in efficiency. The analysis further reveals that, as expected, the k_{system} and the β_3 have decreased. While the k_{system} has decreased by nearly 35%, the β_3 has dropped by 3%, resulting in the 20% rise in c_x and a modest 2.4% increase of Δc_u .

4.3.1. Discussion on the behaviour of internal control variables

4.3.1.1. Decrease of k_{system} or k_{runner} . As seen from the inlet velocity triangles plotted in Fig. 16, the incidence effect between the two stages is marginal (from 6° to 3°). Hence, this large change of k_{runner} can be mainly attributed to modification to the flow passage.

4.3.1.2. Decrease of β_3 . This change in β_3 is very interesting. It can be seen from Fig. 16 that relative flow direction is deviating away from the modified blade direction. Further, the deviation is in the direction of rotation of the blade. This is against the principles of

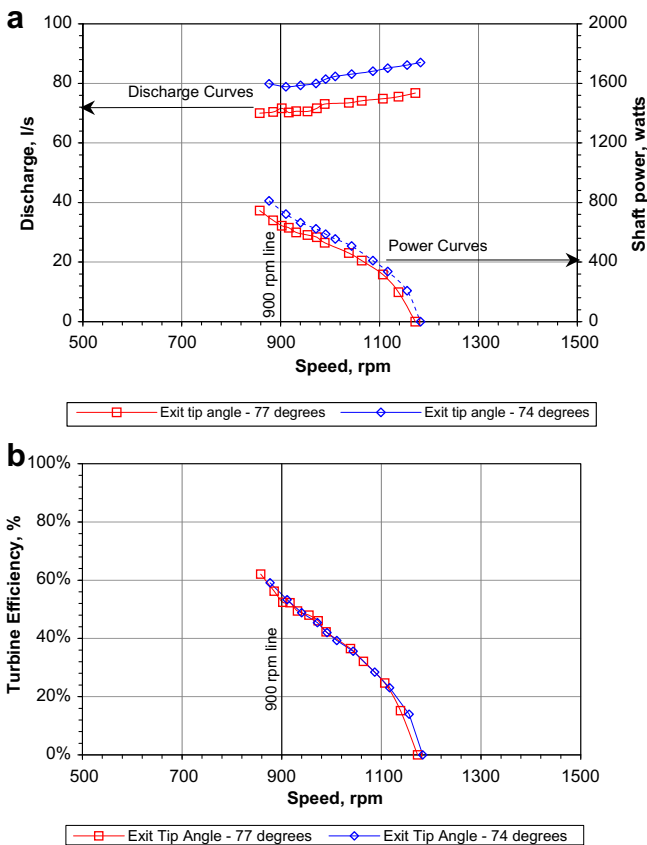


Fig. 11. (a) Discharge and power curves of runner A ($\beta_{3t} - 77^\circ$ to 74°). (b) Efficiency curves of runner A ($\beta_{3t} - 77^\circ$ to 74°).

Table 5 Percentage analysis of the major and minor variables of runner A ($\beta_{3t} - 77^\circ$ to 74°).

Modification stage	Summary of main variables								Summary of the internal variables											
	Control variables				Dependent variables				Independent variables					Dependent variables						
	H (m)	N (rpm)	Q (l/s)	δQ (%)	P (w)	δP (%)	η (%)	$\delta \eta$ (%)	k_{system} ($1/m^4$)	δk (%)	β_3 ($^\circ$)	$\delta \beta_3$ (%)	c_x (m/s)	δc_x (%)	Δc_u (m/s)	$\delta \Delta c_u$ (%)	α_3 ($^\circ$)	$\delta \alpha_3$ (%)	kQ^2 (m)	$\delta(kQ^2)$ (m)
$\beta_{3t} - 77^\circ$	1.75	900	70.6	+12.2%	658	13.7%	54.3%	+0.7%	1574	-21.8%	74.3	-3.0%	2.4	+12.2%	0.99	+1.3%	20.2	+9.8%	0.80	-1%
$\beta_{3t} - 74^\circ$	1.75	900	79.2		748		55.0%		1231		72.1		2.7		1.00		22.2		0.79	

Table 6
Sensitivity analysis for changes to c_x and Δc_u on runner A ($\beta_{3t} - 77^\circ$ to 74°).

Overall change in δc_x (m/s)	δc_x due to k_{system}				δc_x due to β_3			
	$\partial(c_x)/\partial(k)$	δk (m^{-4})	$[\delta c_x]_k$ (m/s)	% Contribution	$\partial(c_x)/\partial(\beta_3)$	$\delta\beta_3$ (Rads)	$[\delta c_x]_{\beta_3}$ (m/s)	% Contribution
+0.29	-1.1E-04	-343	+0.04	12%	-6.59	-0.039	+0.26	88%
Overall change in $\delta \Delta c_u$ (m/s)	$\delta \Delta c_u$ due to k_{system}				$\delta \Delta c_u$ due to β_3			
	$\partial(\Delta c_u)/\partial(k)$	δk (m^{-4})	$[\delta \Delta c_u]_k$ (m/s)	% Contribution	$\partial(\Delta c_u)/\partial(\beta_3)$	$\delta\beta_3$ (rads)	$[\delta \Delta c_u]_{\beta_3}$ (m/s)	% Contribution
+0.01	-4.6E-04	-343	+0.15	1185%	3.69	-0.039	-0.14	-1085%

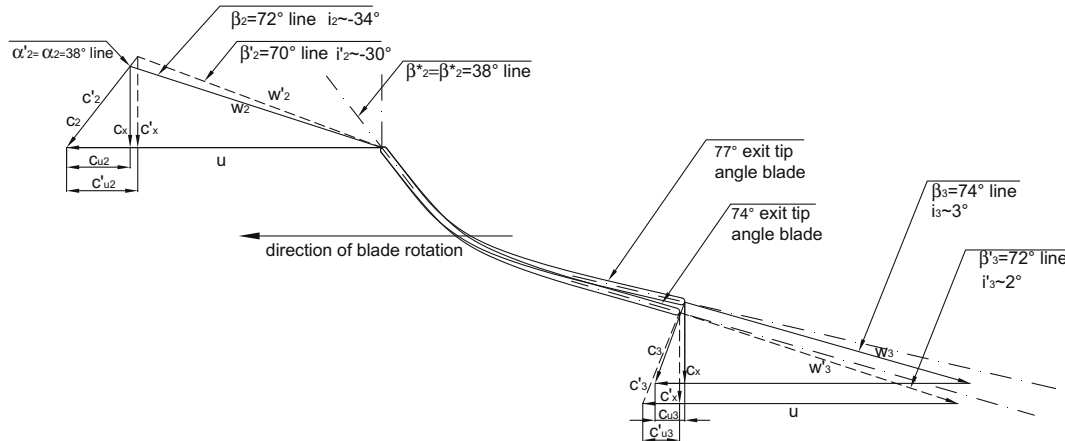


Fig. 12. Consolidated velocity triangles for the 77° and 74° exit tip angle stages of runner A.

Table 7
Percentage analysis of the major and minor variables of runner B ($\beta_{3t} - 75^\circ$ to 70°).

Modification stage	Summary of main variables								Summary of the internal variables											
	Control variables				Dependent variables				Independent variables					Dependent variables						
	H (m)	N (rpm)	Q (l/s)	δQ (%)	P (w)	δP (%)	η (%)	$\delta \eta$ (%)	k_{system} ($1/m^4$)	δk (%)	β_3 (°)	$\delta\beta_3$ (%)	c_x (m/s)	δc_x (%)	Δc_u (m/s)	$\delta \Delta c_u$ (%)	α_3 (°)	$\delta \alpha_3$ (%)	kQ^2 (m)	$\delta(kQ^2)$ (%)
$\beta_{3t} - 75^\circ$	1.75	900	56.8	+19.7	685	+22.6%	70.2	+1.8	1583	-34.2	77.8	-3.5	1.99	+19.7	1.28	+2.4	6.5	+80	0.52	-3%
$\beta_{3t} - 70^\circ$	1.75	900	68.0		840		72.0		1041		75.1		2.38		1.31		11.7		0.49	

slip phenomena. Therefore, the cause of this effect is difficult to ascertain.

4.3.2. Discussion on the behaviour of internal dependent variables
 4.3.2.1. Increase of c_x . The increase of c_x is solely coming from the changes to the β_3 and the influence of k_{system} on c_x is negligible as seen from Table 8.

4.3.2.2. Increase of Δc_u . It can be seen from Table 8 that the positive influence of k_{system} on Δc_u is slightly more than the negative impact of β_3 , resulting in a small increase of the net tangential velocity.

4.4. Swirl effect and draft tube losses

The draft tube losses for all the runner stages are compared in Table 9. Eq. (14) and the exit velocity triangles in Figs. 9, 12 and 16 are used to determine the loss components. It can be seen that the overall draft tube losses form a small component of the total losses. Further, between runner stages changes to the absolute losses is also observed. It has been seen that the draft tube losses have consistently increased following the exit tip modification. This result can be attributed to an increase in both the swirl velocity and the axial velocity of the modified runner.

More interestingly, the increase of draft tube losses would mean that the turbine losses (in the upstream stationary zone and the runner zone) have actually significantly decreased. This methodology could pave way for separating the draft tube loss coefficient from the system loss coefficient. However, it is clearly seen from Table 9 that the draft tube coefficient is rather small compared to the system loss coefficient and changes to its value between runner stages is minimal. These results clearly justify the methodology of attributing the changes in performance to runner effects only (as mentioned in Section 3.4.2).



Fig. 13. Runner B with ($\beta_{3t} - 70^\circ$)

Table 8
Sensitivity analysis for changes to c_x and Δc_u on runner B (β_{3t} – 75° to 70°).

Overall change in δc_x (m/s)	δc_x due to k_{system}				δc_x due to β_3			
	$\partial(c_x)/\partial(k)$	δk (m^{-4})	$[\delta c_x]_k$ (m/s)	% Contribution	$\partial(c_x)/\partial(\beta_3)$	$\delta \beta_3$ (Rads)	$[\delta c_x]_{\beta_3}$ (m/s)	% Contribution
+0.39	-6.1E-05	-542	+0.03	9%	-7.54	-0.048	+0.36	91%
Overall change in $\delta \Delta c_u$ (m/s)	$\delta \Delta c_u$ due to k_{system}				$\delta \Delta c_u$ due to β_3			
	$\partial(\Delta c_u)/\partial(k)$	δk (m^{-4})	$[\delta \Delta c_u]_k$ (m/s)	% Contribution	$\partial(\Delta c_u)/\partial(\beta_3)$	$\delta \beta_3$ (Rads)	$[\delta \Delta c_u]_{\beta_3}$ (m/s)	% Contribution
+0.03	-3.3E-04	-542	+0.18	567	+3.06	-0.048	-0.15	-467

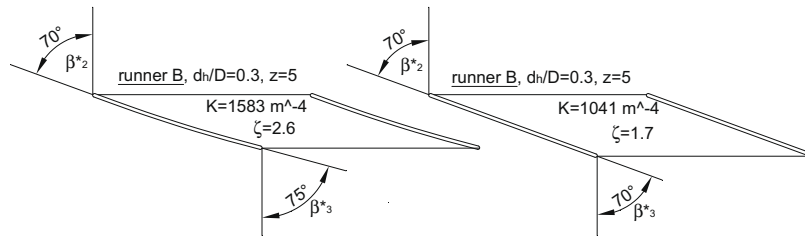


Fig. 14. Cascade for the exit tip modification stages in runner B (β_{3t} – 75° to 70°).

Table 9
Composition of draft tube losses in different runner stages.

Modification stage	H (m)	η_{hyd}	$H_{loss-system}$ (m)	c_{u3} (m/s)	$c_{u3}^2/2g$ (m)	c_{x3} (m)	$H_{loss-diffuser}$ (m)	$H_{loss-draft tube}$ (m)	$H_{loss.turbine}$ (m)	k_{system} (m^{-4})	$k_{draft tube}$ (m^{-4})	$k_{turbine}$ (m^{-4})	
Runner A	Exit tip angle – 85°	1.75	47.0	0.93	0.63	0.02	1.90	0.04	0.06	0.87	2901	178	2722
	Exit tip angle – 77°	1.75	54.3	0.80	0.88	0.04	2.40	0.06	0.10	0.70	1574	194	1381
Runner A	Exit tip angle – 77°	1.75	54.3	0.80	0.88	0.04	2.40	0.06	0.10	0.70	1574	194	1381
	Exit tip angle – 74°	1.75	55.0	0.79	1.10	0.06	2.69	0.07	0.14	0.65	1231	212	1020
Runner B	Exit tip angle – 75°	1.75	70.2	0.52	0.23	0.00	1.99	0.04	0.04	0.48	1583	130	1453
	Exit tip angle – 70°	1.75	72.0	0.49	0.49	0.01	2.38	0.06	0.07	0.42	1041	149	893

4.5. Comparisons with vortex runner

The comparisons are undertaken only for the runner B, since its tip geometry is reasonably similar to the free vortex design. Table 10 compares the performance of both the stages of runner B with the free vortex design. It can be seen that the free vortex head requirement of 1.42 m is not being met. This deviation could be attributed to larger inlet vortex angle of 37.2° of the experimental runners (as seen in Section 3.3) compared to the free vortex specification of 26.6°. The mean axial velocity of the 75° exit tip angle stage is below that of the free vortex runner, while discharge of the 70° exit tip is comparable.

The other reason for this deviation could be due to the fact that the comparisons have not been made at the BEP. However, as seen from the characteristics, the probable BEP of the two runner stages would have lower operating speed compared to 900 rpm and a slightly lower discharge at the same head of

1.75 m. This would decrease the specific speeds of the experimental runners further and the deviations with free vortex runner would still hold.

On the whole, the non-matching of the specific speeds is primarily attributed to the higher head requirement. It would be an important step to consider a change to the guide vane design and evaluating if the free vortex specifications can be achieved.

4.6. Limitations of the theoretical model

The possible errors in the model need to be analyzed, since important conclusions have been interpreted from this model. A free vortex flow characteristics is assumed between the guide vane exit and runner inlet. It can be seen from Fig. 3 that the flow changes from radial to axial direction in a relatively short length. The prime criterion for the validity of free vortex flows is radial

Table 10
Comparison of the runner B stages with the free vortex specifications.

Runner type	N (rpm)	H (m)	c_x (m/s)	α_2	c_{u2} (m/s)	c_{u3} (m/s)	Δc_u (m/s)	η_m (%)	Specific speed (rpm)
Free vortex runner, $\beta_2^* - 74^\circ \beta_3^* - 76^\circ$	900	1.42	2.36	26.6°	1.18	0.00	1.18	80.0	138
Runner B, $\beta_2^* - 70^\circ \beta_3^* - 75^\circ$	900	1.75	1.99	37.2°	1.51	0.23	1.28	70.2	93
Runner B, $\beta_2^* - 70^\circ \beta_3^* - 70^\circ$	900	1.75	2.38	37.2°	1.80	0.49	1.31	72.0	101

equilibrium and constant axial velocity. It is difficult to imagine a zero radial flow component in reality. These deviations would naturally affect the inlet vortex angle predictions, and the shape of inlet velocity triangles.

The other source of error could come from the fact that the entire conclusions are based on velocity triangles at the blade tip. It would be interesting to repeat the analysis at different sections along the blade length. Further, the leakage losses have not been considered in the model, which is reasonable since only relative changes are being analyzed.

4.7. Limitations of the experimental study

As discussed in Section 3.1, the test-rig is not being able to measure the net or dynamic head across the runner. The dynamic head

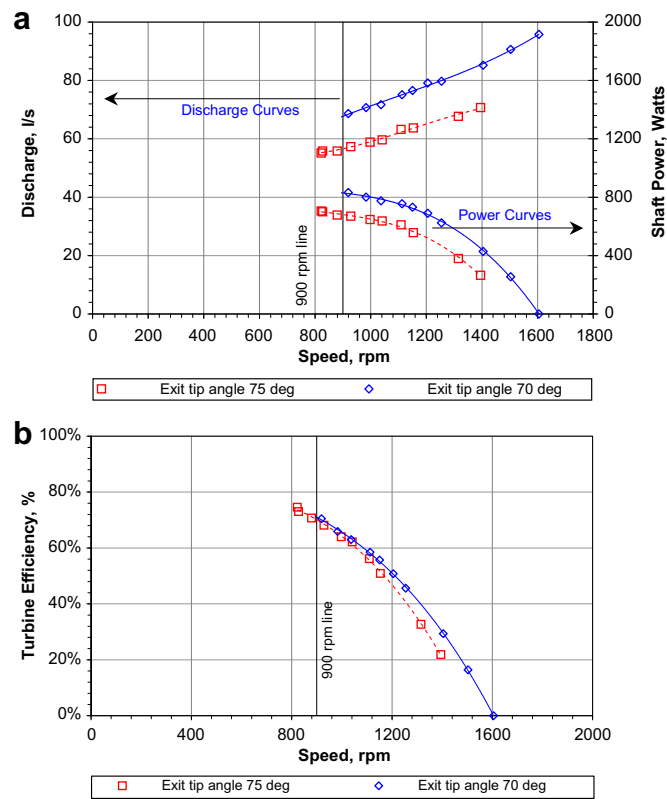


Fig. 15. (a) Discharge and power curves of runner B ($\beta_{3t}^* - 75^\circ$ to 70°). (b) Efficiency characteristics of runner B ($\beta_{3t}^* - 75^\circ$ to 70°).

would be of great value, as the losses would then comprise of runner losses alone and eliminating the probable draft tube effects in the analysis. The determination of runner losses would guide the internal hydraulic study more accurately with respect to the runner loss coefficient rather than the system loss coefficient, which includes other hydraulic loss coefficient within the draft tube amongst others.

In addition, the swirl flow profiles at the upstream and downstream of the runner will also be very useful to validate the free vortex assumptions before the runner inlet and also confirm deviation/slip at the exit respectively.

Further, it can be seen that comparisons have been carried out at points that do not correspond to the BEP of the respective runners. It is known that meaningful study of geometric effects can be determined at the BEP. Nevertheless, the present analysis based on 'point of comparison', which is still in the part-load region is technically correct. This is so because the analysis takes place at a fixed load condition (defined by the control variables-gross head and speed) for both runner stages.

Moreover, the comparison at this point is also meaningful as seen in Appendix A.2 (that brings out a case study on 'pump as turbine optimization'), which shows that the hydraulic behaviour brought about at the 'part-load point' is similar to the that at the BEP and overload points provided the trend lines of the discharge and power curves at constant head of the given runner stage do not intersect their counterparts of the modified stage.

5. Conclusions and recommendations

The preliminary study concluded that while the free vortex design provided the layout for the blade profiles, it did not however specify how the blade angles would influence the performance, which initiated research on evaluating the influence of the exit blade tip.

The theoretical model developed to investigate the internal runner parameters was very useful and brought about functional relationships for these parameters. While the model identified system loss coefficient (or runner loss coefficient) and relative exit flow angle as the primary control variables, it specified mean axial flow velocity and the net tangential flow velocity as the dependent variables. The methodology sensitivity analysis helped in understanding the relative influences of the control variables on the dependent variables.

The results of exit tip modification on all the three runner stages consistently showed that the reduction of the exit tip blade angle increased flow and output shaft power, and positively affecting the efficiency at constant speed and head conditions in the part-load operating condition. With respect to internal flow variables,

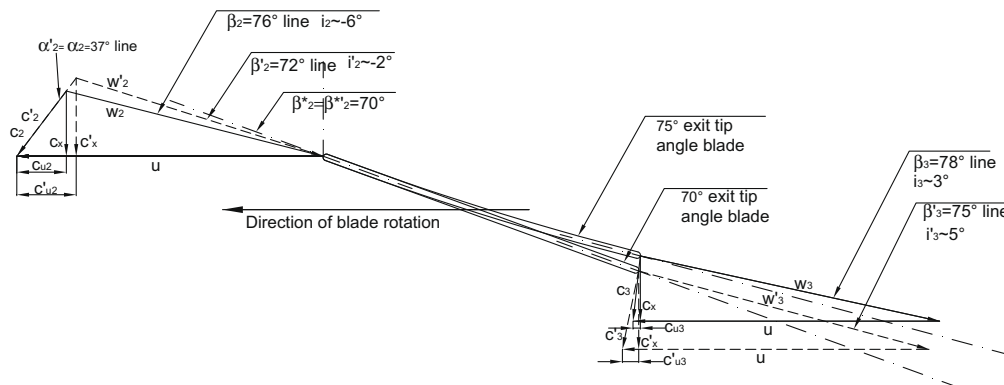


Fig. 16. Consolidated velocity triangles for the 75° and 70° exit tip angle stages of runner B.

it was found that the runner loss coefficient for the modified exit stage decreased considerably owing to the opening of the flow passage rather than the incidence effects. The other significant control parameter, the relative exit flow angle for the modified exit stage showed tendencies to deviate in a direction opposite to blade rotation, which proved the influence of both slip and exit blade angle. However, the relative flow direction for one exit tip modification stage deviated in the direction of blade rotation, which was contrary to the slip phenomena.

The influence of these control parameters on the runner's internal dependent variables was very significant. The increase of mean axial velocity (or discharge) was found to be mainly influenced by the decrease of relative flow angle rather than by the decrease of the runner loss coefficient. On the other hand the net tangential flow velocity was influenced by two control parameters in starkly different ways. While decrease in runner loss coefficient caused the net tangential flow velocity to increase, the decrease relative flow angle caused the net tangential flow velocity to decrease. Both these effects nearly cancelled each other with the runner loss coefficient effect slightly outweighing that of the exit relative flow angle causing the tangential flow velocity to slightly rise.

On the whole, the decrease of the exit tip angle has had a positive effect on the runner performance and this technique can be conveniently used to increase discharge and power through the turbine for the same head without any compromise in efficiency. Thus, this modification can play a role in matching system boundary conditions, if needed.

It could be concluded from the draft tube analysis that the draft tube loss coefficient (comprising of the swirl and diffuser effects) for all the stages was insignificant compared to the system loss coefficient and that major transformation of losses occurred in the turbine zone (upstream stationary and runner zones) only.

It was also found that free vortex conditions could not be realized for any of the runner stages for reasons of non-matching of the inlet vortex angle requirement. It is, therefore, recommended to study the performance of these runners under varying vortex flow conditions by incorporating adjustable guide vanes. This study would enhance the scope of runner application under different combinations of flows.

Ultimately, the complete analysis of exit blade modification was carried out at part-load point that did not correspond to the BEP. Even though it was shown that there would some similarity between the behaviour at part-load and BEP, it is still desirable to carry out analysis at the BEP.

It has also been noticed that there are some limitations in the theoretical model adopted pertaining to the assumptions of the upstream flow conditions. This calls for a stronger need to enhance the experimental setup and study the actual flow condition (velocity and angle) at the upstream and downstream of the runner in order to take corrective measures. The other issue that is recommended for future study is that of slip, which underlines

the importance of relative exit flow angle as controlling parameter. The slip effect can be studied by determining the exit swirl angle across the blade profile along with the help of available slip models.

While furthering experimental investigation is vital for an accurate optimization study, the theoretical model should also be simultaneously validated using well-calibrated CFD techniques. It is important to continue the combined experimental and computational study in order to scrutinize the theoretical model further and make accurate system design tools. This tool should comprise accurate models that characterize the behaviour the control variables (runner loss coefficient and relative exit flow angle) for different geometries of exit blade angle. The pattern of behaviour of these control variables will then enable the determination of other internal variables (internal like mean axial velocity and net tangential velocity) and main variables (discharge, shaft power and efficiency). This kind of system design tool will come in a long way to enable an optimum and sustained solutions for low-head micro-hydro propellers.

Acknowledgements

The authors would like to acknowledge the contributions of Erfried Berger, Boris Lehmann, Frank Seidel, Gerard Close, Günther Kühn, Manfred Lösche, Marcus Plate, Martin Gabi, Michael Ritzmann, Michael Ziegler, Jürgen Ullrich, Peter Oberle, Ramesh, Ravichandran, Saban Caglar, Werner Helm and many others without whom the work of propeller research would not have been accomplished.

Appendix A

A.1. Experimental uncertainty analysis

The overall uncertainty analysis is carried out using the 'single sample study' proposed by Moffat [12] and Kline [13] at various 'points of comparison' for the different runner stages (as in Sections 4.1–4.3) and summarized in Table A1. The evaluation combines the results from two separate test-rigs namely, generator test-rig used for characterizing the generator and turbine test-rig used to study the complete turbine-generator unit. The overall random error for all the variables is summarized in Table A2.

Table A2
Maximum random error for each variable.

ΔV (V)	ΔI (A)	ΔN (rpm)	ΔT (Nm)	ΔQ (l/s)	ΔH (m)
±0.1	±0.1	±1	±0.1	±0.1	±0.005

Table A1
Uncertainty table for all the runner stages.

Runner	Optimization stage	Generator parameters										Turbine parameters									
		V	$\Delta V/V$ (%)	I (%)	$\Delta I/I$ (%)	N (%)	$\Delta N/N$ (%)	T (%)	$\Delta T/T$ (%)	η_g (%)	$\Delta \eta_g/\eta_g$ (%)	$\Delta P_m/P_m$ (%)	P_m (%)	Q (%)	$\Delta Q/Q$ (%)	H (%)	$\Delta H/H$ (%)	η_m (%)	$\Delta \eta_m/\eta_m$ (%)	$\Delta \eta_m$ (%)	
Runner A	85° Exit tip	100.0	±0.1	3.5	±2.9	900	±0.1	4.8	±2.1	77.4	±3.5	±4.6	452	56.0	±0.2	1.75	±0.3	47.0	±4.6	±2.1	
	77° Exit tip	90.0	±0.1	5.3	±1.9	900	±0.1	7.0	±1.4	72.5	±2.4	±3.0	658	70.6	±0.1	1.75	±0.3	54.3	±3.1	±1.7	
Runner A	77° Exit tip	90.0	±0.1	5.3	±1.9	900	±0.1	7.0	±1.4	72.5	±2.4	±3.0	658	70.6	±0.1	1.75	±0.3	54.3	±3.1	±1.7	
	74° Exit tip	85.5	±0.2	6.2	±1.6	900	±0.1	7.9	±1.3	70.4	±2.1	±2.6	748	79.2	±0.1	1.75	±0.3	55.0	±2.6	±1.5	
Runner B	75° Exit tip	88.2	±0.1	5.8	±1.7	900	±0.1	7.3	±1.4	74.7	±2.2	±2.8	685	56.8	±0.2	1.75	±0.3	70.2	±2.8	±2.0	
	70° Exit tip	81.0	±0.1	7.0	±1.4	900	±0.1	8.9	±1.1	67.5	±1.8	±2.3	840	68.0	±0.1	1.75	±0.3	72.0	±2.3	±1.7	

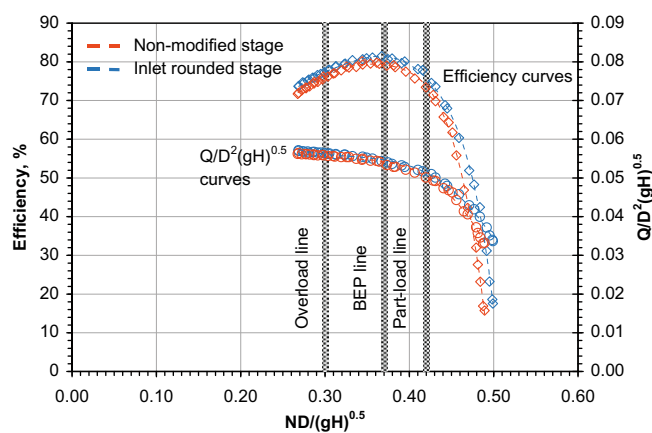


Fig. A1. Effects of inlet rounding: Comparison of the discharge and efficiency characteristics for the 35.3 rpm PAT.

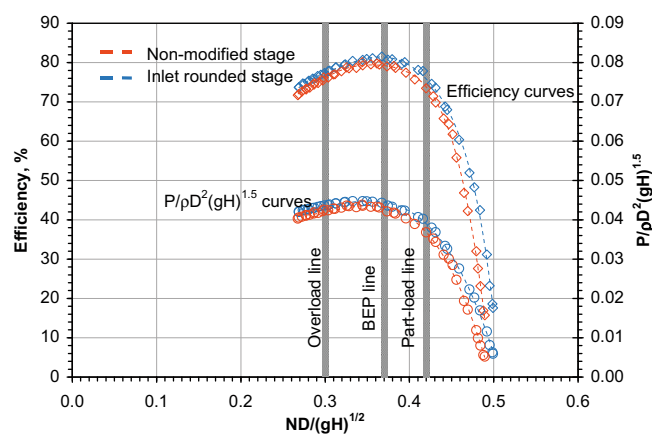


Fig. A2. Effects of inlet rounding: Comparison of the power and efficiency characteristics for the 35.3 rpm PAT.

A.2. Connecting the performance at part-load, BEP and overload points in a turbine

The objective of this section is to show that there is some similarity of the hydraulic effects at the different operating points of a turbine undergoing geometric optimization. Experimental results of an optimization study in pumps as turbines [14] will be used for this purpose. The hydraulic effects include change of discharge, change of shaft power and change of efficiency at constant speed conditions, similar to the hydraulic analysis carried in the propeller turbine optimization study and sensitive analysis in the current manuscript.

Table A3
Analysis of the performance at part-load, BEP and overload points.

Operating point	Unit speed	Unit discharge	% Change in discharge	Unit power	% Change in power	Efficiency	Change in efficiency (%)
Part-load	0.42	0.0500	+2.4	0.0408	+3.4	74.0	+2.0
		0.0512		0.0422		76.0	
BEP	0.37	0.0542	+0.9	0.0434	+2.8	79.1	+2.4
		0.0547		0.0446		81.5	
Overload	0.30	0.0556	+0.7	0.0420	+2.9	76.0	+1.5
		0.0560		0.0432		77.5%	

A.2.1. Hydraulic analysis of operating points in 'pumps as turbines'

This section presents experimental data of the 'inlet runner rounding' optimization stage of a 35.3 rpm PAT as discussed in [14]. Figs. A1 and A2 show the operating characteristics of the non-modified and inlet impeller rounded stage. Three different operating points (defined by the unit speed) that characterize the part-load, BEP and overload regions of the characteristics are analyzed in both the figures as well as in Table A3.

At the part-load unit speed, it is found that the inlet rounding has caused the discharge to increase by 2.4% and the power to increase by 3.4%. The effect of the increased power compared to effect of increased discharge results in an approximate increase in efficiency of 2%. The hydraulic effect at the BEP is quite similar to that of the part-load point, in that the increase of shaft power is maintained at around 3%, while increase of discharge is slightly lower at 0.9%. However, in terms of internal hydraulic effects on parameters like runner loss coefficient and net tangential flow velocity, they are essentially similar. The analysis at the overload point is also found to be similar to that at the BEP.

These findings are important to point out that the change in performance at the part-load is not mutually exclusive to that in the other regions of the characteristics like the BEP and overload conditions. There is a hydraulic similarity of flow phenomenon at these points, which must be recognized.

A.2.2. Relevance of the findings of 'pumps as turbines' to 'propeller turbines'

It can be argued that the hydraulic effects at different operating points of the characteristics depend on the type of modification carried out. This may be true to a certain extent. But, the most important observation to be made from the 'pump as turbine' optimization in Section A.2.1 is that there was no intersection of the unit discharge or the unit power curves of the two stages, which is one of the reasons of the repetitive behaviour of the hydraulic effects.

A closer look into all the optimization stages of the propeller runners in the manuscript (Fig 8a and b, Fig 11a and b, Fig 15a and b) will reveal that respective discharge and power curves for the two stages are separated well from each other and there is no possibility of intersection in the BEP or overload region. Even if an extrapolation was to be carried out, the trend of the curves are such that intersection is ruled out.

In light of the above, it can be confidently interpreted that hydraulic effects due to the exit angle modification of runner tip would be similar at the BEP and part-load points. The magnitude of the relative changes (on a percentage scale) of discharge and power numbers may be different at these two points, but there will be similitude in terms of the changes to performance, i.e. change of discharge will always be positive and change of power will also be positive. This has been consistently seen in the test results of the three runner stages presented in the manuscript.

References

- [1] G.J. Rao, R. Prasad, J.K.S. Rao, Investigation of an axial flow runner for micro hydro power development, In: Proceedings of 8th Fluid Machinery Conference, Budapest, Hungary, 1988, pp. 616–623.
- [2] S. Soundranayagam, A. Suryanarayanan, Ultra Low-head Propeller Turbines for Small Canal Drops, Turbomachines Laboratory Report, Indian Institute of Science, Bangalore, India, 1988.
- [3] G.M. Demetriades, Design of Low-cost Propeller Turbines for Standalone Micro-hydroelectric Generation Units, Ph.D. Thesis, University of Nottingham, United Kingdom, 1997.
- [4] D. Upadhyay, Low Head Turbine Development Using Computational Fluid Dynamics, Ph.D. Thesis, University of Nottingham, United Kingdom, 2004.
- [5] R.G. Simpson, A.A. Williams, Application of computational fluid dynamics to the design of pico propeller turbines, In: Proceedings of the International Conference on Renewable Energy for Developing Countries, 2006.
- [6] K.V. Alexander, E.P. Giddens, A.M. Fuller, Axial-flow turbines for microhydro systems, *Journal of Renewable Energy* 34 (2009) 35–47.
- [7] P. Singh, F. Nestmann, Experimental optimization of a free vortex propeller runner for micro hydro application, *Journal of Experimental Thermal and Fluid Science* 33 (2009) 991–1002.
- [8] S.L. Dixon, *Fluid Mechanics and Thermodynamics of Turbomachinery*, Elsevier, Oxford, UK, 2005 (Chapters 2, 6 and 9).
- [9] C. Pfeleiderer, H. Petermann, *Strömungsmaschinen*, Springer-Verlag, 1964 (Chapter 1).
- [10] N. Watson, M.S. Janota, *Turbocharging of the Internal Combustion Engine*, The Macmillan Press, 1982 (Chapter 5).
- [11] D. Cohrs, Untersuchungen an einer mehrstufigen rückwärtslaufenden Kreiselpumpe im Turbinenbetrieb, *Verlag und Bildarchiv, W.H. Faragallah*, 1997. pp. 8–41.
- [12] R.J. Moffat, Contributions to the theory of single-sample uncertainty analysis, *Journal of Fluids Engineering* (1982) 250–260.
- [13] S.J. Kline, The purposes of uncertainty analysis, *Journal of Fluids Engineering* (1985) 153–160.
- [14] P. Singh, Optimization of the Internal Hydraulics and of System Design for Pumps as Turbines with Field Implementation and Evaluation, Ph.D. Thesis, University of Karlsruhe, Germany, 2005, pp. 76–84.
- [15] Asian Pheonix Resources Ltd. (APRL), *Powerpal Brochure*, 2001, <<http://www.powerpal.com>> (accessed .02.09).



Contents lists available at ScienceDirect

Renewable Energy

journal homepage: www.elsevier.com/locate/renene

Experimental investigation of the influence of blade height and blade number on the performance of low head axial flow turbines

Punit Singh*, Franz Nestmann

Institute for Water and River Basin Management (IWG), University of Karlsruhe, Kaiser Str. 12, D 76128, Karlsruhe, Germany

ARTICLE INFO

Article history:

Received 1 March 2010

Accepted 23 June 2010

Available online 24 July 2010

Keywords:

Micro-hydro

Propeller runner

Blade height

Blade number

Relative flow angle

Runner coefficient

ABSTRACT

Investigations regarding the influence of design parameters in low head axial flow turbines like blade profiles, blade height and blade number for micro-hydro application continue to be inadequate, even though there is a need and potential for the application of such turbines. This inadequacy provides a good ground to make a detailed experimental study to characterize these influences.

The paper presents a holistic theoretical model that attempts to bring out a functionality of the internal performance parameters of the runner and attempts to establish a physical relationship between the two design parameters (blade height and blade number) and the performance parameters.

The experimental results on 3 runners showed that with an increase in the number of blades, the efficiency of the runner dropped drastically due to the change in direction of the relative flow vector at the runner exit, which decreased the net rotational momentum and increased the axial flow velocity. The decrease of blade height on the other hand decreased the overall runner loss coefficient quite drastically but this could not result in major performance gains.

The study concluded that the influence of blade number is more dominating compared to that of the blade height and that choice of blade number should be carefully made. On the hydraulic level, the study found interesting effects like the slip phenomenon and loss mechanisms within the runner. The paper also looks into the possible errors within the theoretical model developed and the extent of their influence on the conclusions. The paper suggests more experimental studies to separately study the effects of blade number and blade height. It further makes a strong case to initiate a computational work to validate all the experimental findings, fill the gaps in the theoretical model and use it as an optimization and standardization tool for axial flow turbines in the specialized application of micro-hydro.

© 2010 Elsevier Ltd. All rights reserved.

1. Introduction

1.1. Background

The overall research and development of low head axial flow turbines of micro-hydro application has been limited. Further, the optimization studies of the design parameters like blade profiles, blade number, blade height (or hub to tip ratio) and others have been even more scarce.

The focus of the major scientific community is on large axial flow turbines, where the design and operating requirements are completely different. In the special context of micro-hydro, the optimization study becomes extremely important because of

challenging boundary conditions, like large variation of flow and yet optimum power generation, notwithstanding the economic constraints that emphasize on simplicity of design and manufacture. Hence, there is need for an all-together different approach for the optimization study where experimentation will be the central theme.

In the recent years there has been a revival of interest of micro-hydro propellers from few researchers like Rao et al. [1], Soundar-nayagam and Suryanarayanan [2], Demitriades [3] and APRL [17] who all focused on developing the runner designs and evaluating their performance. Upadhyay [4] carried out some hydraulic optimization using computational models, while Simpson and Williams [6] employed blade optimization for a field project, but did not analysis of the results with respect to the geometric modification. A notable contribution comes from Alexander et al. [5], who prescribed standard designs of few propeller runners, however they too did not report any kind of optimization. Singh and Nestmann [7] demonstrated how the efficiency of a low head propeller runner could be improved to ideal free vortex conditions by carrying out a series of optimization on the inlet and exit blade geometry.

Abbreviations: BEP, Best Efficiency Point; CFD, Computational Fluid Dynamics.

* Corresponding author.

E-mail addresses: punit.singh@iwg.uka.de (P. Singh), nestmann@iwg.uka.de (F. Nestmann).

Nomenclature		Greek symbols	
<i>Full Scripts</i>		η	efficiency, %
c	absolute velocity, m/s	ρ	density, kg/m ³
d	local diameter, m	α	absolute flow angle, degrees
D	tip diameter, m	β	relative flow angle, degrees
g	acceleration due to gravity, m/s ²	ζ	pressure loss coefficient
H	head parameter, m	<i>Subscripts</i>	
i	angle of incidence, deg	1	guide vane exit
I	current, amps	2	runner inlet
l	blade chord length	3	runner exit
m	mass flow rate, kg/s	g	generator
N	speed, rpm	h	hub region
P	power, kW	m	mechanical
Q	discharge, l/s or m ³ /s	t	tip region
s	blade pitch	u	tangential component
T	torque, Nm	x	axial direction
u	tangential blade velocity, m/s	<i>Superscripts</i>	
V	voltage, volts	*	blade condition
w	relative velocity, m/s		
z	blade number		

Some special design parameters like blade number and blade height have not been elaborately studied at an experimental level and hence the designer has to rely on correlations available for large axial flow turbines (as in [10]) used in the gas turbine applications. Some correlations for hydro turbines are also available in Nechelba [14] and Hothersall [15], but without any experimental proof of their influences. This inadequacy gives sufficient reason to study the accurate influences of these two parameters (blade number and blade height), with an objective to bring out optimum solutions and standardization of axial flow turbine designs for micro-hydro application.

1.2. Objectives and problem outline

- To develop a theoretical model that develops an overall functionality of all the internal hydraulic variables of the propeller runner control volume and tries to physically relate the two design parameters namely, the blade number and the blade height with these variables.
- To design propeller runners with varying blade number and blade heights, but having approximately identical blade profiles and to test them experimentally under similar boundary conditions.
- To use the theoretical model along with experimental results and establish exact influences of the two design variables.
- To evaluate the limitation of the theoretical model and identify the sources of errors and how they would affect the results, and further to recommend alternative methods for studying these effects.
- To determine if these design parameters can be used for optimum matching of system boundary conditions.

2. Theoretical model

2.1. Main variables and functionalities in propeller turbines

The functionality of the main variables of a hydro turbine control volume can be represented by Eq. (1), which classifies the speed and the available head as the independent or control variables and the discharge, shaft power and overall efficiency as the dependent variables.

$$Q, P_{\text{shaft}}, \eta = f(N, gH) \quad (1)$$

2.2. Internal variables and functionalities

The classification of internal variables and their functionalities is done by defining and expanding the main variables without changing the functionality of Eq. (1). The classical velocity triangles along with the cascade approach are then utilized to develop a deeper understanding of the physical significance of the internal variables in the context of propeller geometry. A typical inlet and velocity triangle for a low-pressure axial stage is shown in Fig. 1 at the tip blade profile.

2.2.1. Specifying the internal variables

- Discharge (Q):** The discharge is a dependent variable as seen from Eq. (1) and is given by the mean axial flow velocity and the flow area in Eq. (2). If the diameter (D) is taken as an independent geometric variable and the blade height parameter (hub to tip ratio, d_h/D) taken as a design variable, then the axial flow velocity (c_x) becomes a function of both Q and d_h/D and can be taken as internal dependent variable. The d_h/D is treated as an internal control variable, whose effects are analyzed in this paper.

$$Q = c_x \cdot \left(\pi \cdot D^2 / 4 \right) \cdot \left(1 - (d_h/D)^2 \right) \quad (2)$$

$$c_x = f(Q, d_h/D)$$

- Shaft Power, P_{shaft} :** Based on the Euler turbine fundamentals discussed by Pfleiderer [9] and Dixon [8], the shaft power, which is a mechanical quantity is completely represented by the Euler momentum, $\Delta c_u \cdot u$ and leakage flow losses as shown in Eq. (3).

$$P_{\text{shaft}} = m \cdot (\Delta c_u \cdot u) - \text{leakage losses} \quad (3)$$

If leakage effects are neglected especially while comparing two optimization stages of the runner, the shaft power's proportionality can be represented by Eq. (4). The net tangential flow velocity, Δc_u , is a very important parameter, which represents the energy

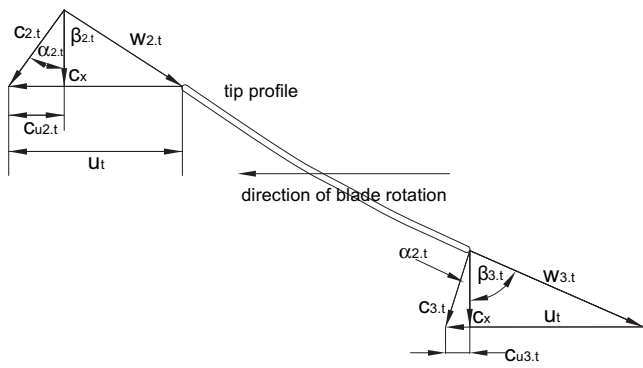


Fig. 1. Typical velocity triangles of a low-pressure axial turbine at the runner hub and tip.

transfer or rotational momentum. For a given blade velocity and tip diameter, Δc_u becomes a function of the dependent variable P_{shaft} and the d_h/D , and can be termed as an internal dependent variable.

$$P_{\text{shaft}} \approx (\rho \cdot Q) \cdot (\Delta c_u \cdot u) = (\rho \cdot A \cdot c_x) \cdot (\Delta c_u \cdot u) = \left(\rho \cdot \left(\pi \cdot D^2 / 4 \right) \cdot \left(1 - (d_h/D)^2 \right) \cdot c_x \right) \cdot (\Delta c_u \cdot u) \quad (4)$$

$$\Delta c_u = f(P_{\text{shaft}}, d_h/D) \text{ for constant } u \text{ and } D$$

Using the velocity triangles in Fig. 1, the Δc_u is represented as in Eq. (5) and for constant blade velocity (u), a functionality for the Δc_u in terms of c_x , β_3 and α_2 can be established. For the fixed guide vane design, α_2 is again a function of d_h/D (Section 2.3.3).

$$\Delta c_u = c_{u2} - c_{u3}$$

$$\Delta c_u = (c_x \cdot \tan \alpha_2) - (u - c_x \cdot \tan \beta_3) = c_x \cdot (\tan \alpha_2 + \tan \beta_3) - u \quad (5)$$

$$\Delta c_u = f(c_x, \beta_3, \alpha_2) \text{ for constant } u \text{ and } D$$

c) Head, gH : The available head is an independent variable as defined section 2.2 and can be represented by the Euler shaft work ($\Delta c_u \cdot u$) and the total system losses, of which runner losses are an important component, as represented in Eq. (6). The system loss coefficient (ζ_{system}) is based on the runner mean axial velocity (c_x) and is another internal variable whose role in the performance of the runner will have to be established.

$$gH = \Delta c_u \cdot u + h_{\text{losses}} = \Delta c_u \cdot u + \zeta_{\text{system}} \cdot \frac{c_x^2}{2} \quad (6)$$

The above methodology of expanding the 3 main variables (discharge, shaft power and head) identifies the internal variables as the axial flow velocity, net tangential flow velocity, relative exit flow angle, inlet vortex angle and system loss coefficient.

2.2.2. Functionality for the mean axial velocity

Combining Eq. (5) and Eq. (6), a second-degree polynomial for c_x can be developed as shown in Eq. (7). If u and gH are kept constant, then c_x would depend only on ζ_{system} , β_3 and α_2 . This is a very important functionality for analyzing the results of geometric changes to blades. The relative influences of ζ_{system} (or ζ_{runner} as will be later seen), β_3 and α_2 can be obtained by performing the sensitivity analysis on Eq. (7).

$$\frac{\zeta_{\text{system}}}{2} \cdot (c_x^2) + u \cdot (\tan \alpha_2 + \tan \beta_3) \cdot (c_x) - (gH + u^2) = 0 \quad (7)$$

$$c_x = f(\zeta_{\text{system}}, \beta_3, \alpha_2) \text{ given that } gH \text{ and } u \text{ are kept constant}$$

2.2.3. Functionality for the net tangential flow velocity

Putting Eq. (5) into Eq. (7) and simplifying, a relationship between Δc_u and the other variables can be determined as in Eq. (8). It can be seen that Δc_u will again remain a function of the three control variables of ζ_{system} , β_3 and α_2 . The individual influences of these three control variables can be studied by carrying out a sensitivity analysis on Eq. (8).

$$\Delta c_u^2 \cdot \frac{\zeta_{\text{system}}}{2} + \Delta c_u \cdot u \cdot (\zeta_{\text{system}} + (\tan \alpha_2 + \tan \beta_3)^2) + \frac{\zeta_{\text{system}}}{2} \cdot u^2 - gH \cdot (\tan \alpha_2 + \tan \beta_3)^2 = 0 \quad (8)$$

$$\Delta c_u = f(\zeta_{\text{system}}, \beta_3, \alpha_2) \text{ for constant } u, gH$$

2.2.4. Overall functionality of internal variables

The preceding analysis leads to the internal functionality of the axial flow turbine control volume given by Eq. (9), which will be the basis of analyzing the hydraulic phenomenon within the runner. The control variables are represented by ζ_{system} , β_3 and α_2 while the dependent variables are taken as c_x and Δc_u . The next step is to physically relate these control variables to the blade height and blade number, which is illustrated in section 2.3.

$$c_x, \Delta c_u = f(\zeta_{\text{system}}, \beta_3, \alpha_2) \text{ for constant } u, gH \quad (9)$$

2.3. Internal control variables

2.3.1. Runner loss coefficient (ζ_{runner})

The overall loss coefficient (ζ_{system}) represents the losses in components like the spiral volute, guide vane ring, runner itself and draft tube. Since modifications are carried out on the runner, the changes to the loss coefficients in the components other than the runner are negligible and overall loss coefficient can be replaced by runner loss coefficient henceforth in the analysis.

The runner loss coefficient (ζ_{runner}) for axial blade profiles is generally evaluated using the cascade and wind tunnel approach as discussed in [8] and [10], where this coefficient is treated primarily as a function of the angle of incidence and flow separation effects. However, the ζ_{runner} also depends on local boundary layers, which is influenced by geometry of blade passage, the blade height (or d_h/D), the blade number (or blade pitch to chord length ratio), the chord length of the blade at different radial sections and other factors. The behaviour of the ζ_{runner} is complex and a detailed experimental analysis will help in getting greater insights about the relative dependence of different parameters on the ζ_{runner} . It can be seen from the functional relationship in Eq. (10) that both the blade number and blade height can influence the runner loss coefficient.

$$\zeta_{\text{runner}} = f(\text{angle of incidence, flow passage geometry, blade height, blade number and others}) \quad (10)$$

2.3.1.1. Blade height. Watson and Janota [10] have discussed the role of blade height very briefly for axial flow turbines for aircraft engines in which they discussed the vibration issues in blades with large height (smaller d_h/D) and leakage effects in blades of smaller height (larger d_h/D). From the perspective hydro turbines, in addition to its role in the frictional characteristics, the parameter d_h/D would also play an important role in the determination of the inlet vortex profile (discussed in section 2.3.3) and hence, the axial flow velocity (Eq. (2)).

2.3.1.2. Blade number. The influence of blade number has been studied in great detail using a dimensionless number, pitch to chord length ratio (s/l) by Ainley and Mathieson [16]. They showed that a compromise has to be made between the flow guidance and friction while selecting this ratio. They brought out charts giving the relationship between profile loss coefficient and pitch to chord length ratio for different vortex angles. In hydro turbines it will be interesting to first ascertain the guidance effect of the relative flow at the runner exit and then evaluate the behaviour of the frictional losses due to changing blade number.

2.3.1.3. Incidence. Incidence losses form the major component of losses in axial flow rotor blades with fixed nozzle designs at varying load conditions. The influence of incidence can be determined from the inlet velocity triangle at the given load point.

2.3.2. Relative flow angle at runner exit (β_3)

The relative flow angle primarily depends on two parameters namely, the blade angle at the exit and the complex slip mechanism at the exit (as reported by Cohrs [11] at the exit of pumps operating as turbines). Slip is governed by circulation within the blade passages and is dependent on the space between the two consecutive blades, which is associated with blade number. The theoretical study of the slip is not the goal of the paper. Rather, it will be attempted to establish the dependence of the relative flow angle on the exit blade angle and slip with the help of velocity triangles.

$$\beta_3 = f(\text{blade angle at the exit, slip effects, blade number}) \quad (11)$$

2.3.3. Inlet vortex angle (α_2)

The vortex angle profile ahead of the runner can be theoretically determined using the continuity and the free vortex equation. The runner flow area is a function of hub ratio, d_h/D and hence α_2 will also become a function of d_h/D as seen by Eq. (12). Fig. 2 describes the absolute flow triangles at the guide vane exit, at the runner tip inlet and the runner hub inlet for a particular runner (runner A) used in the testing. It can be seen that α_2 is increasing from the tip to the hub. One of the prime conditions to develop the free vortex theory is the constancy of the axial flow velocity.

From continuity equation, $A_{\text{guide vane}} \cdot c_{r1} = A_{\text{runner}} \cdot c_{x2}$

$$= (\pi \cdot D^2 / 4) \cdot (1 - (d_h/D)^2) \cdot c_{x2}$$

From free vortex equation, $c_{u1} \cdot r_1 = c_{u2} \cdot r_2$

$$\alpha_{2t} = \tan^{-1} \left(\frac{c_{u2}}{c_{x2}} \right) = \tan^{-1} \left(\frac{c_{u1} \cdot (D_1/D)}{A_{\text{guide vane}} \cdot c_{r1} / (\pi \cdot D^2 / 4) \cdot (1 - (d_h/D)^2)} \right) \quad (12)$$

$$= \tan^{-1} \left(\frac{\tan \alpha_1 \cdot (D_1/D)}{A_{\text{guide vane}} / (\pi \cdot D^2 / 4) \cdot (1 - (d_h/D)^2)} \right),$$

since $(c_{u1} = c_{r1} \cdot \tan \alpha_1)$

Hence for a given guide vane design and runner tip diameter, the vortex angle at inlet tip $\alpha_{2t} = f(d_h/D)$

Further, since $c_{u2} \times r_2 = \text{constant}$, the inlet vortex angle over the entire blade profile is given by, $\alpha_2 = \tan^{-1}(\tan \alpha_{2t} \cdot D/d)$

2.4. Construction of velocity triangles

The inlet and the exit velocity triangles are constructed only at the tip blade profile for the actual operating conditions and help in establishing the two control parameters namely, the angle of incidence (i) and the relative flow angle at the exit (β_3).

Inlet velocity triangle: The inlet velocity triangle is constructed for a known inlet vortex angle, α_2 (refer Fig. 2), the axial velocity c_x (obtained from the Eq. (2)) and the tangential blade velocity, u (given the speed and tip diameter).

Exit velocity triangle: The important parameter to be determined for the construction of the exit velocity triangle is the exit tangential flow velocity c_{u3} , which is obtained from Eq. (5)

provided Δc_{u1} and c_{u2} are known. Δc_{u1} is obtained from Eq. (4) for a measured P_{shaft} and c_x . The exit velocity triangle gives both the relative (β_3) and absolute flow (α_3) directions. It is important to note that the exit blade angle (β^*_3) is not used for the construction of the triangle.

3. Means of solution

3.1. Experimental test-rig

The experimental test-rig for characterizing the propeller stages is discussed in detail in [7], which comprises of the open loop hydraulic test bed along with the required instrumentation. The mechanical assembly of the propeller turbine unit that is used for all the runner stages is illustrated in Fig. 3.

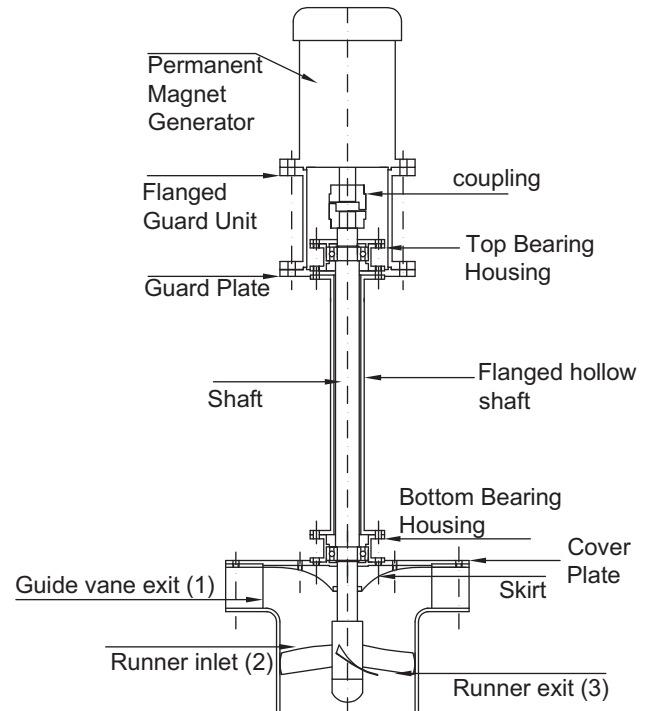


Fig. 3. Assembly of the propeller turbine unit.

Table 1
Summary of the specifications of the experimental runners.

Parameters	Runner A	Runner B	Runner C
d_h/D	0.25	0.3	0.42
α_{2h}	71.8°	68.4°	61.0°
α_{2t}	38.0°	37.2°	34.5°
β^*_{2t}	65.0°	66.0°	63.0°
β^*_{3t}	74.0°	70.0°	71.0°
z	5	5	6
s/l	1.17	1.17	1.15

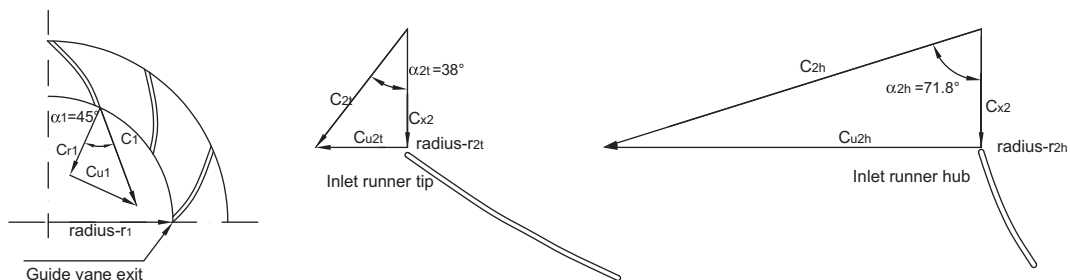


Fig. 2. Velocity triangles at the guide vane exit, inlet runner hub and inlet runner tip.

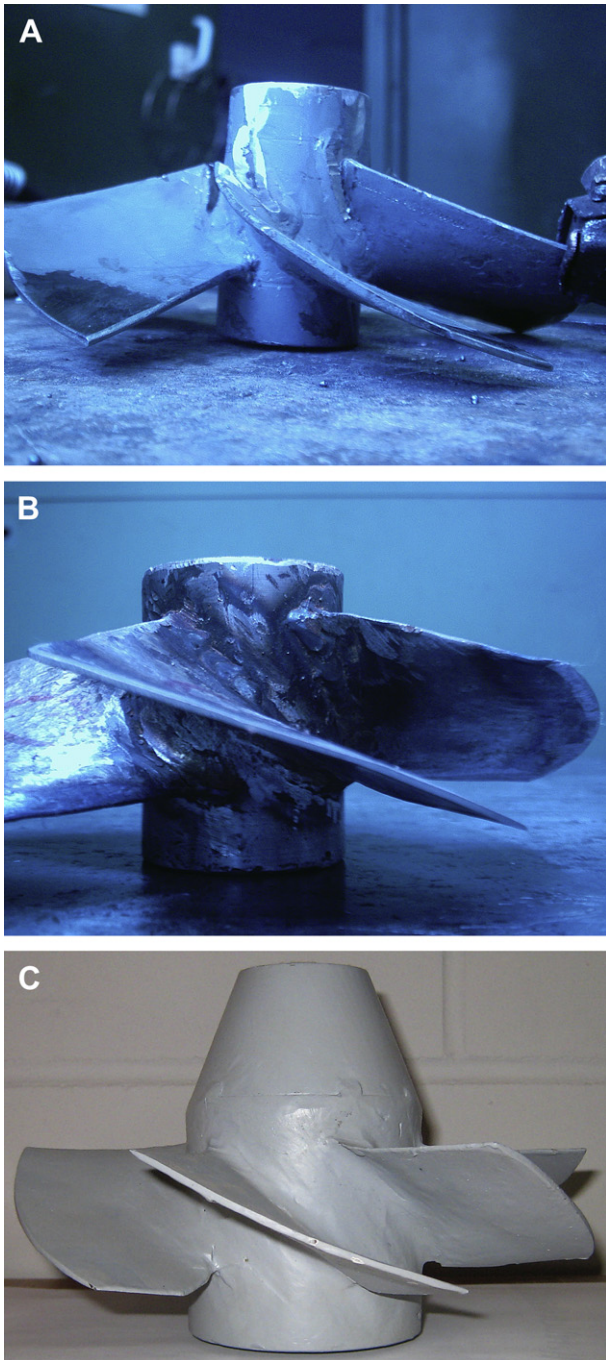


Fig. 4. Picture of runner (A). Picture of runner (B). Picture of runner (C).

3.2. Experimental runners

The chief design parameters of the 3 experimental runners are summarized in Table 1 and their pictures in Fig. 4A–C respectively. The runner A and runner B have 5 blades and nearly same d_h/D , while runner C has 6 blades and a higher d_h/D ratio. Though, the blade angles are slightly different, the effect of blade height (d_h/D) and blade number (s/l) will be studied in following two optimizations stages.

1. Runner A vs runner C
2. Runner B vs runner C

3.3. Analysis of the internal variables

The performance analysis between two runner stages is carried out at a gross head of 1.75 m and a constant speed of 900 rpm, which includes the study of the behaviour of both the main and the internal variables using the theory in Section 2. The percentage deviations of the main variables are graphically read out from the constant head characteristics, which are related to the internal variables by the following analytical equations.

- a) Change in axial velocity, $\delta(c_x)$: Physically, the change in axial velocity can be caused by a specific behaviour of the internal control variables ζ_{runner} , β_3 and α_2 . The exact pattern of behaviour can be determined only by solving the quadratic polynomial in Eq. (7). However, sensitivity analysis can be performed on Eq. (7) using the experimental change of c_x (Eq. (13)) and the relative influences of ζ_{runner} , β_3 and α_2 can then be obtained from the individual slopes $\partial(c_x)/\partial(k)$, $\partial(c_x)/\partial(\beta_3)$ and $\partial(c_x)/\partial(\alpha_2)$ for fixed changes of ζ_{runner} , β_3 and α_2 respectively.

$$\delta(c_x) \approx |Q / (\pi \cdot D^2 / 4) \cdot (1 - (d_h/D)^2)|_A - |Q / (\pi \cdot D^2 / 4) \cdot (1 - (d_h/D)^2)|_B \quad (13)$$

- b) Change in net tangential flow velocity, $\delta(\Delta c_u)$: This component can be evolved from the differential form of Eq. (4) as shown in Eq. (14) using experimental results and further combined with the differential form of Δc_u (given by Eq. (8)) to evaluate the relative influences of ζ_{runner} , β_3 and α_2 using individual slopes $\partial(\Delta c_u)/\partial(k)$, $\partial(\Delta c_u)/\partial(\beta_3)$ and $\partial(c_x)/\partial(\alpha_2)$ for fixed changes of ζ_{runner} , β_3 and α_2 .

$$\delta(\Delta c_u) \approx |P_{shaft} / (\rho \cdot Q) \cdot u|_A - |P_{shaft} / (\rho \cdot Q) \cdot u|_B \quad (14)$$

- c) Change in runner loss coefficient, $\delta(\zeta_{runner})$: The change in runner coefficient can be determined from Eq. (15), which is a differential form of Eq. (6). For identical flow conditions within guide vanes, draft tubes and other components, the change in ζ_{runner} can be taken as proportional to ζ_{runner} .

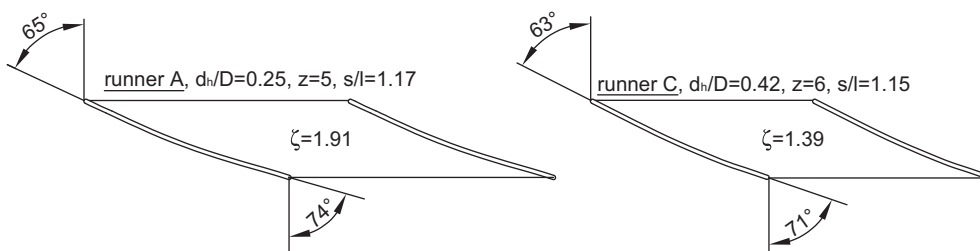


Fig. 5. Cascades of the runner A and runner C.

$$\delta(\zeta_{\text{system}}) \approx \delta(\zeta_{\text{runner}}) = |2 \cdot (gH - \Delta c_u \cdot u) / c_x^2|_A - |2 \cdot (gH - \Delta c_u \cdot u) / c_x^2|_B \quad (15)$$

d) Change in exit relative flow angle ($\delta\beta_3$) and angle of incidence at inlet (i_2): are respectively determined from velocity triangles.

4. Results and discussion

4.1. Comparison between runner A and runner C

The comparison of the cascades of the two runners is illustrated in Fig. 5 and the performance characteristics are summarized in Fig. 6A and B. It can be clearly seen that the discharge capacity of the runner C is more than that of the runner A over the complete operating range. The power has marginally improved, but the efficiency has taken a decreasing trend. The percentage analysis carried out in Table 2 reveals that while the discharge has increased by 18%, the power has risen only by 5%, which is resulting in the overall efficiency drop of nearly 9%. The summary of the internal control variables reveals that ζ_{runner} has considerably decreased (by over 27%), while the β_3 has decreased by 7% (nearly 5°) and α_2 has also decreased. Amongst the internal dependent variables, c_x has increased in the range of 35% and Δc_u has decreased by 11%, while the overall losses have increased by 14%. The velocity triangles at the inlet and exit for the two stages are plotted in Fig. 7.

4.1.1. Discussion on the internal control variables

a) Change in ζ_{runner} : The drastic decrease of the ζ_{runner} needs to be studied with respect to the blade height, blade number (s/l) and incidence effects. However, Ainley and Mathieson [16] have

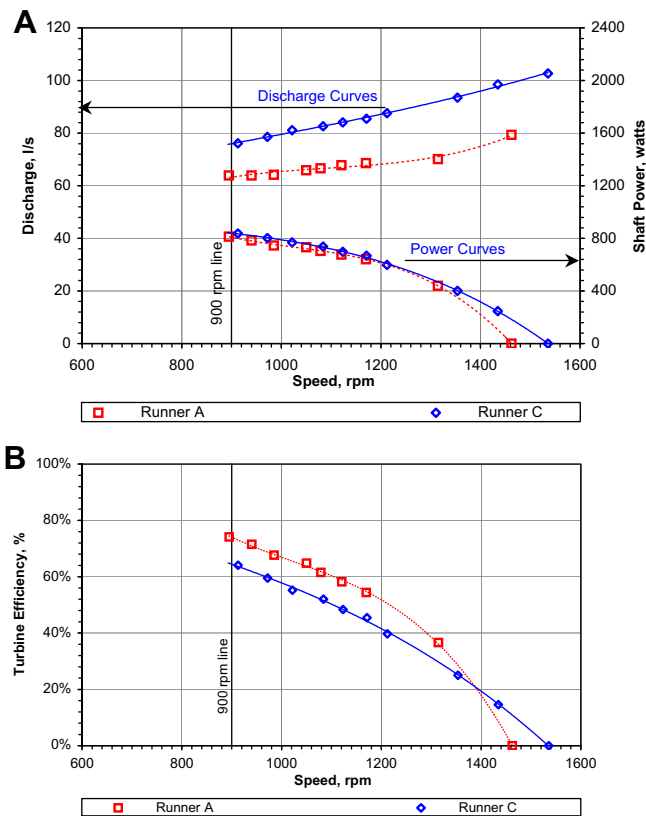


Fig. 6. (A) Discharge and power curves for runner A and runner C. (B) Efficiency curves for runner A and runner C.

Table 2
Percentage analysis of the major and internal variables for runner A and runner C.

Runner type	Summary of main variables					Summary of the internal variables												
	Control		Dependent			Control		Dependent										
	H (m)	N (rpm)	Q (l/s)	δQ (%)	η (%)	$\delta\eta$ (%)	ζ	$\delta\zeta$ (%)	β_3 (deg)	$\delta\beta_3$ (%)	α_2 (deg)	$\delta\alpha_2$ (%)	δc_x (%)	c_x (m/s)	Δc_u (m/s)	$\delta\Delta c_u$ (%)	kQ^2 (m)	$\delta(kQ^2)$ (m)
Runner A	1.75	900	64.0	+18.0%	73.9%	-8.9%	1.91	-27.4%	76.5	-6.8%	38.0	-9.3%	+34.3%	2.173	1.34	-11.0%	0.460	+14.3%
Runner B	1.75	900	75.5		65.0%		1.39		71.3		34.5			2.918	1.19		0.602	

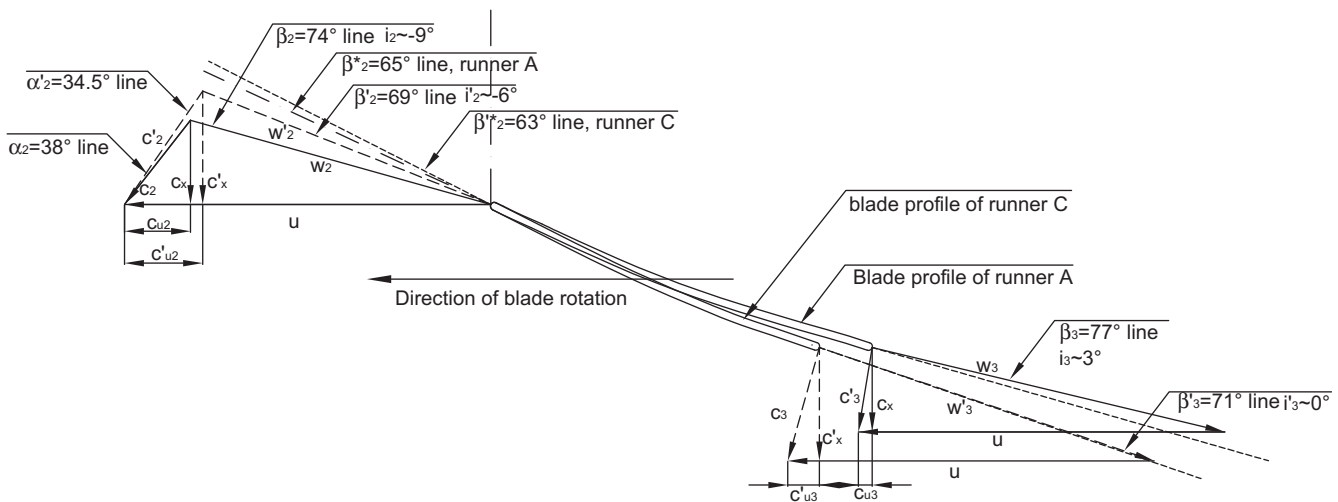


Fig. 7. Consolidated velocity triangles at the blade tip for runner A and runner C.

Table 3
Sensitivity analysis for changes to c_x and Δc_u for runner A and runner C.

Overall change in δc_x (m/s)	δc_x due to ζ_{runner}				δc_x due to β_3				δc_x due to α_2			
	$\partial c_x / \partial \zeta$	$\delta \zeta$	$[\delta c_x]_{\zeta}$	% Contribution	$\partial c_x / \partial \beta_3$	$\delta \beta_3$	$[\delta c_x]_{\beta_3}$	% Contribution	$\partial c_x / \partial \alpha_2$	$\delta \alpha_2$	δc_{x2}	% Contribution
0.74	-4.7E-02	-0.52	+0.02	+3%	-7.45	-0.091	+0.68	+91%	-0.65	-0.062	+0.04	+5%
Overall change in $\delta \Delta c_u$ (m/s)	$\delta \Delta c_u$ due to ζ_{runner}				$\delta \Delta c_u$ due to β_3				$\delta \Delta c_u$ due to α_2			
	$\partial \Delta c_u / \partial \zeta$	$\delta \zeta$	$[\delta \Delta c_u]_{\zeta}$	% Contribution	$\partial \Delta c_u / \partial \beta_3$	$\delta \beta_3$	$[\delta \Delta c_u]_{\beta_3}$	% Contribution	$\partial \Delta c_u / \partial \alpha_2$	$\delta \alpha_2$	$\delta \Delta c_u$	% Contribution
-0.15	-2.3E-01	-0.52	0.12	+81%	2.75	-0.091	-0.25	-169%	0.29	-0.06	-0.02	-12%

showed that the profile loss coefficient does not change for such small change in s/l (1.17–1.15). On the other hand, with the large d_h/D , the blade surface is reduced, which reduces the friction. From Fig. 7, the incidence line for runner B has moved 3° closer to blade angle, which could have slightly reduced the loss coefficient. It has to be seen how this drop in ζ_{runner} would affect the behaviour of the dependent variables like c_x and Δc_u .

- b) Change in β_3 : It can be seen from Fig. 7 that the β_3 for runner C (6 blade) has decreased considerably and is nearly coinciding with the exit blade direction. This result validates the reduced slip and better guidance theory proposed in [16] to a certain extent. The relative flow direction for runner A has moved considerably in the opposite direction of the blade rotation clearly due slip effects. But, it has to be also pointed out that the change in exit blade angle β'_3 (from 74° to 71°) between the two runners will also influence the change in β_3 to an extent. Therefore, the change in β_3 is due to both blade number and exit blade angle. It will be interesting to see how this overall guidance effect will influence the performance.
- c) Change in α_2 : As discussed in Section 2.3.3, the α_2 is influenced by the d_h/D for given guide vane area and runner tip diameter.

It can be seen from Fig. 7 that with increase in d_h/D , the α_2 has decreased. The relative influence of this change in α_2 on the other dependent variables will be interesting to analyze.

4.1.2. Discussion on the internal dependent variables

- a) Change in c_x : The sensitivity analysis carried in Table 3 clearly shows that the single most contributing factor for the increase in axial flow velocity is the relative flow angle at exit. Nearly 91% of the increase in velocity is coming from decrease of β_3 . The changes in α_2 and ζ_{runner} have marginally contributed to the rise in axial velocity. It is really surprising that a substantial decrease in ζ_{runner} of more than 27% has had a relatively insignificant effect on c_x .
- b) Change in Δc_u : Table 3 shows that ζ_{runner} is increasing the Δc_u by 0.12 m/s, but both β_3 and α_2 are bringing down the Δc_u considerably and resulting in the overall decrease of Δc_u by 0.15 m/s. It can be also observed that β_3 is playing a dominating role in reducing the velocity by 0.25 m/s compared to α_2 , which brings the velocity down by only 0.02 m/s.

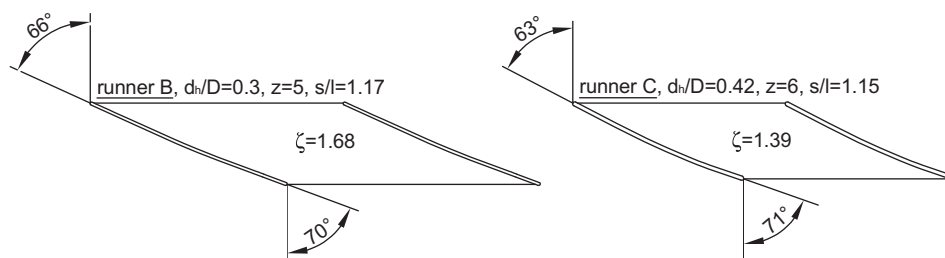


Fig. 8. Cascades of the runner B and runner C.

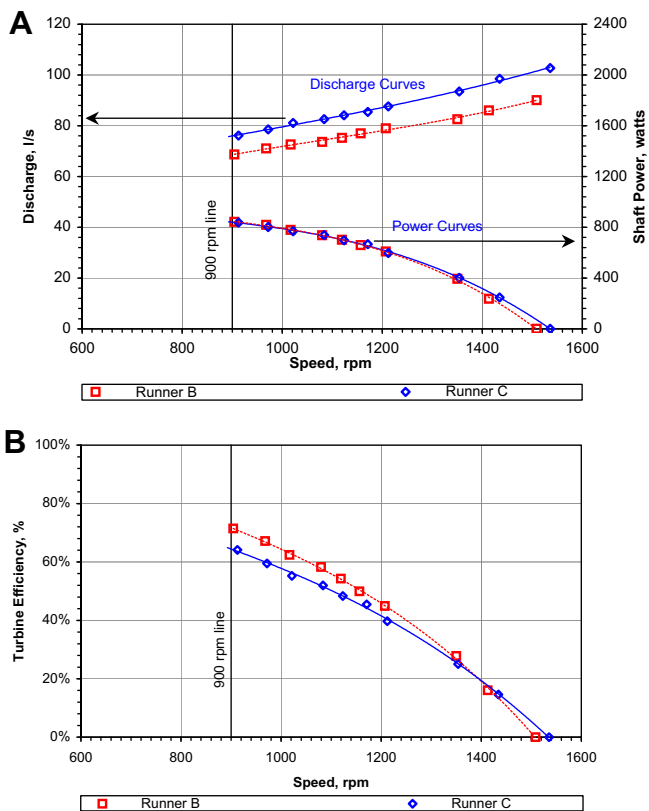


Fig. 9. (A) Discharge and power curves for runner B and runner C. (B) Efficiency curves for runner B and runner C.

4.1.3. Summary of discussion for runner A and runner C

It can be clearly seen that the decrease of runner friction coefficient in runner C has not been able to play a dominating role in controlling the performance compared to the change in relative flow direction at exit. The increase in blade number and to an extent the change in the exit blade angle has improved guidance of runner C, but in the process this has reduced the net tangential flow velocity and increased axial flow velocity, thus bringing down the efficiency considerably. Therefore, more number of blades has created a negative influence on the overall performance. Another conclusion for this particular case is that the influence of blade number on performance is much more compared to the influence of blade height. The blade height has only influenced the friction coefficient and the inlet vortex angle. The runner loss coefficient may have positively affected the net tangential velocity to an extent but it has not been able to influence the behaviour of axial flow velocity. But, the inlet vortex angle could hardly affect the dependent variables.

4.2. Comparison between runner B and runner C

The cascade profiles of the two runners are shown in Fig. 8. The performance characteristics compared in Fig. 9A and B show that the discharge for the runner C is greater than that of runner B over the complete range, but the power characteristics are identical and efficiency behaviour of the runner C is showing a decreasing trend. The percentage analysis in Table 4 shows that the discharge of runner C has increased by 10%, while power has marginally changed and efficiency has decreased from 72% to 65%. The comparison of the internal variables reveals that the ζ_{runner} has decreased by nearly 18%, while the β_3 dropped by 5% (nearly 3.7°) and α_2 has decreased by 7%. The internal dependent variable c_x has increased by nearly 22%, while the other dependent variable Δc_u

Table 4
Percentage analysis of the major and internal variables for runner B and runner C.

Runner type	Summary of main variables		Summary of the internal variables																	
	Control	Dependent	Control			Dependent														
H (m)	N (rpm)	Q (l/s)	δQ (%)	P (W)	δP (%)	η (%)	$\delta \eta$ (%)	ζ ($1/m^4$)	$\delta \zeta$ (%)	β_3 (deg)	$\delta \beta_3$ (%)	α_2 (deg)	$\delta \alpha_2$ (%)	c_x (m/s)	δc_x (%)	Δc_u (m/s)	$\delta \Delta c_u$ (%)	kQ^2 (m)	$\delta(kQ^2)$ (m)	
Runner B	1.75	900	68.5	+10.2%	845	+0.6%	72.0%	-7.0%	1.68	-17.5%	75.0	-4.9%	37.2	-7.3%	2.396	+21.8%	1.31	-8.7%	0.493	+11.0%
Runner C	1.75	900	75.5		850		65.0%		1.39		71.3		34.5		2.918		1.19		0.602	

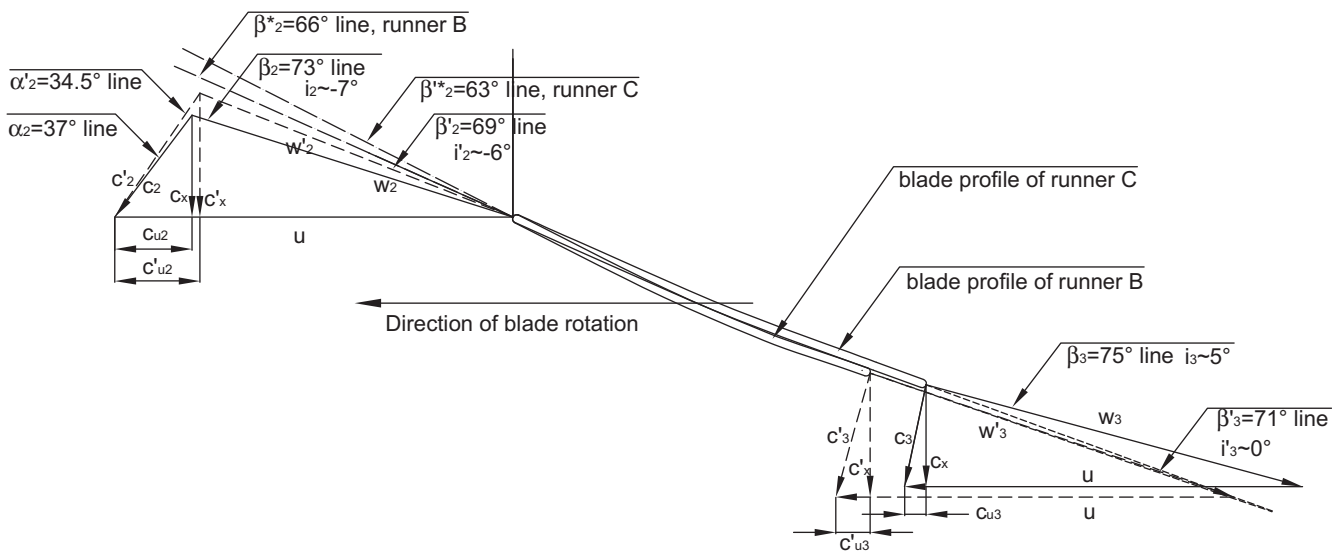


Fig. 10. Consolidated velocity triangles at the blade tip for runner B and runner C.

has fallen by 9%. The velocity triangles for the two runners are constructed in Fig. 10.

4.2.1. Discussion on the internal control variables

- a) Change in ζ_{runner} : The reduction of ζ_{runner} can be attributed mainly to the reduced blade height. The comparison of incidence effects in Fig. 10 shows no major change, which proves that incidence is not playing a major role in reducing ζ_{runner} . Another influence to the runner coefficient could also be the shape of the blade passage.
- b) Change in β_3 : The exit blade angles of the two runners are comparable (70° and 71°), hence the nearly perfect guidance of the exit flow for runner C could be directly owed to increase in the number of blades (reduced slip).
- c) Change in α_2 : The d_h/D ratio has influenced the decrease of inlet tip swirl from 37.2° to 34.5° for runner C.

4.2.2. Discussion on the internal dependent variables

- a) Change in c_x : The sensitivity analysis illustrated in Table 5 reveals that the increase in axial velocity is primarily coming from the relative flow direction effects. The influence of ζ_{runner} and α_2 are negligible.
- b) Change in Δc_u : It can be seen that the decrease in Δc_u is resulting from two contrasting effects. While ζ_{runner} is increasing the Δc_u , both β_3 and α_2 are contributing to the fall in Δc_u . Table 5 shows that the influence of β_3 is very dominating.

4.2.3. Summary of discussion for runner B and runner C

The analysis of the results shows that the perfect flow guidance at the exit of runner C is playing a major role in increasing the axial

velocity and decreasing the net tangential flow velocity, both of which eventually reduces the efficiency. The results also suggest that the relative flow direction at exit is influenced mainly by the number of blades compared to the exit blade angle. As seen with the previous stage comparison (Section 4.1), the influence of runner loss coefficient, a parameter depending on the blade height, is restricted only in the improvement of the net tangential velocity. On the whole the blade number seems to be controlling the performance more than the blade height for this comparison stage (runner B and runner C).

4.3. Discussion of the model's limitations

The possible errors in the model need to be analyzed, since important conclusions have been interpreted from this model. A free vortex flow characteristics is assumed between the guide vane exit and runner inlet. It can be seen from Fig. 3 that the flow changes from radial to axial flow in a relatively short length. The prime criterion for the validity of free vortex flows is radial equilibrium and constant axial velocity. It is difficult to imagine a zero radial flow component in reality. These deviations would naturally affect the inlet vortex angle predictions, which would affect the shape of velocity triangles. However, it is seen from the study both in Section 4.1.2 and 4.2.2 that the influence of inlet vortex angle on the performance is rather small.

The other source of error could come from the fact that the entire conclusions are based on velocity triangles at the blade tip. It would be interesting to repeat the analysis at different sections of the blade. Further, the leakage losses have not been considered in the model, which is reasonable since only relative changes between runner stages are being analyzed.

Table 5 Sensitivity analysis for changes to c_x and Δc_u for runner B and runner C.

Overall δc_x (m/s)	$\delta \Delta c_u$ due to ζ_{runner}				δc_x due to β_3				δc_x due to α_2			
	$\partial c_x / \partial \zeta$	$\delta \zeta$	$[\delta c_x]_\zeta$	% Contribution	$\partial c_x / \partial \beta_3$	$\delta \beta_3$	$[\delta c_x]_{\beta_3}$	% Contribution	$\partial c_x / \partial \alpha_2$	$\delta \alpha_2$	δc_{x2}	% Contribution
0.52	-6.7E-02	-0.30	+0.020	+4%	-7.29	-0.064	+0.47	+89%	-0.77	-0.047	+0.04	+7%
Overall $\delta \Delta c_u$ (m/s)	$\delta \Delta c_u$ due to ζ_{runner}				$\delta \Delta c_u$ due to β_3				$\delta \Delta c_u$ due to α_2			
	$\partial c_x / \partial \zeta$	$\delta \zeta$	$[\delta c_x]_\zeta$	% Contribution	$\partial c_x / \partial \beta_3$	$\delta \beta_3$	$[\delta c_x]_{\beta_3}$	% Contribution	$\partial c_x / \partial \alpha_2$	$\delta \alpha_2$	δc_{x2}	% Contribution
-0.11	-0.41	-0.30	+0.08	+71%	2.81	-0.064	-0.18	-157%	0.33	-0.047	-0.02	-14%

5. Conclusions and recommendations

It can be concluded that the theoretical model developed for propeller turbines along with the sensitivity analysis was very useful to accurately study the influences of the two geometric design parameters, the blade height and blade number. Based on principles of classical turbomachinery, the model evolved a functionality of the internal variables. The two design parameters, blade height and blade number were respectively related to two internal control variables, the inlet vortex angle and the relative flow angle at the exit. These functionalities were further validated using the experimental data.

The experimental study carried out on 3 runners broadly concluded that influence of blade number was much more than the influence of blade height (or hub to tip ratio). It was found that with an increase of the blade number, the flow guidance improved. However, this improved guidance, surprisingly had an overall negative effect on the performance with efficiency decreasing by 8–10%, arising due to an increased axial velocity and reduced net tangential velocity.

Table A1
Uncertainty table for all the runner stages.

Runner	Generator parameters									Turbine parameters									
	V	$\Delta V/V$	I	$\Delta I/I$	N	$\Delta N/N$	T	$\Delta T/T$	η_g	$\Delta \eta_g/\eta_g$	$\Delta P_m/P_m$	P_m	Q	$\Delta Q/Q$	H	$\Delta H/H$	η_m	$\Delta \eta_m/\eta_m$	$\Delta \eta_m$
Runner A	82.5	$\pm 0.1\%$	6.7	$\pm 1.5\%$	900	$\pm 0.1\%$	8.6	$\pm 1.2\%$	68.2%	$\pm 1.9\%$	$\pm 2.4\%$	810	64.0	$\pm 0.2\%$	1.75	$\pm 0.3\%$	73.9%	$\pm 2.4\%$	$\pm 1.8\%$
Runner B	81.0	$\pm 0.1\%$	7	$\pm 1.4\%$	900	$\pm 0.1\%$	9.0	$\pm 1.1\%$	67.1%	$\pm 1.8\%$	$\pm 2.3\%$	845	68.5	$\pm 0.1\%$	1.75	$\pm 0.3\%$	72.0%	$\pm 2.3\%$	$\pm 1.7\%$
Runner C	80.7	$\pm 0.1\%$	7.05	$\pm 1.4\%$	900	$\pm 0.1\%$	9.0	$\pm 1.1\%$	66.9%	$\pm 1.8\%$	$\pm 2.3\%$	850	75.5	$\pm 0.1\%$	1.75	$\pm 0.3\%$	65.0%	$\pm 2.3\%$	$\pm 1.5\%$

It was further found that the runner loss coefficient decreased considerably in the range of 20–30% for the runner having smaller blade height and greater blade number. This decrease was attributed mainly to the shortened blade height and improved flow passage geometry, since increased blade number would instead contribute to the rise in friction. However, this large decrease in runner loss coefficient could hardly influence the axial flow velocity, though it positively contributed to the increase of the net tangential flow velocity.

The results were very interesting and helped in concluding that the blade number should not be increased until there is need to increase the flow through the turbine at the same head, but with comprise of a large drop in efficiency. For the boundary conditions considered in this paper, it is strongly recommended to use propellers with smaller blade height but fewer blades in order to combine the positives of these two design parameters.

The model's limitation were also discussed in which the free vortex assumptions of flow before the runner were found to be debatable. However, given the limited influence of the inlet vortex angle on the performance as found from the experimental analysis, this assumption would not derail the major conclusions of the study. Though this study brought out the separate influence of the blade height and blade number with certain amount of clarity, it is still recommended to independently verify these two effects.

The experimental study has presented very important and interesting results concerning flow hydraulics within runner under the change of some design parameters. The validation of these results using a calibrated and reliable CFD model is vital, as this could reveal certain deficiencies in the theoretical model used. Once the results are validated, it can be extended to the standardization of the design parameters in low head axial flow turbines and serve as a platform for sustainable application in micro-hydro and other energy recovery systems.

Acknowledgements

The authors would like to acknowledge the contribution of Erfried Berger, Boris Lehmann, Frank Seidel, Gerard Close, Günther Kühn, Manfred Lösche, Marcus Plate, Martin Gabi, Michael Ritzmann, Michael Ziegler, Jürgen Ullrich, Peter Oberle, Ramesh, Ravichandran, Saban Caglar and Werner Helm, without whom the work of propeller research would not have been accomplished.

Appendix. Experimental uncertainty analysis

The overall uncertainty analysis is carried out using the single sample study proposed by Moffat [12] and Kline [13] at the BEP points of the 3 runner and is summarized in Table A1. The evaluation combines the results from two separate test-rigs namely, the generator test-rig used for characterizing the generator and the turbine test-rig used to study the complete turbine generator unit. The overall random error for all the variables is summarized in Table A2.

Table A2
Maximum random error for each variable.

ΔV (V)	ΔI (A)	ΔN (rpm)	ΔT (Nm)	ΔQ (l/s)	ΔH (m)
± 0.1	± 0.1	± 1	± 0.1	± 0.1	0.005

References

- [1] Rao GJ, Prasad R, Rao JKS. Investigation of an axial flow runner for micro hydro power development. In: Proceedings of 8th fluid machinery conference, Budapest, Hungary, pp. 616–23, 1988.
- [2] Soundarnayagam S, Suryanarayanan A. Ultra low-head propeller turbines for small canal drops. Turbomachines Laboratory Report. Bangalore, India: Indian Institute of Science; 1988.
- [3] Demetriades GM. Design of low-cost propeller turbines for standalone micro-hydroelectric generation units, Ph.D Thesis, University of Nottingham, United Kingdom, 1997.
- [4] Upadhyay D. Low head turbine development using computational fluid dynamics, Ph.D Thesis, University of Nottingham, United Kingdom, 2004.
- [5] Alexander KV, Giddens EP, Fuller AM. Axial-flow turbines for microhydro systems. Journal of Renewable Energy 2009;34:35–47.
- [6] Simpson RG, Williams AA. Application of computational fluid dynamics to the design of pico propeller turbines. In: Proceedings of the international conference on renewable energy for developing countries, Washington, DC, USA, 2006.
- [7] Singh P, Nestmann F. Experimental optimization of a free vortex propeller runner for micro hydro application. Journal of Experimental Thermal and Fluid Science 2009;33:991–1002.
- [8] Dixon SL. Fluid mechanics and thermodynamics of turbomachinery. Oxford, UK: Elsevier; 2005 [chapters 2, 6 and 9].
- [9] Pfeleiderer C, Petermann H. Strömungsmaschinen. Springer-Verlag; 1964 [chapter 1].
- [10] Watson N, Janota MS. Turbocharging of the internal combustion engine. The Macmillan Press; 1982 [chapter 5].
- [11] Cohrs D. Untersuchungen an einer mehrstufigen rückwärtslaufenden Kreiselpumpe im Turbinenbetrieb. Verlag und Bildarchiv, W.H. Faragallah; 1997. pp 8–41.
- [12] Moffat RJ. Contributions to the theory of single-sample uncertainty analysis. Journal of Fluids Engineering; 1982:250–60.
- [13] Kline SJ. The purposes of uncertainty analysis. Journal of Fluids Engineering; 1985:153–60.
- [14] Nechleba M. Hydraulic turbines: their design and equipment. Prague: ARTIA; 1957.
- [15] Hothersall R. Hydrodynamic design guide for small Francis and propeller turbines. Vienna, Austria: United Nations Industrial Development Organization; 2004 [chapter 2, 3 and 10].
- [16] Ainley DG, Mathieson GCR. A method for performance estimation for axial flow turbines. ARC R&M2974; 1957.
- [17] Asian Phoenix Resources Ltd (APRL). Powerpal brochure, <http://www.powerpal.com>; 2001 (accessed in February 2009).

Influence of the Blade Hub Geometry on the Performance of Low-Head Axial Flow Turbines

Punit Singh¹ and Franz Nestmann²

Abstract: The influence of geometric parameters, such as blade profile and hub geometry on axial flow turbines for micro hydro application remains poorly characterized. This paper first introduces a holistic theoretical model for studying the hydraulic phenomenon resulting from geometric modification to the blades. It then describes modification carried out on two runner stages, of which one has untwisted blades and the other has twisted blades obtained by modifying the inlet hub. The experimental results showed that the performance of the untwisted blade runner was satisfactory with a maximum efficiency of 68%. However, positive effects of twisted blades were clearly evident with an efficiency rise of more than 2%. This study also looks into the possible limitations of the model and suggests the extension of the experimental work and the use of computational tools to conduct a progressive validation of all experimental findings, especially on the flow physics within the hub region and the slip phenomena. The paper finally underlines the importance of developing a standardization philosophy for axial flow turbines specific for micro hydro requirements. DOI: 10.1061/(ASCE)EY.1943-7897.0000060. © 2012 American Society of Civil Engineers.

CE Database subject headings: Hydropower; Head (fluid mechanics); Experimentation; Optimization; Turbines.

Author keywords: Hydropower; Low head; Turbines; Blade twist; Experimentation; Optimization; Slip phenomena.

Introduction

Background

Optimization studies for axial flow turbines comprised of the influence of geometric parameters, such as blade angles, blade height, blade number, and other geometric constants, especially for low-head and smaller power capacities (below 10 kW), has been very limited. The general layout of the blade profiles and specification of other geometries can be obtained by the standard design theories, such as free vortex theory or the constant nozzle angle theory; however, this design information is not enough to evaluate how the geometric parameters would individually affect the performance of the turbine. In the special context of micro hydro, the optimization study becomes extremely important because of challenging boundary conditions, such as large variation of flow, and also has the challenge to generating optimum power notwithstanding the economic constraints that emphasizes on simplicity. Further, the study is also significant to initiate standardization of designs.

Propeller turbine research, although limited, has attracted the attention of few researchers that include Rao et al. (1988); Soundarnayagam and Suryanarayanan (1988); APRL 2001; Demitriades (1997); Upadhyay (2004); Simpson and Williams (2006) and Alexander et al. (2009). Among them, Upadhyay

(2004) carried out optimization studies at a computational level, whereas Simpson and Williams (2006) reported an improvement in the performance of the field propeller turbine after carrying geometric modification to the runner. However, there has been no holistic approach from either the experimental or computational methods to study the influence of individual design parameters.

Singh and Nestmann (2009) made an attempt to study the effects of inlet and exit blade geometry on one runner. They attempted to qualitatively analyze internal hydraulic phenomena within the runner caused by these geometric modifications and presented interesting results. However, they could not numerically quantify the exact behavior pattern of these variables. In spite of this, their work is a good starting point for studying the geometrical influences, which need to be enhanced and given a holistic character.

The blade twist feature of an axial flow turbine blade is said to be the prime consideration for the optimum performance of the runner. The degree of this twist is primarily decided by design approaches employed. Further, it was found that there is a difference between the performance of a design and an actual runner, as reported in Singh and Nestmann (2009). The study of the influence of blade twist therefore becomes important not only to validate the design theories but also to evaluate the degree of improvement of performance that the twist of the blades would affect.

From the perspective of micro hydro, it is necessary to actually state the level of performance alleviation that can be attained with the help of twist to justify the complicated manufacture of a twisted blade profile. This study will further help to answer the question of using untwisted or constant blade angle runners for small power outputs.

Objectives and Problem Outline

1. To build a holistic theoretical model based on the principles of classical turbomachinery for studying the influence of blade design parameters of a propeller turbine system and for numerically characterizing the behavior of the internal hydraulic parameters by employing functionalities;

¹Research Associate, Divecha Centre for Climate Change, Indian Institute of Science, Bangalore, 560012, India; and Visiting Fellow, Institute for Water and River Basin Management (IWG), Karlsruhe Institute of Technology, Kaiser Str. 12, D 76128, Karlsruhe, Germany (corresponding author). E-mail: punit.singh@iwg.uka.de

²Professor and Director, Institute for Water and River Basin Management (IWG), Karlsruhe Institute of Technology, Kaiser Str. 12, D 76128, Karlsruhe, Germany. E-mail: nestmann@iwg.uka.de

Note. This manuscript was submitted on August 25, 2009; approved on September 16, 2011; published online on September 19, 2011. Discussion period open until February 1, 2013; separate discussions must be submitted for individual papers. This paper is part of the *Journal of Energy Engineering*, Vol. 138, No. 3, September 1, 2012. © ASCE, ISSN 0733-9402/2012/3-109-118/\$25.00.

- To experimentally compare the performance of an untwisted blade runner with a runner that incorporates blades certain amount of twist introduced by modifying the inlet hub region only;
- To use the developed theoretical model and experimental results to ascertain the internal hydraulic phenomena with respect to the runner loss coefficient and velocity vectors; and
- To evaluate the limitations of the model and find out the possible sources error and to make suitable recommendations for further study of twist effects.

Theoretical Model

Main Variables and Functionalities of Propeller Runner

The primary working variables for any hydro turbine are classified as input variables, which include the available head and discharge, and the output variables, comprised of the shaft power and speed. By using the standard dimensional analysis, the control (or independent) variables for this system are the head and speed, whereas the dependent variables are represented as the discharge and shaft power. Another performance parameter is the efficiency, which is, again, a dependent variable. The overall dimensional functional equation is represented by Eq. (1):

$$Q, P_{\text{shaft}}, \eta = f(N, gH) \quad (1)$$

Singh and Nestmann (2009) attempted to give a greater physical meaning to the behavior of these dependent variables (discharge, power, and efficiency) individually with respect to the two important internal hydraulic variables; namely, the Euler shaft work, or net rotational momentum, and the runner loss coefficient. They further related the resulting hydraulic phenomena to the geometric modifications carried out on the runner.

Internal Variables and Functionalities

The classification of internal variables and their functionalities is obtained by defining and expanding the primary variables, as conducted in the section "Identifying the Internal Variables," without altering the functionality of Eq. (1). The velocity triangle along with the cascade approach is then utilized to develop a deeper understanding of the physical significance of the internal variables with respect to geometrical design parameters.

A typical inlet and exit velocity triangles for a low-pressure axial stage having hub to tip ratio (d_h/D) of 0.5 is shown in Fig. 1 for

both the hub and tip profiles. The hub profiles at the blade inlet have large incidence effects because a free vortex flow characteristics are assumed, which calls for uniform angular momentum along the blade height from hub to tip. The velocity triangle shapes at the hub and tip will be the focus of the experimental analysis for the twisted and untwisted runner blades.

Identifying the Internal Variables

- Discharge (Q): The discharge is a dependent variable, as shown in Eq. (1), and is given by the mean axial flow velocity and the flow area in Eq. (2). If the diameter (D) is taken as an independent geometric variable and hub to tip ratio (d_h/D) taken as a design variable, then the axial flow velocity (c_x) directly corresponds to Q and becomes an internal dependent variable:

$$Q = c_x \cdot (\pi \cdot D^2/4) \cdot [1 - (d_h/D)^2] \quad c_x \propto Q \quad (2)$$

- Shaft power (P_{shaft}): As shown in Singh and Nestmann (2009), who used the basis of Euler turbine fundamentals proposed by Pfleiderer and Petermann (1991) and Dixon (2005a), it is appropriate to represent the shaft power by the Euler shaft work ($\Delta c_u \cdot u$ or change of rotational momentum) and leakage losses, as shown in Eq. (3):

$$P_{\text{shaft}} = m \cdot (\Delta c_u \cdot u) - \text{leakage losses} \quad (3)$$

If leakage effects are neglected, especially while comparing two optimization stages, then the shaft power's proportionality can be written as Eq. (4). Further, it can be easily shown that the net tangential flow velocity, Δc_u is another internal dependent variable that represents the energy transfer or rotational momentum and hence, the shaft work:

$$\begin{aligned} P_{\text{shaft}} &\approx (\rho \cdot Q \cdot u) \cdot (\Delta c_u) = (\rho \cdot A \cdot c_x \cdot u) \cdot (\Delta c_u) \\ &= \{ \rho \cdot (\pi \cdot D^2/4) \cdot [1 - (d_h/D)^2] \cdot c_x \cdot u \} \cdot (\Delta c_u) \end{aligned} \quad (4)$$

By using the velocity triangles in Fig. 1, the Δc_u is given by Eq. (5), and for constant blade velocity (u) and inlet vortex angle (α_2), a functionality for the net tangential velocity (Δc_u) in mean axial velocity (c_x) and relative flow angle at exit (β_3) can be established. The swirl angle at inlet (α_2) is a function of the blade height (or d_h/D ratio), whose characteristics are discussed in the section "Inlet Vortex Angle (α_2):"

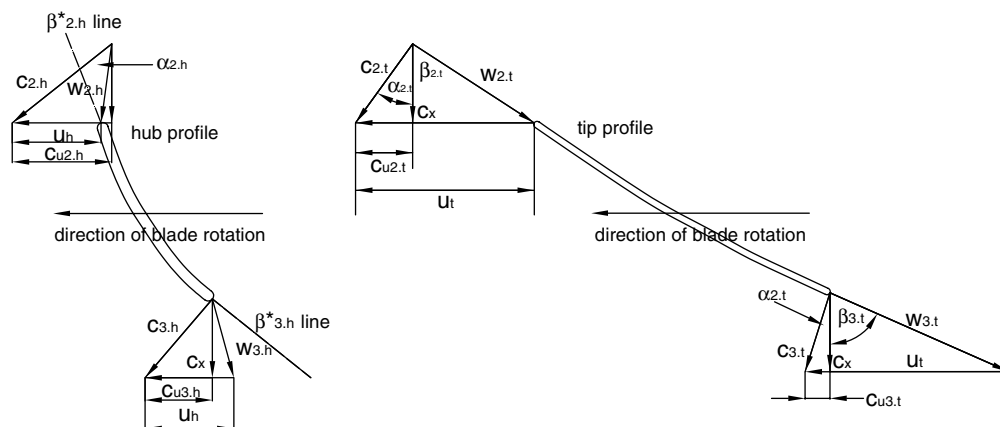


Fig. 1. Typical velocity triangles of a low pressure axial turbine at the blade hub and tip

$$\begin{aligned}
\Delta c_u &= c_{u2} - c_{u3} \\
\Delta c_u &= (c_x \cdot \tan \alpha_2) - (u - c_x \cdot \tan \beta_3) \\
&= c_x \cdot (\tan \alpha_2 + \tan \beta_3) - u \\
\Delta c_u &= f(c_x, \beta_3) \text{ for constant } u \text{ and } \alpha_2
\end{aligned} \tag{5}$$

3. Head (gH): The available head is an independent variable of the turbine control volume and can be represented by the Euler shaft work and the total system losses [Eq. (6)], of which runner losses are an important component. The system losses are represented by the system loss coefficient (k_{runner}) and the discharge:

$$\begin{aligned}
gH &= \Delta c_u \cdot u + h_{\text{losses}} = \Delta c_u \cdot u + k_{\text{system}} \cdot Q^2 \\
&= \Delta c_u \cdot u + k_{\text{system}} \cdot A^2 \cdot c_x^2
\end{aligned} \tag{6}$$

Therefore, the expansion of the main variables (discharge, shaft power, and head) have helped in the identifying internal variables of the propeller system that include the mean axial velocity, net tangential flow velocity, runner loss coefficient, exit relative flow angle, and inlet vortex flow angle.

Functionality for the Mean Axial Velocity

Combining Eqs. (5) and (6), a second-degree polynomial for c_x can be developed that is represented by Eq. (7). If tangential blade speed, the available head, and the inlet swirl angle are kept constant, then c_x would depend only on k_{system} and β_3 . This is a very important functionality for analyzing the results of geometric changes to blades. The relative influences of k_{system} (or k_{runner}) and β_3 can be obtained by performing the sensitivity analysis on Eq. (7):

$$\begin{aligned}
k_{\text{system}} \cdot A^2 \cdot (c_x^2) + u \cdot (\tan \alpha_2 + \tan \beta_3) \cdot (c_x) - (gH + u^2) &= 0 \\
c_x &= f(k_{\text{system}}, \beta_3) \text{ given that } gH, u, \text{ and } \alpha_2 \text{ are kept constant}
\end{aligned} \tag{7}$$

Functionality for the Net Tangential Flow Velocity

By putting Eq. (5) into Eq. (7) and simplifying, a relationship between Δc_u and the other variables can be determined, as illustrated in Eq. (8). The Δc_u will, again, remain a function of the two control variables of k_{system} and β_3 . The individual influences of these two control variables can be studied by carrying out a sensitivity analysis on Eq. (8):

$$\begin{aligned}
\Delta c_u^2 \cdot (k_{\text{system}} \cdot A^2) + \Delta c_u \cdot u \cdot [2 \cdot k_{\text{system}} \cdot A^2 \\
+ (\tan \alpha_2 + \tan \beta_3)^2] + k_{\text{system}} \cdot A^2 \cdot u^2 - gH \\
\cdot (\tan \alpha_2 + \tan \beta_3)^2 = 0 \quad \Delta c_u = f(k_{\text{system}}, \beta_3)
\end{aligned} \tag{8}$$

for constant u , gH and α_2

Overall Functionality of Internal Variables

Combining functionalities for c_x and Δc_u , the internal functionality can be specified with k_{system} and β_3 as the control variables and c_x and Δc_u as the dependent variables, as illustrated in Eq. (9), that will be the basis of analyzing the hydraulic phenomenon within the runner. The internal functionality calls for a better understanding of the two control variables, the system (or runner loss) coefficient and the exit relative flow angle. Further, the inlet swirl angle, which is

also a control variable but taken as a fixed variable in the present analysis, needs a special discussion:

$$c_x, \Delta c_u = f(k_{\text{system}}, \beta_3) \text{ for constant } u, gH, \text{ and } \alpha_2 \tag{9}$$

Internal Control Variables: Runner Loss Coefficient

The overall loss coefficient (k_{system}) is comprised of coefficients within different components like the spiral volute, guide vane ring, runner itself, and the draft tube. Because the modifications are carried out on the runner, the changes to the loss coefficients in the components other than the runner are negligible. Furthermore, the runner loss coefficient can be related to the pressure loss coefficient ζ , as shown in Eq. (10). Physically, there is no difference between ζ and k_{runner} :

$$k_{\text{runner}} \cdot Q^2 = \zeta \cdot /2 \cdot c_x^2 \tag{10}$$

The runner loss coefficient for axial blade profiles is generally evaluated by using the cascade and wind tunnel tests, as discussed in Dixon (2005b) and Watson and Janota (1982), in which this coefficient is treated primarily as a function of the angle of incidence and flow separation effects. However, the ζ_{runner} also depends on local boundary layers, which is influenced by geometry of blade passage, the blade height (or d_h/D), the blade number (or blade pitch to chord length ratio), the chord length of the blade at different radial sections, and other factors. The behavior of the k_{runner} , is complex and a detailed experimental analysis can reveal more information about the relative dependence of k_{runner} on these parameters:

$$k_{\text{runner}} = f(\text{angle of incidence, flow passage geometry, blade length, hub to tip ratio, blade pitch to chord length ratio}) \tag{11}$$

In the present study, in which the twist of the blade is analyzed, the only parameters that can influence the k_{runner} are the angle of incidence, which depends on the respective inlet blade angles, and flow passage geometry, which is, again, a function of the blade angles.

Internal Control Variables: Relative Flow Angle at Runner Exit

The relative flow angle depends primarily on two parameters, namely the exit blade angle and the complex slip mechanism [as reported by Cohrs (1997) at the exit of pumps operating as turbines]. Slip is governed by circulation within the blade passages. The theoretical study of the slip is not the goal of this paper. Rather, it will be attempted to establish the dependence of the relative flow angle on the exit blade angle and slip effects with the help of velocity triangles:

$$\beta_3 = f(\text{blade angle at the exit, slip effects}) \tag{12}$$

Internal Control Variables: Inlet vortex angle

The inlet vortex angle is a control variable but a fixed variable, as shown in the internal functionality in Eq. (9). The vortex angle ahead of the runner can be theoretically determined by using the continuity and the free vortex equation. It can be proved that α_2 is a function of d_h/D [refer to steps in Eq. (13)].

$$\text{From the continuity equation, } A_{\text{guide vane}} \cdot c_{r1} = A_{\text{runner}} \cdot c_{x2} = (\pi \cdot D^2/4) \cdot [1 - (d_h/D)^2] \cdot c_{x2}$$

From the free vortex equation, $c_{u1} \cdot r_1 = c_{u2} \cdot r_2$

$$\begin{aligned} \alpha_2 &= \tan^{-1} \left(\frac{c_{u2}}{c_{x2}} \right) \\ &= \tan^{-1} \left\{ \frac{c_{u1} \cdot (D_1/D)}{A_{\text{guide vane}} \cdot c_{r1} / (\pi \cdot D^2/4) \cdot [1 - (d_h/D)^2]} \right\} \\ &= \tan^{-1} \left\{ \frac{\tan \alpha_1 \cdot (D_1/D)}{A_{\text{guide vane}} \cdot / (\pi \cdot D^2/4) \cdot [1 - (d_h/D)^2]} \right\}, \end{aligned}$$

because $(c_{u1} = c_{r1} \cdot \tan \alpha_1)$ (13)

For a given guide vane design and runner tip diameter, the functionality for inlet vortex angle is represented as, $\alpha_2 = f(d_h/D)$.

If d_h/D is maintained constant, the vortex angle profile will also be constant. Fig. 2 describes the absolute flow triangles at the guide vane exit, at the runner tip inlet, and the runner hub inlet for the experimental runner used in the testing. The α_2 is increasing from the tip to the hub. One of the prime conditions to develop the free vortex theory is the constancy of the axial flow velocity and no influence of radial or secondary flows. Any deviations in these conditions will affect the profile of the inlet vortex angle striking the runner.

Construction of Velocity Triangles

The construction of the inlet and exit velocity triangles for the actual operating conditions helps in establishing the two important parameters, namely the angle of incidence (i) and the relative flow angle at the runner exit (β_3). As shown in Eqs. (11) and (9), both angles are controlling the internal performance parameters. The velocity triangles are constructed both at the tip and hub for the twisted and untwisted runner blades by using the following principles:

- Inlet velocity triangle: The inlet velocity triangle can be constructed with the known inlet vortex angle, α_2 (refer to Fig. 2), the axial velocity, c_x [obtained from Eq. (2)], and the tangential blade velocity, u (given the speed and tip diameter).
- Exit velocity triangle: The important parameter to be determined for the construction of the exit velocity triangle is the exit tangential flow velocity c_{u3} , which can be obtained from Eq. (5) provided Δc_u and c_{u2} are known. The Δc_u is obtained from Eq. (4) for a measured shaft power and axial velocity. The exit velocity triangle gives both the relative (β_3) and absolute flow (α_3) directions. The exit blade angle (β_3^*) is not used for the construction of the triangle.

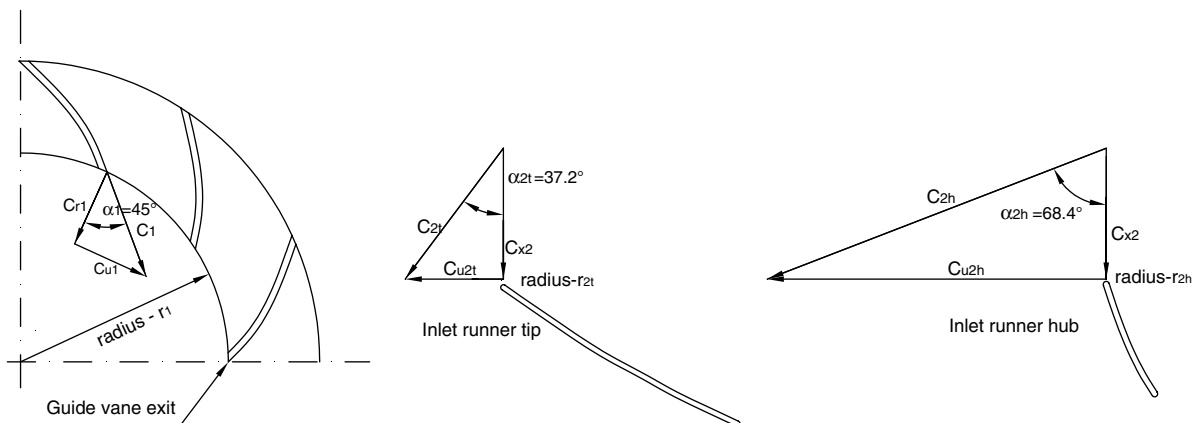


Fig. 2. Velocity triangles at the guide vane exit, inlet runner hub, and inlet runner tip

Means of Solution

Experimental Runner Stages

The basic profile of the blades is obtained from the free vortex design methodology for the boundary conditions of 1.75 m and 75 L/s, as shown in Singh and Nestmann (2009). The recommendation of the free vortex theory for the blade design is summarized in Table 1, which specifies a twist of the blade from hub to tip and different inlet and exit flow angles. However, the basic experimental runner incorporates a constant blade angle design of 70° against the free vortex recommendation of 74° at the inlet tip and 76° at the exit tip.

The actual design parameters of the two runner stages studied in this paper are summarized in Table 2 and the hub modification is illustrated in Figs. 3(a–c), respectively. Stage 1 of the runner is having a constant blade angle from hub to tip, and Stage 2 has been modified in the hub region only, without any changes to the major portion of the blade.

Experimental Test Rig

The experimental test rig for characterizing the propeller stages is shown in Fig. 4 and discussed, in detail, in Singh and Nestmann (2009). The complete propeller unit, comprised of the runner, mechanical assembly, and the generator, is shown in Fig. 5.

Table 1. Free Vortex Specifications of the Relative and Absolute Flow Angles at the Inlet and Exit of the Blade

Flow angles ($^\circ$)	Hub to tip ratio, d_h/D								
	0.3	0.4	0.5	0.6	0.65	0.7	0.8	0.9	1
α_2	59.1°	51.4°	45.0°	39.9°	37.6°	35.6°	32.0°	29.1°	26.6°
β_2	-25.3°	19.0°	44.8°	57.3°	61.3°	64.3°	68.7°	71.8°	74.0°
α_3	0°	0°	0°	0°	0°	0°	0°	0°	0°
β_3	50.1°	57.9°	62.4°	67.3°	68.9°	70.3°	72.6°	74.4°	75.9°

Table 2. Summary of the Specifications of the Experimental Runners

Runner stage	Design parameters of the runner							z
	d_h/D	α_{2h}	β_{2h}^*	β_{3h}^*	α_{2t}	β_{2t}^*	β_{3t}^*	
Runner-stage 1	0.3	68.4°	70°	70°	37.2°	70°	70°	5
Runner-stage 2	0.3	68.4°	60°	70°	37.2°	70°	70°	5

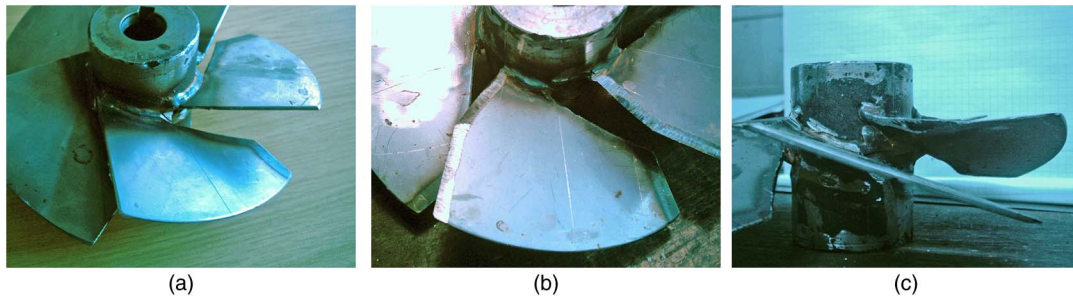


Fig. 3. (a) Untwisted blade runner—Stage 1; (b) modification at the hub; (c) twisted blade runner—Stage 2 (images by Günther Kühn/Punit Singh)

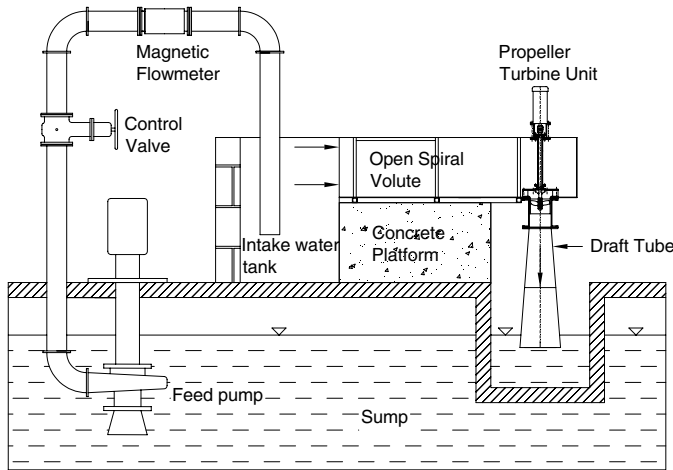


Fig. 4. Hydraulic test rig for propeller turbines

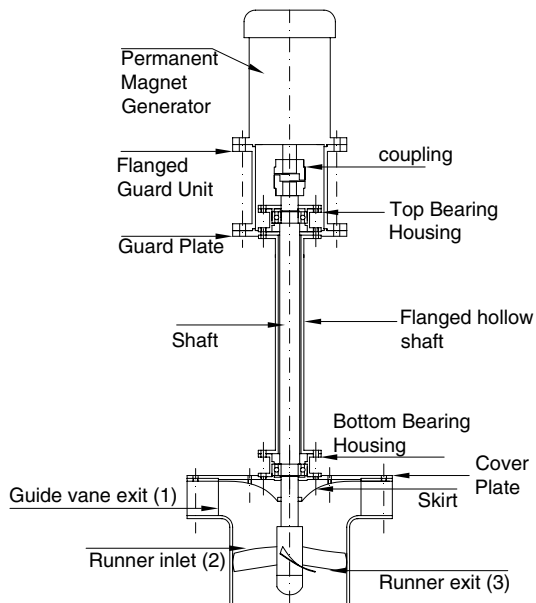


Fig. 5. Assembly of the propeller turbine unit

Analysis of the Internal Variables

The performance analysis between the two stages is carried out at a gross head of 1.75 m and a speed of 900 rpm, which includes the study of the behavior of both the main and the internal variables by using the theory highlighted in the section “Theoretical Model.”

The percentage deviations of the primary variables are graphically read out from the constant head characteristics and are related to the internal variables by the analytical equations described in the following:

1. Change in axial velocity, $\delta(c_x)$: From Eq. (2), c_x is proportional to Q for the same d_h/D . Hence, $\delta(c_x)$ is also proportional to $\delta(Q)$:

$$\delta(c_x) \approx \delta(Q) \quad (14)$$

Physically, the change in axial velocity implies some change caused by either k_{runner} or β_3 or both, as shown in Eq. (7). The exact pattern of the behavior can be determined only by solving the quadratic polynomial in Eq. (7). However, sensitivity analysis can be performed between any two stages of optimization, and the relative influences of both k_{runner} and β_3 can be obtained from the individual slopes $\partial(c_x)/\partial(k)$ and $\partial(c_x)/\partial(\beta_3)$ for fixed changes of k_{runner} and β_3 .

2. Change in net tangential flow velocity, $\delta(\Delta c_u)$: This component can be evolved from Eq. (15) by using experimental results of two stages, which is then combined with the differential form of Δc_u [given by Eq. (8)] to determine the relative influences of k_{runner} and β_3 , by using the sensitivity analysis approach once again that comprises of determining the slopes, $\partial(\Delta c_u)/\partial(k)$ and $\partial(\Delta c_u)/\partial(\beta_3)$ for fixed changes of k_{runner} and β_3 :

$$\delta(\Delta c_u) \approx |P_{shaft}/(\rho \cdot Q) \cdot u|_A - |P_{shaft}/(\rho \cdot Q) \cdot u|_B \quad (15)$$

3. Change in runner loss coefficient, $\delta(k_{runner})$: This can be determined by using the differential form of Eq. (6), as shown in Eq. (16). For identical flow conditions within guide vanes, draft tubes, and other components, the change in k_{system} can be taken as proportional to the change in k_{runner} :

$$\begin{aligned} \delta(k_{system}) &\approx \delta(k_{runner}) \\ &= |(gH - \Delta c_u \cdot u)/Q^2|_A - |(gH - \Delta c_u \cdot u)/Q^2|_B \end{aligned} \quad (16)$$

4. Change in exit relative flow angle ($\delta\beta_3$) and the angle of incidences at the inlet (i_2): These are determined from the velocity triangles.

Results and Discussion

Influence of Inlet Hub

The cascades at the hub of the two runner stages are shown in Fig. 6, whereas the unaltered tip blade profile is represented in Fig. 7. The performance characteristics are compared in Figs. 8(a–b), which reveal that power characteristics of the modified hub (twisted stage)

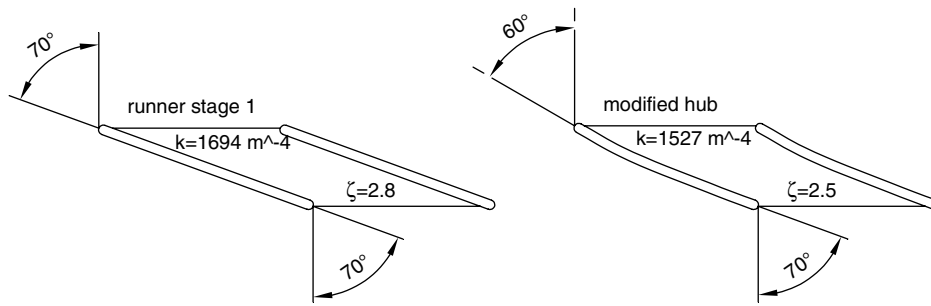


Fig. 6. Cascades of the hub blade profiles for the two runners' stages

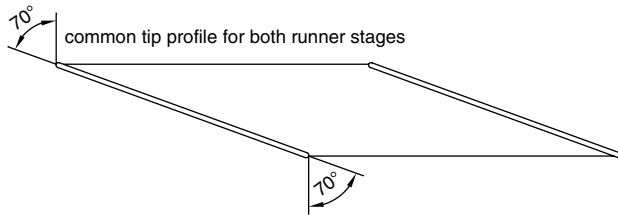


Fig. 7. Cascade of the tip blade profiles

have significantly improved over the complete operating range, whereas the discharge capacity has marginally increased, and the efficiency has risen. However, the performance of the constant blade angle runner is reasonably good, which reaches a maximum efficiency of 68% at 800 rpm. This is an important result when the objective is to keep the design and manufacturing of the runner as simple as possible.

The percentage analysis in Table 3 shows that the power of the modified hub has increased by 5.3%, whereas the discharge has risen by 1.7%, resulting in an efficiency improvement from 66 to 68% at 900 rpm. Among the internal control variables, the k_{runner} has dropped by nearly 10%, whereas the β_3 has changed by only 0.2%. However, the internal dependent variables, c_x and Δc_u , have increased by 1.7 and 3.5%, respectively. It will be interesting to see how changes to the two control variables (k_{runner} and β_3) have relatively affected the dependent variables. The velocity triangles for the two stages, on the basis of experimental results and assumptions described in the section "Construction of Velocity Triangles," were plotted at the tip and hub profiles, respectively, in Figs. 9 and 10.

Discussion on the Behavior of Internal Control Variables

1. Change in k_{runner} : The decrease of the k_{runner} can be primarily attributed to better flow passage geometry in the hub and adjoining regions because incidence effects do not seem to have altered, as shown in both the inlet triangles of the tip and hub blade profiles from Figs. 9 and 10, respectively.
2. Change in β_3 : The marginal change in the direction of the blade rotation, which signifies a decreased slip effect. It will be interesting to see how this small change in relative flow direction will influence the other two dependent variables, c_x and Δc_u , respectively.

Discussion on the Behavior of Internal Dependent Variables

1. Change in c_x : The sensitive analysis in Table 4 reveals some unexpected results. A minute change of 0.2° in β_3 is contributing to a 68% rise in c_x , whereas the large change of 10% in k_{runner} is resulting in a rise of only 32% in c_x . This result clearly shows that the axial flow velocity is very sensitive to the change in the relative flow angle at the exit.
2. Change in Δc_u : The 3.5% (+0.042 m/s) rise in Δc_u results from two contrasting effects, as shown in Table 4. Although the decrease in k_{runner} is playing a dominating role and causing the Δc_u to rise by 0.057 m/s, the decrease in β_3 is contributing to the drop in Δc_u by 0.015 m/s. This result indicates that the net tangential velocity is more sensitive to the runner loss coefficient than the exit relative flow angle.

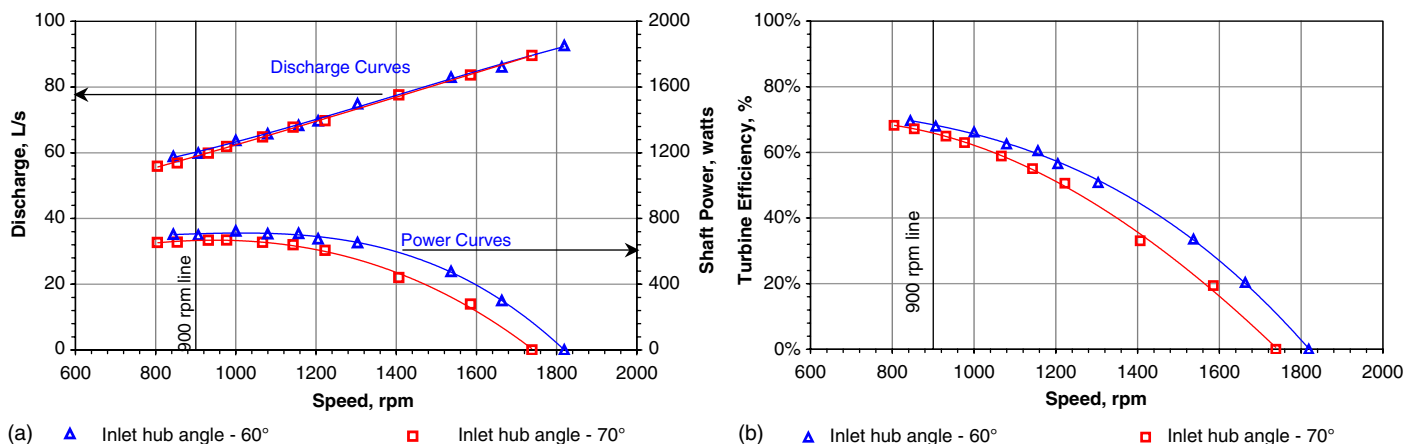


Fig. 8. (a) Discharge and power curves for the two runner stages; (b) efficiency curves for the two runner stages

Table 3. Percentage Analysis of the Major and Internal Variables for the Two Runner Stages

Modification Stage	Summary of the internal variables																	
	Summary of main variables					Control					Dependent							
	H (m)	N (rpm)	Q (L/s)	δQ (%)	P (w)	δP (%)	η	$\delta \eta$ (%)	k_{runner} (1/m ⁴)	δk_{runner} (%)	β_3 (°)	$\delta \beta_3$ (%)	c_x (m/s)	δc_x (%)	Δc_u (m/s)	$\delta \Delta c_u$ (%)	kQ^2 (m)	$\delta(kQ^2)$ (m)
$\beta_{3h} - 70^\circ$	1.75	900	58.7	+1.7	665	+5.3	66.0%	+2.0	1,694	-9.9	77.24	-2.0	2.053	+1.7	1.20	+3.5	0.595	-4.0
$\beta_{3h}^t - 60^\circ$	1.75	900	59.7		700	68.0%		1,527		77.06		2.088		1.24		0.555		

Discussion on the Shape of Velocity Triangles

The velocity triangles can be compared at the tip and at the hub, which were constructed based on the principles laid out in the section “Construction of Velocity Triangles” and the experimental data. The tip velocity triangles (Fig. 9) resemble that of a low-pressure stage with the relative velocity increasing from the inlet to the exit. This behavior is in accordance to the principle of rothalpy introduced by Dixon (2005a), in which the flow within a turbine should accelerate. However, the velocity triangles at the hub (Fig. 10) resemble that of a high-pressure axial turbine stage, but the relative velocity is decreasing from the inlet to the exit, signifying flow deceleration and a negative reaction effect.

This uncommon phenomenon needs further investigation. There could be a possibility of errors in the construction of the velocity triangles. The inlet vortex profile, which is theoretically determined by using the principles mentioned in the section “Inlet Vortex Angle (α_2)” could be faulty. Because of radial and secondary flows, the inlet vortex angle at the hub may be different from that predicted by Eq. (13). The constancy of the axial velocity is also debatable. The sensitivity analysis of the dependent variables with respect to the inlet vortex angle could give an indication on the influence of change in inlet vortex angle on the axial velocity and the net tangential flow velocity, which are both the components of the velocity triangle.

Nevertheless, the energy transfer in the hub region and flow within these passages remains an interesting topic of study and cannot be pursued with the limited experimental data available. Experimental evaluation of the vortex profiles at the inlet will be important to carry the investigation of the hub energy transfer further.

Discussion of the Model's Limitations

As mentioned in the previous section, there could be a possibility of errors in the construction of the velocity triangles, which also forms a part of the theoretical proposed in this paper. The sources of these errors need to be analyzed because important conclusions were interpreted by using this model. Although the classical turbine theory cannot be disproved, one of the possible uncertainties could be with respect to the free vortex flow characteristics assumed between the guide vane exit and runner inlet. As shown in Fig. 5, the flow in this region changes from radial to axial flow in a relatively short length. The prime criteria for the validity of free vortex flows are radial equilibrium and constant axial velocity. It is difficult to imagine a zero radial flow condition in reality. These deviations would naturally affect the inlet vortex angle predictions, which would affect the shape of velocity triangles and conclusions made.

Further, the leakage losses were not considered in the model. However, this is a reasonable assumption because only relative changes of different parameters are analyzed.

Conclusions and Recommendations

The theoretical model developed on the principles of classical turbomachinery for the specific case of propeller turbines was very useful in comprehensively studying the hydraulic phenomenon within the runner. It developed the functionality of the internal variables and identified the runner loss coefficient and the exit relative flow direction as the control variables and the axial flow and net tangential flow velocities as the dependent variables for constant speed and head operation. Further, these functionalities were validated by using experimental techniques.

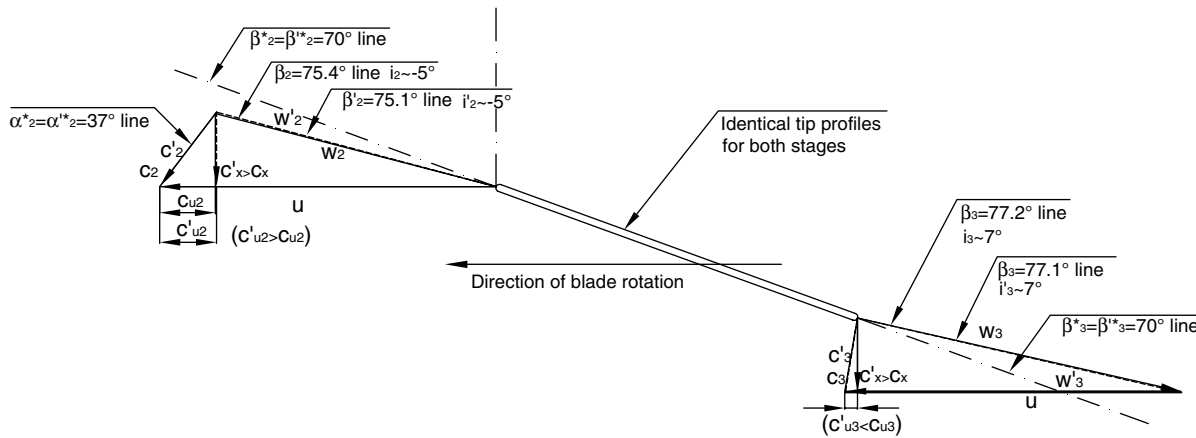


Fig. 9. Consolidated velocity triangles at the blade tip for the two runner stages

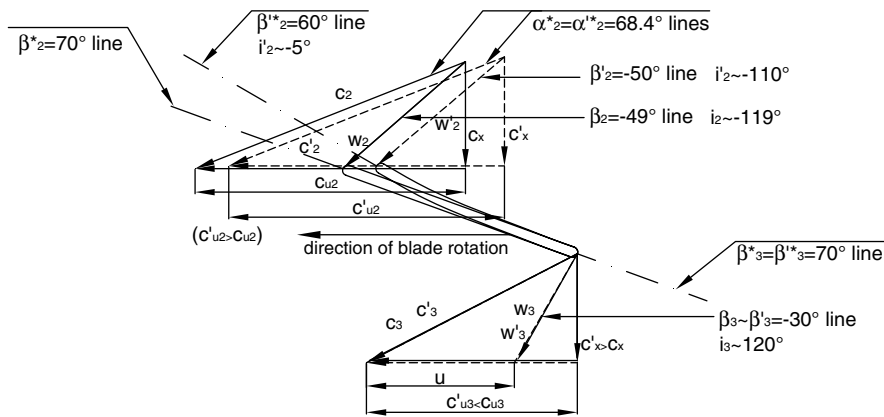


Fig. 10. Consolidated velocity triangles at the blade hub for the two runner stages

The experimental results of untwisted and twisted blades were very interesting. It was heartening to see an untwisted blade with a constant blade angle of 70° achieving an efficiency of over 68%. This simplistic design can be employed for smaller projects, in which efficiency does not play a deciding role. However, the results also clearly showed the value addition obtained by incorporating a twist in the blades. A modification of the inlet hub angle from 70 to 60° certainly created positive effects, causing the efficiency to improve over 2%, nearly reaching the 70% mark. There were clear indications of enhanced power generation and a slight increase of discharge capacity of the modified runner.

The study of the internal hydraulic parameters showed that there was considerable decrease in the runner loss coefficient, which contributed to rise of net tangential flow velocity (or rotational momentum) in a major way and slightly increased the axial velocity. The decrease in the runner loss coefficient was attributed to the improvement in the flow passage geometry near the hub region. The most interesting find was the role of the exit relative flow velocity direction on the axial flow velocity. A very marginal decrease of 0.2° caused a substantial increase of axial velocity and a drop in the net tangential velocity. This change of the relative flow direction was attributed to the reduced slip in the modified hub runner.

The overall results of the study underlined the importance of twist in the design of axial flow turbine blades and agreed with various design theories of axial turbine blades.

The velocity triangle analysis found an uncommon flow phenomenon near the hub region, where flow deceleration was observed instead of the normal flow acceleration in turbine blading. This phenomenon was discussed in the prediction uncertainties of the inlet vortex flow, which could affect the shape of the velocity vectors. However, the energy transfer in the hub region remained inconclusive.

The observations lead to several recommendations from the perspectives of both experimental and computational studies. On the experimental side, it is recommended to measure the inlet vortex flow and mean axial flow velocity profiles along the blade height and compare the results with the theoretical prediction made in the study. The second experimental study is to determine swirl flow characteristics throughout the radial cross section of the blade at the runner exit and compare it with the exit flow direction obtained from the theoretical model.

The study found some limitations in the model primarily with respect to free vortex flow assumptions made between the guide vane exit and runner inlet, which need to be verified by using a calibrated and reliable computational model. The chief objectives of the computational fluid mechanics (CFD) model should be to verify all the results of the experiments. It should also focus on studying the quality of flow and energy transfer mechanisms at different sections of the blade, especially near the hub region that showed flow deceleration in the experimental study. The CFD model should further help in understanding the sensitivity of the

Table 4. Sensitivity Analysis for Changes to c_x and Δc_u for the Two Runner Stages

	δc_x caused by k_{runner}			δc_x caused by β_3			
	$d(c_x)/d(k)$	$\delta k (m^{-4})$	$[\delta c_x]_k (m/s)$	$d(c_x)/d(\beta_3)$	$\delta \beta_3 (rad)$	$[\delta c_x]_{\beta_3} (m/s)$	% contribution
Overall $\delta c_x (m/s)$	-6.7E-05	-168	+0.011	-7.23	-0.003	+0.024	68%
Overall $\delta \Delta c_u (m/s)$	$d(\Delta c_u)/d(k)$	$\delta k (m^{-4})$	$\delta \Delta c_u$ caused by k_{runner} $[\delta \Delta c_u]_k (m/s)$	$d(\Delta c_u)/d(\beta_3)$	$\delta \beta_3 (rad)$	$\delta \Delta c_u$ caused by β_3 $[\delta \Delta c_u]_{\beta_3} (m/s)$	% contribution
0.042	-3.4E-04	-168	+0.057	+4.65	-0.003	-0.015	-36%

Table 5. Uncertainty Table for the Two Runner Stages

Runner	Generator parameters							Turbine parameters											
	V	$\Delta V/V$	I	$\Delta I/I$	N	$\Delta N/N$	T	$\Delta T/T$	η_g	$\Delta \eta_g/\eta_g$	$\Delta P_m/P_m$	P_m	Q	$\Delta Q/Q$	H	$\Delta H/H$	η_{lm}	$\Delta \eta_{lm}/\eta_{lm}$	$\Delta \eta_{lm}$
Runner Stage 1	90.0	$\pm 0.1\%$	5.35	$\pm 1.9\%$	900	0.1%	7.1	$\pm 1.4\%$	72.4%	$\pm 2.4\%$	$\pm 3.0\%$	665	58.7	$\pm 0.2\%$	1.75	$\pm 0.3\%$	66.0%	$\pm 3.0\%$	$\pm 2.0\%$
Runner Stage 2	88.5	$\pm 0.1\%$	5.7	$\pm 1.8\%$	900	0.1%	7.4	$\pm 1.3\%$	72.1%	$\pm 2.2\%$	$\pm 2.8\%$	700	59.7	$\pm 0.2\%$	1.75	$\pm 0.3\%$	68.0%	$\pm 2.8\%$	$\pm 1.9\%$

Table 6. Maximum Random Error for Each Variable

ΔV (V)	ΔI (A)	ΔN (rpm)	ΔT (Nm)	ΔQ (L/s)	ΔH (m)
± 0.1	± 0.1	± 1	± 0.1	± 0.1	0.005

performance parameters to the change in relative flow direction at the runner exit.

Once the CFD model is calibrated to a satisfactory level, it can then be used as an optimization tool and further help in realizing the bigger objective of standardizing the design of optimum blade profiles required for special operating conditions of low-head axial flow turbines in micro hydro application.

Appendix. Experimental Uncertainty Analysis

The overall uncertainty analysis is carried out by using the single sample study proposed by Moffat (1982) and Kline (1985) at the best efficiency points (BEP) points of the two runner stages and is summarized in Table 5. The evaluation combines the results from two separate test rigs, namely the generator test rig used for characterizing the generator and the turbine test rig used to study the complete turbine generator unit. The overall random error for all the variables is summarized in Table 6.

Acknowledgments

The authors would like to acknowledge the contribution of Erfried Berger, Boris Lehmann, Frank Seidel, Gerard Close, Günther Kühn, Manfred Lösche, Marcus Plate, Martin Gabi, Michael Ritzmann, Michael Ziegler, Jürgen Ullrich, Peter Oberle, Ramesh, Ravichandran, Saban Caglar, and Werner Helm, without whom the work of propeller research would not have been accomplished.

Notation

The following symbols are used in this paper

- c = absolute velocity m/s;
- D = tip diameter, m;
- d = local diameter, m;
- g = acceleration caused by gravity, m/s²;
- H = head parameter, m;
- I = current, A;
- i = angle of incidence, deg;
- k = loss coefficient, 1/m⁴;
- m = mass flow rate, kg/s;
- N = speed, rpm;
- P = power, kW;
- Q = discharge, L/s or m³/s;
- T = torque, Nm;
- u = tangential blade velocity, m/s;
- V = voltage, V;
- w = relative velocity, m/s;
- z = number of blades;
- α = absolute flow angle, degrees;
- β = relative flow angle, degrees;
- ζ = pressure loss coefficient;

- η = efficiency, %; and
- ρ = density, kg/m³.

Subscripts

- g = generator;
- h = hub region;
- m = mechanical;
- t = tip region;
- u = tangential direction;
- x = axial direction;
- 1 = guide vane exit;
- 2 = runner inlet; and
- 3 = runner exit.

Superscripts

- * = blade condition.

References

- Alexander, K. V., Giddens, E. P., and Fuller, A. M. (2009). "Axial-flow turbines for microhydro systems." *Renewable Energy*, 34(1), 35–47.
- Asian Phoenix Resources Ltd. (APRL). (2001). "Powerpal brochure." (<http://www.powerpal.com>) (Feb. 17, 2009).
- Cohrs, D. (1997). *Untersuchungen an einer mehrstufigen rückwärtslaufenden kreiselpumpe im turbinenbetrieb*, W. H. Faragallah, ed, Verlag und Bildarchiv, Sulzbach, Germany, 8–41 (in German).
- Demetriades, G. M. (1997). "Design of low-cost propeller turbines for standalone micro-hydroelectric generation units." Ph.D. thesis, Univ. of Nottingham, Nottingham, UK.
- Dixon, S. L. (2005a). "Basic thermodynamics, fluid mechanics: Definition of efficiency." *Fluid mechanics and thermodynamics of turbomachinery*, Elsevier, Oxford, UK, 24–35.
- Dixon, S. L. (2005b). "Two dimensional cascades." *Fluid mechanics and thermodynamics of turbomachinery*, Elsevier, Oxford, UK, 56–90.
- Kline, S. J. (1985). "The purposes of uncertainty analysis." *J. Fluids Eng.*, 107(2), 153–160.
- Moffat, R. J. (1982). "Contributions to the theory of single-sample uncertainty analysis." *J. Fluids Eng.*, 104(2), 250–260.
- Pfleiderer, C., and Petermann, H. (1991). "Der strömungsmechanismus im laufrad." *Strömungsmaschinen*, Springer-Verlag, Berlin (in German).
- Rao, G. J., Prasad, R., and Rao, J. K. S. (1988). "Investigation of an axial flow runner for micro hydro power development." *Proc., 8th Fluid Machinery Conf.*, Scientific Society of Mechanical Engineers–Section of Technical Sciences, Hungarian Academy of Sciences, Akadémiai Kiadó, Budapest, Hungary, 616–623.
- Simpson, R. G., and Williams, A. A. (2006). "Application of computational fluid dynamics to the design of pico propeller turbines." *Proc., Int. Conf. on Renewable Energy for Developing Countries*, School of Engineering and Applied Science, Univ. of the District of Columbia (UDC), Washington, DC.
- Singh, P., and Nestmann, F. (2009). "Experimental optimization of a free vortex propeller runner for micro hydro application." *Exp. Therm. Fluid Sci.*, 33(6), 991–1002.
- Soundarnayagam, S., and Suryanarayanan, A. (1988). "Ultra low-head propeller turbines for small canal drops." *Turbomachines Laboratory Rep.*, Indian Institute of Science, Bangalore, India.
- Upadhyay, D. (2004). "Low head turbine development using computational fluid dynamics." Ph.D. thesis, Univ. of Nottingham, Nottingham, UK.
- Watson, N., and Janota, M. S. (1982). "The axial flow turbine." *Turbocharging of the internal combustion engine*, Macmillan, London, 209–225.

Impeller performance

Axial flow impeller shapes: Part 1

The increasing importance of low head applications necessitates a study of the different axial flow pump impellers used for both pump and turbine operations. In this first of two articles, Punit Singh and Franz Nestmann of Karlsruhe Institute of Technology survey the available impeller shapes and present a theoretical model that reveals the behaviour of the impellers' internal hydraulic variables.

Low head applications of turbomachinery (both pumps and turbines) are gaining increasing importance in modern day engineering. This is particularly true for turbine operation for energy recovery and decentralized power applications^{1,2}. While the requirements for pumping have been handled well by the industry, by comparison the technology

for low head turbine applications has not yet been optimized.

The pumps for low head applications are mainly of the axial flow type, which are manufactured with either forward or backward curved blades. These two blade shapes have different influences on the performance of the pumps.

However, neither experimental nor theoretical investigations on these influences have been effectively compared or presented. In addition, the total pump characteristics (four-quadrant analysis), which have become a norm for the industrial use of pumps under specialized operating conditions after Stepanoff³, have not been published for all the axial flow pumps available on the market. One of the quadrants of these characteristics pertains to turbine operation. However, it is not clear whether forward or backward curved blades are more suitable for turbine applications. In order to clarify both pump and turbine operations with these impeller shapes, a theoretical study would be beneficial before detailed experimental work is initiated.

The objectives and problem outline of this two-article series are summarized as follows:

a) To survey the different axial flow pumps available with forward and backward curved impeller shapes.

b) To develop a theoretical model based on turbomachinery fundamentals for both pump and turbine operation and to study the behaviour of the internal hydraulic variables in these impellers.

c) To study the implications for turbine operation of both these impeller shapes and recommend suitable impellers for further experimental optimization.

d) To initiate a simulation model for the four-quadrant analysis of both these impeller shapes.

Part 1 analyses the forward curved blades, while part 2 will focus on backward curved blades and compare the pump and turbine operations for the two blade shapes.

Means and methods

The study collates classical and modern-day literature on the development of optimum axial flow impeller shapes. Further, a theoretical model based on the Euler theory of turbomachines is developed to study the internal hydraulic behaviour of the two impeller

Definition of parameters and subscripts

- c absolute velocity, m/s
- g acceleration due to gravity, m/s²
- H head, m
- k_a, k_b , etc. constants of the Euler line
- Q discharge, l/s or m³/s
- u tangential blade velocity, m/s
- w relative velocity, m/s
- α absolute flow angle, degrees
- β relative flow angle, degrees
- ζ pressure loss coefficient

- * blade direction
- f,p forward curved pump impeller
- ft forward curved turbine impeller
- p pump mode
- t turbine mode
- u tangential direction
- x axial direction

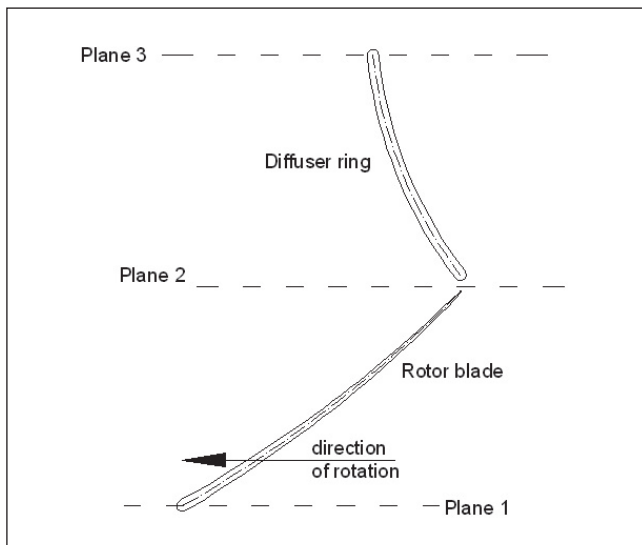


Figure 1. Blade section of a forward curved impeller and diffuser.

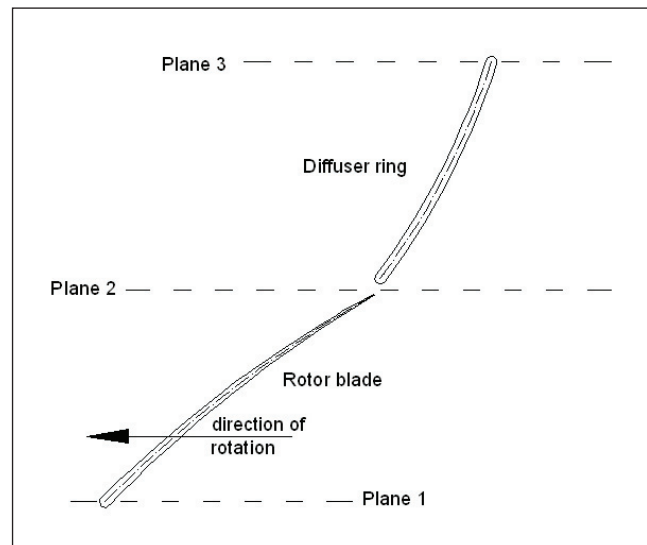


Figure 2. Blade section of a backward curved impeller and diffuser.

shapes for both pump and turbine operations. The model will be useful in evaluating the influences of the blade shapes and also help in studying suitable shapes for dedicated turbine operation.

Survey of axial flow impellers

The basic shape of the axial blade is defined based on the relationship of the curvature with respect to the direction of the blade rotation. The forward curved variety is the most common type of axial flow pump

impeller available on the market and is also seen in the blade shapes of fans and compressors. Figure 1 shows a section of a forward curved axial impeller stage (impeller and diffuser ring). This type of impeller has been investigated by Baumgarten et al. and Stark and Siekmann^{4a&b} for axial flow pumps, while Dixon⁵ has carried out studies on axial flow fans and compressors with forward curved blade designs. The energy transfer and internal hydraulics for this blade shape in pumps and turbines are discussed in the next section.

The shape of the backward curved impeller along with the diffuser blade is shown in Figure 2. This peculiar shape of axial impeller has been widely used by KSB (for example, in the Amacan P series; www.ksb.com) and has also been reported by Springer^{4c}. The energy transfer and behaviour of the internal variables for both pump and turbine modes will be examined in the second article.

Theoretical model and analysis

A theoretical model is derived here for pump and turbine operations using forward curved impellers. The model relies on Euler fundamentals for axial machines as suggested by Singh and Nestmann⁶.

Pump operation

The construction of the velocity triangles in pump mode involves certain assumptions, namely, that the absolute flow entry to the impeller is swirl-free, and that there is zero flow incidence at the blade entry. Further, the deflection of the relative velocity at the blade exit is neglected, which is a reasonable assumption provided the entry is incidence free, as pointed out by Dixon for compressor cascade results⁵. In addition, the flow areas at the exit and the entry are identical, making the axial flow velocities identical as the compressibility effects of the working fluid, which is liquid, have been neglected.

The velocity triangles for the complete stage of a forward curved impeller are plotted in Figure 3. The shape of the diffuser is based on the resulting direction of the absolute flow velocity at the rotor exit and the need

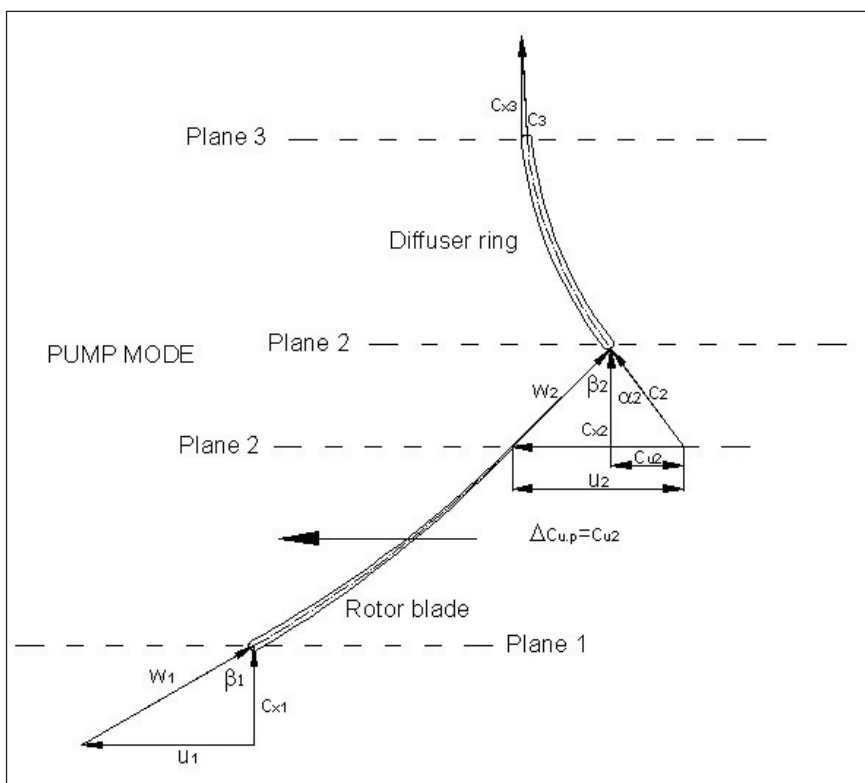


Figure 3. Internal flow analysis of a forward curved blade in pump mode.

to make the flow swirl-free (to have c_{u3} as small as possible) at the stator exit. It can also be seen that the relative velocity is reduced across the rotor blade. The hydraulic shaft power or Euler momentum is positive with respect to the blade velocity, as shown in Equation 1:

$$(\Delta C_u \cdot u)_{f,p} = (c_{u2} - c_{u1}) \cdot u = c_{u2} \cdot u \text{ (as } c_{u1} \text{ is zero)}$$

$$(\Delta C_u \cdot u)_{f,p} = k_{a,f,p} - k_{b,f,p} \cdot Q \quad (1)$$

In addition, internal variables such as the impeller profile loss coefficient result in losses that have to be accounted for before arriving at the actual momentum gained by the fluid (Equation 2). On the whole, the velocity triangles in forward curved pump impellers behave in accordance with the established theory of diffusion through the rotor and positive pressure gradient.

$$(\Delta C_u \cdot u)_{fluid\ f,p} = c_{u2} \cdot u - \zeta_{f,p} \cdot c_x^2 / 2 \quad (2)$$

Turbine operation

The internal hydraulic analysis of the two blade shapes in turbine mode also entails some assumptions. Firstly, it is assumed that the axial flow velocity required to operate the turbine at its best efficiency point (BEP) and at the same speed as the pump would be higher (by 1.4 to 1.6 times) than the corresponding pump axial flow velocity⁷. The flow within the static nozzles (or diffusers in pump mode) follows the respective geometries without any deviation. Further, as the first step it

is assumed that the relative flow at the rotor exit is deflection-free, which is quite contentious as will be seen as the analysis progresses. Another important assumption is that the direction of blade rotation is in the direction of the inlet swirl to the rotor.

The construction of the velocity triangles in Figure 4 and the analysis in Equation 3 show that all the parameters follow the turbomachinery principles with positive angular momentum and increase of relative velocity across the rotor. The behaviour of the internal flow variables for relative flows with and without deflection at the turbine exit is examined in the discussion section.

$$(\Delta C_u \cdot u)_{ft} = (c_{u2} - c_{u1}) \cdot u = \text{positive value}$$

$$(\Delta C_u \cdot u)_{ft} = k_{c,ft} + k_{d,ft} \cdot Q \quad (3)$$

$$(\Delta C_u \cdot u)_{fluid\ ft} = (\Delta C_u \cdot u)_{ft} + \zeta_{ft} \cdot c_x^2 / 2 \quad (4)$$

Results

The theoretical Euler line for forward curved pump impellers (Equation 1), along with the actual head gained by the fluid, is plotted in Figure 5 for a wide range of flows. The losses mainly include the profile losses through the rotor given by Equation 2. The magnitude of these losses will depend purely on the profile loss coefficient, which is a function of the angle of incidence at different flow conditions of the pump. There is a zone of instability in the partial-flow region for these impellers.

The turbine mode characteristics for forward curved impellers, comprising the Euler line (Equation 3), actual pressure line (Equation 4), zero speed ($N = 0$) and zero torque ($T = 0$) lines, are plotted in Figure 6. The extents of zone C (energy generation zone) and zone D (energy consumption zone) are also shown. The operating point with a positive head is also indicated. The Euler line can extend into the negative head zone, but this is not shown in Figure 6.

Discussion

The main discussion point concerns the turbine operation of forward curved impellers. The results (Figure 4) revealed that, for the present design of the diffuser blades (in pump mode), the flow entry would cause considerable incidence effects and would also probably result in deflection effects at the exit. Following the conventional direction of deflections in turbine blades, it is seen that the natural deflection would cause the net Euler torque to increase, but the profile loss coefficient would also increase, resulting in higher net head across the turbine stage. An experimental study of incidence, deflection and profile losses would clarify this phenomenon, which cannot be ascertained with the present theoretical model. The model also places the operating point of the turbine in the safe operating region (zone C), but the actual efficiency of this point would be a function of incidence

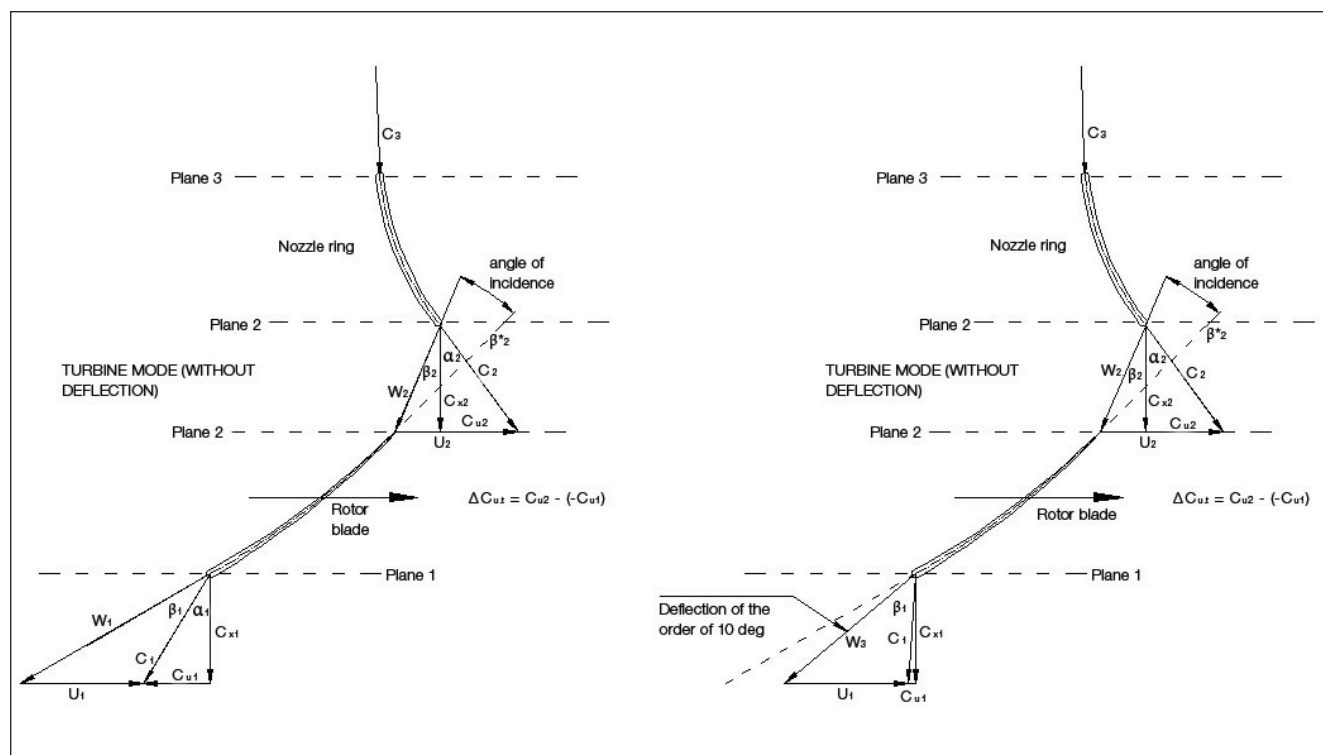


Figure 4. Internal flow analysis of a forward curved blade in turbine mode, with and without deflection.

and deflection effects and the profile loss coefficient.

Conclusions and recommendations

This detailed survey of impellers reveals that manufacturers are using both forward and backward curved impellers primarily intended for pump mode operation. The application of the theoretical model to pump operation did not show any deviation from the expected performance, but the turbine operation of forward curved impellers showed evidence of considerable levels of incidence effects and possible deflection effects at the exit. One of the recommendations for the future study of forward curved impellers would be to carry out elaborate experimental studies at both the cascade and dynamic levels to determine the exact behaviour of incidence, deflection and profile losses.

The remaining objectives of the study, including evaluation of the optimum turbine impeller shape, will be addressed in the second article of this two-part series. ■

References

[1] P. Singh and F. Nestmann, 'Experimental Optimization of a Free Vortex Propeller Runner for Micro Hydro Application', *J. Experimental Thermal & Fluid Science*, 33, pp. 991–1002, (2009).

[2] R.R. Mankbadi and S.A. Mikhail, 'A turbine-pump system for low-head hydropower', *J. Energy Conversion & Management*, 25, pp. 339–344, (1985).

[3] A.J. Stepanoff, *Centrifugal and Axial Flow Pumps*, John Wiley & Sons Inc, Ch. 8 and 16, (1957).

[4] (a) S. Baumgarten, H. Krasmann and J. Rösener, pp. 147–160; (b) U. Stark and H. Siekmann, pp. 87–96; (c) P. Springer, pp. 109–118, *Publication 1 of the Pfleiderer Institute of Turbomachines*, University of Braunschwig, Verlag und Bildarchiv W. H. Faragallah, Sulzbach, Germany, (1994).

[5] S.L. Dixon, *Fluid Mechanics and Thermodynamics of Turbomachinery*, Elsevier, Ch. 3, (2005).

[6] P. Singh and F. Nestmann, 'Exit Blade Geometry and Part-Load Performance of Small Axial Flow Propeller Turbines: An Experimental Investigation', *J. Experimental Thermal & Fluid Science*, 34, pp. 798–811, (2010).

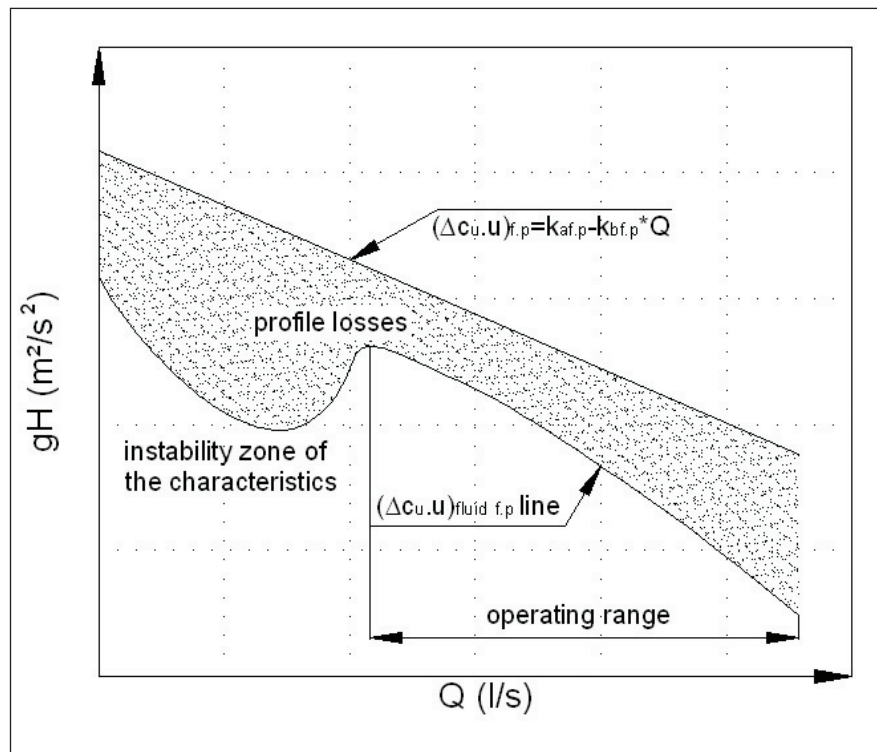


Figure 5. Behaviour of the H-Q line in forward curved pump impellers.

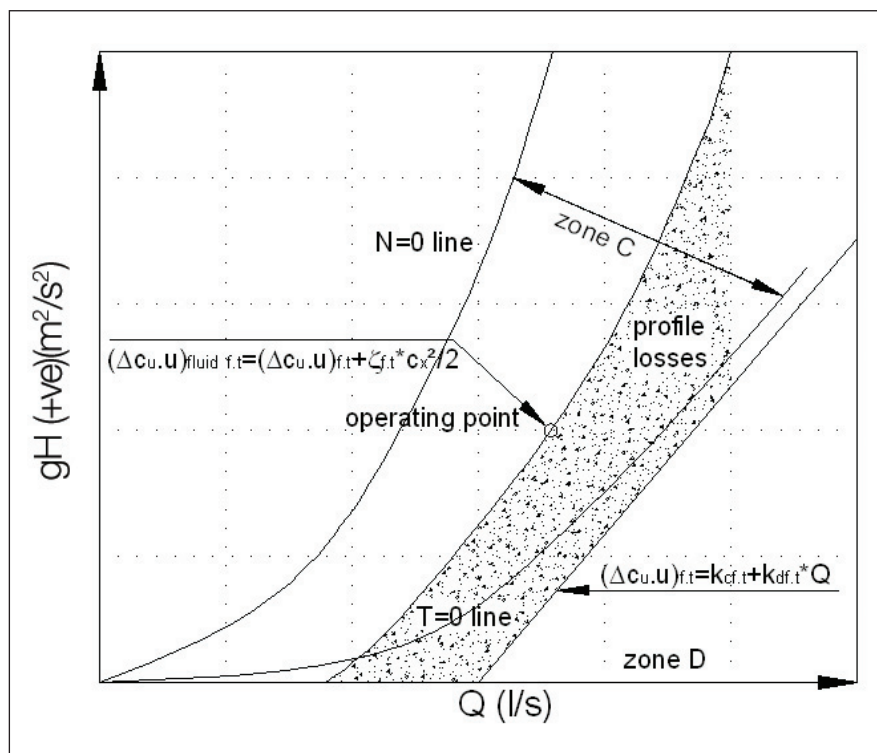


Figure 6. Behaviour of the H-Q line in forward curved turbine impellers.

[7] P. Singh and F. Nestmann, 'An optimization routine on a prediction and selection model for the turbine operation of centrifugal pumps', *J. Experimental Thermal & Fluid Science*, 34, pp. 152–164, (2010).

Contact
 Punit Singh (Postdoctoral researcher) and Franz Nestmann (Director)
 Institute for Water and River Basin Management (IWG)
 Karlsruhe Institute of Technology
 Kaiser Str. 12, Karlsruhe D-76131, Germany
 Tel: +49 721 608 2194
 Fax: +49 721 608 606 026
 Email: punit.singh@iwg.uka.de and nestmann@iwg.uka.de

Impeller performance

Axial flow impeller shapes: part 2

In this second of two articles concerning axial flow impellers, Punit Singh and Franz Nestmann of Karlsruhe Institute of Technology focus on backward curved impellers, revealing hydraulic behaviour that is interesting and unexpected in pump and turbine operations respectively. They also compare the performance of forward and backward curved impellers to determine the optimum impeller shape for turbines.

The background and objectives of this two-part series were discussed in detail in the previous article¹. As mentioned, this second article will closely analyse the performance of backward curved axial flow impellers for both pump and turbine operations, as well as covering the remaining objectives of the study, namely:

- To apply the theoretical model (developed in part 1) to backward curved impellers and look at nuances within the internal hydraulics in both pump and turbine operations.
- To search for the optimum turbine impeller after comparing the turbine operations of forward and backward curved impellers.
- To establish steps for modelling the four-quadrant characteristics of pumps with both forward and backward curved impellers.

Theoretical model and analysis

Pump operation

The pump mode velocity triangles in backward curved impellers are certainly very peculiar (Figure 1). It can be seen that the net hydraulic momentum is negative (Equation 1) since the exit angular momentum is in the opposite direction

to the blade velocity. There is an increase of relative velocity across the rotor, which is a clear deviation from the principles of pump and compressor designs. This represents a negative reaction blade design. The practical ramification of negative fluid torque does not affect the power supply direction; the pump will still be a work-absorbing device. In addition, the shape of the diffuser must undergo a major change to accommodate this negative swirl velocity at the exit, but this condition is still acceptable, as the pump will continue to impart energy and pressure to the fluid.

$$\begin{aligned} (\Delta c_u \cdot u)_{b,p} &= (c_{u2} - c_{u1}) \cdot u = |-c_{u2} \cdot u| \approx -c_{u2} \cdot u \\ (\Delta c_u \cdot u)_{b,p} &= k_{a,b,p} - k_{b,b,p} \cdot Q \end{aligned} \quad (1)$$

Turbine operation

The analysis of the internal hydraulics in backward curved impellers in turbine mode reveals a complex behaviour of the variables (Figure 2). It can be seen that the magnitude of the exit swirl (c_{u1}) is greater than that of the inlet swirl (c_{u2}), causing the outlet hydraulic torque to exceed the inlet torque. This gives a negative value to the net hydraulic momentum, which relates to the condition of energy dissipation and is represented by zone D or zone E (external work done on the shaft) in the four-quadrant pump characteristics (Stepanoff²).

$$(\Delta c_u \cdot u)_{b,t} = (c_{u2} - c_{u1}) \cdot u = \text{negative value}$$

$$(\Delta c_u \cdot u)_{b,t} = k_{c,b,t} + k_{d,b,t} \cdot Q \quad (2)$$

This result ($c_{u1} > c_{u2}$) can be argued on the basis of the principles of deflection under severe incidence conditions in turbine cascades. It can be seen from Figure 2 that a large angle of incidence is created that would necessarily cause deflection of the exit relative velocity in addition to the losses

Definition of parameters and subscripts

c	absolute velocity, m/s
g	acceleration due to gravity, m/s ²
H	head, m
k_a, k_b , etc.	constants of the Euler line
Q	discharge, l/s or m ³ /s
u	tangential blade velocity, m/s
w	relative velocity, m/s
α	absolute flow angle, degrees
β	relative flow angle, degrees
ζ	pressure loss coefficient
*	blade direction
b.p	backward curved pump impeller
b.t	backward curved turbine impeller
p	pump mode
t	turbine mode
u	tangential direction
x	axial direction

within the blade section. If the results of some researchers such as Ainley³ and Okiishi *et al.*⁴ are considered, the relative velocity will be deflected in the opposite direction to the blade velocity, which has also been observed in Figure 2. The deflection could be so severe that it could even result in a reduction of c_{u1} in comparison to c_{u2} and eventually cause the net angular momentum to become positive. However, it will be interesting to investigate practically how these phenomena actually work.

Results

The theoretical Euler line (Equation 1) for backward curved impellers in pump operation mode is plotted in Figure 3. The actual fluid pressure line would depart further from the Euler line owing to both the fluid acceleration effect within the rotor (negative reaction) and profile losses. Further, compared to forward curved impellers there would be greater instability of the actual characteristics due to the negative reaction effects.

In contrast, the turbine characteristics for the backward curved impellers are plotted in two quadrants in Figure 4, comprising three operating zones (C, D and E) for turbine operation. From Equation 2, it is obvious that the operating point of the turbine would be in the negative head region of zone E. Operation at this point would not be useful for optimum power generation.

Discussion

Complex mechanisms in backward curved impellers

The energy mechanisms and internal hydraulics revealed by the model for backward curved impellers, whether for turbine or pump operation, have proved very interesting and an important point for discussion as far as the objectives of this article are concerned.

Turbine operation of the backward curved impellers witnessed severe incidence effects resulting in higher profile losses and causing deflections at the blade exit, which together cause a greater Euler momentum at the exit compared to the inlet. This peculiar or special situation was seen to convert the turbine into a work-absorbing machine rather than work-generating machine. This operating condition has been classified as the 'energy dissipation' zone (D and E) of the total pump characteristics², which is definitely not desirable if useful torque is required from such impellers. These findings are based entirely on the assumed curvature of the rotor and diffuser blades. However, experimental validation of these results is important. The phenomenon of deflection and the transition from power-consuming (c_{u1} greater than c_{u2}) to power-generating (c_{u1} less than c_{u2}) mode would be very interesting to study and to standardize the effects for different blade geometries and individual load points (no load to full load).

The theoretical model and subsequent analysis of backward curved blades in pump operation have also indicated abnormal behaviour, especially with respect to the fluid acceleration within the blade from inlet to exit. Such behaviour is not expected in pump or compressor profiles. The negative reaction created and its implications on the performance cannot be determined from the theoretical model. In addition to the fluid acceleration, another phenomenon observed was the negative swirl created at the rotor

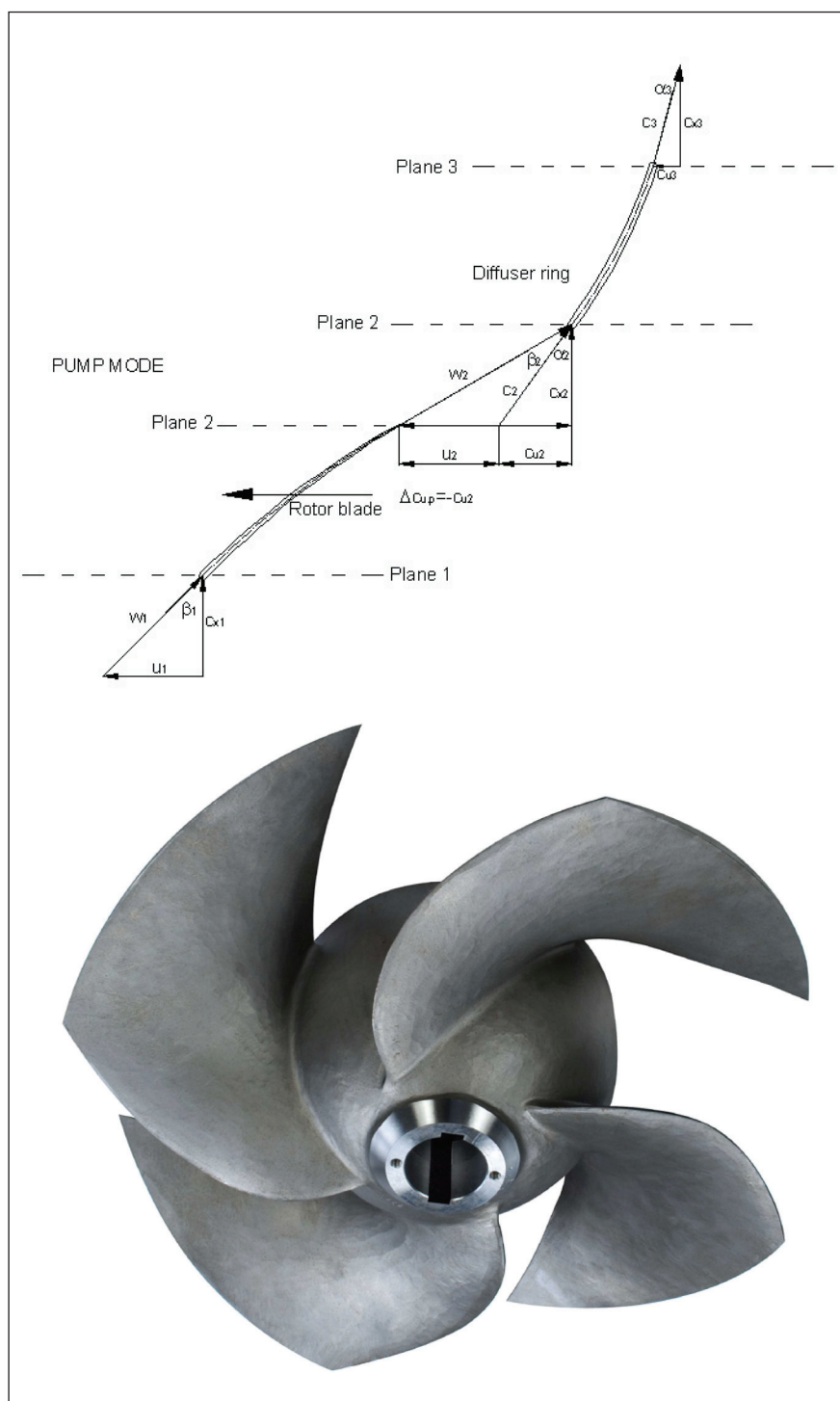


Figure 1. (above) Internal flow analysis of a backward curved blade in pump mode. (below) An example of a pump impeller with backward curved blades (copyright KSB Aktiengesellschaft, Germany).

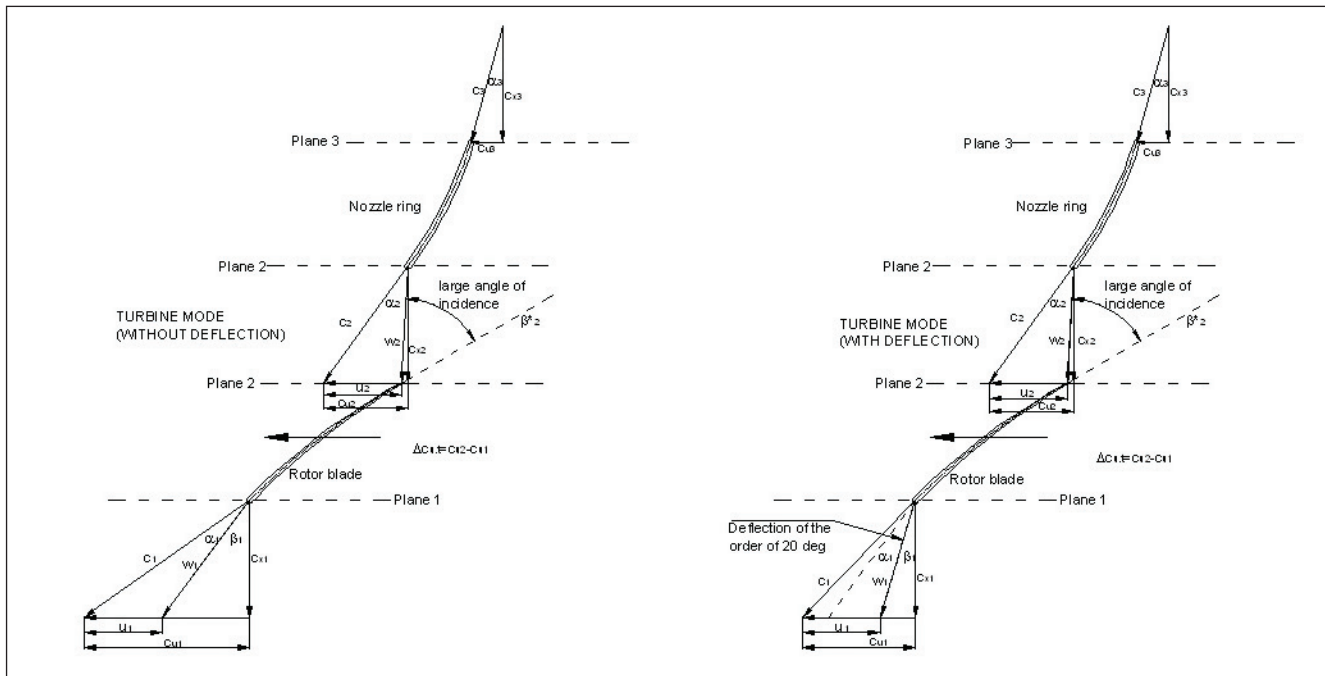


Figure 2. Internal flow analysis of a backward curved blade in turbine mode, with (right) and without (left) deflection.

blade exit. This is not such a big problem because energy is still imparted to the fluid and the shape of the static diffuser would reduce the velocity and enhance the delivery pressure. However, both the fluid acceleration and the negative swirl in pumps need to be studied experimentally.

The optimum turbine impeller

The present analysis based on the theoretical laws of turbomachinery clearly indicates that it would be safer to adopt forward curved axial impellers for optimum turbine operation instead of backward curved impellers. This is mainly owing to the guarantee of performance and fewer uncertainties with respect to incidence and deflection effects along with no likelihood that the operating point will fall in zones D or E. Forward curved impellers may be the first choice for turbine operation, but the study of backward curved impellers for suitability in turbine mode should still be pursued.

Four-quadrant analysis

Some manufacturers have already initiated four-quadrant analysis for selected pumps to meet specialized customer requirements. Nevertheless, a theoretical model to establish these characteristics would be an important development. If the pump and turbine performances could be modelled accurately, then a simple program that connects the operating lines in the remaining zones could be obtained without elaborate experimentation. The

usefulness of the total pump characteristics will be felt in future and working towards this end is recommended, provided the internal hydraulic issues that have been discussed can be resolved satisfactorily.

Conclusions and recommendations

A simple theoretical model based on the Euler theory of turbomachines has been useful in studying the internal hydraulics

of the complex blade shapes in both pump and turbine operating modes. Pump operation for both forward and backward curved blade shapes is well established, but the application of the model clearly showed a difference in the hydraulic behaviour of the two impeller types. While the forward curved pump impeller followed the principles of flow diffusion through the rotor while imparting enthalpy to the fluid, as discussed in the first article, the backward curved impeller

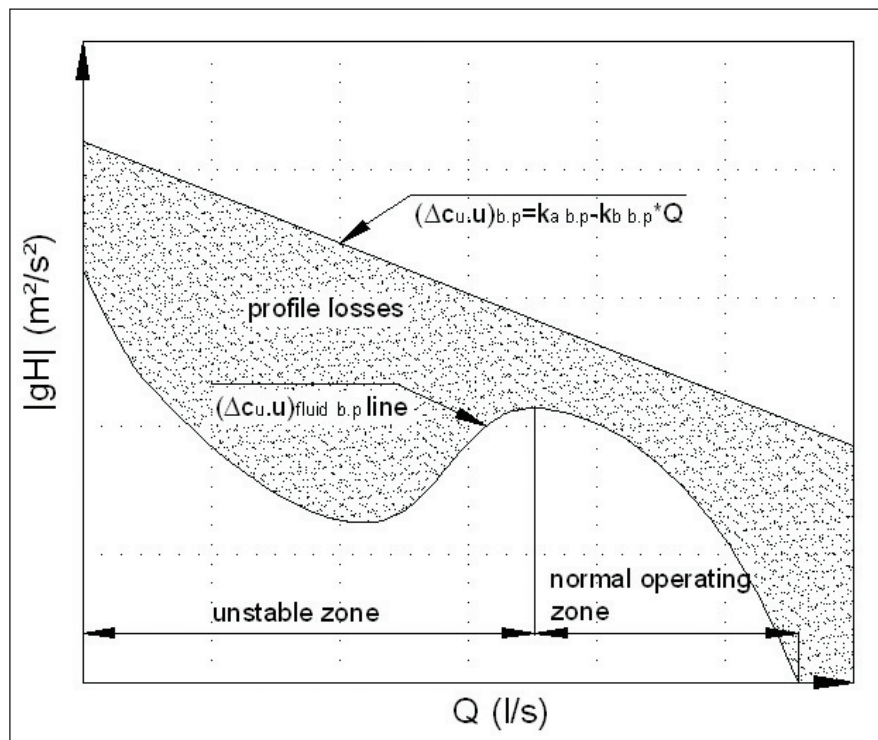


Figure 3. Behaviour of the H-Q line in backward curved pump impellers.

in contrast showed flow acceleration across the rotor, resulting in greater instabilities of the characteristics.

The analysis of the internal hydraulic behaviour of these blade shapes during turbine operation has been startling. For both shapes it has been clearly seen that the turbine blade would be subject to a considerable degree of incidence effect problems as well as fluid deflection, leading to a higher profile loss coefficient. However, the study of the backward curved turbine impeller also established that the hydraulics would become altered to such an extent as to take the turbine into the energy-consumption (input

torque supply) zone, meaning that its turbine mode operation would be highly counterproductive.

It was concluded beyond doubt that forward curved rather than backward curved impellers should be selected for turbine operation. However, we would in no way recommend a halt to the further investigation of backward curved impellers for turbine applications, especially of the interesting effects of incidence and deflection and the power-consuming mode of operation. Such a study would in any case be integral to building the four-quadrant analysis of both backward and forward curved impellers.

The main recommendations from both parts of the current study are summarized below.

- There is a strong case for experimental study particularly focusing on the internal hydraulics of both impeller shapes, especially in turbine mode since turbine hydraulics is yet to be precisely documented. The experimental work should also include cascade studies.
- The theoretical model needs to be made foolproof by standardizing the behaviour of these blade shapes for both pump and turbine applications.
- A programme should be initiated to develop the four-quadrant characteristics of all types of axial flow impellers.
- The survey of the impellers could be enhanced and also extended to other types of turbomachines such as fans and compressors. ■

References

- P. Singh and F. Nestmann, 'Axial flow impeller shapes: part 1', *World Pumps*, No. 533, pp. 32–35, (2011).
- A.J. Stepanoff, *Centrifugal and Axial Flow Pumps*, John Wiley & Sons Inc, Ch. 8 and 16, (1957).
- D.G. Ainley, 'Performance of Axial Flow Turbines', *Proc. Institution Mechanical Engineers*, 159, pp. 230–244, (1948).
- T.H. Okiishi, M.J. Miller, P. Kavanagh and G.K. Serovy, 'Axial-flow pump: blade-element loss and deviation angle prediction', *International J. Mechanical Sciences*, 17 (10), pp. 633–641, (1975).

Contact

Punit Singh (postdoctoral researcher) and Franz Nestmann (director)
Institute for Water and River Basin Management (IWG)
Karlsruhe Institute of Technology
Kaiser Str. 12, Karlsruhe D-76131, Germany
Tel: +49 721 608 2194
Fax: +49 721 608 026
Email: punit.singh@iwg.uka.de and nestmann@iwg.uka.de

Acknowledgements

The authors are indebted to their industry partners KSB AG both in Germany and India for their support. The contribution of the research staff and workshop of the Institute of Water and River Basin Management at the Karlsruhe Institute of Technology is also acknowledged.

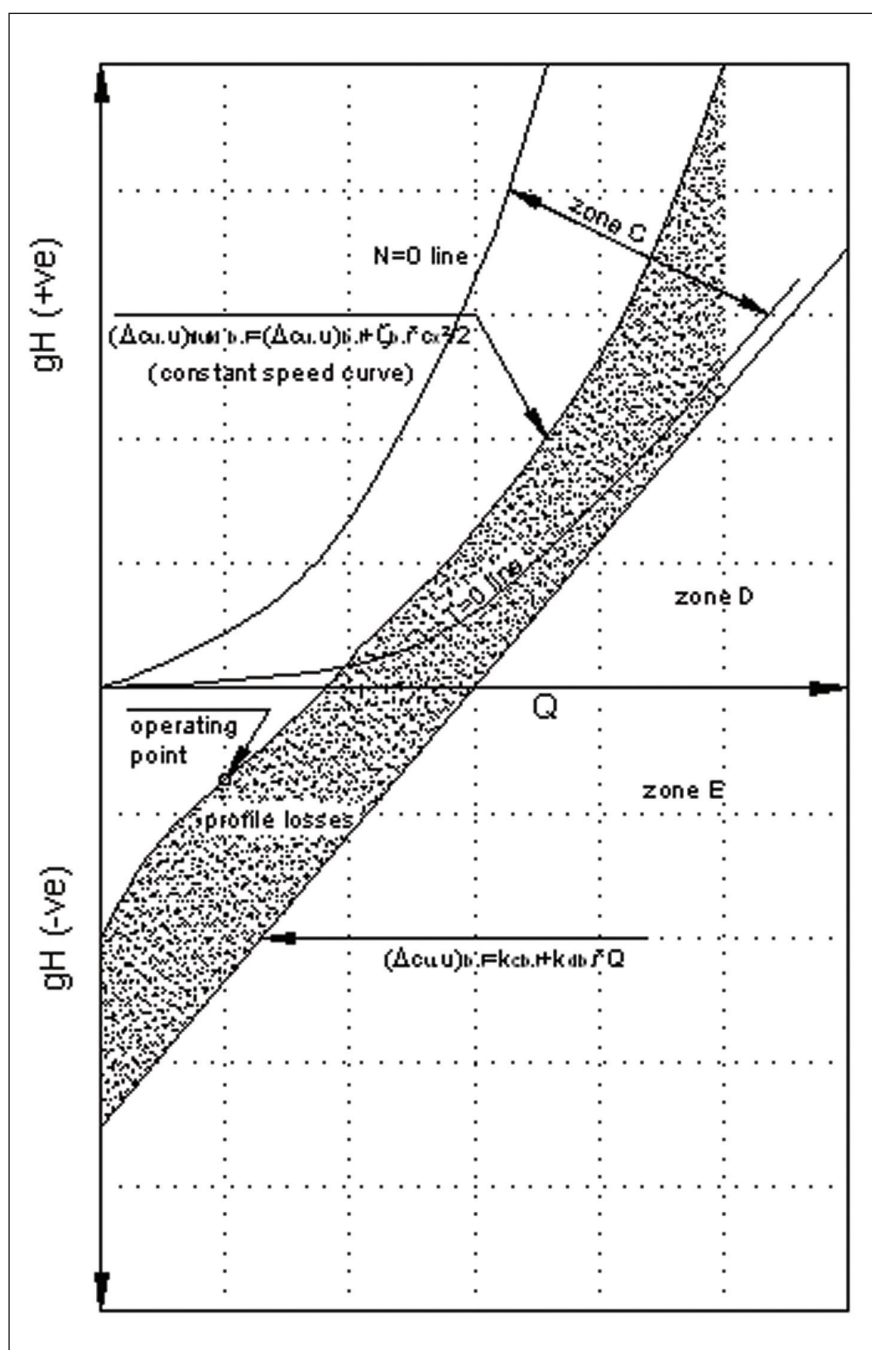


Figure 4. Behaviour of the H-Q line in backward curved turbine impellers.

5.4 CONFERENCE PAPERS

- [15] Franz Nestmann, Peter Oberle, Mohammad Ikhwan, Punit Singh, Bau eines Höhlenkraftwerks zur Trinkwassergewinnung auf, Betonbauwerke im Untergrund - Infrastruktur fuer die Zukunft, 5. Symposium Baustoffe und Bauwerkserhaltung, University of Karlsruhe, pp 109 - 120, (2008)
-

Bau eines Höhlenkraftwerkes zur Trinkwassergewinnung auf Java

Teil 1: Gesamtkonzept zur energetischen Nutzung unterirdischer Wasserressourcen in Karstgebieten

Franz Nestmann, Peter Oberle, Muhammad Ikhwan, Punit Singh

Zusammenfassung

Der Beitrag behandelt ein aktuelles vom Bundesministerium für Bildung und Forschung (BMBF) gefördertes Vorhaben der Universität Karlsruhe (TH) zum Bau einer unterirdischen Wasserförderanlage in einem Karstgebiet auf Java, Indonesien. Wie in vielen Karstgebieten weltweit herrscht auch dort insbesondere während der Trockenzeit ein akuter Wassermangel. Gleichzeitig existieren jedoch große unterirdische Wasserressourcen, die bisher weitgehend ungenutzt über ein weitreichendes Höhlensystem in den Indischen Ozean abfließen. Eine nachhaltige Lösung zur Nutzung dieser unterirdischen Wasserströme wurde bislang nicht gefunden.

Zielsetzung des aktuellen Verbundprojektes ist es, die Trink- und Brauchwasserversorgung der Bevölkerung während der Trockenzeit durch den Bau eines unterirdischen Speichers unter Nutzung regenerativer Energiequellen sicherzustellen. Das erarbeitete Lösungskonzept sieht den Aufstau des unterirdischen Flusses um ca. 10 bis 15 Meter durch den Bau eines Sperrbauwerkes vor. Mittels Wasserkraft soll über den Basisabfluss des Höhlenflusses (ca. 1-2 m³/s) die Energie zum Betrieb von Pumpsystemen bereitgestellt werden, die ausreichend Trink- und Brauchwasser für ca. 80.000 Menschen an die Oberfläche fördern.

Das Projekt wird neben dem BMBF von den Industriepartnern Herrenknecht AG, KSB AG, VAG GmbH sowie Walcher Wasserkraft GmbH unterstützt. Der Bau des Höhlenkraftwerkes soll Ende 2008 abgeschlossen sein.

In dem vorliegenden ersten Teil des Beitrages wird ein Überblick über das Verbundprojekt gegeben. Der zweite Teil des Beitrages beschreibt die Konzeption und Realisierung des Sperrwerkes aus Beton.

1 Hintergrund

Wasser ist die Grundlage jeglichen Lebens – eine zuverlässige Wasserversorgung die Grundlage jeglicher Zivilisation! Für derzeit etwa 1,1 Mrd. Menschen – etwa ein Sechstel der Weltbevölkerung – ist unzureichender Zugang zu Trinkwasser Bestandteil des täglichen Kampfs ums Überleben.

Der Inselstaat Indonesien wird landläufig nicht mit Wasserknappheit assoziiert. Knapp vier Fünftel der indonesischen Bevölkerung besitzen einen gesicherten Zugang zu Trinkwasser. Allerdings existieren auch in Indonesien räumliche Disparitäten hinsichtlich der Versorgung mit Trinkwasser. Auf dem aus Kalkstein aufgebauten Südrand des Archipels ist wegen der weit fortgeschrittenen Verkarstung des Untergrundes eine natürliche Speicherung des Niederschlags, welcher hier fast ausschließlich zwischen den Monaten Oktober bis April fällt, kaum möglich.

Die Gunung Sewu, das Land der „tausend Hügel“, an der Südküste der Insel Java ist eine solche Region (Abbildung 1). Insbesondere während der Trockenzeit herrscht in der landwirtschaftlich geprägten Gegend ein akuter Wassermangel (Abbildung 2). Gleichzeitig existieren jedoch große unterirdische

Wasserressourcen, die bisher weitgehend ungenutzt über ein weitreichendes Höhlensystem in den Indischen Ozean abfließen. Aufgrund der Speicher- bzw. Pufferkapazität des Karstaquifers führen die unterirdischen Flüsse auch in der Trockenzeit eine beträchtliche Abflussmenge. Seit Jahrzehnten wurden von Seiten der indonesischen Regierung große Anstrengungen unternommen, die unterirdischen Wasserströme nutzbar zu machen. Eine nachhaltige Lösung wurde nicht gefunden.



Abb. 1: Lage des Karstgebietes Gunung Sewu auf der Insel Java, Indonesien



Abb. 2: Die Karsthügellandschaft in der Regen- und Trockenzeit

Im Jahr 2002 wurde vom Institut für Wasser und Gewässerentwicklung (IWG) der Universität Karlsruhe ein vom Bundesministerium für Bildung und Forschung (BMBF), sowie deutschen Industriepartnern gefördertes Verbundprojekt initiiert, mit dem Ziel, das Höhlenwasser über regenerative Wasserkraft zu fördern [10]. Hierdurch können Wirtschaftlichkeit und Ökologie in idealer Weise verbunden werden, was gerade in den bzgl. der Wasserqualität hochsensiblen Karstgebieten von besonderer Bedeutung ist. Ganz bewusst konzentrieren sich die Forschungs- und Entwicklungsarbeiten auf einfach handhabbare Technologien, die an die Bedürfnisse von Mensch und Natur angepasst sind. Im Rahmen der deutsch-indonesischen Kooperation wird in der Höhle Gua Bribin zurzeit ein Lösungsansatz erprobt. Mitte 2008 soll an dieser Demonstrationsanlage das erste Wasser über eine Steigleitung in ein 220 m höher gelegenes Verteilerbecken auf einem Karsthügel gefördert werden und 80.000 Menschen in den umliegenden Hüttensiedlungen versorgen. Weitere Projekte in angrenzenden Regionen sind geplant.

Die Projektumsetzung erfordert eine enge Zusammenarbeit unterschiedlicher Fachdisziplinen. So sind neben dem IWG insgesamt fünf weitere Institute der Fakultät für Bauingenieur-, Geo- und Umweltwissenschaften beteiligt: Das Geodätische Institut, das Institut für Massivbau und Baustofftechnologie, das Institut für Mineralogie und Geochemie, die Versuchsanstalt für Stahl, Holz, Steine sowie das Institut

für Boden und Felsmechanik. Weitere Verbundpartner sind das Institut für Geographie der Universität Gießen sowie die Industriepartner Herrenknecht AG (Tunnelvortriebstechnik), KSB AG (Pumpentechnologie), VAG GmbH (Grundablassarmaturen) sowie Walcher Wasserkraft GmbH (Steuer- und Regelungstechnik).

In Indonesien wurde über die Aktivitäten der letzten Jahre unter Einbeziehung aller bedeutenden regionalen und nationalen Behörden und Industriepartner ein gut funktionierendes Netzwerk aufgebaut. Zudem bestehen intensive Kooperationen mit mehreren Universitäten und Forschungseinrichtungen sowie enge Kontakte zur lokalen Bevölkerung und ansässigen Nichtregierungsorganisationen. Die große Bedeutung und Akzeptanz der deutschen Aktivitäten wurde Ende 2004 mit der Besichtigung der Baustelle durch den indonesischen Staatspräsidenten S. B. Yudhoyono und drei Monate später durch die Höhlenbegehung von Bundesforschungsministerin Edelgard Bulmahn unterstrichen.

2 Untersuchungsgebiet Gunung Kidul

Der Verwaltungsdistrikt Gunung Kidul liegt in Zentraljava etwa 100 km südöstlich der Stadt Yogyakarta am Fuße des Vulkans Merapi. Naturräumlich besteht Gunung Kidul aus drei Teilregionen. Im Norden erhebt sich eine Vulkankette, die Gunung Baturagung, die den Distrikt Gunung Kidul nach Norden hin von den eigentlich für Java typischen fruchtbaren Reisbauebenen abgrenzt. Im Zentrum Gunung Kiduls befindet sich das auf Mergelkalken aufgebaute Wonosari Plateau, im Süden und Osten schließt sich eine 1400 km² große Karstlandschaft, die Gunung Sewu an.

Das gesamte Gebiet der Gunung Sewu ist von hunderten, miteinander vernetzten Höhlen durchzogen, welche im Laufe der Jahrhunderte durch Korrosion (Lösungsprozesse) und Erosion (mechanischer Abrieb) entstanden sind; daraus resultiert der komplette Austausch jeglichen Oberflächenabflusses durch ein weit verzweigtes Abflusssystem im Untergrund. Das Wasser dieser unterirdischen Flüsse tritt fast vollständig erst wieder in Quellen an der Küste zutage. Nur in den Talsenken finden sich stellenweise Bereiche mit undurchlässigem Tonboden, welche zu kleinen Seen („Telagas“) aufgestaut sind. Diese flachen Karstwannen können aufgrund der hohen Verdunstungsrate jedoch nur während der Regenzeit von der Bevölkerung als Wasserquelle genutzt werden. [3]

Wegen der naturräumlichen hydrogeologischen Gegebenheiten sowie dem Mangel an nachhaltigen Technologien zur Wassergewinnung wird Gunung Kidul mit seinen 750.000 Einwohnern als das „Armenhaus Javas“ bezeichnet. Besonders betroffen

sind die ländlichen Hüttensiedlungen der Gunung Sewu. [12]

Bereits Anfang der 80er Jahre hat die indonesische Regierung begonnen, die unterirdischen Wasserressourcen zu erschließen. Es wurden mit großem Aufwand dieselbetriebene Pumpanlagen errichtet, Speicherreservoirs gebaut und Wasserleitungen verlegt. Aufgrund von Fehlplanungen, Defekten und mangelnden Energie- bzw. Finanzmitteln zum Betrieb der Pumpen ist durch viele dieser Leitungen allerdings bis heute kein Wasser geflossen. Abgesehen von den ökologischen Risiken beim Einsatz von Dieselgeneratoren sind für die Bevölkerung aufgrund der hohen Betriebs- und Wartungskosten der Pumpanlagen ohnehin nur geringe Wassermengen bezahlbar. Dies gilt auch für die Möglichkeit, sich über Tanklastwagen mit Wasser versorgen zu lassen. Daher ist ein Großteil der ländlichen Bevölkerung auf Alternativen, wie Brunnen, Zisternen und Telagas angewiesen. Diese Versorgungsquellen reichen aber bei Weitem nicht aus, den Bedarf zu decken. Während der Trockenzeit wird das Wasser oftmals direkt aus den Höhlen in stundenlanger Arbeit mit Kanistern nach Hause getragen. Viele Haushalte müssen während der Trockenzeit mit weniger als 10 Liter pro Kopf und Tag auskommen.

3 Erkundung der Höhlensysteme

Seit vielen Jahren besteht von Seiten des Instituts für Wasser und Gewässerentwicklung (IWG) durch Stipendiaten und ehemalige Doktoranden ein enger Kontakt zu mehreren Universitäten und Forschungseinrichtungen in Indonesien, speziell in Mitteljava. So wurde von Seiten der Regierung der Yogyakarta Special Province im Jahr 2000 die konkrete Bitte um Unterstützung bei der Entwicklung nachhaltiger Lösungskonzepte zur Nutzung der unterirdischen Wasservorkommen in Gunung Kidul herangetragen und somit das Initial zu einer vom BMBF geförderten Machbarkeitsstudie gegeben.

Im Rahmen der Vorstudie konnte auf die Berichtsbände einer in den 80er Jahren durchgeführten interdisziplinären Datenerfassung des britischen Consulting-Büros Sir MacDonald & Partners zurückgegriffen werden [5,6]. Von besonderem Interesse waren die Aufzeichnungen einer 2-jährigen Höhlenerkundung durch 5 britisch-indonesische Expeditionsteams. Insgesamt wurden 160 von damals 246 bekannten Höhlen erkundet. Auf Basis dieser Aufzeichnungen konnte die Auswahl der im Rahmen der Machbarkeitsuntersuchung des IWG zu untersuchenden Höhlen getroffen werden. Die weiteren Erkundungen und Datenerhebungen durch das IWG erfolgten mit Unterstützung ortskundiger Speleologen (Abbildung 3).



Abb. 3: Einstieg in das Höhlensystem zur Erkundung der unterirdischen Wasserressourcen

4 Rückwärtslaufende Pumpen als angepasste Technologie

Im Rahmen der Vorstudie wurde folgende Grundkonzeption zur nachhaltigen Nutzung der unterirdischen Wasserressourcen entwickelt:

Durch ein Sperrwerk, über welches der Höhlenquerschnitt komplett geschlossen werden kann, soll das kontinuierlich zuströmende Wasser aufgestaut und die notwendige Druckhöhe erzeugt werden, um einen Teil des Abflusses über ein wasserkraftbetriebenes Pumpsystem an die Oberfläche zu fördern. Der unterirdische Stausee kann dem Bedarf entsprechend bewirtschaftet werden.

Um dem Gedanken der „angepassten Technologie“ Rechnung zu tragen, ist zur Energiegewinnung anstelle von Turbinen der Einsatz invers betriebener Pumpen vorgesehen, die ihrerseits über eine Welle bzw. ein mechanisches Getriebe direkt mit Pumpen für die Wasserförderung gekoppelt werden. Der Vorteil von Pumpen als Turbinenersatz ist, dass sie weltweit leicht verfügbar, kostengünstig und zudem sehr robust und wartungsfreundlich sind.

Mit dem Einsatz von „Pumpen als Turbinen“ (PAT) lassen sich bei Wahl geeigneter Pumpentypen Wirkungsgrade von über 80% erreichen. Um die Eignung verschiedener Pumpentypen für den Einsatz im Turbinenbetrieb zu ermitteln und deren Wirkungsgrade weiter zu optimieren wurde im Theodor-Rehbock-Wasserbaulaboratorium des IWG eine umfassende Studie durchgeführt (Abbildung 4, [13]). Über gezielte Modifikationen an der Laufrad- bzw. Gehäusegeometrie der Pumpen konnten die Strömungsverluste beim inversen Betrieb signifikant reduziert werden und Wirkungsgrade erreicht werden, die im optimalen Betriebspunkt an die von Turbinen heranreichen.

Ein wesentlicher Nachteil von PAT gegenüber echten „Turbinen“ ist das Fehlen einer regelbaren Leiteinrichtung zur Anpassung an ein schwankendes Wasserangebot. Durch parallelen Einbau mehrerer

und großemäßig unterschiedlicher Pumpenmodule, die mit einem Minimum an Regelaufwand je nach verfügbarer Abflussmenge zu- oder abgeschaltet werden, kann jedoch ein beliebig großes Abflussspektrum mit optimalem Wirkungsgrad durchfahren werden. Abflüsse größer dem Bemessungswert der Gesamtanlage werden über Entlastungsrohre mit entsprechend großen Querschnitten durch das Sperrwerk abgeführt.



Abb. 4: Teststand zur Optimierung von Pumpen im Turbinenbetrieb am Theodor-Rehbock-Wasserbaulaboratorium des IWG [13]

5 Pilotprojekt Gua Bribin

Bezüglich einer pilothaften Umsetzung des Wasserförderkonzeptes stellte sich die Höhle Gua Bribin als besonders geeignet heraus (Abbildung 5). Über einen ca. 350 m langen engen Zugangsstollen, erreicht man einen unterirdischen Flusslauf, den Kali

Bribin. Hier wurde bereits in den 80er Jahren eine ca. 2,5 m hohe Wehranlage errichtet, die den Fluss auf einer Länge von 1,5 km rückstaut (Abbildung 6). Einziger Zweck dieses Bauwerkes ist die Sicherstellung einer ausreichenden Überdeckung der oberhalb der Wehranlage installierten Pumpen, welche über Dieselgeneratoren am Höhleneingang betrieben werden. Spätestens hier wird deutlich, welche enormen Anstrengungen in der Region bisher unternommen wurden, um das Höhlenwasser nutzbar zu machen. Leider stehen die Pumpen aufgrund der hohen Wartungs- und Betriebskosten die meiste Zeit still.



Abb.6: Alte unterirdische Wehranlage mit Radarmesspegel des IWG

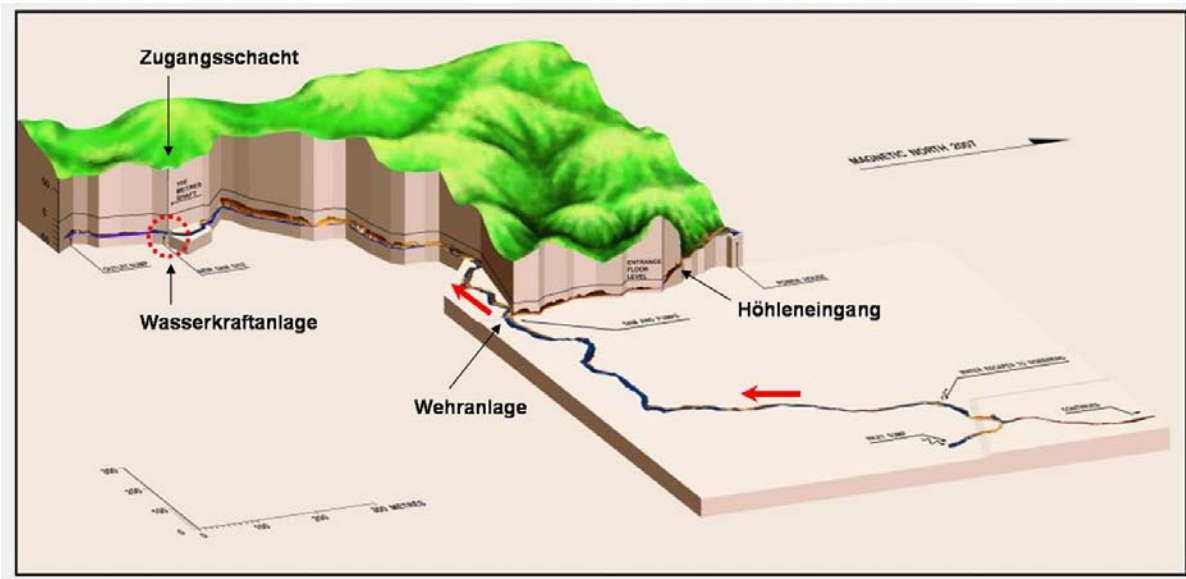


Abb. 5: Lageplan der Höhle Gua Bribin

Der durchflossene Höhlenstrang hat eine Gesamtlänge von etwa 3 km mit einem Gesamtvolumen von

ca. 500.000 m³. Während der Trockenzeit betragen die Abflussmengen zumeist über 1,5 m³/s, in der

Regenzeit können die Abflüsse auf ein Mehrfaches anschwellen. Die Höhle wird am oberen und unteren Ende durch Siphons begrenzt. Vor dem unterstromigen Siphon staut sich das Wasser auf einer Länge von ca. 300 m zu einem natürlichen See zurück. Die elliptische Querschnittsfläche hat eine Breite von 10 m und eine Höhe von 6 m. Aufgrund der vorhandenen geometrischen Randbedingungen und den Ergebnissen einer geologischen Voranalyse wurden hier gute Voraussetzungen für die bautechnische Realisierung eines Einstaubauwerkes erwartet. Das Sperrwerk soll das natürliche Gefälle der Höhle ausnutzen und das Wasser des Kali Bribin auf ein Niveau von 10 bis 15 m über den Wasserstand des Höhlensees aufstauen (Abbildung 7). Der Bemessungsabfluss der Gesamtanlage liegt bei ca. 2 m³/s. Unter Vollauslastung könnte die Anlage genügend mechanische Leistung erzeugen, um pro Sekunde über 65 Liter Wasser in ein ca. 220 m höher liegendes Speicherbecken zu fördern. Von dort wird das Wasser in die umliegenden Dörfer verteilt.

Im 24 Stunden Betrieb sollen somit 80.000 Bewohner mit 70 Liter pro Kopf und Tag (lpcd) versorgt werden. Die WHO-Richtlinie fordert eine Mindestversorgung von 50 lpcd.

Dass Gua Bribin das Wasser auch halten wird, lassen Sedimentablagerungen vulkanogenen Ursprungs unter der Höhlendecke sowie mm- bis cm-

mächtige schwarzbraune Mn-/Fe- reiche Oxidlagen, welche die Kalksteine umkrusten, erwarten. Beides sind Hinweise darauf, dass die Höhle bereits in früheren Zeiten auf natürliche Weise bis unter die Decke eingestaut war. Des Weiteren können auch während der Regenzeit keine lateralen Wassereinträge oder größere Mengen an Sickerwasser beobachtet werden. Weitere Anzeichen einer geringen Durchlässigkeit des Felskörpers ergab die Auswertung von Tracerversuchen und Abflussbilanzierungen zwischen den vernetzten Höhlen. So kann der Fließweg des Kali Bribin über eine Länge von 17 km bis zum Indischen Ozean verfolgt werden, ohne Hinweise auf signifikante Mengenverluste zu finden [1]. Auch die bereits seit Jahrzehnten existierenden Einstaubereiche der kleineren Wehranlagen wie z.B. in Gua Bribin weisen keinerlei Wasserverluste auf. Einen gewissen Abdichtungseffekt könnten auch die genannten Feinsedimentablagerungen bewirken, welche flächendeckend die Böschungen überziehen und stellenweise eine Mächtigkeit von > 1 m aufweisen. Die Prognose der Einstaumöglichkeit wurde im Verlauf der Projektarbeiten durch umfassende Bohrkernanalysen sowie Wasserschluckversuche im Bereich des Sperrwerkes unterstützt (siehe Teil 2, [7]).

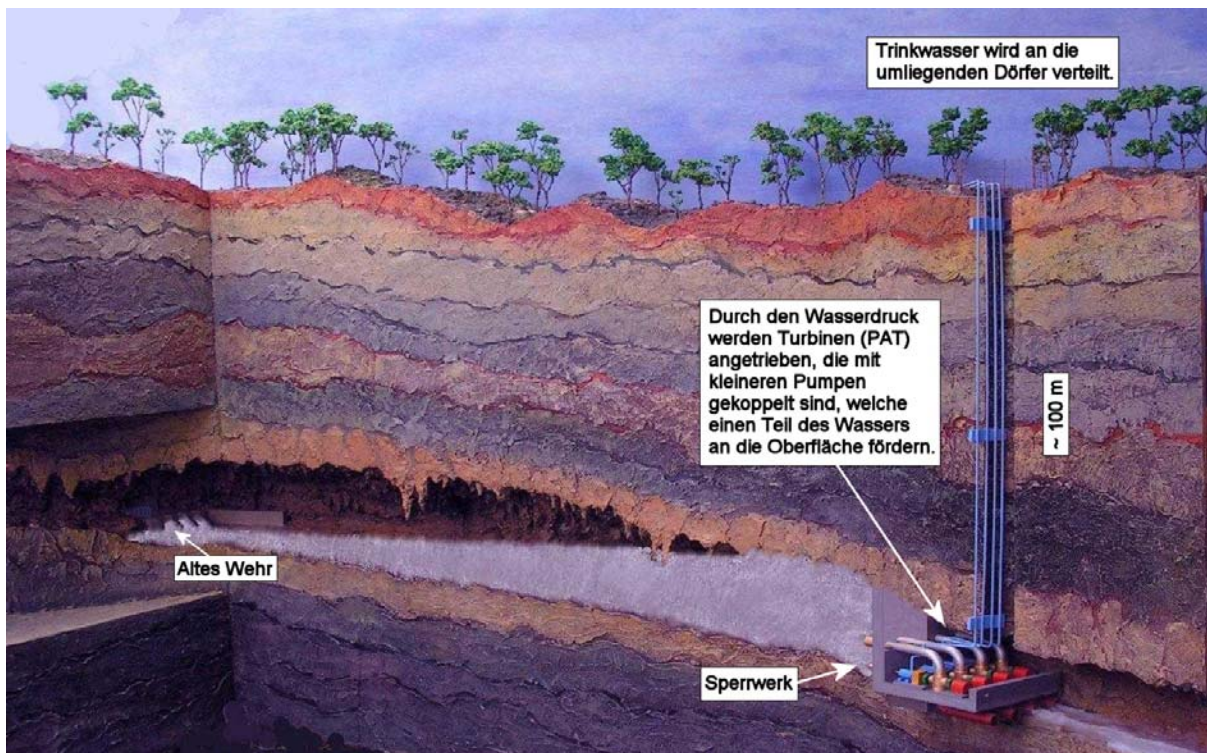


Abb. 7: Prinzipskizze der unterirdischen Wasserförderanlage

5.1 Geodätische Messkampagne

Für den Ausbau der Höhle war die Errichtung eines vertikalen Zugangsschachtes zum Einbringen von Baumaterialien, Rohrleitungen und Fördermodulen sowie für die späteren Betriebs- und Wartungsarbeiten notwendig. Zur Festlegung der Bohrstelle wurde 2003 vom Geodätischen Institut der Universität Karlsruhe (GIK) ein insgesamt 2,4 km langer Polygonzug mittels moderner Laser-Tachymetrie durch die Höhle und oberirdisch durch die felsige Karsthügellandschaft abgesteckt. In dem ca. 200 m langen Seebereich am Höhlenende konnten Standpunkte nur von Schlauchbooten aus über selbstgefertigte Wandkonsolen realisiert werden. Die Anforderungen an die Messgenauigkeit waren enorm da der Schacht die Höhlenwand exakt tangential anschnitten musste.

Die numerische Analyse der zu erwartenden Fehlerfortpflanzung ergab eine relative Fehlerellipse mit den Halbachsen 19,5 und 1,6 cm. Das bedeutete, dass die ermittelte Bohrstelle an der Oberfläche mit einer Wahrscheinlichkeit von etwa 40 % weniger als 20 cm gegenüber dem Bohrziel in der Höhle verschoben lag. Die Bohrtiefe wurde auf 98,5 m ermittelt.

5.2 Bau des Zugangsschachtes

Als weltweit agierender Spezialist in der horizontalen Tunnelvortriebstechnik stellte die Entwicklung von Vertikalbohrmaschinen für die Firma Herrenknecht AG aus Schwanau ein interessantes Entwicklungsfeld dar. Die speziell für den Einsatz in Indonesien entwickelte Schachtabsenkanlage mit einem Durchmesser von 2,5 m ist mit einem Bohrgerät („Schräme“) ausgerüstet, welches vom Maschinenfahrer direkt darüber sitzend mit Steuerhebeln bedient wird [4]. Der hydraulisch angetriebene Schräm Kopf hat eine Leistung von 110 kW und rotiert am Schrämarm kreisförmig um seine eigene Achse, um den Fels abzubauen. Die hohen Gesteinsfestigkeiten (Würfeldruckfestigkeit 80 MPa) machten den Einsatz spezieller Rundschafftmeißel (Bits) notwendig. Das Abbauwerkzeug führt das abgebaute Material einem Schalengreifer zu, der von einer zweiten Person auf einer Plattform oberhalb bedient wird. Über einen seitlich befindlichen Förderschacht wird das Bohrgut 6 m nach oben befördert und über eine Rutsche in einen Förderkübel mit einem Fassungsvermögen von 1,5 m³ geleitet. Dieser wird nach vollständiger Füllung mit einem Kran an die Oberfläche gezogen (Abbildung 8).



Abb. 8: Schachtabsenkanlage der Herrenknecht AG [4]

Zur Sicherung des Schachtes werden sukzessive Stahlsegmente („Tübbinge“) nach einer gebohrten Tiefe von 0,7 – 1 m in den Schacht abgelassen, dort zu einem Ring verschraubt und mit Spezialankern im Fels verdübelt (Abbildung 9). Der Zwischenraum, der durch den Überschneid zwischen Fels und Stahlmantel entsteht, wird mit Mörtel kraftschlüssig verpresst. Die Maschine ist über vier Zugstangen mit einem Stahlrahmen am Schachtkopf verbunden und wird nach jedem Bohrabchnitt über Hohlkolbenzylinder gleichmäßig abgeteuft. Während des Bohrvorganges sind hydraulisch betriebene Grippereinheiten aktiv, die den Schild im Gestein in Position halten. Das Vermessungssystem zum lotrechten Abteufen wurde vom GIK eingerichtet und besteht aus zwei Laserloten an der Schachtoberfläche und einer Zieltafel an der Maschine.

Mit den Bohrarbeiten wurde im Juli 2004 begonnen. Die Bohrarbeiten wurden von der Firma Herrenknecht zusammen mit der indonesischen Baufirma PT Wijaya Karya durchgeführt. Der Schachtdurchbruch in die Höhle erfolgte Anfang Dezember 2004.



Abb. 9: Blick in den Zugangsschacht

5.3 Anlagenplanung

Parallel zu den Vermessungs- und Schachtbohrarbeiten wurden die Entwurfsplanungen für die Dimensionierung und konstruktive Ausführung des Sperrwerkes sowie Felssicherungsmaßnahmen in enger Kooperation mit dem Institut für Massivbau und Baustofftechnologie (IfMB) sowie dem Institut für Boden- und Felsmechanik (IBF) vorangetrieben. Hierbei mussten die besonderen Randbedingungen bezüglich des geringen Platzangebots und der eingeschränkten Zugänglichkeit bei Bau und Betrieb, aber auch die personellen und maschinentechnischen Möglichkeiten der ausführenden indonesischen Bau-firma PT Wijaya Karya berücksichtigt werden. Dies erforderte eine enge Abstimmung mit den indonesischen Kooperationspartnern und war ein äußerst zeitintensiver iterativer Prozess.

Die Geometrie der dreidimensional gekrümmten Mauer wurde am IfMB mit Hilfe numerischer Methoden so optimiert, dass zur Lastabtragung nahezu keine Stahlbewehrung erforderlich ist. Trotzdem ist das Bauwerk mit durchschnittlich 1,5 m Dicke relativ schlank, um die beim Betonieren auftretenden Wärmespannungen möglichst gering zu halten. Als besonders schwierig stellte sich eine erste Beurteilung der Tragfähigkeit der Höhlenwände dar, da aufgrund des kilometerlangen unterirdischen Zugangs zum geplanten Sperrwerksbereich nur leichtes Gerät zur Erkundung eingesetzt werden konnte.

Neben der Dimensionierung des Sperrwerkes mit ausreichender Einbindetiefe in das Karstgefüge (Felswiderlager) konzentrierte sich das IfMB auch auf die Analyse der vor Ort verfügbaren Baustoffe sowie die Entwicklung speziell angepasster Betonrezepturen in Zusammenarbeit mit der Gadjah Mada Universität Yogyakarta.

Besonders innovativ im Sinne „angepasster Technologie“ war zudem die Entwicklung einer unter Tage anwendbaren Methode zur Herstellung von Kofferdämmen zur Baugrubenentwässerung. Da Spundwände, wie sie an oberirdischen Fließgewäs-

sern einsetzbar sind, in der Höhle nicht eingebracht werden können, sollte die Wasserhaltung im langsam durchflossenen Höhlensee über Unterwasserbeton im Ausgussverfahren („prepacked concrete“) umgesetzt werden. Die Optimierung der entmischungsfreien Rezeptur sowie Einbringtechnik erfolgte im Rahmen einer umfangreichen Versuchsreihe.

Eine ausführliche Darlegung zur bautechnologischen Konzeption des Sperrwerkes findet sich in Teil 2 dieses Beitrages. [7]

Vom Institut für Mineralogie und Geochemie (IMG) wurden weitere geologische Analysen u. a. unter Einsatz geoelektrischer und seismischer Messmethoden in Zusammenarbeit mit dem Institute of Technology Surabaya zur Exploration von Hohlräumen und potentiellen Wasserwegsamkeiten durchgeführt. Zudem wurden der Wasserchemismus sowie die Verwitterungsresistenz des Karstgesteins analysiert. Nach Fertigstellung der Schachtbohrung konnten im Bereich des geplanten Sperrwerkes in Zusammenarbeit mit dem IBF und dem IfMB Kernbohrungen ausgewertet sowie Wasserschluckversuche zur Prognose der zu erwartenden Umläufigkeit durchgeführt werden. Als kritisch stellten sich eine den massiven Riffkalkfelsen horizontal durchlaufende Schicht aus Gesteinstrümmern und Tonmergel („Brekzie“) sowie Bereiche kollabierten Kalkgesteins mit jeweils ca. 1 m Mächtigkeit dar. Monitoringkonzepte sowie mögliche Maßnahmen gegen Umläufigkeiten (Felsinjektion, Nachverpressung) wurden gemeinsam mit den indonesischen Partnern entwickelt. [8]

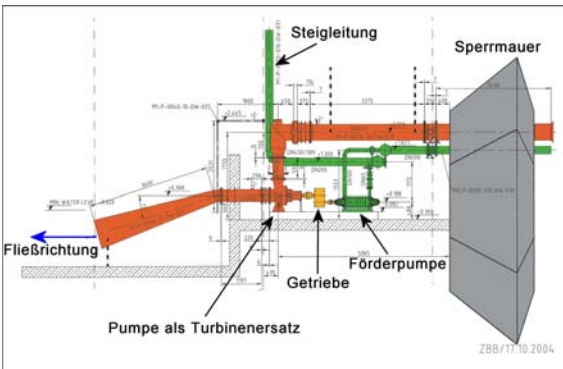
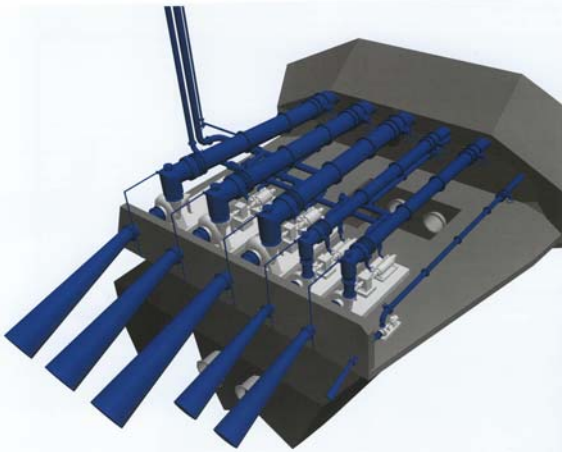


Abb. 10: Modular aufgebaute Wasserförderanlage (Planungszustand; untere Abbildung ohne Grundablassrohre)

Die Dimensionierung der Förderanlage erfolgte unter Berücksichtigung der in Gua Bribin gegebenen hydrologischen und geodätischen Randbedingungen. In Zusammenarbeit mit dem Pumpenhersteller KSB AG wurden Standardmaschinen als Systemkomponenten ausgewählt. Der optimale Wirkungsgrad der Gesamtanlage soll über parallelen Betrieb von maximal 5 Modulen, jeweils bestehend aus PAT, Getriebe und Förderpumpe, erreicht werden. Hierbei sind zwei Modultypen mit unterschiedlichem Schluckvermögen bzw. Förderleistungen vorgesehen. Hinzukommt eine kleineres Aggregat, welches mit einer Leistung von ca. 5 kW einen Drehstrom-Synchrongenerator zur Eigenstromversorgung der Anlage (Inselbetrieb) antreibt. Die elektrische Energie wird u. a. zur Versorgung des Steuerungssystems für die Schieberarmaturen von Modulen und Hochwasserentlastungsrohren (Absperklappe DN800, Ringkolbenventil DN600/700 der Fa. VAG) genutzt (Abbildung 10, 11).



Abb. 11: Endabnahme der Grundablassarmatur (Ringkolbenventil) im VAG-Werk Mannheim (2006)

Die genaue Konstellation der Fördermodule wird erst nach einem Testeinstau zur Ermittlung der möglichen Einstauhöhe festgelegt. Zunächst wurde ein Modultyp bestehend aus einer Spiralgehäusepumpe (als PAT), einem Getriebe und einer 9-stufigen Gliederpumpe auf einem Prüffeld der KSB AG getestet und optimiert (Abbildung 12).



Abb. 12: Fördermodul (Spiralgehäusepumpe als PAT, Stirnradgetriebe, neunstufige Gliederpumpe) auf dem Prüffeld der KSB AG

Die modifizierte PAT besitzt bei 15 m Fallhöhe ein Schluckvermögen von 375 l/s und einen Wirkungsgrad von 81 %. Somit gibt die Pumpe im Turbinenbetrieb an der Welle rd. 45 kW Leistung ab. Ihre Nenn-drehzahl beträgt 1200 U/min und treibt über das Getriebe (Stirnradgetriebe mit Übersetzungsfaktor 1 zu 1,83) die Förderpumpe an. Diese fördert im Nennpunkt bei ca. 2200 U/min rd. 13,5 l/s in den 220 m höher gelegenen Hochbehälter (Abbildung 13). Mit dem Wirkungsgrad der Förderpumpe von 70 % und des Getriebes von 95 % hat das Fördermodul einen Gesamtwirkungsgrad von 54 %. Dieser hohe Wirkungsgrad wird durch die mechanische Kupplung der Pumpe im Turbinenbetrieb mit der Förderpumpe ermöglicht. Bei der Verwendung von elektrischer

Energie (Pumpe im Turbinenbetrieb: Generator; Förderpumpe: Motor) würde sich ein weitaus geringerer Gesamtwirkungsgrad einstellen.

Die Firma Walcher Wasserkraft GmbH entwickelte das SPS-gestützte Steuerungssystem für den modularen Anlagenbetrieb. Dieses ermöglicht durch Einbindung der Fördermodule in das übergeordnete System der Schaltzentrale (Betriebsgebäude am Schachtkopf) die Überwachung und den automatisierten Betrieb der Anlage. Jedes Fördermodul ver-

fügt über einen Schieber mit elektrischem Stellantrieb zum An- und Abfahren. Somit werden die einzelnen Module in Abhängigkeit von Messgrößensignalen (Stauhöhe, Abfluss und Füllstand des Hochbehälters) automatisiert zu- und abgeschaltet. Hierdurch kann der Betriebspunkt der gesamten Förderanlage optimal an die schwankenden hydraulischen Randbedingungen (Wasserdargebot und Wasserbedarf) angepasst werden.

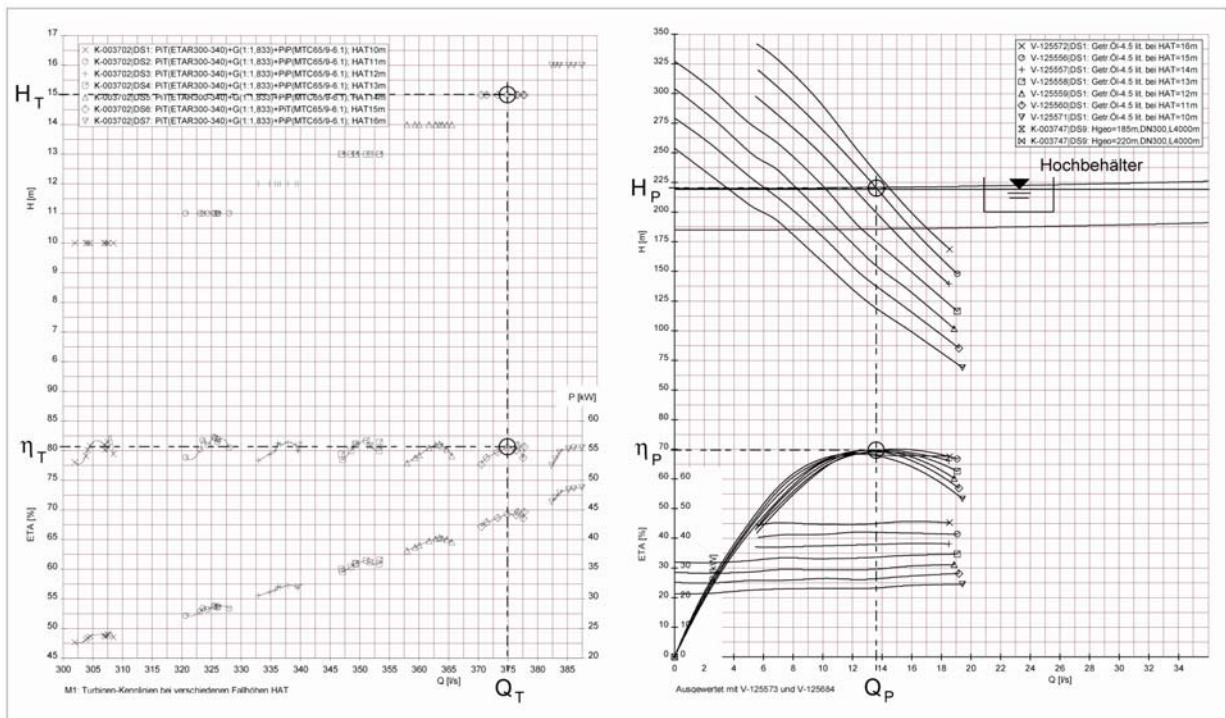


Abb. 13: Kennlinien des Fördermoduls für Fallhöhen von 10 bis 16 m. Links: Turbinenkennlinie der PAT. Rechts: Pumpenkennlinie der Förderpumpe. Beispielhaft ist jeweils der Betriebspunkt für 15 m Fallhöhe (Planungszustand) hervorgehoben (Quelle: KSB AG)

5.4 Beginn der Bauausführung unter Tage

Nach Fertigstellung des Zugangsschachtes im Dezember 2004 konnte am Ende der Regenzeit im April 2005 mit den Ausbaurbeiten in der Höhle begonnen werden. Auf einer Plattform aus Bambus wurde mit Felsausbrucharbeiten und Ankerbohrungen begonnen. Als problematisch stellte sich die Abtragung der stark konsolidierten Schlamm- und Kalzitablagerungen mittels Druckluftanlagen und Saugpumpen an der Gewässersohle heraus, um die Aufstandsfläche für die Wasserhaltungsdämme vorzubereiten. Die bautechnische Realisierung der Wasserhaltung unter Einsatz eines speziellen Verfahrens für Unterwasserbeton ist in Teil 2 des Beitrags dargelegt. [7]

Mitte August war die Baugrube zum ersten Mal wasserfrei. Segmentweise wurden die Hochwasserentlastungsrohre (DN800; DN700/900) von jeweils 18,6 m Länge eingebracht, durch die während der

Bauphase das anströmende Wasser geleitet werden sollte. Nun wurden die Bauarbeiten im Mehrschichtbetrieb Tag und Nacht vorangetrieben. Über 250 m³ Gestein wurden zur Aufweitung der Kaverne und im Bereich des Felswiderlagers mittels Pressluftmeißeln ausgebrochen, weitere 150 m³ an Schlamm- und Geröllablagerungen abgebaut und an die Oberfläche gefördert. Insgesamt wurden 310 Felsankerbohrungen durchgeführt, das Fundament für die Plattform geschüttet, Drainageleitungen verlegt, Bewehrungen vorbereitet. Nach 2-wöchigem Baustillstand während der Ramadan-Feiertage wurden Anfang November die Plattform gegossen sowie die rückwärtige Mauer, welche die Module später während der Regenzeit vor hohen Unterwasserständen schützen soll, errichtet (Abbildung 14).



Abb. 14: Stand der Bauarbeiten Dezember 2005

Anfang Dezember 2005 begann die Regenzeit mit tagelangen Starkniederschlägen unerwartet früh. Am 3. und 11. Dezember 2005 wurde die unterirdische Baustelle durch Hochwasserwellen mit Abflussspitzen von fast 10 m³/s überflutet. Aufgrund des hohen Sicherheitsrisikos wurde in Abstimmung mit den indonesischen Partnern eine Unterbrechung der Arbeiten bis Ende der Regenzeit vereinbart.

5.5 Das Erdbeben im Mai 2006

Kurz nachdem die Arbeiten im Mai 2006 wieder aufgenommen wurden, ereignete sich in der Region Yogyakarta ein katastrophales Erdbebenereignis der Stärke 6,3 (Richterskala). Das Epizentrum lag südöstlich der Stadt Yogyakarta, ca. 30 km von der Höhlenbaustelle entfernt. Es zerstörte über 100.000 Häuser, 6.300 Menschen verloren ihr Leben, über 200.000 Menschen wurden obdachlos.

Zur Zeit des Bebens befanden sich zwei Mitarbeiter des IWG vor Ort und nahmen umgehend Kontakt mit den Karlsruher Kollegen auf. Über persönliche Verbindungen aus dem Projektverbund zu „Komitee Cap Anamur – Deutsche Notärzte e.V.“, war es möglich bereits drei Tage nach der Katastrophe gemeinsam mit einer Hilfsorganisation vor Ort zu sein. Über das bestehende deutsch-indonesische Netzwerk, welches in den letzten Jahren im Rahmen des BMBF-Verbundprojektes aufgebaut wurde, konnten umgehend Soforthilfemaßnahmen mit den verantwortlichen Partnerinstitutionen der Provinzregierung abgestimmt und zielgerichtet initiiert werden. U. a. wurde durch die Universität Karlsruhe mit Unterstützung des BMBF und Cap Anamur ein Sofortprojekt zum Wiederaufbau einer Schule sowie Sanierung eines Krankenhauses gestartet.

Die Baustelleneinrichtung und der Zugangschacht in Gua Bribin blieben weitestgehend unversehrt. Jedoch stieg nach dem Beben der Wasserstand an der Baustelle um ca. 2 m an, so dass eine Fortführung der Baumaßnahme unmöglich war. Wie sich durch den Einsatz deutscher Berufstaucher im

August 2006 herausstellte, war der Wasserspiegelanstieg auf einen durch das Beben ausgelösten Versturz hinter dem Siphon zurückzuführen. Insgesamt blockierten über 1000 m³ Geröllmassen den Fließquerschnitt. Im Rahmen intensiver Untersuchungen der Höhle Gua Bribin sowie weiterer benachbarter Höhlensysteme konnten keine weiteren Einstürze oder hydrogeologischen Veränderungen nachgewiesen werden. Auch die in den 80er Jahren erstellte unterirdische Wehranlage überstand das Extremereignis vollkommen schadlos.

5.6 Fertigstellung des Sperrwerkes

Ende 2006 wurde in Zusammenarbeit deutscher und indonesischer Spezialisten eine Schneise in den Versturz hinter dem Siphon gesprengt. Eine zweite Sprengkampagne und weitere Freilegung des Fließquerschnittes folgte im April 2007 und führte zu einer entsprechenden Reduzierung des Rückstauinflusses. Im Juni 2007 konnten die Arbeiten zum Höhlenkraftwerk wieder aufgenommen werden. [9]

Im Dezember 2007 wurde das unterirdische Sperrwerk fertig gestellt. Wenige Tage nach Abschluss der Betonierarbeiten ereignete sich ein starkes Hochwasser, dessen Abflussscheitel von ca. 11 m³/s bei einer Druckdifferenz am Sperrwerk von ca. 1,5 mWs über die Grundablassrohre und Mauerdurchlässe schadlos abgeführt werden konnte (Abbildung 15).

Eine ausführliche Darlegung zur bautechnologischen Konzeption und Realisierung des Sperrwerkes findet sich in Teil 2 dieses Beitrages. [7]



Abb. 15: Partieller Einstau des Sperrwerkes während eines Hochwasserereignisses wenige Tage nach Abschluss der Betonierarbeiten

5.7 Installation der Fördermodule und Inbetriebnahme

Mit der Installation des ersten Fördermoduls, des Moduls zur Eigenstromversorgung sowie der Grundablassarmaturen und des SPS-gestützten Steue-

nungssystem (entwickelt in Zusammenarbeit mit der Firma Walcher GmbH) wurde direkt nach Fertigstellung des Sperrwerkes begonnen (Abbildung 16). Der Probeeinstau soll im April 2008 stattfinden. Im Anschluss daran erfolgt die Festlegung und Fertigung der weiteren Fördermodule. Die vollständige Inbetriebnahme des Höhlenkraftwerkes soll bis Ende 2008 erfolgen.



Abb. 16: Installiertes KSB-Fördermodul

6 Ausblick

Das laufende Projekt konzentriert sich auf angepasste Technologien zur Wasserförderung. Seit etwa einem Jahr laufen in Zusammenarbeit der Universität Karlsruhe und dem Forschungszentrum Karlsruhe im Auftrag des Bundesministeriums für Bildung und Forschung (BMBF) Vorbereitungen zu einem weiteren mehrjährigen Verbundprojekt in der Region Gunung Kidul. Hierbei geht es um den Aufbau eines „Integrierten Wasserressourcen-Managements (IWRM)“, welches neben der Erschließung der Wasservorkommen auch die Aspekte der optimierten Wasserverteilung, der Wasseraufbereitung sowie der Abwasserentsorgung in der ländlichen Gunung Sewu aber auch den urban geprägten Gebieten des angrenzenden Wonosari Plateaus aufgreifen soll [11].

Zur Gewährleistung der Nachhaltigkeit eines IWRM sind die Entwicklungsarbeiten und Umsetzungen der verschiedenen Fachdisziplinen durch einen intensiven Wissenstransfer zu begleiten. Die exemplarische Entwicklung und Umsetzung eines IWRM in einer überschaubaren Modellregion sollte darauf ausgerichtet sein, die Grundlagen für die konzeptionelle und technologische Übertragung der F&E-Arbeiten auf viele weitere Standorte mit ähnlichen Bedarfssituationen zu schaffen und eine möglichst breitgefächerte Multiplikation anzustoßen.

Die Auswahl der Modellregion favorisiert aus geologischer Sicht eine Karstregion. Gunung Kidul ist hierbei keine Ausnahmegegend. Von den Regie-

rungen der Nachbarprovinzen sowie den kleinen Sundainseln Sumba und Timor wurden bereits Anfragen an das Forscherteam aus Karlsruhe bezüglich der Erschließung der dortigen unterirdischen Flüsse gestellt. Erste Untersuchungen wurden bereits durchgeführt.

Die Nutzung von Karstaquiferen zur Trinkwasserversorgung hat aber auch globale Relevanz [2]. In vielen Regionen der Erde (so z.B. in Südchina, Japan, Philippinen, Thailand, Laos und Südamerika) fließen derzeit tausende von Flüssen, wie Bribin oder Seropan, ungenutzt ins Meer, während die Menschen der Regionen unter Wassermangel leiden. Vor allem in Entwicklungs- und Schwellenländern besteht bezüglich angepasster Technologien zur Erkundung und Bewirtschaftung der unterirdischen Wasserressourcen sowie wirksamen Schutzstrategien des vulnerablen Karstwassers ein enormer Handlungsbedarf.

Die Erschließung des unterirdischen Fließgewässersystems in Verbindung mit der gesamtheitlichen Erarbeitung eines IWRM in Gunung Kidul wird einen wichtigen Beitrag zur Lösung weltweit existierender Wasserknappheit in Karstgebieten liefern. Eine Vielzahl an Forschungsergebnissen des IWRM-Projektes werden sich zudem auch auf Gegenden mit nicht verkarstem Untergrund übertragen lassen. Nicht zuletzt wird das Projekt auch die interkulturelle Verständigung fördern, was gerade vor dem Hintergrund der weltpolitischen Situation von existentieller Bedeutung ist.

Weitere aktuelle Informationen finden sich unter: www.hoehlenbewirtschaftung.de

7 Literatur

- [1] Benischke, R. (2000): „Application of Tracer Methods in the Hydrogeologic Investigation of Karst Systems of Gunung Sewu, Yogyakarta Special Province, Indonesia“. Schlussbericht, Institut für Hydrogeologie und Geothermie, Joanneum Research GmbH, Graz
- [2] Bundschuh, P., Lauer, K. (2005): „Unterirdische Karstfließgewässer als Ressource zur Trinkwasserversorgung“. Literaturstudie, Institut für Mineralogie und Geochemie der Universität Karlsruhe (TH)
- [3] Flathe, H., Pfeiffer, D. (1965): „Grundzüge der Morphologie, Geologie und Hydrologie im Karstgebiet Gunung Sewu/Java (Indonesien)“. In: Geologisches Jahrbuch, Band 83, S. 533-562, Hannover
- [4] Meyer, L. (2005): „Entwicklung und Einsatz einer Vertikalbohrmaschine in Indonesien“. In: Glückauf 141 (2005) Nr.1/2 S.58–63
- [5] MacDonald&Partners (1984): „Greater Yogyakarta Groundwater Resources Study, Volume 3, Cave Survey“, Schlussbericht

- [6] MacDonald&Partners (1984): "Greater Yogyakarta Groundwater Resources Study, Volume 2, Hydrology", Schlussbericht
- [7] Müller, H. S., Fenchel, M., Bohner, E., Mutschler, T. (2008): „Bau eines Höhlenkraftwerkes zur Trinkwassergewinnung auf Java, Teil 2: Konzeption und Realisierung des Sperrwerks unter Berücksichtigung örtlich verfügbarer Baustoffe und Technologien“. In: Symposium Baustoffe und Bauwerkserhaltung, 13. März 2008, Universität Karlsruhe (TH)
- [8] Mutschler, T., Berner, Z. (2005): „Report on Site Inspection of ‚Gua Bribin‘-Project, 14-23 October 2005“. Universität Karlsruhe (TH)
- [9] Mutschler, T., Bohner, E. (2007): „Report on Inspection of ‚Bribin‘-Project and ‚Seropan‘-Project, 5-13 June 2007“. Universität Karlsruhe (TH)
- [10] Nestmann, F., Oberle, P. (2002): „Erkundung und Grenzen der Wasser- und Energiebewirtschaftung großer unterirdischer Wasservorräte in Wonosari, Yogyakarta, Java, Indonesien“. Machbarkeitsuntersuchung im Auftrag des BMBF, Institut für Wasserwirtschaft und Kulturtechnik, Universität Karlsruhe (TH)
- [11] Oberle, P., Kappler, J., Unger, B. (2005): „Integriertes Wasserressourcen-Management (IWRM) in Gunung Kidul, Java, Indonesien“. Schlussbericht zur Machbarkeitsuntersuchung im Auftrag des BMBF, Institut für Wasser und Gewässerentwicklung, Bereich Wasserwirtschaft und Kulturtechnik, Universität Karlsruhe (TH)
- [12] Scholz, U., Unger, B., Lux, T. (2004): „Sozio-ökonomische Analyse potenzieller Wassernutzer in Mitteljava, Indonesien“. Forschungsbericht (unveröffentlicht) im Auftrag des BMBF; Institut für Geographie, Justus-Liebig-Universität Gießen
- [13] Singh, P. (2005): „Optimization of Internal Hydraulics and of System Design for Pumps as Turbines with Field Implementation and Evaluation“. Dissertation, Institut für Wasser und Gewässerentwicklung, Universität Karlsruhe (TH)

Anschrift der Autoren:

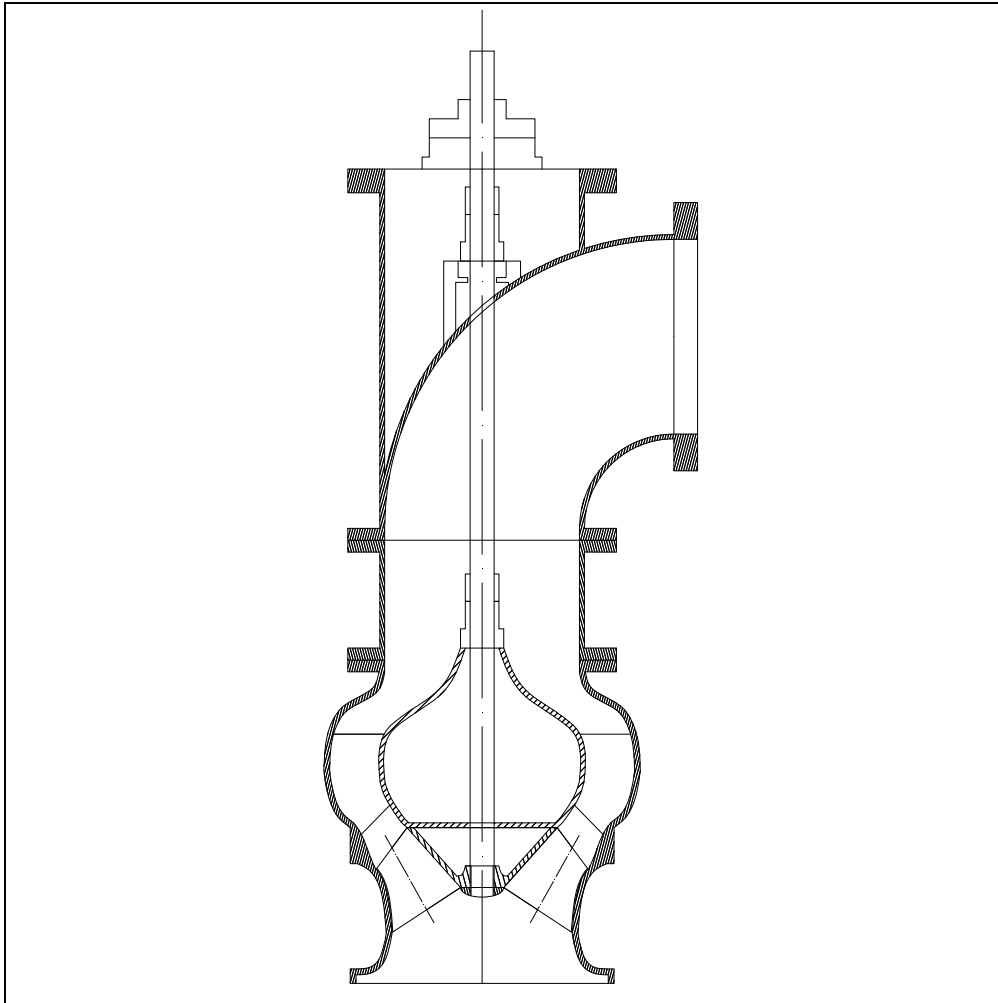
Prof. Dr.-Ing. Dr. h.c. mult. Franz Nestmann
Dr.-Ing. Peter Oberle
Dr.-Ing. Muhammad Ikhwan
Dr.-Ing. Punit Singh

Universität Karlsruhe (TH)
Institut für Wasser und Gewässerentwicklung
Bereich Wasserwirtschaft und Kulturtechnik
Kaiserstr. 12
76131 Karlsruhe

5.5 RESEARCH REPORTS AND PROPOSALS

- [16] Punit Singh, Preliminary Development Stage of the Prediction Model for Mixed Flow Pumps as Turbines, 2011
 - [17] Punit Singh, A Proposal for a Preliminary Prediction Model for Axial Flow Pumps as Turbines, 2011
 - [18] Punit Singh, Critical Review of a Prediction Model for Axial Flow Pumps as Turbines and a Proposal to Optimize the Model, 2011
 - [19] Punit Singh, Field Research Laboratory for Low Head (Micro) Hydro Powered Water Pumping and Electricity Generation Technologies at Taipadar, Chhattisgarh, 2014
-

**Research Report on the
Preliminary Development Stage of the
Prediction Model for Mixed Flow Pumps as Turbines**



Dr. Punit Singh

**Institute of Water and River Basin Management
Karlsruhe Institute of Technology, Germany**

March 2011

Table of Contents

Abstract	3
1. Introduction and Objectives	3
2. The Turbine Plan of the Authors	3
3. Theory of the Prediction Model	4
3.1 Predictions of the BEP.....	4
3.2 Predictions of the 'No-load' point.....	6
3.3 Construction of operating line between no-load and the BEP	7
4. Model Testing	7
4.1 Model testing on the 72.8 rpm PAT	7
4.2 Model testing on the 94.4 rpm PAT	8
5. Application of the Model on a range of Mixed Flow Pumps	9
6. Discussion	10
6.1 Model Limitations.....	10
6.2 Range of Specimen Mixed Flow PATs within the Turbine Space	10
7. Conclusions and Recommendations	11
8. References	11
Nomenclature	12
Abbreviations	12
Appendix	12
A1. Diameter Specifications of Mixed Flow PAT Impeller	12
A2. Conversion Equations used in the Prediction Model	12
A3. Model equations and Spline constants for the specimen MF PATs	12
A4. Muschel curves for the range of specimen MF PATs	13

Abstract

The initiation for this research report is primarily driven by the non-availability of reliable prediction models for mixed flow pumps as turbines, which are seen to be useful and potential turbine solutions for low to medium heads (5 to 15 meters).

The report begins with an illustration of the turbine plan that authors have been working on and highlights the 'unsolved' flow zones on a 'head-flow space' that don't have reliable modeling laws for the turbine design and operation. This background forms the motivation for the search of mixed flow or diagonal pumps to be considered as turbines.

The report describes the development of the prediction model based on 10 experimentally tested radial flow PATs and 2 mixed flow PATs. It accepts the fact that the inclusion of radial flow PATs could lead to some errors in prediction. However, terming this reality as a precursor or preliminary model, the prediction laws for best efficiency point and no-load point are developed.

The report also carries out an interesting comparison of the model predictions with the experimental curves of the two authentic mixed flow machines and shows that both the no-load and best efficiency point predictions are within errors bands of $\pm 15\%$, which is reasonable considering the uncertainties arising due to the inclusion of radial flow PATs.

The report further applies the preliminary prediction model on a wide range of mixed flow pump designs (covering a specific speed from 50 rpm to 130 rpm) from a leading manufacturer and brings out the turbine operating line (including Muschel field curves) for all the pumps. The inclusion of these cruves on authors turbine plan shows that this range of mixed flow PATs cover at least 40% of open or unsolved flow zones (4 to 10 meter and 200 l/s to 1250 l/s).

The study also selects a series of pumps of favorable size to carryout detailed experimental evaluation of the turbine behaviour, which is vital for optimizing the modeling laws for developing a consolidated prediction model that will have predictions errors within the range of $\pm 1-2\%$. The report finally concludes with an immediate recommendation of designing a testrig to carryout the needful experimentation.

1. Introduction and Objectives

While there are models predicting the turbine performance of radial flow pumps as discussed in [1] and [2], there are no exclusive models for mixed flow or diagonal pumps operating as turbines. Mixed flow pumps find useful application in low and medium head turbine applications where radial flow pumps are not suitable for operation. This application area covers heads range from 5 meters to 15 meters in both micro hydro and energy recovery projects. These projects are gaining importance for both decentralized and grid-integrated due to their enormous potential in solving energy deficit, encouraging energy efficiency and helping in the mitigation of climate change effects.

The objectives of this report will be to plan the initial steps for the development of a reliable and robust prediction model using turbomachinery fundamentals combined with experimental results. It would then be required to test this basic model on mixed flow pumps whose turbine performance is already known and then to carryout a detailed error analysis. Further to this, the report will have to undertake a massive application of this model on available mixed flow pumps and publish their turbine characteristics. Following this, the study should identify the H-Q zone where mixed flow pumps as turbines can be adapted and optimized. To conclude, this research report should be able to recommend further steps for the development of a consolidated predicion model for mixed flow pumps as turbines.

2. The Turbine Plan of the Authors

The turbine plan that has been the forefront driver of the authors' research activity for over 12 years has been illustrated in [Fig. 1](#). This plan comprises of several turbine zones on the H-Q space, which cover the turbine research already taken place and also shows the open or unsolved turbine zones. The Ph.D (2000-2005) and postdoc 1 (2005-2009) zones are those in which the authors have sufficient experience and the model laws are capable of making predictions within $\pm 3\%$ error bands. The turbine plan also plots the surveyed zones of new micro hydro and energy recovery projects for which accurate turbine models are not available that the authors could be confident about.

In order to extend the turbine plan with an objective to obtain localized and unique turbine solutions, eight separate zones are identified as specified in [Fig. 1](#). The focus will be to cover 1 to 15 meters of head and 150 l/s to 10000 l/s of discharge with power limits not exceeding 100 KW_e or 140 KW_{shaft}. It is the endeavor of the authors to bring out accurate modeling laws for each of these zones in a strategic way using theoretical models and simulations, but would like to stress on the need for experimental studies.

The authors understand that the solutions in these ‘future zones’ would essentially cover diagonal (mixed flow) and axial flow turbines of different shapes. This characterizes one of the reasons to initiate work on the mixed flow PAT prediction model and to define the spread of these diagonal machines on this H-Q space.

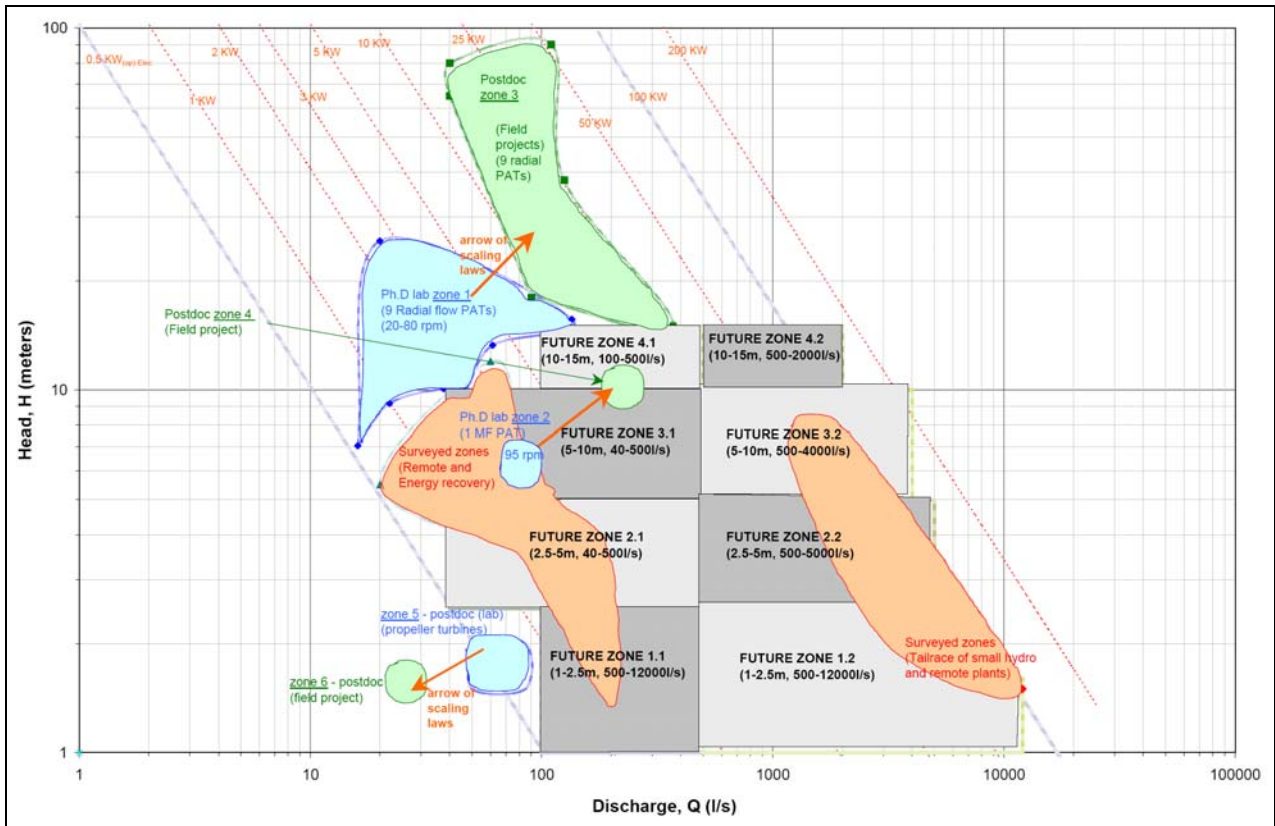


Fig. 1, The authors’ turbine plan on a H-Q space

3. Theory of the Prediction Model

The principles of developing the prediction model for mixed flow PATs will be on the lines of the prediction model proposed in [1] and [2] for centrifugal (radial) flow pumps as turbines that covered a specific speed range of 20 to 80 rpm. There are two significant steps of the model development consisting of ‘best efficiency point’ predictions of a given mixed flow pump shape and ‘no-load’ predictions respectively, which eventually help in constructing the operating characteristics.

3.1 Predictions of the BEP

Since experimental data on mixed flow PATs are available only for two pumps shapes (72.8 rpm and 94.4 rpm as studied in [1]), the preliminary model development will be based on a group of medium specific speed radial flow pumps along with the two mixed flow pumps. This is not the ideal situation to use a combination of two different pump shapes, but this is the only available alternative at the moment. However, the quality of this model will be put to test and detailed scrutiny in [section 4.1](#) for progressing further from this preliminary model stage.

The list of the experimental PATs used in the model has been summarized in [Table 1](#) along with the turbine mode BEP and no-load points (used in [section 3.2](#)). The dimensionless constants of these PATs will be used to develop the different model equations as described in forthcoming sections.

Table 1, Summary of the BEP and NLP of the experimental PATs used in the preliminary prediction model

Sr. No.	N_{qp} (rpm)	Pump type	Best Efficiency Point					No-Load Point	
			ϕ_t	ψ_t	N_{qt} (rpm)	σ	Δ	ϕ_{nl}	ψ_{nl}
1	33.4	Radial flow	0.165	7.468	29.9	0.190	4.283	0.058	3.598
2	35.3	Radial flow	0.151	7.640	28.1	0.178	4.509	0.062	4.050
3	36.4	Radial flow	0.185	8.000	30.1	0.191	4.121	0.072	3.500

4	37.6	Radial flow	0.224	8.400	31.9	0.202	3.791	0.080	3.800
5	39.4	Radial flow	0.200	6.700	35.7	0.226	3.791	0.078	3.100
6	45.2	Radial flow	0.235	6.180	41.1	0.261	3.428	0.115	3.200
7	46.4	Radial flow	0.275	7.600	38.1	0.241	3.337	0.105	2.180
8	55.6	Radial flow	0.323	6.300	47.5	0.301	2.938	0.140	3.000
9	61.3	Radial flow	0.414	5.748	57.6	0.365	2.537	-	-
10	79.1	Radial flow	0.480	4.900	70.0	0.443	2.263	0.250	1.800
11	72.8	Mixed flow	0.446	6.451	54.9	0.348	2.515	0.218	1.897
12	94.4	Mixed flow	0.515	4.522	76.9	0.488	2.143	0.292	1.530

3.1.1 Relating the pump shape to the turbine shape

The plot of the pump mode and turbine mode specific speeds of the experimental PATs has been illustrated in Fig. 2 and its relationship in Eq. (1). It can be seen that there is a considerable scatter of the $N_{q,t}$ points, which will naturally be a source of error in the predictions. However, these deviations can be accommodated within uncertainty bands of the Cordier line (as illustrated in section 3.1.2). The specific speed equation is the very important first step of the model application used to convert the available pump shape to the corresponding turbine shape.

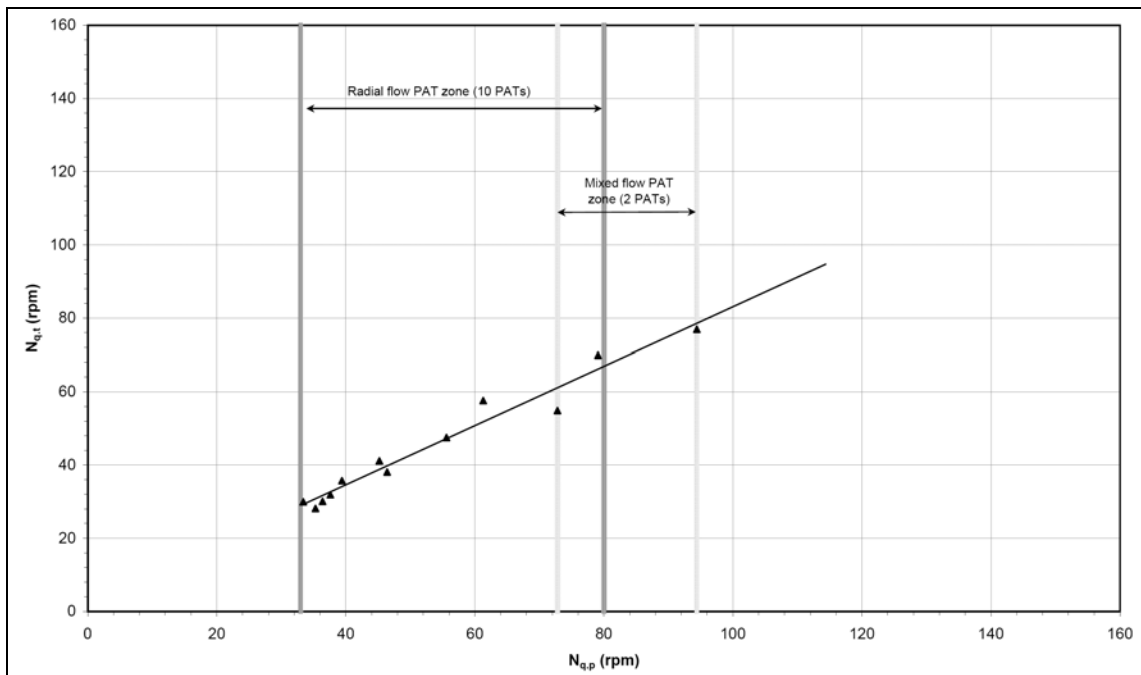


Fig. 2, The mixed flow PAT specific speed line

$$N_{q,t} = 0.8081 \cdot N_{q,p} + 2.2664 \quad (1)$$

3.1.2 The Cordier MF PAT line

The Cordier line that signifies the movement of the BEP of turbomachines is plotted in Fig. 3 for all the experimental PATs and illustrated in Eq. (2). To the mean Cordier line, uncertainty bands are introduced to include the errors that may arise from the specific speed prediction (section 3.1.1) or from the estimation of the specific diameter for a given specific speed. This is done through the addition of random error term R_{Δ} , which can be chosen depending on the confidence levels of the experimental results and different variables influencing the predictions. With the background of radial flow PATs included in the preliminary prediction model, a higher magnitude of error is assumed ($R_{\Delta} = 0.1$). The Cordier line would be used to bring out the turbine BEP operating parameters (head number and discharge number) of given pump shape using the conversion equations discussed in Appendix A2.

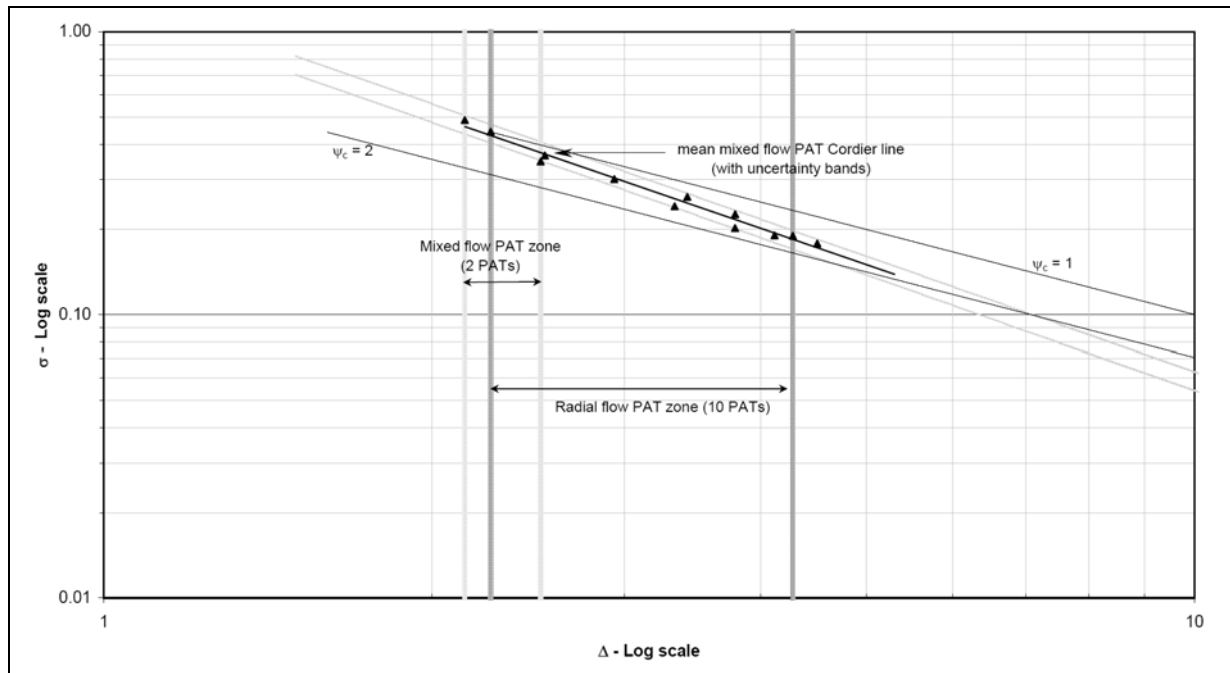


Fig. 3, The Cordier line for the preliminary mixed flow PAT model

$$\sigma = (1.2692 \pm R_{\Delta}) \cdot \Delta^{-1.326} \quad (2)$$

3.2 Predictions of the 'No-load' point

The no-load predictions will be developed from the identical group of experimental PATs used in the BEP predictions. The steps of prediction comprise of determining the no-load discharge number for given turbine shape (N_{qt} or σ) and then to determine the no-load head number from the obtained discharge number.

3.2.1 Specific speed and no-load discharge number

Figure 4 brings out the ϕ_{nl} - σ relationship for all the experimental PATs (the 61.3 rpm PAT results are left out due to its enormous scatter from the field of other PATs). Further, to account for errors in prediction (as done in section 3.1.2) and $R_{\sigma,nl}$ factor is added to ϕ_{nl} - σ equation in Eq. (3). Following some trials a value of 0.06 is given to the error factor $R_{\sigma,nl}$.

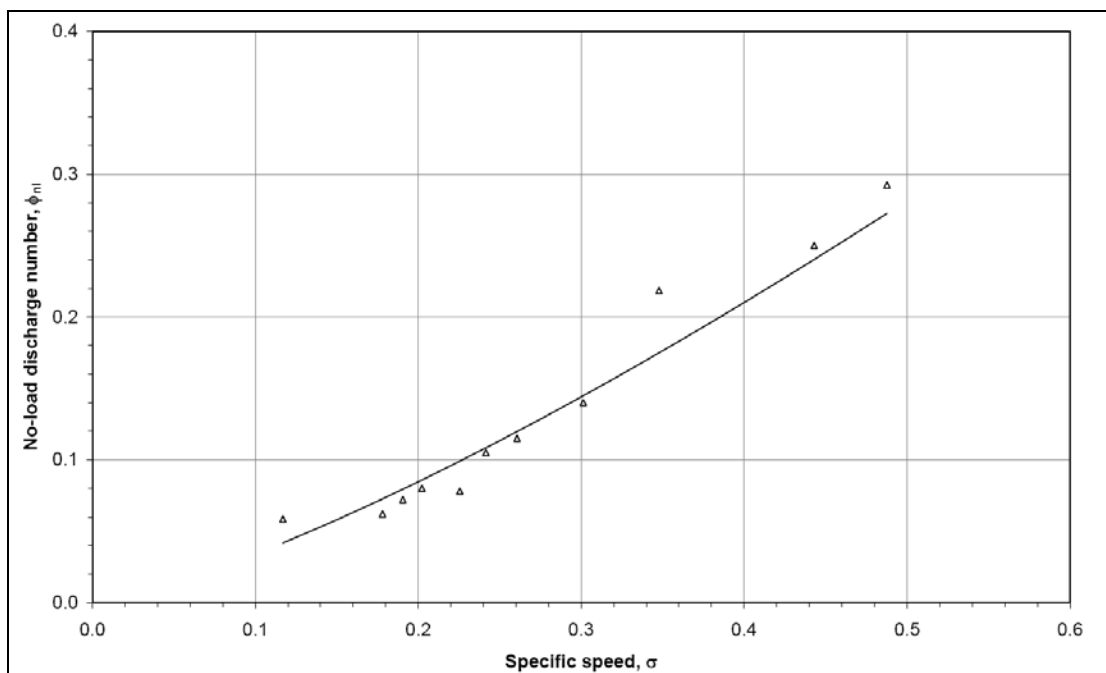


Fig. 4, The no-load line of specific speed and discharge number

$$\phi_{nl} = (0.6998 \pm R_{\sigma_{nl}}) \cdot \sigma^{1.3131} \quad (3)$$

3.2.2 No-load discharge number and no-load head number

The plot of no-load head and discharge numbers is shown in Fig. 5 and the scatter of these points are quite significant across the mean line (Eq. (4)). The errors of these predictions are included within the error factor $R_{\sigma_{nl}}$ of Eq. (3).

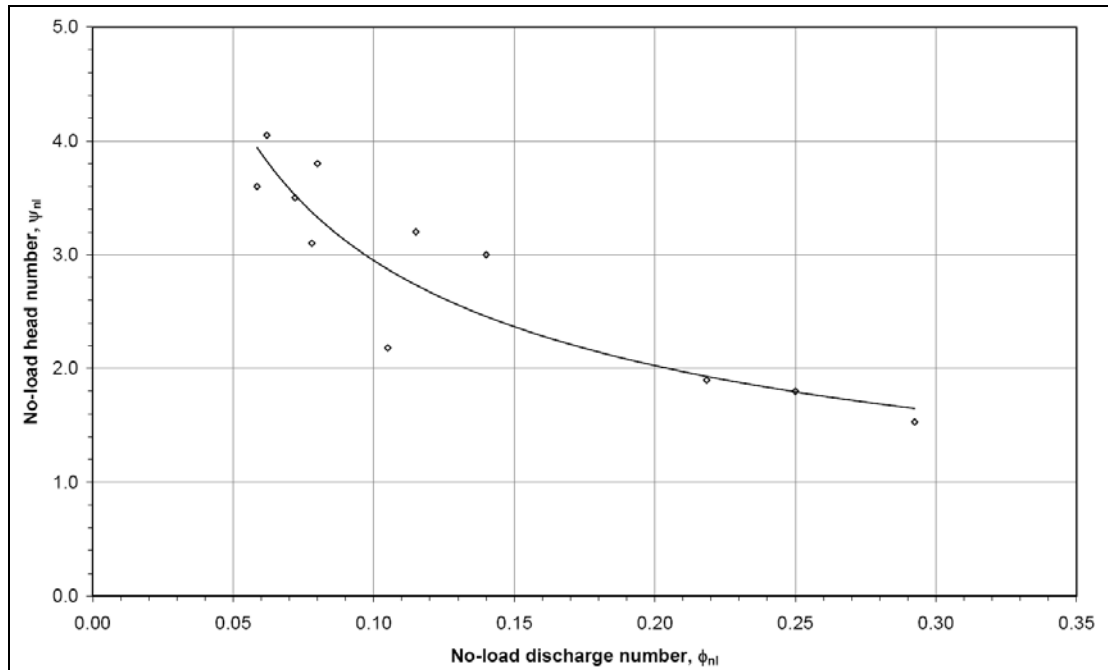


Fig. 5, The no-load line for head and discharge number

$$\psi_{nl} = 0.8464 \cdot \phi_{nl} - 0.5421 \quad (4)$$

The no-load zone for all PATs is quite a difficult zone with uncertain hydraulics. However, the error bands should be able to cover all these uncertainties. The model testing to be carried out in section 4 would reflect on the quality and accuracy of predictions in this zone.

3.3 Construction of operating line between no-load and the BEP

The shape of the operating lines for the head number, efficiency and power number parameters is very important in addition to the accurate prediction of the BEP and no-load points, particularly beyond the BEP into the overload region. This is because most of the PATs are preferred to work near the BEP or slightly in the overload zone.

The construction of these characteristics is carried out with help of Hermite spline interpolation illustrated in in [2]. This methodology requires the slopes of the head number and efficiency parameters with respect to the discharge number. For the preliminary model stage these constants are based on the 12 experimental PATs (Table 1) used in the model.

4. Model Testing

One of the objectives of this report was to test the preliminary prediction model on the available experimental mixed flow PATs. This evaluation will be help in determining the problems in the model and in identifying the sources of errors to recommend further optimization. The model testing will be carried out for complete range from no-load to BEP on two experimentally tested mixed flow PATs (72.8 rpm and 94.4 rpm PATs) in section 4.1 and section 4.2 respectively. The deviations between the model and experimental results along with subsequent optimization of the prediction model will be discussed in section 6.1.

4.1 Model testing on the 72.8 rpm PAT

The experimental and model prediction curves for head number and efficiency parameters are plotted in Fig. 6. It can be seen that the experimental head number curve lies within the uncertainty bands, but is slightly deviated from the mean prediction line. The no-load prediction and the BEP numbers of the two methodologies are summarized in Table 2 along with their deviations.

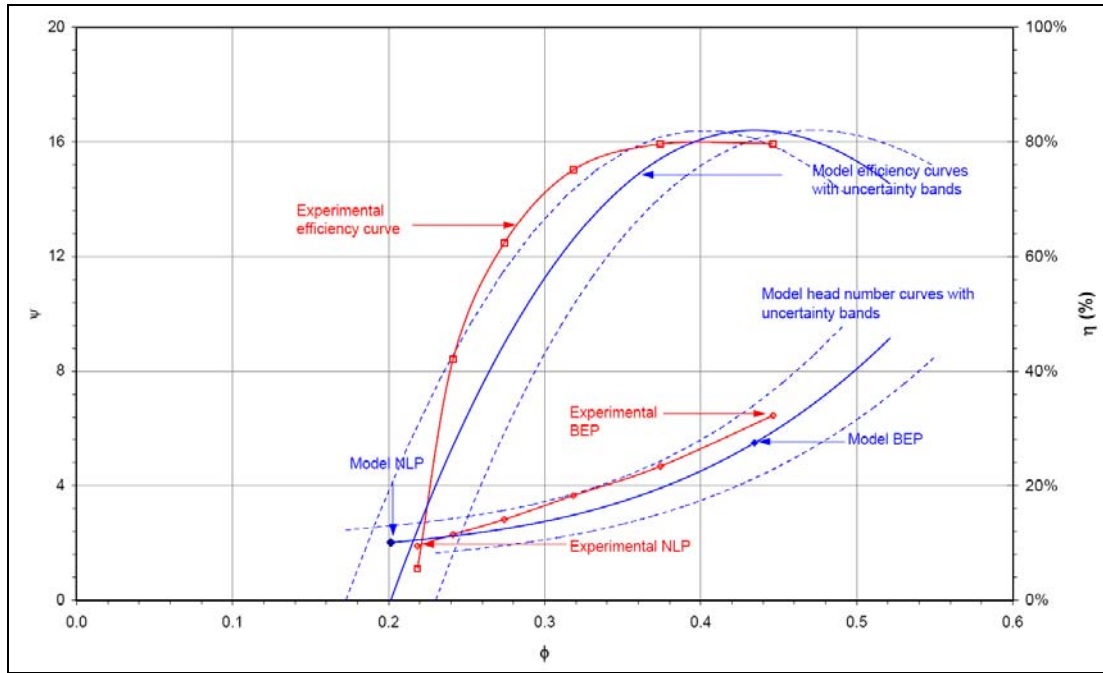


Fig. 6, Comparison of the model and experimental curves for the 72.8 rpm MF PAT

Table 2, Model testing on 72.8 rpm PAT at the BEP and no-load point

Method	Best Efficiency Point					No-load point	
	N_{qt}	σ	Δ_m	ϕ_t	ψ_t	ϕ_{nl}	ψ_{nl}
Model	61.1	0.387	2.448	0.434	5.491	0.201	2.018
Experimental	54.9	0.348	2.515	0.446	6.451	0.218	1.897
Percent change		+11.4%	-2.7%	-2.6%	-14.9%	-7.8%	+6.3%

For the BEP comparisons, it can be seen that prediction model is estimating specific speed with an error of +11.4% and the specific diameter with an error of -2.7%. These errors lead to predictions of -2.6% and -15% for the discharge and head number respectively. The predictions of discharge number are moderate but the error on the head number is considerable. The no-load predictions other the other hand are much better with -7.8% for discharge number and +6.8% for the head number.

4.2 Model testing on the 94.4 rpm PAT

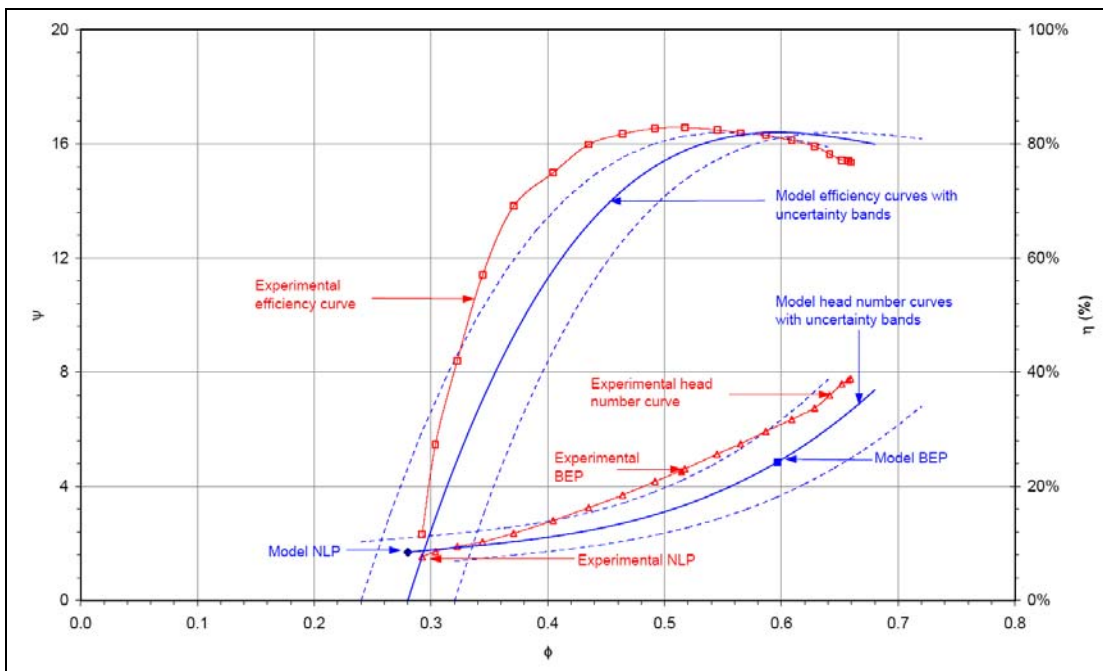


Fig. 7, Comparison of the model and experimental curves for the 94.4 rpm MF PAT

The comparison of the model and experimental curves in Fig. 7 show that the experimental head and efficiency curves are displaced from the mean prediction line and is closer to the upper limiting curves. The comparisons of the BEP in Table 3 reveal that the BEP discharge number is displaced over +15%, while the head number is overestimated by 7%. The origin of these errors is due to an error in estimating in the turbine specific speed and specific diameter respectively. The no-load zone comparison shows at discharge number under-estimation by 4% and an over-estimation of head number by 10%.

Table 3, Model testing on 94.4 rpm PAT at the BEP and no-load point

Method	Best Efficiency Point					No-load point	
	N_{qt}	σ	Δ_m	ϕ_t	ψ_t	ϕ_{nl}	ψ_{nl}
Model	78.6	0.498	2.025	0.597	4.853	0.280	1.687
Experimental	76.9	0.488	2.143	0.515	4.522	0.292	1.530
Percent change		+2.1%	-5.5%	+16.0%	+7.3%	-4.2%	+10.3%

5. Application of the Model on a range of Mixed Flow Pumps

The preliminary prediction model is applied on a mixed flow pump range of 17 pumps (available in four size categories) having specific speeds ranging from 54 rpm to 130 rpm obtained from the manufacturer's catalogue [3] using the relationships illustrated in section 3. The mean predictions of these pumps in turbine mode along with the pump operating parameters are summarized in Table 4. The comparative head and discharge ratios (turbine to pump performance) at BEP are also illustrated in Table 4.

The Cordier parameters (σ and Δ) for all these PATs are plotted in the original Codier diagram (discussed in section 3.1.2) in Fig. 8. This plot also shows the radial flow, mixed flow and overlap zones.

Table 4, Summary of the mixed flow pump parameters and mean predictions in turbine mode

Sr. No.	Pump code		Pump geometry and pump mode data										Turbine mode data after application of model								
			D_1	D_2	D_m	N	Q	H	ψ_p	ϕ_p	N_{qp}	η_p	N_{qt}	σ	Δ_m	ψ_t	ϕ_t	ψ_t/ψ_p	ϕ_t/ϕ_p	ψ_{nl}	ϕ_{nl}
1	400/365	400 series	363	278	320.5	1480	525	16.5	2.59	0.65	131	84.5	108	0.69	1.592	4.148	0.893	1.60	1.38	1.344	0.426
2	400/405		420	335	377.5	1480	600	28.0	3.17	0.45	94	84.0	78	0.50	2.029	4.859	0.595	1.53	1.32	1.690	0.279
3	400/420		427	364	395.5	1450	500	27.0	2.90	0.33	87	83.0	72	0.46	2.158	5.058	0.536	1.74	1.60	1.791	0.251
4	400/430		425	375	400.0	1480	525	33.0	3.33	0.33	78	83.0	65	0.41	2.331	5.319	0.472	1.60	1.42	1.927	0.219
5	400/450		450	410	430.0	1450	500	43.0	3.91	0.26	61	85.0	52	0.33	2.780	5.967	0.351	1.53	1.35	2.275	0.161
6	500/505	500 series	500	428	464.0	980	650	21.0	3.59	0.40	81	85.0	67	0.43	2.274	5.235	0.491	1.46	1.23	1.883	0.229
7	500/515		502	345	423.5	960	825	14.0	2.99	0.68	120	84.0	100	0.63	1.693	4.318	0.805	1.44	1.19	1.425	0.383
8	500/560	610	570	590.0	980	750	36.5	3.86	0.22	57	86.0	48	0.31	2.916	6.155	0.324	1.60	1.45	2.380	0.148	
9	600/550	600 series	557	483	520.0	980	900	24.2	3.29	0.39	85	86.0	71	0.45	2.183	5.096	0.526	1.55	1.34	1.811	0.246
10	600/575		547	429	488.0	960	1100	20.0	3.22	0.59	106	89.0	88	0.56	1.854	4.582	0.691	1.42	1.17	1.553	0.327
11	600/600		605	525	565.0	980	1120	28.5	3.28	0.38	84	86.0	70	0.45	2.204	5.129	0.518	1.56	1.36	1.828	0.242
12	600/650		647	593	620.0	990	910	42.0	3.94	0.23	57	84.5	49	0.31	2.912	6.150	0.325	1.56	1.40	2.378	0.149
13	600/700		700	635	667.5	980	1000	47.5	3.92	0.21	54	85.0	46	0.29	3.030	6.312	0.304	1.61	1.48	2.468	0.139
14	600/720	728	771	749.5	980	1200	51.5	3.37	0.17	56	85.0	47	0.30	2.965	6.222	0.315	1.85	1.81	2.418	0.144	
15	700/655	700 series	704	486	595.0	735	1650	17.0	3.14	0.64	113	84.5	93	0.59	1.777	4.457	0.742	1.42	1.16	1.492	0.352
16	700/715		704	606	655.0	725	1375	21.5	3.37	0.40	85	86.0	71	0.45	2.184	5.098	0.526	1.51	1.30	1.812	0.246
17	700/755		776	607	691.5	725	2000	23.5	3.30	0.50	96	87.0	80	0.51	2.000	4.813	0.609	1.46	1.22	1.667	0.286

The operating line is developed between the no-load and BEP predictions for the mean as well as for the lower and upper band of curves using the spline fitting methodology as mentioned section 3.3 (discussed in detail in [2]) and the constants for all the specimen PATs are summarized Appendix A3. The prediction equations for each of these PATs along with their absolute or Muschel characteristics are presented in Appendix A3 and Appendix A4 respectively.

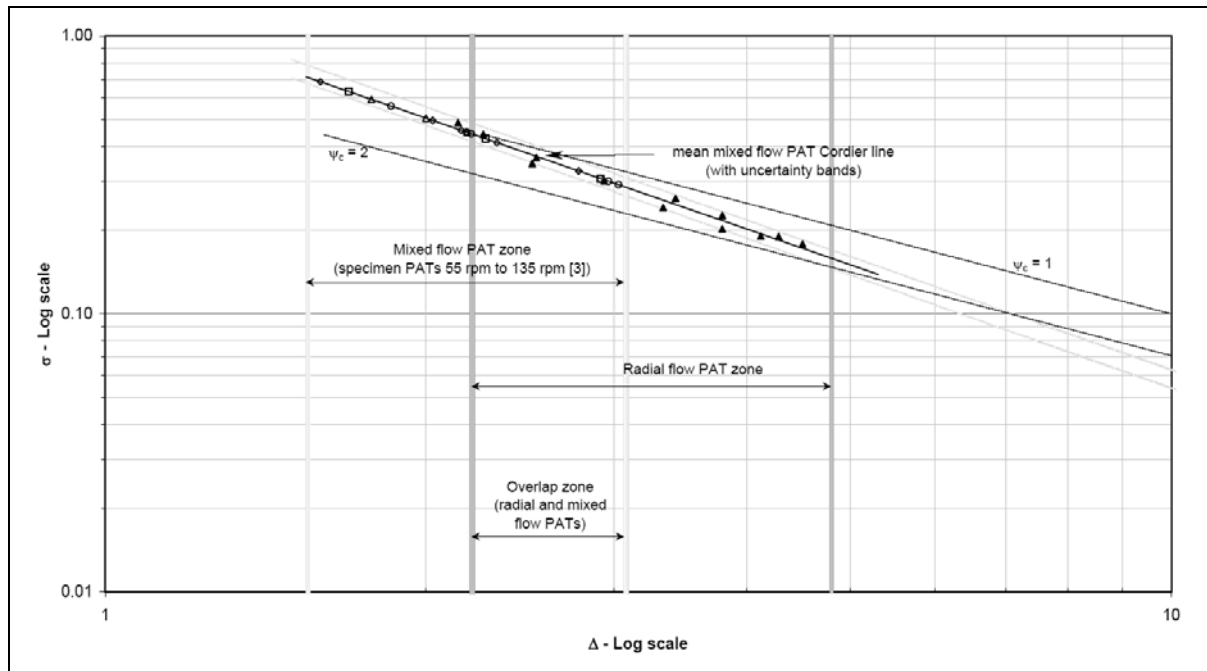


Fig. 8, Cordier diagram for mixed flow PATs with the specimen PATs (adapted from Fig. 2)

6. Discussion

6.1 Model Limitations

It has been seen from the model testing in [section 4](#) that the predictions based preliminary model, which comprised of group of 10 radial flow PATs and 2 mixed flow PATs has been unable to give a desired level of accuracy of $\pm 2\%$ on the head number and discharge number scales. However, it has to be emphasized that this preliminary model is a very initial stage of the development of mixed flow prediction model.

The source of error of the present model is in its incapability to accurately determine the turbine specific speed from the pump shape and then to evaluate the specific diameter from the specific speed using the two relationships (Eq. (1) and Eq. (2)). Both these sources lead to the over or under estimation of the BEP operating discharge and head numbers. It has become quite clear that if these two errors are minimized or eliminated, there is nothing that can prevent the model to bring down the errors on the final predictions to less than $\pm 2\%$.

One of the reasons for the problems with the specific speed and Cordier predictions is the inclusion of the radial flow pumps in the model whose hydraulics are different from the mixed flow pumps. Further, it also has to be emphasized that the developing a model on the two mixed flow pumps is not a conceivable option and the basic predictions made using this preliminary model are not all the bad to reject it. This discussion highlights the need for refinement that will be considered in [section 7](#).

6.2 Range of Specimen Mixed Flow PATs within the Turbine Space

The turbine range of the 17 specimen mixed flow PATs covering 4 series of different sizes (400, 500, 600 and 700) is plotted on the turbine H-Q space of the authors (discussed in [section 2](#)) in Fig. 9. It can be seen that the 400 series PATs extend from future zone 2.1 and 3.1 into zone 4.1 as well, while the 500 series PATs overlaps between zones 3.1/3.2 and 4.1/4.2. The 600 series turbines are seen to cross the head limits of zone 4.1/4.2 though they are still extend partially into the future zones 3.2 and 4.2. The largest PATs of the series (700) are also having higher operating heads but are still seen to penetrate into the turbine zones 3.2 and 4.2.

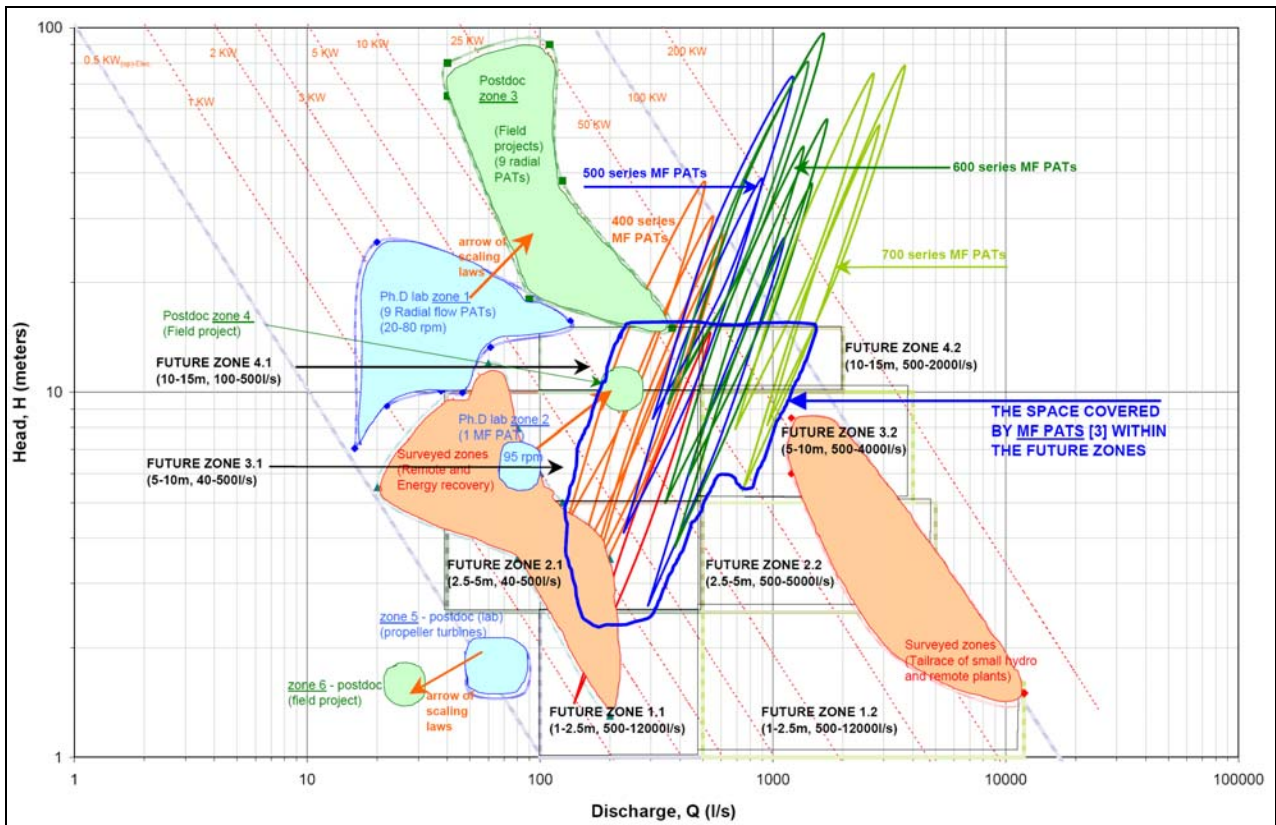


Fig. 9, Operating range of the specimen mixed flow PATs on the H-Q space

This study indicates that the selected type of mixed flow PATs would cover at least 5 of the future zones of the authors' turbine plan, if not completely. It has to be pointed out that this being a 'preliminary development stage' of the prediction model as discussed in section 6.1, the extent of coverage of this type of turbines on the H-Q space should be considered as approximate until an accurate model has been proposed.

7. Conclusions and Recommendations

The mixed flow prediction model development from fundamentals of turbomachinery is yet to reach its final destination as far as the accuracy of predictions are concerned. The reason for the errors in the present model is due to the lack of experimental data. It is obvious that accurate laboratory studies on a range of mixed flow pumps will help in realizing the optimized modeling laws namely, the specific speed relationship and the Cordier line respectively. It is therefore recommended to select the smallest size category (400 series) of the surveyed pumps that cover a specific speed range of 60 to 130 rpm and carryout rigorous experimentation.

There is no other way to develop the model but to design a testrig and determine the turbine operating points. These results can then be introduced to the Cordier diagram and specific speed diagram to bring out a new set of model equations.

Despite the prevailing inaccuracies of the model, it has been able to identify the H-Q operating zone for the specimen PATs on the authors' turbine plan. The reach of mixed flow pumps is quite significant with respect to the unsolved or open hydraulics zones proposed by the authors. It will be an endeavor to standardize the prediction model for mixed flow zones and clearly specify zones in which these types of PATs give optimum performance compared to other types. The only way forward is to script a test program and carry out real time analysis for mixed flow pumps as turbines.

8. References

- [1] Punit Singh, Optimization of the Internal Hydraulic and of System Design in Pumps as Turbines with Field Implementation and Evaluation, Ph.D. Thesis, University of Karlsruhe, Germany, 2005.
- [2] P. Singh, F. Nestmann, An optimization routine on a prediction and selection model for the turbine operation of centrifugal pumps, J. Experimental Thermal and Fluid Science 34, 152-164, 2010.
- [3] KSB Catalogues, 'Performance characteristics of SNW Series pumps', KSB AG, Frankenthal, Germany, 2010.

Nomenclature

Full Scripts

D	Runner diameter, mm or m
g	Gravitational acceleration, m/s ²
h	Hermite basis function
H	Head, m
n	Speed, rps
N _q	Specific Speed, NQ ^{1/2} /H ^{3/4} (N in rpm, H in m, Q in m ³ /s)
Q	Discharge, l/s or m ³ /s
R	Random error
S	Slope between head and discharge number
u	Tangential runner velocity, m/s

Greek symbols

Δ	Turbine Specific diameter, (in A3, Eq. (A4))
φ	Discharge number, Q/nD ³ (Q in 'm ³ /s', n in 'rps', D in 'm')
η	Efficiency, %
σ	Turbine specific speed, (in A3, Eq. (A3))
ψ	Head number, gH/n ² D ² (gH in m ² /s ² , n in 'rps', D in 'm')

Subscripts

1	outer diameter reference
2	inner diameter reference
c	Cordier definition
m	mean
nl	no-load
p	pump mode
t	turbine mode

Abbreviations

PAT	Pump as Turbine	MF	Mixed Flow
BEP	Best Efficiency Point	NLP	No Load Point

Appendix

A1. Diameter Specifications of the Mixed Flow PAT Impeller

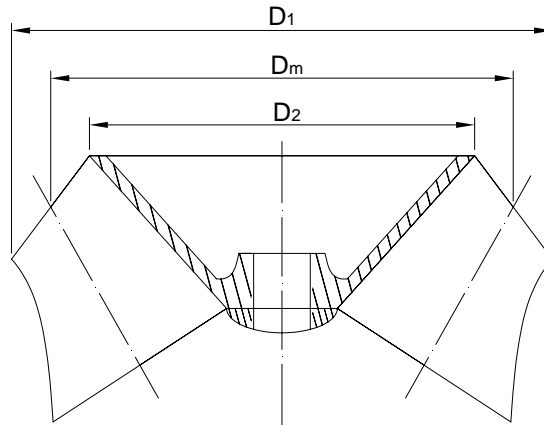


Fig. A1, Cross-section of the mixed flow impeller

A2. Conversion Equations used in the Prediction Model

(A1) Head number, $\psi_c = \frac{2gH}{u^2} = \frac{2}{\pi^2} \frac{gH}{n^2 D^2} = \frac{2}{\pi^2} \psi$	(A2) Discharge number, $\phi_c = \frac{4Q}{\pi D^2 u} = \frac{4}{\pi^2} \frac{Q}{n D^3} = \frac{4}{\pi^2} \phi$
(A3) Turbine Specific speed, $\sigma = \frac{\phi_c^{1/2}}{\psi_c^{3/4}} = 2^{1/4} \pi^{1/2} \frac{\phi_t^{1/2}}{\psi_t^{3/4}}$	(A4) Specific diameter, $\Delta = \frac{\psi_c^{1/4}}{\phi_c^{1/2}} = \frac{\pi^{1/2}}{2^{3/4}} \frac{\psi_t^{1/4}}{\phi_t^{1/2}}$
(A5) The relationship between the Cordier σ and N _q (SI) is given by, $\sigma = \frac{2^{1/4} \pi^{1/2}}{g^{3/4} 60} \frac{NQ^{1/2}}{H^{3/4}} = 6.3383 \times 10^{-3} N_{qt}$	

A3. Model equations and Spline constants for the specimen MF PATs

Table A1, Head number and power number equations and spline slopes for the MF PATs

Sr. No.	Pump code	N _{qp}	Head number equation	Power number equation	Hermite Spline slopes at BEP and NLP			
					S _{bep-ψ}	S _{nl-ψ}	S _{bep-η}	S _{nl-η}
1	400/365-1	131	$\psi = 27.479\phi^3 - 37.229\phi^2 + 17.759\phi - 1.5894$	$p = 28.698\phi^3 - 43.498\phi^2 + 24.914\phi - 4.9541$	17	1	0	4.4
2	500/515-1	120	$\psi = 24.119\phi^3 - 26.414\phi^2 + 11.62\phi - 0.5055$	$p = 22.099\phi^3 - 26.525\phi^2 + 13.917\phi - 2.6897$	16	2	0	5.0
3	700/655-1	113	$\psi = 38.122\phi^3 - 43.351\phi^2 + 19.346\phi - 1.6079$	$p = 24.873\phi^3 - 26.266\phi^2 + 12.422\phi - 2.2083$	18	3	0	5.0

4	600/575-1	106	$\psi = 74.316\phi^3 - 84.028\phi^2 + 33.605\phi - 3.0487$	$p = 53.107\phi^3 - 63.037\phi^2 + 28.311\phi - 4.3897$	24	2.5	0	5.5
5	700/755-1	96	$\psi = 81.677\phi^3 - 78.802\phi^2 + 29.039\phi - 2.1045$	$p = 43.727\phi^3 - 39.871\phi^2 + 15.728\phi - 2.269$	24	4	0	6.0
6	400/405-1	94	$\psi = 79.518\phi^3 - 72.578\phi^2 + 25.932\phi - 1.6234$	$p = 37.612\phi^3 - 29.914\phi^2 + 11.167\phi - 1.607$	24	4	0	6.0
7	400/420-1	87	$\psi = 111.87\phi^3 - 90.109\phi^2 + 28.088\phi - 1.35$	$p = 40.756\phi^3 - 24.664\phi^2 + 7.3767\phi - 0.9371$	28	4	0	6.0
8	600/550-1	85	$\psi = 108.97\phi^3 - 83.41\phi^2 + 25.253\phi - 0.9752$	$p = 43.225\phi^3 - 26.157\phi^2 + 7.8287\phi - 0.9848$	28	4	0	6.0
9	700/715-1	85	$\psi = 108.82\phi^3 - 83.08\phi^2 + 25.117\phi - 0.9575$	$p = 42.956\phi^3 - 25.778\phi^2 + 7.6818\phi - 0.9668$	28	4	0	6.0
10	600/600-1	84	$\psi = 106.09\phi^3 - 77.385\phi^2 + 22.815\phi - 0.6639$	$p = 38.043\phi^3 - 19.056\phi^2 + 5.125\phi - 0.6589$	28	4	0	6.0
11	500/505-1	81	$\psi = 166.31\phi^3 - 128.2\phi^2 + 37.546\phi - 1.9891$	$p = 74.269\phi^3 - 55.551\phi^2 + 17.915\phi - 2.0888$	32	5	0	7.5
12	400/430-1	78	$\psi = 158.81\phi^3 - 111.07\phi^2 + 30.803\phi - 1.1619$	$p = 59.294\phi^3 - 35.692\phi^2 + 10.636\phi - 1.2424$	32	5	0	7.5
13	400/450-1	61	$\psi = 30.043\phi^3 + 55.985\phi^2 - 15.41\phi + 3.1783$	$p = -6.1902\phi^3 + 36.102\phi^2 - 8.236\phi + 0.4237$	35	5	0	10.5
14	600/650-1	57	$\psi = -93.114\phi^3 + 151.39\phi^2 - 33.866\phi + 4.3716$	$p = -77.273\phi^3 + 89.489\phi^2 - 19.624\phi + 1.2088$	35	5	0	10.5
15	500/560-1	57	$\psi = -96.73\phi^3 + 153.98\phi^2 - 34.332\phi + 4.3996$	$p = -79.876\phi^3 + 91.328\phi^2 - 20.003\phi + 1.234$	35	5	0	10.5
16	600/720-1	56	$\psi = -154.08\phi^3 + 193.93\phi^2 - 41.331\phi + 4.8069$	$p = -94.279\phi^3 + 100.79\phi^2 - 21.447\phi + 1.2946$	35	5	0	10.5
17	600/700-1	54	$\psi = -241.68\phi^3 + 251.39\phi^2 - 50.835\phi + 5.327$	$p = -133.32\phi^3 + 126.12\phi^2 - 25.993\phi + 1.5519$	35	5	0	10.5

A4. Muschel curves for the range of specimen MF PATs

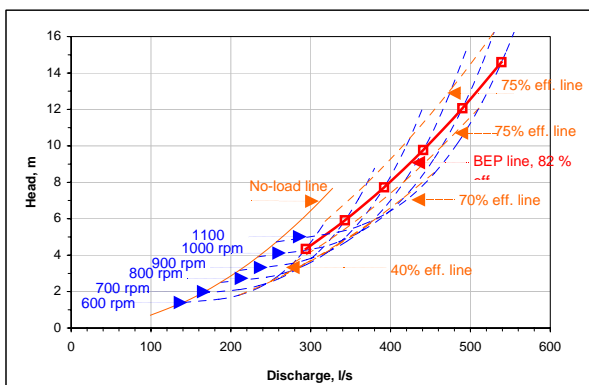


Fig. A2, 400-1 (131 rpm)

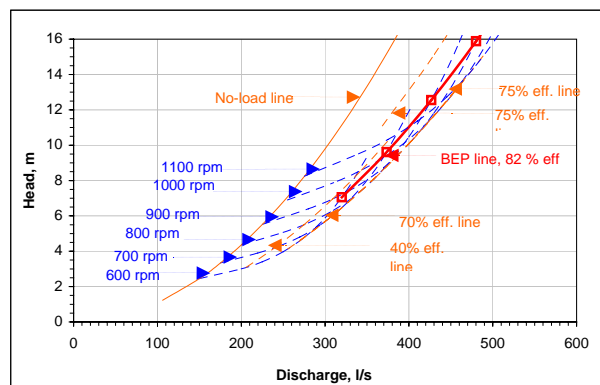


Fig. A3, 400-2 (94 rpm)

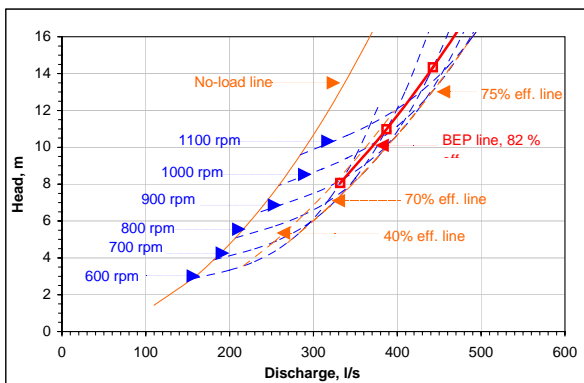


Fig. A4, 400-3 (87 rpm)

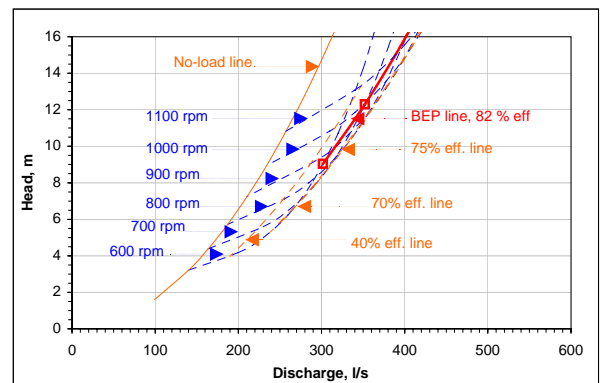


Fig. A5, 400-4 (78 rpm)

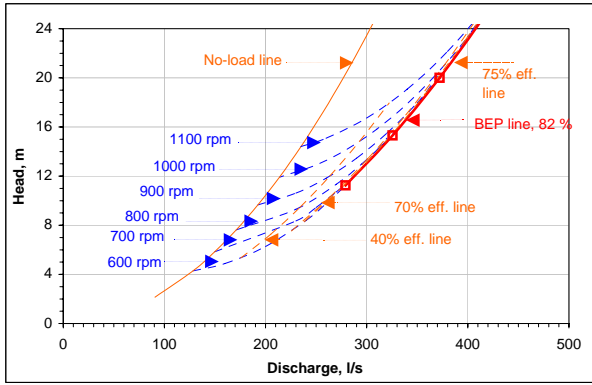


Fig. A6, 400-5 (61 rpm)

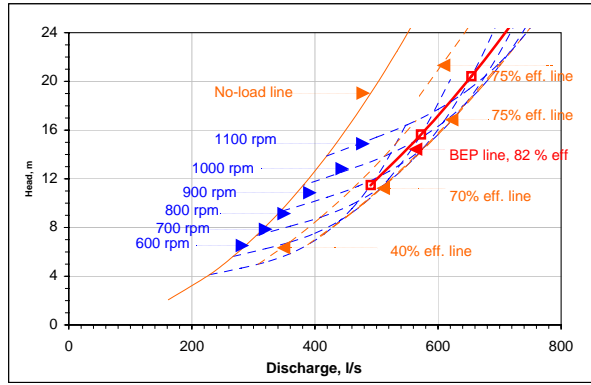


Fig. A7, 500-1 (81 rpm)

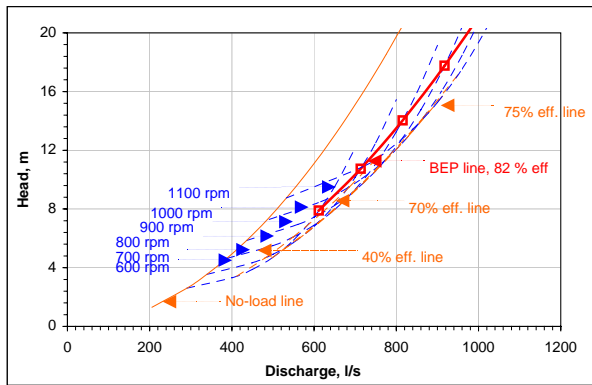


Fig. A8, 500-2 (120 rpm)

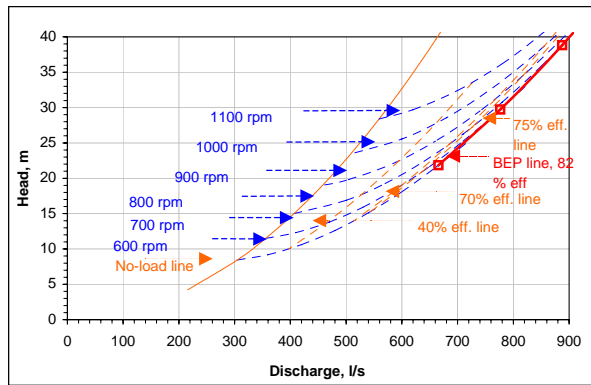


Fig. A9, 500-3 (57 rpm)

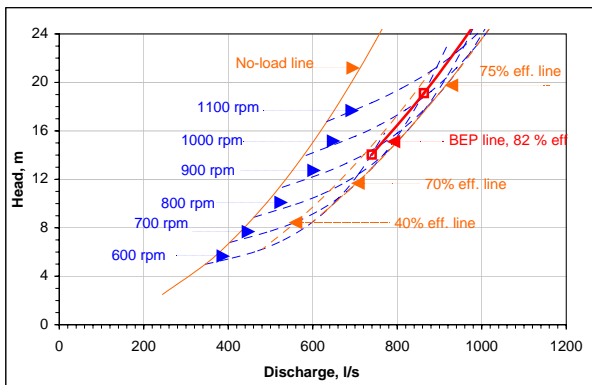


Fig. A10, 600-1 (106 rpm)

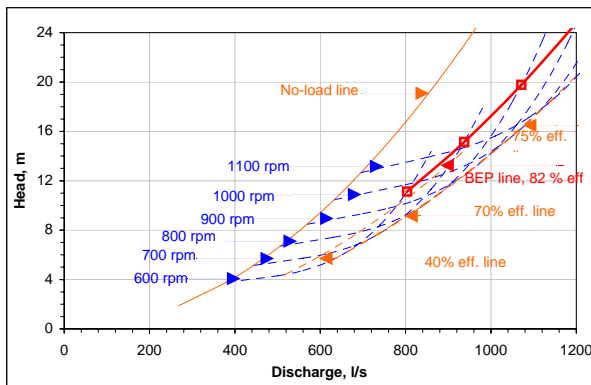


Fig. A11, 600-2 (85 rpm)

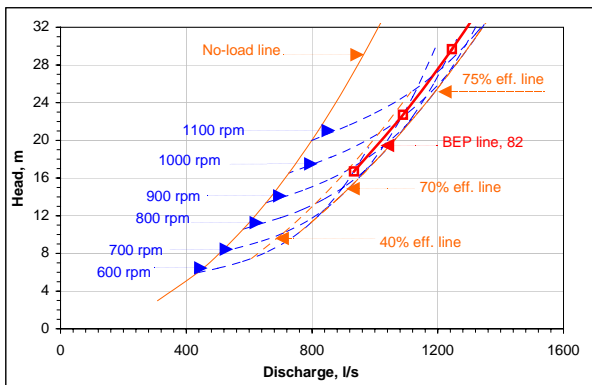


Fig. A12, 600-3 (84 rpm)

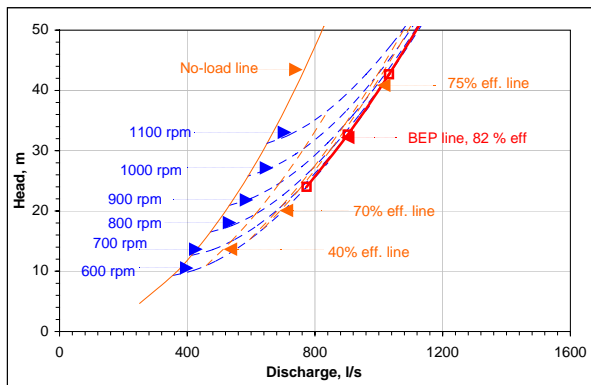


Fig. A13, 600-4 (57 rpm)

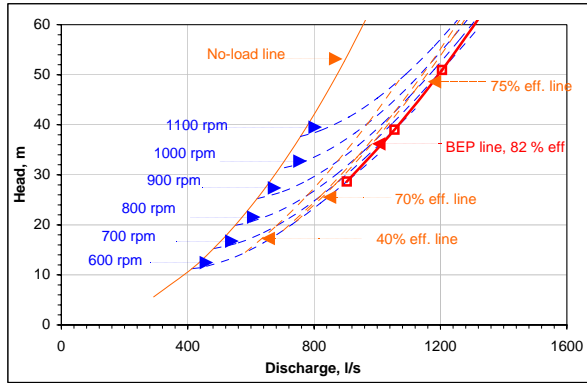


Fig. A14, 600-5 (54 rpm)

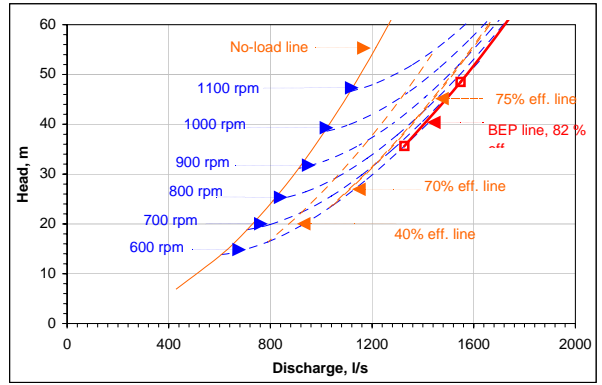


Fig. A15, 600-6 (56 rpm)

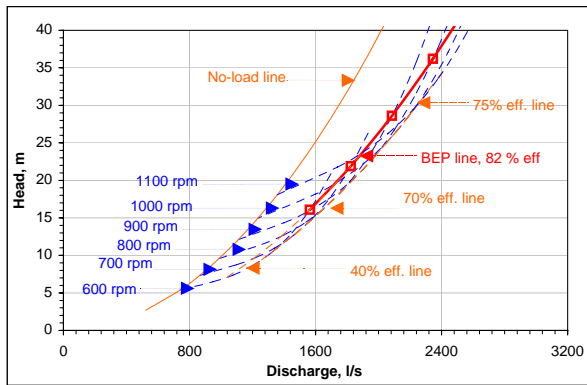


Fig. A16, 700-1 (113 rpm)

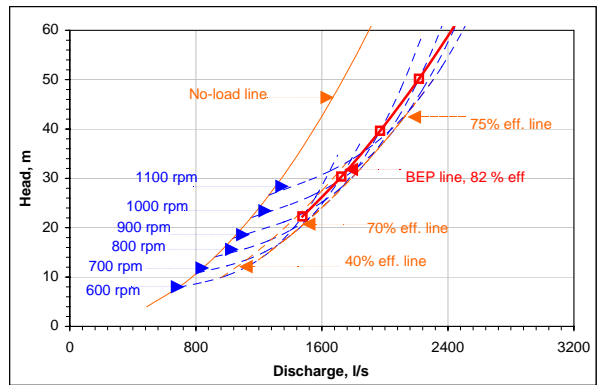


Fig. A17, 700-2 (96 rpm)

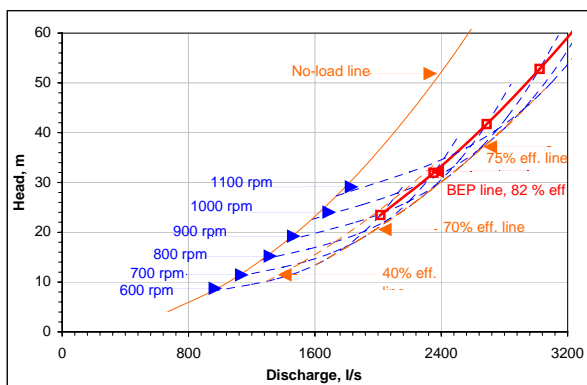
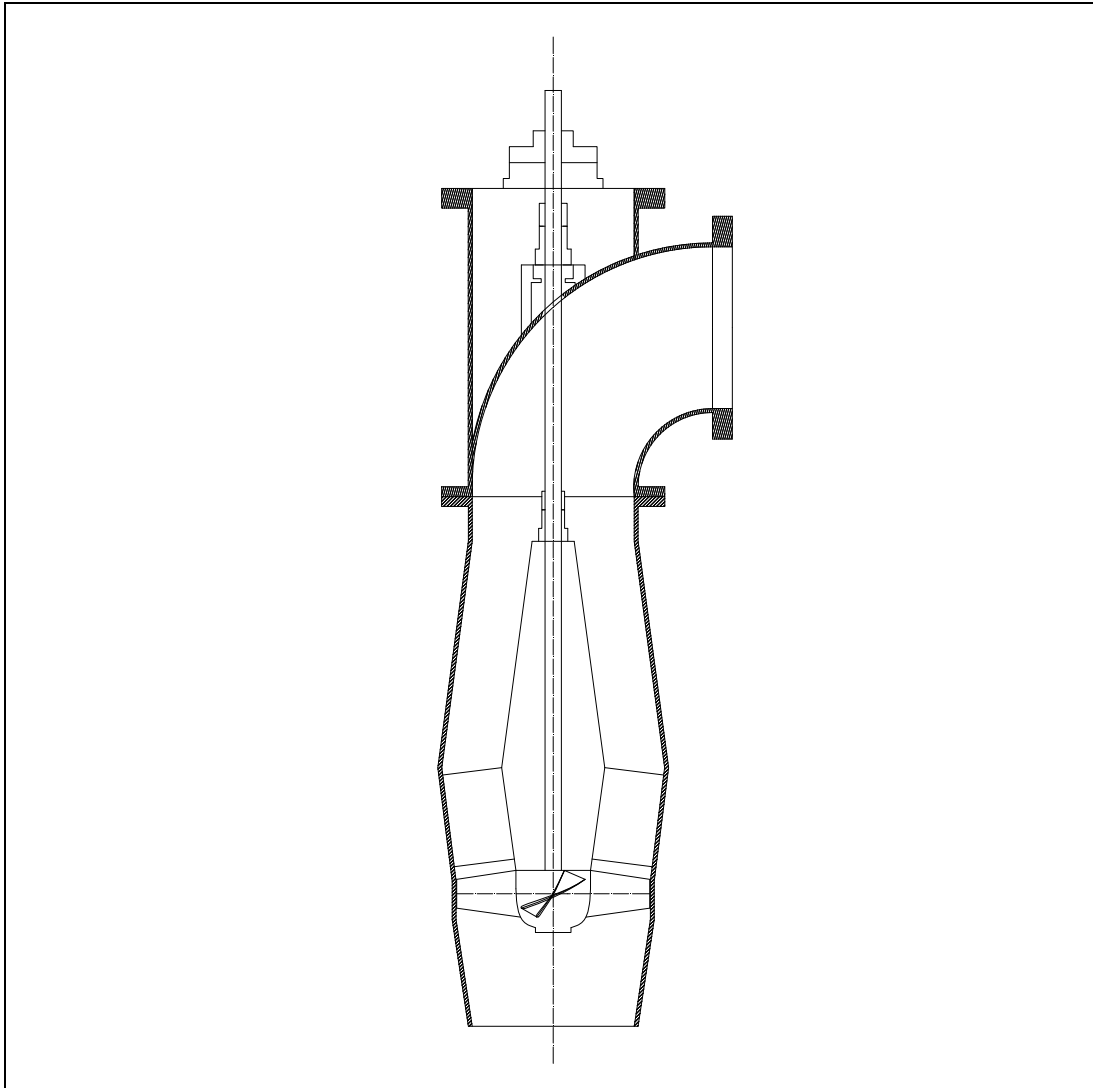


Fig. A18, 700-3 (85 rpm)

**A Proposal for a
Preliminary Prediction Model for
Axial Flow Pumps as Turbines**



Dr. Punit Singh

**Institute of Water and River Basin Management
Karlsruhe Institute of Technology, Germany**

April 2011

Table of Contents

Abstract	3
1. Background and Objectives	3
2. The Theoretical Model	3
2.1 Prediction of the Best Efficiency Point.....	3
2.2 Prediction of the No-load operating zone	5
3. Application of Model and Evaluation of the spread on the H-Q Plane	5
4. Effects of Blade Shapes on the Prediction Model	6
5. Conclusions and Recommendations	8
6. References	9
Nomenclature	9
Abbreviations	9
Appendix	10
A1 Conversion Equations used in the Prediction Model	10
A2 Tabulations for the development of prediction model	10
A3 Muschel Family and Individual Curves	11

Abstract

The task of proposing a turbine prediction model for axial flow pumps arises out of the need of finding optimum turbine solutions in the low head range of 2 to 10 meters and power capacities restricted to 100 KW_e and also due to the fact that there are no calibrated models available for axial flow pumps as turbines.

A preliminary model is proposed, which comprises of experimental data of a mixture of turbine shapes ranging from radial flow PATs, mixed flow PATs, propeller turbines and large Kaplan turbines. It was found that the previously proposed mixed flow prediction modeling laws at the optimum efficiency point showed tremendous conformance with that of the axial flow turbine parameters. This result in a way justified the approach of using diverse turbine shapes for the axial flow PAT model.

The proposed model is applied on a series of standard available axial flow pumps and its range was investigated on the head-flow plane (on the authors' turbine plan). The results were very encouraging to particularly see the spread from 2 to 9 meters and 200 to 2500 l/s, even though higher flows (which was desired at lower heads) could not be achieved by the specimen range of axial pumps.

The report also brought out some interesting influences with respect to the axial blade shapes in axial pump runners, which could have an impact on the proposed prediction model. A theoretical analysis revealed that forward and backward shaped blades popularly incorporated in the design of axial pump runners could have divergent turbine characteristics, which leads to the recommendation for accurately characterizing the effects of blade shapes on the model.

The paper concludes with a sincere recommendation of carrying out an elaborate experimental study to achieve two goals, firstly to develop a robust prediction given the large uncertainties in the current procedure of using diverse turbine shapes and secondly to evaluate the influence of blade shapes.

1. Background and Objectives

There is a significant dearth of optimum turbine solutions for low heads ranging 2 to 8 meters and flows covering 200 to 5000 l/s for power capacities below 100 KWs as elaborately discussed using a 'Turbine Plan' in [1]. One of the turbine solutions that could be adopted for this low-head range is the operation of axial flow pumps as turbines that are easily available in the market [2]. The experience of using radial flow pumps as turbines has been quite positive as seen in many field projects in [3] with the help of good prediction models. Hence, to achieve any success with axial flow pumps as turbines, it would be necessary to develop accurate models of their turbine operation. With wide range and designs of axial flow pumps manufactured there would always be a possibility and hope of using some of them efficiently as turbines.

Singh and Nestmann in [4] and [5] have particularly looked at the influence of blade shape of axial flow impellers on both the pump and turbine mode performances and have recommended the use of forward shaped axial flow impellers for turbine operation. However, their study was restricted to a theoretical workout based on Euler laws and it could not bring out modeling laws for predicting the turbine operation of these blade shapes.

The present status of prediction model development in pumps as turbines particularly for mixed and axial flow pumps is not very encouraging in spite of the fact that there is a need for such models. The diverse requirement for such low head applications from both energy recovery and remote hydro schemes [6] is a sufficient basis to initiate a program for developing a robust prediction model that will be characterized by accuracy on one hand and parsimony with respect to input geometric variables on the other hand.

Based on the above background, the objectives of this study would be to firstly lay foundations for a raw or preliminary prediction model for axial flow pumps using experimental data from similar shapes of 'conventional' turbines and other pumps as turbines that are available. The second objective of the study would be to apply this preliminary model on the standard available axial flow pump shapes and evaluate the spread or reach on their turbine characteristics on the authors' 'turbine plan' illustrated in [1]. It would also be required to investigate the influences of blade shape (forward and backward) on the proposed prediction model. Finally, the study should conclude with discrete recommendations to develop a consolidated and optimized prediction model for axial flow pump as turbines.

2. The Theoretical Model

2.1 Prediction of the Best Efficiency Point

2.1.1 The proposed Cordier Line for Axial Flow PATs

In a very interesting exercise the Cordier line developed for mixed flow PATs in [1] is integrated with the Cordier data points from small propeller turbines developed by authors [7] and Kaplan turbine data available [8] in Fig. 1. As seen from the plot, there is great degree of conformance of the MF PAT line with that of the propeller and Kaplan turbine points. This is indeed a significant and quite a fascinating result that

reveals and proves that on a scale of Cordier parameters, there is negligible difference in the hydraulics of the BEP zone of radial flow and mixed flow PATs in comparison with that of the axial flow turbines. It has to be underlined that the developed MF PAT model in [1] used some radial flow PAT as well. This positive result can be used as a basis for proposing a new axial flow PAT model. A new Cordier line for the axial flow PATs is hence proposed considering all these different turbine shapes as shown in Fig. 1 and represented in Eq. (1). The data for all these turbine shapes have been illustrated in Appendix A2.

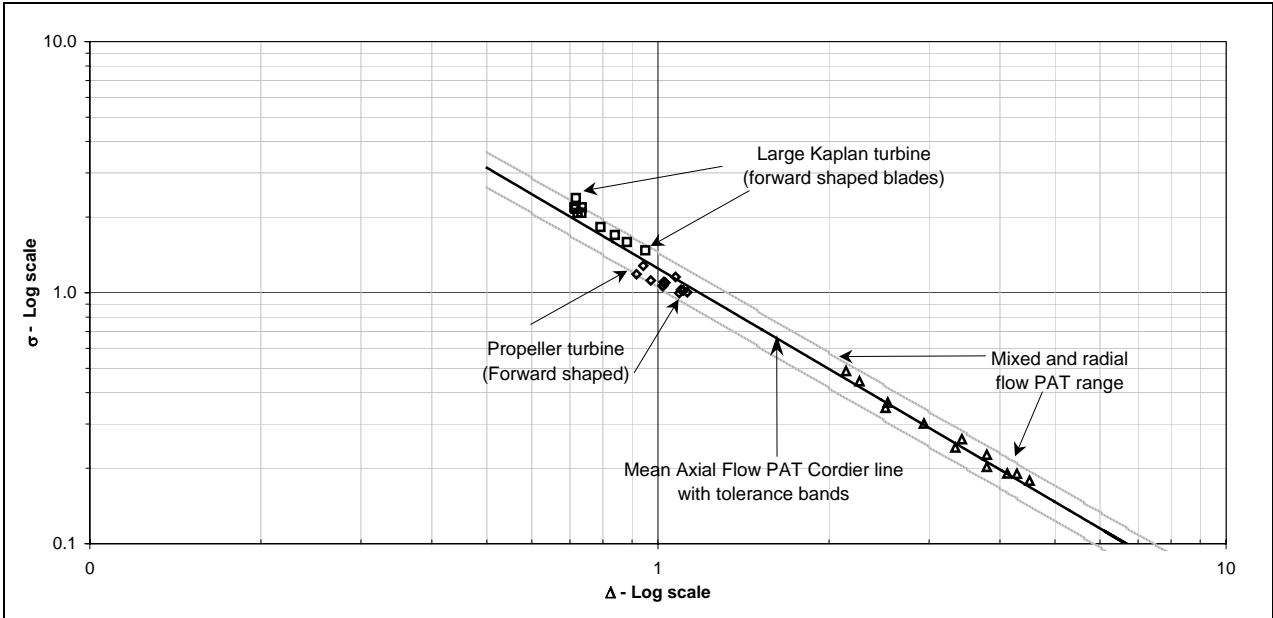


Fig. 1, A proposal for Cordier Axial Flow PAT line

$$\sigma = (1.2497 \pm R_{\Delta}) \cdot \Delta^{-1.3311} \tag{1}$$

$$\sigma = (1.2497 \pm 0.2) \cdot \Delta^{-1.3311}$$

The methodology of using different turbine shapes to predict the BEP of axial flow PATs may not have a strong scientific basis, but the proof of the concurrence of Cordier line gives hope for the model and to an extent justifies the procedure adopted.

2.1.2 The Specific Speed Line for Axial Flow PATs

One of the fundamental requirements of a prediction model for pumps as turbines is to make a fairly accurate determination of the turbine specific speed from the pump specific speed. Given the background that no axial flow PAT data is available and a reasonably good conformance of the MF PAT Cordier line for axial flow turbines is observed in Fig. 1, the specific speed relationship for mixed flow PATs is retained for axial flow PAT prediction model as well and presented in Fig. 2 and Eq. (2).

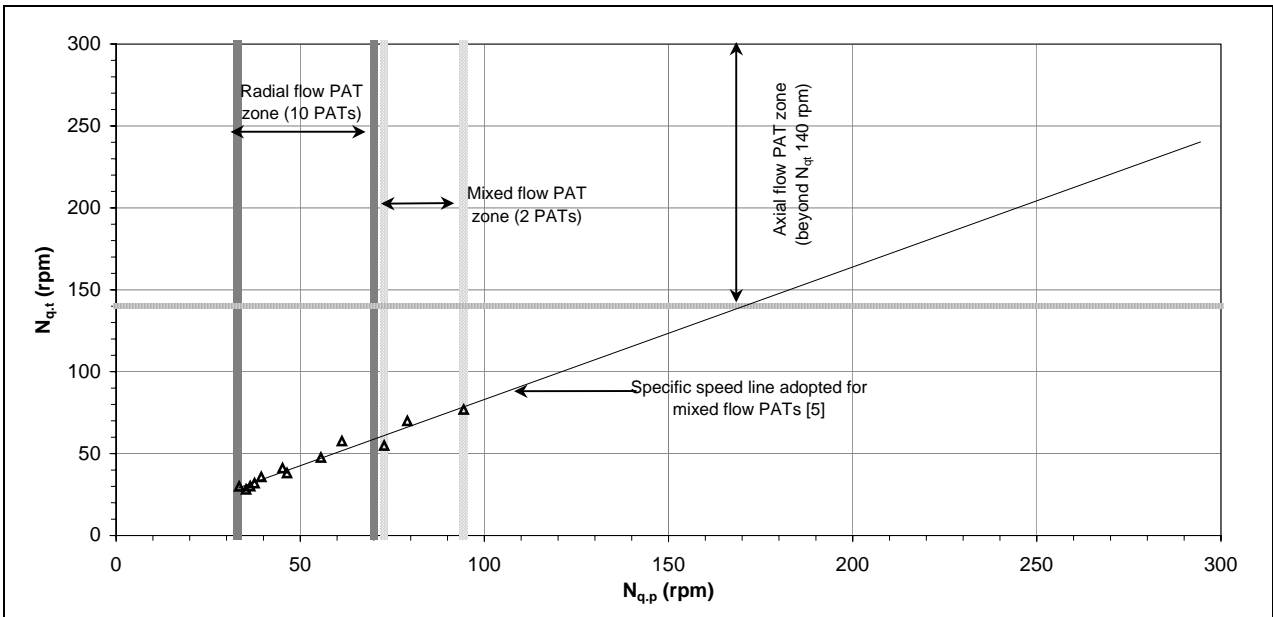


Fig. 2, The Specific speed line for axial flow PATs

$$N_{q,t} = 0.8081 \cdot N_{q,p} + 2.2664 \quad (2)$$

There could be some uncertainties because the Cordier line deals with the turbine operating parameters only and the specific speed line (in Fig. 2) brings in pump performance parameters into the picture. But, at this stage the influence of uncertainties between mixed flow and axial flow pump parameters cannot be accurately ascertained. However, a broad based uncertainty is considered in the Cordier line with the random error factor in Eq. (1). The tolerance bands on the Cordier line would also inherently include the uncertainties in specific speed prediction as well.

2.2 Prediction of the No-load operating zone

The beautiful conformity of the BEP parameter of radial flow PATs, mixed flow PATs, fixed propeller and large axial flow turbines on the Cordier line gave sufficient belief that there would be a reasonable similarity of the hydraulics of these turbines within the no-load operating zone as well. However, there was tremendous scatter especially for the radial and mixed flow PATs in relation with the available no-load information for propeller turbines.

After due consideration, it was concluded that the no-load zone is completely different from the BEP zone and there need not be any repeatability in the respective behaviours. It was also felt that it would be better to leave out the no-load points of the radial and mixed flow PATs completely and develop the no-load model based on the propeller turbine data only. This is carried out under the assumption that the no-load hydraulics of two types of axial flow turbines would be similar.

The no-load graphs comprising of no-load discharge number-specific speed and the no-load head number-no-load discharge number for the selected propeller turbines are illustrated in Fig. 3 and Fig. 4 respectively. The different model equations are summarized in Eq. (3) and Eq. (4). The data for these turbines are provided in Appendix A2. Similar to the exercise in the Codier line, the no-load uncertainties are considered within the specific speed parameter as shown in Eq. (3).

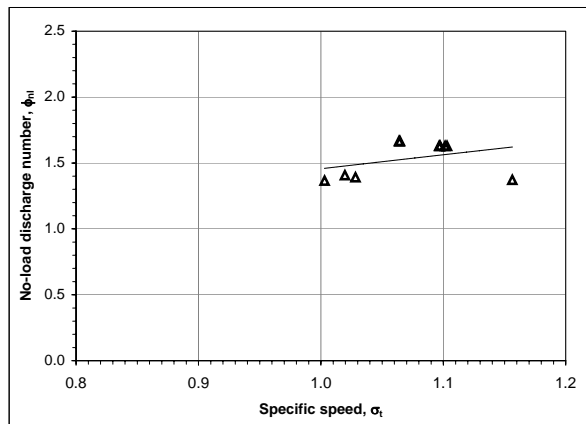


Fig. 3, No-load discharge number Vs Specific speed for axial flow PATs

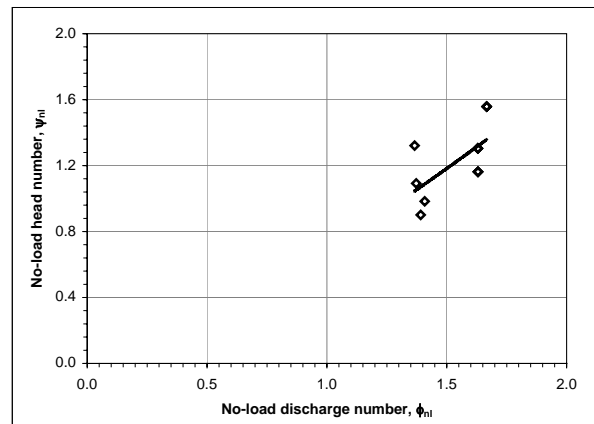


Fig. 4, No-load head number Vs No-load discharge number for axial flow PATs

$$\begin{aligned} \phi_{nl} &= (1.4562 \pm R_{\sigma_{nl}}) \cdot \sigma^{0.7391} \\ \phi_{nl} &= (1.4562 \pm 0.1) \cdot \sigma^{0.7391} \end{aligned} \quad (3)$$

$$\psi_{nl} = 0.6933 \cdot \phi_{nl}^{1.3171} \quad (4)$$

3. Application of Model and Evaluation of the spread on the H-Q Plane

The preliminary axial flow prediction model described in section 2 is applied on a standard range of axial flow pumps (drainage pumps manufactured by KSB [2] that comprises of 6 pumps of different sizes and each pump having 7 or 8 configurations of blade pitch). A typical representation of the internal hydraulics of this type of pump is shown in Fig. 5.

The model evaluates the turbine BEP and no-load points for each of these pumps at their different blade pitch positions (summarized in Appendix A3). The operating characteristics (both non-dimensional and absolute) are plotted using a spline interpolation technique used in [3]. The absolute or muschel curves for each of these pumps at different positions of blade and operating speeds in presented in Appendix A3.1 to Appendix A3.6. A consolidated muschel family curves comprising of absolute characteristics for all the blade positions of each pump at a fixed speed is also illustrated in Appendix A3.

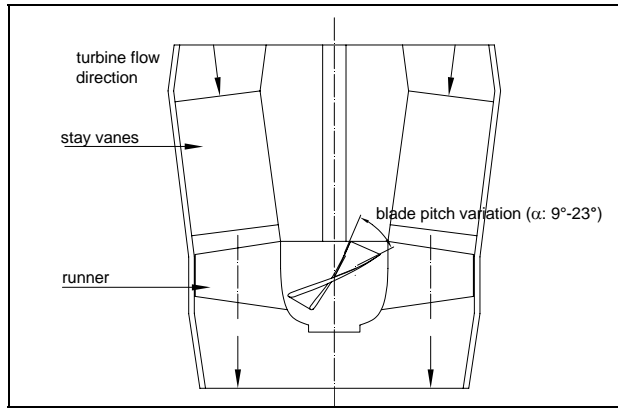


Fig. 5, The internal hydraulics of an axial flow pump

The spread of the turbine operating characteristics of these 6 pumps is plotted on turbine plan in Fig. 6. It can be seen that the operating curves dominate in zones 2.1, 2.2 and 3.2 respectively. However, they fail to penetrate into the ‘critical’ low head zone of 1.2, though certain regions of zone 1.1 are covered. It is naturally an encouraging result to cover a range for 2 to 9 meters and discharge of 200 to 2500 l/s.

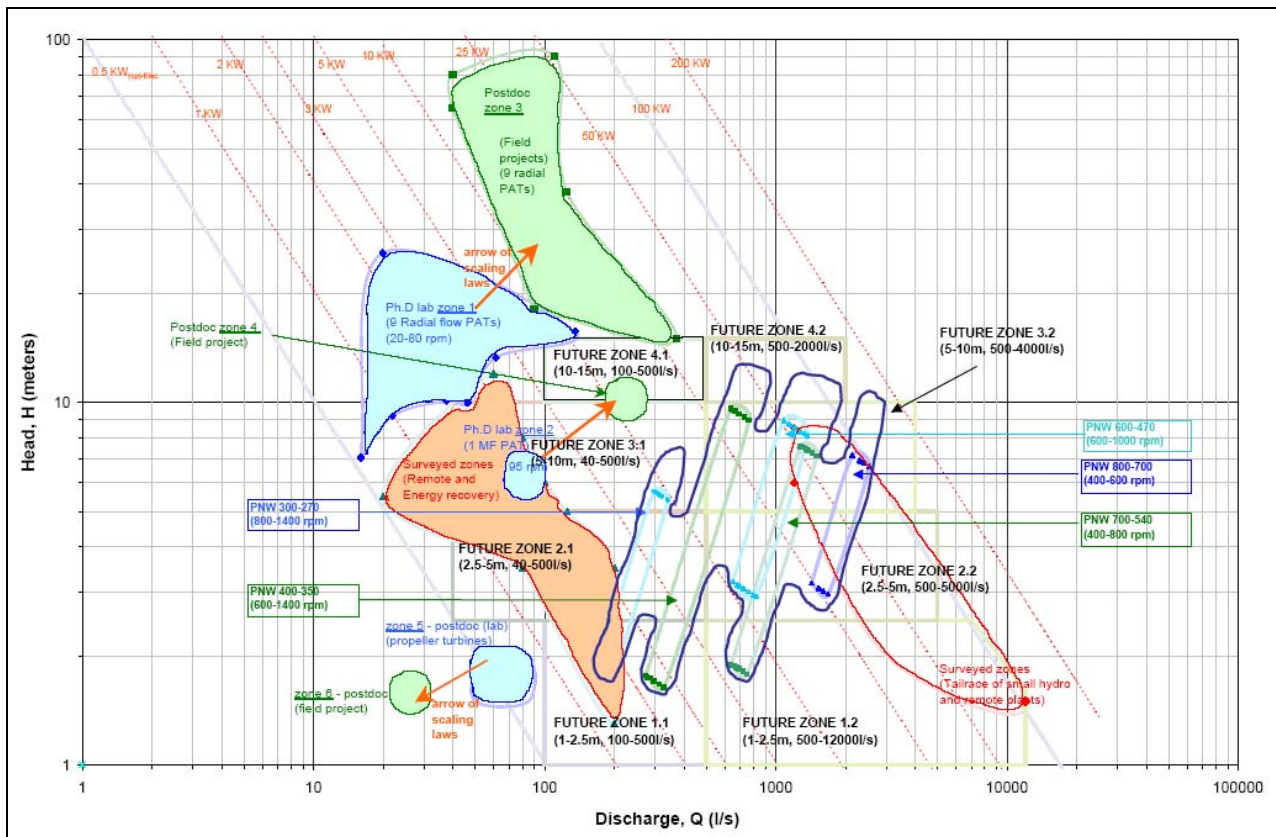


Fig. 6, The spread of the turbine characteristics of Axial flow pumps [2]

It has to be emphasized that these are predicted characteristics based on a very preliminary model and will be subjected to issues of accuracy and uncertainty. Further, this model has not given consideration to the shape of the blades, which will be dealt in the following section (section 4).

4. Effects of Blade Shapes on the Prediction Model

As mentioned in section 1, the authors in [4] and [5] have shown that the shape of the blade plays a very significant role for both the turbine and pump performances respectively. With the help of their theoretical model, they showed that backward shaped blades would result in a negative performance especially in the turbine mode. The turbine operating point for such backward blades would be characteristically positioned in the energy dissipation zone, which would make the turbine a net consumer of shaft power rather than a generator. The shape of the backward blade and its turbine operating point is illustrated in Fig. 7 and Fig. 8 respectively.

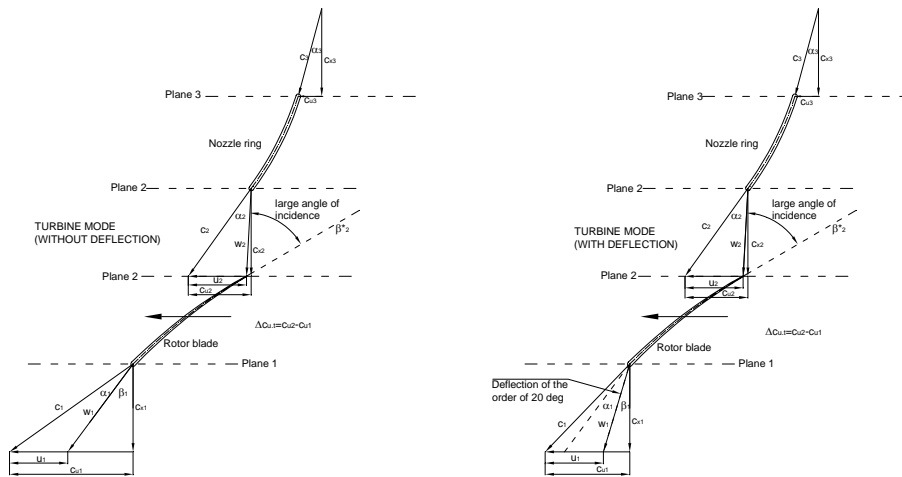


Fig. 7, A backward shaped axial flow pump blade in turbine mode [5]

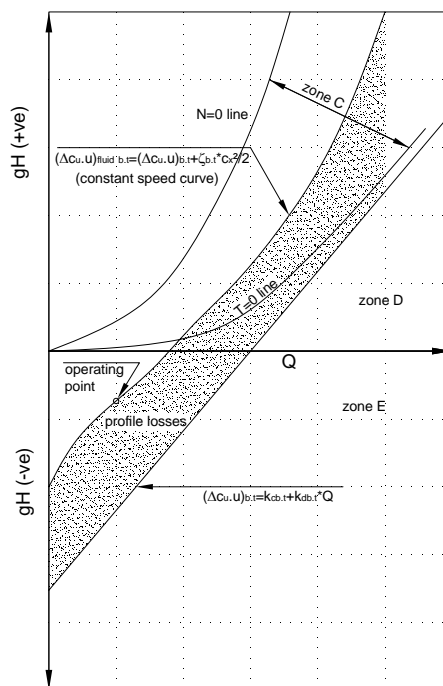


Fig. 8, Probable turbine operating point of the backward shaped pump blade [5]

The study in [4] and [5] however found that forward shaped blades would be more suitable for turbine operation, which is illustrated in Fig. 9 and Fig. 10 respectively.

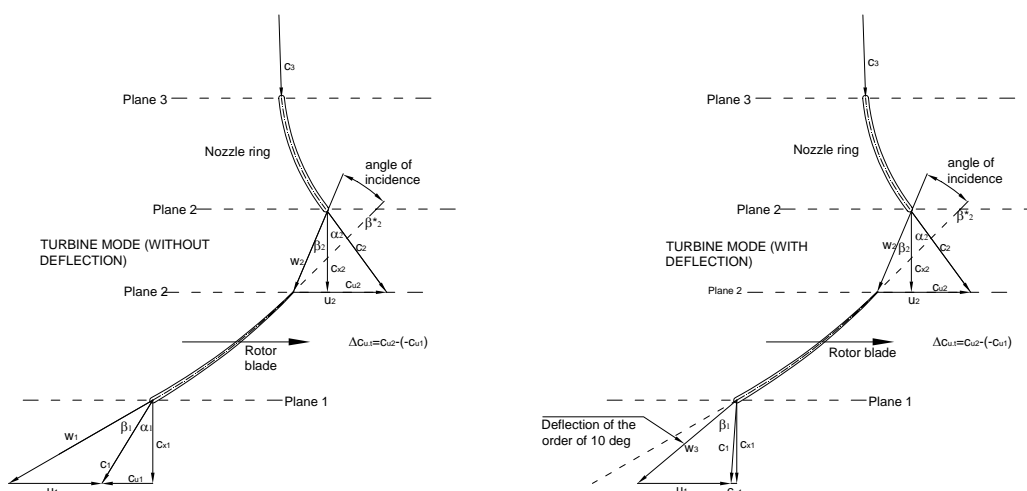


Fig. 9, A forward shaped axial flow pump blade in turbine mode [4]

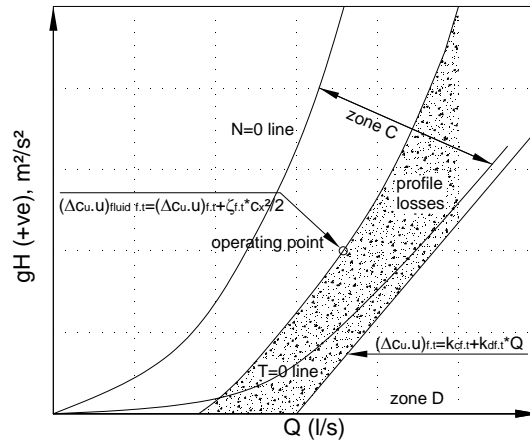


Fig. 10, Probable turbine operating point of the forward shaped pump blade [4]

It is not sure the impellers of the present series of axial flow pumps [2] are forward or backward shaped, though there are indications that they could have a backward shaped blade as gathered from information in [2]. Based on the above hypothesis, the shape is definitely going to have a bearing on the turbine characteristics and this would have to be taken into consideration for the prediction model proposed in section 2.

However, it has to be also pointed out that in spite of the complex mixture of turbine shapes in the Cordier line in section 2 (radial flow, mixed flow and axial flow machines), they found some kind of adherence at least at the best efficiency operating zone. Hence, it would be hard to believe that backward and forward shaped axial blades would have totally divergent characteristics as explained in [4] and [5].

Another aspect to be considered, which could argue well with the findings of the authors in [4] and [5] is that both the propellers and Kaplan turbines used in the model have a forward shaped impeller. The only way to evaluate this interesting behaviour of backward and forward blades is to make a thorough review of the geometry of the currently investigated axial flow pumps and carryout detailed experimental study in turbine mode to get more clarity.

5. Conclusions and Recommendations

The proposal made for the prediction model for axial flow pumps as turbines in this study report has used experimental from very diverse shapes of turbines. On one hand the model considered categories of regular turbines and unconventional pumps as turbines for the 'best efficiency point' predictions and on the other hand it preferred only axial flow propeller turbines for the determination of the no-load operating zone. This approach or preferential selection in a model for different operating zones is debatable and the accuracy of such modeling laws would be obviously questionable. Unfortunately, no test or published data for axial flow pumps operating were available for any kind of investigation to be carried out in the context of model accuracy. This proposed model will need to go through a thorough calibration process through an experimental study and computational simulations to arrive at a robust consolidated model.

The application of this raw prediction model on a series of axial flow pumps showed that these pumps could cover a decent range of unsolved turbine zones in the range of 2 to 9 meters and flow in the range of 200 to 2500 l/s. If the expected accuracy would lie in the zone of $\pm 15\%$ to $\pm 25\%$, it would yet be a encouraging and significant result for finding turbine solutions in the low head and large flow range.

However, there still remains a catch in the model. Despite its simplicity and parsimony features, it still can't clearly determine the influence of forward or backward blade shapes in axial flow pumps. The considerations for blade shapes assumes significance and importance because many axial flow pump manufacturers use backward vanes in their axial flow pump designs, which is reported to have negative impact on the turbine operation.

For both the development of a consolidated robust model and evaluation of blade shape effects, there would be a need for a detailed experimental study. The only recommendation this study can make at this stage is to design a testrig for the smallest series of pumps (DN300-270 range that cover a good range of specific speeds at all blade positions) and carryout elaborate tests in turbine mode. The results will serve a basis of a new prediction model, though the procedures for the determination of the Cordier line, specific speed line and no-load zone will remain intact as entailed in this preliminary model.

The present model should be used for only trial and reference purposes and not for actual project implementation until a consolidated model is not developed.

6. References

- [1] P. Singh, F. Nestmann, Research Report on the Preliminary Development Stage of the Prediction Model for Mixed Flow Pumps as Turbines, Internal Technical Report, IWG, KIT, March 2010.
- [2] KSB Catalogues, 'Performance characteristics of PNW Series pumps', KSB AG, Frankenthal, Germany, 2010.
- [3] P. Singh, F. Nestmann, An optimization routine on a prediction and selection model for the turbine operation of centrifugal pumps, J. Experimental Thermal and Fluid Science 34, 152-164, 2010.
- [4] Punit Singh, Franz Nestmann, Axial flow impeller shapes: Part 1, World Pumps (Elsevier), Vol. 2011, Issue 2, 2011.
- [5] Punit Singh, Franz Nestmann, Axial flow impeller shapes: Part 2, World Pumps (Elsevier), Vol. 2011, Issue 3, 2011.
- [6] Punit Singh, Franz Nestmann, Experimental Optimization of a Free Vortex Propeller Runner for Micro Hydro Application, J. Experimental Thermal and Fluid Science, 33, 991-1002, 2009.
- [7] Punit Singh, Franz Nestmann, Low Head Propeller Turbine Research-Detailed Test Report, IWG, KIT, 2007.
- [8] Voith Hydro, Operating points of field based Kaplan Pit Turbines, Voith Hydraulics Laboratory, Heidenheim, 2010

Nomenclature

Full Scripts

c	absolute velocity, m/s
D	Runner diameter, mm or m
g	acceleration due to gravity, m/s ²
H	head parameter, m
k	constants of the Euler line
n	Speed, rps
N _q	Specific Speed, $NQ^{1/2}/H^{3/4}$ (N in rpm, H in m, Q in m ³ /s)
Q	discharge, l/s or m ³ /s
R	Random error
u	tangential blade velocity, m/s
w	relative velocity, m/s

Greek symbols

α	absolute flow angle, degrees
β	relative flow angle, degrees
σ	Turbine specific speed, (in A3, Eq. (A3))
ϕ	Discharge number, Q/nD^3 (Q in 'm ³ /s', n in 'rps', D in 'm')
η	Efficiency, %
ψ	Head number, gH/n^2D^2 (gH in m ² /s ² , n in 'rps', D in 'm')
Δ	Turbine Specific diameter, (in A3, Eq. (A4))
ζ	pressure loss coefficient

Subscripts

*	blade direction
1	outer diameter reference
2	inner diameter reference
c	Cordier definition
m	mean
nl	no-load
b.p	backward pump impeller
b.t	backward turbine impeller
f.p	forward pump impeller
f.t	forward turbine impeller
p	pump mode
t	turbine mode
u	tangential direction
x	axial direction

Abbreviations

PAT	Pump as Turbine	MF	Mixed Flow	AF	Axial Flow
BEP	Best Efficiency Point	NLP	No Load Point		

Appendix

A1 Conversion Equations used in the Prediction Model

(A1) Head number, $\psi_c = \frac{2gH}{u^2} = \frac{2}{\pi^2} \frac{gH}{n^2 D^2} = \frac{2}{\pi^2} \psi$	(A2) Discharge number, $\phi_c = \frac{4Q}{\pi D^2 u} = \frac{4}{\pi^2} \frac{Q}{n D^3} = \frac{4}{\pi^2} \phi$
(A3) Turbine Specific speed, $\sigma = \frac{\phi_c^{1/2}}{\psi_c^{3/4}} = 2^{1/4} \pi^{1/2} \frac{\phi_t^{1/2}}{\psi_t^{3/4}}$	(A4) Specific diameter, $\Delta = \frac{\psi_c^{1/4}}{\phi_c^{1/2}} = \frac{\pi^{1/2}}{2^{3/4}} \frac{\psi_t^{1/4}}{\phi_t^{1/2}}$
(A5) The relationship between the Cordier σ and N_q (SI) is given by, $\sigma = \frac{2^{1/4} \pi^{1/2}}{g^{3/4} 60} \frac{NQ^{1/2}}{H^{3/4}} = 6.3383 \times 10^{-3} N_{qt}$	

A2 Tabulations for the development of prediction model

A2.1 Data for the Axial Flow Cordier PAT Line (Fig. 1)

Sr. No.	Turbine Type	N_{qp} (rpm)	Best Efficiency Point				
			ϕ_b	ψ_t	N_{qt} (rpm)	σ	Δ
1	Radial flow pump	33.4	0.165	7.468	29.9	0.190	4.283
2		35.3	0.151	7.640	28.1	0.178	4.509
3		36.4	0.185	8.000	30.1	0.191	4.121
4		37.6	0.224	8.400	31.9	0.202	3.791
5		39.4	0.200	6.700	35.7	0.226	3.791
6		45.2	0.235	6.180	41.1	0.261	3.428
7		46.4	0.275	7.600	38.1	0.241	3.337
8		55.6	0.323	6.300	47.5	0.301	2.938
9		61.3	0.414	5.748	57.6	0.365	2.537
10		79.1	0.480	4.900	70.0	0.443	2.263
11	Mixed Flow pump	94.4	0.515	4.522	76.9	0.488	2.143
12		72.8	0.446	6.451	54.9	0.348	2.515
1	Low head propeller turbine	-	2.304	3.390	202.0	1.281	0.942
2		-	1.911	4.186	157.1	0.996	1.090
3		-	2.410	4.186	176.4	1.118	0.971
4		-	2.703	4.186	186.8	1.184	0.917
5		-	1.724	3.870	158.2	1.003	1.126
6		-	2.063	3.870	173.1	1.097	1.029
7		-	2.181	4.186	167.8	1.064	1.021
8		-	2.085	3.870	174.0	1.103	1.024
9		-	2.060	3.870	173.0	1.097	1.030
10		-	2.185	4.186	168.0	1.065	1.020
11		-	1.721	3.198	182.4	1.156	1.074
12		-	2.079	3.870	173.8	1.101	1.025
13		-	1.781	3.870	160.9	1.020	1.108
14		-	1.812	3.870	162.2	1.028	1.098
1	Large specific speed Kaplan turbines	-	2.812	1.693	375.8	2.382	0.717
2		-	3.114	2.028	345.3	2.189	0.713
3		-	3.119	2.072	340.1	2.155	0.716
4		-	2.844	1.909	345.3	2.189	0.735
5		-	3.153	2.192	327.8	2.078	0.722
6		-	3.009	2.121	328.2	2.080	0.733
7		-	2.713	2.352	288.4	1.828	0.792
8		-	2.455	2.430	267.7	1.697	0.840
9		-	2.259	2.503	251.2	1.592	0.882
10		-	1.951	2.514	232.6	1.474	0.950

A2.2 Data for the no-load modeling laws (section 2.2)

Sr. No.	Turbine Type	N_{qt}	σ_t	ϕ_{nl}	ψ_{nl}
1	Low head propeller turbines	158.2	1.003	1.365	1.322
2		173.1	1.097	1.630	1.163
3		167.8	1.064	1.666	1.558
4		174.0	1.103	1.630	1.305
5		173.0	1.097	1.630	1.163
6		168.0	1.065	1.666	1.558
7		182.4	1.156	1.372	1.092
8		173.8	1.101	1.630	1.305
9		160.9	1.020	1.408	0.984
10		162.2	1.028	1.391	0.901

A3 Muschel Family and Individual Curves

A3.1 300-270 series

A3.1.1 Summary of the operating points

Sr. No	Pump geometry and pump mode data												Turbine mode data after application of model								
	α	d/D	D ₁	D ₂	D _m	N	Q	H	ψ_p	ϕ_p	N _{qp}	η_p	N _{qt}	σ	Δ_m	ψ_t/ψ_p	ϕ_t/ϕ_p	ψ_t	ϕ_t	ψ_{nl}	ϕ_{nl}
1	9	0.35	270	94.5	182.3	1450	175	3.2	1.62	1.20	254	76.5	207	1.31	0.964	1.91	1.76	3.083	2.100	1.483	1.781
2	11	0.35	270	94.5	182.3	1450	193	3.3	1.67	1.32	260	78.0	213	1.35	0.945	1.82	1.64	3.044	2.169	1.520	1.815
3	13	0.35	270	94.5	182.3	1450	212	3.4	1.72	1.45	267	79.0	218	1.38	0.928	1.75	1.54	3.008	2.236	1.556	1.848
4	15	0.35	270	94.5	182.3	1450	228	3.6	1.82	1.56	265	79.0	216	1.37	0.933	1.66	1.42	3.017	2.218	1.547	1.839
5	17	0.35	270	94.5	182.3	1450	250	3.5	1.77	1.71	283	79.0	231	1.47	0.887	1.65	1.41	2.919	2.411	1.650	1.932
6	19	0.35	270	94.5	182.3	1450	262	4.0	2.02	1.79	262	79.0	214	1.36	0.939	1.50	1.22	3.031	2.192	1.533	1.826
7	21	0.35	270	94.5	182.3	1450	278	4.0	2.02	1.90	270	79.0	221	1.40	0.919	1.48	1.20	2.987	2.274	1.577	1.866
8	23	0.35	270	94.5	182.3	1450	295	4.3	2.17	2.02	264	79.0	215	1.37	0.936	1.39	1.09	3.024	2.206	1.540	1.833

A3.1.2 Muschel family curve

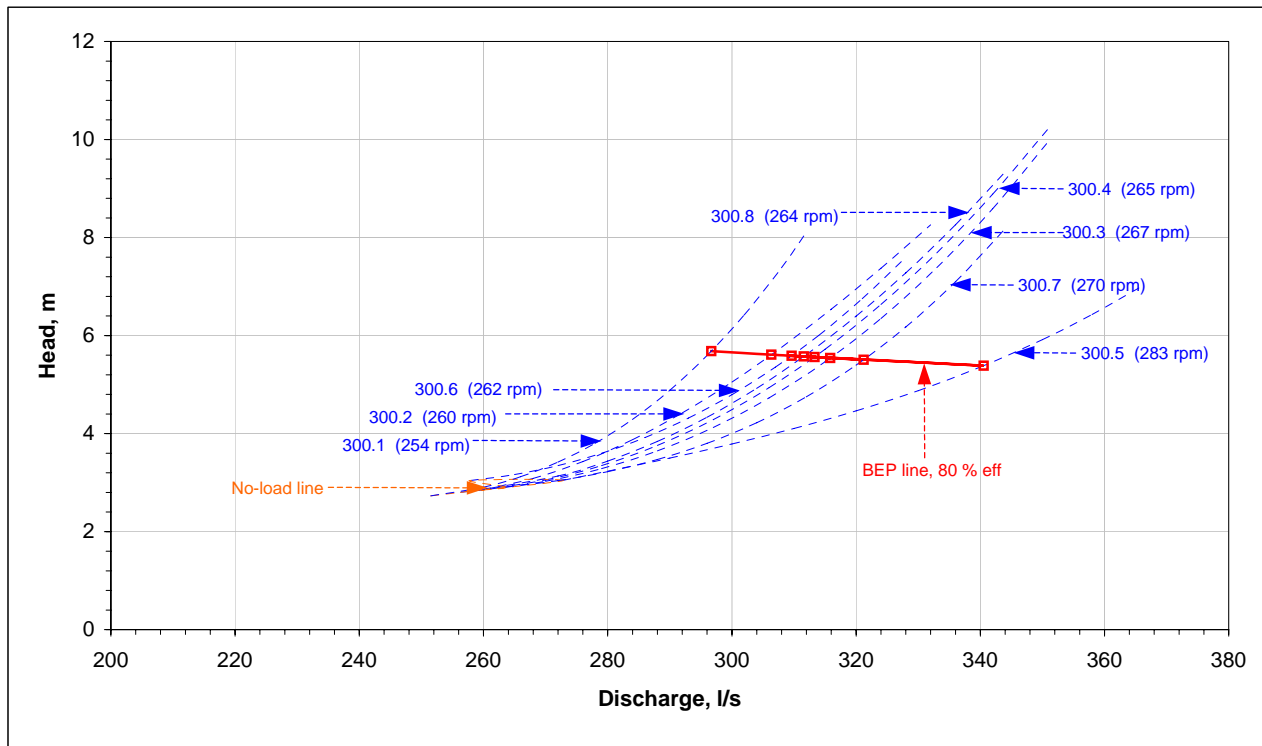


Fig. A3.1, Muschel family curves for 300-370 AF PAT at 1400 rpm

A3.1.3 Muschel individual curves

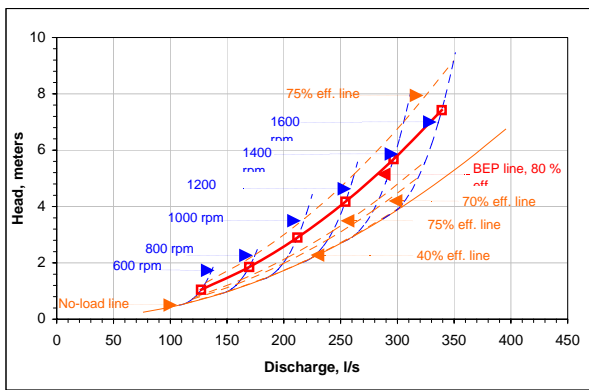


Fig. A3.2, 300-270 (9) (254 rpm)

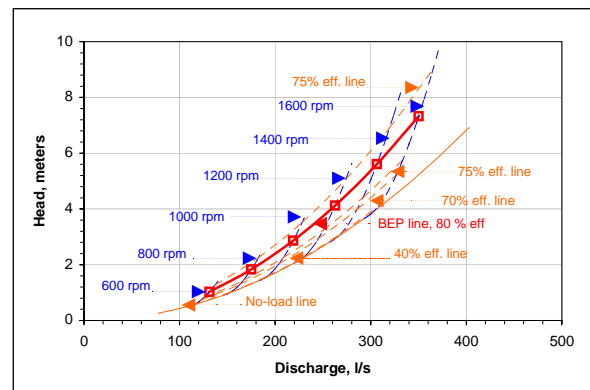


Fig. A3.3, 300-270 (11) (260 rpm)

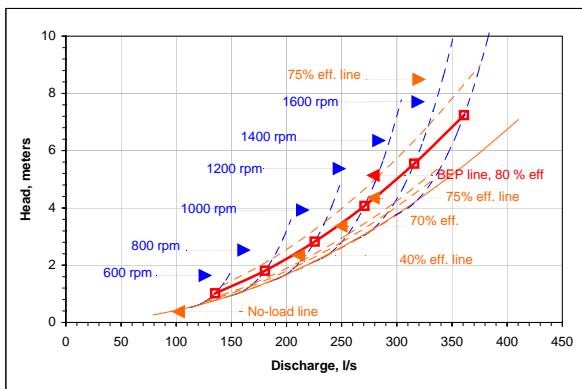


Fig. A3.4, 300-270 (13) (267 rpm)

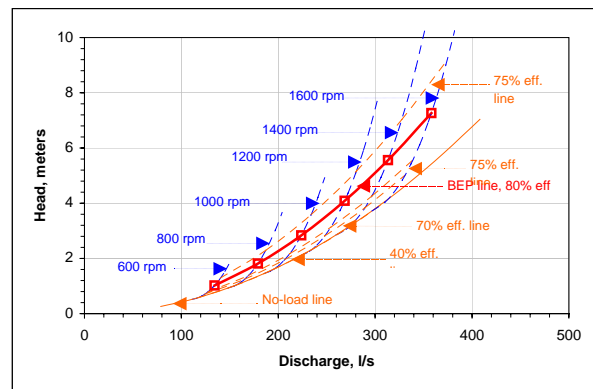


Fig. A3.5, 300-270 (15) (265 rpm)

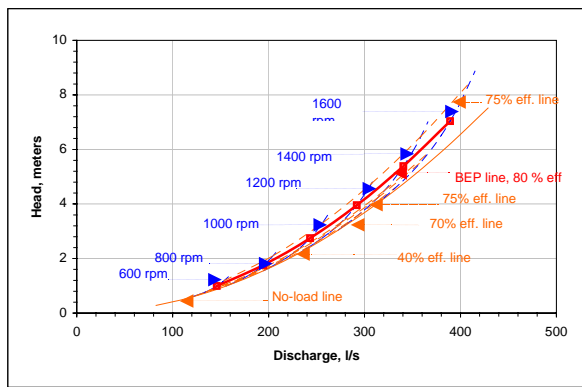


Fig. A3.6, 300-270 (17) (283 rpm)

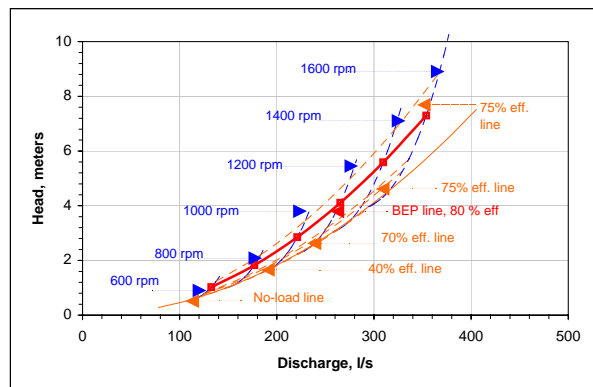


Fig. A3.7, 300-270 (19) (262 rpm)

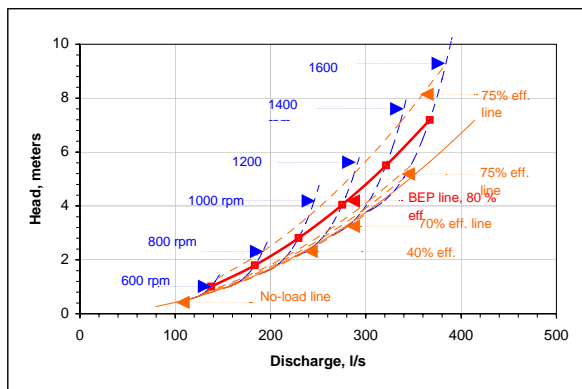


Fig. A3.8, 300-270 (21) (270 rpm)

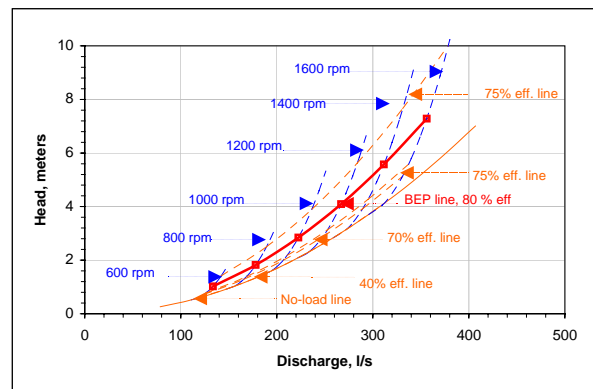


Fig. A3.9, 300-270 (21) (264 rpm)

A3.2 400-350 series

A3.2.1 Summary of the operating points

Sr. No	Pump geometry and pump mode data												Turbine mode data after application of model								
	α	d/D	D ₁	D ₂	D _m	N	Q	H	ψ_p	ϕ_p	N _{qp}	η_p	N _{qt}	σ	Δ_m	ψ_r/ψ_p	ϕ_r/ϕ_p	ψ_t	ϕ_t	ψ_{nl}	ϕ_{nl}
1	9	0.35	350	122.5	236.3	960	260	2.2	1.48	1.23	276	79	225	1.43	0.905	2.00	1.89	2.959	2.331	1.607	1.893
2	11	0.35	350	122.5	236.3	960	270	2.3	1.58	1.28	267	79	218	1.38	0.927	1.90	1.75	3.005	2.241	1.559	1.850
3	13	0.35	350	122.5	236.3	960	280	2.4	1.61	1.33	268	80	219	1.39	0.926	1.86	1.69	3.002	2.246	1.562	1.853
4	15	0.35	350	122.5	236.3	960	312	2.8	1.89	1.48	251	80	205	1.30	0.971	1.64	1.40	3.098	2.076	1.469	1.768
5	17	0.35	350	122.5	236.3	960	340	2.8	1.89	1.61	262	81	214	1.36	0.940	1.61	1.36	3.033	2.189	1.531	1.825
6	19	0.35	350	122.5	236.3	960	370	2.8	1.89	1.75	273	81	223	1.41	0.911	1.57	1.32	2.970	2.307	1.595	1.882
7	21	0.35	350	122.5	236.3	960	390	2.9	1.96	1.85	273	80	223	1.41	0.911	1.52	1.25	2.971	2.306	1.594	1.881
8	23	0.35	350	122.5	236.3	960	408	3.0	2.06	1.93	269	80	220	1.39	0.922	1.45	1.17	2.995	2.261	1.570	1.860

A3.2.2 Muschel family curve

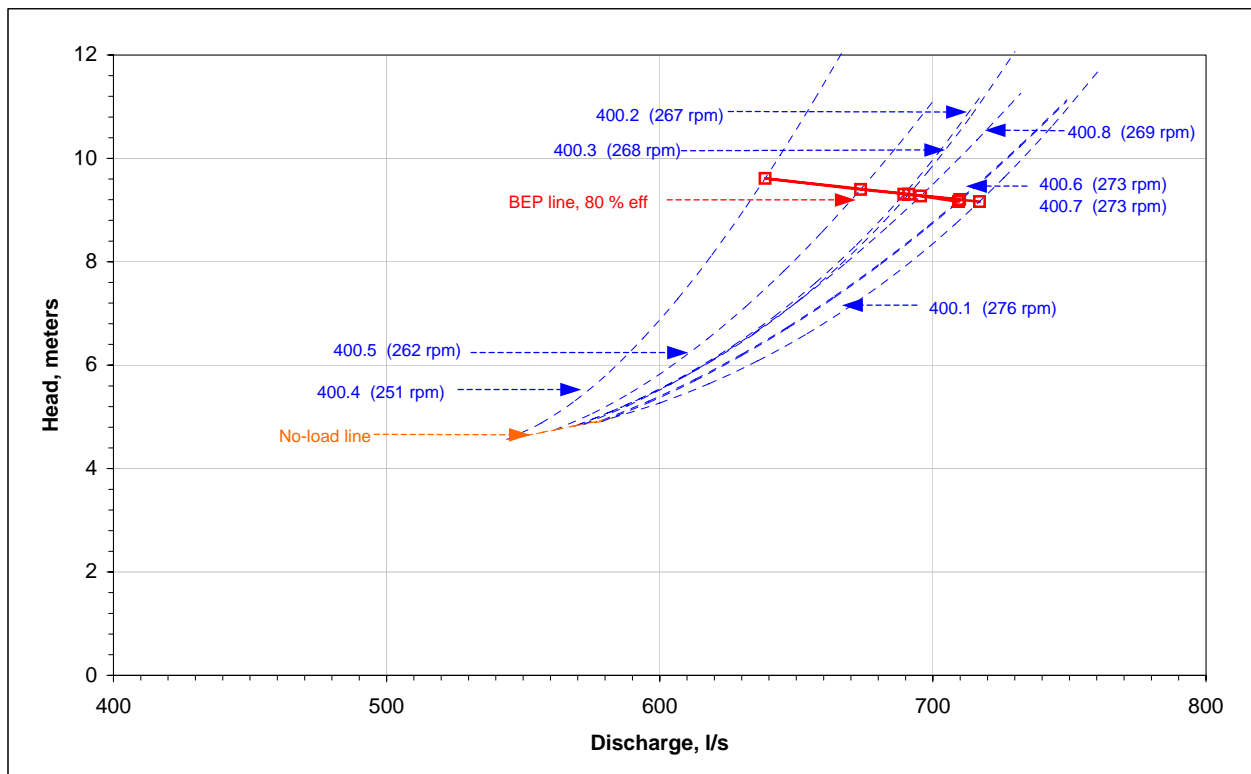


Fig. A3.10, Muschel family curves for 400-350 AF PAT at 1400 rpm

A3.2.3 Muschel individual curves

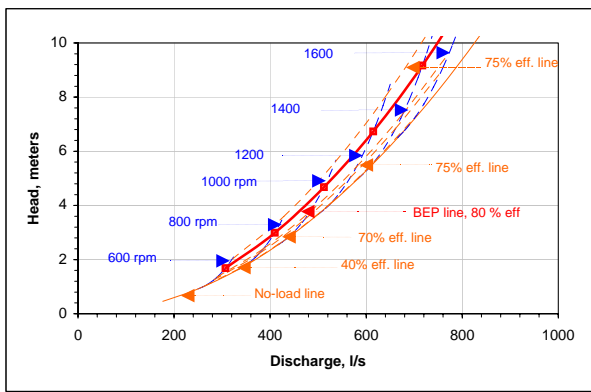


Fig. A3.11, 400-350 (9) (276 rpm)

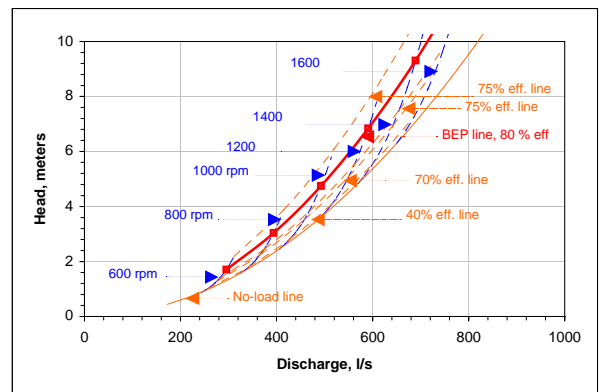


Fig. A3.12, 400-350 (11) (267 rpm)

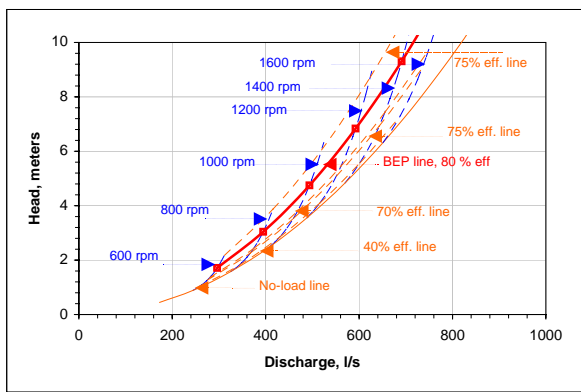


Fig. A3.13, 400-350 (13) (268 rpm)

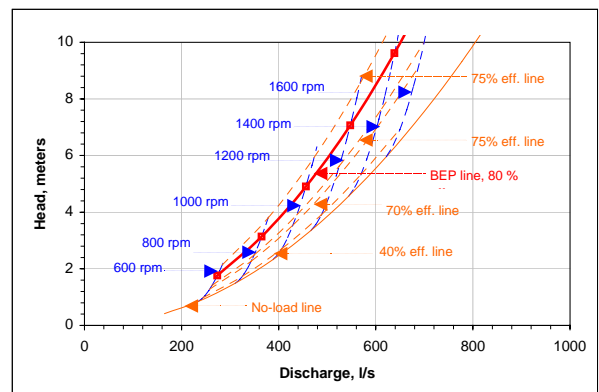


Fig. A3.14, 400-350 (15) (251 rpm)

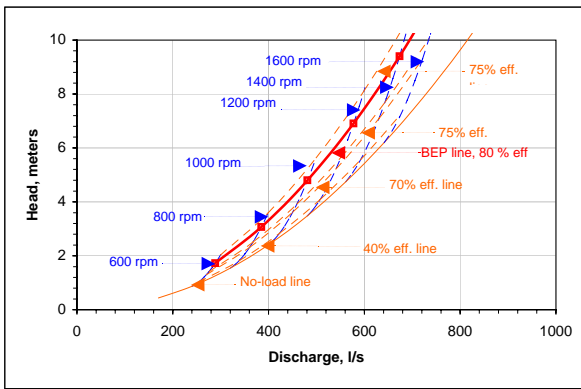


Fig. A3.15, 400-350 (17) (262 rpm)

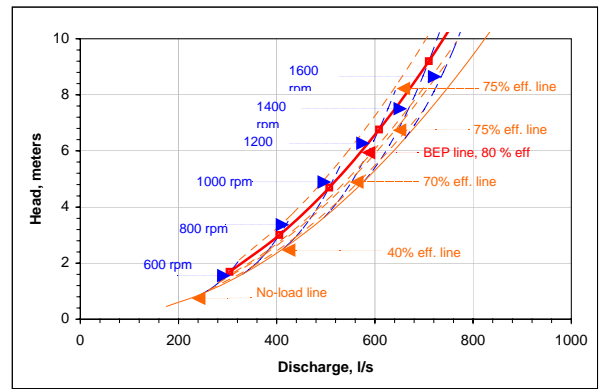


Fig. A3.16, 400-350 (19) (273 rpm)

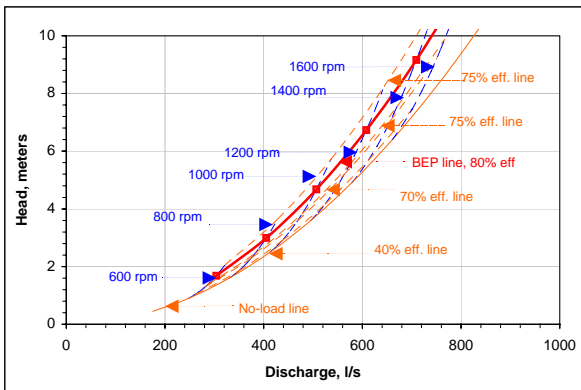


Fig. A3.17, 400-350 (21) (273 rpm)

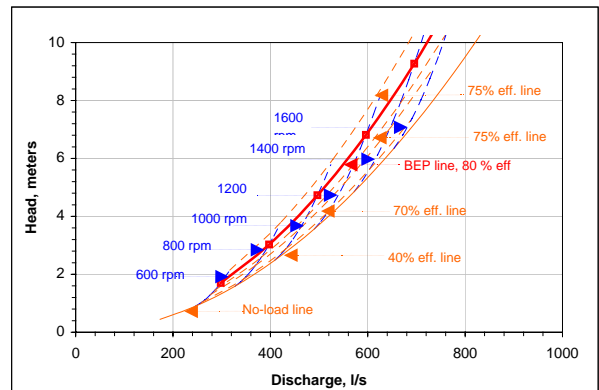


Fig. A3.18, 400-350 (23) (269 rpm)

A3.3 500-350 series

A3.3.1 Summary of the operating points

Sr. No	Pump geometry and pump mode data											Turbine mode data after application of model									
	α	d/D	D ₁	D ₂	D _m	N	Q	H	ψ_p	ϕ_p	N _{qp}	η_p	N _{qt}	σ	Δ_m	ψ_s/ψ_p	ϕ_s/ϕ_p	ψ_t	ϕ_t	ψ_{nl}	ϕ_{nl}
1	9	0.35	350	122.5	236.3	1450	375	5.4	1.63	1.18	251	80	205	1.30	0.972	1.91	1.76	3.100	2.071	1.466	1.766
2	11	0.35	350	122.5	236.3	1450	412	5.5	1.66	1.29	259	80	212	1.34	0.948	1.84	1.67	3.050	2.158	1.514	1.810
3	13	0.35	350	122.5	236.3	1450	450	6.0	1.81	1.41	254	81	207	1.31	0.963	1.71	1.49	3.082	2.102	1.484	1.782
4	15	0.35	350	122.5	236.3	1450	500	6.0	1.81	1.57	267	81	218	1.38	0.926	1.66	1.43	3.003	2.244	1.561	1.852
5	17	0.35	350	122.5	236.3	1450	545	6.0	1.81	1.71	279	81	228	1.44	0.897	1.63	1.38	2.940	2.368	1.627	1.911
6	19	0.35	350	122.5	236.3	1450	587	6.0	1.81	1.84	290	80	236	1.50	0.872	1.60	1.35	2.887	2.479	1.686	1.964
7	21	0.35	350	122.5	236.3	1450	620	6.2	1.87	1.95	291	80	237	1.50	0.871	1.55	1.28	2.883	2.488	1.691	1.968

A3.3.2 Muschel family curve

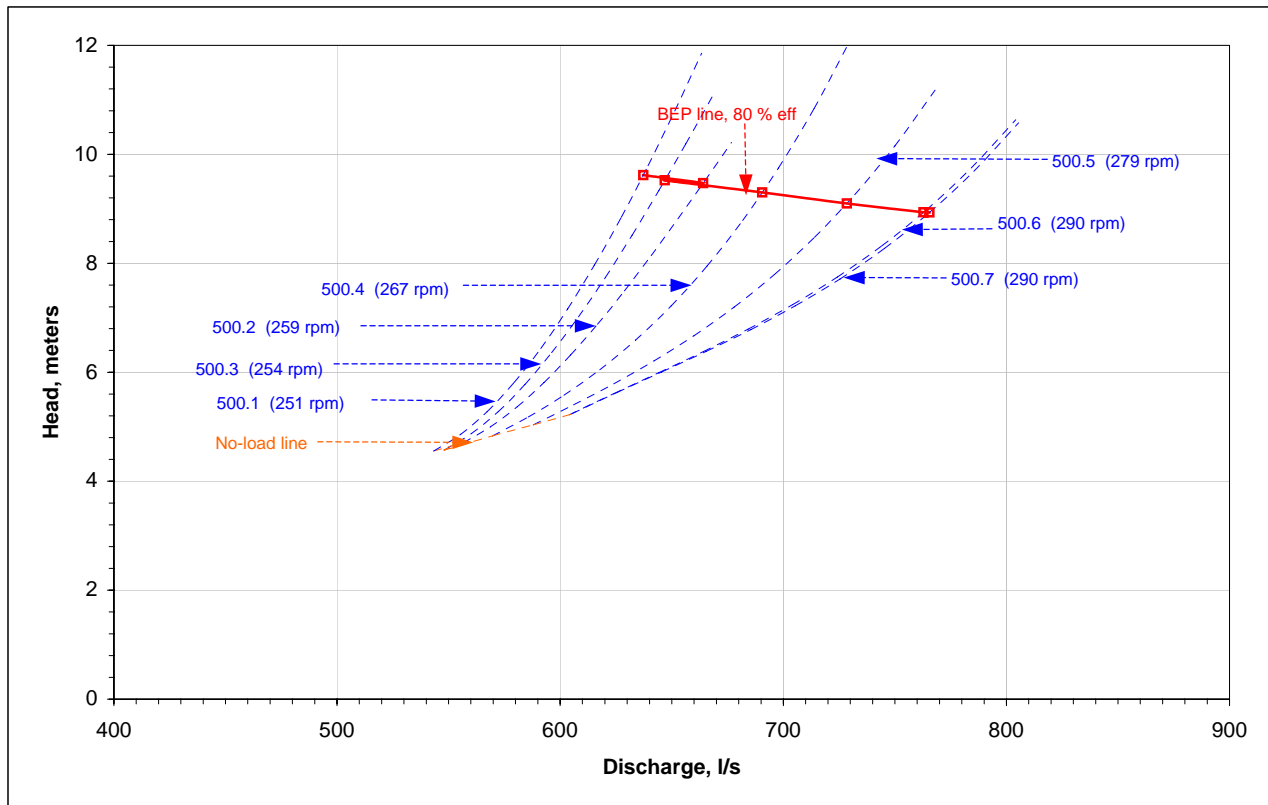


Fig. A3.19, Muschel family curves for 500-350 AF PAT at 1400 rpm

A3.3.3 Muschel individual curves

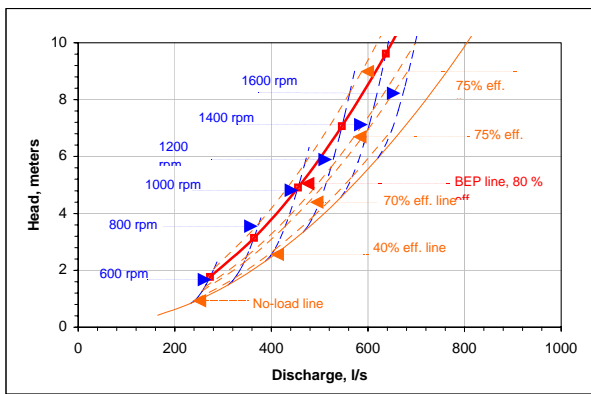


Fig. A3.20, 500-350 (9) (251 rpm)

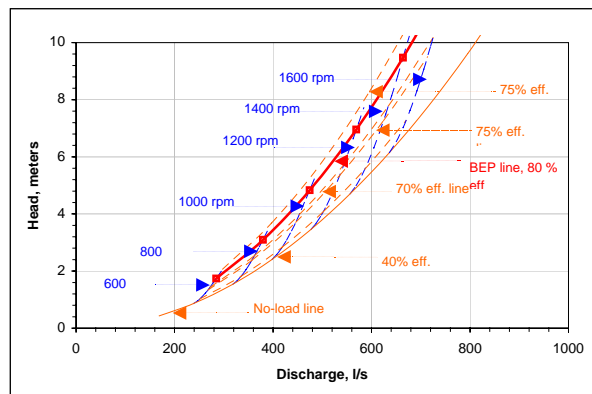


Fig. A3.21, 500-350 (11) (259 rpm)

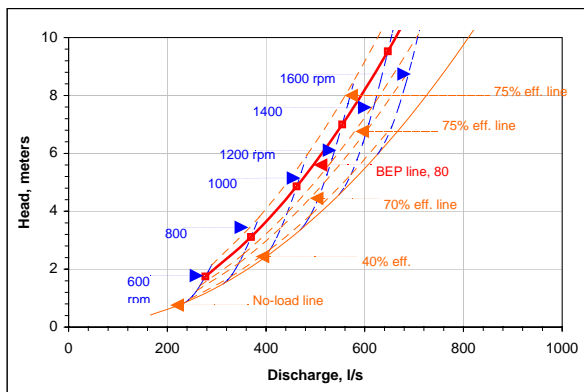


Fig. A3.22, 500-350 (13) (254 rpm)

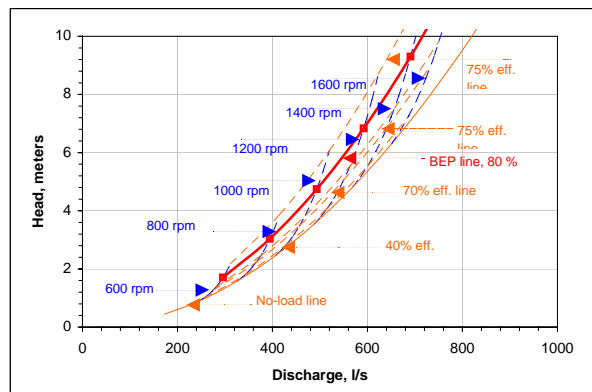


Fig. A3.23, 500-350 (15) (267 rpm)

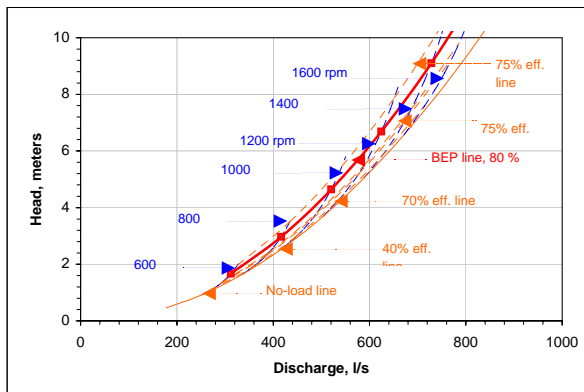


Fig. A3.24, 500-350 (17) (279 rpm)

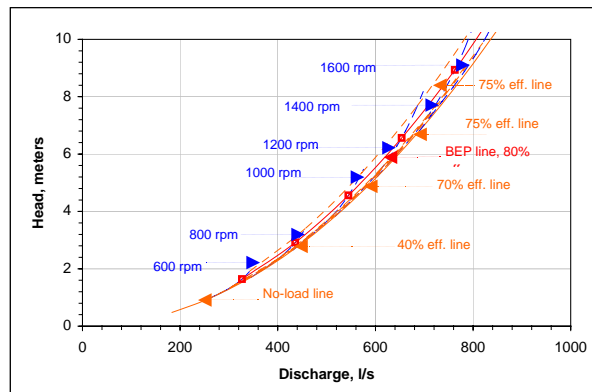


Fig. A3.25, 500-350 (19) (290 rpm)

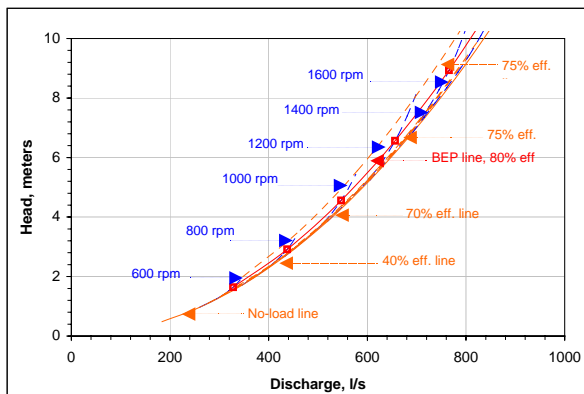


Fig. A3.26, 500-350 (21) (291 rpm)

A3.4 600-470 series

A3.4.1 Summary of the operating points

Sr. No	Pump geometry and pump mode data											Turbine mode data after application of model									
	α	d/D	D ₁	D ₂	D _m	N	Q	H	ψ_p	ϕ_p	N _{qp}	η_p	N _{qt}	σ	Δ_m	ψ_s/ψ_p	ϕ_s/ϕ_p	ψ_t	ϕ_t	ψ_{nl}	ϕ_{nl}
1	9	0.35	470	164.5	317.3	960	625	4.3	1.62	1.22	256	81	209	1.33	0.956	1.89	1.74	3.066	2.130	1.499	1.796
2	11	0.35	470	164.5	317.3	960	675	4.7	1.79	1.32	247	82	202	1.28	0.982	1.74	1.54	3.122	2.034	1.446	1.748
3	13	0.35	470	164.5	317.3	960	750	4.7	1.79	1.47	260	82	213	1.35	0.944	1.70	1.48	3.043	2.172	1.522	1.816
4	15	0.35	470	164.5	317.3	960	825	4.8	1.81	1.61	271	83	221	1.40	0.917	1.65	1.41	2.984	2.282	1.581	1.870
5	17	0.35	470	164.5	317.3	960	885	5.0	1.90	1.73	270	83	221	1.40	0.919	1.57	1.31	2.989	2.272	1.576	1.865
6	19	0.35	470	164.5	317.3	960	960	5.0	1.90	1.88	281	83	230	1.46	0.892	1.54	1.27	2.929	2.390	1.639	1.922
7	21	0.35	470	164.5	317.3	960	1030	5.0	1.90	2.02	291	82	238	1.51	0.869	1.51	1.24	2.879	2.496	1.695	1.972
8	23	0.35	470	164.5	317.3	960	1080	5.0	1.90	2.11	298	82	243	1.54	0.854	1.49	1.22	2.846	2.571	1.734	2.006

A3.4.2 Muschel family curve

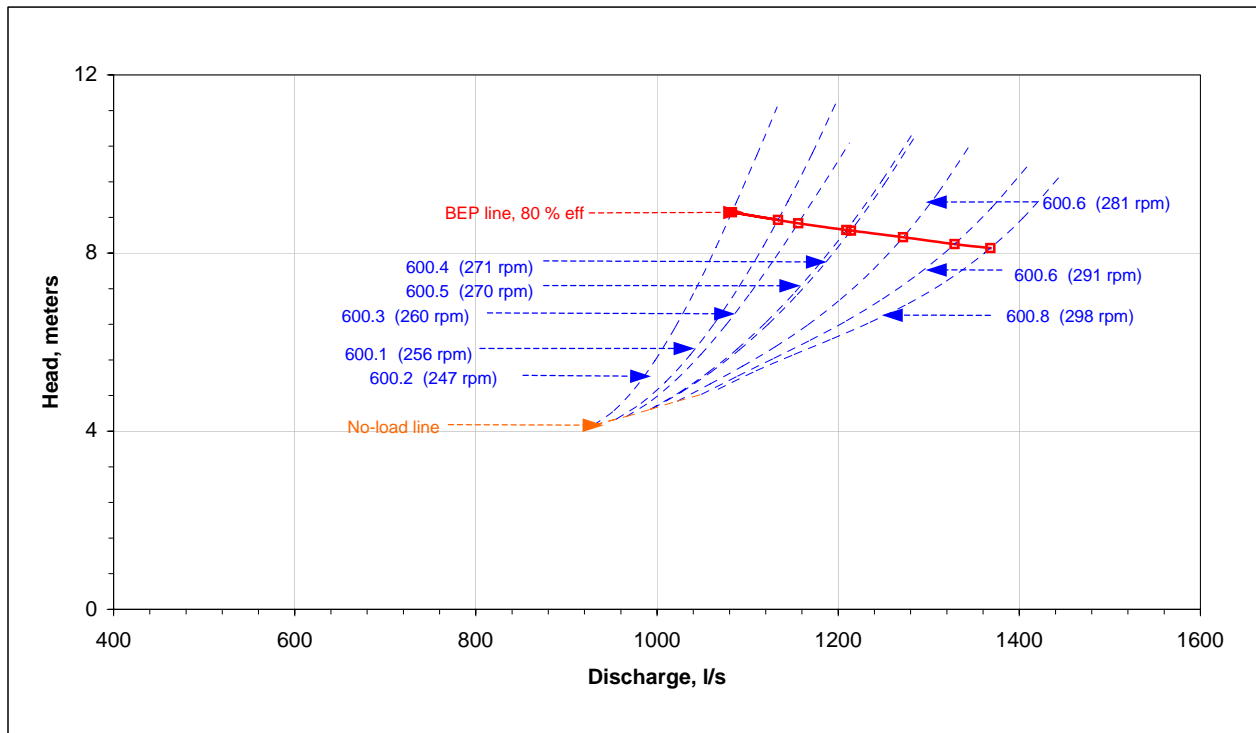


Fig. A3.27, Muschel family curves for 600-470 AF PAT at 1000 rpm

A3.4.3 Muschel individual curves

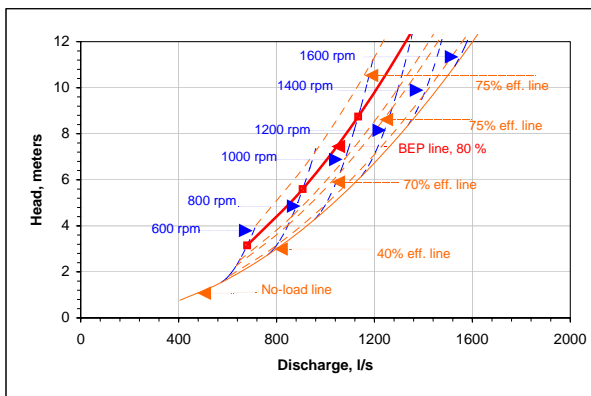


Fig. A3.28, 600-470 (9) (256 rpm)

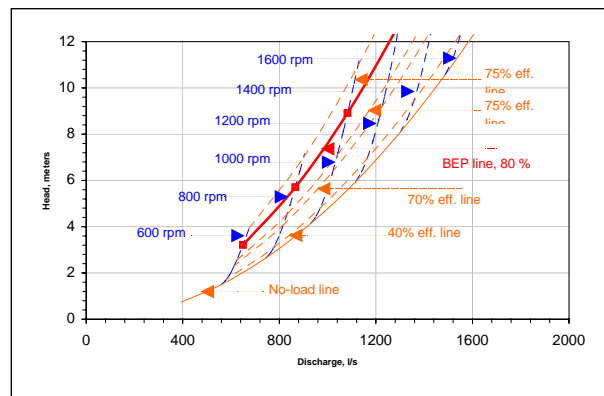


Fig. A3.29, 600-470 (11) (247 rpm)

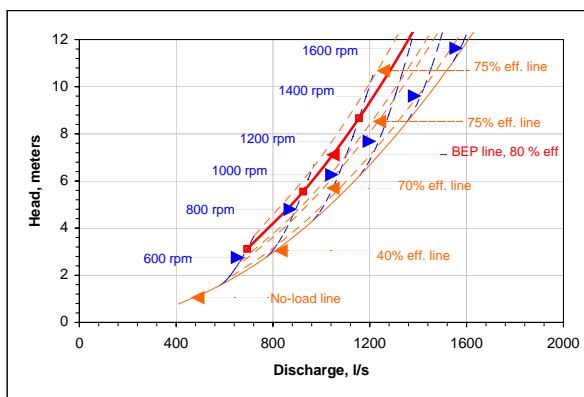


Fig. A3.30, 600-470 (13) (260 rpm)

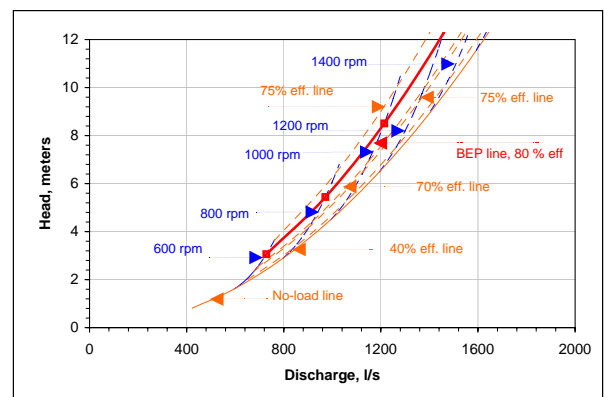


Fig. A3.31, 600-470 (15) (271 rpm)

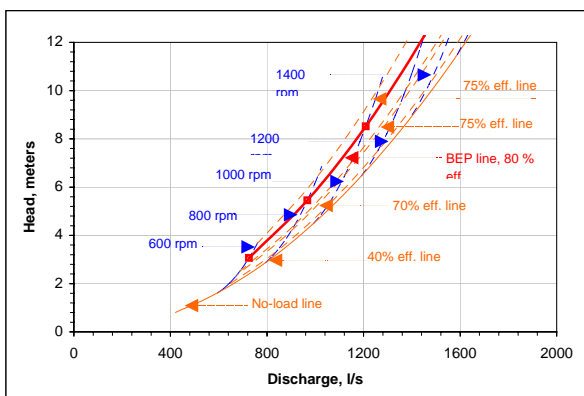


Fig. A3.32, 600-470 (17) (270 rpm)

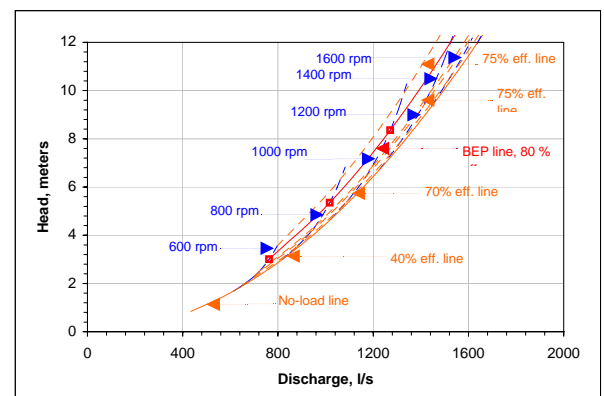


Fig. A3.33, 600-470 (19) (281 rpm)

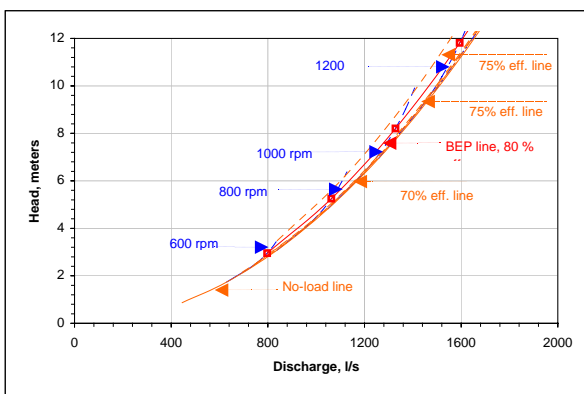


Fig. A3.34, 600-470 (21) (291 rpm)

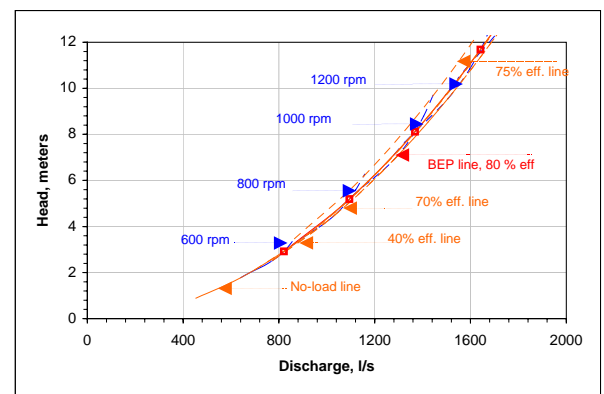


Fig. A3.35, 600-470 (23) (298 rpm)

A3.5 700-540 series

A3.5.1 Summary of the operating points

Sr. No	Pump geometry and pump mode data											Turbine mode data after application of model									
	α	d/D	D ₁	D ₂	D _m	N	Q	H	ψ_p	ϕ_p	N _{qp}	η_p	N _{qt}	σ	Δ_m	ψ_s/ψ_p	ϕ_s/ϕ_p	ψ_t	ϕ_t	ψ_{nl}	ϕ_{nl}
1	9	0.35	540	189	364.5	960	950	5.6	1.62	1.23	257	82	210	1.33	0.954	1.90	1.74	3.062	2.137	1.502	1.799
2	11	0.35	540	189	364.5	960	1030	6.2	1.79	1.33	248	82	203	1.28	0.980	1.74	1.54	3.117	2.043	1.451	1.752
3	13	0.35	540	189	364.5	960	1100	6.7	1.93	1.42	242	83	198	1.25	0.998	1.63	1.40	3.156	1.980	1.416	1.720
4	15	0.35	540	189	364.5	960	1220	6.8	1.96	1.57	252	83	206	1.30	0.968	1.58	1.32	3.093	2.083	1.473	1.772
5	17	0.35	540	189	364.5	960	1320	7.0	2.02	1.70	256	84	209	1.33	0.956	1.52	1.25	3.067	2.129	1.498	1.795
6	19	0.35	540	189	364.5	960	1420	7.0	2.02	1.83	266	83	217	1.38	0.930	1.49	1.22	3.012	2.228	1.552	1.844
7	21	0.35	540	189	364.5	960	1520	7.0	2.02	1.96	275	83	225	1.42	0.907	1.47	1.18	2.962	2.324	1.603	1.890

A3.5.2 Muschel family curve

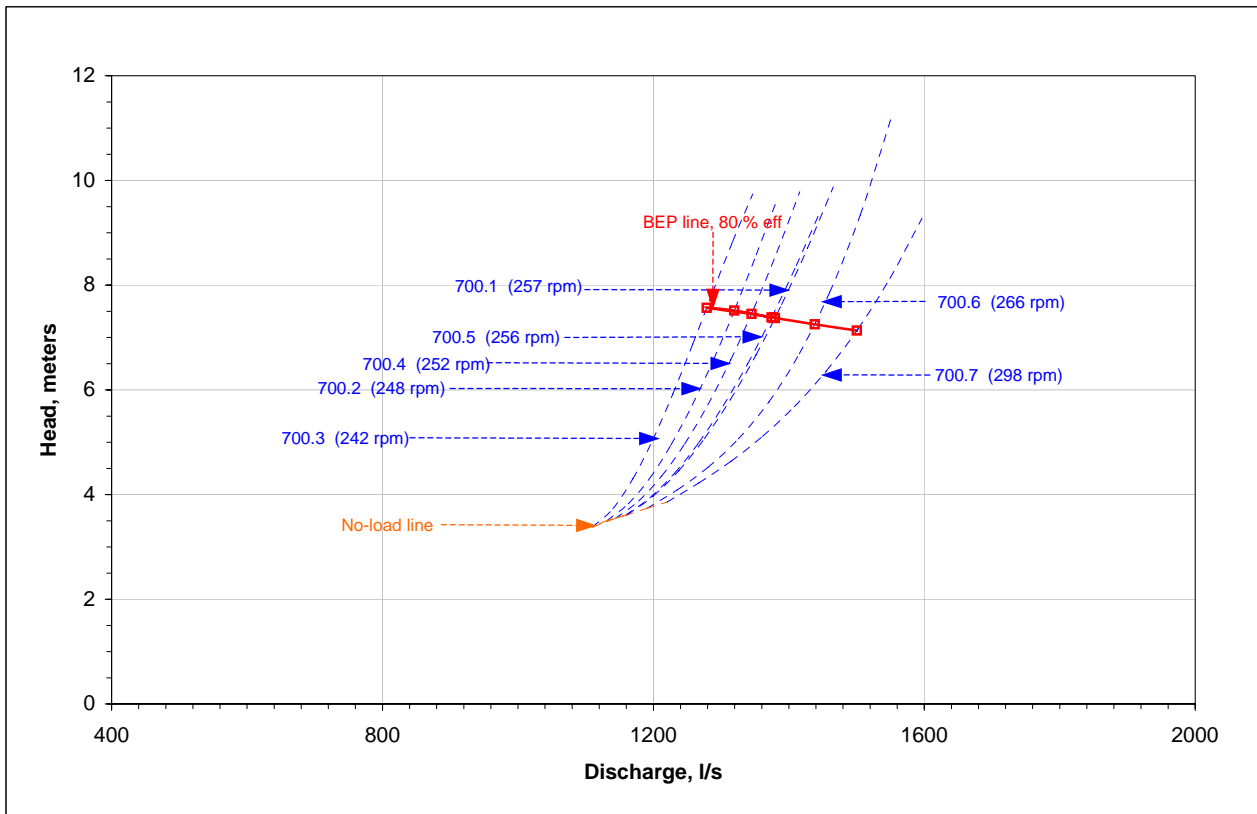


Fig. A3.36, Muschel family curves for 700-540 AF PAT at 800 rpm

A3.5.3 Muschel individual curves

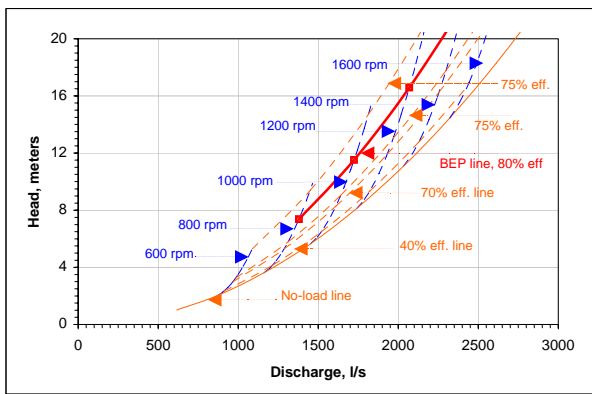


Fig. A3.37, 700-540 (9) (257 rpm)

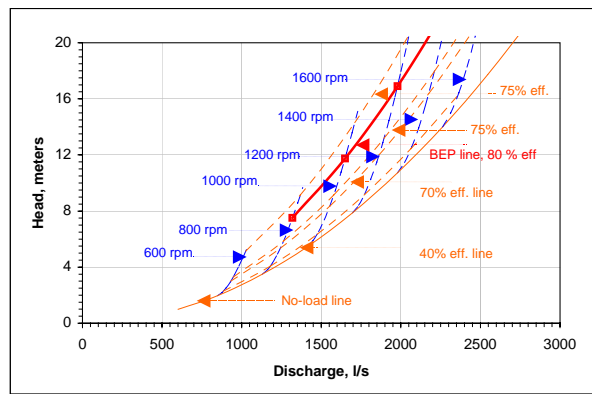


Fig. A3.38, 700-540 (11) (248 rpm)

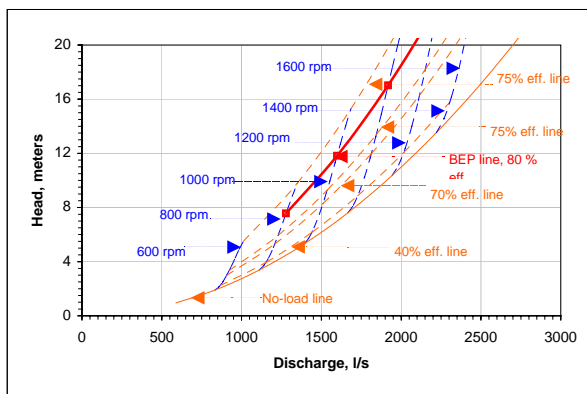


Fig. A3.39, 700-540 (13) (242 rpm)

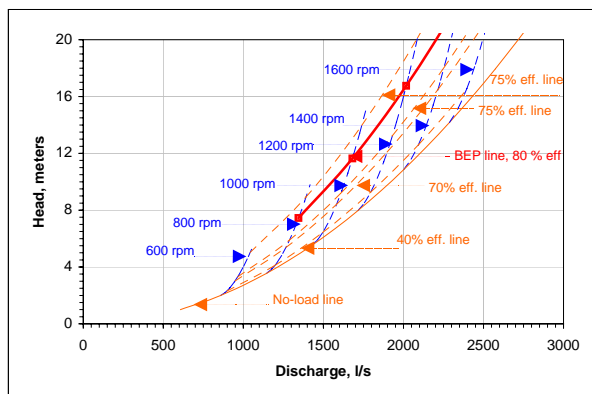


Fig. A3.40, 700-540 (15) (252 rpm)

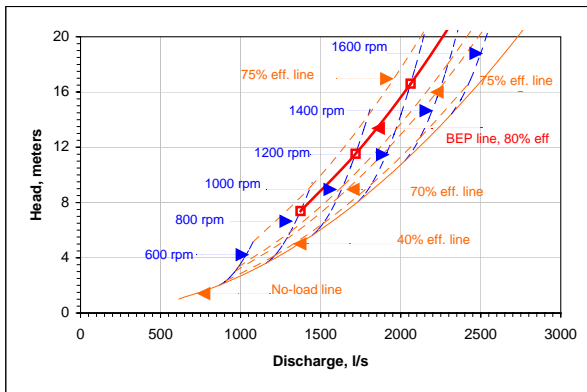


Fig. A3.41, 700-540 (17) (256 rpm)

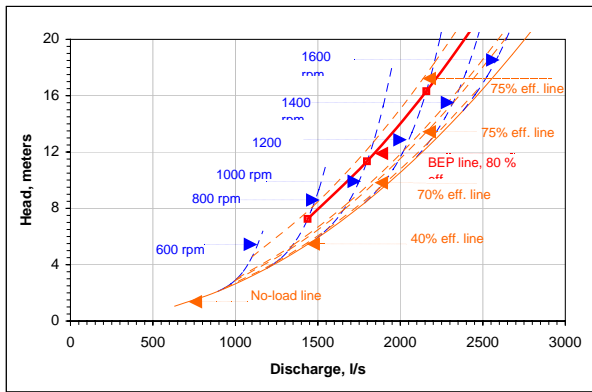


Fig. A3.42, 700-540 (19) (266 rpm)

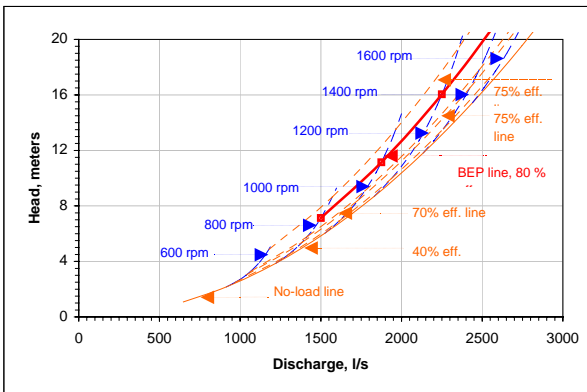


Fig. A3.43, 700-540 (21) (275 rpm)

A3.6 800-700 series

A3.6.1 Summary of the operating points

Sr. No	Pump geometry and pump mode data											Turbine mode data after application of model									
	α	d/D	D ₁	D ₂	D _m	N	Q	H	ψ_p	ϕ_p	N _{qp}	η_p	N _{qt}	σ	Δ_m	ψ_s/ψ_p	ϕ_s/ϕ_p	ψ_t	ϕ_t	ψ_{nl}	ϕ_{nl}
1	9	0.35	700	245	472.5	725	1530	5.6	1.69	1.20	246	83	201	1.28	0.984	1.86	1.69	3.127	2.027	1.442	1.744
2	11	0.35	700	245	472.5	725	1760	5.6	1.69	1.38	264	83	216	1.37	0.934	1.79	1.60	3.021	2.211	1.543	1.835
3	13	0.35	700	245	472.5	725	1830	5.8	1.75	1.44	262	84	214	1.36	0.939	1.74	1.53	3.031	2.192	1.533	1.826
4	15	0.35	700	245	472.5	725	2000	6.2	1.87	1.57	261	84	213	1.35	0.943	1.63	1.39	3.040	2.177	1.524	1.819
5	17	0.35	700	245	472.5	725	2150	6.5	1.96	1.69	261	84	213	1.35	0.943	1.55	1.29	3.039	2.179	1.525	1.820
6	19	0.35	700	245	472.5	725	2320	6.5	1.96	1.82	271	85	221	1.40	0.916	1.52	1.26	2.982	2.284	1.582	1.871
7	21	0.35	700	245	472.5	725	2500	6.5	1.96	1.96	282	84	230	1.46	0.891	1.50	1.22	2.928	2.393	1.640	1.923

A3.6.2 Muschel family curve

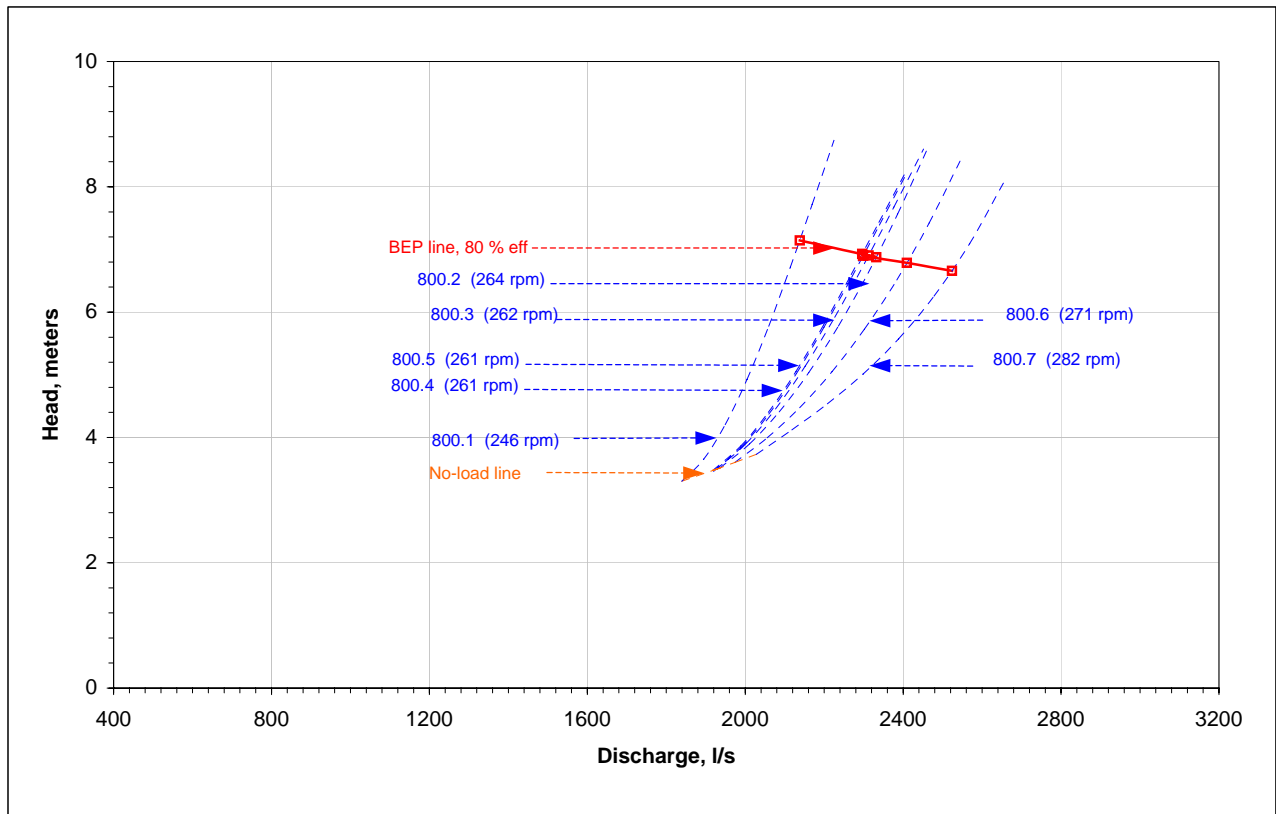


Fig. A3.44, Muschel family curves for 800-700 AF PAT at 600 rpm

A3.6.3 Muschel individual curves

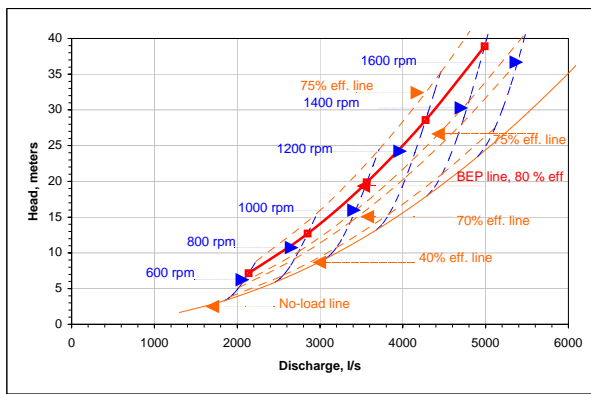


Fig. A3.45, 800-700 (9) (246 rpm)

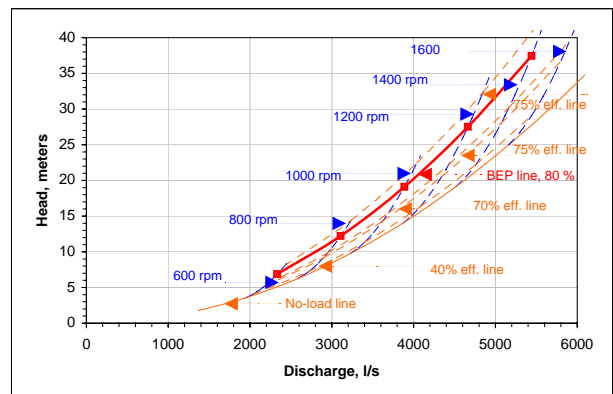


Fig. A3.46, 800-700 (11) (264 rpm)

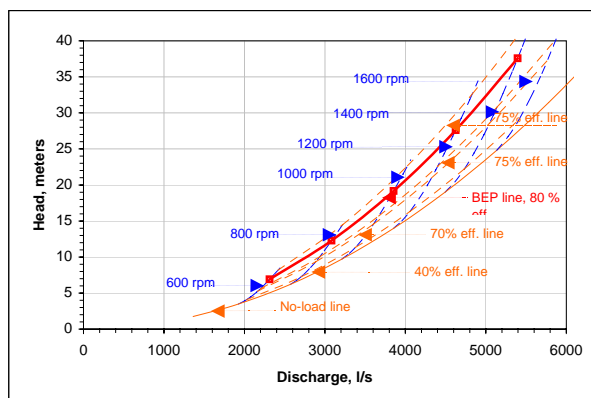


Fig. A3.47, 800-700 (13) (262 rpm)

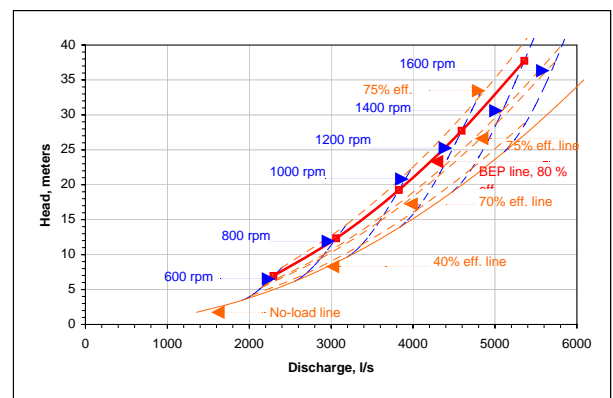


Fig. A3.48, 800-700 (15) (261 rpm)

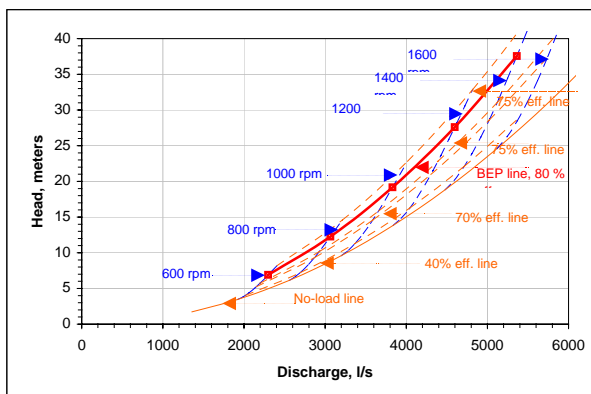


Fig. A3.49, 800-700 (17) (261 rpm)

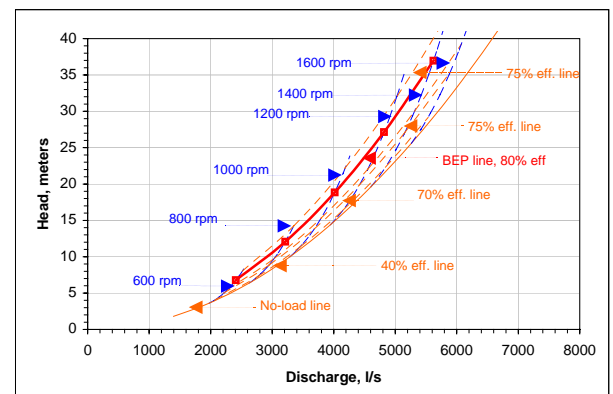


Fig. A3.50, 800-700 (19) (271 rpm)

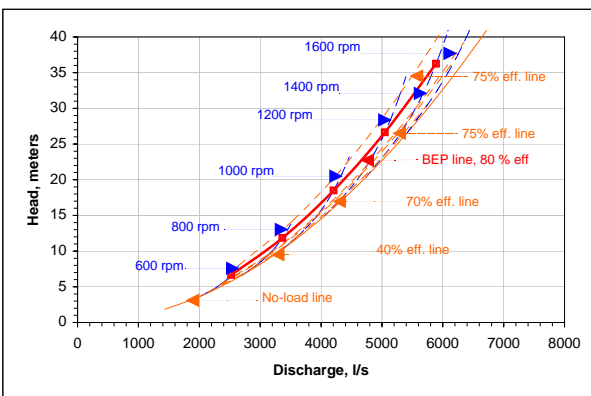
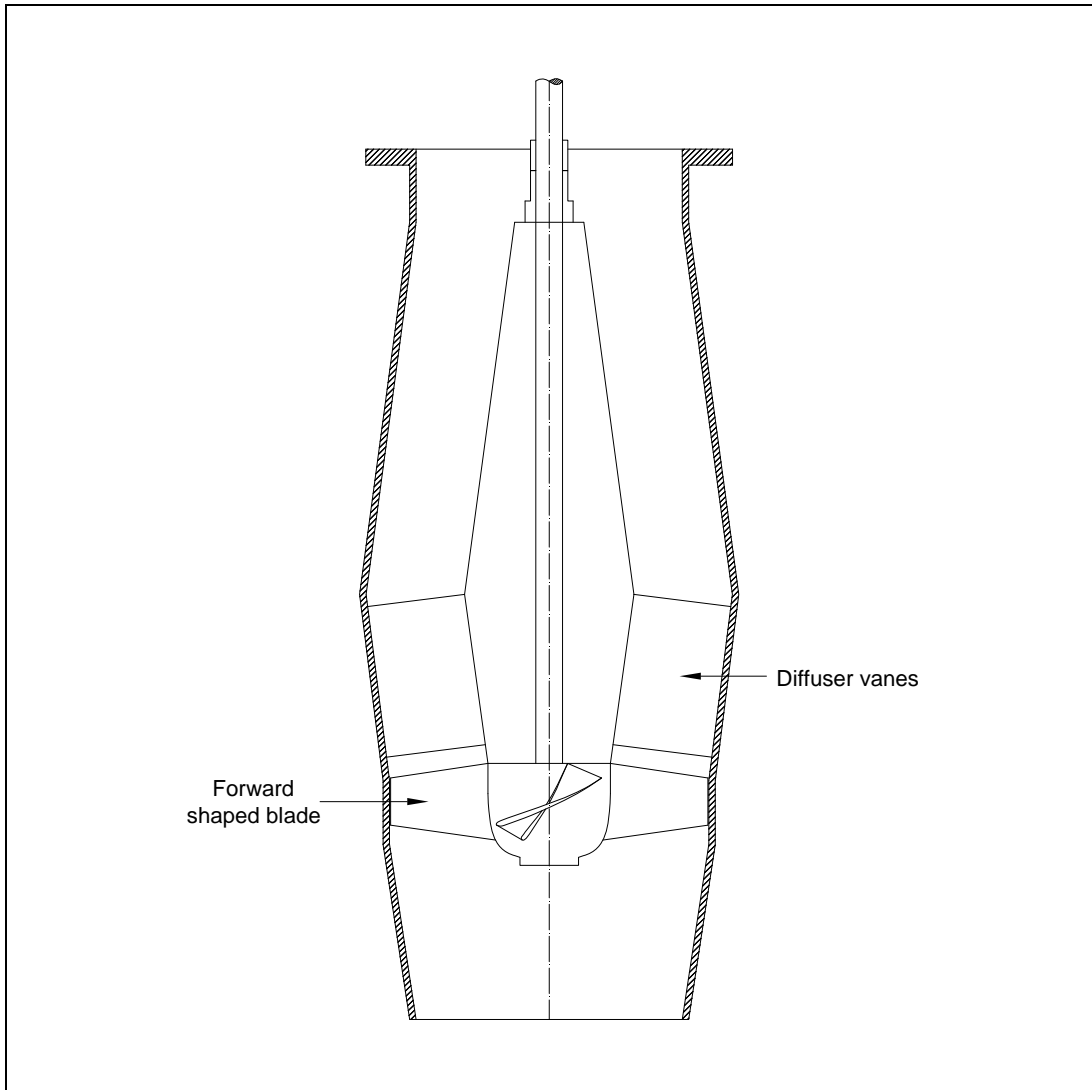


Fig. A3.51, 800-700 (21) (282 rpm)

**Critical Review of a
Prediction Model for Axial Flow Pumps as Turbines and
A Proposal to Optimize the Model**



**Dr. Punit Singh
Divecha Center for Climate Change,
Indian Institute of Science, Bangalore**

May 2011

Table of Contents

Abstract	3
1. Introduction and Objectives	3
2. Special Case of Backward Pump Impellers – Negative $\Delta c_{u,u}$	3
3. Forward Shaped Impellers Positive – $\Delta c_{u,u}$	4
4. Critical Analysis of the Axial Flow Model [1]	5
4.1 The Conversion of pump shape to turbine shape	5
4.2 Validity of Cordier PAT Line for forward and backward shape impellers	6
4.3 Translation of Δ and σ errors on ϕ and ψ values	7
5. Roadmap for the development of shape specific prediction model	7
5.1 Theoretical workout	7
5.2 Experimental investigation	7
6. Conclusions and Recommendations	8
7. References	8
Nomenclature	9
Abbreviations	9
Appendix	9
A1 Conversion Equations used in the Prediction Model	9

Abstract

This paper is aimed to carefully investigate the fundamentals of a proposed prediction model for the turbine operation of axial flow pumps and make specific proposals to amend the model in order to reach the acceptable level of accuracy of $\pm 2\%$ on the head and discharge scales.

The study has particularly focused on how to differentiate the blade shape factor while analyzing the turbine performance and develop independent modeling equations for forward and backward blade shapes respectively. Using experimentally tested data for radial flow and mixed flow pumps as turbines, it has shown that the theoretical approach of assessing the performance of backward shape blades was flawed in which the rotational momentum was stated to be negative instead of being positive.

The paper also found that there could be significant errors introduced in the overall predictions by adopting a generalized modeling law for a wide range of blade shapes that was being recommended by the existing model. It was also seen that the two step model involving the prediction of turbine specific speed and turbine specific diameter respectively cannot make errors beyond $\pm 0.5\%$ in order to keep the prediction errors of the turbine mode head and flow within $\pm 2\%$ range.

The paper also proposes a methodology that comprises of a theoretical workout on the geometries of existing pump designs and the existing prediction model, both backed by elaborate experimental investigations to developed two independent models that will be more sensitive to the shape factor and bring down the uncertainties to the acceptable limits.

The paper concludes with an immediate recommendation of associating with reliable pump manufacturers and to initiate the data acquisition of diverse pump shapes.

1. Introduction and Objectives

The preliminary prediction model [1] for axial flow pumps as turbines developed from the recommendations of the detailed study of axial flow impellers in both pump and turbine operations ([2] and [3]) had left several open topics to be discussed and investigated carefully before making the model usable.

Firstly, the model was based on multiple geometries of turbine shapes and secondly, it could not differentiate between forward shape and backward shape pump impellers while predicting the turbine performance. It was also not clear as to which of the modeling equations (specific speed relation of the Cordier Line) would need to be modified in order to incorporate the change in the blade shape.

The importance of developing a separate prediction models for the two blade shapes arise due to the fact that manufacturers have preferred both these shapes for varied pump applications ([2] and [3]). In particular, this study also gives a very pessimistic picture about the performance of backward shaped impellers in turbine mode. Further, it pointed out that the Euler rotational momentum of the fluid and the net head should be negative for the backward blade shapes and also warned that the turbine would tend to operate in the energy dissipation zone instead of the energy generation zone. Nevertheless, the study recommended that the research should be continued especially in investigating the effects of geometry (guide vane and blade curvature along with pitch effects) of such pumps that are available.

Hence, the objective of this paper will be to analyze the reasons for the generation of negative Euler momentum in backward vanes and confirm the validity of this behavior. Secondly, the paper will have to carefully introspect the various steps in the prediction model [1] and identify those steps (modeling equations) that would be directly influenced by the shape of the blade. It should also try to find out the relative contribution of these equations on the accuracy of prediction. Finally, the paper should provide a clear direction for evolving an optimized shape specific prediction model for axial flow pumps as turbines and also define the acceptable error limits for prediction.

2. Special Case of Backward Pump Impellers – Negative $\Delta c_{u,u}$

The study in [2] and [3] proved negative $\Delta c_{u,u}$ for backward impellers on the basis of velocity triangles that assumed that the turbine axial flow velocity would be 1.5 times that of the pump operation and that the fluid entry into the rotating impellers would be guided by the diffuser shape of the pump, which will now act as a nozzle. The exit condition of the fluid considered both deflection and no-deflection scenarios, however in both cases the net rotational momentum was found to be negative even though it became slightly positive (less negative) for the scenario with fluid deflection.

But, the analysis seems to have an internal flaw since the pump mode Euler momentum generated for this very blade shape was positive (exit fluid momentum $>$ inlet fluid momentum) and it cannot be possible for the turbine mode to give a negative momentum. One of the primary reasons for this is the fact that all pumps that operate as turbines have nearly comparable net momentums at the same conditions of speed at the best efficiency point. This result has been investigated by the author after surveying his own

performance data of radial flow [5] and mixed flow pumps [6] in both pump and turbine modes, which have been summarized in Table 1. There are some deviations in the two rotational momentums, which lie within the range of $\pm 10\%$ for most of the pumps. Hence, this assumption of equivalence of momentum can be held reasonably valid. The net head that composes of losses pump in the pump and turbine mode bring out the famous prediction ratios (turbine parameter to pump parameter) used by PAT scientists worldwide.

Table 1, Investigation of the constancy of pump and turbine $\Delta C_u \cdot u$ on radial flow and mixed flow PATs

Sr. No.	PAT (N_{qp})	ψ_p	η_p	$(\Delta C_u \cdot u)_p$	ψ_t	η_t	$(\Delta C_u \cdot u)_t$	%errors
1	35.3	4.75	0.79	6.0	7.64	0.81	6.2	+3%
2	36.4	4.65	0.74	6.3	8.00	0.73	5.8	-7%
3	39.4	4.79	0.81	5.9	6.70	0.83	5.6	-6%
4	45.2	4.41	0.81	5.4	6.18	0.80	4.9	-9%
5	46.4	4.84	0.77	6.3	7.60	0.75	5.7	-9%
6	61.3	3.94	0.76	5.2	5.75	0.77	4.4	-15%
7	79.1	3.55	0.83	4.3	4.90	0.79	3.9	-10%
8	72.8	2.58	0.81	3.2	4.52	0.80	3.6	+13%
9	94.4	4.22	0.82	5.1	6.45	0.81	5.2	+2%

This condition of numerical equality of rotational fluid momentums can be used in determining the actual velocity triangles for the backward shape impellers. It should be noted that the while determining the velocity triangle shapes using this condition the assumption of turbine axial velocity (proposed in [2]) is not required.

Figure 1 plots the velocity triangles using the constancy of rotational momentums and also assumes a small degree (20% to 40% inlet swirl) positive swirl at the impeller exit. This assumption was required because there is another experience from PAT research that turbine axial velocity is always greater than the pump axial velocity at the same blade speed and best efficiency conditions. It can be seen that this assumption causes considerable angle of incidence and large deflection. Both these changes (incidence and deflection) cause large profile losses, which will naturally increase the net head ($\Delta C_u \cdot u + \text{losses}$). The large angles of incidence and deflection are actually related, which has been documented in different cascade studies of axial blade shapes [4] showing large incidences causing considerable fluid deflection.

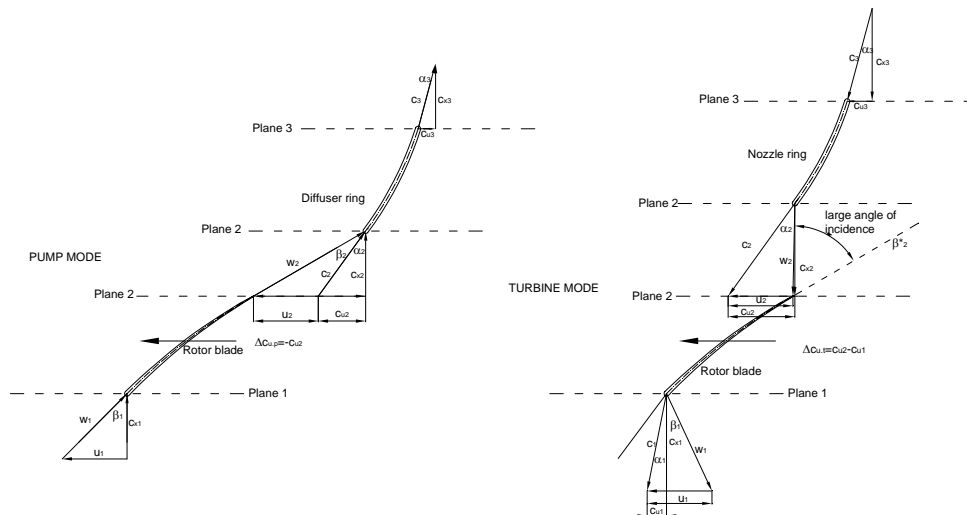


Figure 1, Velocity triangles in backward shaped impellers (pump and turbine) assuming equal $\Delta C_u \cdot u$

The above study shows firstly that Euler momentum cannot be negative for backward shaped blades and secondly that the equality of momentums is pump and turbine mode can be used to predict the turbine performance without having to making assumptions on the turbine axial velocity factor.

3. Forward Shaped Impellers – Positive $\Delta C_u \cdot u$

The authors in [2] and [3] however showed that the forward shaped impellers will not have any special case of negative rotational momentum in turbine mode and had recommended the use of these impellers for turbine application.

Based on the new condition imposed in [section 2](#) concerning the constancy of the rotational momentums in pump and turbine modes, new velocity triangles are constructed in [Figure 2](#). These triangles also indicate a smaller degree of incidence and deflection compared to the backward blades.

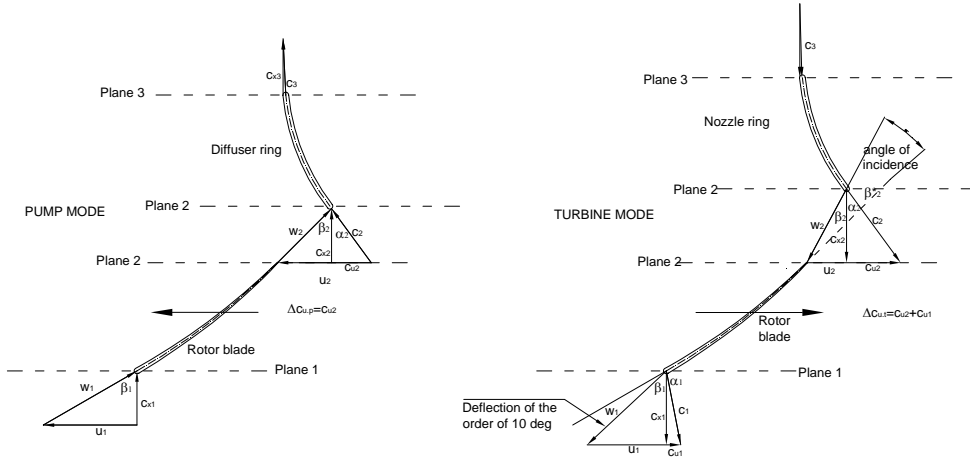


[Figure 2](#), Velocity triangles in forward shaped impellers (pump and turbine) assuming equal $\Delta c_u \cdot u$

4. Critical Analysis of the Axial Flow Model [1]

4.1 The Conversion of pump shape to turbine shape

The previous section showed that with comparable rotational momentums between the pump and turbine modes of operation it is possible to have backward shaped turbine impellers to operate with a positive net head, however with greater degree of hydraulic losses (larger incidence and deflection). Therefore, the comparison of the two velocity triangles gives the first indication of how pump shape can be converted to turbine shape.

The specific speed number has axial velocity (in the form of discharge), rotational momentum and hydraulic losses (in the form of net head) as shown in [Eq. \(1\)](#).

$$N_q = \frac{N \cdot \sqrt{Q}}{gH} \sim \frac{\sqrt{c_x}}{\Delta c_u \cdot u + H_{Loss}} \text{ at constant speed} \quad (1)$$

If the rotational momentums are nearly equal (as seen in [Table 1](#)), the magnitude of axial velocity and the hydraulic losses become the two main parameters that would be required to convert the pump shape to turbine shape.

It has also been seen that the incidence and deflection effects are unique for a given blade shape ([Fig. 2](#) and [Fig. 3](#)), which will make the losses and axial velocity take different values for different blade shapes. Therefore, the turbine shape is very closely influenced by the shape of the blade (forward and backward) and generalized prediction equation for both shapes cannot be assumed. This is exactly carried out in the model developed in [1], which proposes a single relationship for N_q prediction over wide range of axial pump shapes, given by [Eq. \(2\)](#).

$$N_{q,t} = 0.8081 \cdot N_{q,p} + 2.2664 \quad (2)$$

4.1.1 An example showing prediction errors on N_q in radial flow and mixed flow PATs

The errors due to a similar prediction equation developed exclusively for radial flow PATs [5] in the N_q range from 20 rpm to 80 rpm and mixed flow PATs [6] in the range of 70 to 100 rpm have been illustrated in [Fig. 3](#), which use the true turbine shape (experimental) as the reference and compares it with the model turbine shape. It can be seen that the model is making significant prediction errors.

4.1.2 Relevance on Axial Flow PAT model [1]

The magnitude of N_q errors in radial flow and mixed flow PATs can come up in the modeling of axial flow PATs as well. These errors can further influence in the Cordier predictions (that is ultimately used to predict the BEP numbers of the turbine, ϕ and ψ), which is the next important step of the model that uses the specific speed value (σ) as an input variable. The errors in N_q can be termed as the first source of error in prediction.

The hydraulics of backward and forward shape impellers are so different that it is not possible to have identical prediction laws for both these shapes of axial impellers. Even within backward shaped blade designs there could be several variations like guide vane angle, blade pitch and curvature that would have an influence on operating hydraulics, which will make specific speed predictions even more challenging.

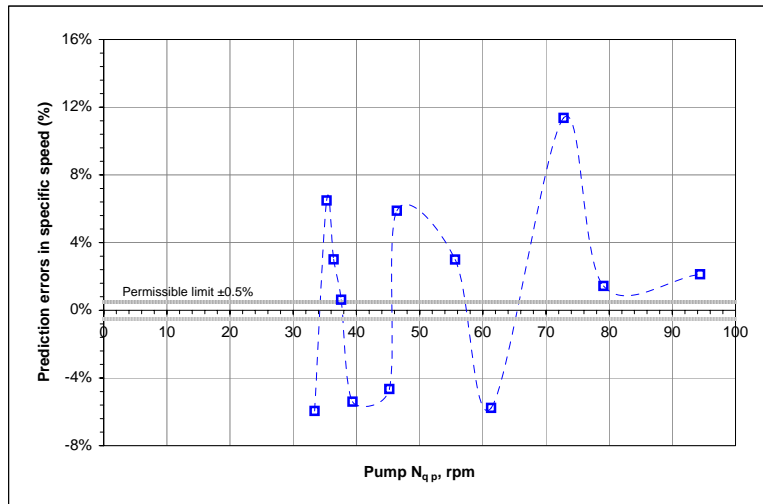


Fig. 3, Errors in the prediction turbine specific speed in radial flow and mixed flow PATs

4.2 Validity of Cordier PAT Line for forward and backward shape impellers

As mentioned in [1] the axial flow PAT model used a mixture of turbine shapes (radial flow PATs, mixed flow PATs, forward shaped propeller turbine and forward shaped Kaplan blades) to bring out the Cordier relationship (Δ - σ) illustrated in Eq. (2), which could naturally be prone to errors.

$$\sigma = (1.2497) \cdot \Delta^{-1.3311} \quad (2)$$

During the steps of modeling the turbine σ is calculated first from the pump shape and then the Cordier line is used to predict the mean Δ . The Δ and σ are combined to give the head number (ψ) and discharge number (ϕ) respectively.

It will be an interesting study to evaluate the Δ given that the turbine shape has been accurately determined. This has been investigated in Fig. 4 using the authors experimental results of radial flow and mixed flow PATs ([5 and 6]), which shows an inconsistent pattern between specific diameters determined using model prediction and actual specific speed numbers. This result clearly proves that even if the turbine specific speed was to be accurate (equal to that of the experiment), the Cordier line (Eq. (2)) could still make an error in the prediction of Δ .

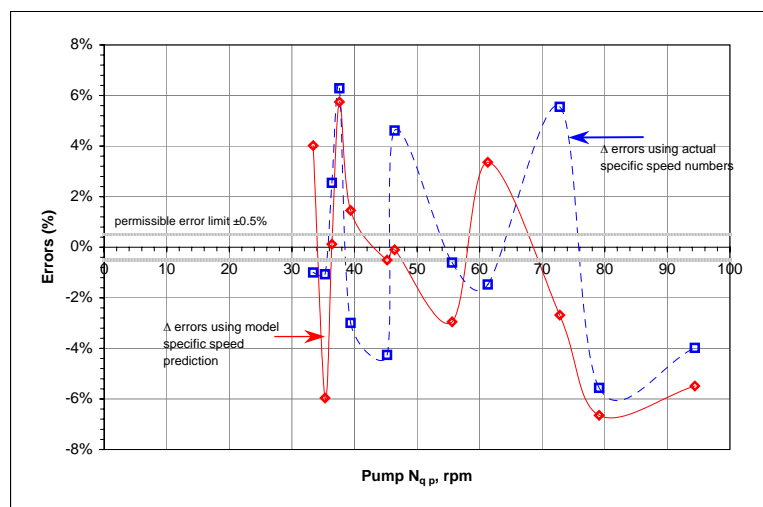


Fig. 4, Studying the validity of the Cordier predictions on radial flow and mixed flow PATs

Hence, in addition to the errors coming from the specific speed equation, the Cordier line too has uncertainties. This aspect needs to be carefully considered in the development of shape specific prediction models for forward and backward shapes impellers respectively.

4.3 Translation of Δ and σ errors on ϕ and ψ values

The most important question that remains is to see how these modeling errors on σ and Δ shown in [Fig. 3](#) and [Fig. 4](#) respectively translate to errors on turbine operating parameters ϕ and ψ (representing the discharge and head values respectively).

This question is once again analyzed using the author's experimental data and a model based the very same experimental PATs. A chart representing these errors has been plotted in [Fig. 5](#) show to errors to be quite significant in the range of $\pm 10\%$ for low specific speed PATs and exceeds $\pm 20\%$ for higher specific speed PATs.

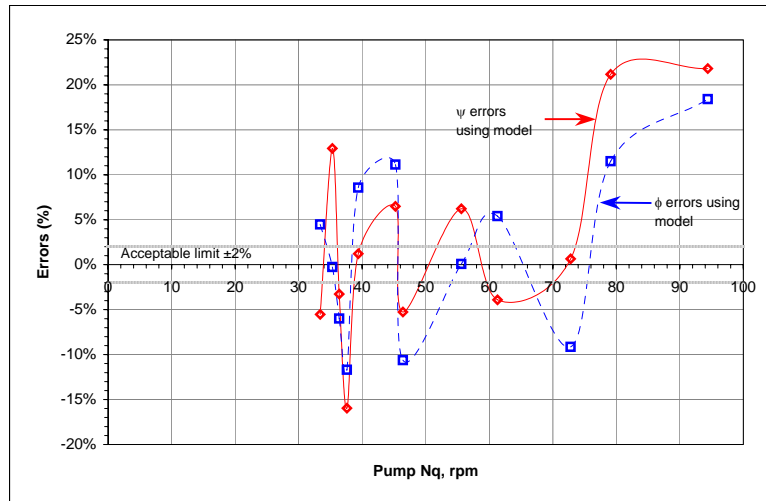


[Fig. 5](#), Errors on ϕ and ψ due to errors in Δ and σ in radial flow and mixed flow PATs

These errors are unacceptable by all standards. However, the findings of this study has a lot of meaning. Firstly, it shows that a prediction model is making very significant errors despite the fact that it was developed from the very same PATs on which the model evaluation has been carried out. This directly implies that the author's [4] approach of generalizing the prediction model for radial flow PATs in the range of 20 rpm to 80 rpm and mixed flow PATs in the range of 70 rpm to 100 rpm is fundamentally flawed and there should be no assumptions of an universal law for large ranges of specific speeds.

Secondly, it has to be clearly underlined that any new model should predict not only an accurate value of σ but also an accurate value of Δ . It has been found that in order to keep the prediction errors on ϕ and ψ within the $\pm 2\%$ error bands, then the prediction errors on Δ and σ should not exceed $\pm 0.5\%$. This certainly adds stringent modeling requirements and the roadmap should be conceived in such a way that models should be independent for both forward and backward blades and should further have categories and sub-categories within them to reflect the diversity of blade shapes.

5. Roadmap for the development of shape specific prediction model

5.1 Theoretical workout

The theoretical procedure in [section 2](#) and [section 3](#) using basic velocity triangles and constant rotational momentum condition revealed that both the pump and turbine hydraulics could be compared, provided the drawings of the guide vane and blade shapes are available. Though, the estimation of hydraulic losses will not be easy, some indication can be obtained from the incidence or deflection effects. This methodology is not foolproof but will certainly help in getting a value of turbine specific speed for both forward and backward shaped blades, without needing to rely on the specific speed equation (Eq. (2)).

The prediction of specific diameter from specific speed can also be realized if the axial velocity and losses are known for given blade geometry. These parameters would have already been estimated in the determination of specific speed.

This is an independent approach for determining specific speed and specific diameter for a given blade shape. This approach can be optimized further if the real flow vectors and their direction along with hydraulic losses are determined using an experimental testrig (discussed in [section 5.2](#)).

5.2 Experimental investigation

It is important realize that the theoretical methodology in [section 5.1](#) cannot be fully relied due to source of errors firstly in the assumption of constant rotational momentum (errors have been witnessed in [Fig. 3](#) for

experimentally tested PATs) and secondly in the determination of hydraulic losses from incidence and deflection effects.

It has also become evident that preliminary model [1] too can be susceptible to large errors and cannot be used in the present form. If it is required to achieve a prediction error of $\pm 0.5\%$ on Δ and σ values, then an elaborate experimental program covering large blade shapes should be conceived.

The model [1] is based on well-established turbine fundamentals and its methodology need not be discarded. The only difference in the new optimized model would be giving out modeling laws in narrower bands of blade shapes, which will also be exclusive for forward and backward blade shapes. It would also take into account intricate geometric details within forward and backward blade designs.

The theoretical workout ([sections 2](#) and [3](#)) should be adopted for initial assessment of turbine predictions. But, with more experimental data on different blade shapes it can be optimized further as mentioned in [section 5.1](#) and may become reliable as well and used as an alternate technique.

The goal of the experimental work should be to add more quality and robustness to the predictions of all axial pump blade shapes.

6. Conclusions and Recommendations

This small introspective study has shown that backward shaped impellers cannot have negative fluid momentum as proposed in previous study [1]. This result could be proved through strong evidences that Euler fluid momentums are comparable for both pumps and turbine modes of operation.

The second conclusion of the study was that the preliminary prediction model [1] has inbuilt errors related to the accurate estimation of turbine specific speed from the pump shape. Even though the Cordier line is very well established line for all types of turbomachines it was seen that even this was not insensitive to turbine shapes.

The study of the prediction errors of similar model developed for radial flow and mixed flow PATs showed the gravity of making wrong predictions of specific speed and specific diameter. It was also found that in order to keep the turbine head and flow predictions in error bands of $\pm 2\%$, the prediction errors on specific speed and specific diameter cannot exceed $\pm 0.5\%$.

Based the above findings, the paper makes the following recommendation.

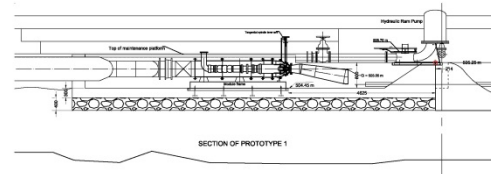
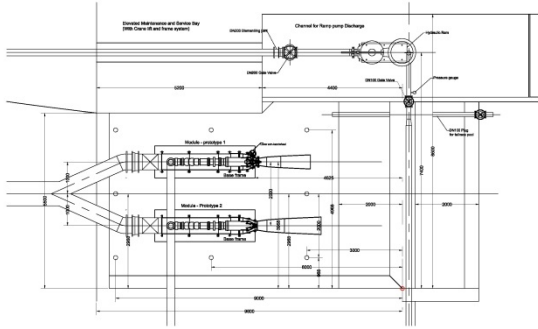
- 1) Firstly, a critical examination of different pump blade shapes needs to be carried. This can be done in association with the manufacturer and a database of these shapes be created for both forward and backward shaped blades. The database should include geometries of the diffuser ring and blade angles at all radial sections.
- 2) Secondly, a well-structured experimental program needs to be made. This would include design of a testrig that will measure a combination of external (head, flow, speed and torque) and internal parameters (velocity vector profiles at the inlet and exit of the blades). While the external parameters will be used for the Cordier based model (model 1), the internal measurements will be very helpful to complete the theoretical approach for the turbine performance estimation highlighted in this paper (model 2). The two modeling approaches should have exclusive categories for forward and backward shapes and sub-categories within them to include any possible geometric deviations.
- 3) Thirdly, as the experimentation is being planned a parallel computational study for the identical goals can also be initiated.

If the above recommendations were to be carried out in its totality there would be two independent prediction models for axial flow pumps as turbines that will be sensitive to the blade shape. This would come in long way it realizing a truly optimized and robust model.

7. References

- [1] P. Singh, F. Nestmann, Research Report on the A Proposal for a Preliminary Prediction Model for Axial Flow Pumps as Turbines, Internal Technical Report, IWG, KIT, March 2010.
- [2] Punit Singh, Franz Nestmann, Axial flow impeller shapes: Part 1, World Pumps (Elsevier), Vol. 2011, Issue 2, 2011.
- [3] Punit Singh, Franz Nestmann, Axial flow impeller shapes: Part 2, World Pumps (Elsevier), Vol. 2011, Issue 3, 2011. [6]
- [4] S. L. Dixon, Fluid Mechanics and Thermodynamics of Turbomachinery, Elsevier, Oxford, UK, Chapter 3, 2005.

**Field Research Laboratory for
Low Head (Micro) Hydro Powered Water Pumping and
Electricity Generation Technologies
at Taipadar, Chhattisgarh**



A Research Proposal by

**Dr.-Ing Punit Singh,
Visiting Scientist,
Karlsruhe Institute of Technology, Germany**

December 2014

Table of Contents

Abstract	3
1. Introduction and Background.....	3
2. The Taipadar Project	4
2.1 Brief Timeline	4
2.2 Review of Survey	5
2.3 Cost Estimates of Project.....	6
3. Prototypes under Investigation.....	7
3.1 Brief Review of available simulation results.....	7
3.2 Hydro Turbine based Pumps	7
3.2.1 Prototype 1 – Axial flow turbine with adjustable guide vanes	8
3.2.2 Prototype 2 – Fixed geometry axial flow pump as turbine	11
3.3 Water Hammer/Ram based Pump	12
3.4 Consolidated Characteristics of turbine pump based and ram pump based prototypes	15
3.5 Generator mode characteristics of Hydro turbine prototypes	16
3.5.1 Operational physics of variable speed controller.....	16
3.5.2 Hydraulic behavior of Axial flow turbines in part-load and no-load regions	17
3.5.3 VSC operation with axial flow turbine in part-loads	17
3.5.4 Generator characteristics of Prototype 1.....	17
3.5.5 Generator characteristics of Prototype 2.....	18
4. Testrig Facility.....	19
4.1 Civil and Hydraulic Structures	19
4.2 Measuring parameters and methods.....	19
4.3 Total Costs of Field Research Station	20
4.4 Testing Protocols	21
4.4.1 Pumping mode	21
4.4.2 Electricity generation mode	23
5. Summary.....	25
6. References	25
7. Nomenclature.....	26

Abstract

The research proposal highlights the need of establishing a field laboratory, which is interfaced with a community based micro hydro project for a specific case of evaluating low head hydropower technologies with twin utilities of water pumping and electricity generation.

The paper introduces the project, its social and environmental context, while reviewing the cost of the total project covering irrigation, power supply and drinking water utilities. There is focus on the pumping operation using two contrasting principles. The first one is based on rotational fluid mechanics (turbine) and the second one on the principles of fluid flow compression (hydraulic ram), both driven by low heads. The paper presents the simulation data for these two categories of prototypes. The results of power generation through turbine methodology with variable speed drive are also described.

The proposal further elaborates the testing infrastructure, instrumentation and protocols for all modes of operation. The cost of establishing the testrig is estimated to be 160 lakhs of rupees, which a third of the total project costs (500 lakhs). It concludes with an introspection on how the various options of chosen technologies, combining modern as well as vintage principles, will fit into the lives of an isolated community living a forest ecosystem having a gradually sloped effluent stream.

1. Introduction and Background

The motivation of building a field research station for low-head micro hydro pumping devices comes from the need of bringing a new thinking for energy and water resources management for regions in the vicinity of gradually sloped streams/creeks. Further to this the lack of verifiable performance of low-head machines working in below 10-15 kW makes the creation of field test-rig important not only from the scientific point of view but also from the social and ecological perspectives.

The project location is within a pristine forest in the southern Bastar district of Chhattisgarh State having a perennial flow stream, named Ganesh Bahar, which is rivulet to River Shabari that eventually joins the larger river Godavari and the Bay of Bengal. The Ganesh Bahar nala is approximately 19 kilometers in length and has three tribal settlements along it, which are over 300 years old. The selected settlement is the smallest amongst the three with a population of over 200 inhabitants and having a cultivable area of about 80 Ha.

The Taipadar and other settlements are not connected to the grid require both electricity and water supply primarily for agricultural purposes, which drives the village economy. Presently, the irrigation based on highly unpredictable monsoon pattern of the subcontinent. Potable water supply is the third vital need of the community. Presently, drinking water is managed by hand pumps, while small photovoltaic plant provides only for basic lighting during evening and night times.

Therefore, the technological innovation was to use the low head water source to efficiently pump water from the same stream to higher levels and also to generate electric power for agricultural related activity along with domestic use. The focus of the innovation was to consider the seasonal variation of flow and intelligently operate the energy devices. The device should preserve the ground water table and promote the interdependence of forest and effluent stream flow, which is the heart of philosophy of the low head hydropower technology.

Two categories of technologies have been considered for this innovation. The first one is the turbine option where both pumping and electricity generation can be achieved and the second technology is based on water hammering phenomena (a 200 year old! Invention), called a Ram pump is only for pumping water. This category of pumping technology even though vintage in some sense, yet has some physical aspects that need to be understood and optimized by contemporary hydraulic scientists.

The present proposal deals with both short-term and long-term performance evaluation, validation of laboratory and simulated results along with implementation of improved methods after evaluation, and thus bringing good to the lives of the people of this hinterland while protecting the forest ecology.

2. The Taipadar Project

The Taipadar settlement along the south flowing Ganesh Bahar Nala is shown in Fig. 1, with two bigger settlements Kavapal towards the north and Tiriya to the south. The rivulet is seen to join River Shabari at southern tip of Tiriya settlement. Figure 2 shows a blow up of the Taipadar village along with a neat spread of cultivation land and some landmarks of the multi-purpose project. A detailed project report [1] for this project has evolved in 3 versions with the final version brought out in September 2014.

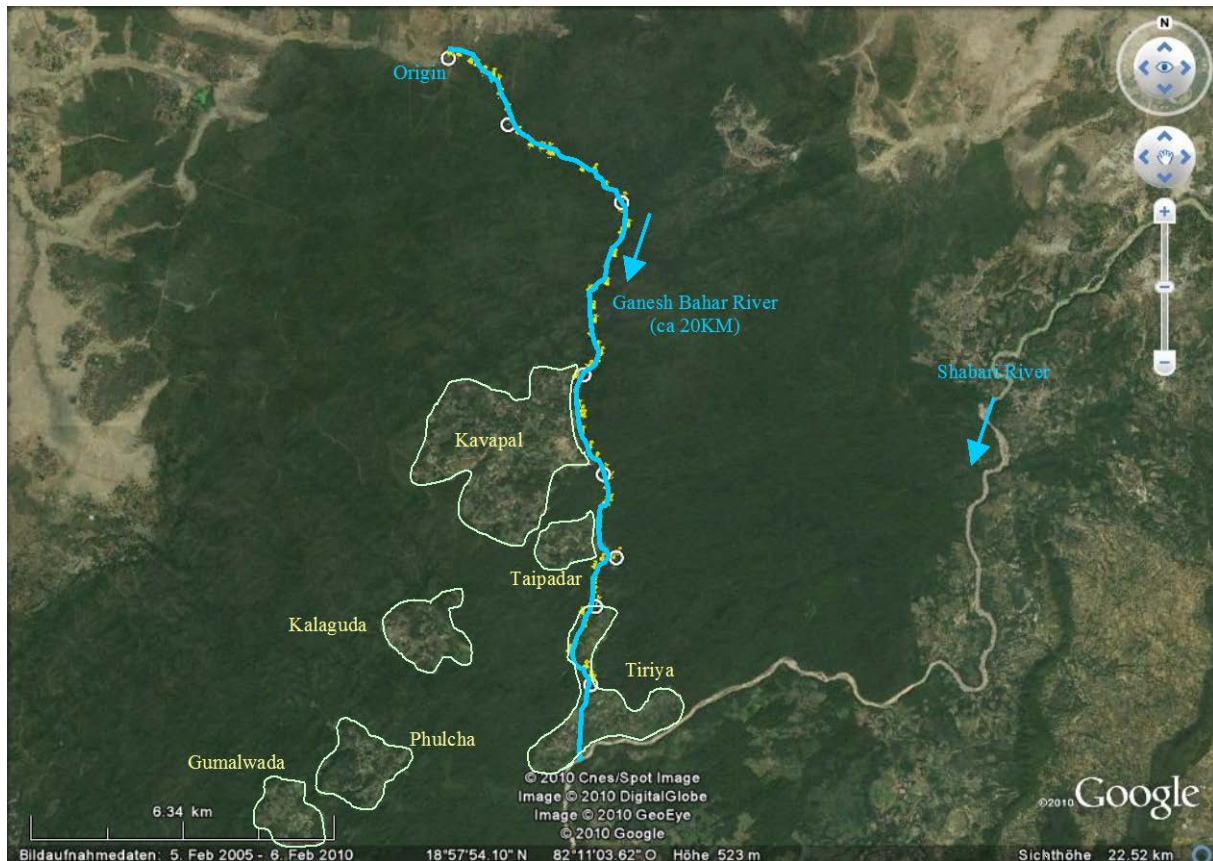


Fig. 1, Ganesh Bahar Nala and its settlements

2.1 Brief Timeline

Table 1, Chronology of the Taipadar Journey

Sr. No.	Particulars	Chronology
1	First visit to the site with CREDA engineers	Nov. 2009
2	Preliminary investigation of flow, bringing out a concept paper	July. 2010
3	3 day expedition on the 20 km river length, from origin to confluence	Dec. 2010
4	Pre-feasibility survey/multiple state reporting/brainstorming the concept/first design of the micro hydel pump	Jan.-Jun. 2011
5	Applying to KSB Foundation for financial support	May 2011
6	Award of a Fellowship from KSB Foundation	Dec. 2011
7	Construction of a measurement weir on Ganesh Bahar Nala	Feb.-Mar. 2012
8	Topographic survey of streambed and command area of Taipadar village	Dec. 2012
9	Detailed Project Report Versions	
	DPR - Edition 1 (with only turbine pumps - 4 nos.)	Mar 2013
	DPR - Edition 2 (two turbine pumps, one with adjustable and other with fixed geometry)	Sept 2013
	DPR - Edition 2.1 (inclusion of Ram Pump as the third prototype)	Jan. 2014
	DPR - Edition 2.2 (relocating the diversion weir, redistribution of costs)	Sept 2014
10	Construction of Riverbed powerhouse	Feb - July 2014
11	Ordering heavy duty Ram Pump from Rife Pump, USA	Apr 2014

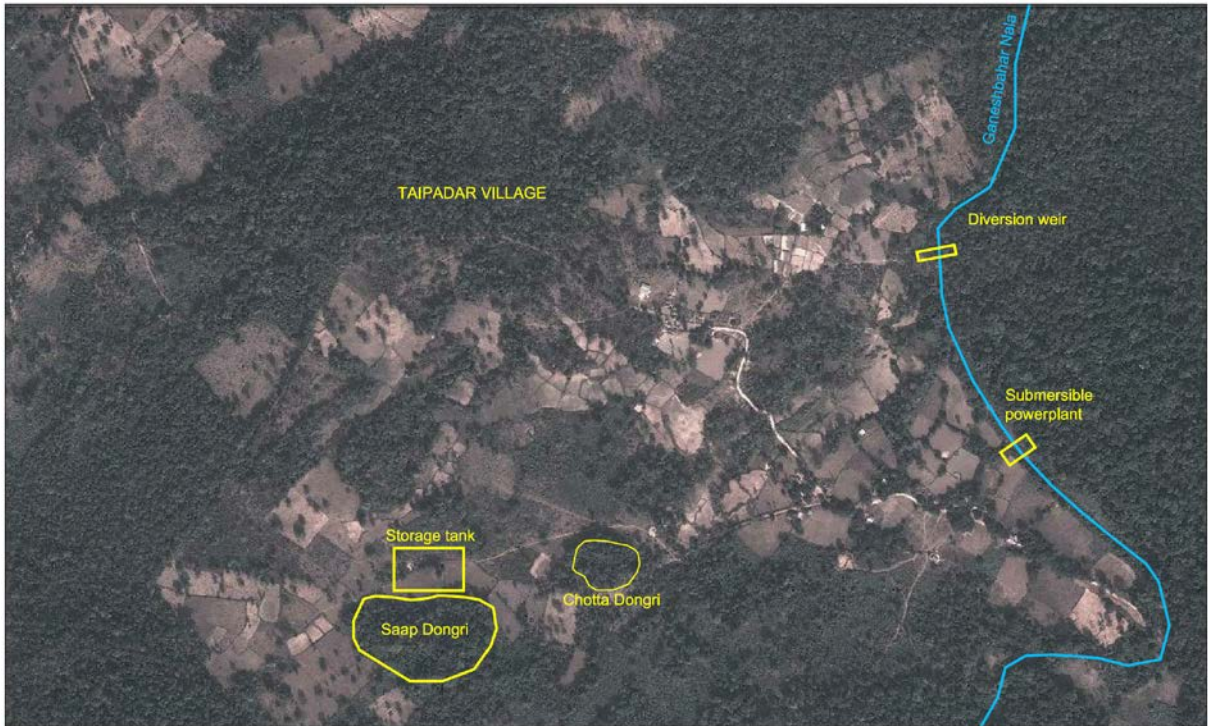


Fig. 2, Satellite image of Taipadar village

2.2 Review of Survey

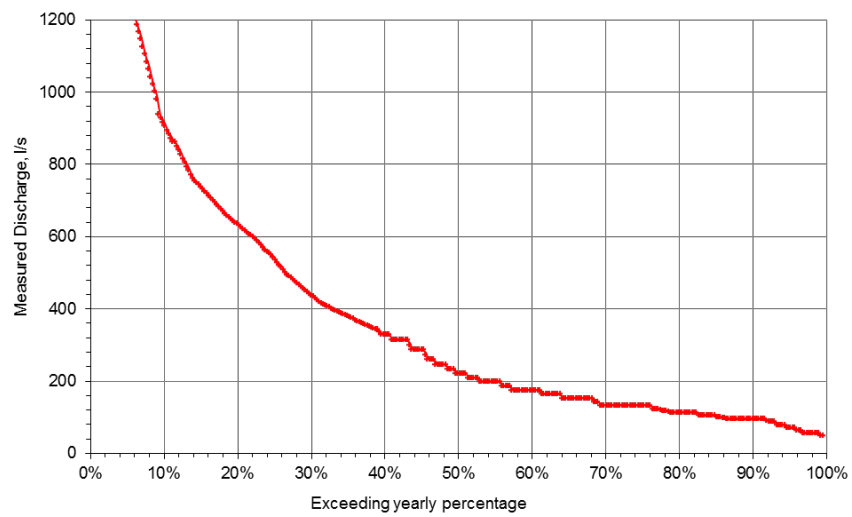


Fig. 3, Measurement weir and flow duration curve

As mentioned in Table 1, the survey comprised of a both hydrological survey and topography study [details in DPR, 1]. A permanent weir/gauge was built as seen m Fig. 3 for flow measurement and a flow duration curve obtained for one year data. The topographic survey is shown in Fig. 4 that illustrates the cultivation, houses, road network, and the section of Ganesh Bahar valley along with the major project components like diversion weir, riverbed powerhouse, storage tank, penstock and various water network lines

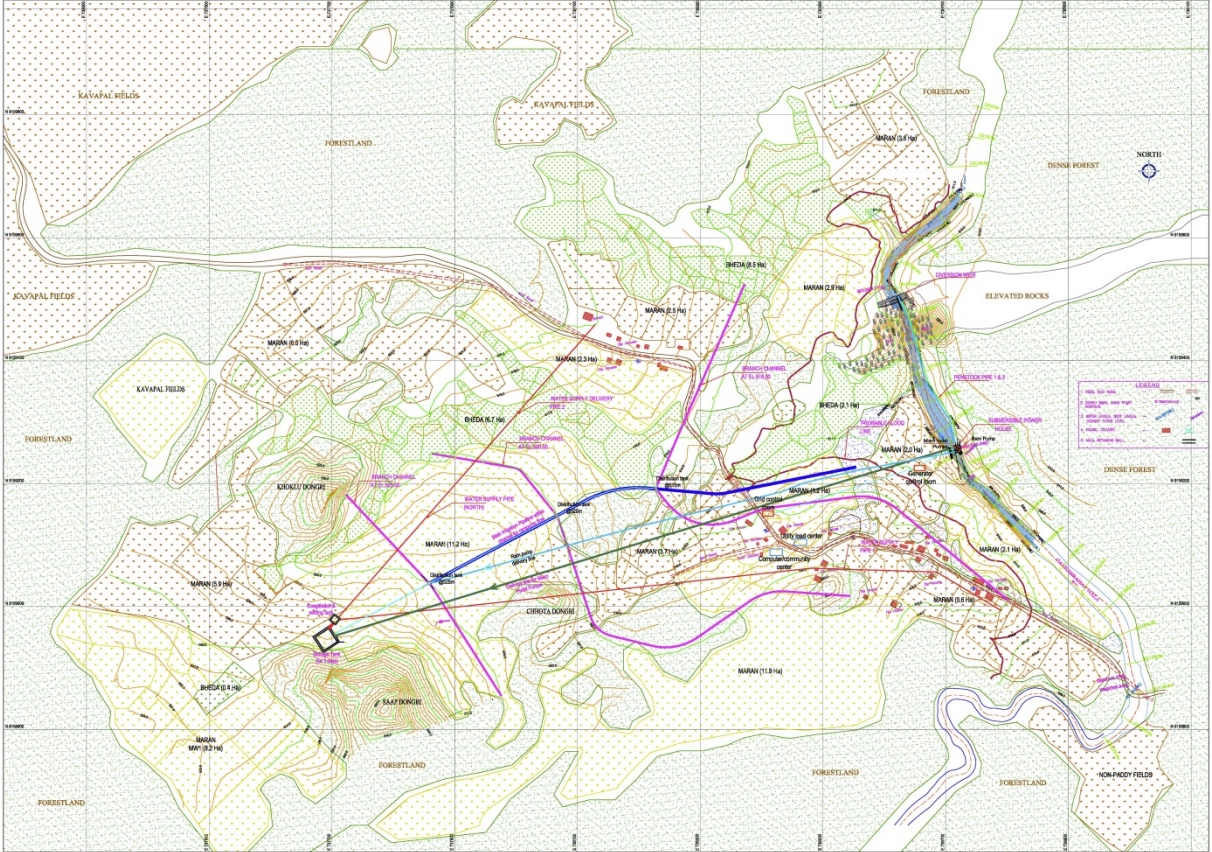


Fig. 4, Topographic survey

2.3 Cost Estimates of Project

The cost estimates for the three utilities have been discussed in detail in DPR 2.2 [1]. A component wise distribution for the three utilities (micro hydel, irrigation and drinking water) is illustrated in Table 2.

The first utility electricity generation (micro hydel) comprises of civil works associated with the two turbine based prototypes along with transmission and load distribution arrangement. This utility costs about 260 lakhs. The second and important utility as far as the village economy is concerned, is irrigation divided into two phases. The first phase of irrigation is with Ram pump is estimated to be 88 lakhs, while second phase with micro hydel pumps will need 118 lakhs. The drinking water supply utility comprising of simple purification techniques is estimated at 34 lakhs.

This brings the total project funding of nearly 500 lakhs. The workout for the ‘bill of quantities and estimates’ has been carried out in the DPR 2.2, [1].

Table 2, Cost Summary for the Taipadar Project

Utility	Components	Costs (in Lakhs)
1 Micro Hydel (without Micro Hydel Pumps costing 100 Lakhs)	Diversion Weir	34
	Penstock Line 1	44
	Powerhouse	32
	Turbine Accessories	25
	Control System	57

		Transmission/Distribution and Loads	47
		Overheads	20
		sub-Total for Micro Hydel	259
2	Irrigation		
	Phase 1 - with Ram Pump	Ram Pump	34
		Penstock Line 2	10
		Delivery Line 2	16
		Branch and Field Channels	28
		sub-total (Phase 1)	88
	Phase 2 - with Micro Hydel Pump	Storage Tank	41
		Pump Delivery Line 2	42
		Main Irrigation Pipeline	27
		sub-total (Phase 2)	110
		Irrigation overheads	8
		Sub-total - Irrigation Utility	206
3	Drinking water		
		Coagulation tank	4
		Supply lines (North and South)	21
		Distribution lines	5
		Overheads	4
		sub-total	34
		TOTAL	499

3. Prototypes under Investigation

As briefly introduced (in section 1), there are three test specimen (termed as prototypes henceforth) of water pumping devices driven by different principles. The first two prototypes fall under the category of turbine or rotary fluid action, while the third prototype works on an entirely of the different physical concept that ensures a perpetual water hammer action and continuous pumping (section 3.3).

Further, the prototypes based on rotary action have different techniques of turbine operation, one based on fixed geometry of blades and other with adjustable gates.

The first two prototypes are subsidized as a part the co-author's postdoctoral research from KSB foundation through Karlsruhe Institute of Technology (KIT), Germany. However, the ram pump is procured from funds of the co-author's firm, Dr. Punit Singh Associates.

3.1 Brief Review of available simulation results

While the KIT will carry out laboratory level experiments on the hydro turbine based prototype before supply, the ram pump will not be tested due to lack of test infrastructure available at the manufacturers end. The turbine prototypes have been simulated based on combined computational and theoretical models, but the Ram pump's performance is predicted based on scaled up laboratory results of smaller pumps that cannot be entirely reliable.

3.2 Hydro Turbine based Pumps

This category of prototypes is an integrated unit of an axial flow turbine as prime mover, an asynchronous generator followed by a submersible multistage pump, which is separated from the turbine-generator assembly by an electro-magnetic clutch. This type of prototype is called a 'micro hydel pump', because it works as alternatively as a generator or a pump depending on the status of the clutch (engaged/disengaged).

3.2.1 Prototype 1 – Axial flow turbine with adjustable guide vanes

The section of prototype 1 is shown in Fig. 5.1 and 5.2, which shows the axial flow turbine, with adjustable guide vanes, generator and pump. The mechanism of the altering gate setting using a lever and rotating ring is also described.

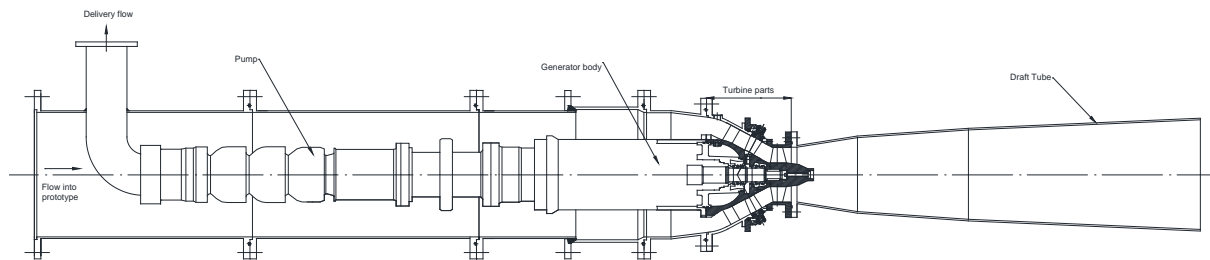


Fig. 5.1, Prototype 1 – Variable geometry turbine

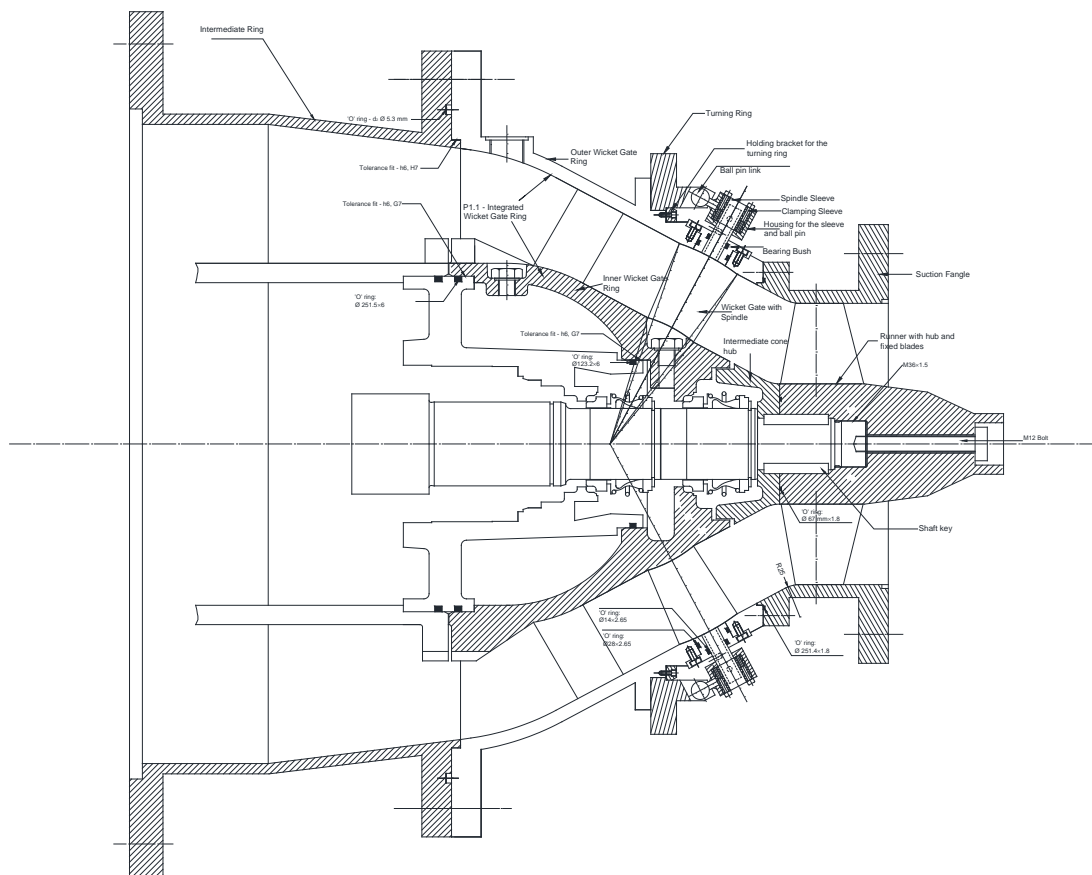


Fig. 5.2, Prototype 1 – Turbine cross-section

The turbine design itself is subject of extensive research to find the most optimum shape on one side and to satisfy the changing operating conditions of the other.

The author went about elaborate experimental work on the influence of geometry, starting from a free vortex runner [2] to inlet blade geometry in [3], exit blade condition in [4] and finally to understand the influence of blade height and number in [5]. Even though research gave an idea about how the operating condition (head and flow) were related to the internal fluid mechanisms of runner, it still left many questions unanswered, especially on the standardizing of the rotating blades and the stationary flow passages including the guide vane.

The propeller is designed for turbine flow of 178 l/s and head of 5 meters based on the classical design proposed by Neschleba [6] and with the help of the adjustable gates, it is hoped that the turbine flow can be reduced to 120 l/s at the same head. The choice of operational conditions is based on the flow duration curve shown in Fig. 3 and description in [1], while targeting medium flow season during the months of December, January, February and March.

The evolution of this turbine design is to make it as flexible as possible with respect to flow at different head conditions and also to give it an operational simplicity. It was decided to pursue with a fixed flow propeller design and adjustable guide vanes. Even though the design of the propeller followed Neschleba's [6] experience, there were certain modifications made based on author's experiments.

The gate exit angles can be changed from a nearly open condition of 15° to a restricted flow condition of 60° . Two such settings (one of 30° and other of 60°) are shown in Fig. 6 for which turbine simulations have been carried out.

The flow representations in Fig. 6 show a larger wake formation at the suction side of the 60° setting compared to a smoother flow for the 30° gate setting. The fluid flow for the 60° setting is more restrictive at the same driving head and helps in achieving reasonable performance at lower flow rates, even though it is less hydraulically optimal compared to the 30° setting.

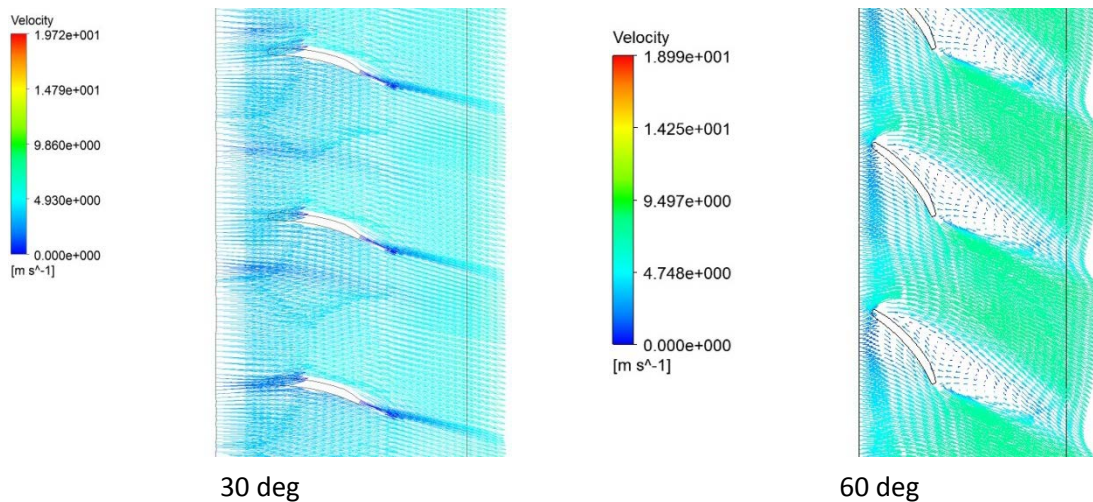


Fig. 6, 30 deg and 60 deg gate setting

For understanding the turbine-pump mode of operation, the constant speed curves of the pump sub-component of the prototype are intersected by the constant head curves of the turbine sub-component. It can be seen from Fig. 7 that the 60° setting brings out lower pumping flow at the same head conditions. The operating zone of the pump is characterized by the 30 m and 19 m pump delivery head lines on the top and bottom, and by the 3 m and 5 meter turbine head lines on the sides.

However, Fig. 7 does not discuss the turbine flows or the operating efficiencies, which matters the most as far as the research motives are concerned. This part is analyzed with the help of an innovative representation of head, flow and efficiency on a logarithmic scale as shown in Fig. 8. The head and flow for the pump and turbine are combined together as the ordinate and abscissa respectively, while the efficiency (turbine-pump) is used as the second ordinate.

There are two turbine (or drive) flow zones corresponded with pump (or delivery flow zones) and the respective efficiency flow zones at the 30° and 60° setting respectively. For obvious reasons, 30° setting provides a higher efficiency range, but the 60° setting is capable of operating under much lower flows at corresponding heads.

It is noteworthy to state that the expected minimum turbine flow in the 60° setting is only 135 l/s as compared to the design requirement of 120 l/s. The peak efficiencies of the turbine-pump barely cross the 60% barrier for the 30° gate setting.

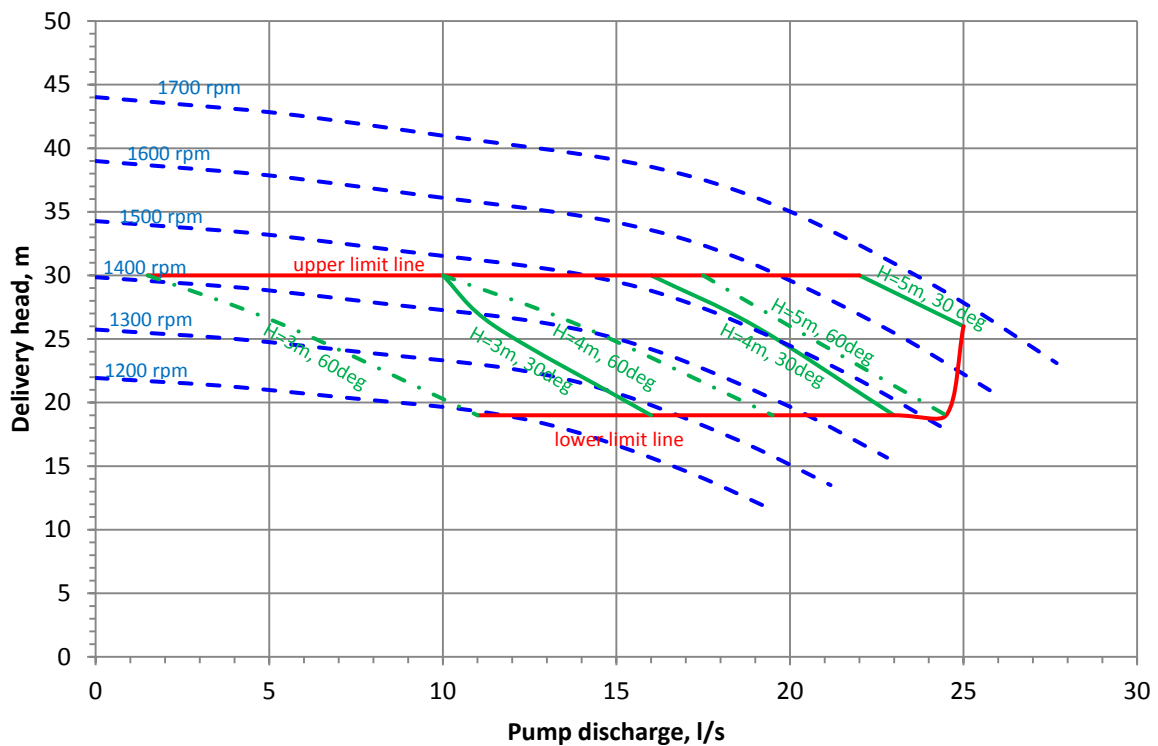


Fig. 7, Constant head turbine and pump curves for 30 and 60 deg setting

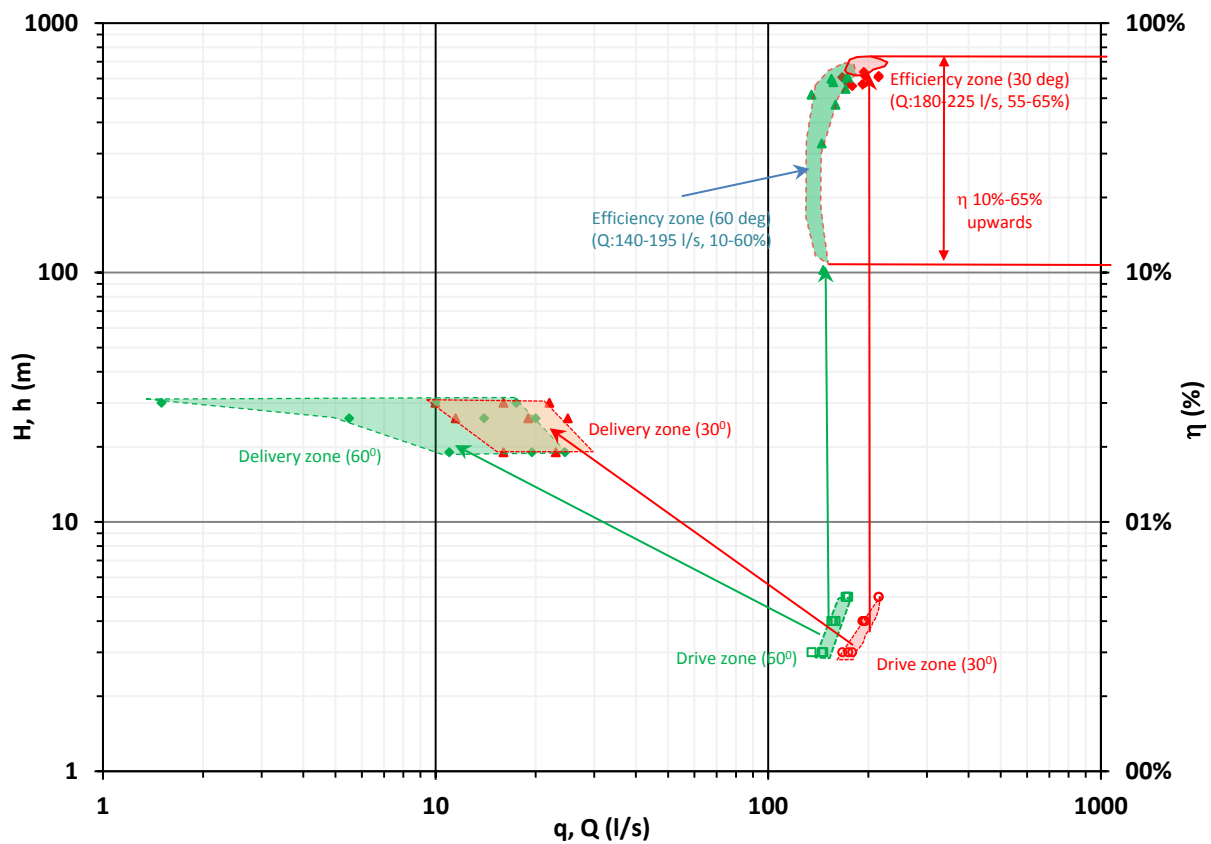


Fig. 8, Range of pump operation of adjustable turbine

3.2.2 Prototype 2 – Fixed geometry axial flow pump as turbine

Figure 9.1 and 9.2 shows the cross-section of the fixed geometry axial pump restricted in operation. The reversed pump propeller is chosen to take 250 l/s of flow at 5 meters. The characteristics in pump mode operation are summarized in Fig. 10 and 11.

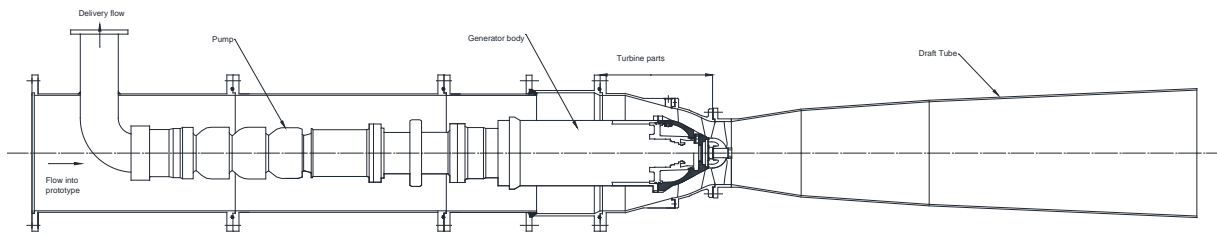


Fig. 9.1, Prototype 2 – Fixed geometry reversible pump as turbine

As mentioned above the prototype 2 is designed for a larger capacity compared to prototype 1 and this is revealed in Fig. 10 and 11. The pump flow range for 5 m turbine head condition spans from 25 l/s to 35 l/s. The efficiencies of this reversible pump is favorable in the range of 60% and 65%, however, the minimum permissible turbine flow is 265 l/s at 5 m turbine head and 200 l/s at 3 m drive head.

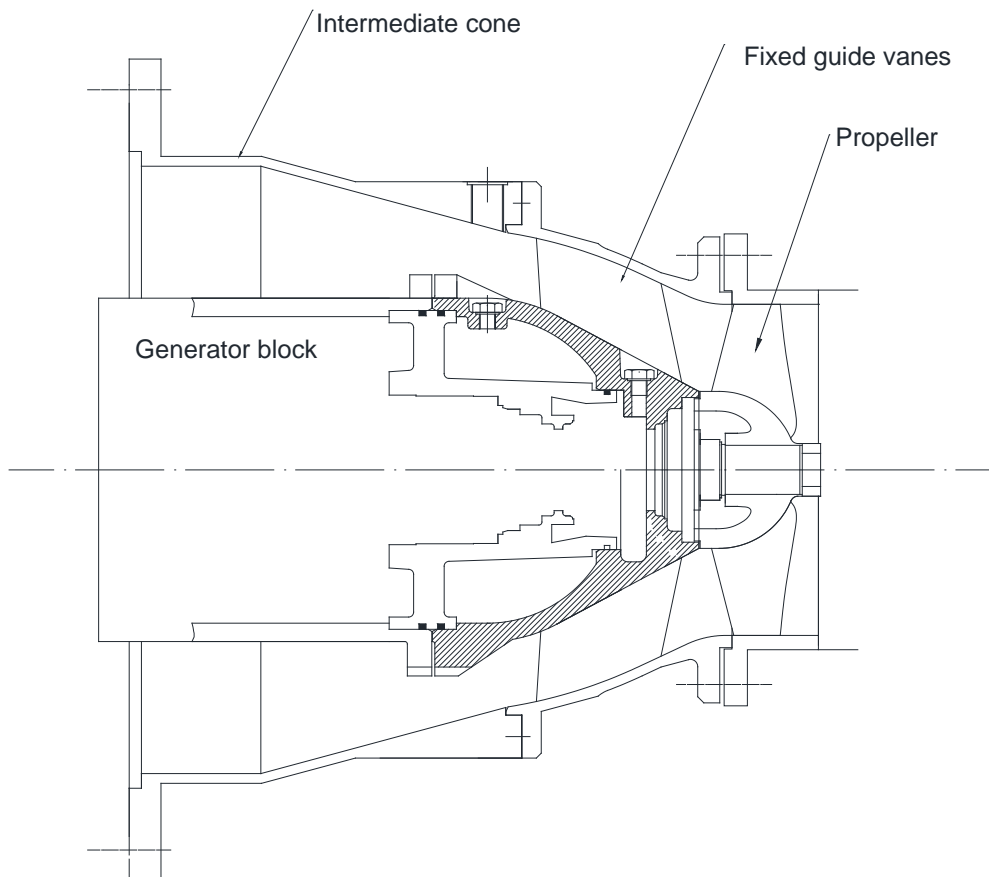


Fig. 9.2, View of Reversible Pump

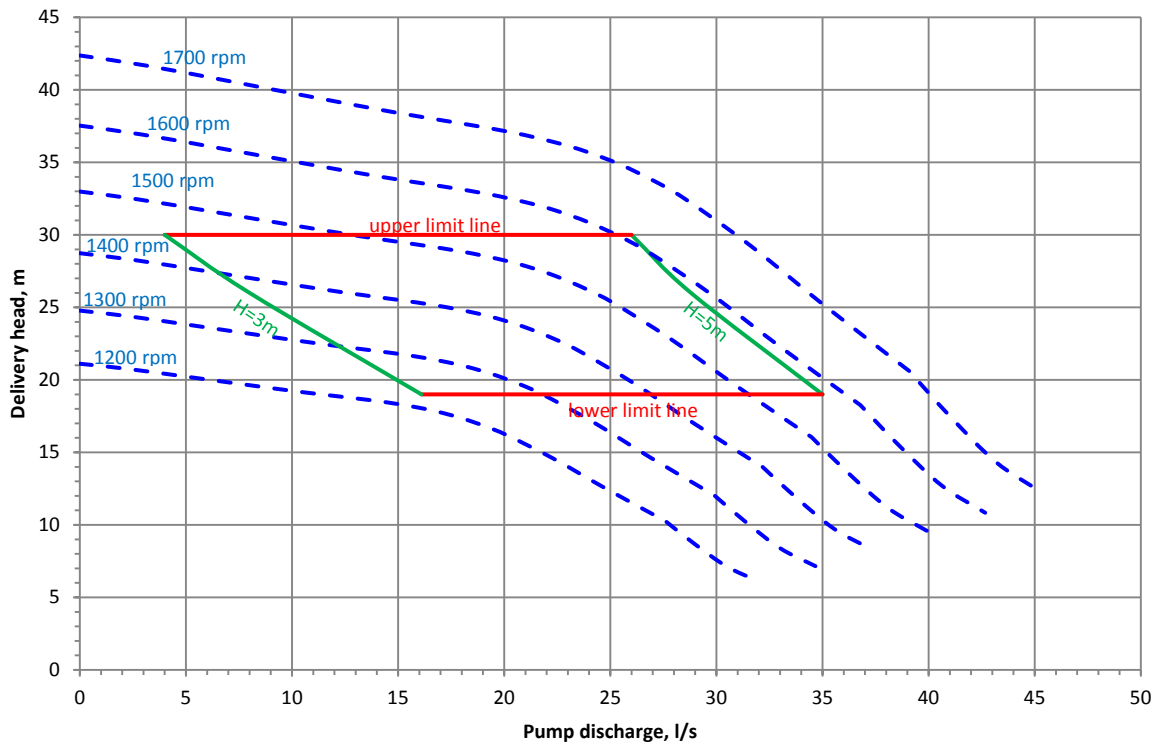


Fig. 10, Pump mode operation of Prototype 2 at constant turbine heads

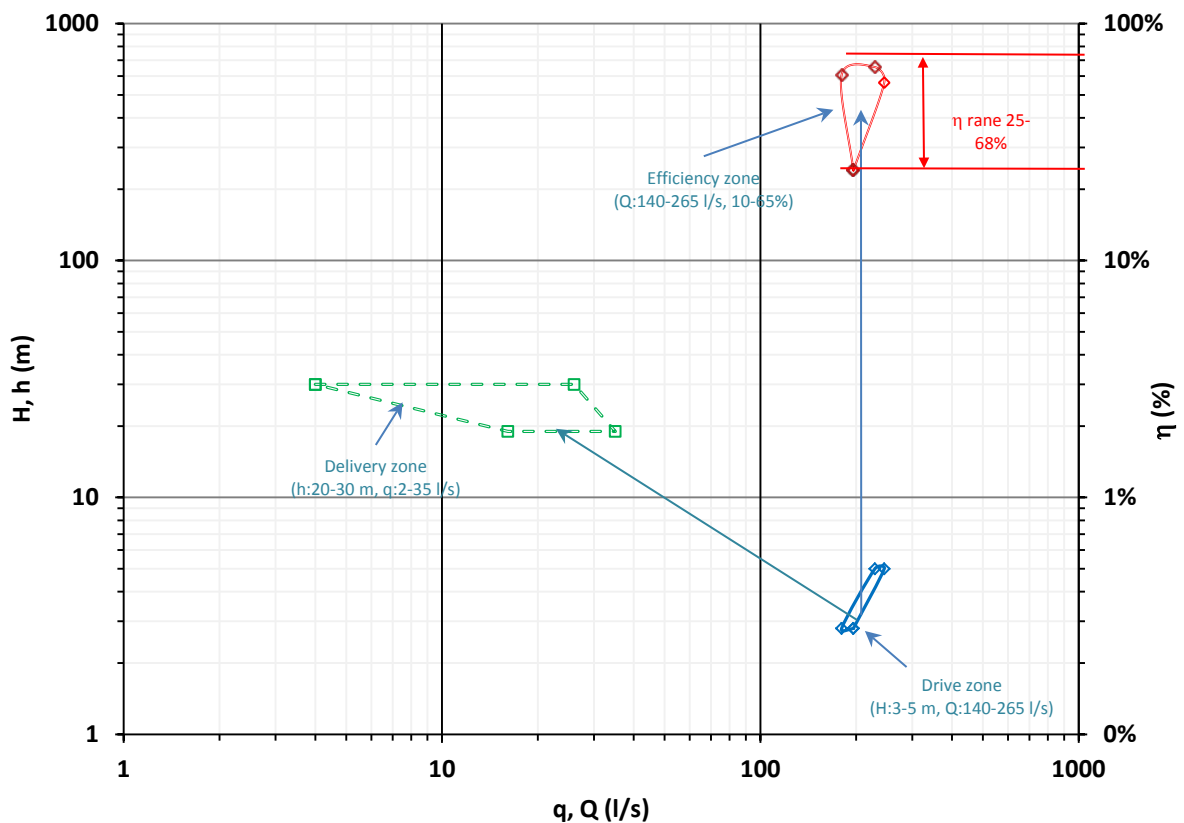


Fig. 11, Pump operating range of prototype 2

3.3 Water Hammer/Ram based Pump

The working principle of a this classic pump briefly covered in preceding sections, which has no rotating parts, is based on the synchronous closing of and opening of two valves (operation briefly

explained in Fig. 12). The subsystems like drive pipe and pressure chamber convert the otherwise damaging/undesirable water hammer to a positive effect of building pressure over a small time delay (lasting for few seconds only).

The first valve known as the outside or waste flow valve creates a continuous sound wave cycles all along the drive pipe (penstock) due to its opening and closing, and the second valve called the inside valve (housed inside the pressure chamber) alternatively opens and closes under the effect of the direction of the pressure wave resulting in a large pressure built over the period of time.

The chamber has multiphase fluids comprising of air at the top and water at the bottom. Once sufficient pressure is built in the vessel, opening of a smaller valve on the water side of chamber causes the water to reach higher levels through the delivery pipe.

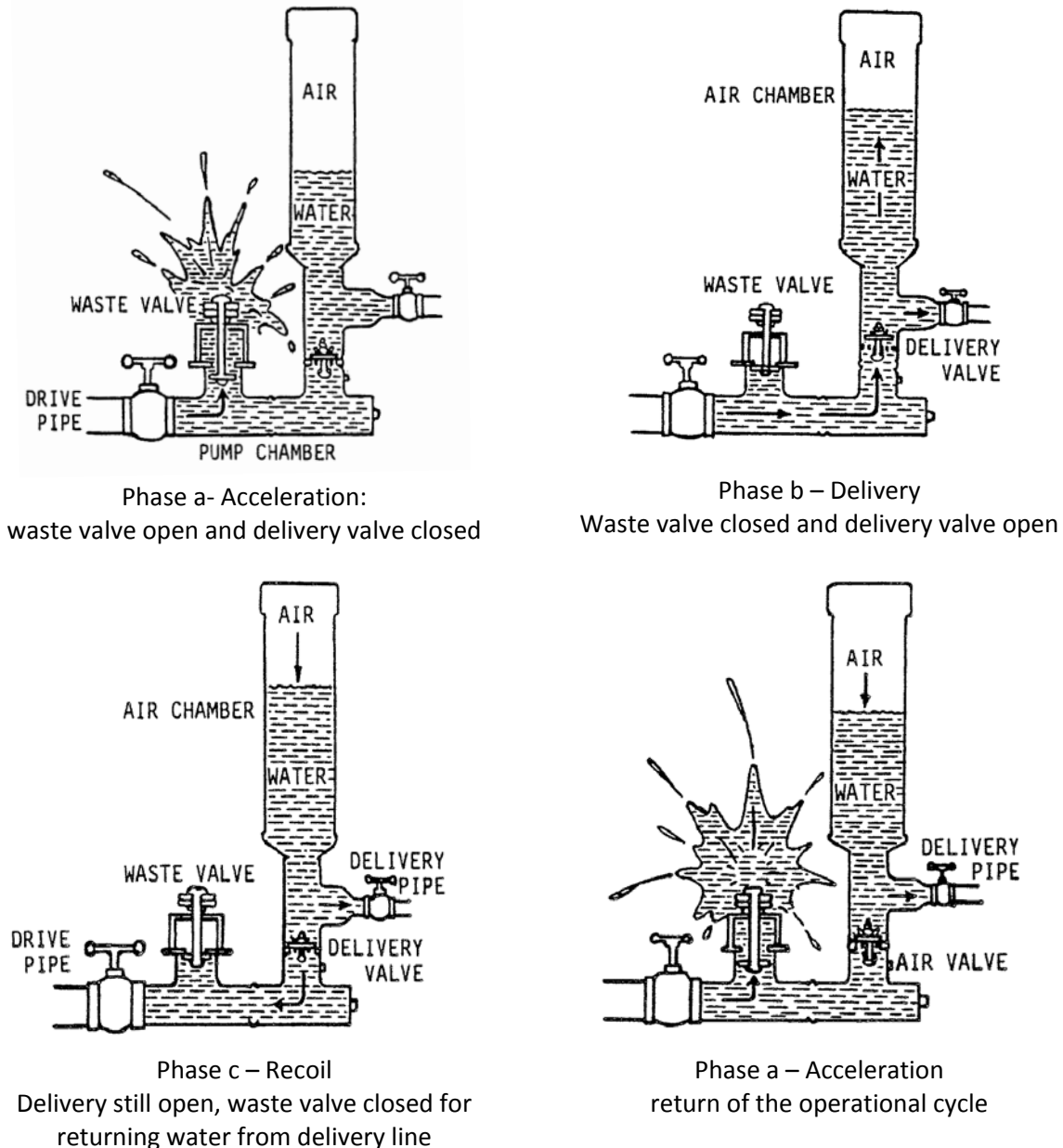


Fig. 12, Synchronized operational cycle of Ram pump valves [Tacke, 8]

If the variables (like the stroke rate and length of the waste valve or the proper positioning of the air vent lines on the chamber) are controlled pump operates on its own with minimum interference from the operator.

Research on these pumps (albeit of smaller pump capacities) has been extensively studied by scientists at Delft University [7], [8] and University of Warwick [9]. While these researchers focused on laboratory results other scientists like [10] and [11] brought out simulation equations for this transient behavior. However, their validation of these simulations was also only on smaller pumps. Moreover, there has been ‘no’ scaling law established for ram pump performance like in turbine pumps. The pump chosen for Taipadar project is a heavy duty (200 mm diameter inlet) and research has been restricted to smaller duty with inlet drive diameter of 50-65 mm only.

The reality is that real data of heavy duty ram pump is the requirement not only to verify the simulation methodology [10, 11] but also to understand the scaling of results of smaller pumps in [8, 9].

Heavy Duty Ram pump selected for Taipadar

The Ram Pump is chosen for that part of flow duration curve (Fig. 3) where turbine based pumps cannot function efficiently, i.e. during peak summer months when the flow falls below 100 l/s. As mentioned in section 3, the hydraulic ram pump is standard product manufactured by Rife [12] with external and internal representation shown in Fig. 13. The performance characteristics based on experimental results of smaller pump is illustrated in a logarithmic scale in Fig. 14.

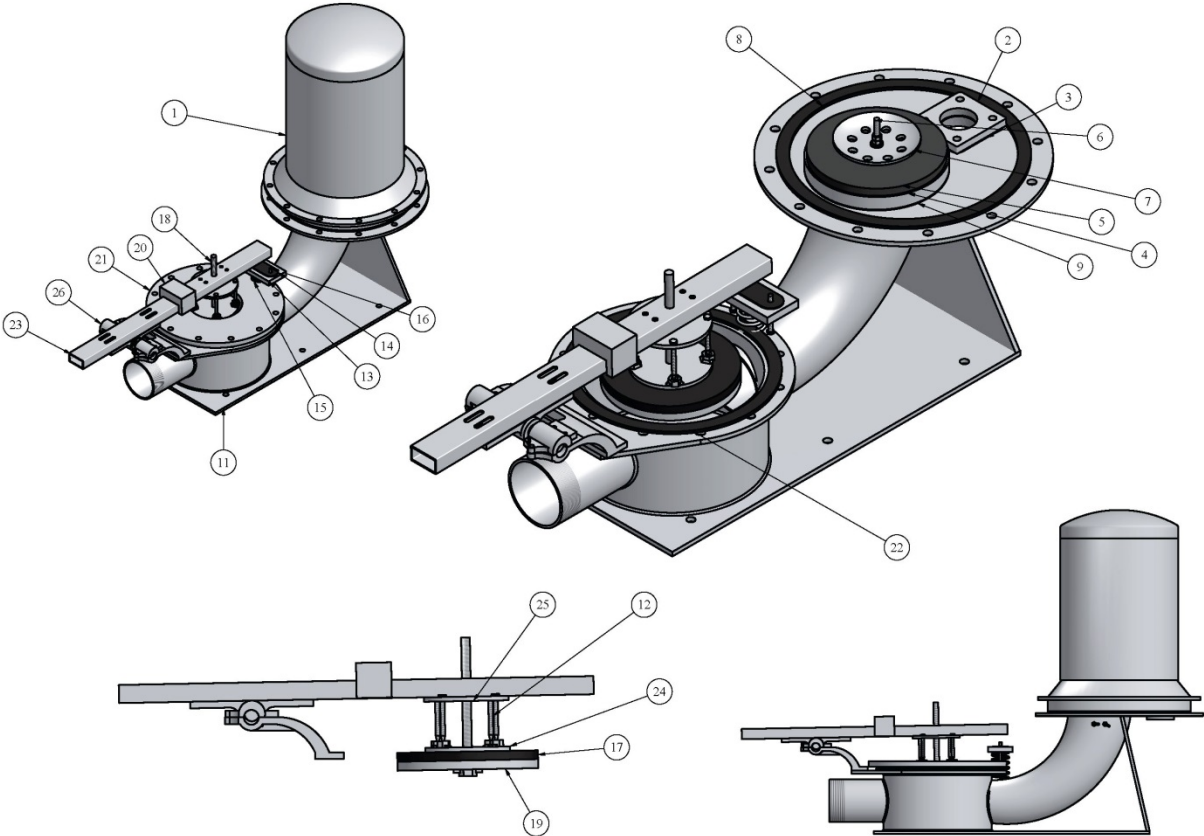


Fig. 13, Cross-section of the Ram Pump (Source, Rife Ram Pumps 2010 [12])

Part No.	Description	Part No.	Description
1	Air chamber (iron)	13	Lever rest studs (2) w/ nuts
2	Outlet flange	14	Lever rest & cushion
3	Outlet flange gasket	15	Lever rest spring
4	Gridiron	16	Lever rest bolts
5	Inside rubber valve	17	Outside rubber valve
6	Inside valve bolt w/ nuts	18	Outside valve center bolt
7	Inside valve washer	19	Lower washer
8	Air chamber gasket	20	Lever weight & bolts

9	Gridiron gasket	21	Valve chamber (iron)
10	Air feed valve body & pin	22	Valve chamber gasket
11	Base (iron)	23	Lever & bolts (2)
12	Adjusting pin (3)	25	Upper washer

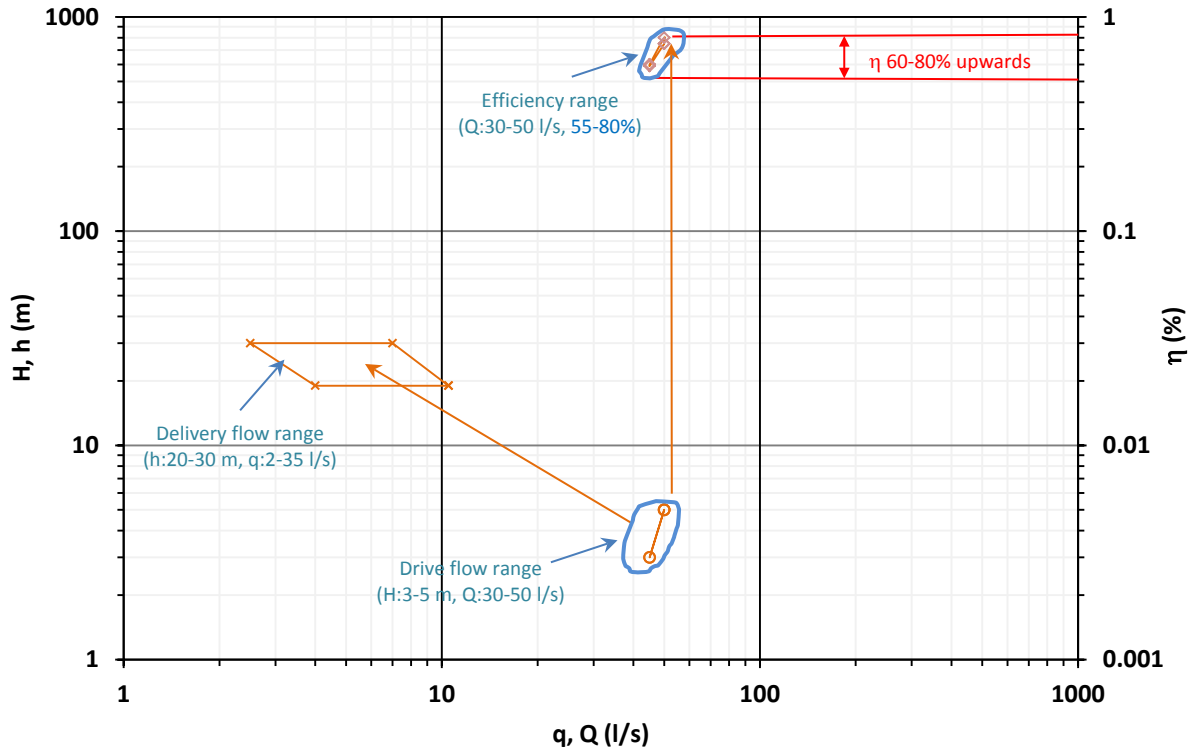


Fig. 14, Characteristics of the Ram Pump

3.4 Consolidated Characteristics of turbine pump based and ram pump based prototypes

The comparative study of the pump performance of the three types of prototypes have to be compared with respect to three parameters, which include the drive or turbine flow range, efficiency range and delivery or pump flow. These three parameters are represented in the form of zones in Fig. 15 and provide interesting revelations.

i) Drive or turbine flow range

Figure 15 shows that the drive flows between 55 l/s (maximum limit for ram pump) and 135 l/s (minimum limit of prototype 1) cannot be utilized by the entire system. Therefore, when the stream flow condition reaches flows more than 135 l/s, the ram pump should be shut off and prototype 1 started.

ii) Efficiency range

If the ram pump with 200 mm drive diameter were to behave exactly similar to the laboratory tested 50 mm drive diameter pump, then efficiency range of the ram pump with smaller flows is much beyond that of the two turbine prototypes. However, the ram pump supports only a drive flow of 45 to 55 l/s and turbine prototypes support drive flows from 135 l/s to 250 l/s.

This goes to prove that for lower flows a ram pump is more efficient and appropriate compared to a turbine pump, but at the same time for larger drive flows, the ram pump will become inherently too bulky and hence more compact models of turbine pumps would be preferred even if their efficiencies might be slightly lower.

iii) Delivery or pump flow range

The delivery flow is a direct result of drive flow and operating efficiency at different drive/delivery heads. The delivery zones of ramp pump and turbine prototype 2 are quite stable, but the zone for the prototype 1 is slightly skewed because of adjustable guide vane design.

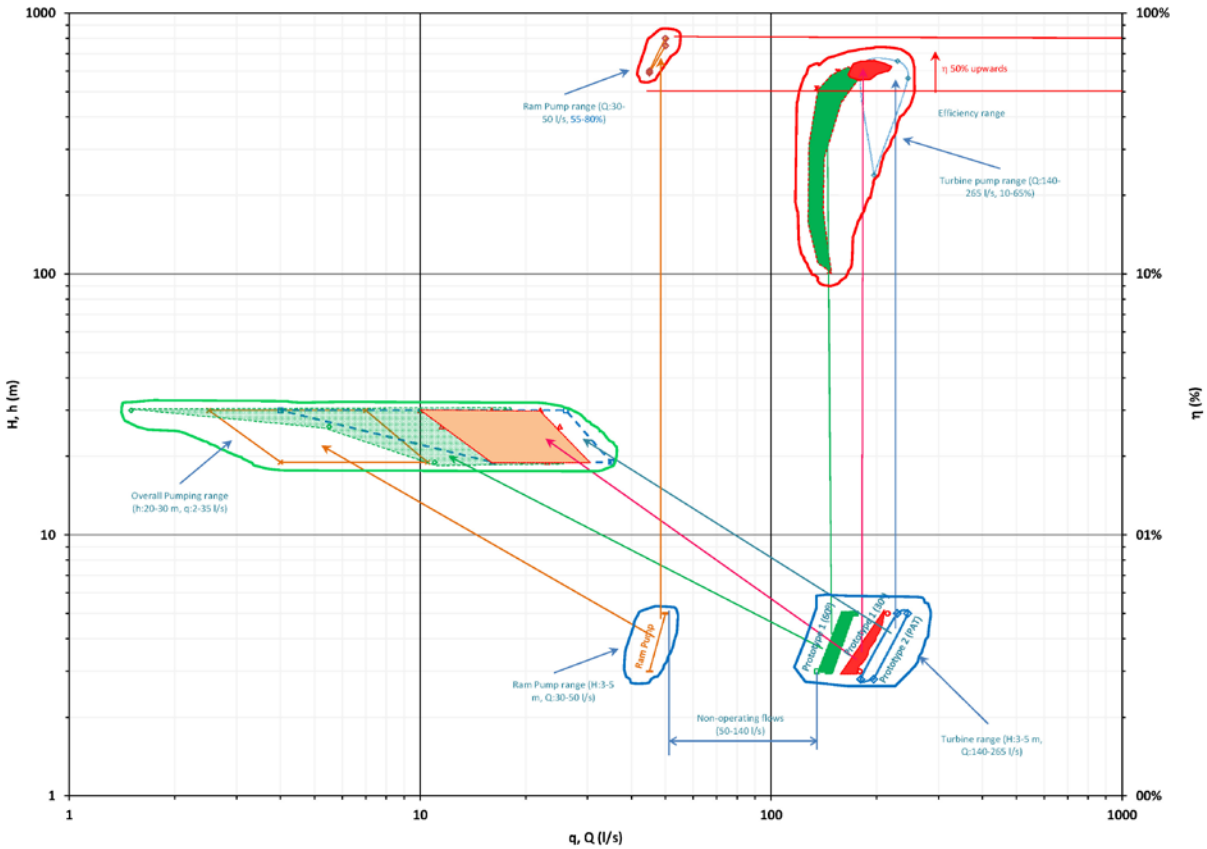


Fig. 15, Pump mode performance of turbine and ram action based prototypes

However, analyzing and interpreting based on simulated and theoretical results will not be of much significance until field validation is carried out.

3.5 Generator mode characteristics of Hydro turbine prototypes

3.5.1 Operational physics of variable speed controller

The electricity generation mode of the micro hydel pump is achieved with the help of a variable speed controller. The physics of a VSC system can be understood by configuration the Fig. 16, which allows for the turbine operating point to be altered based on the exactly load condition of the decentralized grid.

When the load changes the speed of the turbine changes at the first instant. This is used as an input variable to the controller that causes the synchronous speed of the generator to reach the corresponding level turbine condition (defined by a new flow and same or new head). This is done by the generator side controller’s electronics, while grid side’s electronics will ensure stable voltage and frequency. This action eliminates the need of a ballast load on the grid side.

The presence of a pulse-width modulator on the generator side causes appropriate changes the synchronous speed of the motor as seen in Fig. 16. The DC link between the generator side and grid side electronics ensures independent control mechanisms.

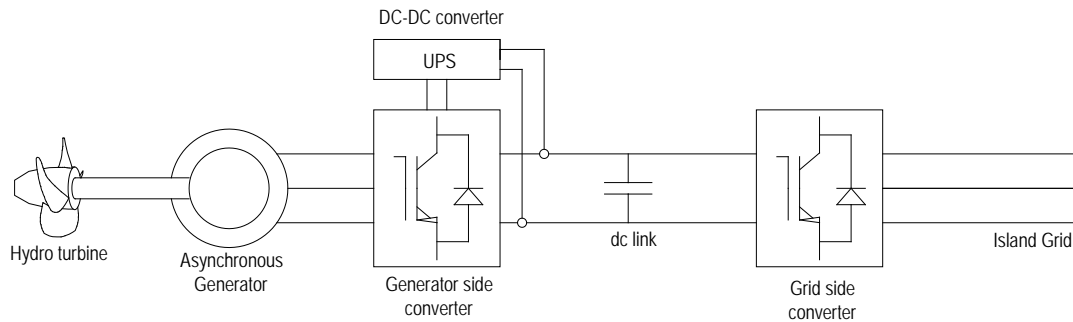


Fig. 16, Configuration of the variable speed full load controller

The asynchronous generator is a 4-pole stator for both the prototypes. The torque-speed characteristics at different synchronous speeds (and correspondingly induced voltages) at constant flux is presented in Fig. 17, 18 (for prototype 1) and 19 (prototype 2). The synchronous speeds are achieved by the frequency modulator of the grid-side converter, while the flux is controlled by the external UPS which supplies a constant reactive power.

3.5.2 Hydraulic behavior of Axial flow turbines in part-load and no-load regions

A peculiar, interesting and yet very important behavior of axial flow turbines (used in both the prototypes) is that operating region between no-load and BEP/max power lines is not only characterized by large speeds but also larger flows. This fact can be partly visualized in torque-speed curves of the respective axial turbines in Fig. 17, 18 and 19. The degree of speed-discharge increase varies depending on the overall turbine geometry (guide vane and propeller).

This behavior is in sharp contrast to radial/centrifugal turbine designs, where the flow reduces as the turbine enters the part-load and no-load region.

3.5.3 VSC operation with axial flow turbine in part-loads

The natural tendency of any turbine on losing load is to overspeed, while VSC's electronics follows this high speed and correspondingly discharge increases at the given head. In the context of Taipadar where stream flow is more or less fixed, the net flow rate ($Q_{\text{turbine}} - Q_{\text{stream}}$) would come into picture. If the net flow rate is negative the head on the turbine will shrink as there is very little storage upstream of the diversion weir, setting up hydraulic transients. The shrinking of head will proceed till a steady system is created with 'zero' net flow rate.

The time duration from unsteady to steady condition and behavior during the transient phase will depend on the system parameters (penstock volume, storage capacity ahead of the weir) along with the machine parameters. The transient behavior could even result in a runaway condition and would adversely impact the hydraulic, mechanical and electrical components.

This time interval cannot be predicted so easily, even though laboratory tests will give a reasonable idea to study the response characteristics. Hence, field trials are vital not only for validation of simulated results, but also for studying the above transient hydraulics at part-load. Section 4.4.2 provides additional information about the field and laboratory tests in power generation mode.

3.5.4 Generator characteristics of Prototype 1

The generator characteristics are intersected by constant head torque speed curves of the turbine along with a field of constant electric power points and maximum power lines. For the 30° gate setting (Fig. 6), the expected peak power is about 7.9 kWe at 5 m and 358 l/s with large speed of operation of about 3400 rpm. But, this condition can hardly met by the stream flow. The ideal point at 5 m head would be 7.5 kWe at lower speed of 2000 rpm and flow of 246 l/s. However, this point is in the overload region of the turbine characteristics.

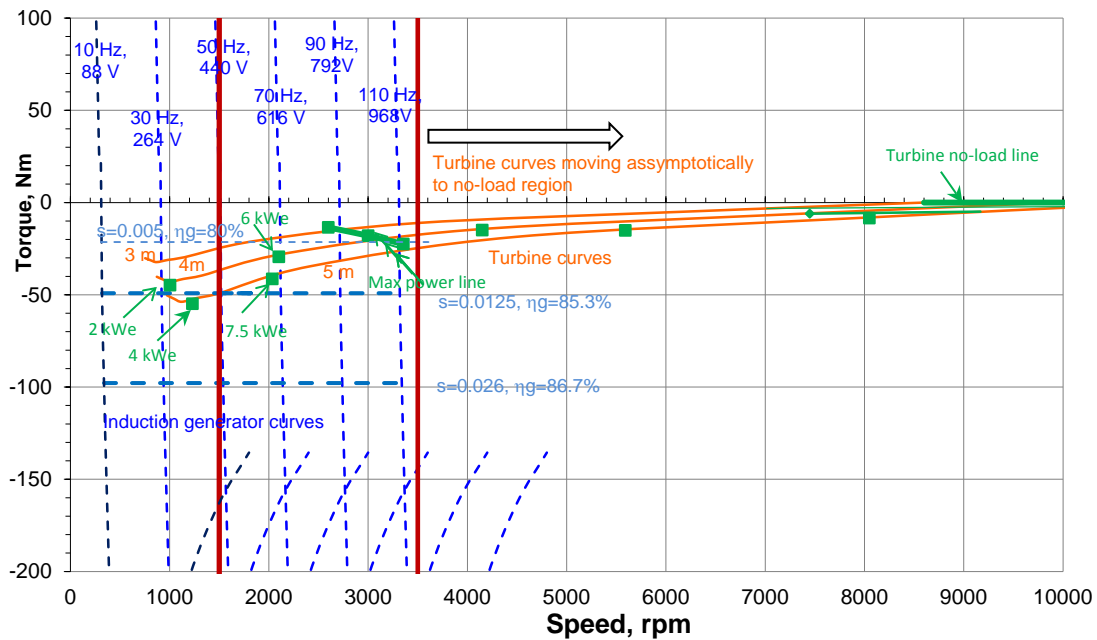


Fig. 17, Simulated characteristics of at 30 deg settings

For the 60° gate setting (as in Fig. 6), it can be seen that the peak power is only about 5.5 kWe at 5 m, 165 l/s and speed of 1409 rpm, which also in the overload region. The restricted flow area provided by the guide vanes results not only in lower power but also lower discharges at same heads.

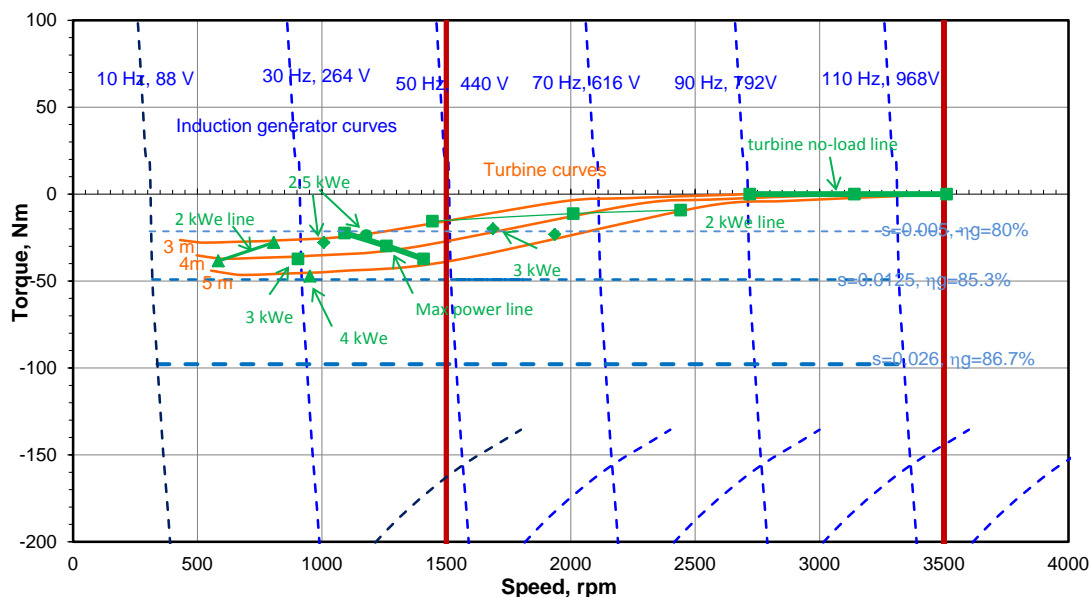


Fig. 18, Simulated characteristics at 60 deg setting

3.5.5 Generator characteristics of Prototype 2

Similar to the torque-speed characteristics in Prototype 1, the prototype 2 will also have same generator characteristics, but with different turbine head and power curves. Fig. 19 reveals the simulated results. The peak power of 8 kWe occurs at speed of 1750 rpm with turbine conditions at 5 m head and 250 l/s flow. Furthermore, the part-load condition of this fixed geometry turbine is also characterized by large speeds and flows at constant heads and hence appropriate safety system is required to be built in the controller architecture.

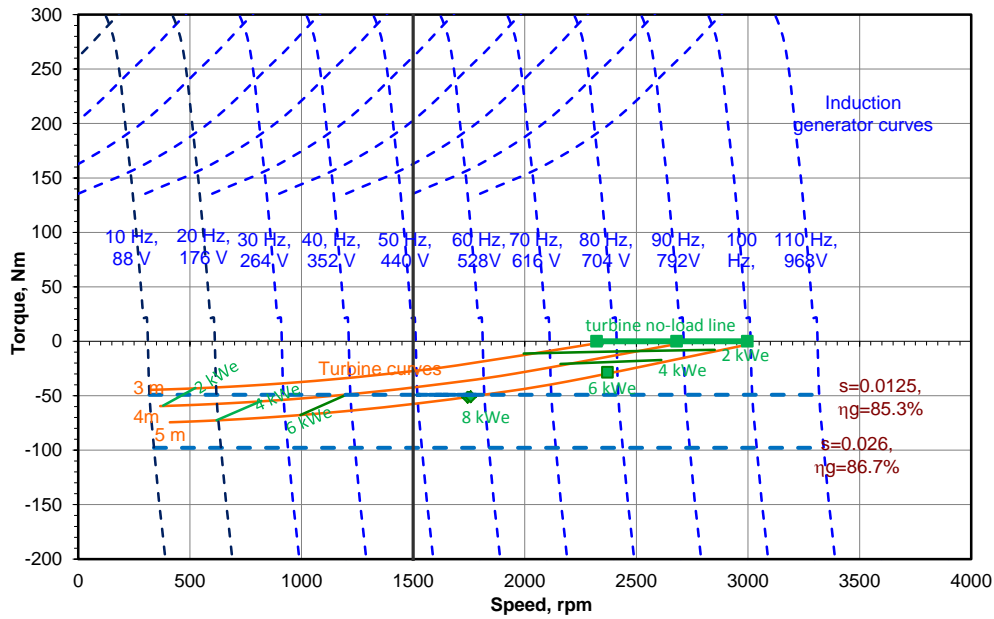


Fig. 19, Generator mode operation of prototype 2

4. Testrig Facility

The broad contour of a ‘field research station’ cannot include only instrumentation and associated inventory, but should encompass the civil infrastructure as well. Since this project is not solely a field station, but also a demonstration cum permanent facility for the village use, it should be looked from a different perspective, especially with respect the cost of the infrastructure components.

4.1 Civil and Hydraulic Structures

The project cost for all the three utilities have been summarized in Table 2. However, the authors have selectively chosen only those critical components from this list required to make the test-rig functional in terms of measurements, interpretation and analysis. The components and their respective costs are summarized in Table 3. It excludes long delivery lines of the turbine and ram pump prototypes, the expansive configuration of the control, transmission and distribution system. It also excludes the storage tanks, irrigation and drinking water supply systems.

Table 3, Infrastructure components of the test-rig

Sr. No.	Component	Sub-components	Cost (in Lakhs INR)
1	Diversion Weir	RCC work , Intake gates, silt flush out, railings, others	34
2	Penstock Line 1	750 mm pipe	44
3	Powerhouse	Foundation, embankments, other	32
4	Turbine Accessories	Manifold, valves on line 1 and 2, crane structure and others	25
5	Penstock Line 2	300 mm pipe with 400 mm standpipe	10
6	Generator side control room	Civil and associated works	2
Total			147

4.2 Measuring parameters and methods

The parameters of measurement for the two modes of operation for the prototypes along with their methods are summarized in Table 4. The financial aid required for setting up instrumentation is mainly associated with procurement pressure gauges and mechanical flow meters for delivery flow. The outflow through the prototypes is measured by weir arrangements that will be part of costing in respective civil infrastructure described in Table 3.

Table 4, Parameters for measurements on the prototypes

Testing Mode	Parameter	Location	Method of measurement
Pumping mode	Head	Turbine inlet head, H	Pressure Gauge
		Turbine pump delivery head, h	Pressure Gauge
		Ram pump inlet head, H	Stand pipe
	Flow	Ram pump delivery head, h	Pressure Gauge
		Turbine exit flow, Q	Overflow weir
		Pump flow, q	Mechanical flow meter
		Ram Pump waste/outlet flow, Q	Rectangular notch
	Ram Pump delivery flow, q	Mechanical flow meter	
Power Generation mode	Voltage	Generator terminals	Inbuild meter displays in control system
		Controller terminals (after AC-DC-AC)	Do
	Current	Load	External voltmeter
		Generator	Inbuild meter displays in control system
	Frequency	Load	External ammeter
		Generator	Inbuild meter displays in control system
		Load	Inbuild meter displays in control system
Active power	Load	do	
Power factor	Load	do	

The electrical measurements are a part of console of the control system being supplied with the ‘micro hydel pump’ prototypes by KIT. However, external load box will have to be arranged for power generation mode of testing.

Table 5, Cost estimates for instrumentation

Sr. No.	Instrument	Position	Cost estimate (in lakhs of INR)
1	Pressure gauge	Inlet of prototype 1	0.15
		Inlet of prototype 2	0.15
		Delivery of Prototype 1	0.15
		Delivery of Prototype 2	0.15
2	Mechanical flow meter	Delivery line of P1 and P2	2.5
		delivery line of Ram pump	2
3	Electric load box	Generator side VSD	0.5
		Total	5.6

4.3 Total Costs of Field Research Station

The infrastructure costs (Table 3) and the instrumentation costs (in Table 5) together would be required for making the test-rig functional. These costs are summarized in Table 6, which includes some unforeseen expenses, overheads. The total requirement for the Taipadar field and demonstration station will be about 160 lakhs.

Table 6, Overall costs of the testrig

Sr. No	Particulars	Cost (in lakhs of INR)
1	Infrastructure components	147
2	Instrumentation	5.6
	Sub-total	152.6
3	Overheads, unforeseen expenses and roundoff (@ca 5%)	7.4
	Total	160

4.4 Testing Protocols

The field testing protocol for the prototypes shall concentrate on the overall performance of the respective mode of operation, either the pumping or the electricity generation. As seen in Table 4, there is no room for the isolated torque measurement at the turbine shaft end. The objective of the field trials is to investigate and ensure smooth operation of the unit under different conditions. The conditions vary from short-term (trials over a few days to check parameters) and long-term (where trials will be monitored over a few months covering seasons).

While short-term trials will enable understand the range of each prototype, long-term monitoring will enable to choose from the different prototypes depending on the stream flow available. In addition, long-term testing will also help in identifying mechanical problems.

4.4.1 Pumping mode

a) Turbine based prototypes

The testing protocol will be same for both the prototypes. It would comprise of constant head maintained on the turbine inlet with varying flow, with varying head and flow conditions at the pump side. The head into the turbine will be controlled by the inlet valve, while the delivery valve on the pump side shall provide loading (no-load to full-load) to the turbine. Figure 20 illustrates the line diagram of the test setup and Table 6 gives a sample of garnering parameters for each constant head load test.

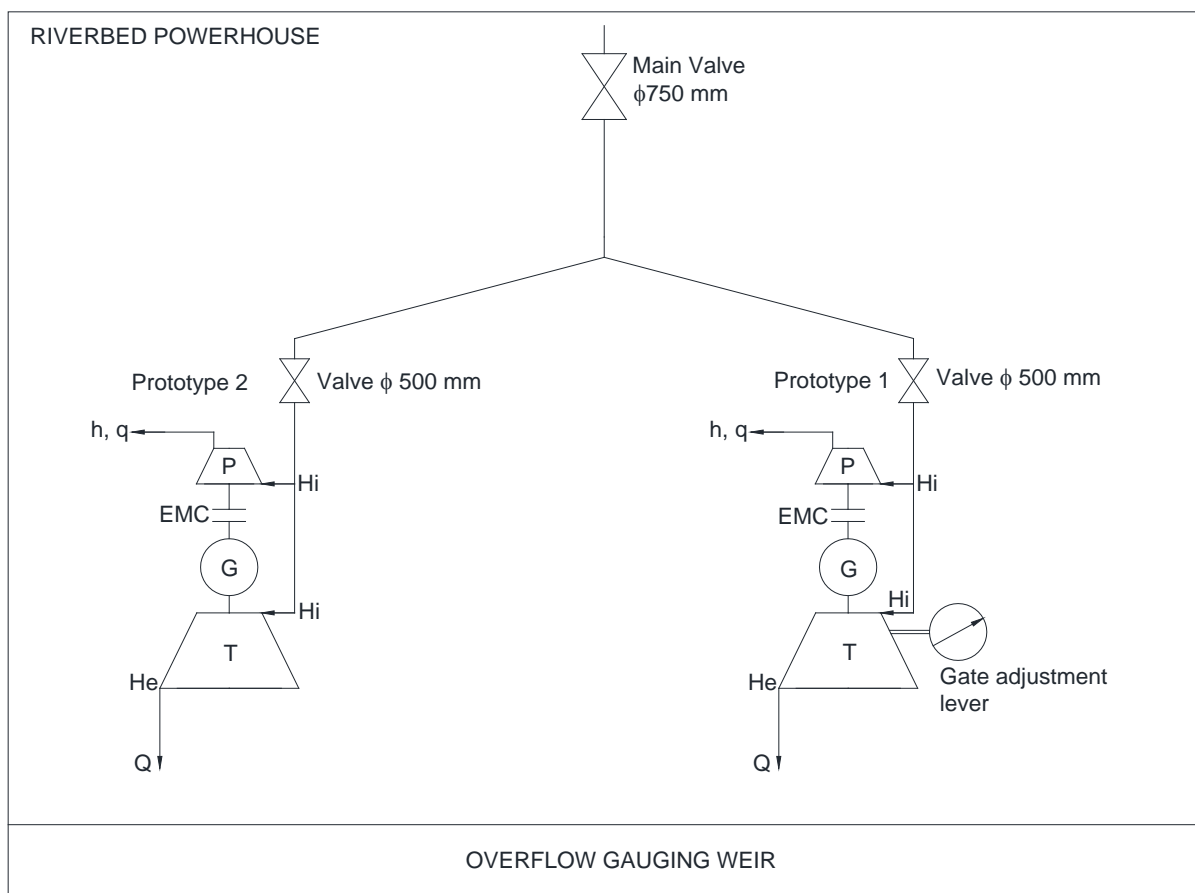


Fig. 20, Line diagram for testing the turbine prototypes

Table 6, Sample data acquisition table for pump mode testing of prototypes

Turbine Inlet Head (m)	Q (l/s)	h (m)	q (l/s)	N (rpm)
3 m	$Q_{3i=1}$			
	$Q_{3i=2}$			
	$Q_{3i=3}$			
	$Q_{3i=n}$			

4 m	$Q_{4i=1}$
	$Q_{4i=2}$
	$Q_{4i=3}$
	$Q_{4i=n}$
5 m	$Q_{5i=1}$
	$Q_{5i=2}$
	$Q_{5i=3}$
	$Q_{5i=n}$

b) Ram pump Prototypes

Unlike the turbine-pump based prototype, the Ram pump prototype will be subjected to tests at a single constant head (depending on the full reservoir level of the diversion weir). This is because of the inclusion of the 400 mm diameter standpipe behind the inlet valve, which will make it cumbersome (even if it is impossible) to vary the head to ram pump as shown in Fig. 21. Further, the tests on the Ram pump will be carried out a full-valve opening (gate/slucice type) while adjustments shall be focused on the outside or waste flow (beating) valve as illustrated below.

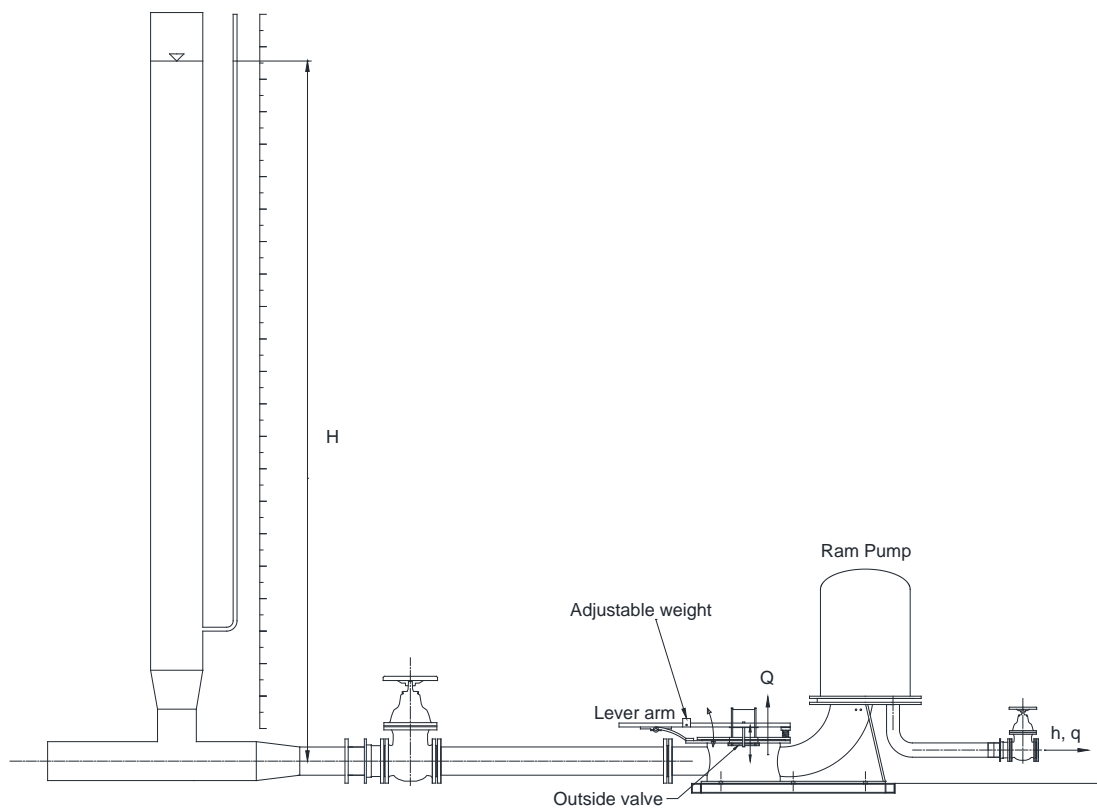


Fig. 21, Line diagram for testing the Ram pump prototype

i) Beat rate or stroke rate tests

This is first type of tests carried out by varying the position of the weight on the lever arm, which will create different torque on the lever arm and force on the reciprocating valve washer and rubber. This force will change the beating rate of the valve accordingly. High beat rate facilitates the lower waste flow and low beat rate allows for larger waste flow. Further, to varying the flow, the beat rate test is essential for the modifying the frequency at which the sound waves move across the system of drive pipe, pressure chamber and the delivery line (albeit to an extent).

The sample data collection chart is described in Table 7. For each stroke rate, the complete load test is accomplished by controlling the delivery valve on the outside of the pressure chamber.

Table 7, Data sampling for testing with various beat rates at constant head

Position of weight on the lever	beats/min	Q in l/s	q (l/s)	h (m)
a				
b				
c				
d				

ii) Stroke length tests

The stroke length is another form of varying the input flow to ram pump. Unlike the beat rate test in described earlier, this methodology can only change the area available for waste flow, but not the water hammer phenomena. Table 8 illustrates the parameter collection, which explains that each stroke length test is carried out under couple of beat rate tests.

Table 8, Data sampling table for stroke length test on the Ram pump

Stroke length, mm	Position weight on lever arm	beats/min	Q in l/s	q (l/s)	h (m)
L1	a				
	b				
	c				
	d				
L2	a				
	b				
	c				
	d				
L3	a				
	b				
	c				
	d				

4.4.2 Electricity generation mode

The power generation test will be carried out with the help of the control system cum console for all the electrical parameters listed in Table 4. Since, the transmission and distribution lines for the village would not be setup by the time of the field tests, a resistive load box will be used to perform the constant turbine head load test.

A line diagram of the electrical mode of testing is shown in Fig. 22. In addition, Table 9 shows the different parameters to be assimilated during each constant head test, include the hydraulic parameters namely flow and head on the turbine.

However, as mentioned in section 3.5.3, the field tests would have to study the hydraulic transients at part-loads in addition to endorsement of the performance at full-load. If the hydraulic transients take last longer than permissible limits of the machinery (runaway speed limits and penstock stability) then an alternative solution of maintaining speed with a traditional load diverter should be contemplated. Though this is a primitive solution and inefficient to certain extent, it is need for safety. The VSC will need additional interfaces relay ports to be activated a pre-set speed values.

It is important to note that the VSC, which itself acts as a load to turbine and the status of the connected UPS (that supplies reactive power to the generator) will define the base load on the turbine at all times. The value of this load can be further investigated in laboratory tests. This may be an inherent advantage to prevent no load on the turbine.

Laboratory tests

Since the hydro turbine based prototypes (prototype 1 and 2) will be tested both in generator and pump mode (section 3.1), these investigations should be comprehensive to study all possibilities of field conditions. Starting the prototypes in generator mode from pump mode (and vice versa) should

be attempted. Load should be varied to verify the transient response. It is important to point out that flow control to the prototype should not be attempted during the transient investigations. However, the condition of the feed pump driving the prototypes will be important to create a situation similar to that in the field. Hence, it will be desirable for the feed pump to operate at fixed flows at varying heads using its own VSC.

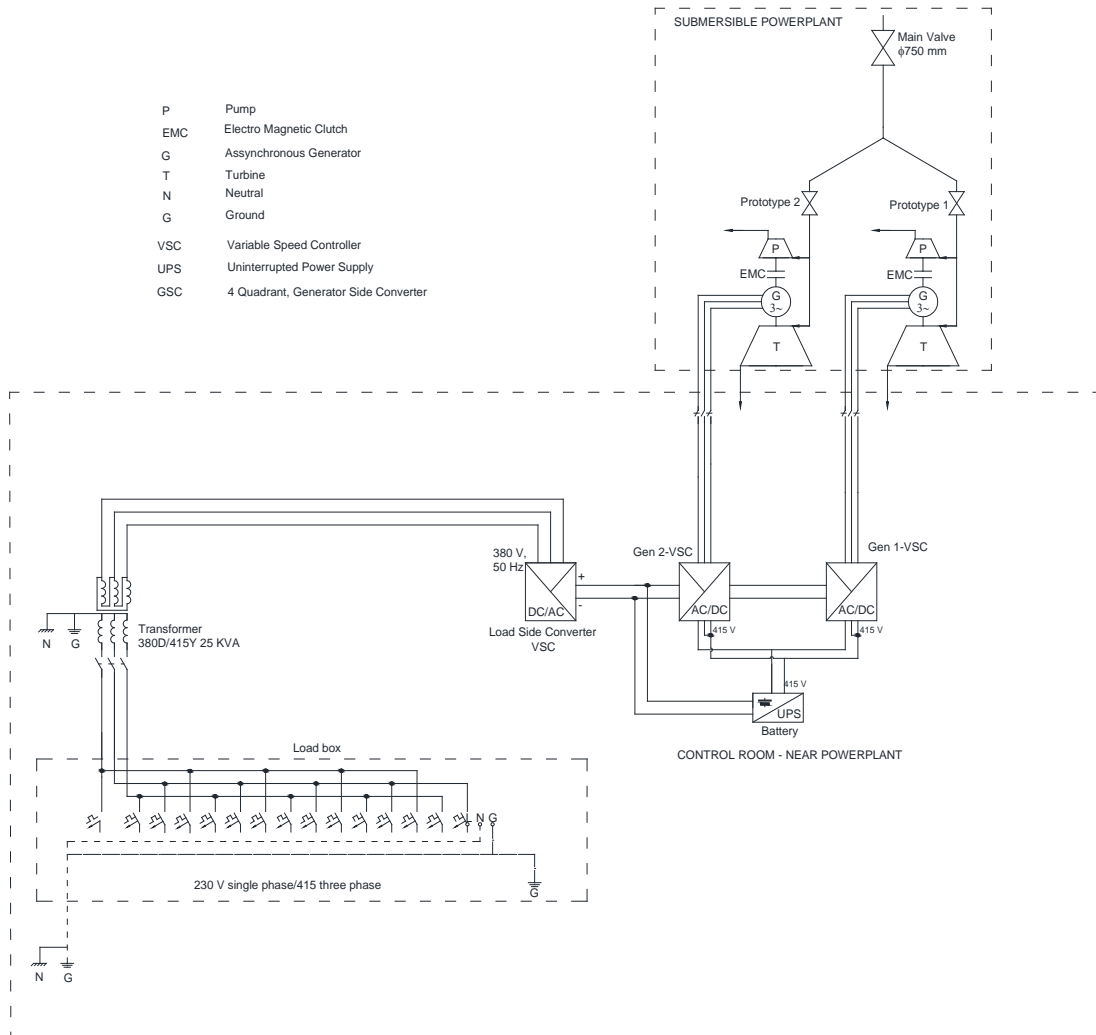


Fig. 22, Line diagram for load tests on the generator mode

Table 9, Electric load test on the asynchronous generator

Testing range	Hi	He	Q	N	f, Hz	Vgen	Igen	Pgen	Vload	Iload	Pload	pf
3 m												
4 m												
5 m												

5. Summary

The field research station exclusively for low head hydro powered devices can serve as a testing ground for better and more efficient prototypes other than the types proposed in this proposal. The modular foundation for the 3 prototypes will allow changeover without any changes to the civil and hydraulic structure of the project.

The two types of technologies though strongly advocated in this proposal as the most optimum solution may have certain deficiencies that will be known only after long-term evaluation and feedback from locals.

Notwithstanding the constraints imposed by low heads, the additional seasonal variation of flow poses severe design challenges especially for micro hydro capacities. This testrig on one hand shall provide answers for the level of technological flexibility and capability to be incorporated, and on the other hand shall provide a roadmap on using an improved age-old ram pump technology or for using modern turbine technology.

More importantly, two more aspects have to be considered. First, the treatment of a community based project as a field research station and second, the costs of setting it up. It may be slightly uncomfortable from the end-users point of view that they should be receiving a product that stills needs some amount of investigation and fine-tuning. This is true with any new technology and since most of the tests are short-term test, it would only for few days during which the system can be validated. The long-term tests will be more symbolic and most of the short-comings of the equipment can be verified in short duration tests.

The cost of the field research station is about 160 lakhs out of 499 lakhs required to set up all the utilities of the project. This large amount can be justified not only from the scientific and social perspective, but also from the environmental perspective. This because the concept of low head water pumping is using the effluent stream flow without tampering with the ground water table and secondly the low head scenario rules out storage and causes minimum harm to the forest's green cover.

6. References

- [1] 'Detailed Project Report, Edition- 2.2, Taipadar Micro Hydro and Water Resources Management Project (Power, Irrigation and Drinking Water Supply Utilities)', Dr. Punit Singh Associates, A Submission to MNRE and CREDA, 2014
- [2] Punit Singh, Franz Nestmann, 'Experimental optimization of a free vortex propeller runner for micro hydro application', *Experimental Thermal and Fluid Science*, Vol. 33, 2009
- [3] Punit Singh, Fran Nestmann, 'Influence of the Blade Hub Geometry on the Performance of Low-Head Axial Flow Turbines', *Energy Engineering*, September 2012
- [4] Punit Singh, Franz Nestmann, 'Exit blade geometry and part-load performance of small axial flow propeller turbines: An experimental investigation', *Experimental Thermal and Fluid Science*, Vol. 34, 2010
- [5] Punit Singh, Franz Nestmann, 'Experimental investigation of the influence of blade height and blade number on the performance of low head axial flow turbines', *Renewable Energy*, Vol. 36, 2011
- [6] Miroslav Neschleba, 'HYDRAULIC TURBINES Their Design and Equipment', ART IA Prague, Czech Republic, 1957
- [7] P de Jong, 'Hydraulic Rams - Consumers Guide', Delft University of Technology, Netherlands, 1988
- [8] JHPM Tacke, 'Hydraulic Rams - A Comparative Investigation' Communication on hydraulic and geotechnical engineering, Delft University of Technology, Netherlands, 1988
- [9] Technological Development Unit, 'Comparison between DTU and Commercial Hydraulic Ram Pump Performance', Working Paper No. 33, Warwick University, 1992

-
- [10] H N Najm, P H Azoury, M Piasecki, Hydraulic ram analysis: a new look at an old problem, Proceedings of the Institution of Mechanical Engineers, Part A: Journal of Power and Energy 1999 213: 127
- [11] Veljko Filipan, Zdravko Virag, Anton Bergant, Mathematical Modelling of a Hydraulic Ram Pump System, Journal of Mechanical Engineering 49(2003)3,137-149
- [12] Rife Hydraulic Engines, 'Universal Heavy Duty Ram pumps – Owner's guide', Nanticoke, PA, USA, 2014, www.riferam.com

7. Nomenclature

EMC	Electromagnetic coupling
f	frequency, hz
G	Generator
h	Delivery or pump head, m
H	Drive or turbine head, m
H _e	Exit turbine head, m
H _i	Inlet turbine head, m
I	Current, amps
N	Rotational speed, rpm
pf	power factor
P	Power, watts
P	Pump
q	Delivery or pump flow, l/s
Q	Drive of turbine flow, l/s
T	Turbine
UPS	Uninterrupted Power Supply
V	Voltage, volts
VSC	Variable Speed Controller

5.6 PROJECT REPORTS

[20] Punit Singh, Taipadar Micro Hydro and Water Resources Management Project (Power, Irrigation and Drinking Water Supply Utilities), 2014

[21] Punit Singh, Mylasandra Hydro Energy Recovery Project, 2013

DETAILED PROJECT REPORT

EDITION – 2.2

Taipadar Micro Hydro and Water Resources Management Project

(Power, Irrigation and Drinking Water Supply Utilities)

**Prepared by
Dr. Punit Singh**

September 2014

Table of Contents

Executive Summary	4
Chapter 1 – Introduction.....	6
1.1 Power Scenario.....	6
1.2 Micro Hydro and the Decentralized Sector	6
1.3 Taipadar Village and Inhabitants	7
1.4 Primary needs of the village	8
1.4 A solution to meet the requirements of the village	8
Chapter 2 – Location, Catchment Area and the Scheme.....	10
2.1 Location of the Project	10
2.2 Catchment Area.....	10
2.3 Features of the Scheme.....	10
Chapter 3 – Surveys and Investigation.....	12
3.1 Topographic Studies	12
3.2 Village and Community Survey.....	12
3.3 Historical Structures and Environment	15
Chapter 4 – Hydrology	16
4.1 General	16
4.2 Flow Duration Studies	16
4.3 Flood Studies	17
Chapter 5 – Power and Energy Studies	19
5.1 System Design – Module Configuration	19
5.2 Power and Energy Duration Curves.....	20
Chapter 6 – Irrigation and Drinking Water Studies.....	21
6.1 Drinking Water Requirements.....	21
6.2 Irrigation Planning	21
6.2.4 Turbine Pumps versus Ram Pump	22
Chapter 7 – Civil Works, Hydro Mechanical Equipment and Construction Materials.....	24
7.1 Civil Structures:.....	24
7.2 Hydro-Mechanical Equipment.....	31
7.3 Construction Materials	31
Chapter 8 – Electromechanical Equipment and Power Evacuation	32
8.1 Rotating Machinery – The Module ‘Micro Hydel Pump’	32
8.2 Ram Pump	37
8.3 Control System	38
8.4 Power Evacuation	39
Chapter 9 – Environment Impacts and Benefits	40
9.1 General Aspects.....	40
9.2 Impact Assessment.....	40
9.3 The Concept of Limited Growth and Environmental Sustainability	42
Chapter 10 – Cost Estimates.....	43
10.1 Abstract of Total Project Costs	43
10.2 Utility-wise distribution of costs.....	43
Chapter 11 – Financial Studies	45
11.1 Economic Value from Benefits	45
11.2 Cost-Benefit Analysis	45
11.3 Larger Aspects of Benefits – Societal Perspective	46
Chapter 12 - Project Implementation Phases.....	47
12.1 Introduction.....	47

12.2 Overview of the Taipadar Project – Components, Cost and Phases of Implementation	48
12.3 Utility-wise distribution of project costs	49
12.4 Implementation Phases of Taipadar Project	50
12.5 Flow Chart for Phase 1 – Hydropower and Irrigation	51
12.6 Planning chart for Phase 1	52
Chapter 13 – Project Management.....	53
13.1 Organization Chart	53
13.2 Constructional Programme	54
13.3 Additional Responsibilities of Implementing Agency	54
Chapter 14 – Future Investigations and Actions.....	55
14.1 Hydrology and Flood Prediction	55
14.2 Geo-technical Studies	55
14.3 Other Investigations	55
14.4 An Independent Economic Study	55
14.5 Other Significant Actions	55
Chapter 15 – Project Overview and Conclusion	56
Nomenclature	57
References	58
Annexure	59
A1 Project at a Glance	59
A2 Salient Features.....	60
A3 Detailed Cost Estimates.....	63
A3 Project Implementation Schedule.....	70
A4 Project Completion Schedule.....	70
A5 Operation and Maintenance cost for 5 years	70
A6 Civil Layouts.....	71

Executive Summary

1. The Promoters and Project

The KSB Foundation, the one of promoter of the Taipadar project is an independent trust based in Germany. The Foundation is supporting the design, manufacture and testing of the rotating machinery. It is also morally supporting the implementation of an integrated (or hybrid) hydro project catering to 3 essential utilities required for human survival namely, drinking water, irrigation and electricity, all of which require more promoters.

The Taipadar project is both renewable and decentralized in nature, aimed at meeting the requirements and provides for growth of a local community in an environmentally sustainable way.

2. Purpose and scope of the DPR

The purpose of the DPR is to study, evaluate and establish the technical feasibility, economic viability along with environmental impacts and sustainability of this proposed project.

The scope of the reports covers the following,

- i. Review and analyze the topography, hydrology, hydraulic and other field parameters along with the requirements of the community.
- ii. Formulation of the alternatives for the water conductor system for the hydro project, irrigation project and drinking water projects respectively that will include pipes, canals and hydro mechanical systems.
- iii. To carry out power, energy, irrigation and drinking water studies to determine the optimum capacity of the scheme and the respective annual generation.
- iv. Selection of the type, number and capacity of the turbine, generator and pump units.
- v. Details of the hydro system covering the civil, mechanical and electrical aspects.
- vi. Details of the irrigation project comprising of tank, main conductor (canals/pipes), branch conductor and field channels.
- vii. Drinking water system covering the treatment tank, supply and distribution lines.
- viii. General layout drawings, project estimates and financial studies.
- ix. Environmental impact assessment studies with a holistic and accurate benefit analysis covering the ecological, social and economic aspects.
- x. Implementation schedule

3. The Stream and Basin

The Taipadar project is planned across a stream named Ganeshbahar Nala, which has an effective length of 19 km and flowing south to become a tributary to River Shabari in the Jagdalpur district of Chhattisgarh State. The Ganeshbahar Nala is an effluent stream (primarily supported by the ground water flow) and part of a river basin situated in the Tiriya reserve forest. Taipadar is one of the 5 settlements of this forest river basin.

4. Hydrology of the Project

The basin of the Ganeshbahar Nala and local catchment area of the proposed project is sandwiched between the Indravathi River basin towards the north and Shabari basin in the south. The stream is perennial in nature and as mentioned it is primarily supported by the water table of the forest river basin that receives both southwest and northeast monsoon. There are smaller tributaries to Ganeshbahar Nala, however inflow from these tributaries is minimal and available only during 4 to 6 months a year.

The peak flow in the stream during monsoon goes beyond 1000 l/s and the minimal available flow is about 100 l/s. The estimated flood flow is between 150 and 250 m³/s.

5. Power and Energy Studies

The basis of the power and energy studies is the flow duration curve that is determined with the help of a measurement weir constructed across the stream. The design head is 5 meters with a peak design flow of 465 l/s and lean flow of 95 l/s respectively. It is found that the monthly variation of flow can be optimally used by 2 units of 6 and 8.0 kWe respectively. The annual generation of energy for 8 hours of operation per day (remaining time for pumping) is found to be 18650 kWh.

6. Irrigation and Drinking Water Studies

The total drinking water requirement for the Taiapadar community with 200 litres per day per head is determined to be 45 m³ per day.

The pump module (two turbine pumps and one ram pump) can pump between 6 and 30 l/s for a net pumping head of 24 meters. The annual pumping volume for irrigation is 51060 mm.Ha with daily availability of water that varying

from 30 mm.Ha in lean season to 265 mm.Ha in peak flows, which is sufficient for an irrigation capacity between 8 ha and 34 ha respectively.

An irrigation yield study based on the crop cultivation model proposed by the villagers is carried out, which estimates 100 quintals of paddy yield, 97 quintals of wheat and 9 quintals of mustard seeds in a year.

7. Mechanical Equipment

In order to accomplish the electricity and water pumping, a compact and encapsulated unit known as the micro hydel pump (also known as turbine pump module) is conceptualized. It encloses a hydro turbine unit directly coupled to an electric generator and a pump which is placed at the rear side of the generator separated by an electromagnetic coupling that can be engaged and disengaged depending on electricity or water pumping modes of operation. There are 2 prototypes of different capacities planned for the optimum utilization of available flow.

The second type of pumping module is based on the principle of water hammer (ram pump), especially for lean flow seasons since the two prototypes (turbine pumps) are designed for flows greater than 120 l/s. The present ram pump chosen is off-the-shelf and designed to handle flows between 40 and 50 l/s. However, the ram pump is exclusively for pumping and cannot generate electricity like the micro hydel pump module.

8. Power Evacuation

The power distribution is planned for the individual households (32 in number), a school along with two newly planned utility centers for building additional value. One of the utility centers comprises of multiple equipment needed for agriculture and food processing (flourmill, dehusking machines and other low capacity machinery as per requirement and available power). The second utility center is called the computer and mass media center where the youth and others in the community can gather for education, resource sharing and entertainment.

The households and the media center will have 230V single phase connection, while the machinery center will be supplied with 415V, 3 phase electricity.

9. Estimates of Project Costs

The quantity estimates of civil works for the power, irrigation and drinking water supply projects are based on the project layout finalized after carefully optimization. The rates are based on the latest version of KPCL schedule of rates. The cost of electromechanical and power evacuation equipment is based on the budgetary offers and quotes from various suppliers. The estimated project cost is found to be nearly 59900000 INR (ca 750000 Euros).

10. Financial Studies

The financial studies are carried out at two levels. Firstly the economic value from benefits (electricity, irrigation yield and drinking water) is determined based on prevailing national average rates, which is comes up to nearly 4850000 INR (60600 euros) annually.

In the second level the cost-benefits analysis is carried out with determination of economic parameters like annual costs, net income, net present value of income for a nominal discount rate of 5 % and life of 20 years. Currently, the net income (present value) is less than the net annual cost indicating a loss.

11. Implementation Schedule

The implementation will be carried out in 3 phases after achieving financial closure of the project. The first phase dedicated for irrigation utility will require an additional 347 lakhs (434000 Euro) since 100 lakhs (125000 Euro) is already sanctioned by one of promoters, KSB Foundation. The Phase 2 for electricity supply utility and Phase 3 for drinking water utility need 118 lakhs (147500 Euro) and 30 lakhs (37500) respectively.

The financial closure for Phase 1 is expected between July and October 2014 and it would approximately take 9 months to commission the project (July 2015).

12. Recommendation

There is a need to pursue investigation pertaining to accurate flood flow determination and geo-technical studies. The detailed engineering study should follow as quickly as possible so that the consultants can release the final drawings to the contractors in time. Above all, the implementing agency needs to make a sincere effort for arranging funds from interested promoters as soon as possible.

13. Environmental, Economic and Societal Impact – Project Rationale

The Taipadar project not only meets the basic environmental norms, but creates an interdependence between sustenance of forest ecology with the livelihood of people with a distinguishing attribute comprising of a defined limit for benefits and growth above which the project cannot be scaled up to overuse any of the resources.

Chapter 1 – Introduction

1.1 Power Scenario

The task of building a national economy to a large extent depends on the development and conservation of the nation's water and land resources. Water resources development, pervading as it does, in most phases of economic activity has some influence on almost every aspect of national economic interest. Thus the coordinated development of water resources has direct and immediate effect on agricultural and forest activities, and vice versa.

India is a land of villages and agriculture is the predominant economic activity in Indian villages. Irrigation, which has emerged as the most important factor in improvement of standard of life, has therefore, an impact on social conditions and economic prosperity. The distributions in growth of food and energy in various regions are unequal. Important regions supporting 40% of the country's population are short in food grains and energy supply. These regions can get their requirement of energy from natural and renewable resources such as water, wind and sun shine only.

It must be remembered that thermal power production requires burning of fossil fuels, which affect the environment adversely. Moreover India has to import the fuel to meet the thermal power needs at a huge cost. Therefore Hydropower which is at present given less priority has to receive its due share in the overall power scenario in the country. With the estimated total Hydro power potential of the country at 1,35,000 MW, major power needs of the country can be met from Hydel power which is renewable, non-polluting, reliable as well as the cheapest form of energy. Integrated water planning and management, based on comprehensive ecosystem assessment taking full account of the use of water in human activities should therefore be the main 'Principle' behind environmentally sound, sustainable development and management of water resources.

The role of Small/Mini/Micro hydel Projects as an attempt to supplement energy generation is well-accepted fact today. Development of small Hydel has been taking place steadily since its first Hydel installation of 130 kW at Darjeeling in 1897. In Northern India in the hilly areas of Himalayan region, Vindhyan region of central India, East & West Coast hilly region along the sea perennial streams with small discharges are available which can be harnessed for power generation.

In the plains the large irrigation system where there are small drops in the canals having considerable discharges can also be harnessed for power generation. Thus there are two distinctive categories in the development in small Hydel in India. Developments of both these are taking place side by side. Government of India has recognized the importance of small Hydel and has included it as one of the items under the 20-point program. The Government had duly notified all the authorities in the country that while planning irrigation systems incidence of small falls in the course of the canals should be considered for development of power and necessary provisions for its development are included in the project reports.

Also India is committed to extensive rural electrification to bring social justice to all the people in the country, especially those residing in remote and far-flung villages to which it is difficult and uneconomical to provide electricity by distribution network. This policy has brought greater attention for the development of small Hydel Schemes. In almost all States a large number of small Hydel schemes are under investigation and a number of projects have been commissioned and power pumped to the Grid.

To develop small Hydro projects Govt. has liberalized the policies for attracting private investment in the power sector. Some State Governments have also decided to introduce reforms and restructure their power supply industry to make it more efficient and economical. This support of government for hydro projects which are grid-connected have drawn private developers to own, operate and sell electricity to local energy supply companies at favorable rates.

1.2 Micro Hydro and the Decentralized Sector

However all these positive vibes of Government interest and support, the micro hydro and decentralized projects have not attracted private players because of high investment costs compared to the returns. These projects are supported by grants but such models are hardly successful. These projects are seen as social commitments are classified as non-profitable by industry. Therefore, such projects are very few, a handful of them have been developed by villagers using low technology themselves and some NGOs. The challenge really lies in making a successful business model for decentralized projects similar to that of Taipadar.

There is acute shortage of electric power generation in the country so much so that the areas already connected to the power grids are subjected to frequent power cuts. The available fuel resources being used for electricity generation are getting fast depleted. This problem and sensitivity coupled with erecting the electric power lines through deep forest, the cost involved in extending power grids and cost & problems in O & M of the line in the

isolated remote villages make it almost impossible for electricity to reach the far flung in accessible and remote villages.

The economic and social conditions of inhabitants of un-electrified remote villages in the state of Chhattisgarh is quite depressive, more so in the tribal populated most backward districts of the State. Electricity being one of the basic infrastructure requirements for development and progress, the only hope in the above scenario is the use of renewable energy sources to generate and supply electricity to remote villages for providing lighting, motive power, creating lift irrigation facility and providing drinking water supply to inhabitants.

In an effort towards the above objective, the Taipadar project has been conceived for immediate electrification of the most backward Taipadar village in Bastar region of Chhattisgarh state, creating sustainable lift irrigation facilities and providing potable water for about 32 tribal family settlements in the village.

1.3 Taipadar Village and Inhabitants

The Taipadar village is situated 51 km east of Jagdalpur city, which is part of the Bastar region of the Chhattisgarh state of the Indian Republic. Taipadar is one of the five tribal settlements in the Tiriya Reserve forest under the Machkot range that is part of the Shabari (or Kolab) river basin. These settlements have come up nearly 200 years ago according to information.

Amongst the five settlements, there are three settlements (Kavalpal, Taipadar and Tiriya), which are on the western banks of Ganeshbahar Nala, a perennial stream that is a tributary to Shabari river as seen in Fig. 1.1. The perennial characteristic of the Ganeshbahar Nala is predominately a resultant of groundwater flow dynamics of the forest river basin (as will be described later in Chapter 4 – Hydrology) and hence qualifying it as an effluent type.

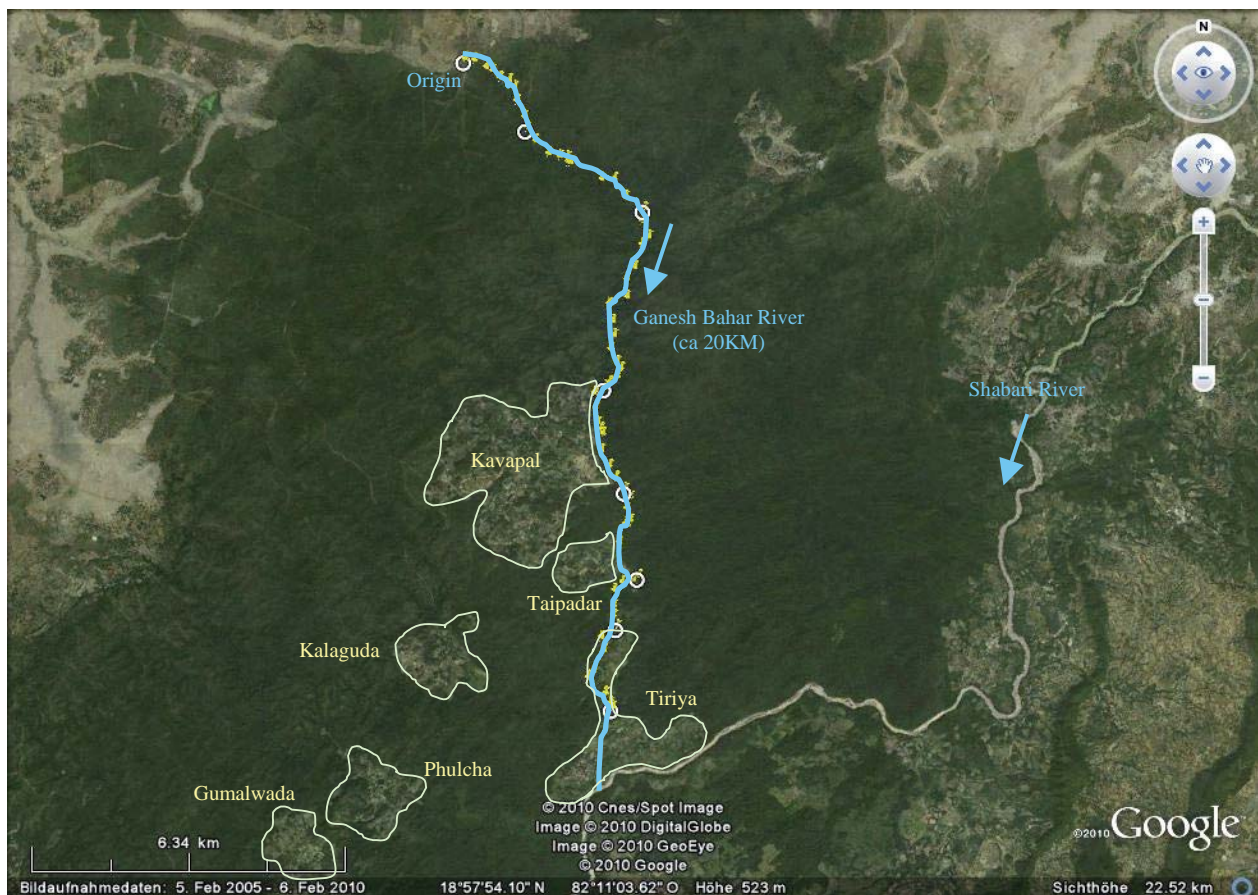


Fig 1.1, Taipadar village in Shabari River Basin

The village comprises of 32 households having a population of approximately 180. Agriculture is the main occupation of the population, which is completely dependent on monsoons. They cultivate mainly paddy with some pulses and very few seeds (described in section 3.2, Chapter 3) during the Kharif season from southwest monsoon (July to October) of the subcontinent's monsoon calendar. The agricultural activity slows down during the Rabi season (between November and February) arising from northeast monsoon.

The stream flow of Ganeshbahar Nala is not being utilized for cultivation since the all the five settlements including Taipadar are not connected with grid electricity. The population (both men and women) are involved for 65% to 70% of year in various activities relating to cultivation (in section 3.2, Chapter 3). During the remaining period of the year

they are work as contract laborers in construction, road repair and other manual works in nearby towns. There is however no guarantee of these kind of external jobs.

The socioeconomic condition of Taipadar village is bad with a per capita income of a household (with 5 to 6 members) is less than 1500 USD (ca 48000 USD for 32 households), equivalent to 75 cents per day per head. This is far below the international economic benchmark of 1.25 USD per day per head that determines the poverty line.

The per capita income of the village is about 240 USD is marginal compared to the national average of 1370 USD [1] provided by World Economic Outlook, which clearly shows underlining poverty situation in Taipadar.

The tribal population of Taipadar is classified under the scheduled tribe category under the Indian law and the state government of Chhattisgarh provides subsidized grains to each family (30 kg rice at 2 INR/kg, 2 kg chickpeas at 10 INR/kg and 2 kg of free iodized salt). The village has a government primary school (until grade 4) with a single teacher. There is no hospital facility in the village. The nearest dispensary is located in Tiriya village. However, for major health issues people have to travel to Jagdalpur.

The communication systems also remain very poor for the village. The blacktopped road ends 24 km prior to the village, which is a manmade cart track and motorable only during dry season. Further to this there is no telecommunication facility including signal waves for mobile network. They have to travel at least 35 km outside to get a reliable mobile network area.

Over generations, this tribal community has converted some parts of the forestland for agriculture. They also use dried wood abundant widely in the forest for cooking purposes. Some of the agricultural lands have land records and some of parts are in the process of being regularized by forest and government authorities. As see from Table 3.3, in section 3.2, Chapter 3, there 32 landowners who own 107 bits or pieces of land having a total cultivable area of 199.5 acres (ca 80.7 Ha) out of which 107 acres (43.3 Ha) have land records and remaining 92.5 acres (37.4 Ha) have to authenticated by the government.

The drinking water requirement is fulfilled from hand pumps at 2 different locations of the village. The women folk are generally responsible for filling and bringing the water back home. There are no toilets or bathing facilities at homes. This water conserved and essentially is used mainly for cooking and drinking. Bathing and washing is done in the stream itself.

The village has a decentralized lighting arrangement using solar photovoltaic panels, which was implemented few years back by a Government agency. It provides for lighting only during early morning and night hours. It is being maintained by young local boys who have been trained from the agency.

1.4 Primary needs of the village

Given the above background and various village meetings conducted (Table 3.4, Chapter 3), the primary requirement of the community can be summarized as follows.

- i. Providing water for irrigation during the Rabi season
- ii. Water supply for irrigation when monsoons fail (there has been a drought in the Indian subcontinent 3 times in the last 10 years)
- iii. Additional water supply in Kharif season even during normal monsoons. The villagers have expressed their desire to more area of paddy since the available rainfall accommodates only 60% of cultivable area.
- iv. Motive power of agricultural related activities like dehusking of paddy. This is currently done manually using traditional methods and is a labour intensive activity carried out again by the women folk. They would also welcome motive power for flour milling, small scale food processing and other farming related operations.
- v. They would also like some electricity for educational requirements like audio-visual and computer training. A community center with television and others facilities that add some entertainment value to their lives during free time has been recommended.
- vi. In addition to all this, the women folk in particular have requested the supply of potable water to homes because they can be saved from the labour required and time consumed in bringing the water.

The above needs shall certainly contribute in improving the quality standards of their lives and shall give them dignity.

1.4 A solution to meet the requirements of the village

The goal of the promoters would be implement an ecologically acceptable, renewable, decentralized and innovative engineering solution that will create interdependence between the forest river basin and the solution itself, which will help in meeting the needs of a human society living within this forest river basin.

The engineering solution should comprise of run-off-river type of hydro project, which will prevent any kind of submergence of the forestland. The solution should further include submersible (underwater application)

hydropower station within the riverbed that will involve no powerhouse construction causing minimum loss to the forest cover.

The innovative part of the solution should be to combine electricity generation and water pumping from the same location using an integrated device. This innovation would result in a ‘critical’ interdependence factor between the forest basin and the solution because it has been established through surveys and investigations (Chapter 3) that the river flow is solely supported by the forest water table. This will cause the solution to essentially use the water from the river flow that is not needed by the forest.

If we were to conceive an idea with only an electricity generation solution and encourage groundwater usage for water management (irrigation and drinking water), we would be depriving the forest of vital support system required for its sustenance and this would gradually result in disturbing the forest ecology over time. In turn it would have cascading affects the characteristics of the river flow and subsequently on the performance of the hydropower station (or engineering solution).

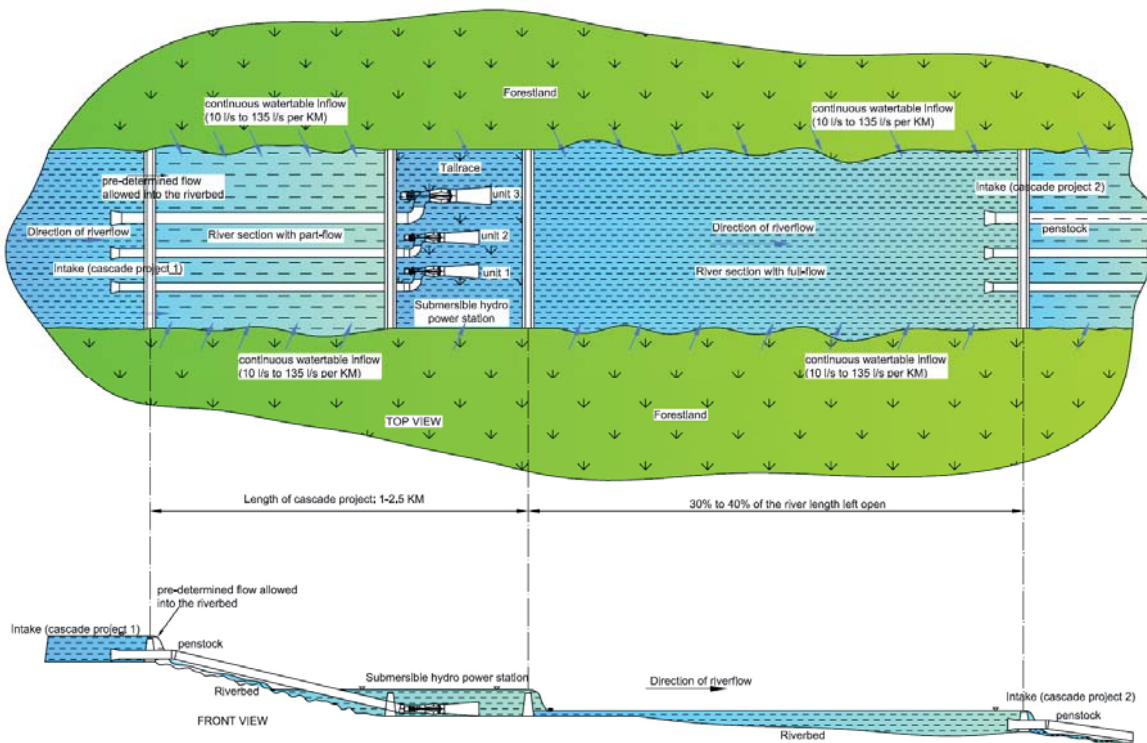


Fig. 1.2, The dynamics of the forest river basin and the hydropower solution

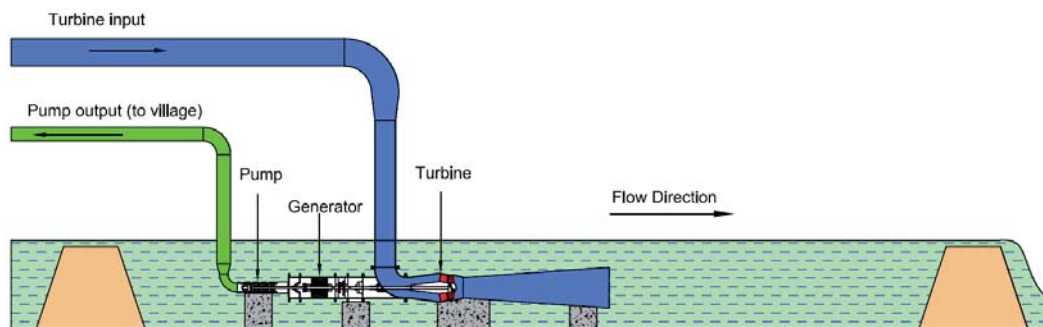


Fig. 1.3, The submersible Micro Hydel Pump or the Module

The concept proposed by the promoters for the engineering solution and its interaction with the forest river basin is illustrated in Fig 1.2 and Fig 1.3 respectively. Figure 1.2 shows the layout of the run-off-river cascade projects and also displays the effluent nature of the basin and quantum range of flow from the forest water table to the river flow. It also shows the submersible concept of the engineering solution. The combined electricity and water pumping application from the micro hydel pump has been illustrated in Fig. 1.3 (further description of this is provided in chapter 2 and a more technical literature is illustrated in Chapter 5 and 8). The micro hydel pump is also referred as ‘module’ within the literature.

Chapter 2 – Location, Catchment Area and the Scheme

2.1 Location of the Project

The location of the major civil components of the Taipadar project is shown in satellite image in Fig. 2.1 that includes the diversion weir, submersible power plant and the storage tanks. The bird's view of the Taipadar village with cultivation fields, Ganeshbahar valley to the east and main village road along with huts beside the internal roads can also be seen. The road intersects the stream at the southeastern tip before making way into the dense forest. There are two hillocks known as Saap Dongri and Chotta Dongri.

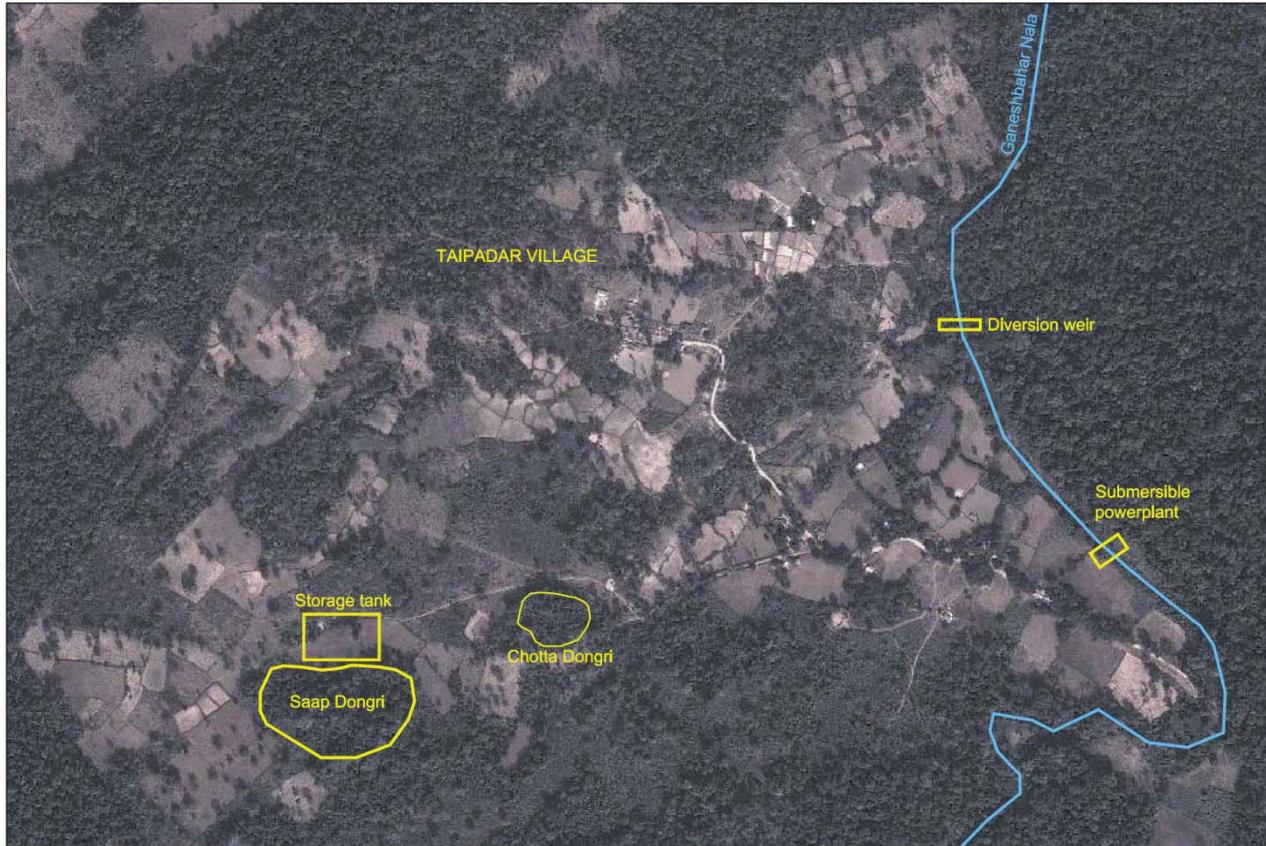


Fig. 2.1 Location of the Project

2.2 Catchment Area

The watershed or catchment area specifically for the chosen location Taipadar project is sketched by joining the ridgelines of the contours provided in the two Topo sheets No. 65 I4 and 65 J1 [2] obtained from the Survey of India illustrated in Fig. 2.2. The catchment area is found to be 135 km².

The catchment area receives an average annual rainfall of 1480 mm. The area is characterized by moderately dense tree growth with patches of barren lands and cultivable lands interspersed and the entire area comes under the Tiriya reserve forest.

2.3 Features of the Scheme

The proposed diversion weir across Ganeshbahar Nala is located at Lat: 18° 56' 43"-N & Long: 82° 10' 36"-E. The weir is constructed to raise the level of water and level difference between the FSL (Full Supply Level) of the weir and the TWL (Tailrace Weir Level) downstream of the submersible powerhouse is utilized for the generation of the power.

The micro hydel pump modules to be installed at the powerhouse with dual operations, providing scope for generation of power when clutch is disengaged and pumping of water when the clutch is engaged and rotor of the generator, which is on no-load providing only a flywheel effect to the unit.

The water from the foreshore of the weir is drawn through a penstock pipe to the powerhouse. After generation the water is led back in to the stream. During operation of the turbine in pump mode, it pumps water to a storage tank situated at a height of about 25 m from the powerhouse through a delivery pipe. The water stored in the tank will be

utilized for irrigating lands to an extent of 9 to 34 ha besides providing drinking water facilities to about 32 families residing in Taipadar village.

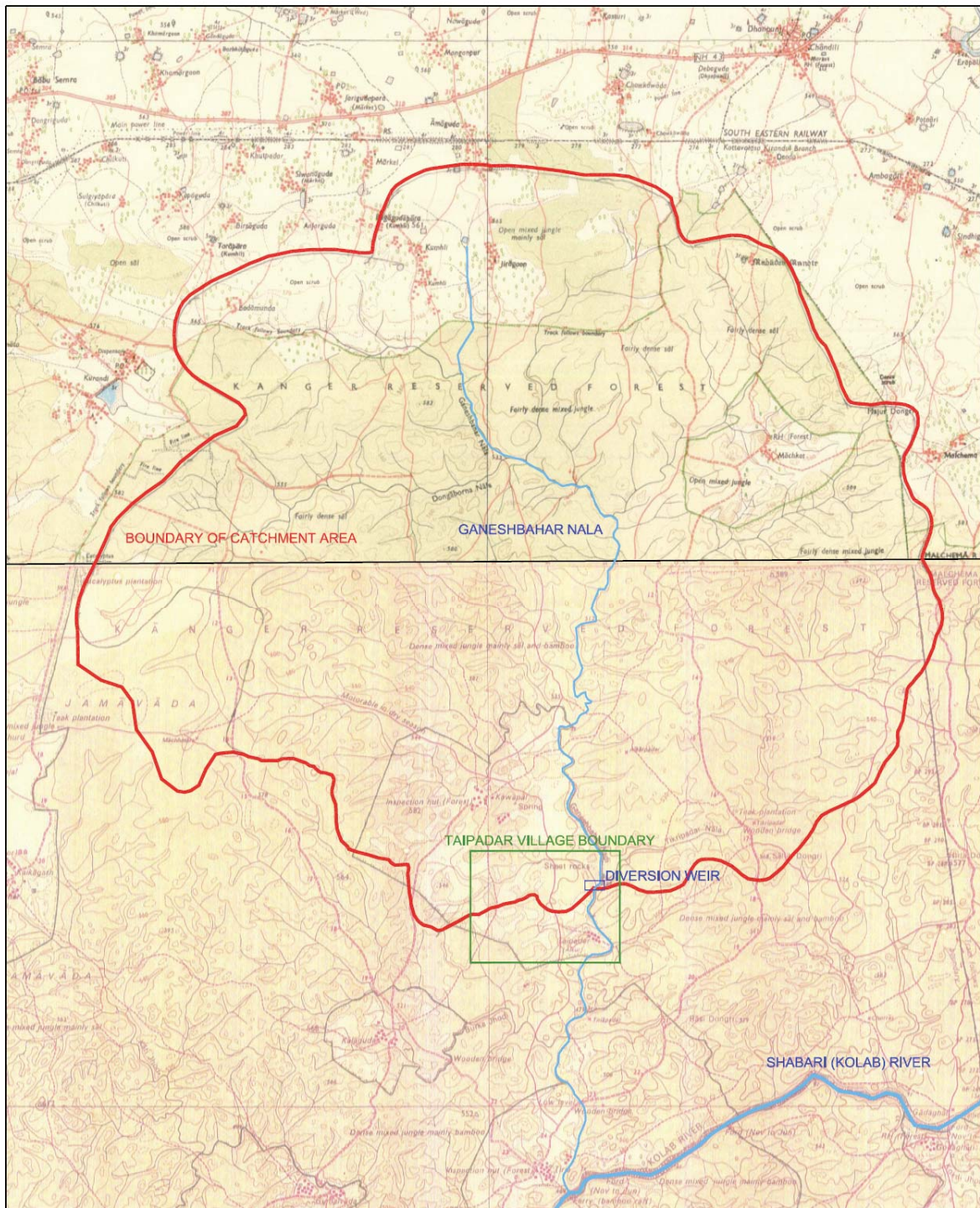


Fig. 2.2 Catchment area of the Taipadar Project

The FSL at the weir site is EL. 511.00 m with respect to MSL. The excess water above EL.511.00mtr discharges into the Nala flowing over the weir. The estimated flood at the proposed weir location is has been investigated in chapter 5 and there are some uncertainties with respect to its true value. The combination of HFL and correlations reveal a wide span of flows between 200 and 475 m³/s.

The minimum tail water level for operation of modules is about EL.504.80 m downstream of the powerhouse location. The Storage tank is situated at a location EL. 530 m in order to command all the land area belonging to families settled in the Taipadar village under irrigation and also providing drinking water through separate distribution system taking off from the coagulation tank.

Chapter 3 – Surveys and Investigation

3.1 Topographic Studies

The topography of a section of the Ganeshbahar Nala and the entire village is determined using ‘total station’ survey equipment in two separate surveys and depicted in Fig. 3.1. The various zones of cultivation are also shown in the plan.

The first survey carried out in December 2011 by VAS Nirman, Raipur focused only on the stream section of 1.3 km, while the second survey was carried out exactly a year later to determine the complete command area of the village. The command area, an important resource for planning the irrigation and drinking water supply systems, comprised of the whole land area in the vicinity of the village belonging to the 32 families including valleys, ridges, cultivable land, Government land and forest land. Benchmarks have been created and the contours at an interval of one meter have been generated as shown in Fig. 3.1.

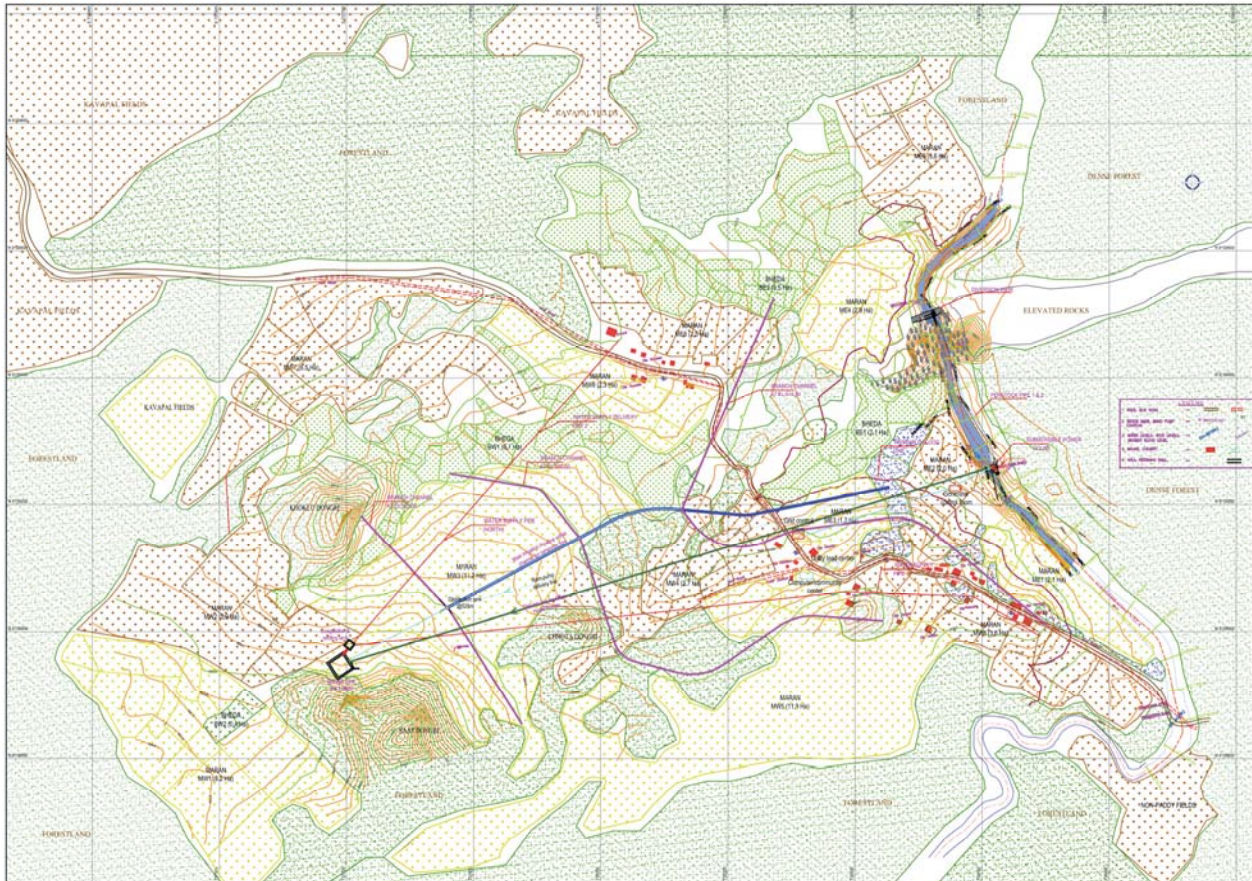


Fig.3.1, Village and Stream Topography

3.2 Village and Community Survey

The village and community survey covers intricate life schedules of the Taipadar villagers, their landholding distribution, and expectations from the project. But, the striking feature is the two village meetings where the farming intelligence and techniques of the villagers (that may be inherited from ancestors) can be understood. The promoters are sure that the Taipadar will work for equitable and honest farming methods amongst each other along with carrying out the maintenance (provided there is elaborate training) of project.

The farmlands are classified into two categories. Paddy or rice fields are known as ‘Bheda(s)’ and non-paddy or other crops are called ‘Maran(s)’ in local tribal language.

3.2.1 Activities of Community in a Year Calendar

Table 3.1, Activity chart of the population during a calendar year

Sr. No.	Month	Activities
1	January	Cutting the bushes and other growths in Maran

2	February	1. Allowing the dry bushes of the Maran to burn and get the maran cleaned. 2. Venturing into the forest to douse natural fires
3	March	1. Clearing the ashes of the Marans fields 2. Going out for work (labor contracts, etc)
4	April	Do
5	May	1. Till the soil of both Maran and Bhedas. 2. In the end of May, the spread manure only for Bhedas begin (cow dung used)
6	June	1. Sowing rice and special rice in Bhedas along with maize, ragi, khosla in Marans. 2. Previous years seeds are used.
7	July	1. Sowing of ragi and khosla continues. In addition sowing of urd begins
8	August	1. Second round of tilling is done with sown seeds to make the land soft. Manure spread once again. In 2012, for the first time they have tried chemical fertilizers obtained from government. 2. Remove weeds that have grown along with rice plants. 3. Sowing of Till and Arava
9	September	Harvesting of Maize
10	October	1. Separate the dried and used maize plants. 2. Starting the harvest of both category of rice and khosla. 3. Sowing of mustard towards the end of October
11	November	1. Continue the harvest of rice, khosla and ragi. 2. Separating the rice and seeds from the plants with the help of rollers. 3. No dedusking yet.
12	December	1. Till and arava are harvested and mustard plants are removed.

3.2.2 Crop Pattern Adopted

Table 3.2, Crop pattern of the Taipadar village

Sr. No.	Crop	Type	Category	Sowing	Harvesting	Delta (over base period)	Mean Gross Irrigation Requirement (mm/day)
1	Rice	Bheda	Kharif Paddy	Jul-Aug	Oct-Nov	1000 mm	10-12 mm
2	Special rice (less water reqd.)	Maran	Kharif Paddy	Jul-Aug	Oct-Nov		7 mm
3	Khosla	Maran	Kharif Paddy	July	Oct-Nov		
4	Till seeds	Maran	Kharif Seed	Aug	Dec	450 mm	5 mm
5	Urad dhal	Maran	Kharif Pulses	Jul-Aug	Nov	300 mm	3.5 mm
6	Kolath/Arava	Maran	Kharif Pulses	Aug	Nov		
7	Maize	Maran	Kharif Grain	Jun	Sept-Oct	450 mm	5 mm
8	Ragi/finger millet	Maran	Kharif Grain	Jun-Jul	Sept-Oct	300 mm	3 mm
9	Radish (with mustard)	Maran	Kharif Vegetable	Jul	Oct		5 mm
10	Ambadi (sour fruit)	Maran	Kharif Fruit	Jul	Oct		5 mm
11	Mustard	Maran	Rabi Seed	Oct	Jan-Feb	450 mm	5 mm

3.2.3 Landholding for Cultivation

Table 3.3, Landholding for cultivation in Taipadar

Sr. No.	Land Owner	Quantity of Land (in bits)	Total Area (acres)
1	Buddharam M	4	6.5
2	Kursu	7	15
3	Dommu	1	5
4	Guru	5	10
5	Durjan	4	8
6	Fagnu	5	8
7	Buddharam C	1	5
8	Gonchu	3	6.5
9	Lakmu	2	2.5
10	Pakhali	4	4.5
11	Aaithu	4	10.5
12	Loknath	3	3.5
13	Mosu	3	5
14	Banmali	3	3.5
15	Sudhu	1	5
16	Sukhman	3	4
17	Hanu	10	18.5
18	Badhu	8	16
19	Sukhram	4	6
20	Guruwari	2	4
21	Churkha	4	5.5
22	Ramprasad	4	6
23	Booty	1	1
24	Fagnu S	3	6
25	Ramsunder	3	3
26	Ramvati	1	1
27	Mahesh	1	2
28	Domayee	5	14
29	Jenuwa	1	1
30	Sonadhar	1	1
31	Manu	1	1
32	Kandra	3	11
Total Land Bits - 105 bits		Total Land units with Records - 56	Total Area of cultivated land (199.5 acres, 80.7 Ha)
		(107 acres, 43 Ha)	

3.2.4 Expectations from the Project

Table 3.4, Summary of village meetings

Sr. No.	Details	Date	Suggestions	Participants
---------	---------	------	-------------	--------------

1	Afternoon meeting	16.01.2013	<ol style="list-style-type: none"> 1. Submergence not a problem. The water will go over the weir, on the forest side as well and shall not come only to the village side. Kursu suggested another gate in the weir, but it was explained to him that the operation of this would be impossible given the short reaction time available in a flood situation. 2. Sharing of water that is available at different times of the year will be done amicably between users. 3. Irrigation canals passing through fields will not be a problem. 4. The cultivable zone highlighted in the map does not exclude any owner. So, nobody will be left out. 5. Drinking water is major boon for women. 	16 land owners participated in the meeting
2	Evening meeting	16.01.2013	<ol style="list-style-type: none"> 1. Submergence at 512 m Submergence due to floods last for few hours only. The water will quickly drain out through the natural slope of the valley. Stagnation of water very rare 2. Cultivation plan with tank irrigation <ol style="list-style-type: none"> i) With additional water available they will convert some Maran fields to Bhedas for more rice cultivation during monsoons ii) Post harvest of Kharif crops (in Oct-Nov), they shall sowing wheat, channa, maize, Ambadi, bringal, tomatoes, radish, lauchi, potatoes, onion, pumpkin, mustard, arsi (small till), kuma, jadha and greens 3. Muddy water pumped in monsoon This will be a problem for drinking and household use. There were suggestions to use olden methods like settling and filtration. However, they requested some 'technical' solution for this. 	There were 10 participants out of 32 landowners.

3.3 Historical Structures and Environment

The proposed Taipadar is located in an area free of any identified historical structure such as temples and archaeological sites etc. The said project does not involve any forestland.

Even though, the project is non-polluting, eco-friendly and does not affect the ecology of the area in anyway, a more elaborate and unbiased environmental assessment is needed (as carried out in Chapter 9).

Chapter 4 – Hydrology

4.1 General

The scope of hydrology pertaining to hydropower project mainly deals with two important parameters viz.

- First, the water yield required for the assessment of power potential, energy generation, design of water conductor system and other hydro power structures.
- Second, the maximum probable flood that may occur at the site for the safe design of weir flood control structures and protective works at the intake and powerhouse sites, taking into account importance of structure and hazard potential downstream of the structures. More than the effect on the project structures, the analysis of submergence levels in both the cultivable and forestlands caused by floods needs to be carried out.

4.2 Flow Duration Studies

The flow duration curve of the stream (Ganeshbahar Nala) is determined using a specially constructed measured weir as shown in Fig. 4.1 and 4.2. The recommendations of Theodore Rehbock's rectangular weir [3] were used at the basis of the design of this weir. The flow (based on the water level above the crest) was measured daily for one year (from March 25th 2012 to March 25th 2013) as shown in the Fig. 4.3.



Fig. 4.1 Overview of the measured weir



Fig. 4.2 The nappe created over the weir

Based on the daily flow data a monthly mean is derived and illustrated in Table 4.1, which is also plotted in Fig. 4.3. The comparison of the daily flow data and monthly mean curve shows good fit. The monthly curve will be used in determination of permissible flow through the micro hydel pump modules in Chapter 5.

Table 4.1, Daily averaged Monthly mean values of flow

Sr. No.	Month	Measured flow (l/s) – Daily averaged monthly mean
1	January	210
2	February	153
3	March	133
4	April	114
5	May	105
6	June	71
7	July	1036
8	August	929
9	September	661
10	October	490
11	November	376
12	December	286

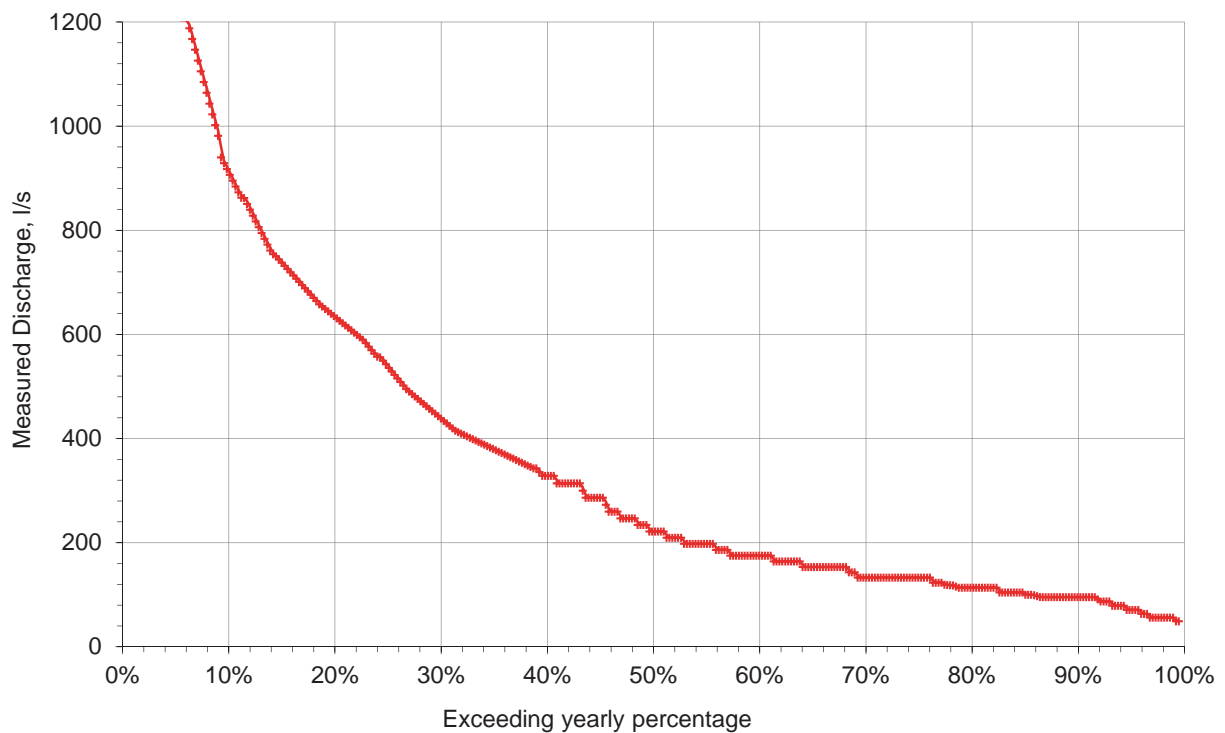


Fig. 4.3, Flow duration curve for the Ganeshbahar Nala

4.3 Flood Studies

4.3.1 Preliminary Investigation

The flood investigation for the Taipadar catchment area is still underway and the promoters are in the process of contemplating an accurate simulation methodology since this can have repercussions on the extent of submergence of forest and farmland. The promoters and its implementing team in no way want to take chances, as there is no accurate data available and all the simulations come with their own levels of uncertainties.

Initial studies include a comparison between the available correlations and highest flood levels pointed out by village elders. This simple comparison is carried out in Table 4.2. It can be seen that the widely used Dickenson’s correlation results in 475 m³/s compared to 215 m³/s, which is determined from the historic HFL.

Table 4.2, Preliminary determination of flood flows

Sr. No.	Methodology	Relation	Q (m ³ /s)
1	Dickenson's correlation [4]	$Q=C*(A)^{3/4}$ with C=12 and A (Catchment Area) = 135 km ²	475
2	Manning's Formula based HFL indicated by village elders [5]	$Q=(1/n)*R^{2/3}*S^{1/2}*A=214$ m ³ /s, with A=115 m ² , S=1/1250, R=3.5 and n =0.035	215

4.3.2 Simulation of Submergence

The submergence levels are determined at different heights (0 to 2 meters) above the diversion weir planned at 511 m based on Manning’s formula and using average cross-sections at different levels from the topography of the village. The slope and friction constants are nominally assumed. The discharges at different levels are summarized in Table 4.3 and the total flow is composed of flow into the farmland and over the weir. However, the flow into forestland is not considered due lack of sufficient levels for contours until 513 m.

Table 4.3, Simulation of submergence

Sr. No	Level	Flow over weir (m ³ /s)	Village flow (m ³ /s)	Total stream flow (m ³ /s)
1	511.5	19.1	22.0	41.1
2	512.0	54.0	73.7	127.7

3	512.5	99.2	147.0	246.2
4	513.0	152.7	258.3	411.0

While 512 m is maximum allowable submergence from the promoter's point of view (given the objective of the project to have no submergence), this would facilitate only about 128 m³/s, which is far below both the methods used for prediction in Table 4.2. There is strong possibility of the submergence level reaching even 513 m, if flood crosses the 400 m³/s mark.

As presented in Chapter 3, the villagers have no objection with this submergence level of 512 m, which they believe would last for only few hours and would not harm the preparatory crops for Kharif season given that floods are expected between July and September only. However, this reassurance does not give a green signal to build the weir to its FSL of 511 m.

A more holistic view has to be undertaken as will be highlighted in the impact assessment study (Chapter 9, section 9.2.4) and future investigation (Chapter 14, section 14.1).

Chapter 5 – Power and Energy Studies

5.1 System Design – Module Configuration

The permissible flow into the modules should factor both ecological and climate variation factors. Despite being an effluent stream (ground water flow nourished), the promoters have decided to allow some flow into the stream, while water is diverted into the penstock for the modules. There is also a possibility of climate changes and flow uncertainties. Since the flow duration curve is based on only one year flow data, there is need to appropriately fix the permissible module flow. Figure 5.1 shows the monthly mean and the permissible flow curves.

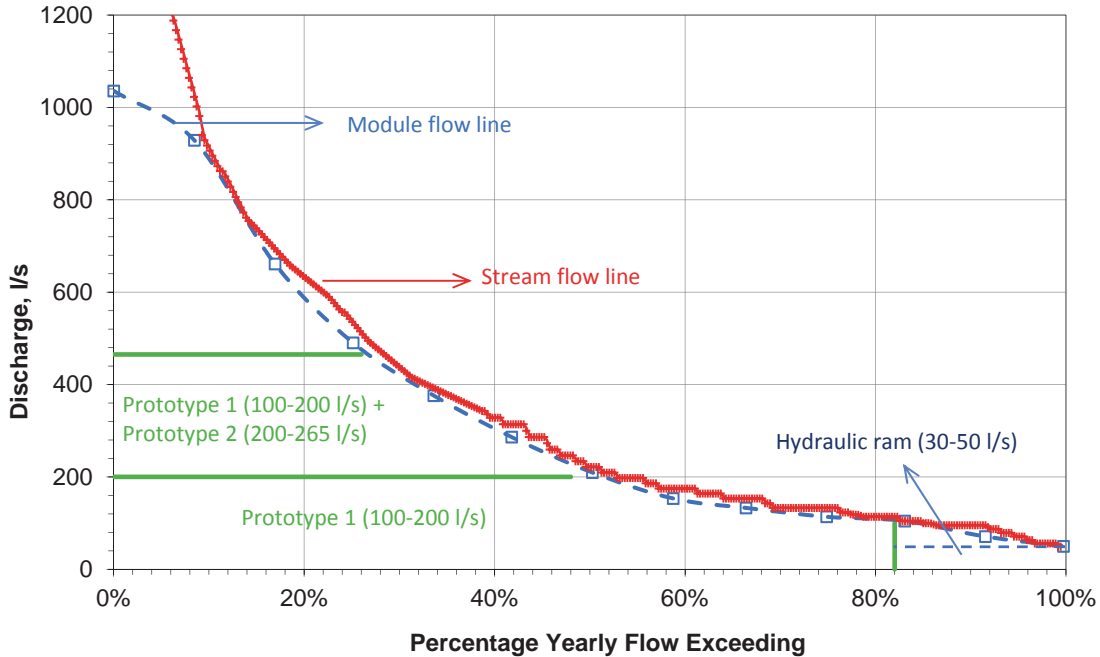


Figure 5.1, Permissible module flow curves and plan for operation

The planning of the module configuration can be understood from Fig. 5.1 where 2 operating zones are plotted. The maximum flow capacity of the modules is restricted to 25% availability of flow (465 l/s). The least flow considered for design corresponds to a little beyond 82% of flow availability (100 l/s) throughout the year.

As will be illustrated in Chapter 8, two different modules (rotating) are planned to be designed and manufactured that can optimally be combined to use the flow pattern as shown in Fig. 5.1. The first module (prototype 1) has an adjustable guide vane fixed on to a fixed axial flow runner and can operate in wide range of flow zone (100 to 200 l/s) translating to flow availability between 52% and 82%. The larger module (prototype 2) has fixed guide vane and runner (axial flow PAT driven module) and is designed to cover a flow of 200-265 l/s.

In addition to the two turbine based modules, a ram pump is selected for the leanest period of flow (85% to 100% of the flow availability abscissa). The objective of selecting the ram pump is to provide minimum water for irrigation and drinking water. The hydraulic ram will not be able to generate electricity unlike the rotating module.

Table 5.1 summarizes the prototype and ram operation in these three zones.

Table 5.1, Module configuration					
Sr. No.	Zone	Flow range	Module Configuration	Flow availability	Months of operation
1	Zone 1	30-50 l/s	Hydraulic Ram	Ca 100%	April, May, June (for pumping application only)
1	Zone 2	100-200 l/s	Prototype 1	ca 50% to 85%	December, January, February, March
2	Zone 3	200-265 l/s	Prototype 1 + Prototype 2	ca 25%	July, August, September, October, November

The permissible flow is shared between the turbine and pump for pump mode operation (section 6.2.1) of the prototype and utilized only by the turbine in the generator mode of operation (section 5.2).

5.2 Power and Energy Duration Curves

The priority of operation of the modules will be for pumping water, as agriculture is seen economic generator (Chapter 1). However, electricity generation is also important and the modules are proposed to operate for about 8 hours a day during evenings and at times when utility loads have to be operated. The power and energy distribution over the year is summarized in Fig. 5.2. The flow duration curve are also plotted along with the power and energy curves.

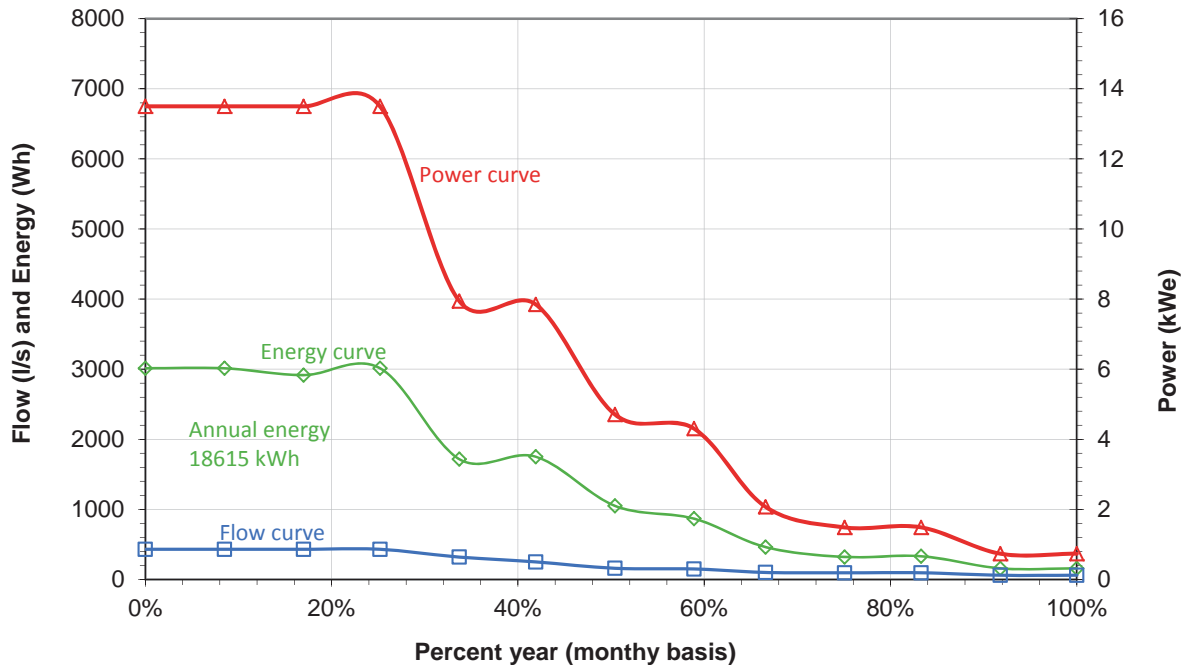


Fig. 5.2, Energy and Power Duration Curves

The power is determined for a net head of 5 meters on the turbine and the energy is calculated with a plant load factor of 90%. The annual energy generated for nominal load operation is approximately 18600 kW h (as illustrated in Table 5.3).

Table 5.3, Monthly distribution of power and electricity generation

Sr. No.	Month	Usable stream flow (l/s)	Module flow (l/s)	Module configuration.	Power (kWe)	Energy (kWh)
1	January	160	160,0	P1	4,7	1051
2	February	150	150,0	P1	4,3	868
3	March	100	100,0	P1	2,1	463
4	April	95	95,0	P1	1,5	321
5	May	95	95,0	P1	1,5	332
6	June	60	60,0	P1	0,7	159
7	July	515	430,0	P1 + P2	13,5	3013
8	August	500	430,0	P1 + P2	13,5	3013
9	September	515	430,0	P1 + P2	13,5	2916
10	October	515	430,0	P1 + P2	13,5	3013
11	November	320	320,0	P2	7,9	1716
12	December	250	250,0	P2	7,8	1752

Annual Energy Generation (kWh) 18615

Chapter 6 – Irrigation and Drinking Water Studies

6.1 Drinking Water Requirements

The potable water for drinking and other purposes forms one of the primary requirements of the Taipadar village as illustrated in Chapter 1 (Section 1.3). Assuming WHO standards [6] of ca 200 litres per day per head for the village is approximately 45 m³/day, which results in an annual 'drinking water' production of 16425 m³.

6.2 Irrigation Planning

6.2.1 Location of Tank and Pumping Capacity of Modules

The planning for the agricultural needs of the community requires careful thought not only from the duration of operation during the day (ca 16 hours/day) but also from the criterion of management like crop selection and the entire farming management.

On one side is the availability and the other side is the farming requirements of the villagers. The critical factor is to have the elevation data between the module location on the streambed and the proposed supply tank location. The selection of this location has to be optimally chosen keeping in mind the topography on one side and mechanical power provided by the turbine for a permissible pump flow. Based the topographic investigations (Chapter 3) a location is chosen as shown in Fig. 3.1 having a ground level of 525 meter, which is around 15 meters from the weir full reservoir level of 511m at the diversion weir.

The pumping capacity of the two prototypes is determined by equating the shaft powers of the turbine and pump units for a mean turbine efficiency of 80% and pump efficiency of 75% with a net head on turbine of 5 meters and net pumping head of 24 (accounting for maximum of 9 meters of head loss) and summarized in Table 6.1.

As discussed in section 5.1, a pump based on water hammer principle is chosen for managing the lean flow during summer season (extending from 15% to 20%). The ramp pump has an overall efficiency of between 60-65%, which have flow capacities lower compared to the turbine modules, but are more efficient than prototype 1 operating in this flow range. Performance characteristics of the ram pump module used is presented in Chapter 8.

Table 6.1, Pumping capacity of the modules under 24 meters of pumping head

Sr. No.	Module	Q _{module} (l/s)	Q _{turbine/drive} (l/s)	Q _{pump} (l/s)
1	Hydraulic Ram Pump (R1)	45-55	38-45	2-10
2	Prototype 1	100-200	90 - 175	5 - 25
3	Prototype 2	200-265	190-235	10 - 30

6.2.2 Annual Capacity of Irrigation

The annual capacity of irrigation (in terms of Delta, Δ , and cultivable land) for a non-paddy crop is summarized in Table 6.2 and in Fig. 6.1. The total volume of water pumped a year is approximately 51000 mm.hectare.

Table 6.2, Available water for irrigation

Sr. No.	Month	Usable stream flow (l/s)	Module Configuration	Turbine (drive) flow (l/s)	Pump (delivery) flow (l/s)	Act. Mod Flow (l/s)	V (m ³ /day)	V (mm.ha/day)
1	January	160	P1	145,0	15	160,0	778	73
2	February	150	P1	142	13,5	155,5	700	65
3	March	100	P1+R1	96.5	12	108.5	622	58
4	April	95	P1+R1	92	11	103.0	570	53
5	May	95	P1+R1	92	11	103.0	570	53
6	June	60	R1	50	7	57.0	518	32
7	July	515	P1 + P2	410	52	462,0	2696	265
8	August	500	P1 + P2	410	52	462,0	2696	265
9	September	515	P1 + P2	410	52	462,0	2696	265
10	October	515	P1 + P2	410	52	462,0	2696	265
11	November	320	P2	235	30	265,0	1555	151
12	December	250	P2	225	25	250,0	1296	125
							Annual Quantity (mm.ha)	51063

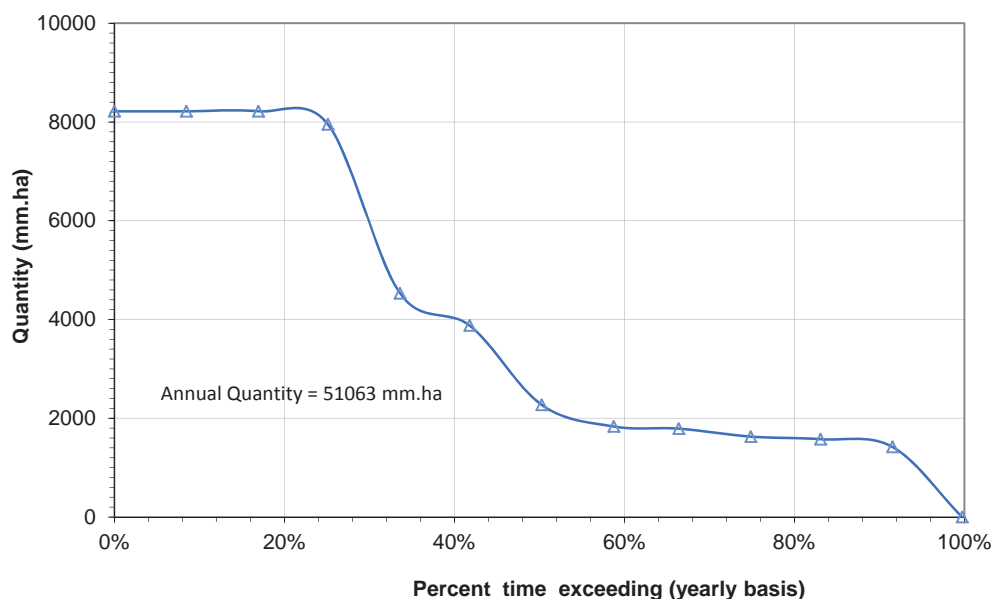


Fig. 6.1, Available water for irrigation

6.2.3 Irrigation Yield

An annual irrigation model is proposed (Table 6.3) based on the discussions with villagers (summarized in Chapter 1) and annual available depth of flow (Fig. 6.2). A base period of 3 months (123 days) during the Kharif season is allocated for high-yielding variety of rice. Wheat is selected as the second crop during Rabi season, while the remaining time of the year is dedicated for other crops (mustard, vegetables and others). The irrigable area and the total yield have been summarized in Table 6.3.

Table 6.3, Irrigation yield as per proposed crop model

Season	Months	Base period	Quantity (mm.ha/month)	Quantity mm.ha/season	Crop	Δ , mm [10]	Ha	Yield (kg/ha)	Yield (kg)
Kharif	August	123	8217	32603	Special paddy (High yielding)	950	34,3	3000	102958
	September		8217						
	October		8217						
Rabi	July	120	8217	12513	Wheat (high yielding)	450	27,8	3500	97326
	November		4531						
	December		3878						
	January		2271						
Summer	February	122	1834	6413	Mustard/vegetable	300	21.4	1000	21377
	March		1789						
	April		1628						
	May		1576						
	June		1420						

6.2.4 Turbine Pumps versus Ram Pump

The ram pump is seen to work for 4 months a year (Table 6.2) out of which in 3 months it works in combination with Prototype 1 pump and in the month of June it works isolated. The volumes of water supplied by the ram pump in comparison with the turbine pumps (P1 and P2) are summarized in Table 6.4.

It can be seen that ram provides only for 8% of total volume, but during the critical dry season phase when the turbine pumps operate with lower efficiency.

Table 6.4, Irrigation water yield (volumetric) of ram pump and turbine pumps

Month	Drive flow (l/s)	Delivery flow (l/s)	Volume (mm.ha)	Comments
March	50	7	985	
April	50	7	954	
May	50	7	985	
June	50	7	954	
		Ram pump (total)	3878	8%
		Turbine pumps	47185	92%
		Total	51063	

Chapter 7 – Civil Works, Hydro Mechanical Equipment and Construction Materials

7.1 Civil Structures:

The Civil and appurtenant Structures that are envisaged for different components of the proposed Taipadar Project are detailed in this Chapter. The components of civil structures

The Main components are

- Diversion Weir including intake and silt excluder arrangement.
- Penstock pipe.
- Power House including Tail end weir.
- Pumping main delivery pipe.
- Storage tank for irrigation
- Main distribution pipe for irrigation
- Branch and Feeder channels
- Settling and coagulation Tank
- Main delivery pipes for drinking water supply
- Distribution pipe for households including individual water tanks and taps

All the components of the proposed scheme are ideally located within the limited area in the vicinity of Taipadar village and are accessible through approach roads to be formed connecting the main road, which will be used to facilitate movement of men machinery and materials.

7.1.1 Project Layout:

The general arrangement of the proposed scheme is shown vide drawing entitled “General Layout- Plan and Section” Fig. A1 (a representation has already been shown in Fig. 3.1). The design features and provisions of different components are discussed in the following paragraphs.

7.1.2 Diversion Weir including intake and silt excluder arrangement:

The diversion weir consists of an over flow ogee weir of top length 25.00 m and non over flow portions of length 3.85 m and 2.00 m on left and right bank respectively. The crest level of the over flow weir is proposed at EL: 511.00 m and the top level of the non-overflow blocks EL: 512.50 m. The deepest foundation level of the over flow weir is at EL: 504.00 m. The Diversion weir is a gravity structure and constructed with cement concrete M20 with skin reinforcement for the overflow and bucket portion of the weir.

It is proposed to embed two circular HDPE pipes in the body of the non-overflow section of the weir on the left bank with necessary transitions at the entry to the pipe. The pipe taking off at the level EL: 508.35 m will continue as penstock for supply of water to the power house and other taking off at EL: 507.35m will terminate immediately d/s of the weir and this will serve as silt excluder for de- silting of the fore shore at regular intervals. Both the penstock and silt excluder are proposed to be provided with control gates for regulation of discharges. The hoisting mechanism of gates consists of screw type hoist located at El: 512.50 m. An operating platform for hoisting arrangement will be constructed at the top level of NOF on the left bank.

7.1.3 Penstock pipe

The penstock pipe takes off from the diversion weir in the left bank and runs for a length of 258.00 m up to the bifurcation point. It is proposed to provide HDPE pipe of 750 mm diameter of designed thickness to withstand the static head and the pressure rise due to load through off on the Unit/Units. The penstock pipe will be branched off into two and each branch pipe is further bifurcated into two to feed the four Units. The penstock partly runs in excavation and balance over ground. It is proposed to provide suitably designed anchor blocks wherever change in direction is there both in plan and sectional elevation. In between the anchor blocks the saddles/ground supports will be provided at maximum intervals of 6 meter with proper fastening into the saddles/ground supports with metal strips. The maximum velocity is limited to 1.2 m/sec

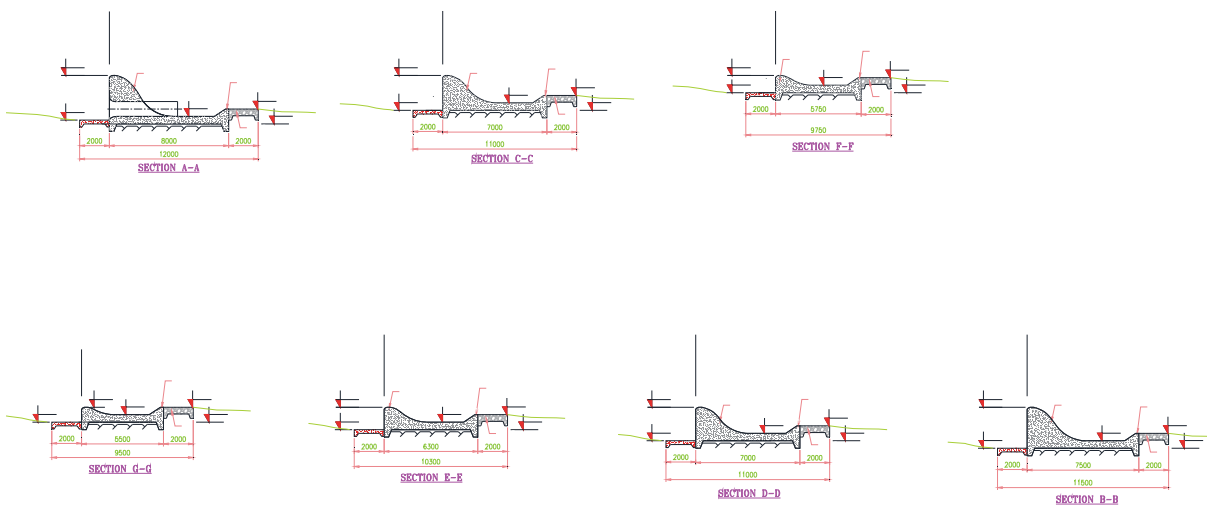
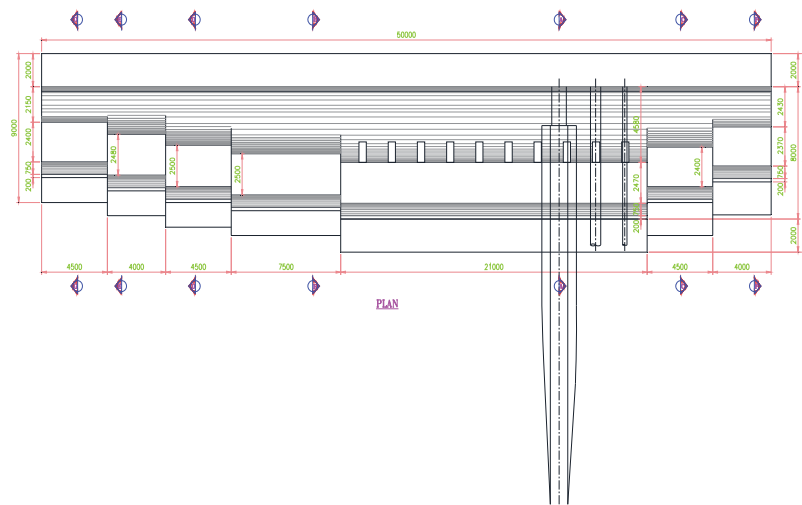
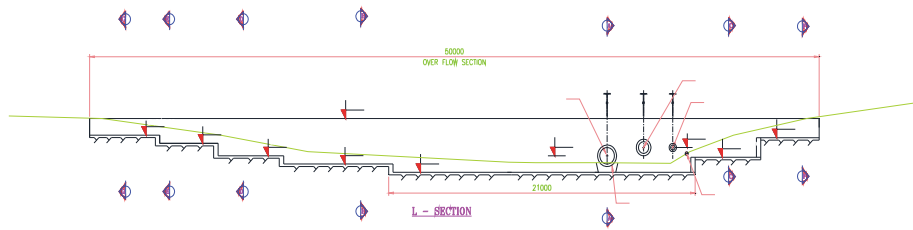


Fig. 7.1, Sections of Diversion Weir

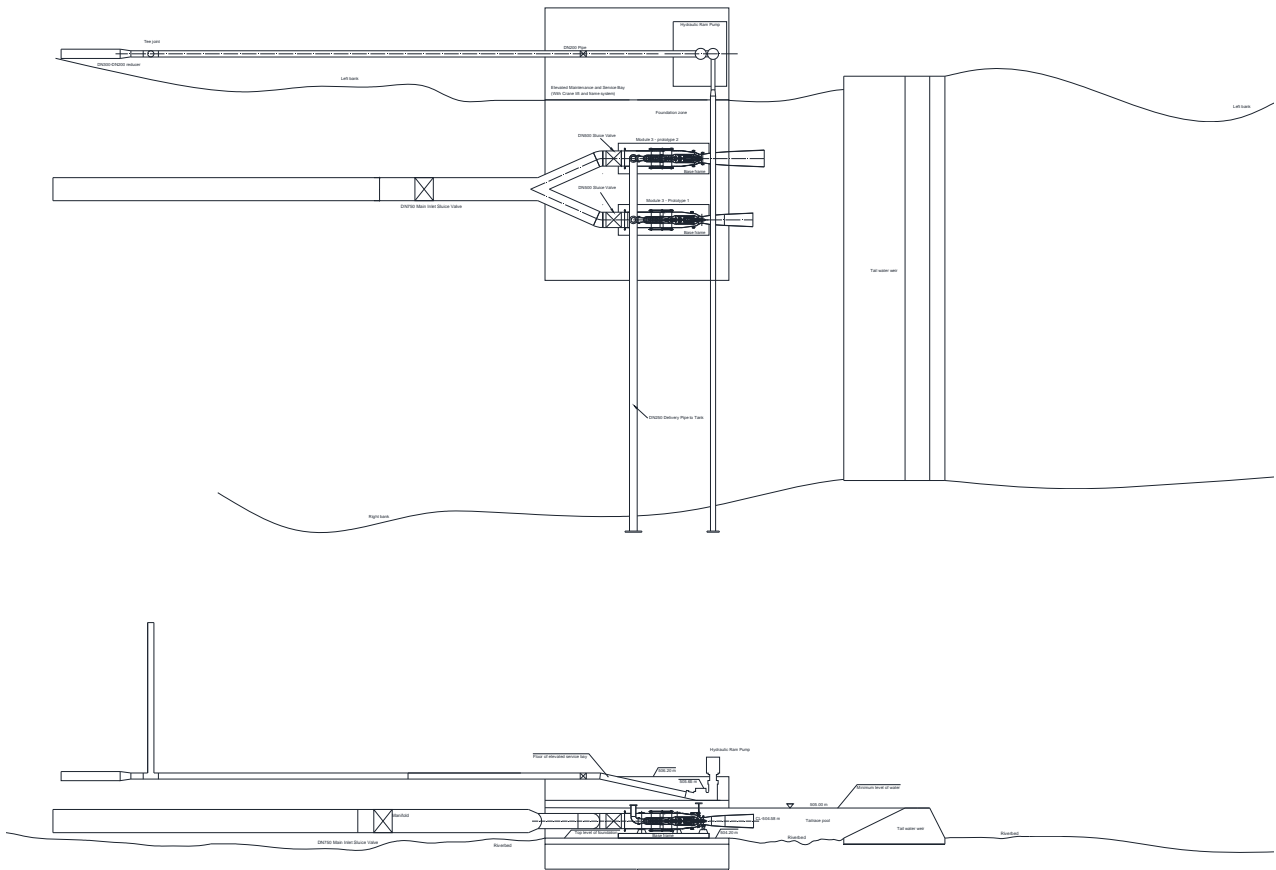


Fig. 7.3, Plan and Elevation of the Submersible Powerhouse

7.1.5 Pumping main delivery pipe

When the Units are working under pump mode, all the Units will be connected with a common manifold and linked to the delivery pipe. The water delivery pipe is of HDPE make of diameter 250 mm and delivers water to the storage tank located at ground elevation EL: 526.00m.

The length of delivery pipe is 1140.00 m and runs partly below ground and balance above ground. It is proposed to provide suitably designed anchor blocks wherever change in direction is there both in plan and sectional elevation. In between the anchor blocks the saddles/ground supports will be provided at maximum intervals of 6 meter with proper fastening into the saddles/ground supports with metal strips. The pumping head is about 32.00 m including suction, delivery head, friction and other losses.

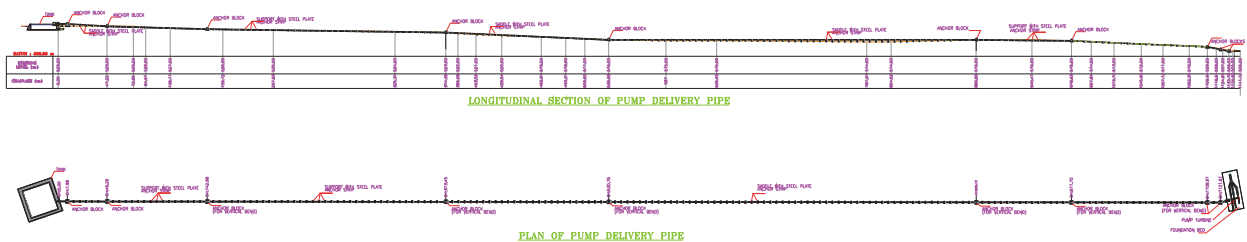
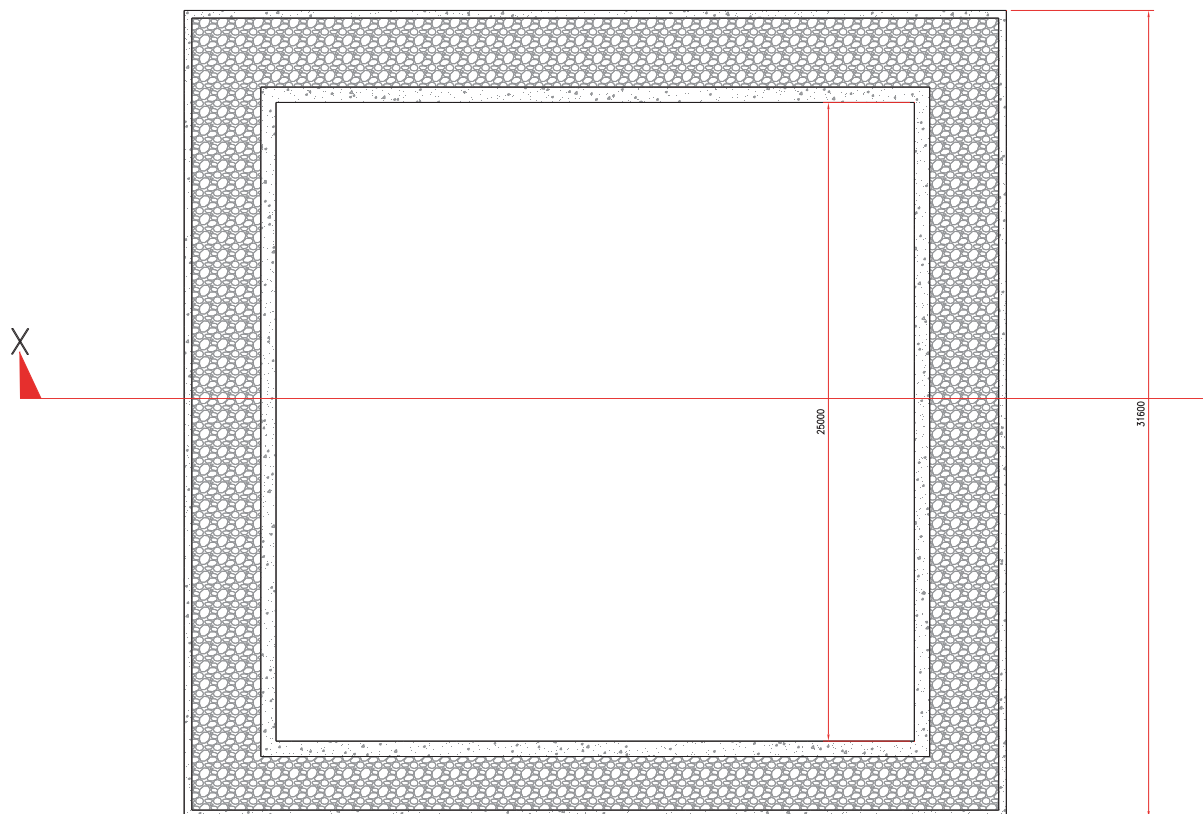
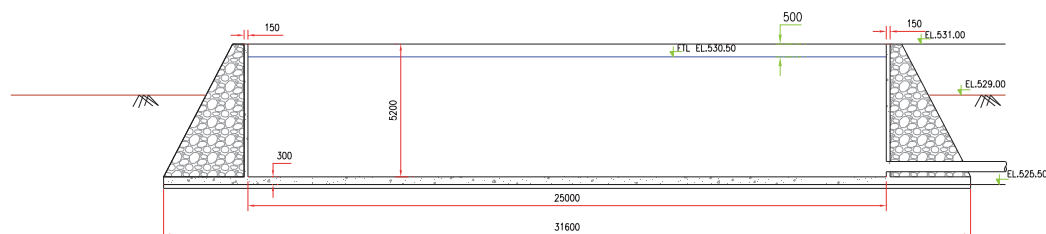


Fig. 7.4, Main Delivery Pipe (Plan and L-section)

7.1.6 Storage tank for irrigation & Water Supply



PLAN OF TANK



C/S OF TANK AT X-X

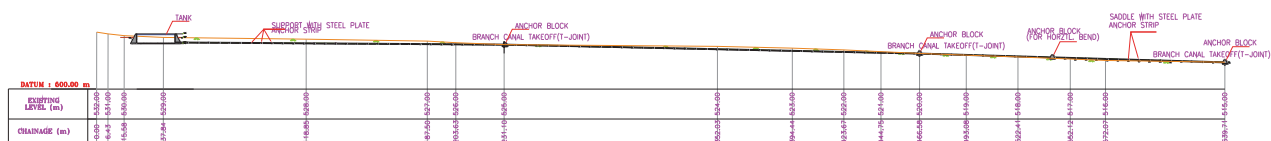
Fig. 7.5, Plan and Cross-section of Irrigation Storage Tank

It is proposed to construct a ground level tank at the highest elevation to command area so that all the lands of the village can be supplied with water for irrigation purposes.

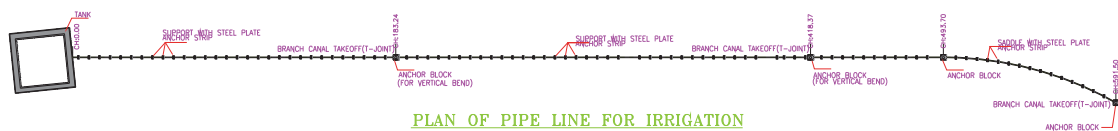
The high ground is at elevation about EL: 529.00m on the right bank about 1.15km away from the power house location. The storage tank is proposed to be constructed with UCR masonry with RCC lining of 150mm thick using water proof agent and plan dimension is 25.00m X 25.00m for storing water for a depth of about 4.8m. The capacity of the tank is about 3125.00cum and will serve the purpose of supply of water for irrigation and water supply to about 35 families of Taipadar village.

7.1.7 Main distribution pipe for irrigation

The water to irrigate about 50 ha of land belonging to the 32 families of Taipadar village and situated close by will be supplied through a main distribution pipe of diameter 250 mm. The total length of this pipe is 645.00 m and runs partly in cutting and balance over ground. It is proposed to provide suitably designed anchor blocks wherever change in direction is there both in plan and sectional elevation. In between the anchor blocks the saddles/ground supports will be provided at maximum intervals of 6 meter with proper fastening into the saddles/ground supports with metal strips. Three numbers of T-joints are proposed along this pipe to draw water at levels EL: 525.00 m, EL: 520.00 m and EL: 515.00m to draw water into contour branch channels at these levels.



LONGITUDINAL SECTION OF PIPE LINE FOR IRRIGATION



PLAN OF PIPE LINE FOR IRRIGATION

Fig. 7.6, Main Distribution Line for Irrigation

7.1.8 Branch and Feeder channels

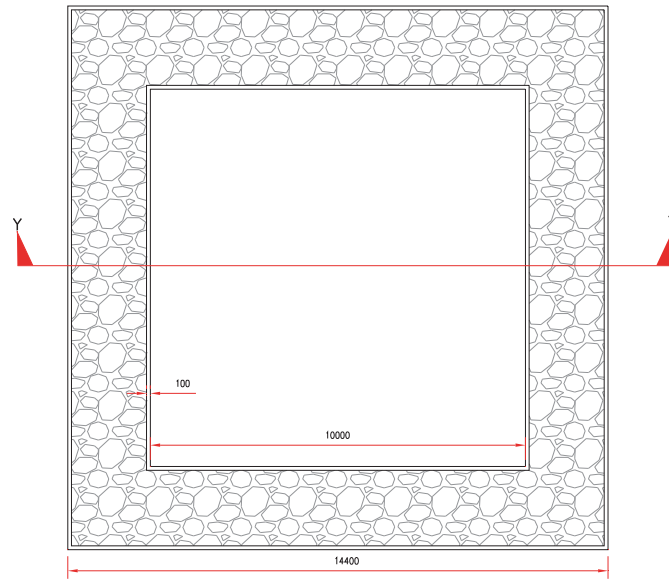
The branch channels take off at the T-joints of the main distribution pipe to carry water to the fields on either side of the main distribution pipe. The length of the branch channels is 234.00 m left side and 211.00 m right side at EL: 525.00 m contour channel. Similarly the lengths are 680.00 m (left) and 260.00 m (right) at EL: 520.00m contour channel and 710.00m (left) and 390.00m (right) at EL: 515.00m contour channel. The branch channels are of trapezoidal section excavated at respective levels as indicated above with 0.5m bed width and 1:1 side slopes. It is proposed to line the channel bed and sides with concrete lining of 100mm thick with nominal reinforcement to take care of temperature variations. The carrying capacity of the channel is sufficient to meet the requirement of irrigation water of the command area under each branch channel. The regulatory valves will be provided at each T-joint to control and regulate the discharge to match the irrigation requirement. The tertiary feeder channels will take off from the branch channel depending on the requirement.

7.1.9 Settling and coagulation Tank

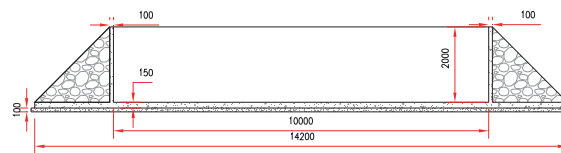
The water in the Ganeshbahar Nala especially during monsoon carries some fine silt. The water pumped to the storage tank needs treatment for removal of suspended sediment before the same is supplied for the purpose of drinking. For this purpose it is proposed to construct a separate settling tank of dimension 10.00 m X 10.00 m X 2.00 m. The water will be drawn from the storage tank to the settling tank and allow for sedimentation process with a certain detention period. The coagulating agent such as alum will be added and after settlement of resulting flock, water will be drawn for potable purpose.

7.1.10 Main delivery pipes for drinking water supply

Two numbers of delivery pipes of make HDPE diameter 150 mm each are provided for supplying water for drinking purposes. One delivery pipe will meet the drinking water for 14 nos. of families and school in northern side along with the two utility centers and other delivery pipe meets requirement 18 nos. of families settled in southern side. These pipes partly run in excavation and balance over ground. It is proposed to provide suitably designed anchor blocks wherever change in direction is there both in plan and sectional elevation. In between the anchor blocks the saddles/ground supports will be provided at maximum intervals of 6 meter with proper fastening into the saddles/ground supports with metal strips. Control valves will be provided to control and regulate the flow.



PLAN OF TANK (DRINKING WATER)

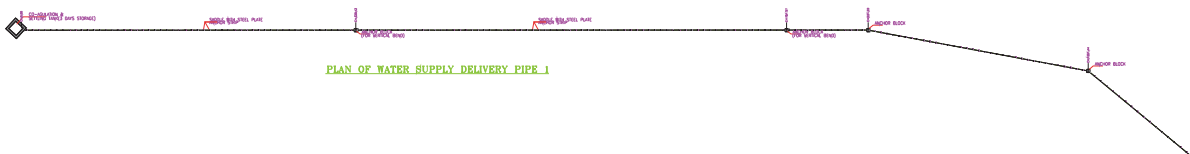


C/S OF TANK Y-Y

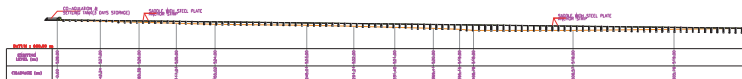
Fig. 7.7, Drinking Water Storage cum Coagulation Tank



LONGITUDINAL SECTION OF WATER SUPPLY DELIVERY PIPE 1



PLAN OF WATER SUPPLY DELIVERY PIPE 1



LONGITUDINAL SECTION OF WATER SUPPLY DELIVERY PIPE 2



PLAN OF WATER SUPPLY DELIVERY PIPE 2

Fig. 7.8, Delivery Pipes for Water Supply

7.1.11 Distribution pipe for households including individual water tanks and taps

The distribution pipe of diameter 75mm connected to the main delivery pipe will supply water to individual households. Valves for regulation purposes will be provided at each tapping. Individual water storage tanks like syntax tanks will be installed at each household with provision of necessary taps.

7.2 Hydro-Mechanical Equipment

The hydro-mechanical equipment primarily comprises of the gates at the diversion weir, valves at the powerhouse, storage tanks and at the branch canal-main irrigation pipe interface.

7.3 Construction Materials

Jagdapur is the nearest major town for the proposed project site at a distance of about 52 km from the project site. The manufactured construction materials like cement, steel, pipes etc will be sourced from this town depending upon the availability and cost effectiveness.

- i. Cement and Steel: Cement and reinforcement steel will be procured and transported by road having lead distance as indicated above. Random sampling will be done from the supplies received from time to time and the tests on the strength and properties of cement and steel will be got done from a reliable testing agency / nearby Engineering College. The structural steel such as I sections, Channels, Angles and Plates required for the fabrication works of gates and hoists will be procured by the contractors to whom the works will be entrusted on contract basis. The fabricators will be asked to get samples tested in reputed laboratories and furnish test reports before the materials go to the shops for fabrication.
- ii. POL: The civil contractors to whom works will be entrusted on contract basis will arrange themselves petrol, oil and lubricants for their machinery plant and equipment.
- iii. Coarse Aggregates: Coarse aggregates required for all the concrete works will be procured and transported by road from a suitable quarry situated nearby the project site. The excavated rock from the power house site is also proposed to be utilized for crushing aggregates, if found suitable. Samples of aggregates will be got tested in the laboratories to establish their suitability.
- iv. Sand: Sand required for the works will be procured from u/s & d/s reaches of Ganeshbahar Nala where sand deposits are abundantly available. The lead involved will be about 3 to 4 kms from the site. Samples of sand will be collected and get them tested at the laboratories for its suitability for use in RCC and other works.
- v. Bricks: Bricks required for the construction will be procured from nearest village where good bricks are available. Alternatively manufactured concrete blocks can also be used depending on its availability and cost effectiveness.

Chapter 8 – Electromechanical Equipment and Power Evacuation

8.1 Rotating Machinery – The Module ‘Micro Hydel Pump’

The concept of the micro hydel pump (also known as the module unit) has already been introduced in Chapter 1 and configuration of these module units was specified in Chapter 5 for the available stream flow conditions.

A more technical description is illustrated in Fig.8.1 in which the only driver unit is the turbine followed by the generator for electricity situated in an encapsulated watertight bulb. The generator shaft is linked to a component known as the clutch that is also housed in the same bulb. The other end of the clutch shaft comes out of the bulb and engages with the pump shaft through a coupling.

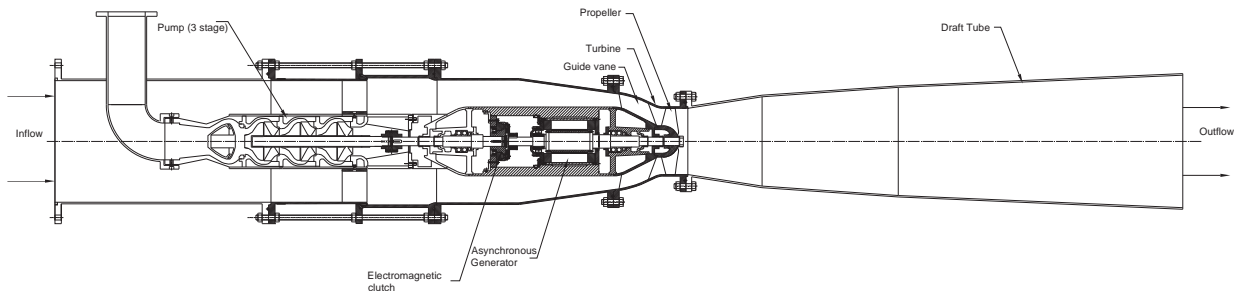


Fig. 8.1, The micro hydel pump module or hydro turbine pump module

8.1.1 Turbine

The turbine component of the micro hydel pump is an axial flow pump operated as a turbine with optimized hydraulics of the runner blades. Though the geometry of both guide vanes and runner blades is fixed, the pitch of the runner blades can be chosen before manufacture. The designers have already chosen an optimum pitch for the modules, but since the propeller is relatively inexpensive 2 or 3 runners with varying blade pitches can be supplied.

One important noticeable feature as seen in Chapter 5 and 7 in the layout of the submersible power plant will be supplied with two prototypes.

8.1.1.1 Prototype 1

The flow range and the adjustable design feature of the prototype 1 has already been illustrated in Chapter 5 (Table 5.1). The turbine mode characteristics of prototype coupled with an asynchronous generator is summarized under two different gate settings (30 deg and 60 deg respectively) in the following sub-sections.

a) 30° Setting of guide vane

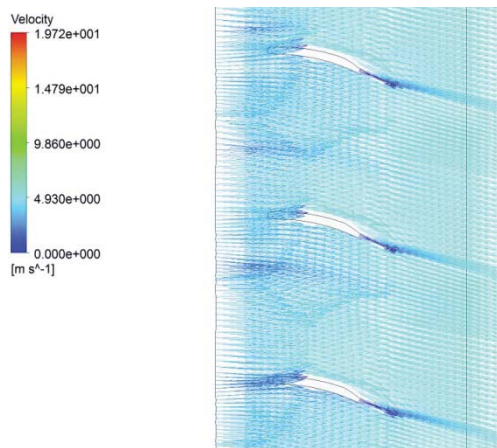


Fig. 8.2, 30° Gate setting of Prototype 1

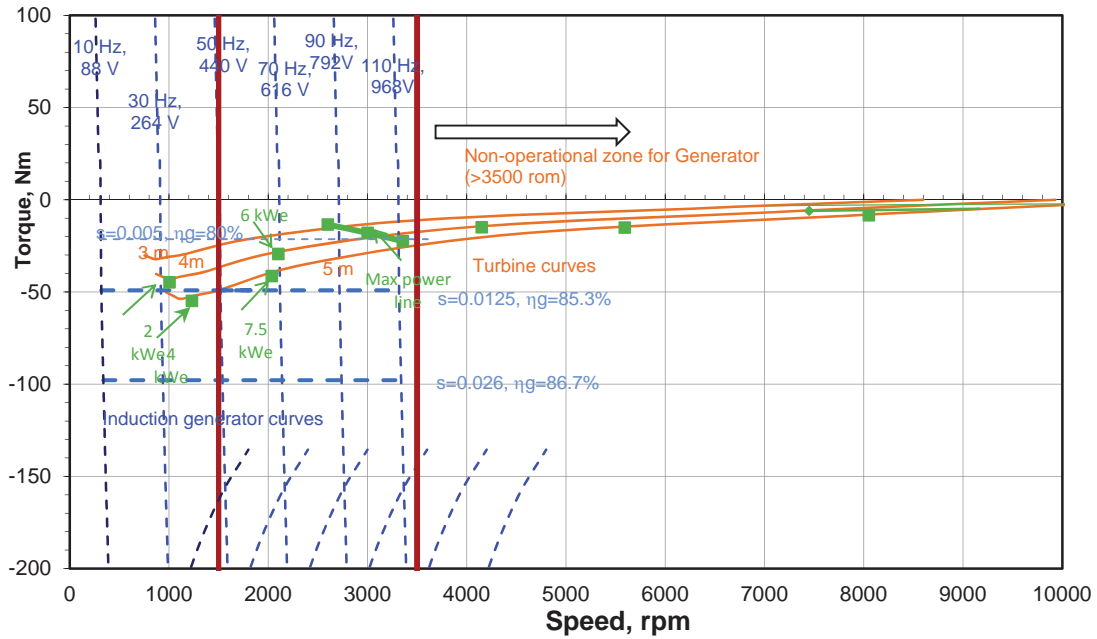


Fig. 8.3, Turbine-Generator characteristics of Prototype 1 -30 deg setting

Table 8.1, Selected points on the Torque-Speed field of 30 deg Prototype configuration

Sr. No.	Power and machine condition	H (m)	N (rpm)	Q (l/s)	T (Nm)
1	2 kWe	5	10141	921.	-2.2
2	(turbine in part load, generator in partload)	4	8720	800	-2.6
3		3	7015	653	-3.2
4	3.5 kWe (turbine in part load, generator in partload)	3	4244	424	-9.3
5	3.5 kWe (turbine in BEP zone, generator in partload)	3	1602	191	-24.5
6	4 kWe	5	9168	850	-4.9
7	(turbine in part load, generator in partload)	4	7450	399	-6.0
8	4 kWe (turbine in BEP zone, generator in partload)	4	1004	160	-44.8
	5.5 kWe (turbine in part load, generator in partload)	4	4150	186	-14.9
9	5.5 kWe (turbine in BEP zone, generator in partload)	4	2100	210	-29.4
10	6 kWe (turbine in part load, generator in partload)	5	8050	762	-8.4
11	6 kWe (turbine in overload, generator in BEP)	5	1230	186	-54.7
12	8 kWe (turbine in part load, generator in partload)	5	5590	559	-15.1
13	8 kWe (turbine in BEP zone, generator in partload)	5	2035	246	-41.4

b) 60° setting of guide vane

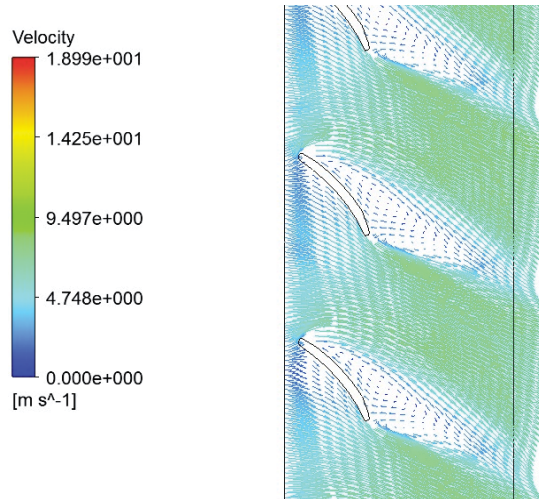


Fig. 8.4, 60° Gate setting pf Prototype 2

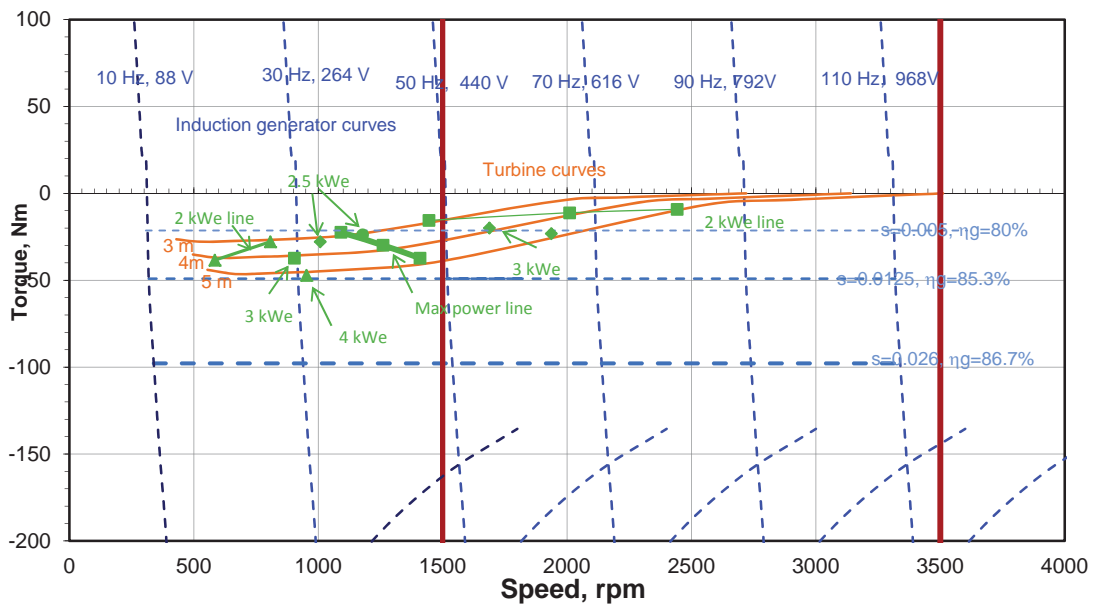


Fig. 8.5 Turbine-Generator Characteristics of Prototype 1 – 60 deg setting

Table 8.2, Selected points on the Torque speed field of 60 deg Prototype configuration

Sr. No.	Power and machine condition	H (m)	N (rpm)	Q (l/s)	T (Nm)
1	2 kWe	5	2442	224	-9.2
2	(turbine in part load, generator in partload)	4	2010	190	-11.2
3		3	1444	146	-15.6
4	2 kWe	4	584	106	-38.5
5	(turbine in overload, generator in BEP range)	3	807	111	-27.8
6	2.5 kWe	3	1178	135	-23.8
7	(Turbine in BEP and generator part load)	3	1008	123	-27.9
8	3 kWe	4	1688	174	-20.0
	(turbine in part load, generator in partload)				
9	3 kWe	4	904	126	-37.3
	(turbine in overload, generator in partload)				

10	4 kWe (turbine in part load, generator in partload)	5	1936	197	-23.2
11	4 kWe (turbine in overload, generator in partload)	5	953	139	-47.2

8.1.1.2 Prototype 2

As discussed the prototype 2 has an axial flow pump operated as turbine, which has fixed geometries of gate setting and runner. The turbine characteristics if prototype 2 is described in Table 8.1 and Fig. 8.3.

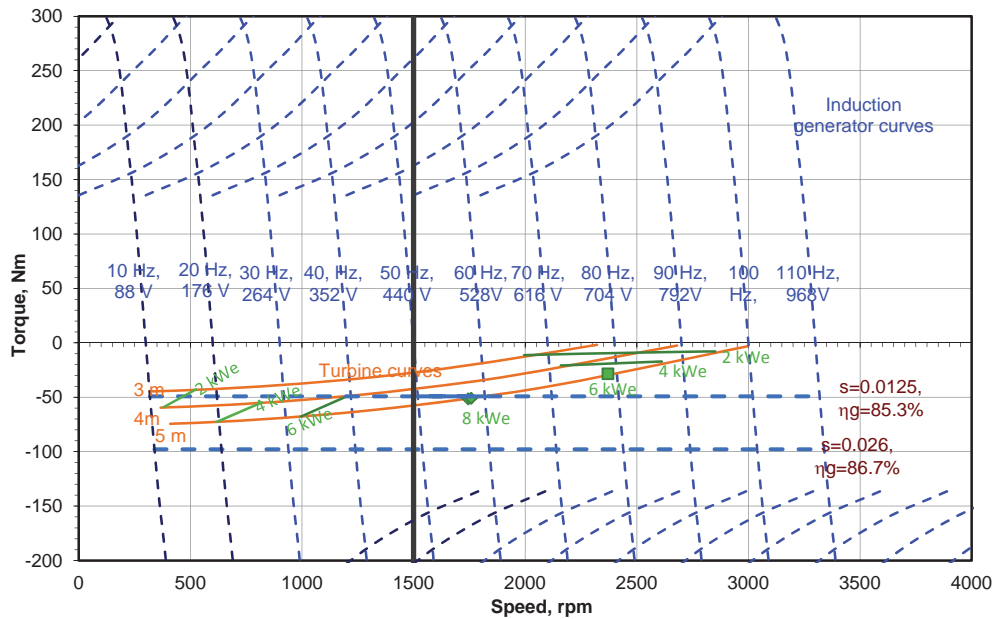


Fig. 8.6, Turbine mode characteristics of Prototype 2

Table 8.1, Summary of the Constant Power lines of Prototype 2

Sr. No.	Power and machine condition	H (m)	N (rpm)	Q (l/s)	T (Nm)
1		5	2851	459	-7.9
2	2 kWe (turbine in partload and generator in partload)	4	2464	415	-9.1
3		3	1995	365	-11.3
4	2 kWe (turbine in overload and generator in BEP)	4	380	140	-59.1
5		3	525	135	-42.8
6	4 kWe (turbine in partload and generator partload)	5	2612	445	-17.2
7		4	2160	399	-20.8
8	4 kWe (turbine in overload and generator in BEP)	5	619	172	-72.6
9		4	820	170	-54.8
10	6 kWe (turbine in partload and generator in partload)	5	2370	295	-28.4
11	6 kWe (turbine in overload and generator in partload)	5	995	197	-67.7

12	generator near BEP)	4	1200	198	-49.1
13	8 kWe (turbine in partload and	5	1744	246	-51.5
14	generator at BEP)	5	1758	250	-51.1

8.1.2 Generator

The generator chosen for this project is an asynchronous generator of class IE4-(Supreme class motors) with very high operating efficiency over wide loads. However, these types of generators will need external excitation that is done via a dedicated battery backup as explained in section 8.2.

8.1.3 Electromagnetic Clutch

The electromagnetic clutch is very critical component of the module. Its performance should be reliable and foolproof. It is normally engaged when electricity is not supplied and operates the pump since pumping is the priority for the people. When electricity supplied to this clutch is gets disengaged and the electricity generation becomes possible.

8.1.4 Pump

The pump is a conventional multi-stage submersible pump. It operates at a same speed as that of the turbine, since the head is less than 25 meters, centrifugal pump designs are adopted. Two different pumps are used for prototype 1 and prototype 2. The overall turbine-pump characteristics for prototype 1 and 2 are shown in Fig. 8.4 and 8.5 respectively.

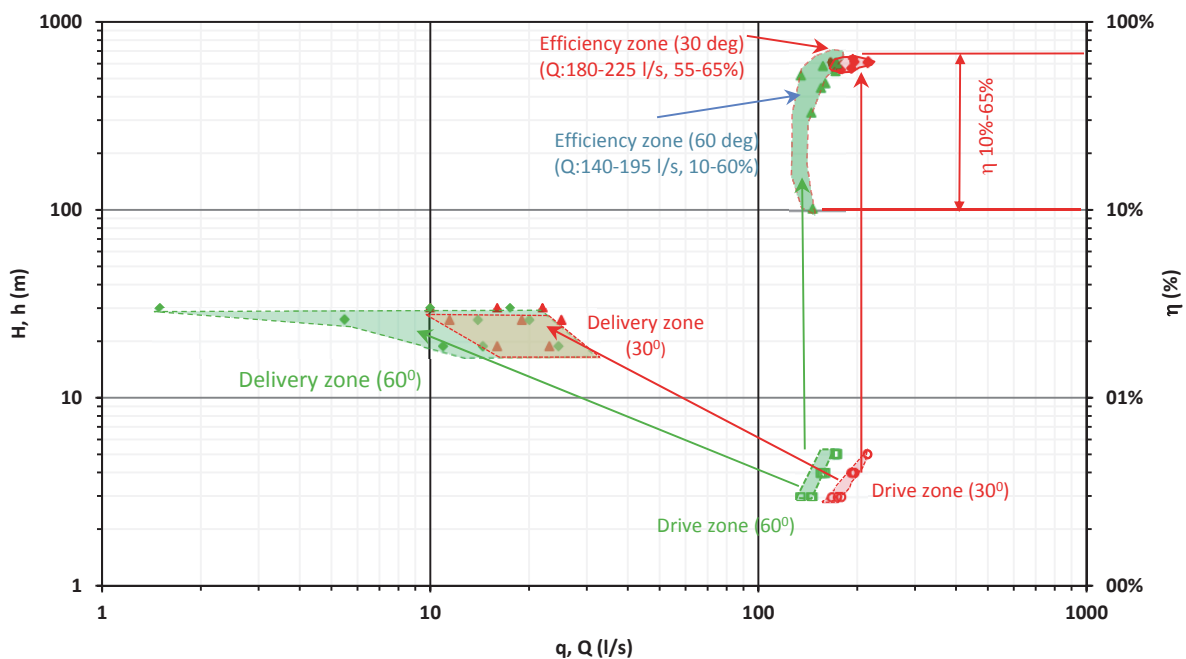


Fig. 8.4, Overall pumping characteristics of Prototype 1

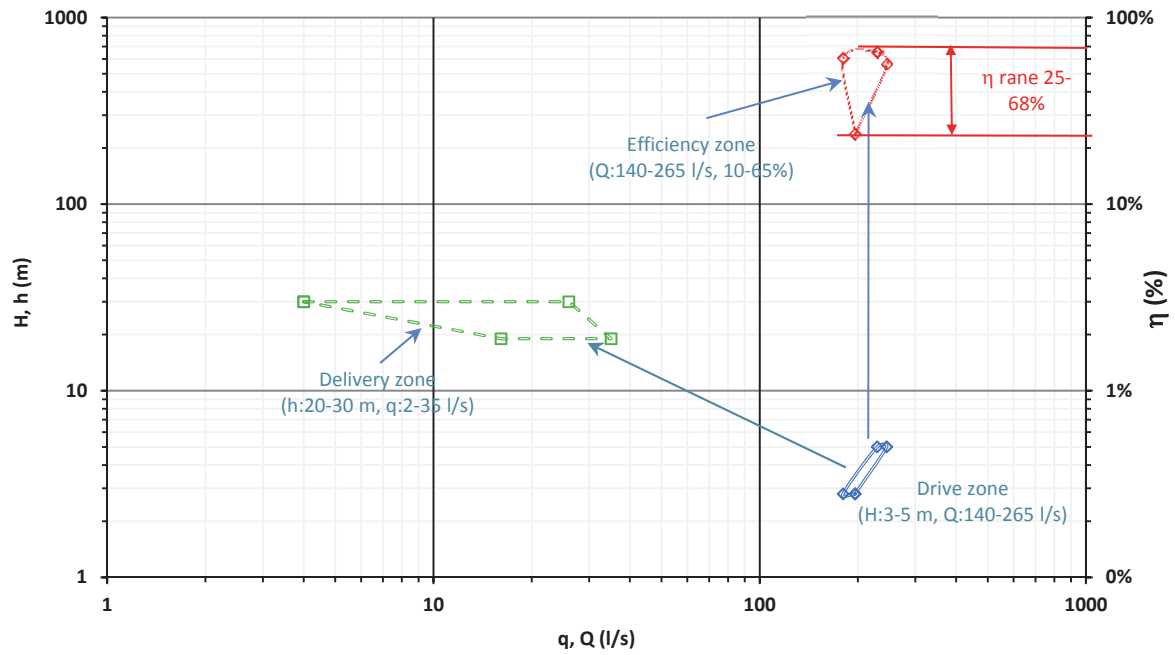


Fig. 8.5, Overall pumping characteristics of Prototype 2

8.2 Ram Pump

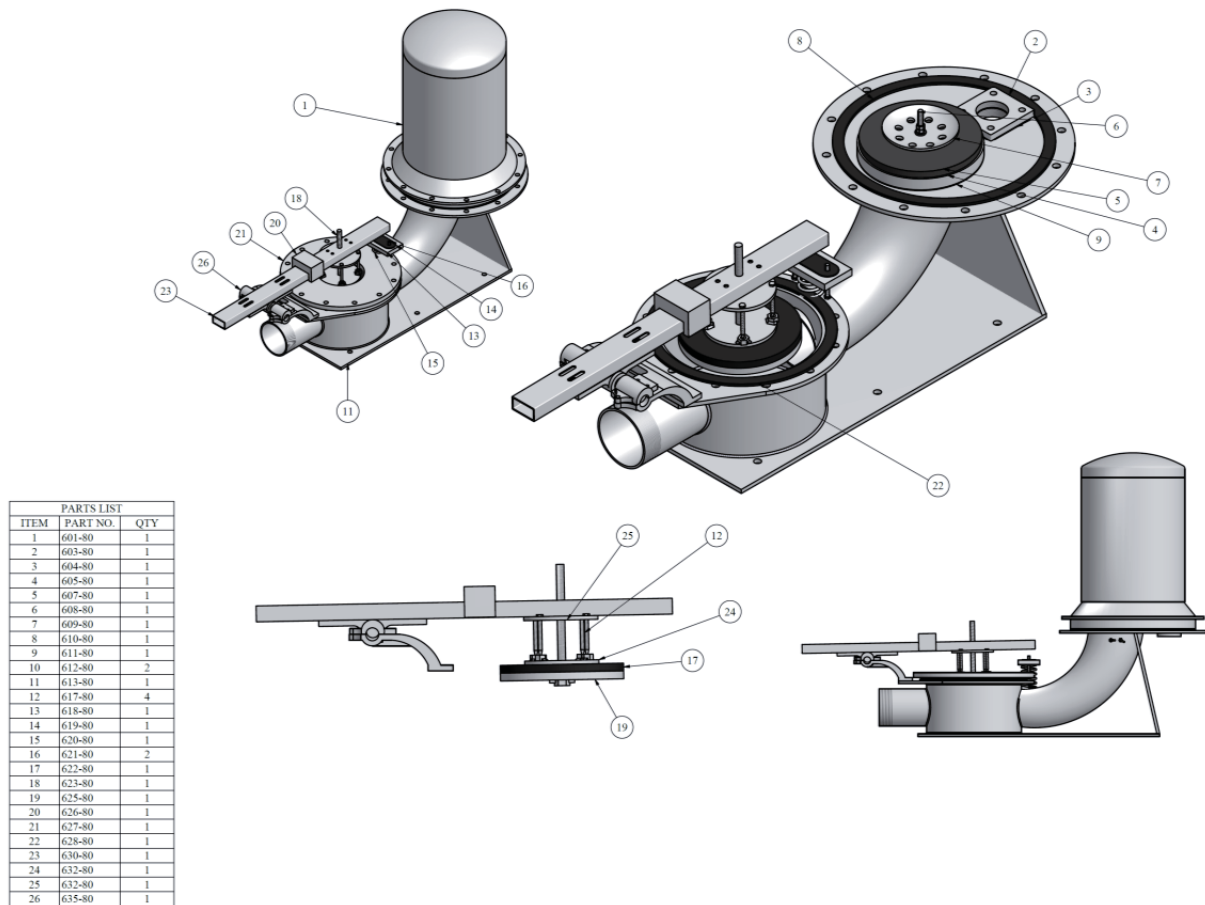


Fig. 8.6, Cross-section of the Ram Pump (Source, Rife Ram Pumps 2010 [11])

Part No.	Description	Part No.	Description
601	AIR CHAMBER (IRON)	619	LEVER REST & CUSHION
602	AIR CHAMBER BOLTS (6)	620	LEVER REST SPRING
603	outlet flange	622	OUTSIDE RUBBER VALVE
604	outlet flange gasket	623	OUTSIDE VALVE CENTER BOLT
605	GRIDIRON	625	LOWER WASHER
606	GRIDIRON BOLTS	626	LEVER WEIGHT & BOLTS
607	INSIDE RUBBER VALVE	627	VALVE CHAMBER (IRON)
608	INSIDE VALVE BOLT W/ NUTS	628	VALVE CHAMBER GASKET
609	INSIDE VALVE WASHER	629	VALVE CHAMBER BOLTS
610	AIR CHAMBER GASKET	630	LEVER & BOLTS (2)
611	GRIDIRON GASKET	632	UPPER WASHER
612	AIR FEED VALVE BODY & PIN	635	ROCKERSHAFT ASSEMBLY COMPLETE
613	BASE (IRON)	638	DRIVEPIPE COUPLING
614	LEG AND BOLT	639	DRIVEPIPE COUPLING BOLTS
615	PIN PIECE & BOLTS (2)	640	DRIVEPIPE COUPLING GASKET
617	ADJUSTING PIN (3)		
618	LEVER REST STUDS (2) w/ NUTS		

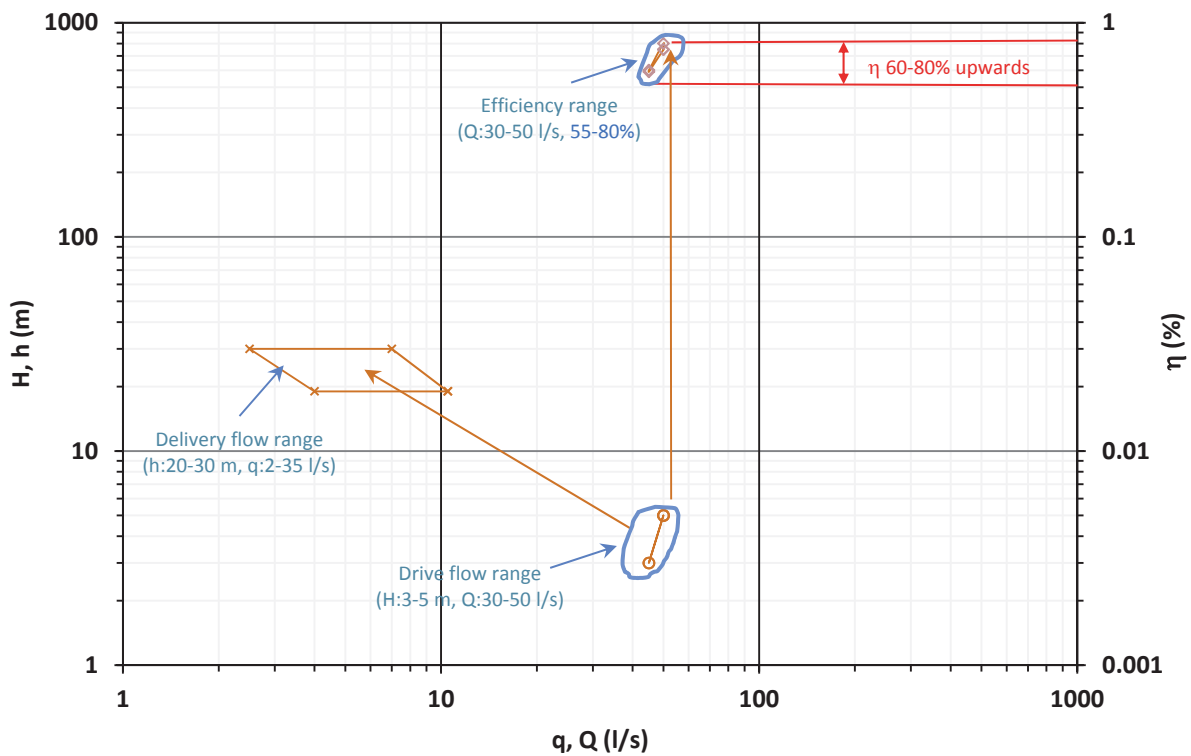


Fig. 8.6, Characteristics of the Ram Pump

8.3 Control System

The control system of the modules comprises of two components. The first component is the 4-quadrant full load converter for the asynchronous generators and the second part is the regulation required for the electromagnetic clutch.

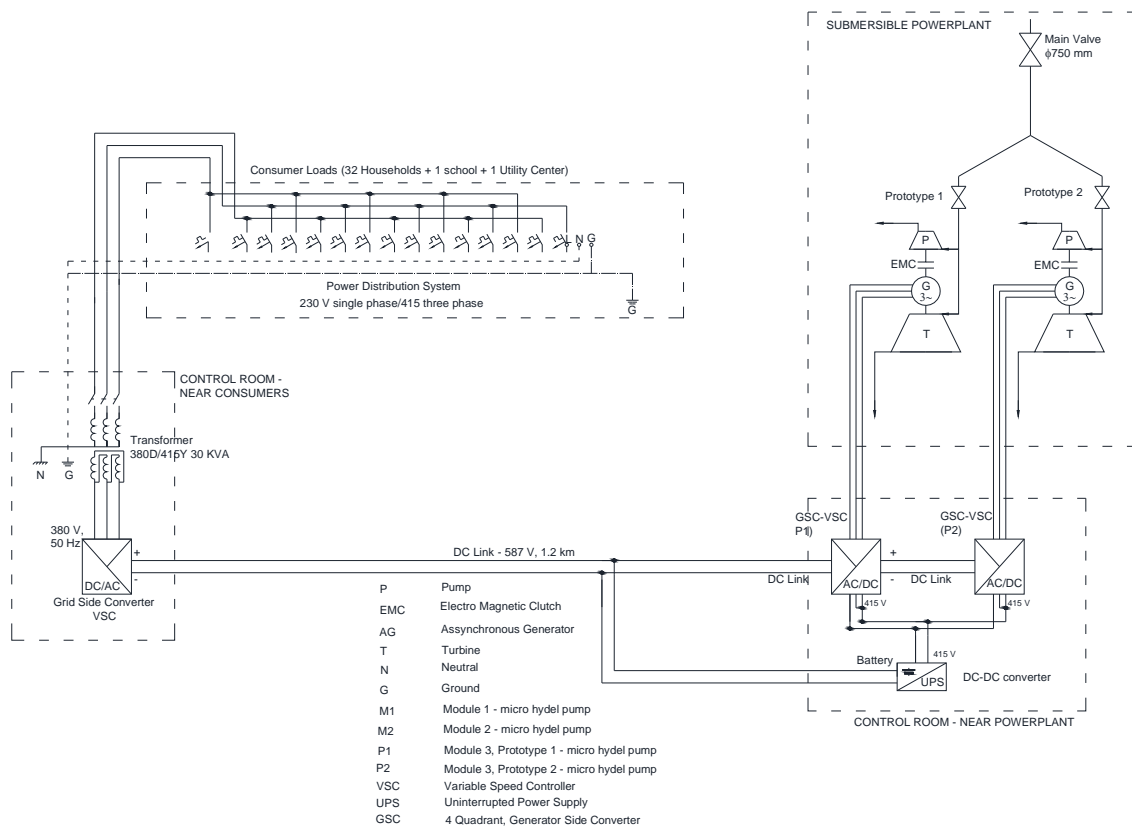


Fig. 8.6 Single Line Diagram of the Electromechanical, Control and power evacuation system

The line diagram in Fig. 8.6 explains the basic function of the control system. The full load converter comprises of two separate controller units known as the variable speed controller. The first VSC, which is closer to the power plant is specially referred to a generator side converter. It senses the speed and flux of the stator coil at various loads and adjust the torque and speed to optimal values corresponding to the hydraulic condition of the turbines (head and flow). The VSC on the grid side regulates the phase and frequency of the load current. The two converters are separated by a DC link that helps the two controllers to work independently.

This technology helps the load to exactly correspond to the turbine output. Hence, the flow and head may change accordingly. This facility eliminates the need of a separate load balancer or controller used in conventional decentralized power projects.

However, there is permanent backup that will be needed to start the generators by supplying the reactive power and the also electricity to the electromagnetic clutch. The battery backup is charged from the DC link as shown in Fig. 8.2.

In addition to these components, there is transformer located at the output the grid side converter for enhance the supply voltage to 415 V. There would be a drop of 10 to 25 V in the DC link that extends for more than 1 km.

8.4 Power Evacuation

The power evacuation system is briefly touched in Fig. 8.6. The loads comprise of the 32 households, one school and two utility centers (A3.3.4) as described in Appendix A3. While all the loads have single phase distribution, the utility center, which comprises of machineries, will be provided with 3 phase supply.

Chapter 9 – Environment Impacts and Benefits

9.1 General Aspects

Small, Mini and Micro Hydel projects are distinct from the conventional and large hydroelectric projects due to simple layout and mostly non-interference with the regime of flowing water. The bulk of small and micro hydro projects in India would be run off River type developments utilizing higher heads with or without small pondage. The other category of low head schemes may utilize the flows as a part of irrigation/drinking water facility and drops available in the course of canal/river. The first category would involve very little submergence, rehabilitation, deforestation etc, and have practically no adverse effect on environmental and ecology of the area. The other category utilizes water from the existing body and hence no additional environmental impacts are associated.

Hydro Projects involving capital outlay up to Rs. 54 Crores (ca 6.7 million euros) has been exempted from obtaining environmental clearance from Ministry Of Environment and Forests. Forest clearance, if applicable and clearance from Pollution Control Board are required to be obtained. Specifically this project is

- i. Free from hazards of pollution.
- ii. There is no submergence of land, and therefore no loss of forest reserves /land
- iii. No resettlement/relocation of people
- iv. No dislocation of habitation, monuments and communication facilities
- v. Up to 50 laborers may be engaged in various construction activities at the site
- vi. The project will be executed entirely by local laborers
- vii. No Flora and Fauna will be affected on account of the project construction.

The area around the powerhouse will be appropriately landscaped keeping sensitivities of forest ecology. These will be undertaken under the advice of qualified personnel, so as to keep up and possibly enhance the beauty of nature around the project area.

On the whole, the project does not create any environmental problem, non- polluting and environmental friendly. On the other hand, it makes a favorable and striking impact on the regional ecology. Irrespective of the above there is a strong need to make a non-biased impact assessment to find out if this project can have even smallest or unnoticeable adverse effect.

9.2 Impact Assessment

As discussed above, the impacts of this unique concept that so strongly supports local ecology (i.e. forest, water table and river basin in total) along with limited economic value have to be truly represented. The promoters foresee 3 major impact categories, first during construction activity, second the diversion of flow through the penstock and third, which is most important impact category concerns the extent of submergence of forest and farmlands during flash floods.

9.2.1 Construction Activity

The major construction activities in this project take place in components like the diversion weir, main supply tank, pipe laying and canals. The forest cover will have to be protected during construction. Felling of grown trees will not be allowed, though bushes and some plantations will have to be selectively removed only after consultation with the villagers.

There would be strict conditions of the contractor to protect local environment while bringing in machinery for construction. There would be no major contract laborers from outside except for few experts like masons or supervisors. The villagers (both men and women) will provide all the labor for the contractor. This in a way will ensure the village's participation at every step of the construction activities. The experience of building the measurement weir and its subsequent repair show how successful construction management can be if the local villagers are used as paid laborers.

Noise pollution is another factor of concern during construction, which will have to be maintained within the permissible limits of the Forest Act.

9.2.2 Diversion of Water to the Power Plant

The chapter 5 (Fig. 5.1) shows that a substantial portion of the stream flow is diverted into the penstock for the use in the modules. In Table 9.1, the monthly averaged module flow for both the modes (water pumping and electricity)

is compared to stream flow in the respective months. It can be seen that module flows are lower compared to the stream flow except in the month of February, indicating residual flow in the riverbed.

Nevertheless, there are three important arguments justifying that this flow diversion from the riverbed will not impact river ecology. Firstly, the river basin is of the effluent category with the water table supporting the stream uniformly over the entire stretch of 20 km. Secondly, the major part of the selected stream section (where diversion takes place) is having a very small slope with large depths resulting in a pond like environment that will always be filled. Thirdly, the length of diversion is only 230 meters before the major flow (except for pumped out flow) joins back after passing through the modules.

Table 9.1, Comparison of module flows (pumping and electricity modes) with stream flows

Sr. No.	Month	Stream flow (l/s)	Module flow (l/s)	
			Water mode	Electricity mode
1	January	210	160	160
2	February	153	156	150
3	March	133	104	100
4	April	114	98	95
5	May	105	98	95
6	June	71	57	60
7	July	1036	462	430
8	August	929	462	430
9	September	661	462	430
10	October	490	462	430
11	November	376	265	320
12	December	286	250	250

9.2.3 Effect of Pumping Water on River basin

The water pumped out of the stream will be primarily used for irrigation, which as discussed in section 9.3 will become a part of the water cycle with some percentage of this flow returning to the basin's water table. However, one has to honestly compare this quantity in comparison with the module flow used by the pump as well as the turbine. This value should not be large to affect the downstream communities (primarily the Tiriya settlement as the Ganeshbahar Nala ends there).

This comparison is carried out in Table 9.2. It can be seen that the pumped flow does not exceed 11% of the stream flow (only during pump operation i.e. 16hr/day or 67% of the time). This will not cause any change in livelihood of the Tiriya settlement. However, the villagers belonging to Tiriya need to be explained about this quantity being pumped out.

Table 9.2, The analysis of quantity of water pumped out from Ganeshbahar Nala

Sr. No.	Month	Q _{pump} (l/s)	Stream flow (l/s) (from Table 5.1)	Pumped flow as percent of stream flow
1	January	15	210	7%
2	February	14	153	9%
3	March	12	133	9%
4	April	11	114	10%
5	May	11	105	11%
6	June	7	71	10%
7	July	52	1036	5%
8	August	52	929	6%
9	September	52	661	8%
10	October	52	490	11%
11	November	30	376	8%
12	December	25	286	9%

9.2.4 Floods and the Issue of Submergence

The flood studies in section 4.2 (Chapter 4) show how uncertain the promoters are with respect the quantity of the historic flood level (for example 100-year high flood level, $HFL_{@100 \text{ years}}$). Despite the assurance from the villagers that entry of flood flow into forestland and farmland is normal and would last for a short duration, the promoters would not like to take chances with nature's fury that may result in any unforeseen tragedy.

To be on the safer side, the promoters have decided to construct the diversion weir in stages. For the first year, the weir will be built at an elevation of 509 meters (2 m below the 511 meter as per design). After being satisfied with the floods during the first years' monsoon, the height of the weir will be gradually increased in next year. It is envisaged to reach the design height of 511 meters in 3 or 4 years of time.

9.3 The Concept of Limited Growth and Environmental Sustainability

The unique interdependence characteristics of engineering solution planned for the requirements of the Taipadar village have already been detailed out in Chapter 1 (section 1.4). However, there is further underlining feature of creating a model for limited growth, which paves way for environmental sustainability.

The three features of the project namely, irrigation, electricity and drinking water will certainly improve the livelihood and economy of the local population, but these cannot contribute to a high economic growth model that can cause either expansion of cultivable land or excessive use of electricity. The renewable characteristics ensure that even with maximum use of the project (16 hours for pumping and 8 hours of electricity a day), this can only facilitate a paddy crop for an area of 34 ha (Section 6.2.3) for 4 months, 28 ha of wheat crop for 4 months and less than 8 ha of land for mustard out of a total available cultivable area of 80.7 ha (section 1.2).

The water that is used for irrigation is taken out of the stream but this does not disturb the ground water dynamics. In fact the water used by the crops will eventually become a part of the water cycle with some percentage evaporated and some entering the water table to eventually find its way back to the stream.

The electricity is used for only utility loads and forbidden to pump out ground water for even for drinking water let alone for irrigation.

This limited growth model is explained and well-understood by the villagers that this unique project cannot be compared to grid connected environment where people can use electricity as much as required when available. The people have no choice and have to adapt to this model of limited growth.

Hence, this engineering solution called the micro hydel pump will always guarantee the total environmental sustainability be it protection of forest cover or groundwater or river basin

Chapter 10 – Cost Estimates

10.1 Abstract of Total Project Costs

This section covers only the basic outline of the capital investment need for the civil works (that includes hydropower, irrigation, drinking water supply utilities), electromechanical equipment along with control system and power evacuation. A detailed 'bill of quantities and cost estimates' for each of items is covered in the Annexure A3.

Table 10.1, Summary of the Total Project Costs

Sr. No.	Particulars	Total Cost (in INR, lakhs)
1	<u>Civil Works (A3.1)</u>	
1.1	Hydro Power component (diversion weir, penstock for two 'turbine-pump' prototypes and one ram pump, powerhouse)	120
1.2	Hydro irrigation component (Delivery pipe for turbine pumps and ram pump, Storage tank, Main irrigation line, Branch & Field channel)	154
1.3	Drinking water supply component Tank and distribution system for each household	30
2	<u>Mechanical Devices</u> (Turbine-pump Prototypes in A3.2.1 and Ram pump in A3.2.2)	159
3	<u>Control System and Power Evacuation (A3.3)</u>	110
4	<u>Other Costs</u>	
4.1	Lands, Preliminaries including Statutory fee payable	10
4.2	Surveys & Investigations	3
4.3	Infrastructure Works	3
4.4	Engineering & Consultancy	5
4.5	Operational Costs during construction - Office administration including establishment	6
Grand Total (in lakhs INR)		599

10.2 Utility-wise distribution of costs

The distribution of projects costs from the perspective of utilities could be of help for evaluation from different funding agencies, since no single department will be able to fund the entire project. This is done in the following table under 3 categories, Micro hydel, irrigation and drinking water. This distribution has also been illustrated in the form of flow charts in Chapter 12 (section 12.3).

Table 10.2, Distribution of Project Costs Utility-wise

Sr. No.	Utility	Components	Costs (in Lakhs)
1	<u>Micro Hydel (without Micro Hydel Pumps costing 100 Lakhs)</u>		
		Diversion Weir	34
		Penstock Line 1	44
		Powerhouse	32
		Turbine Accessories	25
		Control System	57
		Transmission/Distribution and Loads	47
		Overheads	20
		sub-total for Micro Hydel	259

2	<u>Irrigation</u>		
	Phase 1 - with Ram Pump	Ram Pump	34
		Penstock Line 2	10
		Delivery Line 1	16
		Branch and Field Channels	28
		sub-total (Phase 1)	88
	Phase 2 - with Micro Hydel Pump	Storage Tank	41
		Pump Delivery Line 2	42
		Main Irrigation Pipeline	27
		sub-total (Phase 2)	110
		Irrigation overheads	8
		<u>Sub-total - Irrigation Utility</u>	<u>206</u>
3	<u>Drinking water</u>		
		Coagulation tank	4
		Supply lines (North and South)	21
		Distribution lines	5
		Overheads	4
		<u>sub-total</u>	<u>34</u>
		Total of all Utilities	499

Chapter 11 – Financial Studies

11.1 Economic Value from Benefits

The economic value from the 3 utilities (annual electricity in Chapter 5, irrigation yield and drinking water in Chapter 6) has been quantified approximately based on market value [9] and summarized in Table 11.1. The total value (per year basis) of the 3 utilities put together is about 48.5 Lakhs of Indian Rupees (ca 60660 Euros).

Table 11.1, The Economic Value of the Benefits of the Taipadar Integrated Project

Sr. No.	Yearly Benefits	Quantity		Value/unit	Total (INR)
		Value	units		
1	Electricity	18405	kWh	4	73621
2	Irrigation				
	Paddy	102958	kg	20	2059160
	Wheat	97326	kg	20	1946515
	Mustard	21377	kg	35	748196
3	Drinking water	16425	m ³	1,5	24638
Total value benefits in a year			(Indian Rupees)		4852971
			(in Euros)		60662

11.2 Cost-Benefit Analysis

The overall economics of the project is worked under simple parameters of determining the net present value of the scheme (NPV) in Table 12.3 under the conditions (summarized in Table 11.2). It can be seen that the annual net income negative value, which means that the NPV also negative number signifying a 'loss' for the assumed discount rate of 5% and a relatively long project life of 20 years.

Table 11.2, Summary of conditions for determining the economic indices

Sr. No	Particulars	Units	Value
1	Total Project Cost	(in INR)	59917278
		In Euros (80 INR=1 Euro)	748966
2	Discount Rate	(%)	5%
3	Life	(Years)	20
4	Projected revenue/Income	(Euros)	60662

Table 11.3, The Economic Indices of the Taipadar Project

Sr. No.	Parameter	Units	Value	Comments
1	Annual Cost	Euros	60099	
2	Annual maintenance cost	Euros	6000	
3	Net Annual Cost	Euros	66099	
4	Income	Euros	60662	
5	Net Income	Euros	-5437	Loss
6	Present Value of Income			Negative value
7	Net Present Value (Present Value - Net Annual Cost)		- Indeterminate	
8	IRR	%	-Indeterminate	

11.3 Larger Aspects of Benefits – Societal Perspective

The simplified financial analysis (section 11.2) reveals that this project would not make any economic sense and financier will not like to invest in the project, given the negative values of net income, present value and NPV.

The environmental benefits have been discussed elaborately in Chapter 9, which would definitely have an economic value in terms of income (or revenue). Renewable energy projects are entitled for carbon credits, but this has not been considered here. There are sufficient controversies in determining the accurate ecological income. This is not the objective of the study in this 'Detailed Project Report'. However, there is societal aspect that has to be recognized and presented.

The economic value that this project will add, from the irrigation yield alone is 60660 Euros (ca 48.5 lakhs in Table 11.1), is much more than the 48000 Euros per annum (illustrated in section 1.2, Chapter 1) that the village currently earns. This would definitely result in the improvement of the quality of life with more than double the earnings per family.

There would be a great reduction of human drudgery and labor as the time and effort spent in carrying water home is reduced or eliminated. Further, mundane jobs of dehusking and milling, particularly by the women folk, would see sharp decline with use of machinery. The time saved can be used for other activities like working in fields and also in education, in handicrafts like tailoring and others.

There would also be a marked improvement in sanitation conditions with construction toilets and bathing areas within the house, which directly enhances the health standards of the people. Education standards are bound to improve with mass media and computer facility planned. Telecommunication facility that is currently not available can be brought in by the installation of mobile towers using the electricity generated. Further, the villagers will be busy throughout the year and will not need to work as contract laborers. This will pave way for ending the temporary migration.

The above social benefits have to be recognized in addition to the ecological benefits. The conventional economists (market driven) would hardly take such consideration, even though there is an increasing awareness. Therefore, the promoters would underline the need for a debate between conventional and ecological economists.

This project is certainly not discouraging in terms of economy. The villagers can be charged for the benefits (water and electricity) and some methodology of an economically sustainable model can be developed.

Chapter 12 - Project Implementation Phases

12.1 Introduction

The diverse project like Taipadar that attempts to demonstrate 3 different utilities (electricity generation, irrigation and drinking water supply) and is relatively expensive for population of 200 habitants, needs a careful treatment as far as implementation is concerned.

As seen in Table 10.1 in order to realize the three utilities of the project in total, all the four components (civil works, electromechanical equipment, control system and power evacuation, and other costs) would have to be addressed. However, for implementing each of the utilities, the components and sub-components have to be reorganized with an objective of not only realizing a particularly utility completely, but also keeping the investment low.

It is proposed to implement the project in 3 phases as discussed in section 12.2. The Phase 1, which focuses implementing the only irrigation utility, is termed as 'Hydropower and Irrigation'. Irrigation utility cannot be realized without including hydropower and electromechanical components because of the inherent design of the prototype that includes generator as part of the turbine pump system as seen in Chapter 8.

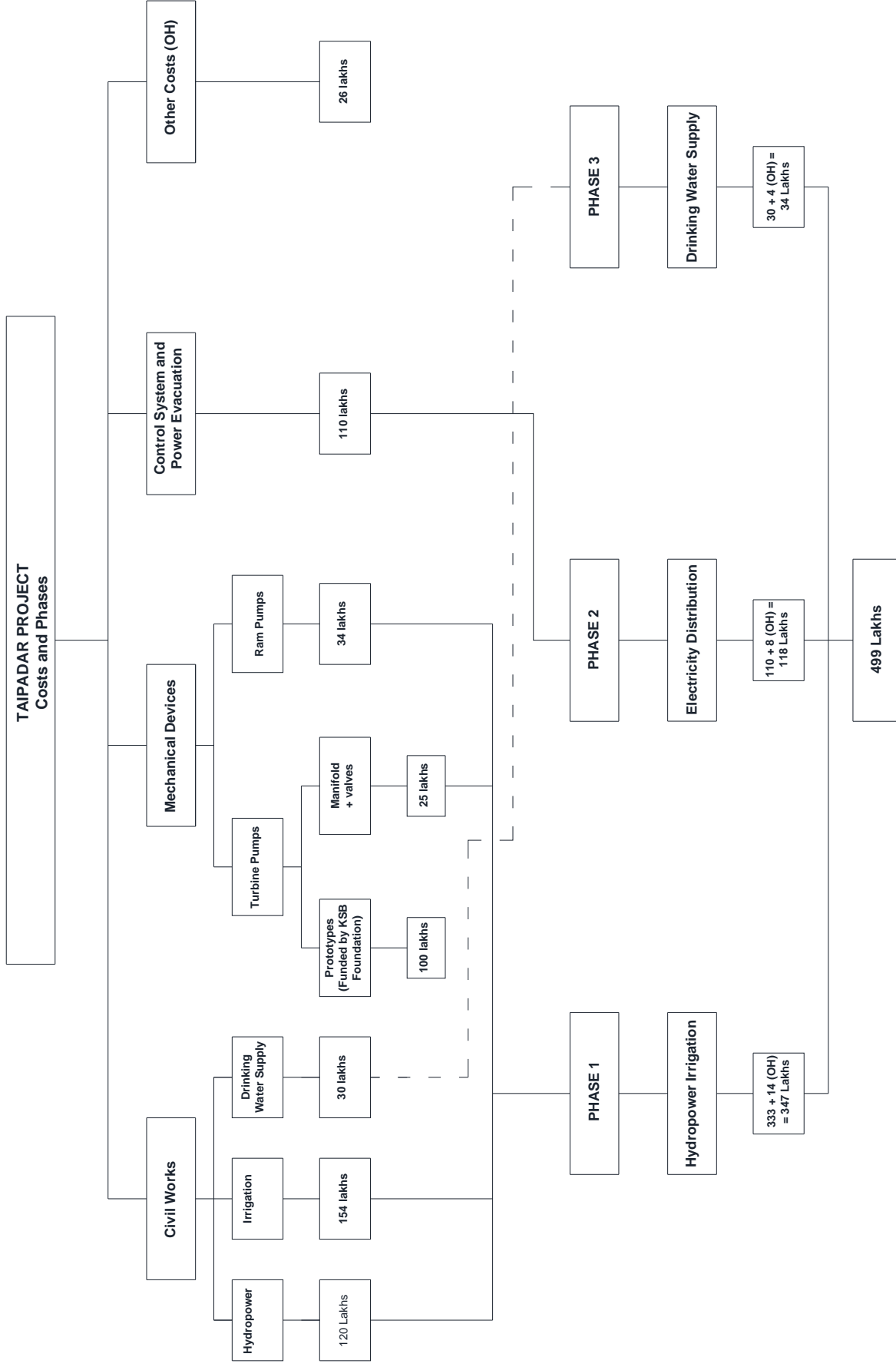
The second phase of implementation (electricity distribution) will have components like control system and power evacuation gears. The final phase (Drinking water supply) includes only the sub-component of civil works.

The fourth component of project costs (i.e. other costs) is proportionally divided to the 3 phases as illustrated in section 12.2 and 12.4. Phase 1 is the most expensive phase of the project (285 lakhs) followed by phase 2 (118 lakhs) and phase 3 (34 lakhs). The cost for the two prototypes (ca 100 lakhs) is excluded in Phase 1 as it is funded by KSB Foundation.

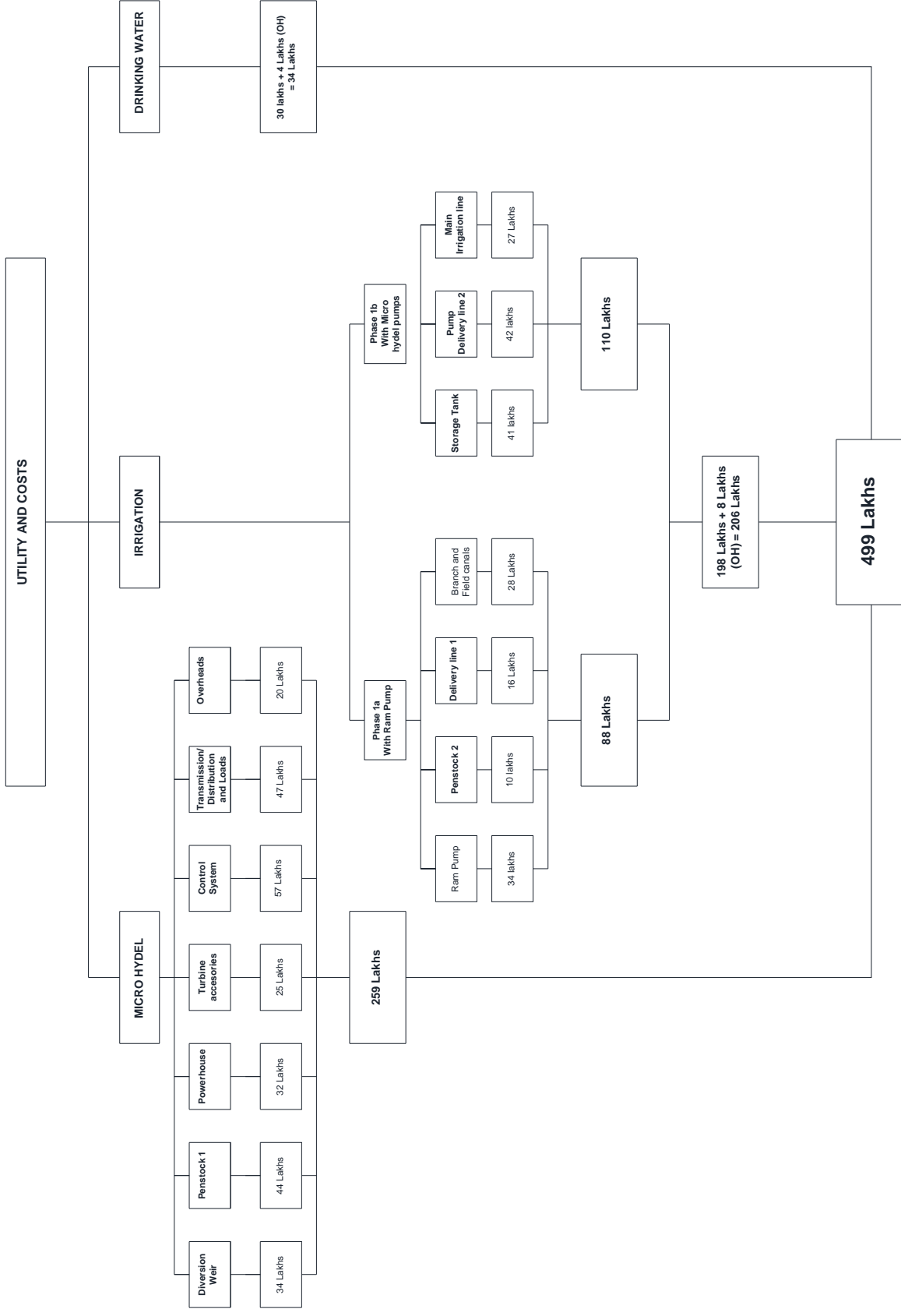
Another flow chart that gives the utility distribution of the project costs (in accordance with Table 10.2, Chapter 10) has been presented in section 12.3.

Section 12.5 gives a detailed outline of the components for Phase 1. It can be seen that without having the hydropower structures in place, the irrigation utility that forms of the backbone of the future revenue (chapter 11) cannot be commissioned.

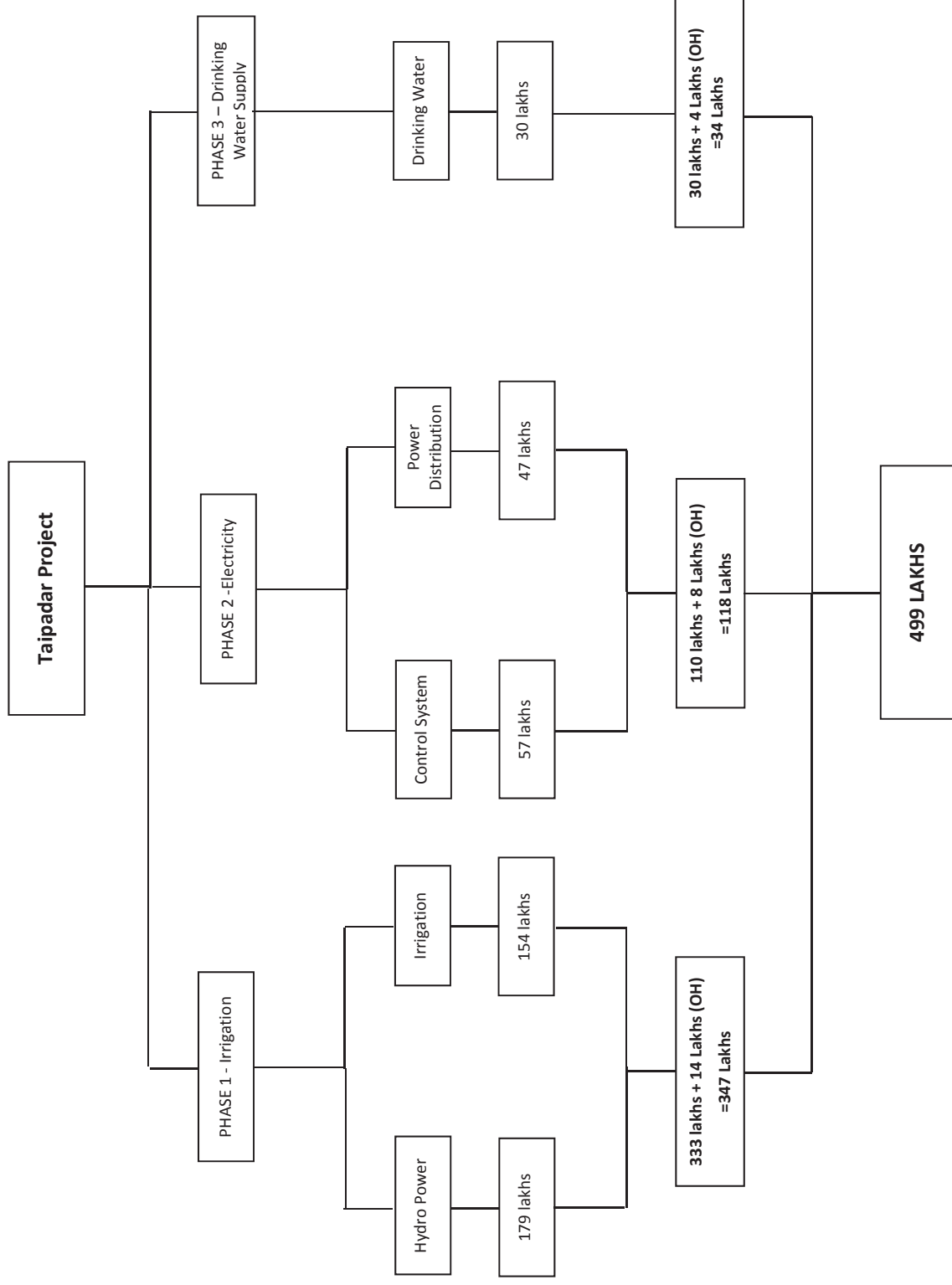
12.2 Overview of the Taipadar Project – Components, Cost and Phases of Implementation



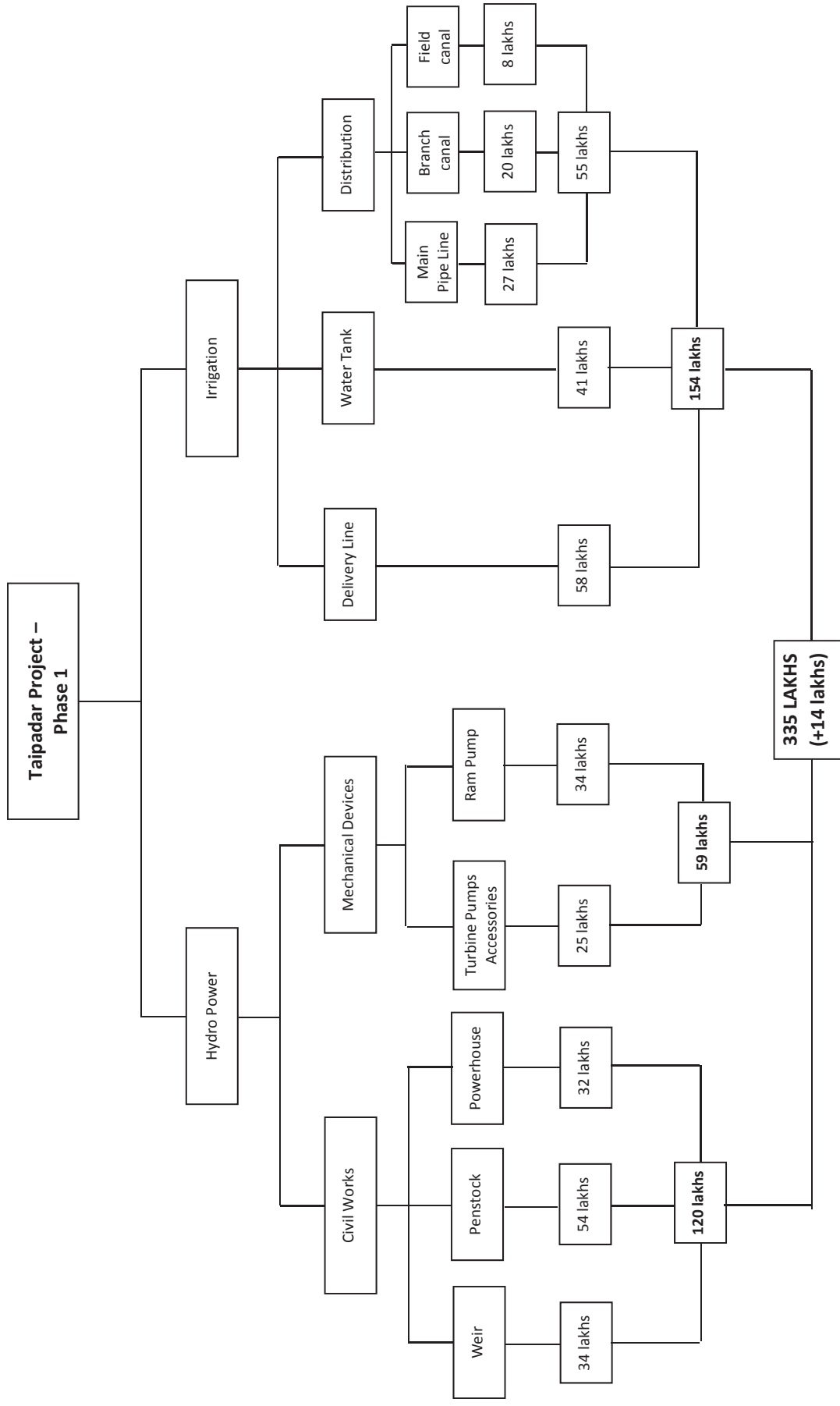
12.3 Utility-wise distribution of project costs



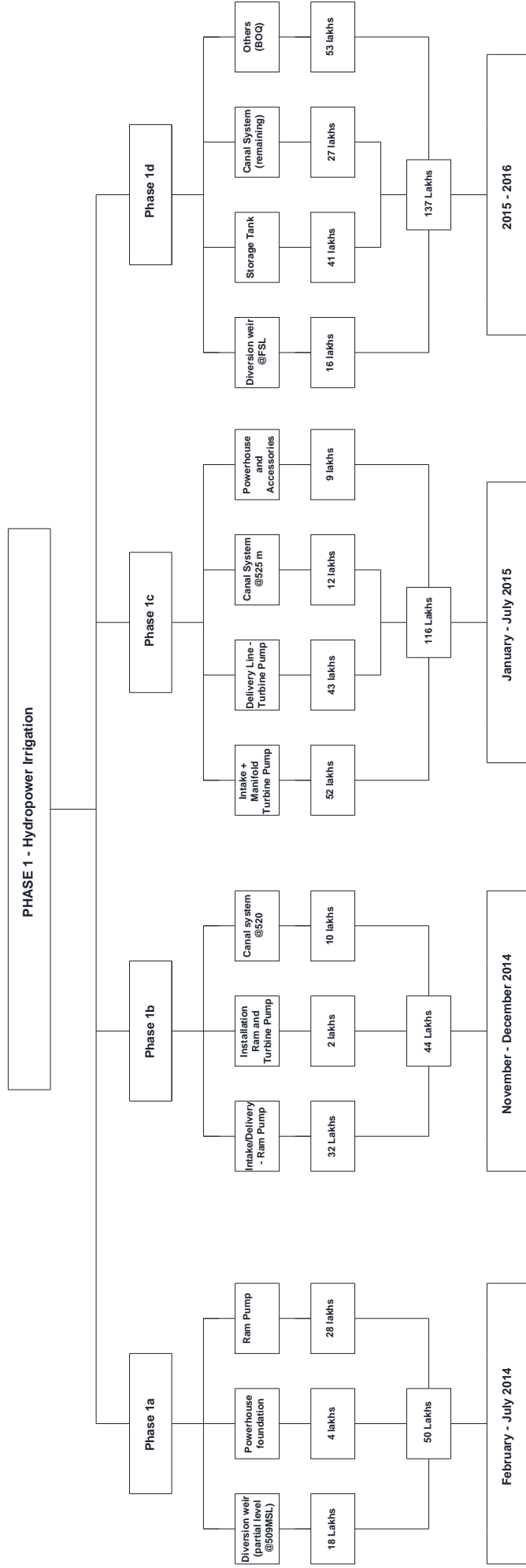
12.4 Implementation Phases of Taipadar Project



12.5 Flow Chart for Phase 1 – Hydropower and Irrigation



12.6 Planning chart for Phase 1



Chapter 13 – Project Management

13.1 Organization Chart

The organization structure for implementing the Taipadar Project would comprise of a 3 tier structure with Funding Agencies occupying the first tier. The second tier would be the implementing agency and followed by the third tier comprising of consultants, contractors and a separate group responsible for running the plant.

Since, the investment for the project is substantial (as seen in Chapters 10 and 11) and with the limited sources as of now (only KSB Foundation has committed to fund the two prototypes of the order of 100 lakhs), additional funding of 499 lakhs needs to be arranged to complete the project. However, for the Phase 1 (Hydropower and Irrigation) an investment of 347 lakhs would be required.

As per the proposal illustrated in Fig. 13.1, the funding agencies will provide funds to the implementing agency, which will be responsible for the design, construction and commissioning of the project along with running the project in the trial phase (duration to be selected after discussion with funders). This agency will also be responsible for training the village committee in operating the plant in cooperation with local government agencies.

Further, the implementing agency will have to appoint consultants and contractors for successfully implementing the project according to standards. The agency will directly report to the funding agencies and ensure smooth working between team members. The spending and accounting will be handled by the implementing agency. In addition to these, there are other responsibilities for the implementing agency as summarized in section 13.3.

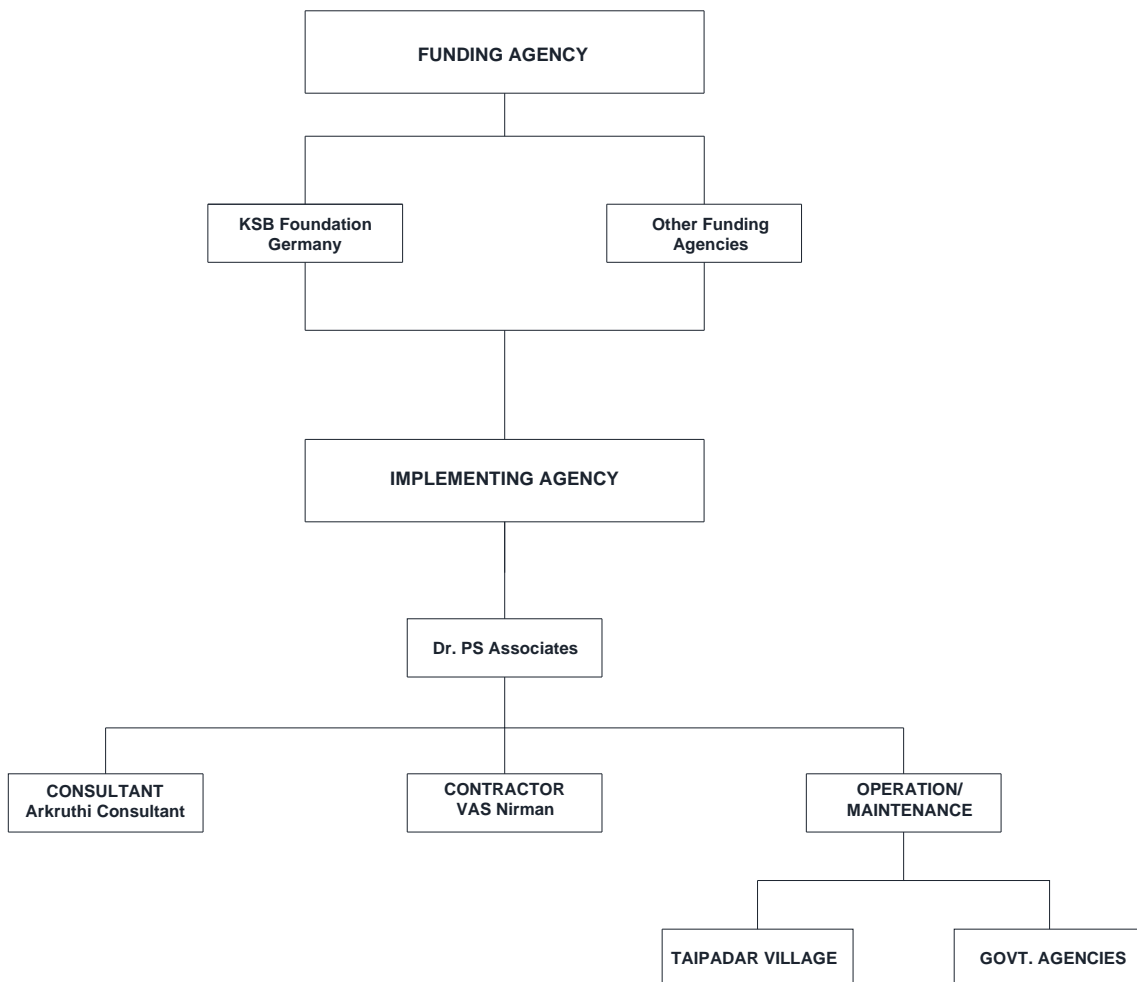


Fig. 13.1, Organizational setup required for the execution of the Taipadar Project

13.2 Constructional Programme

The construction programme of the Taipadar project is reckoned to start from the succeeding month in which all clearances are obtained and financial closure of different phases of the project is achieved.

The detailed drawings required for the execution of various items will be prepared by the consultants and then tenders will be invited for both Civil and E & M works and also for Gate installation etc. This project is programmed to be completed within a period of 12 months. In order to achieve the above goal, all the activities have to be meticulously worked out for taking up the Construction of different components of works. All the major components of the project are proposed to be executed through competent contractors, selected through competitive bidding process, who have the expertise and who have executed similar works in other projects.

Broadly the project activities are divided into following groups.

- Activities related to Civil Works of Power, Irrigation and Water supply components.
- Activities related to Electro Mechanical equipment and power distribution systems
- Other Miscellaneous works

Tenders will be invited for each of the above work separately and agencies will be decided well before commencement of working season.

13.2.1 Material Planning and Procurement:

The works are proposed to be executed by engaging contractors who will be allotted works under various packages. The contractors will be provided with detailed construction drawings, specifications as prepared by the consultants engaged for this purpose. The contractors for each package will have to make their own arrangement for procurement of construction materials steel etc., their transportation, labour procurement, maintenance and operation of the construction equipment. The promoters will acquire all the land required for the various structures, stockyards, workshops, colony etc., and arrange power supply for the construction work as per the terms and conditions agreed upon.

13.2.2 Construction Methodology

The Construction methodology suggested will help the contractors to plan their own construction techniques, based upon the availability of equipment and technical know-how with them. The contractors will however interact and discuss with the promoters and their consultants from time to time to see that the works are executed as per the drawings duly adhering to the construction schedule.

13.3 Additional Responsibilities of Implementing Agency

The implementing agency will be the core party involved to carry forward this project, given the complex nature and requirements. It will have to carry out the normal responsibilities along with special roles. The normal responsibilities include,

- Overall project management
- Financial closure and dealing with financial institutions
- Statutory clearances
- Project planning and achieving the targets
- Coordination between various contractors and consultants
- Inspection and quality control
- Verification of bill of quantities and certification of bills
- Audit and accounting
- Site office management

Above and all, the implementing agency will be responsible for the most important task of building communication links with each and every partner with the villagers at the forefront along with promoters, consultants, contractors, government agencies and any other party involved. Through this communication link honest views and appraisals can be put forth ensuring every utility and component of project is understood and implemented in the right spirit.

Chapter 14 – Future Investigations and Actions

14.1 Hydrology and Flood Prediction

The impact assessment carried out in Chapter 9 show that the studies pertaining to hydrology and floods is inadequate. The future investigation should focus on a multi-pronged strategy in the immediate future.

With the monsoon going to start in July, the floods should be continuously monitored and the HFL gauged. This will give another confirmation to the promoters on the HFL currently used to determine flood (215 m³/s in Chapter 4). This is easiest and practical method available.

However, theoretical simulations should be attempted. The correlations (based on rainfall data) and computer models (from simple hydrological models to more complex ones like the Stanford model) along with other available tools (like synthetic hydrographs) should be used. The models with require intricate data like conditions of catchment area, short term and long term rainfall data, soil moisture content and other meteorological data in addition to rainfall data.

In addition to the theoretical and computational tools, one more study can be initiated, which involves installing several gauges in the catchment area and monitor the ground water dynamics. This may however be very time consuming and expensive affair.

The promoters are adopting a safety measure as discussed in Chapter 9 (section 9.1.4) in which the full height of the diversion weir will be realized after studying the floods for 3 consecutive years (2013, 2014 and 2015).

14.2 Geo-technical Studies

The locations of the diversion weir and the submersible power plant (both on the riverbed) would have be subjected to geo-technical investigations to determine the safe bearing capacity required for the civil structures. The study should also establish the regional geology, type of rock, identify bedrock, firm rock levels and depth of over burden.

14.3 Other Investigations

- Identify the location of faults if any in the area, seismology, ground water and rock stability.
- Identify the suitability for construction materials, earth fill, aggregate, sand etc.
- Make test pits and log results.
- Make bore logs at suitable locations.

14.4 An Independent Economic Study

The future course of action would be to initiate a more comprehensive and independent economic, cost-benefit study for a presentation to potential funding agencies.

The study carried out in this report (in Chapter 12) is far means limited. Firstly, the economic value coming from all the utilities is assumed to be equal to the income generation, which may not be the case. Next, accounting for the environmental cost and its benefits needs to be more elaborately carried out compared to that in Chapter 9. Further, accounting for the societal benefits (presented in section 12.3) need to be accounted in this study.

A revenue model for the different utilities also needs to be proposed under this study. If not on a profit mode, the model should ensure the sustainability of this project.

14.5 Other Significant Actions

The following are the recommended actions:

- Land acquisition
- Approval/clearances by various statutory agencies.
- Arrange for finance through Financial Institutions
- Detailed engineering including detailed designs for the civil works and technical specifications for the electromechanical equipment.
- Implementation of the project including construction of civil works and sourcing of electromechanical equipment and establishment of power evacuation arrangement.
- Erection / installation of the equipment
- Trial runs and Commissioning of the plant.

Chapter 15 – Project Overview and Conclusion

The rationale behind the Taipadar project is provide a local ‘micro hydro power’ solution to meet additional needs of water for irrigation, provide direct drinking water supply and electricity for value addition that together creates three fold benefits with respect to environment, economy and society, ensuring sustenance of each utility.

The priority of the project is clearly the increase of agricultural productivity that is the only source of community’s income, after which comes the direct supply of drinking water to houses along with electricity primarily for small agro-based applications.

The determination of the partners would essentially be to provide a dignified, productive and fruitful life to the community during the inactive irrigation phase. The purpose would also be eliminate the human drudgery particularly for the women folk who have to manually carry drinking water to homes and spend endless time in grain processing like dehusking and milling.

The Taipadar project is located in a forest river basin in the southern tip of Chhattisgarh State in central India. The size of the village in terms of population is approximately 200 people within 32 families and in terms of agriculture land is around 80 ha. The project is designed to cater to the irrigation of additional 8 to 32 ha depending on the river water flow and drinking water (200 liters per person per day) through the year along with electricity in the range of 3 to 15 kWe for various applications.

The beneficiaries of the project are righteous and self-esteemed tribes who presently are not having electricity supply through grid or any method of artificial irrigation and relying only on monsoons.

The overall capital investment for the project is 750000 euros with market value of benefits equal to 60660 euros annually out of which 90 to 95% contribution is from agricultural yield. Detailed economic analysis like revenue models have not been carried out as yet due to the uncertainty in the approach of study.

The economic value through irrigation alone is over 59400 euros compared to the current income of the 48000 euros for the entire village, which means that this project could double the growth rate from the present.

The project team would comprise of an implementing agency executing the project on behalf of the funding agencies and then handing it over to the local community by setting up a village society to operate and manage the project. The local government and forest department will be on board but the project will be managed by the villagers only after due training provided by the promoters.

The main issues of the project yet to be resolved cover some technical validation on flood scenario, arranging finances and creating a mutually acceptable revenue model before the project can take off.

Nomenclature

AC	Alternating Current
DC	Direct Current
DPR	Detailed Project Report
EL	Elevation
EMC	Electro-Magnetic Clutch
FSL	Full Supply Level
G	Ground
GeSC-VSC	Generator Side Converter - Variable Speed Controller (4 quadrant)
GrSC-VSC	Grid Side Converter - Variable Speed Controller (4 quadrant)
HDPE	High Density Polyethylene
HFL	High Flood Level
INR	Indian National Rupees
IRR	Internal Rate of Return
KPCL	Karnataka Power Corporation Limited
LS	Lots
M	Module
P1	Prototype 1
P2	Prototype 2
MCB	Miniature Circuit Breaker
MDR	Mud Road
MSL	Mean Sea Level
MT	Metric Ton
NH	National Highway
NPV	Net Present Value
OM	Operations and Maintenance
P	Pump
PLF	Plant Load Factor
POL	Petrol Oil and Lubricants
RCC	Reinforced Cement Concrete
T	Turbine
TMT	Thermo Mechanically Treated Steel
TWL	Tailrace Weir Level
UCR	Un-Coarse Masonry
UPS	Uninterrupted Power Supply
USD	United States Dollar
VR	Village Road
VSC	Variable Speed Controller
WHO	World Health Organization

References

- [1] Data from World Economic Outlook 2012, <http://www.imf.org/external/data.htm>
- [2] GSI Toposheet, 1982, 'Toposheet 65 J/1' and 'Toposheet 65 I/4', Geological survey of India, 'http://www.portal.gsi.gov.in/portal/page?_pageid=108,717695&_dad=portal&_schema=PORTAL', accessed in October 2010
- [3] Hydraulic Data Handbook for Engineers, Likhi and Sharma, Chapter 9, Flow Measurement, New Age International Publishers, India
- [4] Engineering Hydrology, Varshney, Chapter 11, Empirical Formulae and Envelope Curves, Nem Chand and Brothers Roorkee, India
- [5] Hydraulic Data Handbook for Engineers, Likhi and Sharma, Chapter 8, Flow Through Open Channels, New Age International Publishers, India
- [6] WHO Publication, 'http://www.searo.who.int/LinkFiles/List_of_Guidelines_for_Health_Emergency_Minimum_water_quantity.pdf', accessed in October 2010
- [7] Schedule of Rates for Hydro and Thermal Power Projects, Karnataka Power Corporation Ltd, 2012
- [8] KSB AG and Sub-Suppliers
- [9] Directorate of Marketing & Inspection (DMI), Ministry of Agriculture, Government of India, <http://agmarknet.nic.in/>
- [10] Theory and Design of Irrigation Structures, 2005, Varshney. R.S., Gupta S.C., Gupta R.L. Chapter 3 and 4, Nem Chand and Bros Roorkee, India.
- [11] Heavy Duty Ram Pump, Rife Hydraulic Engine MFG, 1 Line Street, PO Box 95, Nanticoke PA 18634, www.RifeRam.com

Annexure

A1 Project at a Glance

1	Name of the Scheme	Taipadar Micro Hydro and Water Resources Management Project
2	Location	
	2.1 Village	Taipadar
	2.2 District	Jagadapur
	2.3 State	Chhattisgarh
3	Installed Capacity	1×6 kWe + 1×8 kWe
4	Average annual energy generations (8 hours/day, 0.9 PLF)	18,405 kWh
5	Annual Irrigation yield (16 hours/day, 0.9 PLF)	
	5.1 Water available for Irrigation	Annual availability 51,060 mm.Ha/year
	5.2 Cultivable Land	8 ha to 32 ha
	5.3 Yield based on proposed cultivation pattern	103,000 kg of rice, 97,326 kg wheat, 21,377 kg mustard
6	Quantity of Drinking Water available per day	45 m ³ /day
7	Total Project Cost (INR)	59,900,000 (ca 750,000 Euros)
8	Projected Yearly Revenue (INR)	48,50,000 (ca 60,660 Euros)

A2 Salient Features

Sr. No.	Particulars	
1.	Location:	
	State	Chattisgarh
	District	Jagadalpur
	Region	Bastar
	Village	Taipadar
	Nearest State Highway	NH 43, connecting Raipur and Vizag
	Nearest Railway Station	Jagadalpur
	Project Site	Ganeshbahar Nala – 52kms south of Jagadalpur – Connected partly by MDR and Balance by VR
	Category of Project	Hydro and Water Resources Management
2.	Hydrology:	
	Stream:	Ganeshbahar Nala – A tributary to Kolab River (Shabari)
	Catchment Area up to Weir:	131 Sqkms
	Average annual Rain Fall:	1480 mm
	Design Discharge:	95 l/s in lean season and 465 l/s in monsoon
	Maximum Design Flood:	215 – 450 m ³ /s
	Temperature:	
	Max:	38 ⁰ C
	Min:	4 ⁰ C
	Humidity	
	Max:	96 %
	Min:	45 %
3.	Diversion Weir:	
	Co-ordinates:	
	Latitude	18 ⁰ 56' 43"-N
	Longitude	82 ⁰ 10' 36"-E
	Type:	Solid Gravity Concrete Structure with over flow and Non overflow portions
	Full Supply Level:	EL:511.00m (Crest Level of overflow weir)
	Length of over flow weir:	25.00m
	Shape of Crest:	Ogee
	Height of over flow weir:	7.00m
	Deepest bed level:	EL:504.00m
	Total Length of Weir including non- overflow portion:	30.85m
	Top width of NOF:	2.00m
	Centre line of Penstock:	EL:508.875m
	Centre line of De – silting pipe:	EL:507.725m
	Energy Dissipation arrangement:	Roller Bucket – 5m radius
4.	Power Component	
i	Main Penstock:	
	Diameter:	750mm
	Length:	258m
	Type:	HDPE
ii	Control Gate:	
	Numbers	Two – One each for penstock and de-silting pipe
	Type:	Screw type gate at the entrance of penstock and de- silting pipes
iii	Valve:	Main Inlet Valve – One each for four Units

Sr. No.	Particulars	
iv	Power House	
	Number of Units	3 nos of Pumps as Turbines and 1 no. turbine
	Type:	Axial Flow Submersible
	Rated output	
	Prototype 1	6.0 kWe
	Prototype 2	8.0 kWe
	Rated Head	
	Gross	6.20m
	Net	5.00m
	Rated Discharge (power generation)	
	Prototype 1	180 l/s
	Prototype 2	250 l/s
	Rated Speed	
	Prototype 1	1650 rpm
	Prototype 2	1700 rpm
	Runner Diameter	
	Prototype 1	φ218 mm
	Prototype 2	φ270 mm
	Efficiency at rated output	85 % for turbine and 89% for generator
	Generation Voltage	415 volts (3 phase)
	C/L of Pump Turbine	EL:504.37m
	Top of TG Bed level	EL:503.82m
	Service Bay level	EL:506.20m
	Min. Tail Water Level	EL:504.80m
v	Energy Generation	
	Prototype 1	8200 kWh /annum
	Prototype 2	10400 kWh /annum
5.	Irrigation Component	
i	Pumping Capacity:	
	Prototype 1	5-25 l/s
	Prototype 2	10-30 l/s
	Hydraulic Ram R1	4-10 l/s
ii	Delivery Pipe (module to tank)	
	Length	1140.00m
	Diameter	250.00mm
	Type:	HDPE
iii	Storage Tank	
	Size:	25m (l)x 25m(b) x 5.2m(h) Inner Dimension
	Type of Construction	RCC – M25 grade
	Storage Capacity	2940cum
	FTL:	EL:530.50m
iv	Main Irrigation Supply Pipe	
	Length	645.00m
	Diameter	250.00mm
	Type:	HDPE
v	Branch Canal	
	1 st Take Off channel	EL:525.00m
	Length of Left Portion	211.00m
	Length of Right Portion	234.00m
	2 nd Take Off channel	EL:520.00m
	Length of Left Portion	260.00m
	Length of Right Portion	680.00m
	3 rd Take Off channel	EL:515.00m
	Length of Left Portion	390.00m
	Length of Right Portion	710.00m
	Section:	Trapezoidal concrete lined

Sr. No.	Particulars
	Bed Width: 500.00mm
	Depth of Flow: 124.00mm
	Side Slope: 1:1
6	Water Supply Component
i	Sedimentation and coagulation Tank
	Size: 10m (l)x 10m(b) x 2m(h) Inner Dimension
	Type of Construction: RCC – M25 grade
	Storage Capacity: 190cum
	FTL: EL:530.40m
ii	Main Delivery Pipe
	Pipe Line 1
	Length: 1185.00m
	Diameter: 150.00mm
	Type: HDPE
	Pipe Line 2
	Length: 680.00m
	Diameter: 150.00mm
	Type: HDPE
iii	Distribution Pipe Across Village
	Length: 800.00m
	Diameter: 75.00mm
	Type: HDPE
iv	House Connection
	Numbers: 35
	Tank: Syntex Type (HDPE) with Taps

A3 Detailed Cost Estimates

The rates for various items of civil works are based on the schedule of rates of Karnataka Power Corporation Ltd [7], a leading power company of Government of Karnataka and also based on the rates in other similar ongoing power projects with suitable escalation considered where necessary. Costs for various civil structures like diversion weir, penstock and powerhouse etc, are estimated on the basis of layout finalized for the hydro scheme. Similarly structures plan for irrigation and water supply are estimated are based in the general layout finalized.

Cost of the modules including control equipment and control panels is based on budgetary offers received from turbine manufacturers [8]. For electromechanical equipment, provision has been made for spare parts along with the equipment. The estimate also considers freight, insurance and cost of erecting and commissioning. Costs of other mechanical and electrical equipment are based on recent costs for similar items in other similar projects, with suitable escalation where necessary.

A3.1 Civil Works

A3.1.1 Hydropower Component

Sl no.	Particulars	Units	Quantities	Rates	Total cost
1	Weir				
a	Excavation	cum	283,68	352,3	99939
b	PCC	cum	26,06	3328	86736
c	Concrete (RCC)	cum	367,37	6630	2435674
d	TMT steel quantity (Reinforcement)	MT	11,02	50000	551058
e	Foundation Treatment	LS		200000	200000
				Total=	3373406
2	Penstock Pipe				
a	Excavation	cum	187,20	101,79	19055
b	PCC	cum	37,80	3328	125798
c	Concrete (RCC)	cum	48,12	6630	319049
d	TMT steel quantity (Reinforcement)	MT	1,44	50000	72183
e	Penstock Pipe, HDPE 2.5 Kg/cm ² , 750mm Dia	RM	258,00	15000	3870000
				Total=	4406085
3	Penstock Pipe - Ram Pump Module				
a	Total PCC	cum	15.12	6630	100246
b	Total RCC for saddles, support and anchor blocks	cum	19.25	6630	127620
c	TMT steel (Reinforcement)	MT	0.58	50000	28873
d	Penstock Pipe, HDPE 2.5 Kg/cm ² , 300mm Dia	RM	240.00	3000	720000
e	Penstock Pipe, HDPE 2.5 Kg/cm ² , 200mm Dia	RM	25.00	1750	43750
				Total=	1020488
4	Power House				
a	Excavation	cum	63,00	352,3	22195
b	PCC	cum	12,60	3328	41933
c	Concrete (RCC)	cum	26,40	6630	175032
d	TMT steel quantity (Reinforcement)	MT	0,79	50000	39600
				Total=	278760
5	Generator Side Control Room				
a	Excavation	cum	14,92	101,79	1519
b	PCC	cum	2,24	3328	7448
c	Stone Masonry	cum	7,27	1488,5	10827

d	Concrete (RCC)	MT	7,27	5330	38768
e	Brick Masonry	cum	8,39	2203,5	18488
f	Roof Slab	cum	2,00	6630	13260
g	TMT steel quantity (Reinforcement)	MT	0,40	50000	20000
h	Cement Plastering	Sqm	36,48	145,6	5311
i	Flooring				
	Bed Concrete	cum	0,40	2223	889
	Floor Finish	Sqm	12,00	226,2	2714
k	Windows	Sqm	3,00	4862	14586
l	Door	Sqm	2,52	4862	12252
m	Painting	LS		15000	15000
j	Outside Paving	LS		10000	10000
				Sub-Total=	171063
k	Electrification	LS		13685,0164	13685
l	Water Supply & Sanitary	LS		13685,0164	13685
				Total=	198433
6	Manifold for the turbines	LS	1	800000	800000
7	Power station auxiliaries (mechanical)	LS	1	700000	700000
8	Gates & Screw Type Hoist	Nos	2	107186	214372
9	Miscellaneous, unforeseen, contingency and roundoff				1008455
TOTAL IN LAKHS					120

A3.1.2 Irrigation Component

Sl no.	Particulars	Units	Quantity	Rates	Total cost
1	Water Tank				
a	Excavation	cum	2943,50	101,79	299619
b	PCC	cum	99,86	3328	332321
c	UCR	cum	263,19	1488,5	391758
d	Raft Concrete (RCC)	cum	299,57	6630	1986136
e	Concrete (RCC)	cum	78,00	6630	517140
f	TMT steel quantity (Reinforcement)	MT	11,33	50000	566352
				Total=	4093326
2	Pump Delivery Pipe				
a	Excavation	cum	93,71	101,79	9539
b	Back filling	cum	34,99	48,88	1710
c	PCC	cum	136,20	3328	453274
d	Concrete (RCC)	cum	150,75	6630	999486
e	TMT steel quantity (Reinforcement)	MT	4,52	50000	226128
f	Pump Delivery Pipe, HDPE 4 Kg/cm ² , 250 mm Dia	RM	1140,00	2250	2565000

				Total=	4255137
3	Pump Delivery Pipe - Ram pump Module				
a	Excavation	cum	40.00	101.79	4072
b	Back filling	cum	12.00	48.88	587
c	PCC	cum	40.00	3328	133120
d	Concrete (RCC)	cum	50.00	6630	331500
e	TMT steel quantity (Reinforcement)	MT	1.50	50000	75000
a	Pump Delivery Pipe, HDPE 4 Kg/cm ² , 150 mm Dia	RM	800.00	1350	1080000
				Total=	1624278
4	Pipe line for irrigation				
a	Excavation	cum	378,45	101,79	38522
b	Back Filling	cum	301,95	48,88	14759
b	PCC	cum	57,60	3328	191693
c	Concrete (RCC)	cum	63,73	6630	422517
d	TMT steel quantity (Reinforcement)	MT	1,91	50000	95592
e	Pipe line for Irrigation, HDPE 2.5 Kg/cm ² , 300mm dia	RM	645,00	3000	1935000
				Total=	2698083
5	Branch canal				
a	Excavation	cum	497,00	101,79	50590
c	Concrete (RCC)	cum	273,35	6630	1812311
d	TMT steel quantity (Reinforcement)	MT	2,73	50000	136675
				Total=	1999575
6	T Joint Pipes	nos	3,00	165,1	495
7	Gates & Valves	LS		200000	200000
8	Field Channels	LS		350000	350000
				Sub Total	15220894
9	Miscellaneous, unforeseen, contingency and round off	LS			221634
				TOTAL (IN LAKHS)	154

A3.1.3 Drinking Water Supply Component

Sl no.	Particulars	Units	Quantities	Rates	Total cost
1	Water Tank				
a	Excavation	cum	45,00	101,79	4581
b	PCC	cum	20,74	3328	69009
c	UCR	cum	24,40	1488,5	36319
d	Raft Concrete	cum	31,10	6630	206220
e	Concrete (RCC)	cum	8,00	6630	53040
f	TMT steel quantity (Reinforcement)	cum	1,17	50000	58656
				Total=	427825
2	Pipe Line 1				
a	Excavation	cum	199,08	101,79	20264

b	Back filling	cum	174,76	48,88	8542
c	PCC	cum	29,63	3328	98592
d	Concrete (RCC)	cum	63,64	6630	421953
e	TMT steel quantity (Reinforcement)	cum	1,91	50000	95465
f	Pipe Line 1 125mm Dia	RM	1185,00	450	533250
				Total=	1178066
3	Pipe Line 2				
a	Excavation	cum	4,62	101,79	470
b	PCC	cum	17,00	3328	56576
c	Concrete (RCC)	cum	69,26	6630	459161
d	TMT steel quantity (Reinforcement)	cum	2,08	50000	103883
e	Pipe Line 2 125mm Dia	RM	680,00	450	306000
				Total=	926089
4	Pipe Line Across Village 75mm	RM	800,00	200	160000
5	Syntex Tank	Nos	35,00	1000	35000
6	Taps	Nos	35,00	1000	35000
7	Gates & Valves	LS		100000,00	100000
				Sub Total	2861980
8	Miscellaneous, Unforeseen, contingency and Rounding off	LS			117770
GRAND TOTAL (IN LAKHS)					30

A3.2 Mechanical Devices

A3.2.1 Turbine-Pump Modules

Sr. No.	Particulars	Qty	Unit Cost (INR)	Total Cost (INR)
1	Turbine-Pump Modules			
1,1	Prototype 1 An integrated turbine having guide vane adjustability, asynchronous generator connected to a pump via an electromagnetic clutch delivery 9 KW of shaft power and 7.8 KW of electric power with a pumping capacity of 5 to 22 l/s to a tank at a height of 26 m	1 no.	2000000	2000000
1,1	Prototype 2 An integrated turbine having fixed guide vanes, asynchronous generator connected to a pump via an electromagnetic clutch delivery 10 KW of shaft power and 8.5 KW of electric power with a pumping capacity of 10 to 30 l/s to a tank at a height of 26 meters	1 no.	8000000	8000000
2	Main Inlet Valves to Turbine-Pump Modules			
2,1	Common for all modules 750f mm Hand-operated sluice valve	1 no.	400000	400000
2,2	Module 3 - Prototype A 500f mm Hand-operated sluice valve	1 no.	300000	300000
2,3	Module 3 - Prototype B 500f mm Hand-operated sluice valve		300000	300000
3	Delivery Valves from Turbine-Pump Modules			
3,1	Module 3 - Prototype A 200f mm Hand-operated butterfly valve	1 no.	40000	40000
3,2	Module 3 - Prototype B 200f mm Hand-operated butterfly valve	1 no.	40000	40000
4	Spares for 5 years of operation			

4,1	Mechanical Spares	Lot	200000	200000
5	Miscellaneous, unforeseen, contingency and roundoff			1220000
TOTAL (IN LAKHS)				125

A3.2.2 Ram Pump Module

Sr. No.	Particulars	Qty	Unit Cost (INR)	Total Cost (INR)
1	Ram Pump Module			
	8 inch Pump	1	3200000	3200000
2	Main Inlet Valve			
	200 ϕ mm Hand-operated sluice valve	1	80000	80000
3	Delivery Valve			
	100 ϕ mm Hand-operated butterfly valve	1	4000	4000
4	Miscellaneous, unforeseen, contingency and roundoff			116000
Total (in Lakhs)				34

A3.3 Control System and Power Evacuation

A3.3.1 Costs Overview

Sr. No.	Particulars	Cost (In Lakhs, INR)
1	Control Equipment	56,8
2	Power Evacuation and Load centers	32
3	Station auxiliaries (electrical)	14,7
4	Miscellaneous, unforeseen, contingency and round off	6
TOTAL (IN LAKHS)		110

A3.3.2 Control System

Sr. No.	Particulars	Qty	Unit Cost (INR)	Total Cost (INR)	
1	Control System				
1,1	Module 3 - Prototype 1	4 quadrant, variable frequency generator side converter of appropriate rating (having high η ~99% at wide loads) with a AC/DC conversion and a clutch actuating logic	1 no.	1200000	1200000

1,2	Module 3 - Prototype 2	4 quadrant, variable frequency generator side converter of appropriate rating (having high h~99% at wide loads) with a AC/DC conversion and a clutch actuating logic	1 no.	1200000	1200000
1,3	Common for all modules	Uninterrupted Power Source (DC Supply to generator side converters and clutch actuating mechanism	1 no.	50000	50000
1,4	Common for all modules	A variable frequency grid side converter of appropriate rating for the combined load of all modules (ensuring high h~99% at all electrical loads) with DC/AC converter and 440 V output transformer (D-Y)	1 no.	2250000	2250000
1,5	Common for all modules	A Common feeder high voltage DC link of 1.2 km length between all the generator side converters and the single grid side converter with cable specification of 5*20 mm ² , where positive and negative links have 2*20mm ² each and the fifth cable for linking th	1200	650	780000
2	Spares for 5 years of operation				
2,1	Electrical Spares		Lot	200000	200000
TOTAL (IN LAKHS)					56,8

A3.3.3 Powerhouse Auxiliaries and Load Centers

Sr. No.	Particulars	Qty		Unit Cost (INR)	Total Cost (INR)
1	Electrical Auxiliary				
1,1	Power and Control Cables	Lot	1	50000	50000
1,2	Lighting protection, Earthing and Appurtment works at Generator side control room	Lot	1	50000	50000
1,3	440V Distribution board with bus bars, MCBs and other switch gears at Grid side control room	Lot	1	75000	75000
1,4	Lighting protection, Earthing and Appurtment works at Grid side control room	Lot	1	50000	50000
				Total =	225000
2	Grid Side Control Room Plinth Area (28.82 Sqm)	Sqm	6885	28,82	198433
3	Media & Computer Room Plinth Area (46.65Sqm)	Sqm	6885	46,75	321885
4	Utility Centre Room Plinth Area (46.65Sqm)	Sqm	6885	46,65	321197
5	Erection and Commissioning	Lot	1	400000	400000
6	Miscellaneous, unforeseen, contingency and round off				33485
TOTAL (in Lakhs)					15

A3.3.4 Power Evacuation

Sr. No.	Particulars	Qty units	Reqt	Unit Cost (INR)	Total Cost (INR)
1	Distribution lines				
1,1	A single phase distribution configuration for the northern sector comprising of 14 houses and school for a load carrying capacity ranging from 1 kW to 9 KW with copper cable of specification 4×25 mm ²	Meters	1150	800	920000
1,2	A single phase distribution configuration for the southern sector comprising of 18 houses for a load carrying capacity ranging from 1 kW to 12 KW with copper cable of specification 4×25 mm ²	Meters	1350	800	1080000
1,3	A three phase distribution configuration for the utility center for a load carrying capacity ranging from 2 kW to 15 KW with copper cable of specification 4×25 mm ²	meters	100	800	80000
1,4	A single phase distribution configuration for the computer facility and community center for a load carrying capacity ranging from 0.5 kW to 4 KW with copper cable of specification 4×25 mm ²	meters	100	800	80000
2	Pillar Boxes and Supports				
2,1	Households and School: 1 KWh meter (5A, 1% accuracy), overload circuit breaker (4 A) Copper Terminal strip with 6 holes(acc to drawing), all weather proof enclosure and support for each pillar with internal house wiring	lot	33	14000	462000
2,2	Utility Center: 80 KWh meter (40A, 1% accuracy), overload circuit breaker (40 A) Copper Terminal strip with 6 holes(acc to drawing), all weather proof enclosure and support	lot	1	20000	20000
2,3	Computer facility and Community Center: 20 KWh meter (18A, 1% accuracy), overload circuit breaker (18 A) Copper Terminal strip with 6 holes(acc to drawing), all weather proof enclosure and a support	lot	1	15000	15000
3	Utility Center Loads				
3,1	Loads comprising of flour mills, dehulling machines, agricultural machinery and similar as per requirement	lot	1	400000	400000
4	Community and Computer Center Loads				
4,1	Loads comprising of 2 personal computer, mass media with television and similar as per requirement	lot	1	150000	150000
TOTAL (in Lakhs)					32,1

A3 Project Implementation Schedule

Sr. No.	Activity	Duration
1	Diversion Weir	Nov 2014 - Jan 2015
2	Installation of Ram Pump	Dec 2014
3	Penstock for Ram Pump	Jan 2015 - Mar 2015
4	Delivery line for Ram Pump	Jan 2015 - Mar 2015
5	Construction of Branch tank at EL 525 m	March 2015
6	Irrigation distribution - Phase 1	Apr - May 2015
7	Installation Micro Hydrel Pumps	Oct 2015
8	Construction Gen/grid control rooms	Oct 2015- Dec 2015
9	Cable laying and distribution lines	Oct 2015- Dec 2015
10	Buildings for load centers	Dec 2015 - Feb 2016
11	Storage tank and Drinking water tank	Dec 2015 - Feb 2016
12	Irrigation distribution - Phase 2	Jan 2016 - Mar 2016
13	Drinking water supply and Distribution lines	Jan 2016 - Mar 2016

A4 Project Completion Schedule

The project will be commissioned with the two irrigations phase followed by electricity and drinking water supply phases.

Sr. No.	Commissioning Activity	Duration
1	Irrigation Phase 1 - with Ram Pump	May 2015 - Jun 2015
2	Irrigation Phase 2 - with turbine pumps	Mar 2016 - Apr 2016
3	Electricity commissioning	Mar 2016 - Apr 2016
4	Drinking water	Apr 2016 - May 2016

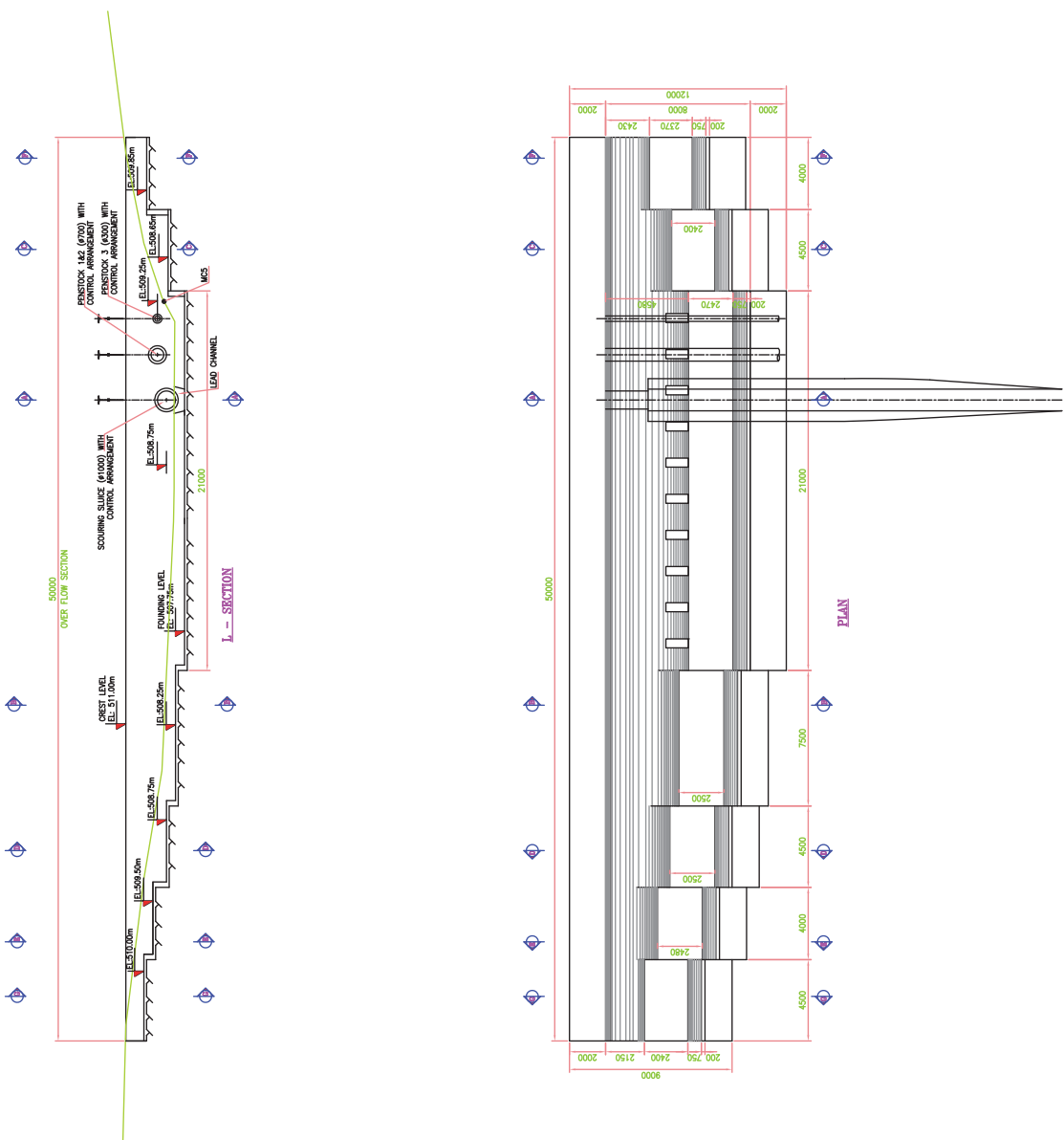
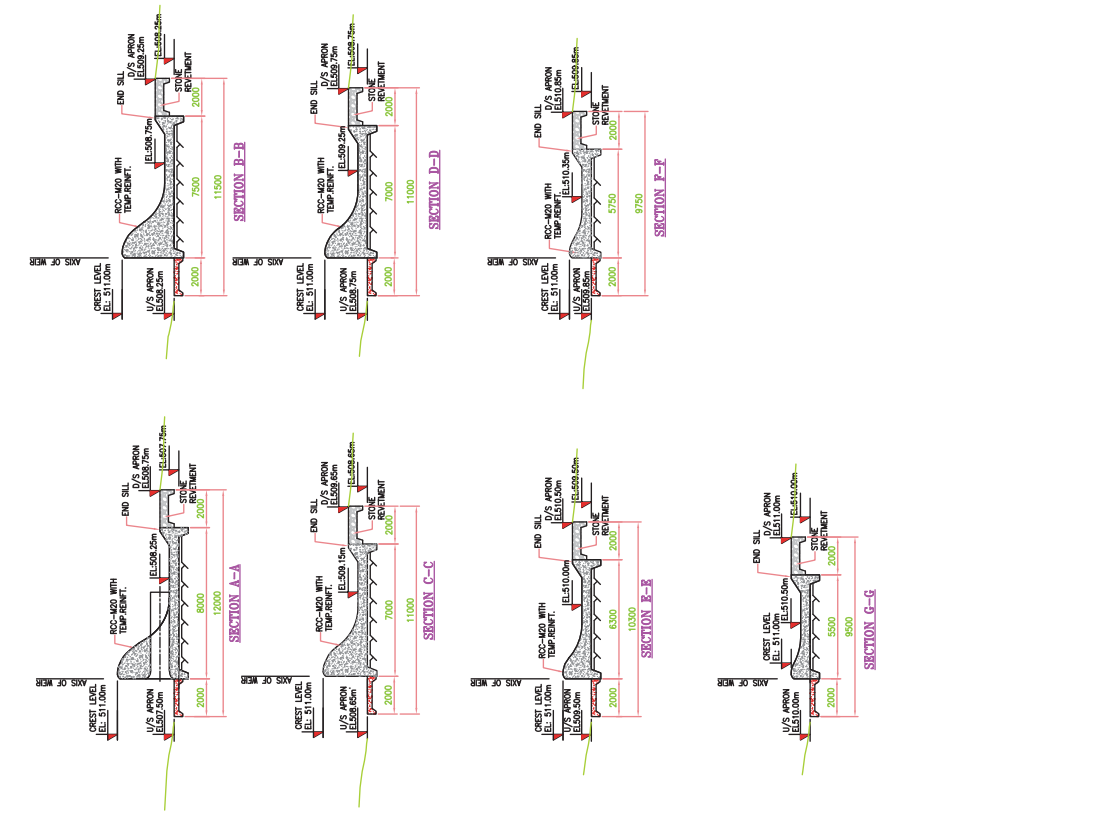
A5 Operation and Maintenance cost for 5 years

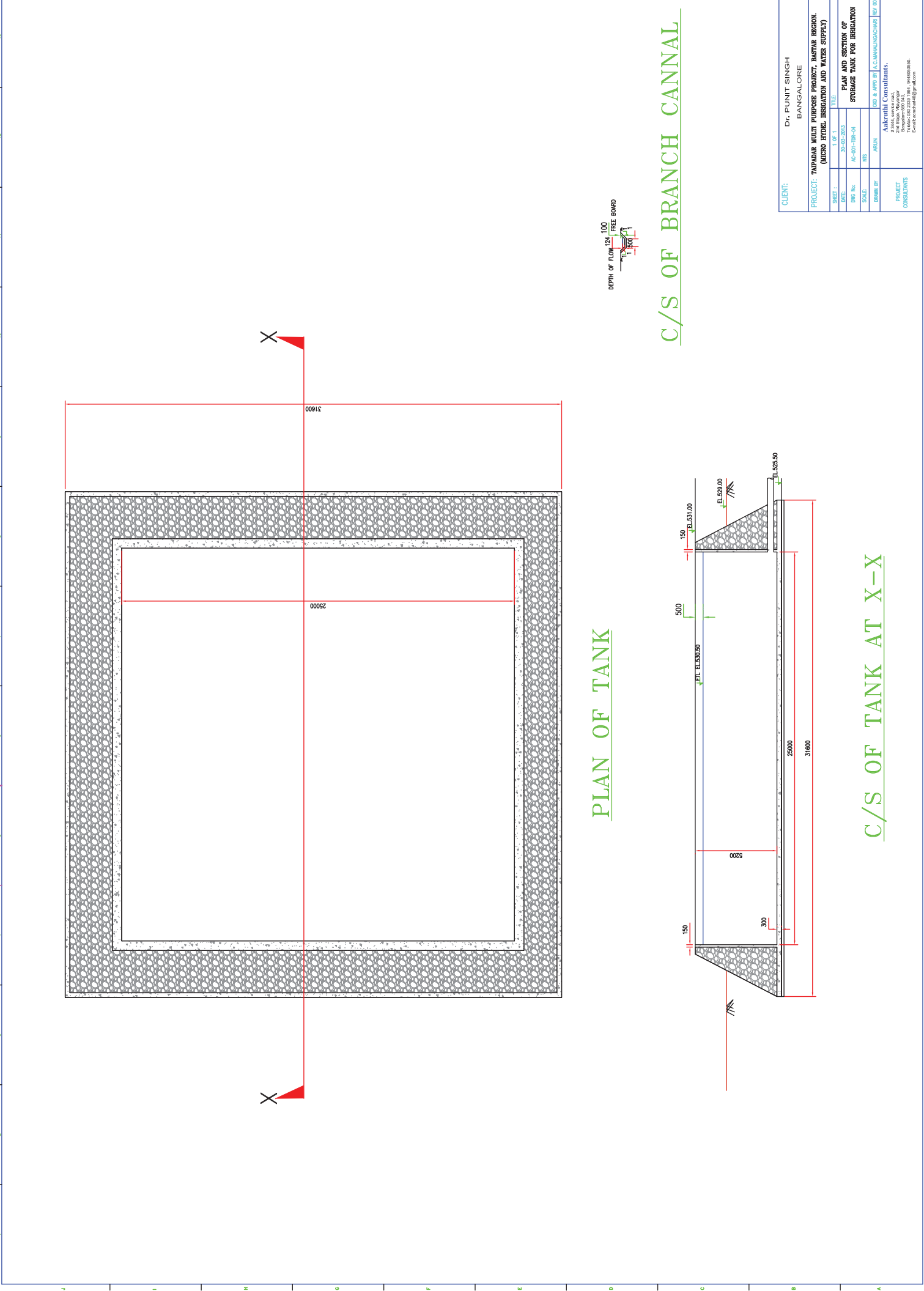
The operation and maintenance costs have been excluded for the total project costs. It is envisaged that the maintenance costs should be generated from the annual revenue that the project generates. The table below provides for the yearly O&M costs with an inflation model of 5% discount rate.

Sr. No.	Year	Annual cost (in lakhs) with 5% discount rate
1	Year 2015	4.8
2	Year 2016	5.0
3	Year 2017	5.3
4	Year 2018	5.6
5	Year 2019	5.8
	Total	26.5

A6 Civil Layouts

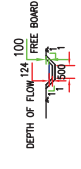
Fig. No.	Title
Fig. A1	General Layout of the Taipadar Project
Fig. A2	Sections of Diversion Weir
Fig. A3	Plan and L-section of Penstock Pipe
Fig. A4	Main Delivery Pipe (Plan and L-section)
Fig. A5	Cross-section of Irrigation Storage Tanks
Fig. A6	Main Distribution Line for Irrigation
Fig. A7	Drinking Water Storage cum Coagulation Tank
Fig. A8	Delivery Pipes for Water Supply





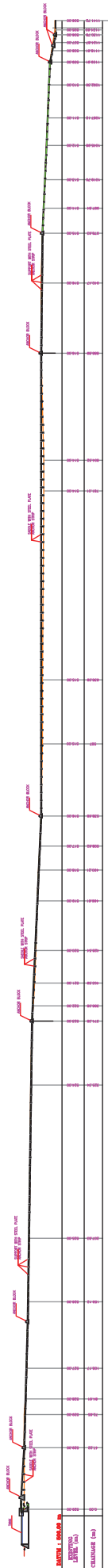
PLAN OF TANK

C/S OF BRANCH CANNAL



CLIENT:		D. PUNIT SINGH BANGALORE	
PROJECT:		TAPADAR MULTI PURPOSE PROJECT, BASTAR REGION, (MICRO HYDRL IRRIGATION AND WATER SUPPLY)	
SHEET :	1 OF 1	TITLE:	
DATE:	30-03-2013	PLAN AND SECTION OF	STORAGE TANK FOR IRRIGATION
DWG No:	AC-01-TDR-04	SCALE:	NS
DRAWN BY:	ARUN	DES. & APPR BY:	A.C.MAHALINGACHAR REV.00
PROJECT CONSULTANTS	Aakrenthi Consultants, A-36, 3rd stage road, Banashankari 3rd stage, Bangalore-560075, Karnataka-560075, E-mail: aakrenthi@gmail.com		

C/S OF TANK AT X-X

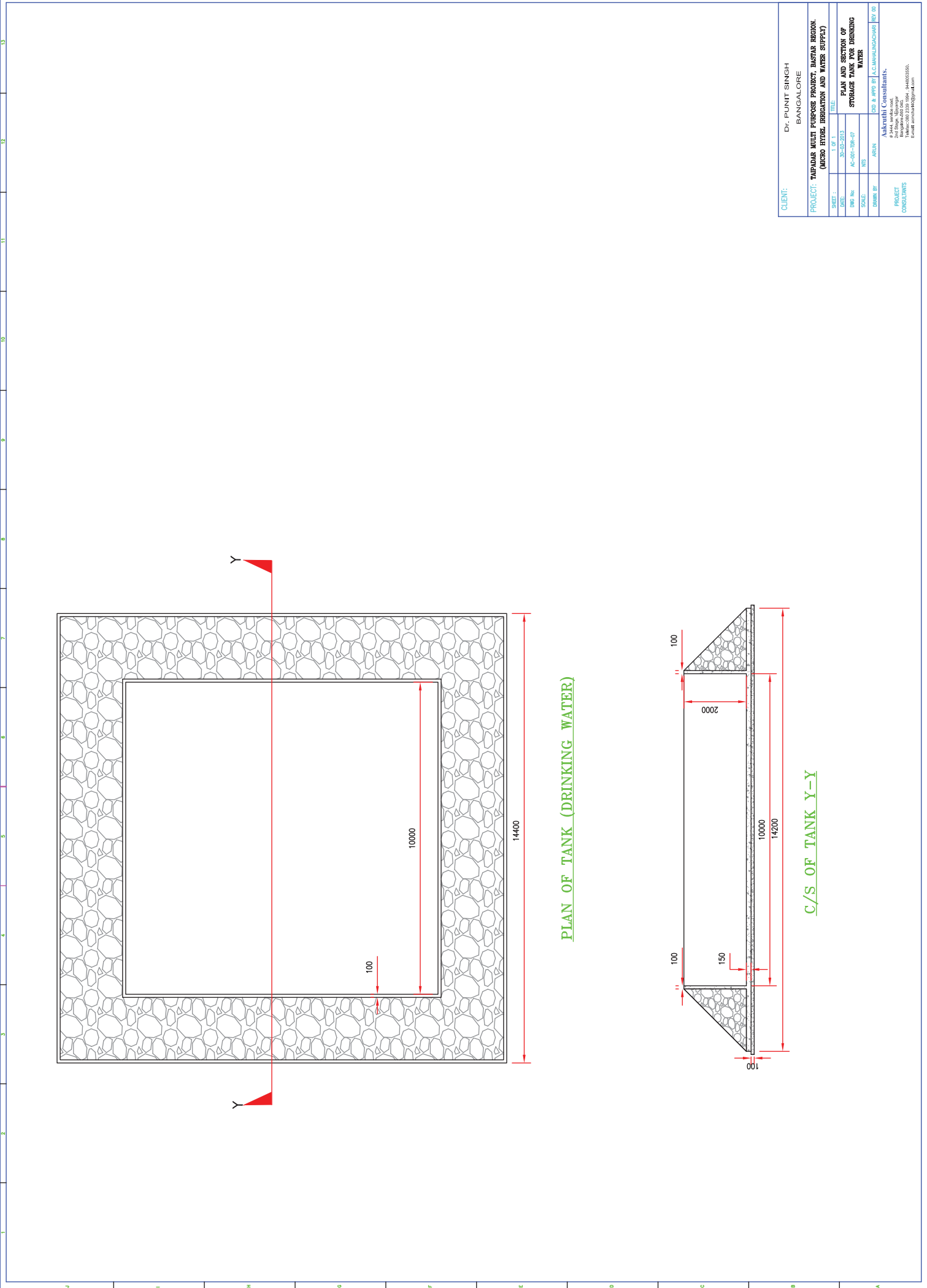


LONGITUDINAL SECTION OF PUMP DELIVERY PIPE



PLAN OF PUMP DELIVERY PIPE

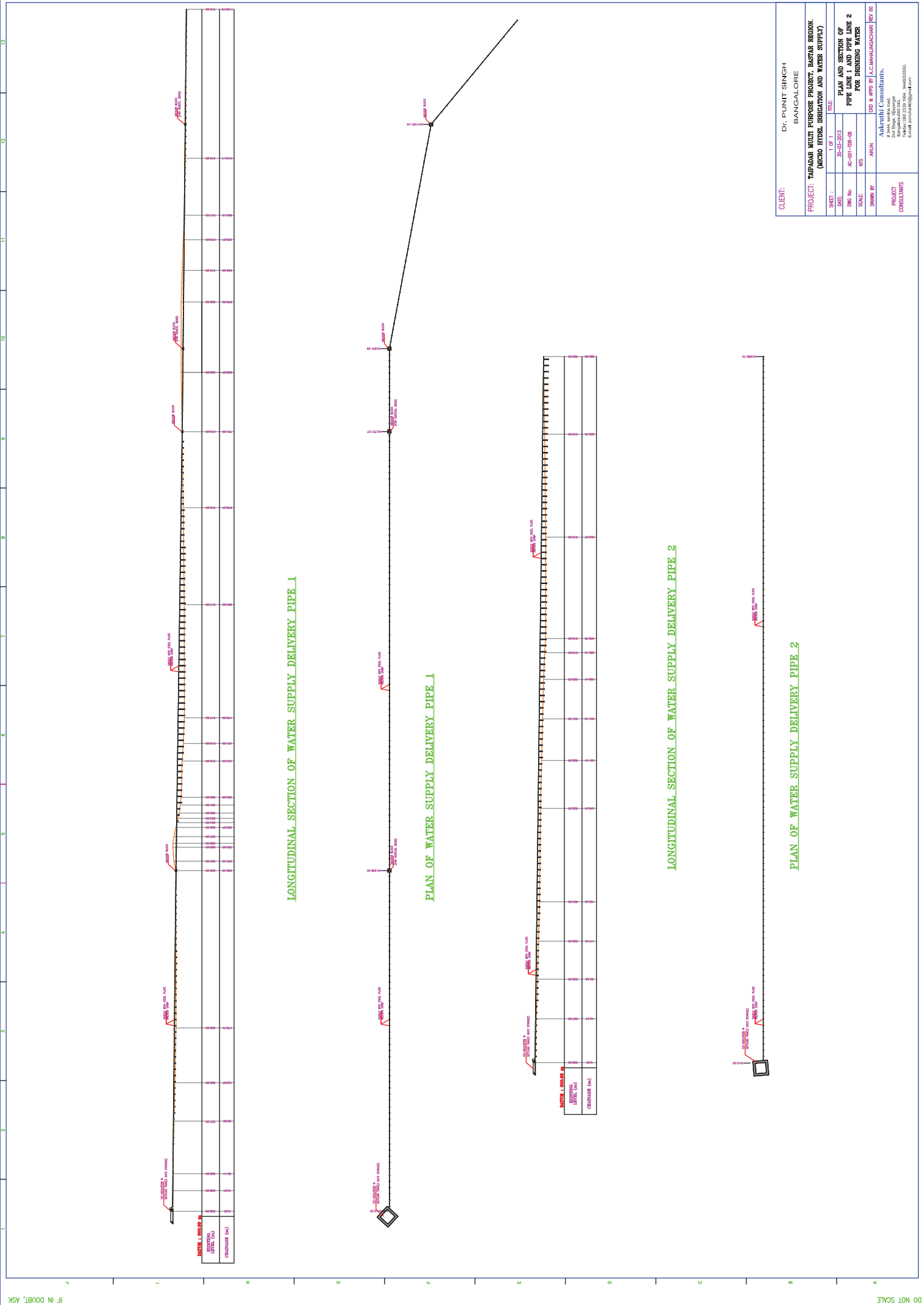
CLIENT: DR. PUNIT SINGH BANGALORE	
PROJECT: TAPPAAR MULTI PURPOSE PROJECT, BASTAR REGION (MICRO IRRIG. IRRIGATION AND WATER SUPPLY)	
SHEET: 1 OF 1	TITLE: PLAN AND SECTION OF PUMP DELIVERY PIPE
DATE: 30-03-2013	DWG No: AC-001-TDR-08
SCALE: 1/50	DESIGNER: ARUN
DRAWN BY: ARUN	CHECKED BY: A.C. MANI MOHAMMED
PROJECT CONSULTANTS: AARVATHI CONSULTANTS, 23/46, 4th cross road, 5th stage, 5th block, Banashankari, Bangalore-560075, KARNATAKA, INDIA. E-mail: aarvathi@aarvathi.com Phone: 9845333333	



PLAN OF TANK (DRINKING WATER)

C/S OF TANK Y-Y

CLIENT:		DR. PUNIT SINGH BANGALORE	
PROJECT:		TAMPANE MULTI PURPOSE PROJECT, BASTAR REGION (MICRO FITZEL IRRIGATION AND WATER SUPPLY)	
SHEET /	DATE:	NO. OF SHEETS	TITLE:
1 / 1	30-03-2013	30-03-2013	PLAN AND SECTION OF STORAGE TANK FOR DRINKING WATER
DWG No:	SCALE:	DATE:	PROJECT
AC-001-TWP-07	1/5	07/03/2013	CONSULTANTS
DRAWN BY:	DATE:	PROJECT NO:	CONSULTANTS
ADAN	07/03/2013	AC-001-TWP-07	Ashraful Consultants, 2nd Stage, Mirangal, Tumkur (Dist: Tumkur), Karnataka (India) 575104. E-mail: ashraful@ashraful.com



LONGITUDINAL SECTION OF WATER SUPPLY DELIVERY PIPE_1

PLAN OF WATER SUPPLY DELIVERY PIPE_1

LONGITUDINAL SECTION OF WATER SUPPLY DELIVERY PIPE_2

PLAN OF WATER SUPPLY DELIVERY PIPE_2

CLIENT: DR. PUNIT SINGH BANGALORE	
PROJECT: TAMPANE MULTI PURPOSE PROJECT, BASTAR REGION, (MICRO IRRIG. IRRIGATION AND WATER SUPPLY)	
SHEET /	1 OF 1
DATE:	30-03-2013
DWG No:	AC-001-TDP-08
SCALE:	1:50
DRAWN BY:	ARUN
PROJECT CONSULTANTS:	Ashwin Consultants, 2nd Stage, Mysore Taluk, Dist: Channarayana, Karnataka E-mail: ashwin@ashwin.com

DETAILED PROJECT REPORT

MYLASANDRA HYDRO ENERGY RECOVERY PROJECT

**Prepared by,
Dr. -Ing Punit Singh**

23th July 2013

Table of Contents

Executive Summary	4
Project at a Glance	6
Chapter 1 – Introduction	7
1.1 Waste Water Scenario in Bangalore	7
1.2 Energy Recovery from Wastewater.....	8
1.3 Mylasandra Sewage Treatment Plant	9
1.4 Scope and Purpose of Hydro Energy Recovery at Mylasandra	9
1.5 A solution to meet the Energy requirements of the Treatment Plant.....	11
Chapter 2 – Surveys and Investigation	12
2.1 Topographic Studies	12
2.2 Normal Grid Operation.....	13
2.2.1 Flow Duration Characteristics of Treated Water	13
2.2.2 Power Consumption Characteristics of Plant	14
2.3 Operation during Utility Grid Failure.....	14
2.3.1 Present Scenario	14
2.3.2 Control Volume and Free flow Discharge Characteristics	15
Chapter 3 – Power and Energy Studies	17
3.1 Grid Mode Operation	17
3.2 Island Mode Operation	17
3.2.1 Summary of System Design of Island Mode	18
Chapter 4 – Civil Works, Hydro Mechanical Equipment and Construction Materials	19
4.1 Civil Structures:.....	19
4.1.1 Project Layout:	19
4.1.2 Intake Pool:.....	20
4.1.3 Penstock pipe.....	21
4.1.4 Power House.....	21
4.1.5 Tail race Pool and End Discharge weir	22
4.2 Hydro-Mechanical Works	22
4.3 Construction Materials	22
Chapter 5 – Electromechanical Equipment and Power Evacuation	23
5.1 Rotating Machinery – The Submersible Hydro Turbine	23
5.1.1 Turbine	24
5.1.2 Generator	25
5.2 System Design and Recovery Plant Performance	25
5.2 Control System	26
5.2.1 Grid Mode Operation.....	26
5.2.2 Island Mode Operation	28
5.3 Instrumentation.....	29
5.3.1 Discharge.....	29
5.3.2 Electrical Energy	29
5.4 Power Evacuation.....	29
Chapter 6 – Environment Impacts and Benefits	31
6.1 Floods and the Issue of Submergence	31
6.2 Environmental Benefits	31
Chapter 7 – Cost Estimates	32
7.1 The Basis for the Cost Estimates	32
7.2 Implementation Options	32

7.3 Abstract of Project Costs	32
7.3.1 Hybrid Mode (Grid and Island Modes)	32
7.3.2 Dedicated Grid Mode	34
7.4 Summary	36
Chapter 8 – Financial Studies.....	37
8.1 Revenue from Benefits	37
8.2 Cost-Benefit Analysis	37
8.2.1 Dedicated Grid Mode	37
8.2.2 Usefulness of Island Mode	37
8.2.2.1 Plant conditions	37
8.2.2.2 Performance of turbine-generator of the recovery unit.....	37
8.2.2.3 Layout and system design.....	38
8.2.2.4 Economic assessment	38
Chapter 9 – Project Management and Schedule	39
9.1 Project Organization	39
9.2 Project Schedule	39
Chapter 10 – Summary, Conclusions and Recommendations.....	41
Nomenclature	42
References	42
Annexure	43
A1 Detailed Cost Estimates	43
A1.1 Civil Works and Hydro-Mechanical Costs	43
A1.2 Hydro-mechanical Works	48
A1.3 Electromechanical and Control System	49
A1.4 Power Evacuation	49
A2 Layouts	51
A2.1 Civil Layouts	51
A2.2 Implementation Options	51

Executive Summary

1. The Promoters, Clients and Developers

This hydro energy recovery project within a wastewater treatment plant is being promoted jointly by KSB AG, Germany and IISc Bangalore. The promoters have decided to fund the project by themselves solely for the purpose of demonstrating a unique and important application in the context of energy efficiency in industries. The promoters are not seeking any commercial benefit from this project once electricity is synchronized with treatment plant's distribution network.

The clients, BWSSB, have provided the facility and land within the treatment plant for implementing the project. They would provide 'non-material' support during survey, investigation and construction. After commissioning of the project, it would be handed over to BWSSB who would maintain and operate the recovery plant.

The developer, Dr. Punit Singh Associates, will provide the complete design, engineering and associated consultancy with his team for this project. The developer would be in charge of preparing the detailed project report, identify contractors and construct the plant in an agreed time frame. The developer will be responsible for commission and carrying out trial runs for 3 months before handing over the project to the clients.

2. Purpose and scope of the DPR

The purpose of the DPR is to study, evaluate and establish the technical feasibility, economic viability and sustainability of this proposed recovery project.

The scope of the report covers the following,

- i. To evaluate the available hydropower potential using available flow duration curves and topography.
- ii. To optimally plan micro hydro energy recovery system for normal grid mode of operation.
- iii. To additionally evaluate the feasibility of an island mode of operation during tripping of utility grid.
- iv. To provide general arrangement drawings of the civil works that include intake pool (forebay tank), penstock, powerhouse and tailrace canal, along with quantity and cost estimates for each.
- v. To design and select appropriate turbine and generator for the available conditions.
- vi. To plan the power evacuation (distribution) in both grid and island mode of operation.
- vii. To prepare the abstract of project costs with different implementing possibilities.
- viii. To make an impartial technical study and recommendations for the cost-effective implementation and commissioning of this project

3. The Vrishabhavati River Basin and Mylasandra Treatment Plant

The Vrishabhavati valley is one of the four and the most prominent of the valleys in Bangalore city because it links Bangalore to River Cauvery, from where drinking water is sourced to the city. Being a monsoon and ground water fed river, it is currently carrying nearly 350 MLD of untreated and treated water back to Cauvery sink.

The Mylasandra wastewater treatment plant is one of the two major treatment plants on the banks of Vrishabhavati. It has a modest capacity of 75 MLD and gets untreated water from northeastern and southeastern parts of the city.

4. Flow Characteristics of Treated Water from the Plant

The average flow handling capacity of the plant varies between 40 million liters to 50 million liters every day, which largely depends on the inflow of wastewater from external sources. The base flow is 20 to 25 MLD and the peak reaches 75 MLD for 6 to 7 hours/day, while an intermediate flow range of 50 MLD is achieved during forenoons and late evenings with the help of 3 feed pumps each having a capacity of 25 MLD. The energy recovery plant is designed for flow duration curve that represents a mean flow capacity of 48 MLD.

In addition to the normal flow characteristics, the plant has a special flow scenario during the failure of grid. The active storage volume of the plant gradually discharges, which can be used for decentralized power distribution. The storage volume varies between 700 and 1100 m³ depending on the pumps operating when tripping occurs.

5. Power and Energy Studies

The power calculations are based on the net head available and flow duration characteristics of the treated water. For each flow step of 25 MLD, 12.5 kWe of power can be generated. Following the 48 MLD flow duration curve, a maximum energy that can be recovered in 595 kWh.

6. Electromechanical Equipment

The electromechanical equipment comprises of an axial flow turbine of fixed guide vanes and propeller coupled to an asynchronous (induction) generator and is designed for submersible operation. The nominal rating of the turbine is defined at 1520 rpm and 6.4 m with a flow of 290 l/s (25 MLD) and 14.5 kWm of shaft power at an efficiency of 80%. The generator with an efficiency of 86.7% delivers 12.6 kWe of electrical power to the terminals.

There are 3 identical recovery units proposed to handle the unsteady flow behavior. For the standard flow duration curve of 48 MLD, the 3 recovery units can generate 555 kWh against the prescribed 595 kWh, mainly due to drop in efficiency while changing operational sequence of the feed pumps.

7. Power Evacuation

Two modes of power evacuation have been proposed. First is the grid mode when the utility electricity is available and the recovery units are feeding the power into the local grid. The second mode of power evacuation is through an island grid when the utility power supply fails. The grid mode power integration is achieved using soft starter and multifunction power sensors, while the units derive reactive power directly from the grid.

However, the distribution with island mode is more complex that involves numerous components automatic valve actuators, 4 quadrant variable speed converters along with extensive wiring and switch gears (interlocking) for creating a dedicated island load from the existing load comprising of lighting, laboratory and control room.

8. Estimates of Project Costs

The estimates are determined for both hybrid mode (grid and island mode together) and dedicated grid mode of operations. Within the hybrid mode, the implementation option with 3 recovery units came up to 124 lakhs and option with one recovery unit was nearly 100 lakhs. On the other hand the dedicated grid mode estimated to 101 lakhs and 73 lakhs for three and single recovery units respectively.

9. Financial Studies

The financial studies were carried with an annual energy generation of 180675 kWh (14.5 lakhs) and 98550 kWh (8 lakhs) for combined and single recovery units respectively at rate of 8 INR/kWh. The investigations revealed that the hybrid option was not only uneconomical but also less useful from the operational aspects, since the power is available only for 30 to 60 mins (linked to storage volume).

The dedicated grid mode on the other hand had favorable economics with a modest annual income 2 lakhs. However, the present value of the project is only 17% of project costs for 15 year life and 5% discount rate,

10. Recommendation

The developer recommends the implementation of dedicated grid mode for this recovery project starting with single unit that would cost about 72 lakhs. Subsequently, the other two units can be added at an additional cost of about 30 lakhs.

11. Environmental and Economic Impact – Project Rationale

The hydro energy recovery as proposed at the Mylasandra treatment plant may not classify as pure renewable energy project since the pumped drinking water is converted to sewage that is landing for treatment in the plant. Nevertheless, it is one of the ways of improving energy efficiency as this project results in energy savings of 4% of the plant's overall energy consumption. This may be a small proportion, but an important step for larger environment perspective and global climate.

The economic impact of this project may be reduced, but with the ever-increasing cost of electricity even this small contribution will be valued in the years to come.

Project at a Glance

1 Name of the Scheme	Mylasandra Hydro Energy Recovery Plant	
2 Location		
	2.1 Village	Mylasandra
	2.2 District	Bangalore
	2.3 State	Karnataka
3 Installed Capacity	3×12.5 kWe	
4 Average annual energy generations (0.9 PLF)	180675 kWh (with 3 units) 98550 kWh (with 1 unit)	
5 Total Project Cost (INR)	<u>1) Dedicated grid mode</u> 3 units – 101 lakhs 1 unit – 73 lakhs <u>2) Hybrid mode</u> 3 units – 124 lakhs 1 unit – 100 lakhs	
6 Projected Yearly Revenue (INR)	3 units – 14.5 lakhs 1 unit – 8 lakhs	

Chapter 1 – Introduction

1.1 Waste Water Scenario in Bangalore

The city of Bangalore has a unique status of being built on a plateau with a maximum elevation being 945 MSL. This plateau is characterized by 4 distinct valleys (Fig. 1) giving rise to many river formations along with several static water bodies (tanks.) The topography with significant elevation has blessed the city with pleasant climate. These favorable conditions allowed policy makers to invite industry and scientific institutions, which lead to an ever-expanding population and also its needs.

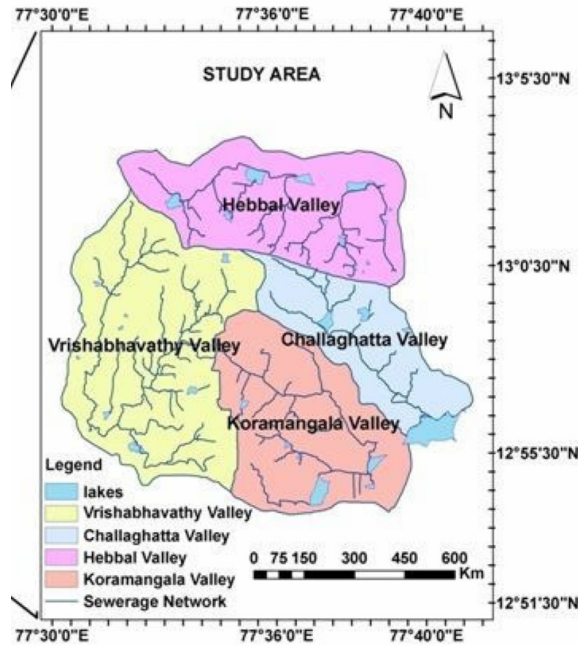


Fig. 1, Bangalore City and its Valleys [1]

Despite the several valleys, none of them are perennial flowing rivers and mainly rain fed or from overflowing tanks. In recent times, these valleys have sadly become the sinks for the city’s sewage. The primary water supply to the city is accomplished from River Cauvery flowing 90 to 100 km south of the city. Figure 2, illustrates block diagram of the path followed by the water where the significance of the Vrishabhavati comes into the problem. From the 900 MLD (until mid 2013) pumped from River Cauvery, nearly 35% of this water (in partly treated form) returns to the river through the Vrishabhavati valley over 85 to 90 km.

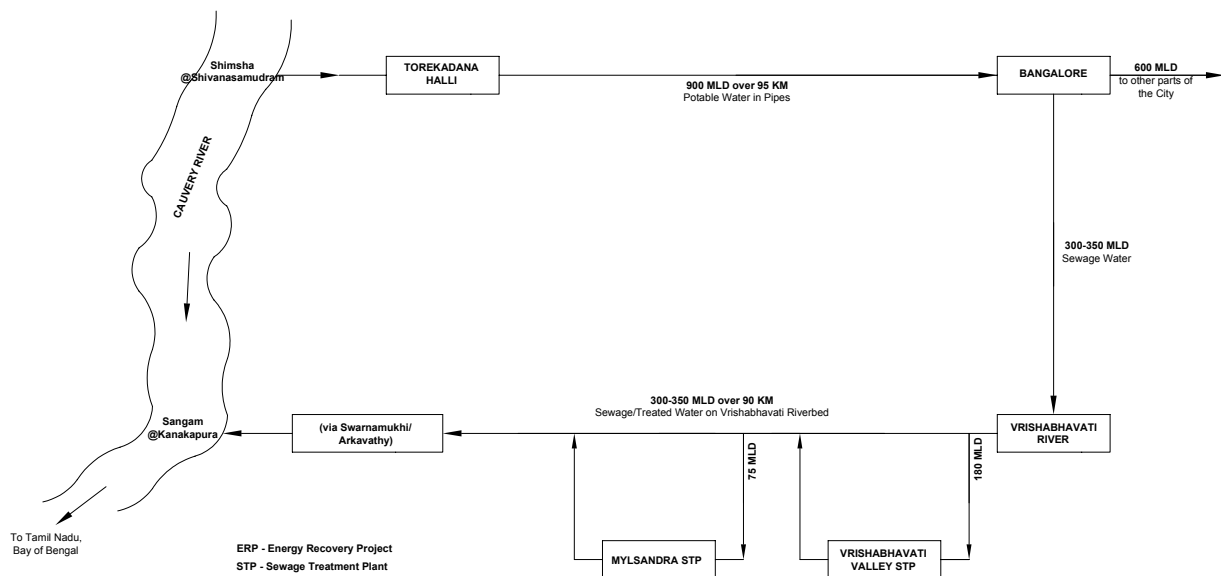


Fig. 2, Journey of drinking water (piped) and wastewater (through Vrishabhavati valley) in Bangalore city

As seen in Fig. 2, there are two sewage treatment plants along the banks of Vrishabhavati River. The first project known as Vrishabhavati STP has a current capacity of 180 MLD, while the second project called the Mylasandra STP has a modest capacity of 75 MLD. These projects are separated by a distance of 5 km and are illustrated in satellite based plan in Fig. 3

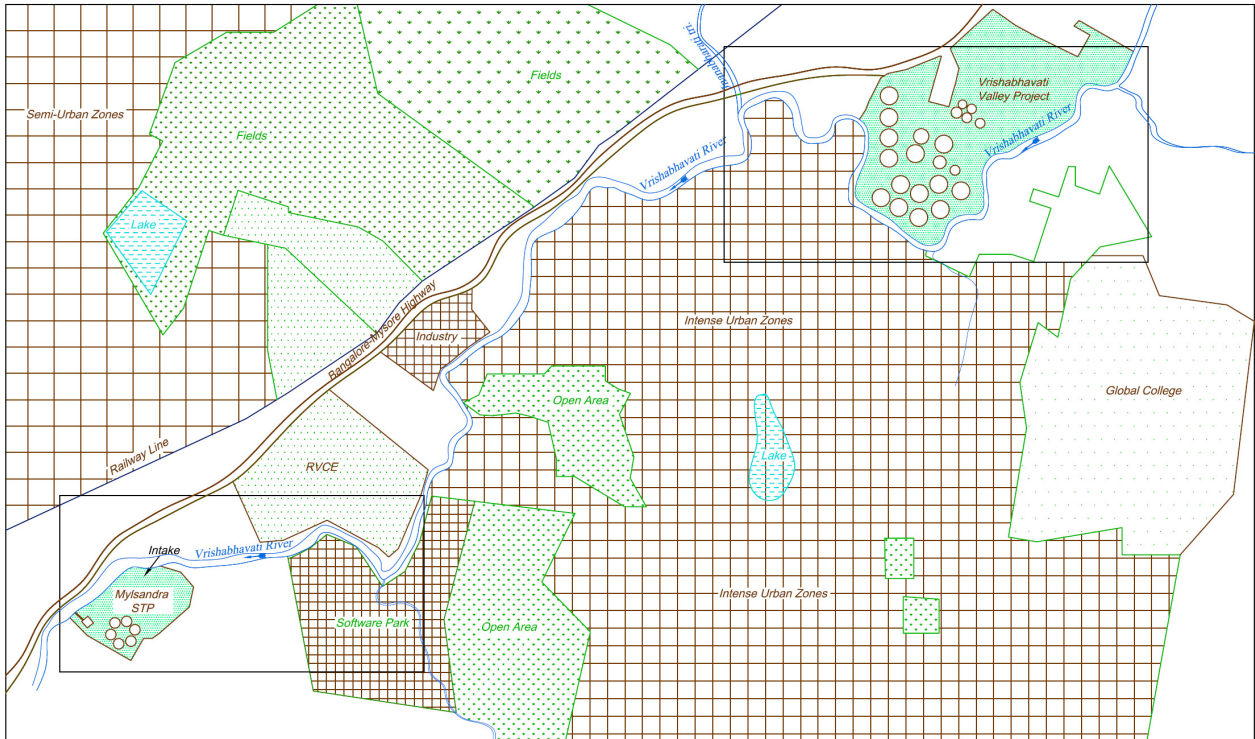


Fig. 3, The plan of the Vrishabhavati Valley and Mylasandra treatment plants on banks of Vrishabhavati River

1.2 Energy Recovery from Wastewater

The treatment of the water is primary concern of the civic authorities, but what is more significant is the scope of energy recovery. Figure 4 gives a perspective of the energy balance involved in pumping water. While pumping energy is equivalent to 2250 kWh/MLD, the energy recovered is estimated at 850 kWh/MLD even with pessimistic recovery factors.

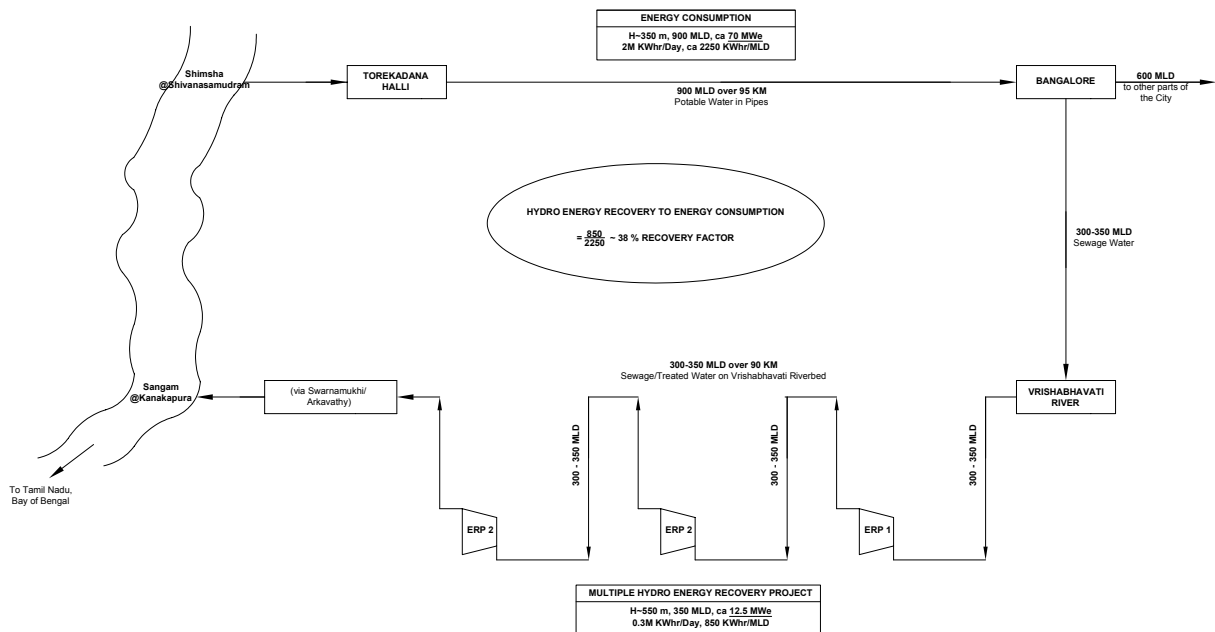


Fig. 4, Energy Balance of drinking water supply and wastewater sink

Hydro energy recovery from wastewater, a relatively new concept, is gaining prominence all over the world given the climate issues becoming dominant since the last decade and half. An illustration of energy recovery specific to Switzerland (a developed country) is shown in Table 1. It can be seen that wastewater (untreated and treated) has potential of 12.5 MW, from which only 1.1 MW was recovery based on 1995 published data [2].

Table 1, An example of Hydro energy recovery in Switzerland [2]

Water network type	Potential type	Number of sites	Output (MW)	Production (GWh/year)	Electricity consumption equivalent households
Drinking water	Operating	90	17.8	80	17780
	Remaining	380	38.9	175	38890
Untreated wastewater	Operating	3	0.4	1.4	310
	Remaining	86	7.1	32	7110
Treated wastewater	Operating	6	0.7	2.9	640
	Remaining	44	4.2	19	4220

In a short summary, Bangalore represents a strong case of investigation for energy recovery from both treated and untreated wastewater.

1.3 Mylasandra Sewage Treatment Plant

As mentioned in Fig. 2 and 3, the Mylasandra STP has been designed to treat 75 MLD, smaller compared to the Vrishabhavati Valley treatment plant, which is primarily designed to treat the entire quantity of wastewater passing through the valley. Even though situated in the valley, the Mylasandra plant is not designed to draw water directly from the Vrishabhavati, but to receive piped sewage coming from 3 different sources (Bangalore University at the northeast, BHEL valley in the north and Subramanyapura at the southwest) integrated few kilometers north of the plant as shown in Fig. 5.

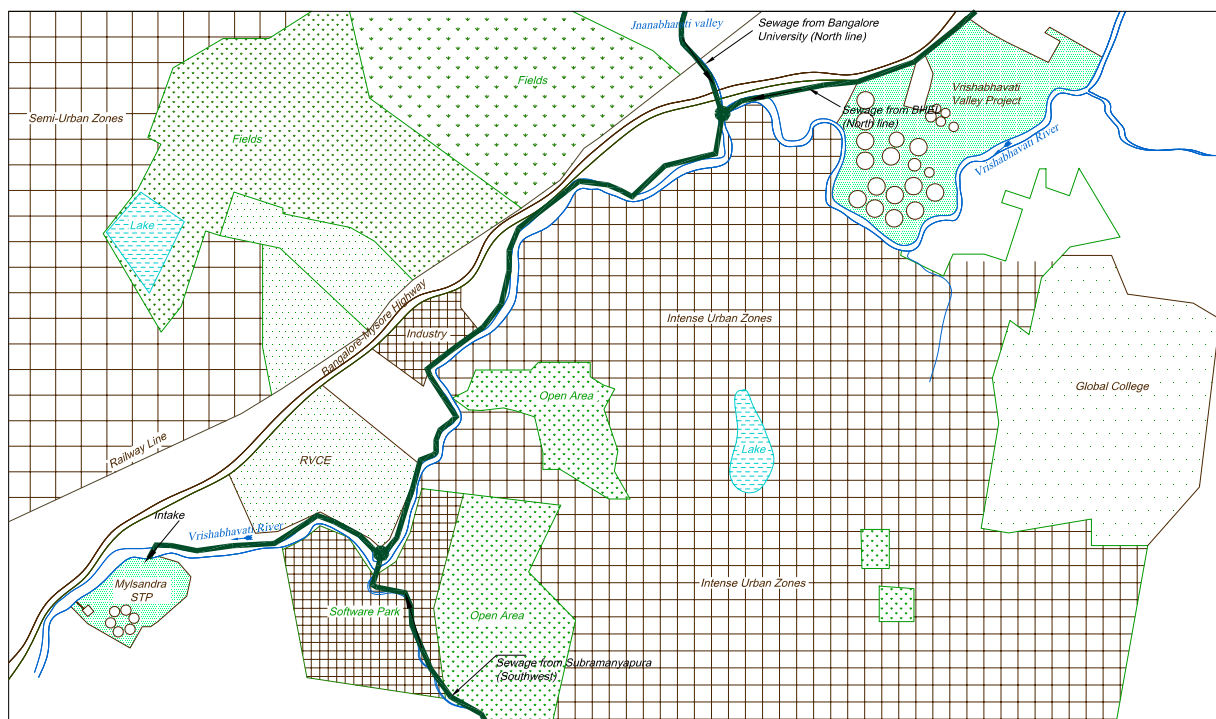


Fig. 5, The Mylasandra treatment plant and its intake

1.4 Scope and Purpose of Hydro Energy Recovery at Mylasandra

The operation of the plant is explained with the help of the plan in Fig. 6 and single line diagram in Fig. 7, which shows the path of untreated water through the plant’s major components (aerators, primary and secondary clarifiers) before the treated water is brought to the chlorination tank and then being discharged through a channel into Vrishabhavati River.

The single line diagram shows load distribution between two major loads, firstly the pump loads known as terminal sewage pump station (TSPS) and the balance of plant loads that comprises of motors that drive the aerators, clarifiers, pumps for reactivated sludge, laboratory, lighting and other supplementary loads required for plant operation.

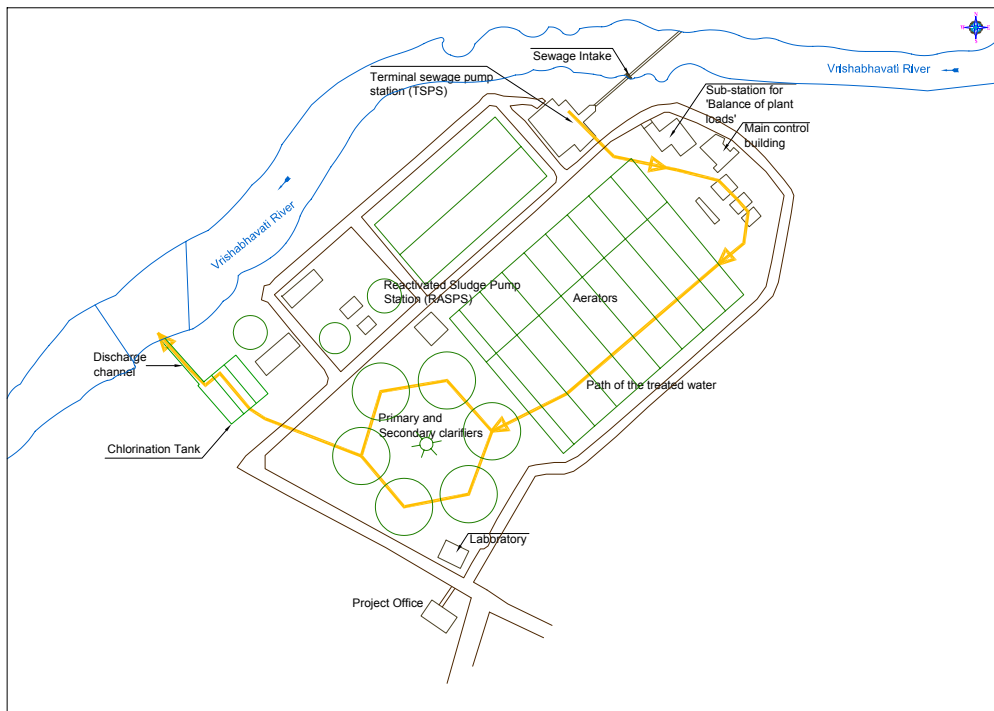


Fig. 6, Operation of Mylasandra treatment plant

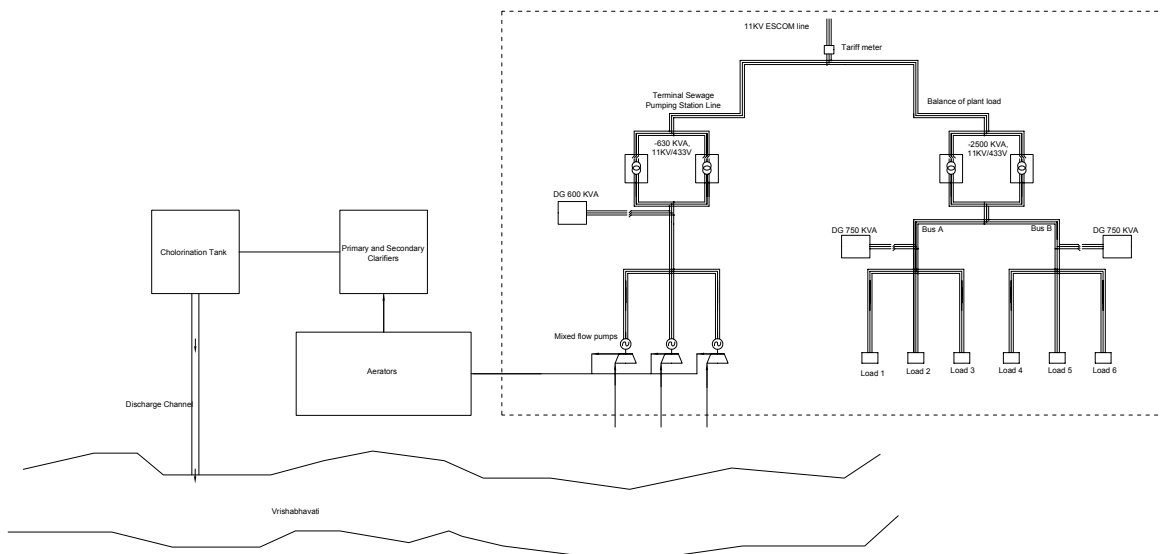


Fig. 7, Single line diagram of the plant operation and load distribution

There is scope of hydro energy recovery from the treated water after it has been released from the chlorination tank to the river. The treated water is falling from a height of nearly 6.8 meters and represents nearly power capacity of 36 kWe for steady flow of 870 l/s (equivalent to 75 MLD with all 3 pumps in operation).

The purpose of the hydro energy recovery plant is to use the generated electricity within the plant during normal operation and in turn to reduce the electricity consumption from the utility grid. The secondary purpose of recovery plant is to provide for emergency power, when the utility grid fails, by using the available storage volume in the various clarifiers at the time of power failure. One prerequisite of the design is that the recovery plant should have not adverse impact in any of the treatment processes of the plant.

1.5 A solution to meet the Energy requirements of the Treatment Plant

A solution for meeting the needs of the limited energy can be devised by installing optimal number of recovery turbines near the exit channel (beside the chlorination tank) to use available the treated water during different times of the day. This solution will not affect the plant’s processes since it will be at the exit after all the treatment has been carried out.

The recovery unit comprises of an axial flow hydro turbine coupled to a generator. Both normal grid operation and island grid operation is possible as shown in Fig. 8.

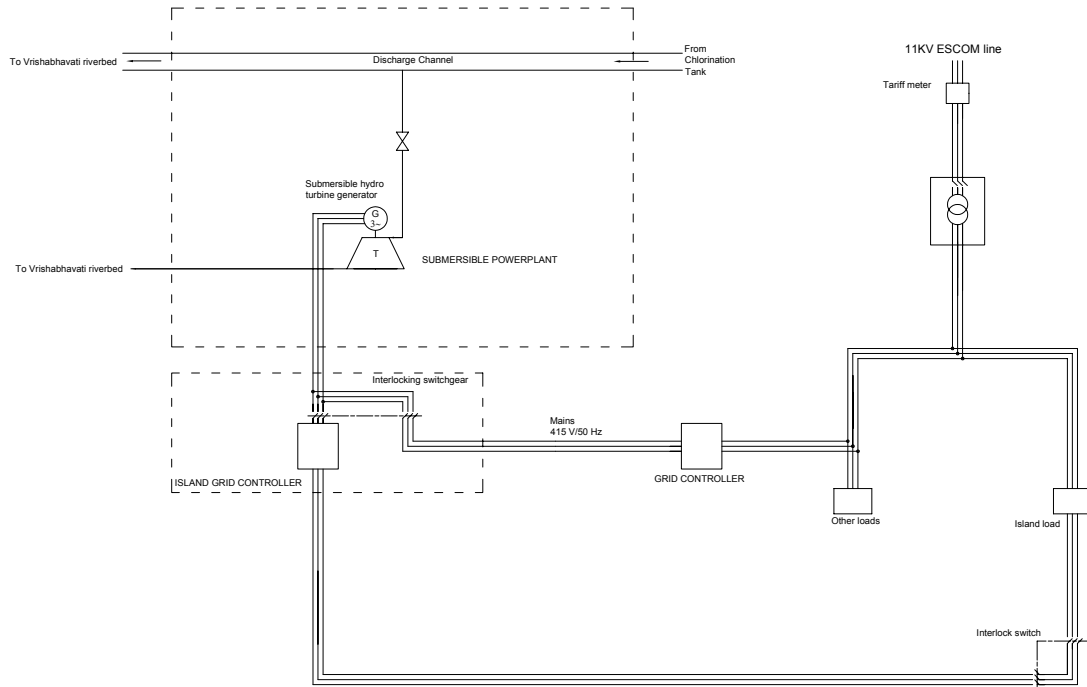


Fig. 8, Hydro energy recovery solution for grid and off-grid application at Mylasandra STP

Chapter 2 – Surveys and Investigation

2.1 Topographic Studies

The topographic investigations were restricted to the area around the exit channel next to the chlorination tank leading to the Vrishabhavati valley that represented the maximum recovery potential during the preliminary studies. The topography of the site is shown in Fig. 9 with contours at intervals of 0.5 meters. The data was compiled from land surface and water levels only. However, the cross-sections of the riverbed were not recorded. This is not important for the designing the plant, since the recovery unit is to be planned on the surface away from the riverbed even though a tailrace canal would lead to the valley bed.

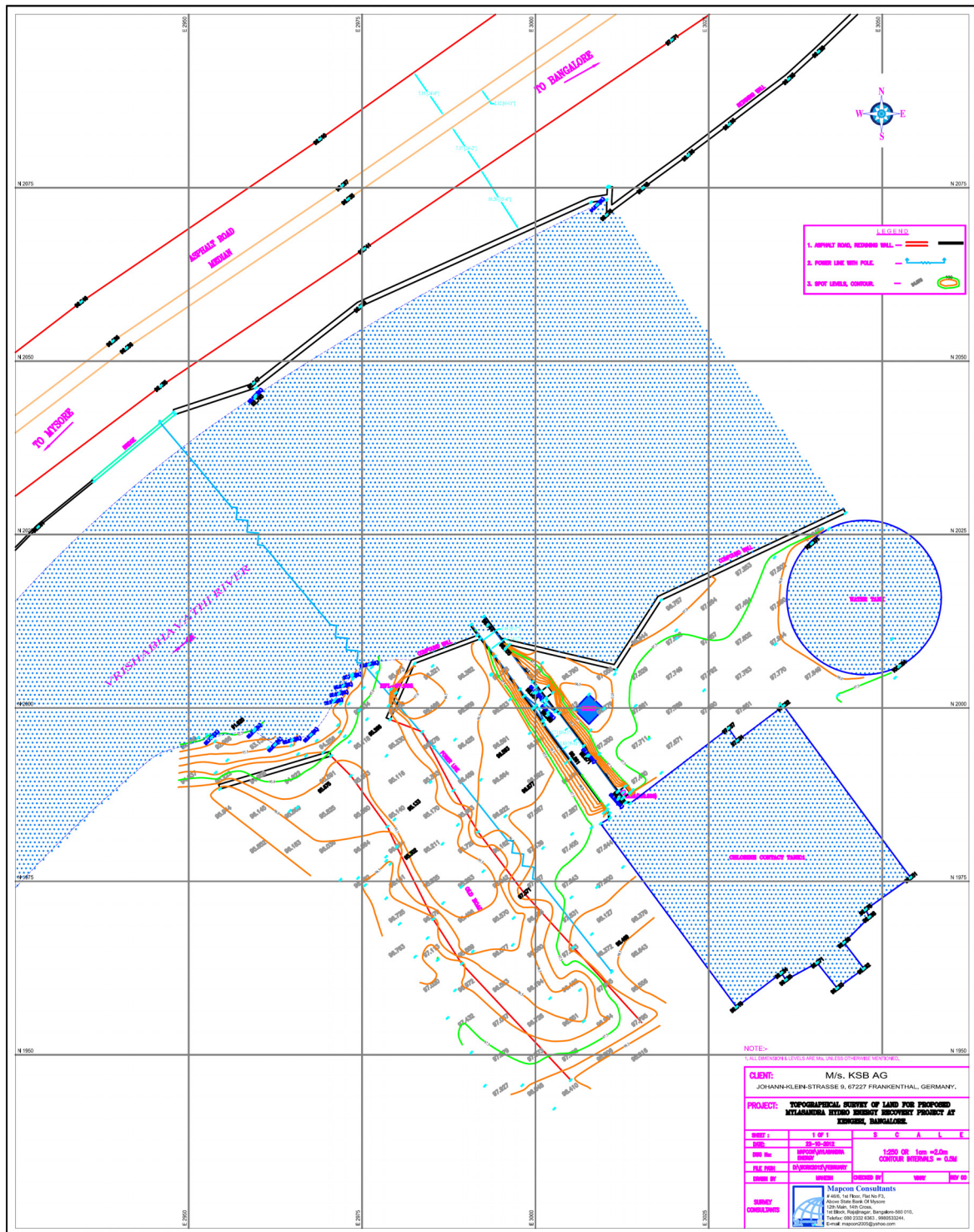


Fig. 9, Topography of the site for the recovery plant

2.2 Normal Grid Operation

The normal grid operation of the treatment plant is defined when all the loads of the plants (pumps, motors, lighting and others) are in direct connection with the utility grid. During this operation, the pumps operate in three different combinations (as explained in 2.2.1) depending on the available inflow of sewage to the plant.

2.2.1 Flow Duration Characteristics of Treated Water

The behaviour of the treated water flow depends on the time of the day, linked with the human and industrial activity of the city (respective locations from where sewage is reaching the plant as explained in Fig. 5). The flow is measured on a rectangular flume (ISO4359) constructed on the exit channel. The design of the flume along with the location of the sensor is shown in Fig. 10.

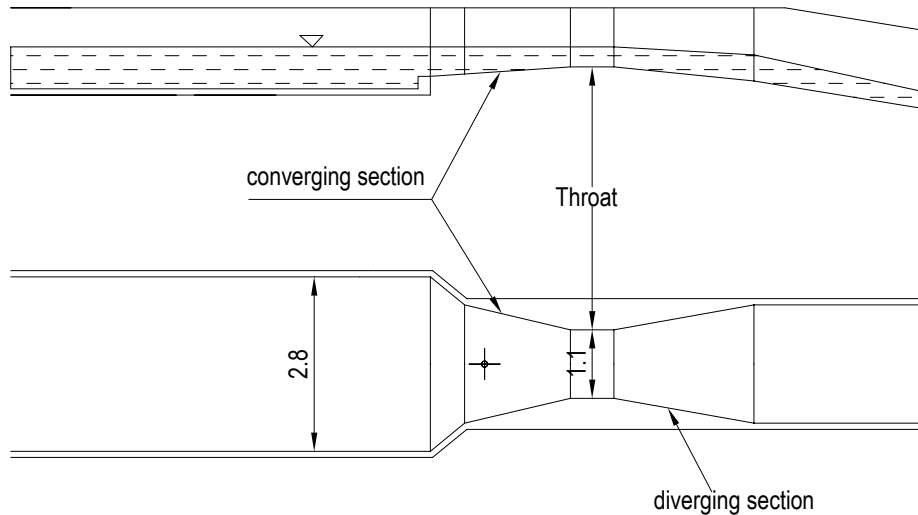


Fig. 10, The rectangular measurement flume on the exit channel at Mylasandra

A typical chart of the treated flow behaviour is shown in Fig. 11, starting from 8 am of a particular day (24th Jan 2012) to 8 am the following day. The total volume of water treated during this day is 43.1 million litres. The flow behaviour is represented on a percentage time scale in Fig. 12, which shows that the base flow for single pump operation (between 200 l/s and 300 l/s) is available for 100% of the time, while the 2 pump operation representing a flow of 540 to 600 l/s is available for 60% time and the peak flow of 850 to 900 l/s when all the 3 pumps are operating is present for 30 to 35% of time.

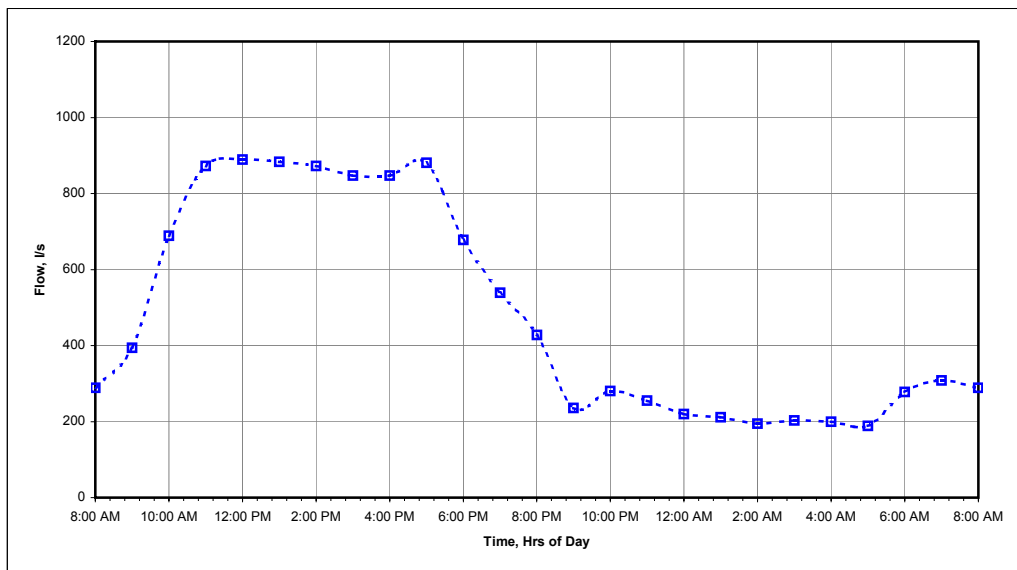


Fig. 11, Flow duration curve of the treated water (on hour scale)

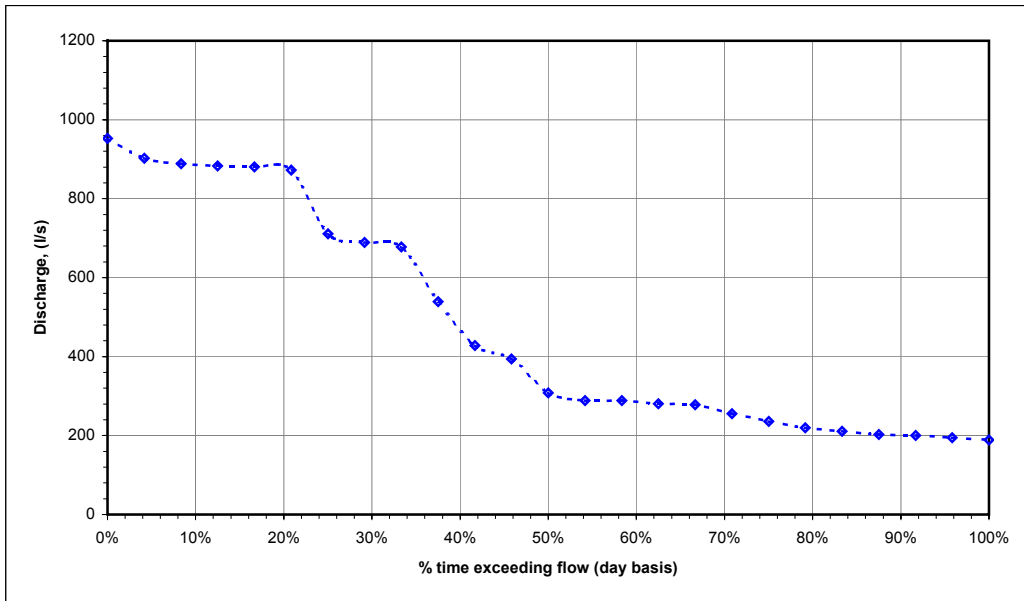


Fig. 12, Flow duration curve of the treated water (on percentage exceeding scale)

2.2.2 Power Consumption Characteristics of Plant

The power consumption (on energy basis) of all the plants loads comprising of the pumps, aerators as primary loads along with other loads has been investigated on the same day of the represented flow characteristics in Fig 11. The hourly power consumption chart is illustrated in Fig. 13 along with the flow curve.

It can be seen that the pattern followed by the mean energy curve does not correspond have a one to one correspondence to the flow curve, because the additional loads with 2 and 3 pumps in operation pertains only to the pumps and on the aerators whose loads are nearly constant at all flows. The total power consumed during the given day's operation is about 13200 kWh (with an average power of 550 kW).

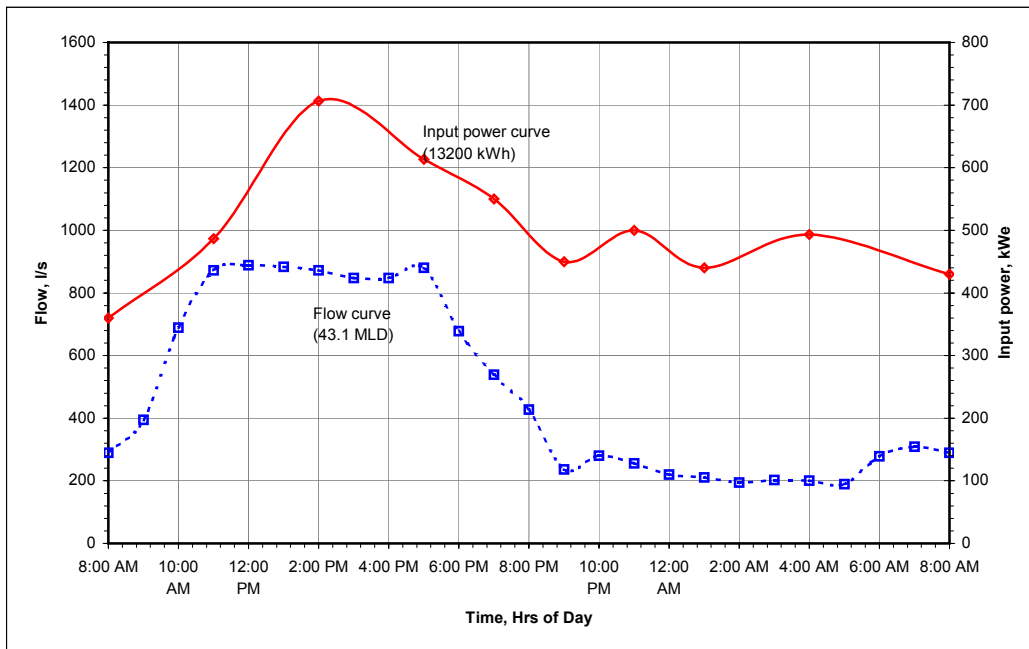


Fig. 13, Power consumption of the treatment plant

2.3 Operation during Utility Grid Failure

2.3.1 Present Scenario

The grid failure at Mylasandra treatment plant is quite common and as discussed in section 1.4, the energy recovery plant should be able to switch to an island grid powering few critically and continuously running loads.

This is notwithstanding the presence of diesel generators, which are planned for backup power supply for running the treatment plant.

The operators prefer to wait for the grid power to return instead of switching to auxiliary sources. The wait is between one hour and eight hours. Only when there are longer blackouts, the diesel generators are used.

In order to design the recovery plant for this scenario, it is important to understand the hydraulics of water flow within the different components of the plant. An exercise is carried out to understand this flow behaviour based on field measurements and simulation as described in subsequent sections.

2.3.2 Control Volume and Free flow Discharge Characteristics

The path of water flow within the plant can be understood from Fig. 14 using a control volume approach. The temporary storage components comprising of the aerators, clarifiers (primary and secondary), chlorination tank and various conduits (pipes and channels) can be defined as the control volume of the plant. Under steady state condition (whether single pump or multiple pumps are in operation), the untreated water is drawn from the sewage pumping station and after treatment it is discharged through the exit channel.

Under standstill condition, the mean level of the residual water in various tanks is lower than that in the running condition. These two levels are shown in Fig. 14 and the difference between the levels signifies to the active volume of the control volume. When the utility grid fails, this active volume causes continuous discharges (essentially due to slope incorporated between intermediate volumes) in an unsteady manner until the minimum volume is reached.

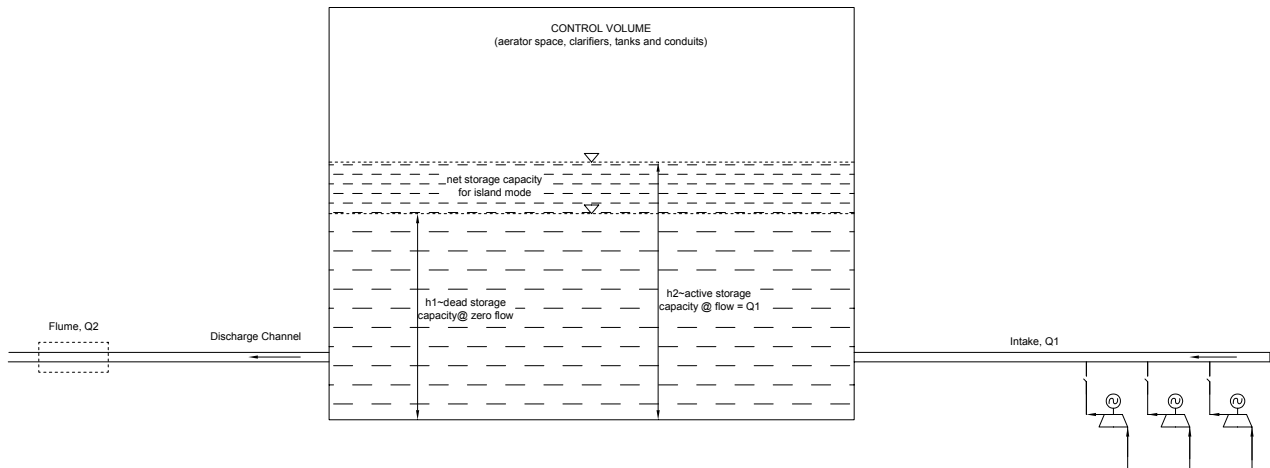


Fig. 14, Control volume approach of the plant's operation

Field investigations would comprise of recording the flows through the discharge channel (with help of the flume) as a function of time under different combinations of the pumps operating at the time the grid trips. The behavior of the discharge in three different scenarios (one pump, 2 pumps and 3 pumps operating) are simulated by switching off the respective pump combinations and the available active volume for island operation of the recovery plant can be determined.

2.3.2.1 Simulation

The actual determination of the discharge behavior could not be carried out, however, a simulation based on past experiences of such tripping situation is illustrated in Fig. 15. The simulated curves representing 3 scenarios are plotted in Fig. 15. The past tests showed that discharge rate fell faster with more number of pumps in operation. It can also be seen that the volume is marginally higher when higher number of pumps in operation due to the additional capacity available in the plant's control volume as explained earlier in Fig. 14.

It is now important to determine the potential available for energy recovery and optimum configuration of these units, which will be carried out in section 2.3.2.2.

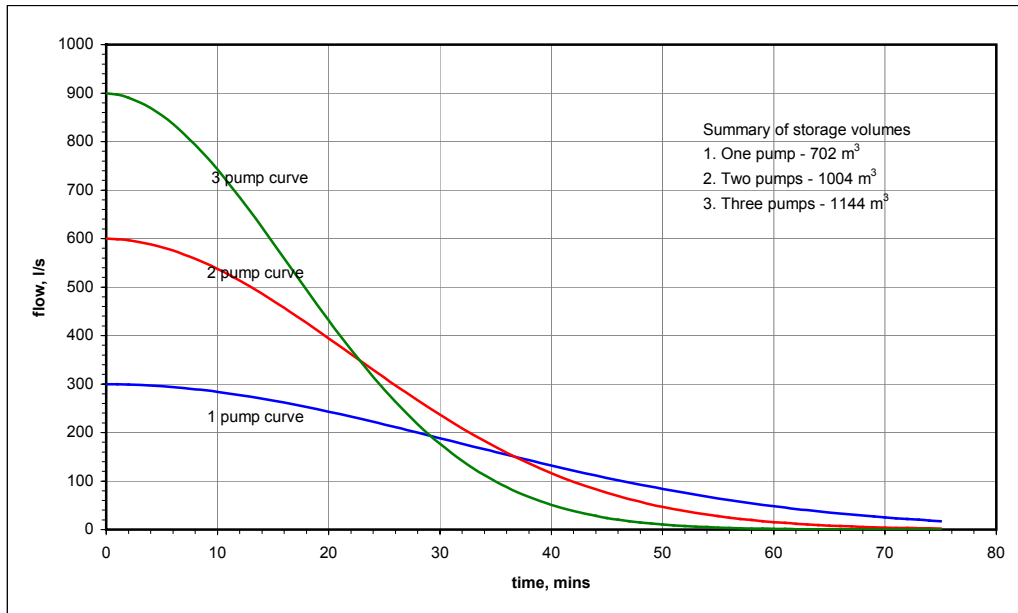


Fig. 15, Tripping behaviour of flow with under different conditions of pump operation

2.3.2.2 Operating scenario of recovery units

The evaluation of the performance of the recovery units is carried out under the assumption that the treated water available within control volume under each tripping scenario is discharged only through the respective recovery units and there is no situation of overflow from the regulating gate.

The results are summarized in Table 2, which helps in arriving at the first conclusion that planning recovery through 2 or 3 modules (turbine units) is not useful since the operating time of the units is limited to less than 30 minutes. However, a single module operation under the 3 scenarios show that the energy available for critical (island) loads varies from 8.4 kWh to 13.7 kWh with operating times between 40 to 60 minutes.

Even though, the analysis below shows that island mode of operation with single recovery unit is possible, the system design and economic considerations needs to be assessed to bring a true picture of benefits.

Table 2, Performance of recovery units at different tripping scenarios

Sr. No.	Tripping state	Active volume (m ³)	Recovery unit	Flow (l/s)	Operating time (min)	Energy (kWh)
1	One pump	702	One module	300	39	8.4
			Two modules	600	19	8.4
			Three modules	900	13	8.4
2	Two pumps	1008	One module	300	56	12.1
			Two modules	600	28	12.1
			Three modules	900	19	12.1
3	Three pumps	1144	One module	300	64	13.7
			Two modules	600	32	13.7
			Three modules	900	21	13.7

Chapter 3 – Power and Energy Studies

3.1 Grid Mode Operation

The discharge characteristics of typical day of operation of the treatment plant has been explained in Fig. 11 and 12 for an average flow capacity of 43.1 MLD. However, according to the plant's operational manual and standards, the treated flow capacity per day should not be less than 48 MLD. Hence, the power and energy studies need to be carried for this flow capacity. Figure 16 integrates the flow duration curve and power generation curves on the percentage scale for 48 MLD flow capacity.

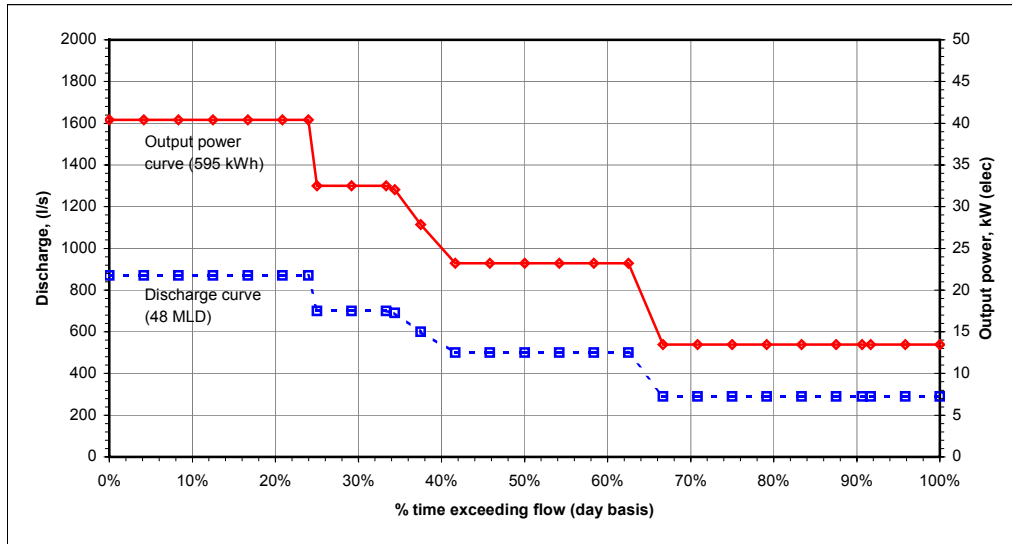


Fig. 16, Recovery power characteristics for a 48MLD flow capacity flow duration curve

The power generation curve is simulated for a net head of 6.4 m on the turbine, turbine efficiency of 85% and generator efficiency of 87% resulting a total energy recovered equal to 595 kWh. It can be seen that the power and flow duration curves follow identical pattern. The system design of the recovery units should try to achieve this value of energy.

The energy recovery per every million liters of flowing water is about 12.4 kWh (595 kWh/48MLD). In comparison to the total energy consumed (13200 kWh/43.1MLD = 306 kWh/MLD), energy recovered per MLD is about 4.05%.

3.2 Island Mode Operation

An accurate simulation of the island mode of operation of the recovery turbine is very important for understanding the usefulness of this mode (section 9.2.2), given the substantial investment it would incur (chapter 8). In the event of selecting the 'single recovery module' having a nominal power of 12.5 kW_e (290 l/s) under the three tripping scenarios, the recovery plant will operate for only 40 to 60 minutes before the water in the control volume gets emptied.

The schematic view of the single recovery unit is shown in Fig. 17. In order to run one recovery unit, the other two turbine valves needs to be immediately closed the moment the power fails (tripping) otherwise there would loss of water. The respective butterfly valves of these turbines will have to be fitted with dead weight actuators in order to isolate the flowing water through them as shown in the configuration proposed in Fig. 20 (section 5.4).

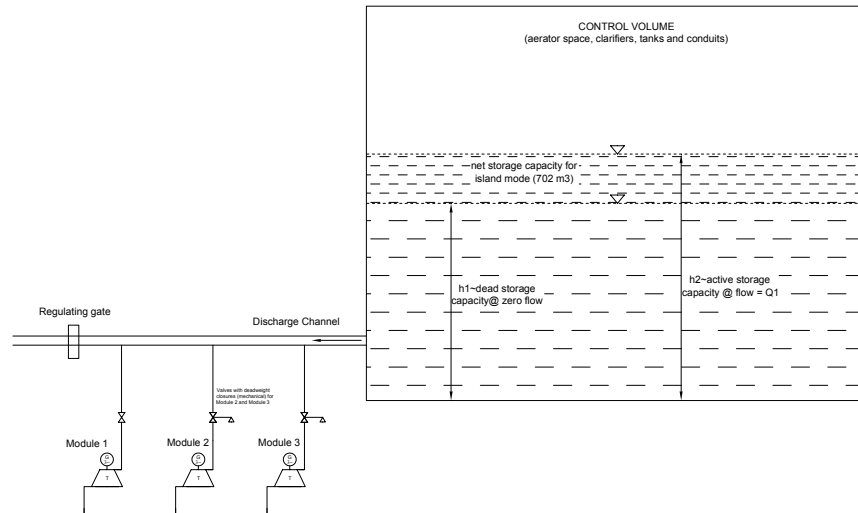


Fig. 17, Recovery units in island mode with available control volume

The cost benefit analysis of this single machine operation will need to consider factors like the delivered performance, system design involved and most importantly economics before re-evaluating the need for island mode.

3.2.1 Summary of System Design of Island Mode

The system design will be discussed in detail in section 6.4 and chapter 8. In short, the island mode of operation will require 3 additional components listed below.

- i) Dead weight actuated open/close valves for two recovery units
- ii) Island mode controller (4 quadrant converter)
- iii) Creation of an island grid with interlocking switching gears

Chapter 4 – Civil Works, Hydro Mechanical Equipment and Construction Materials

4.1 Civil Structures:

The Civil and appurtenant structures that are envisaged for different components of the proposed Mylasandra Hydro Energy recovery Plant are detailed in this Chapter. The Main components are,

- Intake Pool.
- Penstock pipe and connected civil works.
- Powerhouse.
- Tailrace Pool & end discharge Weir.

All the components of the proposed scheme are ideally located on the left side of the discharge channel emanating from the chlorination tank, which is a part of BWSSB's tertiary sewage treatment plant at Mylasandra. These components are accessible through approach roads available within the Mylasandra treatment plant area.

4.1.1 Project Layout:

The general arrangement of the proposed scheme is shown wide drawing (Fig. 18.1 and Fig. 18.2) entitled "General Layout- Plan and L- Section". The broad design features and provisions of different components are discussed in the following paragraphs.

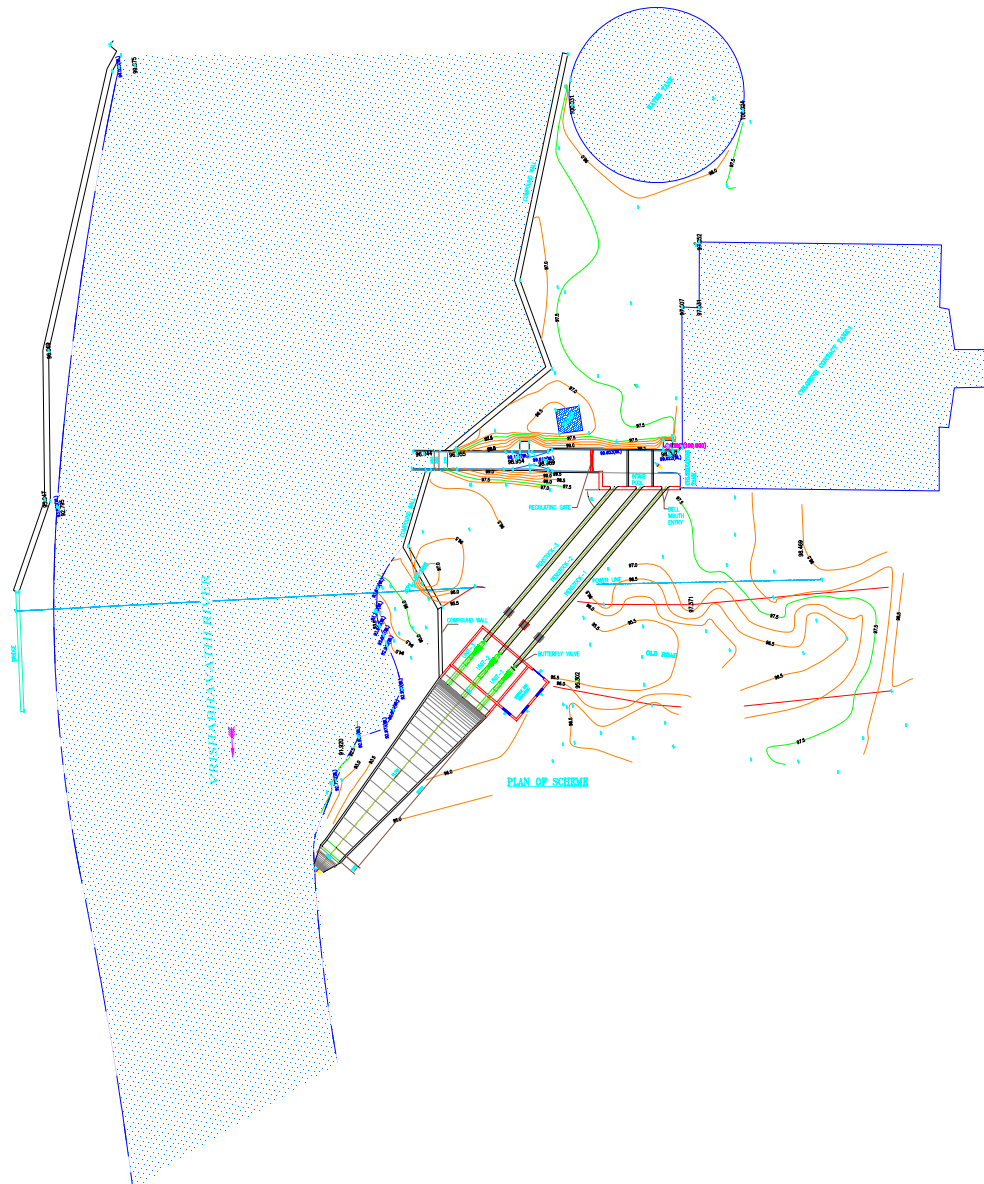


Fig. 18.1, General Layout, Plan of Mylasandra Scheme

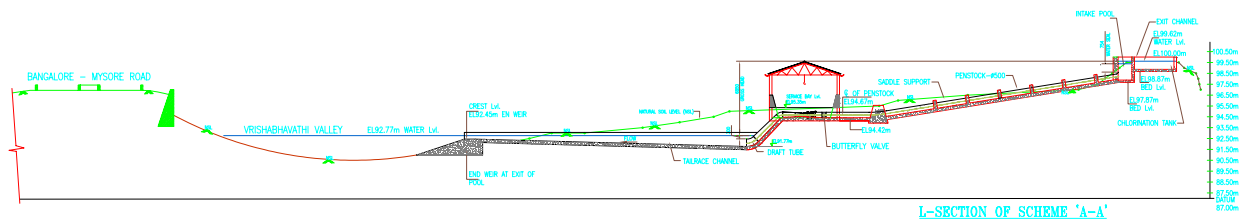


Fig. 18.2 General layout, L – section of the Mylasandra Scheme

4.1.2 Intake Pool:

The Intake pool is proposed to be constructed adjacent to the existing discharge channel as a part of the channel. The pool consists of a cistern with its floor level depressed by one meter with respect to channel floor level as illustrated in Fig. 19.

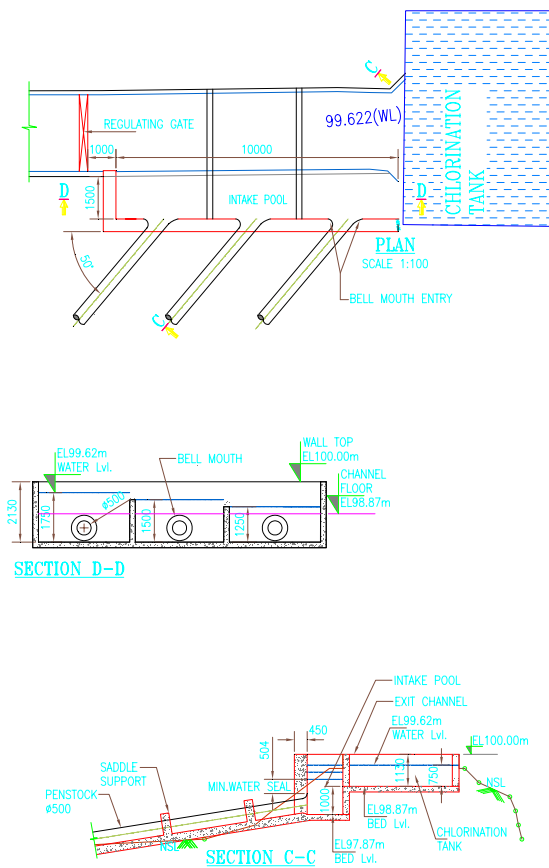


Fig. 19, Intake pool

The size of the pool is 10.0m long and 1.50m wide and sufficient to accommodate the three penstock pipes required to carry the water to the powerhouse. The pool is proposed to be of RCC type construction with the wall thickness of 450 mm. Necessary transition to facilitate smooth entry of flow to the penstock with in the wall thickness is proposed to be provided.

The channel and the cistern are proposed to be divided in to three compartments by constructing divider walls across the discharge channel and the cistern in order to draw the required discharge in to the penstock. The height of divider wall is kept at such a level as to push the design discharge of 300 l/s in to each penstock. Sufficient water seal would be available at the entry to the penstock in order to avoid entry of air and surface vortices.

4.1.3 Penstock pipe

The penstock pipe takes off at an angle of 50° to the longitudinal axis of the discharge channel from the intake pool and runs for a length of 27.50 m up to the Main Inlet Valve (MIV) as shown in Fig. 18.1 and 18.2. It is proposed to provide HDPE pipe of 500 mm diameter of pre-designed thickness to withstand the static head and the pressure rise due to load throw off (runaway) on the unit. Individual penstock pipes are proposed for each unit.

The penstock partly runs in excavation and balance over ground. It is proposed to provide suitably designed anchor block at the change in direction near the power plant in sectional elevation (No bends in plan). In between the anchor block and the intake pool saddle supports will be provided at maximum intervals of 6 meter with proper fastening into the saddle supports with metal strips. The maximum velocity is limited to 1.52 m/sec, which is about 13% of the spouting velocity. The MIV provided near the generator unit would regulate the flow depending on the load. And hence no intake regulatory gate is contemplated at the entry to the penstock.

4.1.4 Power House

The three micro turbo-generator units (TG) of 12.5 kW_e capacity each are proposed to be installed (Fig. 20) in the powerhouse. It is proposed to install axial flow type turbo-generators suitable for limited varying conditions of discharge and head. The TG units are proposed to be installed at the elevation El 94.42m on a common platform over the base plates anchored in to the concrete platform.

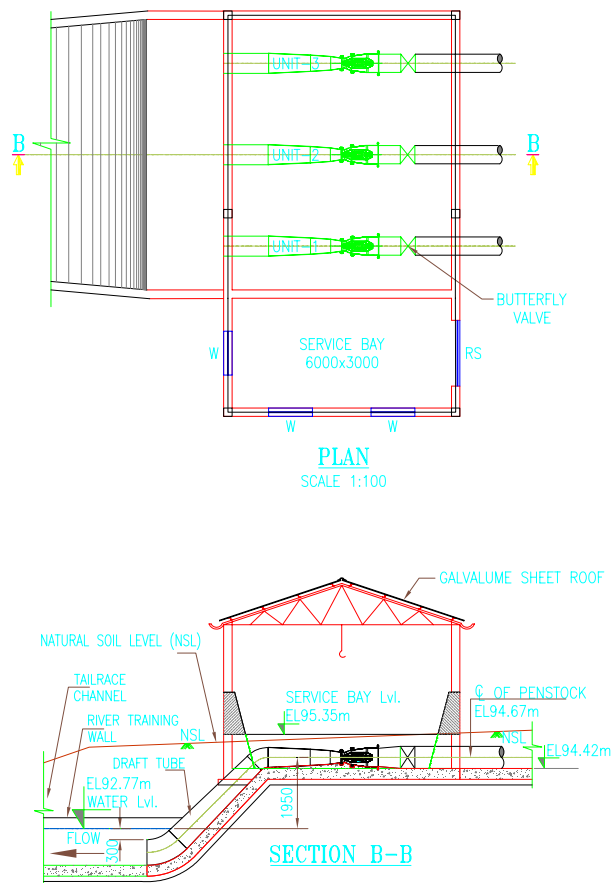


Fig. 20, Plan and elevation of powerhouse

The powerhouse is an open type with service bay provided on the left bank at an elevation of EL: 95.35 m, which is above the likely flood level. The power cable of 440volts capacity will be taken underground to control room proposed on the right bank where control panels, switch gears and batteries etc are proposed to be housed with all protections. The powerhouse platform is of size 11.00m X 6.50m including the service bay and constructed with UCR masonry as core and RCC slab and walls as casing.

It is seen that good foundation strata is available for supporting the structure of the powerhouse in the bed and banks of the stream. The super structure of powerhouse consists of RCC columns, steel roof trusses and AC sheet roofing. The discharge diameter of turbine is 300mm and the end is connected to a circular draft tube of varying diameter from 300mm at the entry to 800mm at the exit end.

4.1.5 Tail race Pool and End Discharge weir

The three independent draft tubes, one for each unit, would discharge the water in to the common tailrace pool. The pool is of RCC type construction and has a length of 25m with width varying from 7.40m at the beginning and 3.0m at the end as illustrated in Fig. 21. The bed has a reverse slope of about 1 in 37. A discharge weir is proposed at the end of the pool with sill level kept at El92.45m. Detailed views are provided in the Annexure (Fig. A1 and A2).

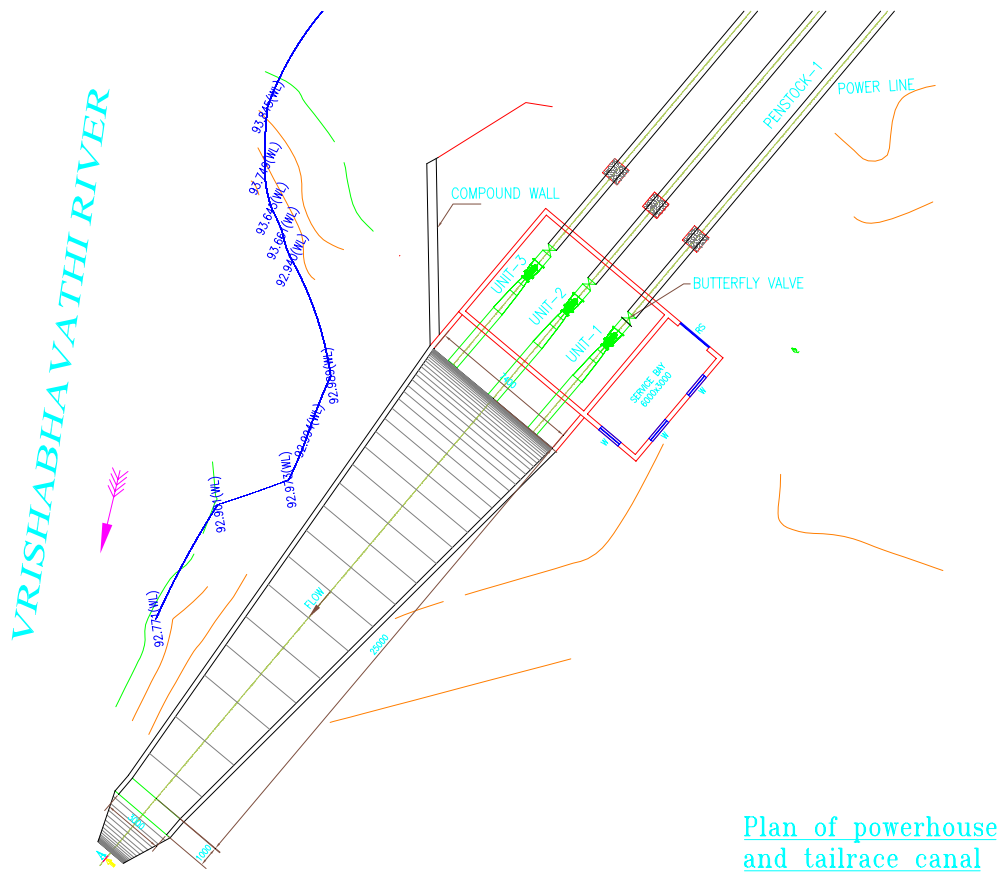


Fig. 21, Plan of the tailrace canal and position of the discharge weir

4.2 Hydro-Mechanical Works

The hydro-mechanical works primarily comprises of the penstock pipe (3Nos) and a regulatory gate across the main discharge channel. The penstock pipe, as already described in foregoing paragraphs, is 500mm internal dia and of HDPE make. The pipe of suitable thickness would be chosen in order to resist the static head and the pressure raise due to load throw off. The gate proposed across the discharge channel would be of simple vertical lift type with screw type hoisting arrangement.

4.3 Construction Materials

The project is situated within the Bangalore urban agglomeration and the manufactured construction materials like cement, steel, pipes etc will be sourced from Bangalore city. Random sampling will be done from the supplies received from time to time and the tests on the strength and properties of cement and steel will be got done from a reliable testing agency / nearby Engineering College. The structural steel such as I sections, Channels, Angles and Plates required for the fabrication works of gates, hoists and roof truss will be procured by the contractors to whom the works will be entrusted on contract basis. The fabricators will be asked to furnish the test certificates taken from the dealers from whom steel materials are procured. The Rubble, Size stone, Bricks, Coarse and fine Aggregates required for the works will be procured and transported by the contracting agency to whom the civil works will be entrusted. Samples of aggregates will be got tested in the laboratories to establish their suitability.

Chapter 5 – Electromechanical Equipment and Power Evacuation

5.1 Rotating Machinery – The Submersible Hydro Turbine

The selection of the hydraulics for the recovery unit is based on the net head and the flow corresponding to the nominal rating of the each sewage pump (illustrated in section 3.2.1). Subsequently, the sizing of the generator is made. The recovery unit comprises of an integrated hydro turbine coupled to a generator as shown in Fig. 19. The unit can be placed either in a submerged or open condition while operating, since the turbine is enclosed within the casing, while the generator is further protected within an airtight housing. The inlet (from tank) and exit (to draft tubes) are shown in Fig. 22.

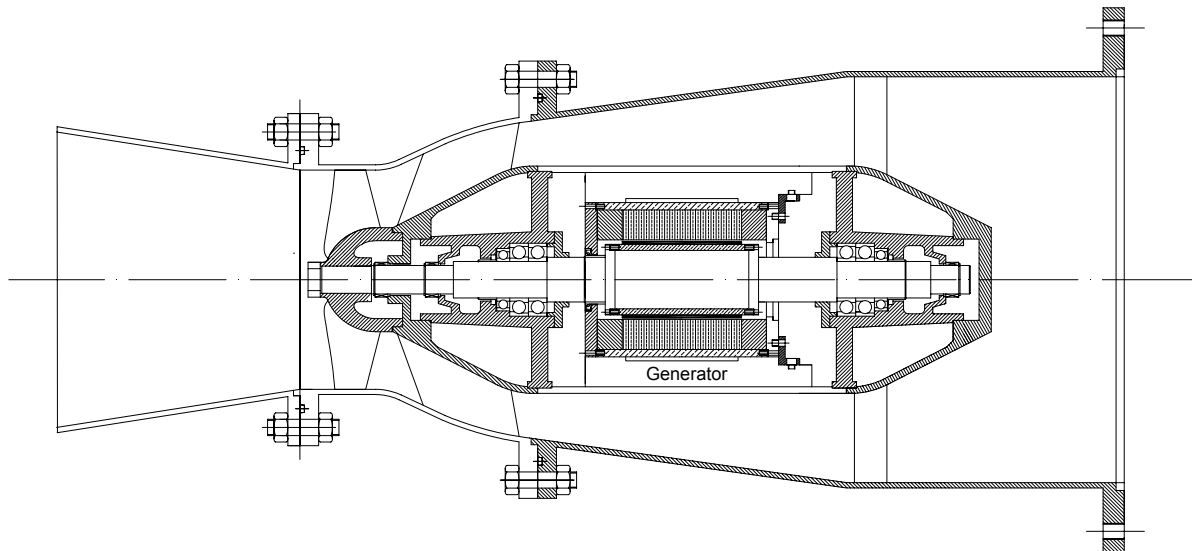


Fig. 22, Cross-section of recovery unit – A submersible hydro turbine

The pictorial representations of the components of the recovery unit comprising of the runner, guide vanes along with intake and exit shapes are shown in Fig. 23.

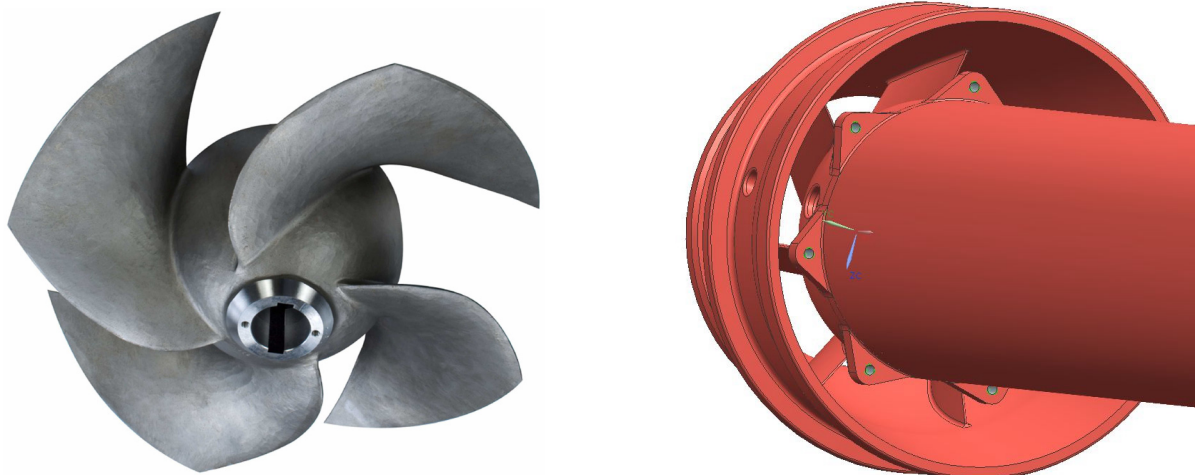




Fig. 23, Representation of the submersible hydro turbine with propeller and fixed gates

5.1.1 Turbine

The type of the turbine for the conditions of 6-6.4 m head and 280-300 l/s is essentially an axial flow propeller. A reverse operating axial flow pump that suits the above conditions and achieves the power values corresponding to the requirements specified section 4.1 is selected. The performance characteristics at 1520 rpm for a given pitch angle of the blade is illustrated in Fig. 24. The nominal point of the turbine is defined at a flow rate of 290 l/s with an overall hydraulic efficiency of the turbine unit is 80%, which is slightly below the required value of 85%.

Flow	290	l/s
Net head	6.4	m
Efficiency	80	%
Shaft power	14.5	kW
Speed	1520	rpm

The Fig. 24 also summarizes the performance of the turbine and generator at different flow rates. It can be seen that small changes in flow will cause a drop of net head and subsequently the shaft and electric powers. The constant speed characteristics in Fig. 24 are representative for grid mode of operation only.

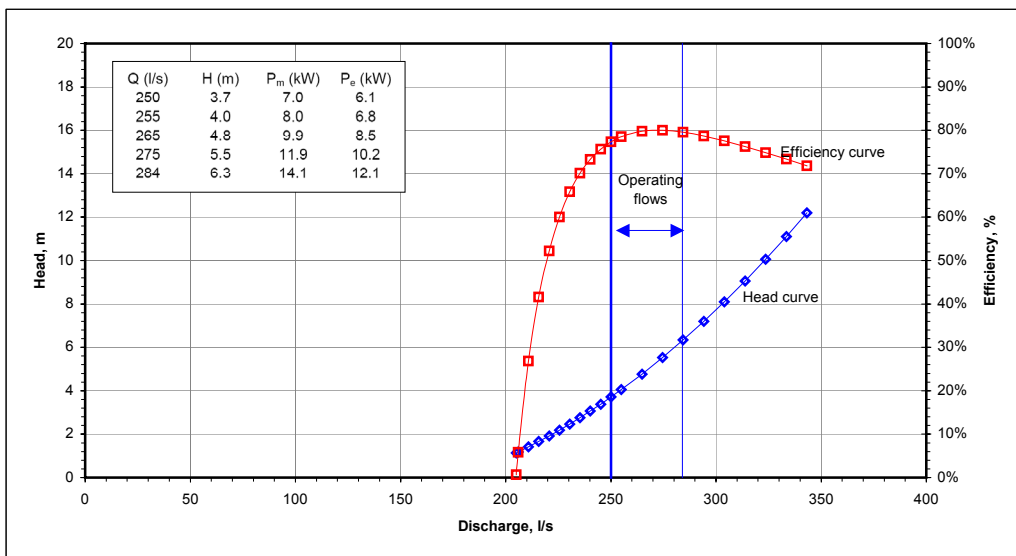


Fig. 24, Performance of the recovery unit at constant speed of 1520 rpm (grid mode)

Another method of representing the performance of the recovery unit is on the basis of constant head as shown in Fig. 25 and 26 will be basis for the island mode of operation (section 5.2.2).

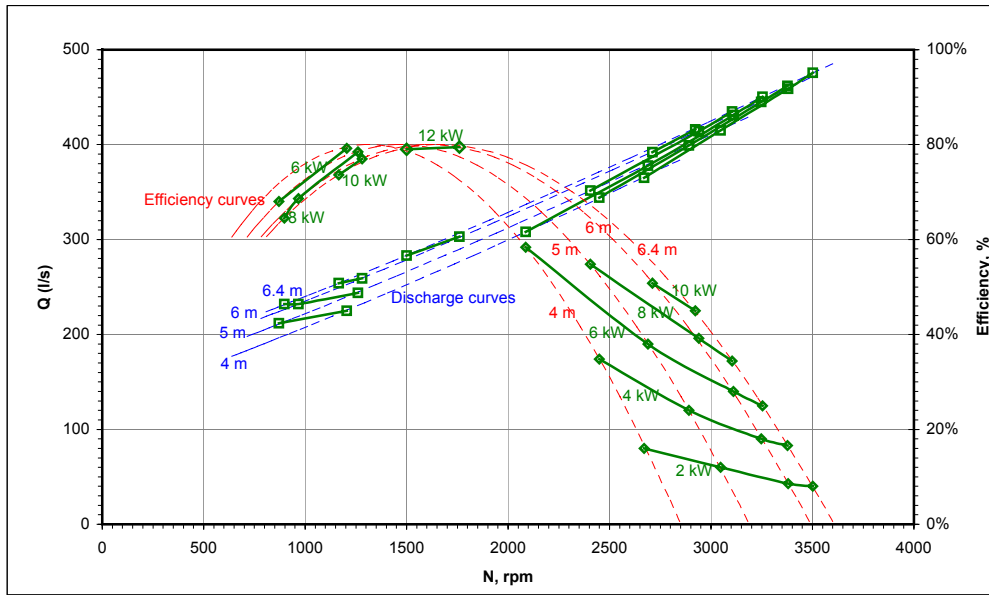


Fig. 25, Discharge and efficiency characteristics of the recovery unit at constant head (island mode)

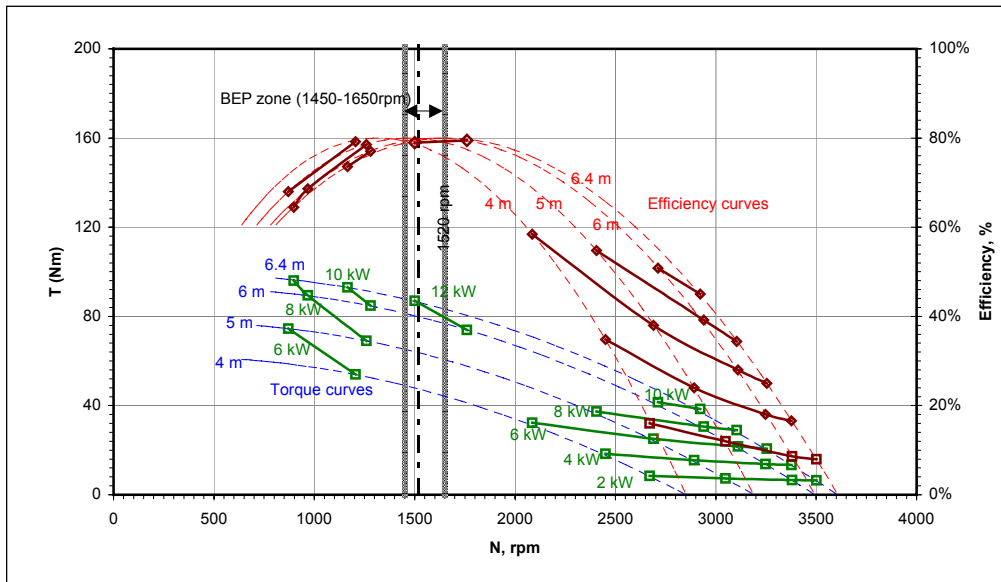


Fig.26, Torque speed characteristics of the turbine at constant heads (island mode)

5.1.2 Generator

The chosen generator for this hydro turbine is an asynchronous generator of a rugged design capable of both grid and off-grid operation, whose performance at nominal point is defined as follows.

Speed	1520	rpm
Input shaft power	14.5	kW
Efficiency	86.7	%
Output power	12.6	kW _e

5.2 System Design and Recovery Plant Performance

The system design for the recovery unit is based on the flow duration curve defined for 48 MLD plant capacity discussed in section 3.1. The proposed system design comprises of 3 recovery units of identical design as illustrated in the preceding section.

The recovery plant performance for this system design is discussed at two levels. The first level is the effectiveness of units to utilize the available flow completely (Fig. 27) and the second level deals with energy generated from these units (Fig. 28).

It can be seen that though the turbines are capable to use the flow at varying capacities completely, the conversion to shaft power at transition flows (from 290 to 580 l/s from single turbine to two turbine operation and 580 to 870 l/s from two turbines to three turbine operation) does not match with the ‘nominal’ values defined in section 5.1.1 and 5.1.2.

This is because the fixed propeller and guide vane design are optimized for nominal flows (290 l/s, 580 l/s and 870 l/s) only and the efficiency along with the useable head falls at transition flows (Fig. 24). However, the duration of transition flows is relatively small and configuration results in a healthy value of energy recovered of 545 kWh compared to 595 kWh required by the plant design protocol (section 4.1). The transition zone can be further narrowed by controlling the feed pump operation and proper maintenance.

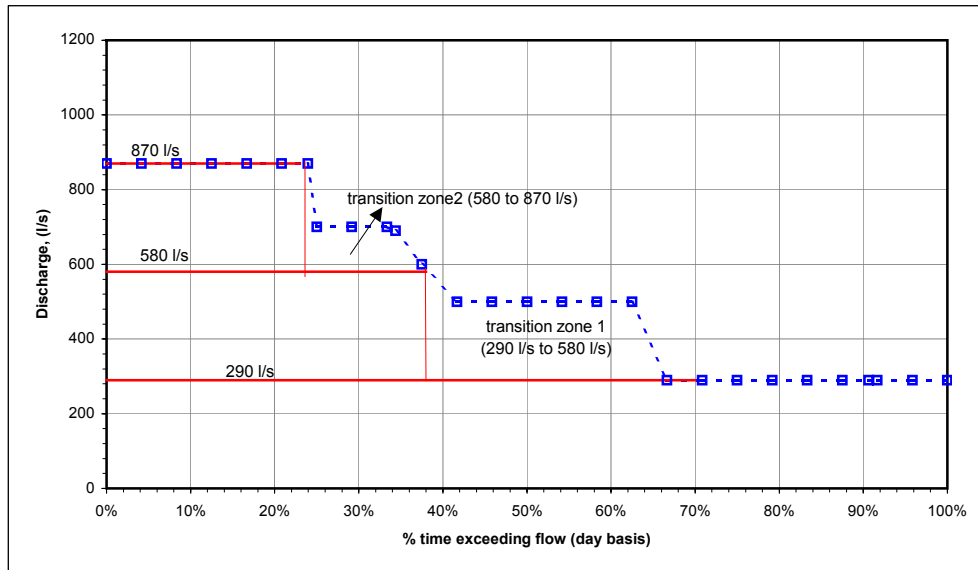


Fig. 27, Operation of the 3 recovery units under the 48 MLD flow duration curve

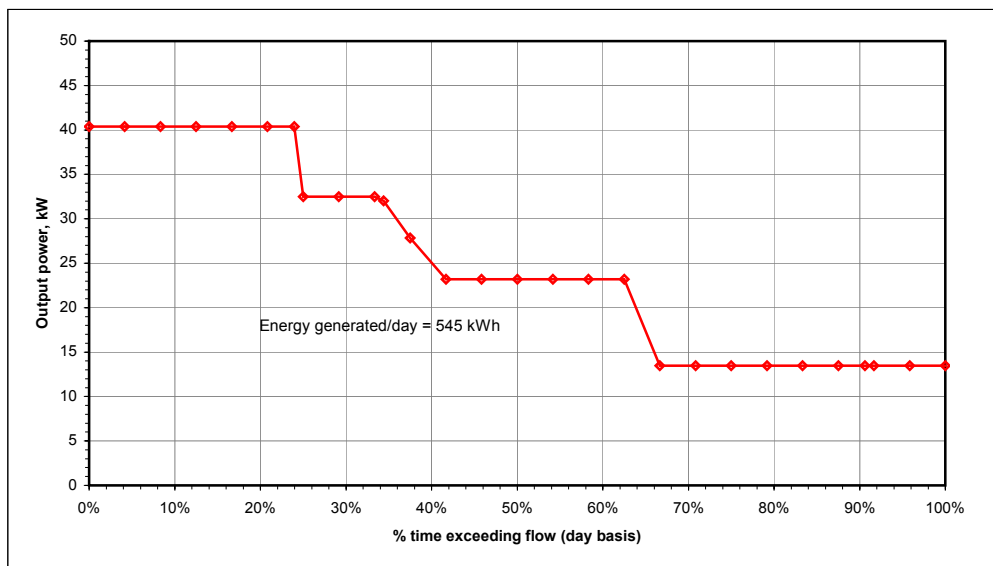


Fig. 28, Energy generation from the 3 recovery units under the 48 MLD power duration curve

5.2 Control System

5.2.1 Grid Mode Operation

The generator mode of operation of an asynchronous (or induction) machines is well known, which is achieved by allowing the generator speed to reach the designated synchronous speed on free run (grid disconnected) first and then allow the speed to progressively increase (grid connected) by monitoring the electromagnetic torque on rotor (consumed) equals the mechanical torque from the prime mover. The operation is explained using the complete torque speed characteristics of a typical asynchronous generator (in Fig. 26).

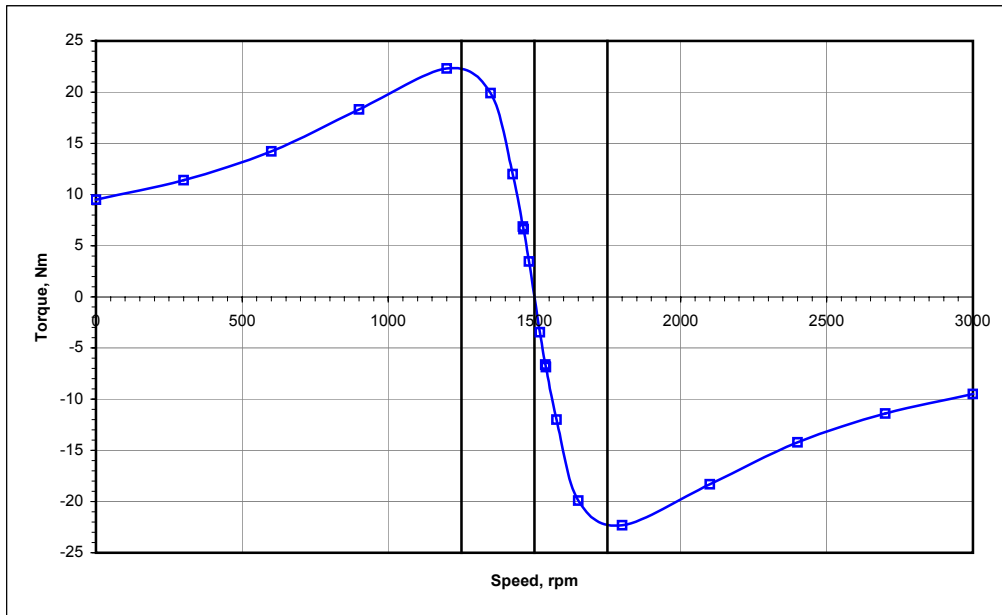


Fig. 26, Complete torque speed characteristics of a 3 phase induction machine at 1500 rpm synchronous speed

As the water is allowed to pass through the turbine, the speed increases from standstill. In case the stator is in contact with the grid (of specified voltage and frequency), the asynchronous machine will first enter the motor mode, where the electromagnetic torque (consumed) is in the opposite direction of the mechanical torque. This is an unstable region that is not advisable for longer running times. As the mechanical torque increases (with increase in speed corresponding to increase in flow and head to the turbine), it overcomes the electromagnetic torque at synchronous speed of the grid. Any increase in speed beyond this point will cause the electromagnetic torque to change direction (generation instead of consumption) and the machine will become a generator supplying electric power to the grid. However, only active power is supplied to the grid, while the small amount of reactive power required for the generator to produce flux is still coming from the grid.

Even though there is no need for an external device to bring the asynchronous generator to synchronous speed, the unstable region of clashing torque needs to be overcome as soon as possible. One of the features of the grid controller used is to sense the direction of the electromagnetic torque at different speeds using a multi-functional power meter. Initially, the asynchronous generator is disconnected with the grid, which makes the turbine run on no-load speed. At different speeds of the turbine, the generator is allowed to interact with the grid to determine the status of the electromagnetic torque. If the torque is positive (according to the Fig. 26), the grid is disconnected and the turbine speed is allowed to increase further. After some trials, the torque becomes negative, signifying that the generator mode is achieved. After this, the generator is left on and it generates power according to turbine load.

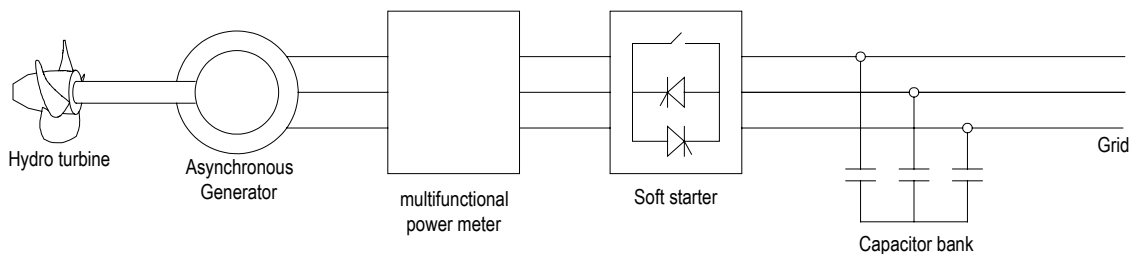


Fig. 27, Schematic diagram of a grid connected asynchronous generator with controller

In addition to torque sensors the grid controller also includes features like control buttons, protection switches and displays for electrical parameters and discharge through the turbine. Each of the 3 recovery units has its own torque sensor (multifunctional power meter) and automatic switchgears. In addition, a reverse energy meter is installed to measure the net energy evacuated to the grid.

The panel also includes interface relays required for any external control requirements (valve controls and others). A grid-protection relay is also included in the control system.

5.2.2 Island Mode Operation

The island mode of operating an asynchronous generator requires a much more advanced controller. One of the controlling techniques is to use variable speed drives powered by advanced switches like pulse width modulators (with high response speeds) such as IGBT (Insulated Gate Bipolar Transistors). A typical variable speed drive, also known as a 4-quadrant full load controller, is shown in Fig. 28.

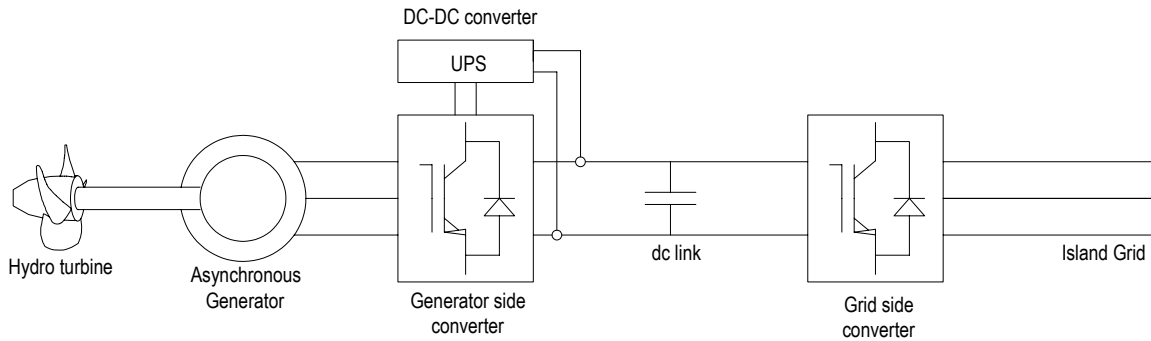


Fig. 28, Island controller using a 4-quadrant full load converter

The line diagram in Fig. 28 explains the basic function of the control system operating on an island load. The full load converter comprises of two separate controller units known as the variable speed converter (VSC). The first VSC, which is closer to the power plant is referred to a generator side converter. It senses the speed and flux of the stator coil at various loads and adjust the torque and speed to optimal values corresponding to the hydraulic condition of the turbines (head and flow). The VSC on the grid side regulates the phase vector and frequency of the load current. The two converters are separated by a DC link that helps the two controllers to work independently.

This technology helps the load to exactly correspond to the turbine output. Hence, the flow and head may change accordingly. This facility eliminates the need of a separate load diverter based control system used in conventional decentralized power projects.

However, there is permanent backup that will be needed to start the generators by supplying the reactive power to the stator. The battery backup is charged from the DC link as shown in Fig. 28. In addition to these components, there is transformer located at the output the grid side converter for enhance the supply voltage to 415 V.

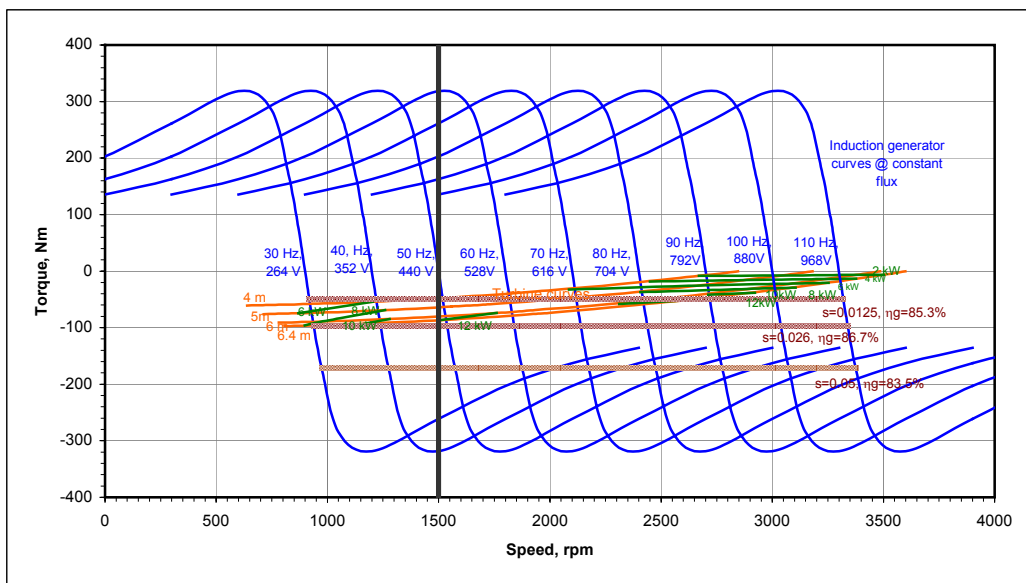


Fig. 29, Application of variable speed converter technology on the submersible recovery unit

The integrated performance of the turbine-asynchronous generator with the full load controller is shown in Fig. 29. It can be seen that a field of torque speed characteristics are formed at different synchronous speeds and

induced voltages at constant flux. While the synchronous speeds are achieved by the firing of the pulse width modulator, the increased voltage by the same factor of synchronous speed rise is due to the fact that voltage is directly proportional to the synchronous speed at constant flux.

The optimum efficiency range (related to the slip limits) are also plotted in Fig. 29. The turbine characteristics described in Fig. 26 are also plotted, with constant output power lines.

It has to be emphasized that the island load be maintained in the range of 10 to 12 kWe for optimum discharge and efficiency values. Reducing the load on the island grid will cause the speed to increase and the controller will settle at this load, but with high discharge through the turbine. Greater flows through the turbine will defeat the purpose of island mode since there is a limit of the available volume (section 3.2).

5.3 Instrumentation

Amongst the different parameters that have to be monitored, there are two important parameters that have to be recorded continuously. The first parameter is the discharge through the turbines and the second parameter is the energy evacuated into the plant load.

5.3.1 Discharge

The quantity of treated water is an important performance parameter of the wastewater treatment plant. Presently, the flume (discussed in section 2.1) is being used to record the flow. Subsequent to the commissioning of recovery plant, major portion of the flow would pass through the turbine units. The regulating gate at exit flow channel will serve as an overflow weir when the recovery plant is not operating. Therefore, at any point of time two flows need to be measured, one through the recovery units and other through the channel.

The ultrasonic level indicator at the flume will be untouched and an additional flow measurement for the turbines can be accomplished in two ways.

- a) The first approach (an internal measure of flow) is to have discharge through the turbine calibrated at different speeds and powers during the 'mandatory' laboratory investigation to be carried out before delivery. Subsequently, a display can be setup in the panel that will give the value of discharge depending on operating the turbine speed and generated power.
- b) The second method is an external measure of flow that would involve setting up of 3 additional flow level indicators at 3 separate channels leading the treated water from the chlorination tank to the header channel before it enters the cisterns.

The selection of the approach will need be based on the reliability on the approach and not necessarily of the economics.

5.3.2 Electrical Energy

The generated and net energy evacuated gives a measure of the recovery plant's performance. Electric energy will be recorded for all the 3 units together and not for individual units separately using a reverse energy meter. The asynchronous generator will draw a small quantity of reactive power, while evacuation active power into the grid system. The difference between the two powers will appear of the display and will be continuously monitored over time.

5.4 Power Evacuation

The power evacuation should accomplish two major requirements of the plant load, first, integrating the recovery units smoothly to the local electrical network during normal operation and second, to commission a dedicated island grid in case of failure of grid and return to normal operation when the grid power returns by automatically switching in and out the island loads.

The second requirement of switching in and out of the island grid needs to be done in a foolproof way since the island loads are also a part of main plant load. In addition to a specialized island controller as discussed in the preceding section, the control system should also incorporate an advanced switchgear solution.

Figure 30, shows the consolidated power evacuation diagram with both the control operations along with the plant load configuration and 3 specific load distribution centers that would be isolated for the island circuit.

The maximum load on the island line will be limited 10 to 12 kWe as discussed in section 2.3, 3.2 and 5.2.2, and will serve only critical loads like laboratory, backup for the master control room, and lighting loads. The switching to the island load centers is achieved by a mechanical interlocking gear as shown in Fig. 30.

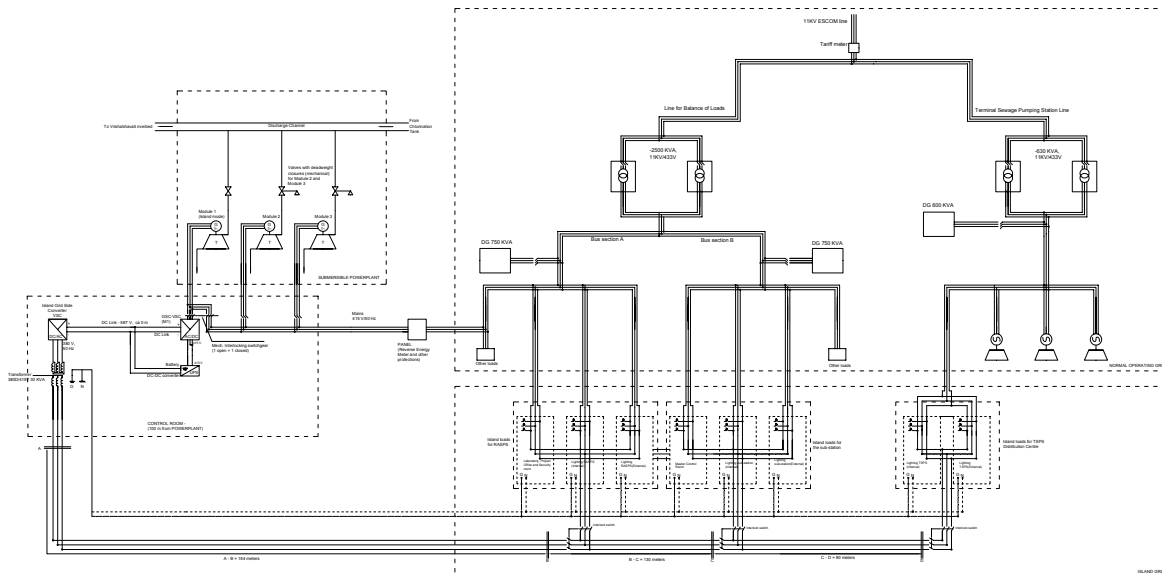


Fig. 30, Power evacuation diagram for hydro energy recovery plant (also in Annexure, Fig. A3)

As discussed in section 2.3.2, the active control volume is only about 700 m³ to 1100 m³, which cannot be stored. The intrinsic design of the variable speed controller that would change the operating speed on the turbine (in other words, the operating point by keeping the head constant and varying the discharge) to generate only that amount of power required by the island grid. When the load is maintained in the range of 10 to 12 kWe, the turbine and generator parameters would be stable operating till the storage volume is emptied (ca 40 to 60 min).

However, reducing the load below 10 kWe would cause the turbine speed to increase and also the flow, which in effect would reduce the duration of island operation. This aspect will have to be taken into serious consideration while making cost-benefit analysis of island grid (as in section 8.2.2).

The actual locations of the powerhouse chamber, control room (where both grid interface and control system for island grid is located) and the three island load centers are shown in Fig. 31.

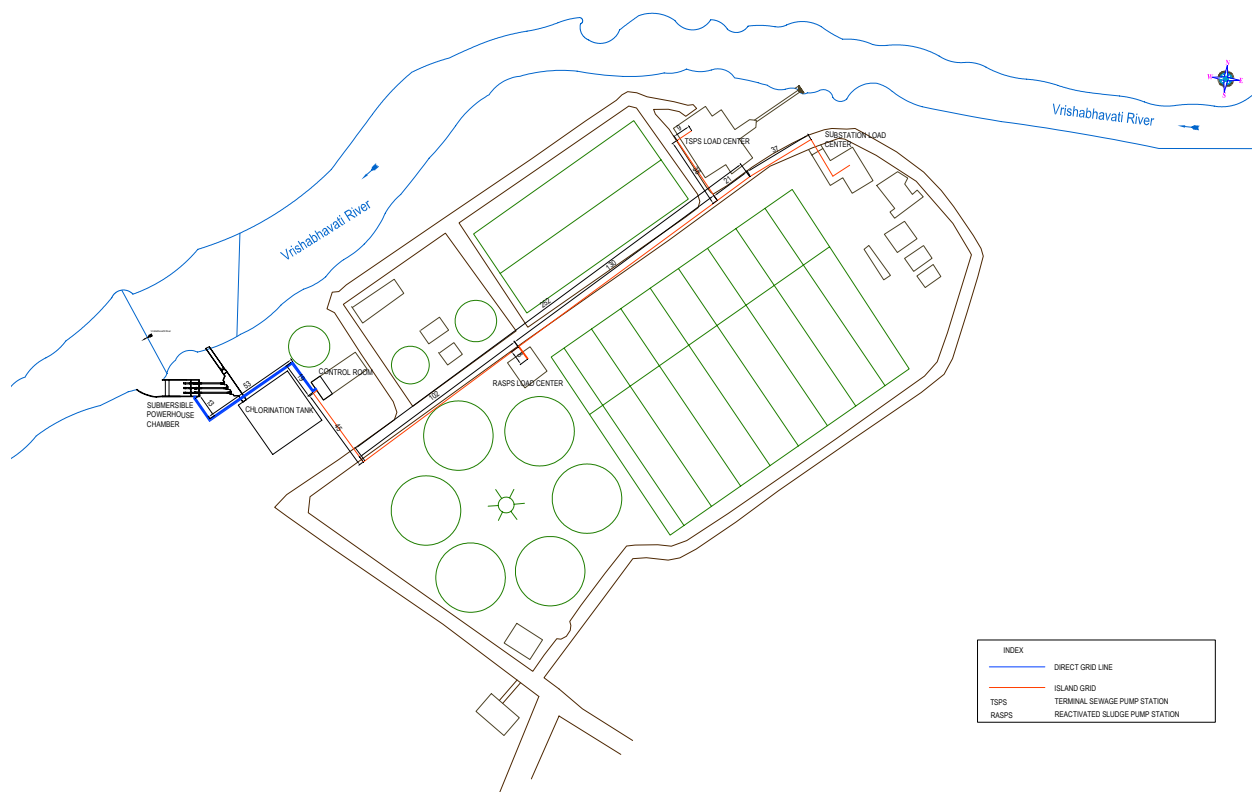


Fig. 31, Locations of the control room and island load centers with respect to powerhouse chamber

Chapter 6 – Environment Impacts and Benefits

6.1 Floods and the Issue of Submergence

As elaborated in chapter 1, the energy recovery plant is situated close to the riverbed and the ‘high flood level’ (97.365 m) recorded is significantly above the centerline of the recovery units (94.669 m). The civil design of the powerhouse walls and floor has taken into consideration this extreme situation. Further, the bed and the embankments of the tailrace canal have accounted for submergence corresponding to this level.

Moreover, the electromechanical equipment comprising of turbine and generator are of submersible design capable to withstand flooding. The valves accommodated in the powerhouse are also insensitive to flooding.

However, the control system is taken nearly 100 meters away from the powerhouse and installed within an enclosed room well above the HFL.

6.2 Environmental Benefits

The hydro energy recovery plant can be classified under renewable energy, even though the treated water is actually drinking water pumped from a river source. Instead of having a free fall of hydropower and losing substantial energy, the recovery plant enables the energy recovery of 550 kWh/day, which represents a saving of nearly 4% of the total energy required.

This may not be significant from economic sense, but environmentally it is a little example of limiting the energy consumption, improving efficiency and mitigating climate change effects in a small way.

Chapter 7 – Cost Estimates

7.1 The Basis for the Cost Estimates

The rates for various items of civil works are based on the schedule of rates of Karnataka Power Corporation Ltd [3], a leading power company of Government of Karnataka and also based on the rates in similar ongoing power projects with suitable escalation considered where necessary. Costs for various civil structures like intake pool, penstock and powerhouse etc. are estimated on the basis of layout finalized for the hydro energy recovery scheme.

Cost of the modules including control equipment and control panels is based on budgetary offers received from turbine manufacturers [4]. For electromechanical equipment, provision has been made for spare parts along with the equipment. The estimate also considers freight, insurance and cost of erecting and commissioning. Costs of other mechanical and electrical equipment are based on recent costs for similar items in other similar projects, with suitable escalation where necessary.

7.2 Implementation Options

The developer proposes the project execution in 4 different options under two categories being discussed in the report. The first category (hybrid mode) pertains to a complete package of grid and island grid operation, while second category (dedicated grid mode) discounts on island grid from the package. Under each category, there are two stages of implementation, one with a single recovery unit and the other with by 3 recovery units.

Cost estimates for the entire project should be evaluated for each of these options and summarized for helping the funding agencies (promoters) to decide the course. Section 7.3 presents the line diagram as well as the cost estimates.

7.3 Abstract of Project Costs

7.3.1 Hybrid Mode (Grid and Island Modes)

7.3.1.1 Option A – Three Recovery Units

The layout for this consolidated ‘hybrid’ option is described in Fig. 30 (section 5.4) has all the 3 recovery units along with provisions for normal operation with grid and island operation. The cost estimates under 5 categories (civil works, hydro-mechanical, electromechanical and controls, power evacuation and miscellaneous) are summarized in Table 4.

This is the most expensive option with an estimated project costs of over 120 lakhs. The island mode operation is contributing significantly to the costs, which includes components like hydraulic operated valves and a dedicated controller in addition of establishing island loads.

Table 4, Project Estimates for Option A

Sr. No.	Category	Sub-category	Estimate (in INR)
1	Civil works	1.1 Intake pool	300003
		1.2 Penstock and Draft Tube	650000
		1.3 Powerhouse	1400000
		1.4 Tailrace canal	799997
		1.5 Boundary wall	200000
		1.6 Landscaping	200000
			3550000
2	Hydro-mechanical	2.1 Regulating gate on exit channel	200000
		2.2 Manually controlled valve	230000
		2.3 Hydraulically operated deadweight valves	1200000
			1630000
3	Electromechanical and control system	3.1 Recovery units	3066000
		3.2 Grid controller	1095000
		3.3 Island controller	1168000
			5694000

		3.4 E and M accessories	365000	
4	Power evacuation	4.1 Grid mode	240000	634000
		4.2 Island mode	394000	
5	Miscellaneous	5.1 Survey and investigation	100000	900000
		5.2 Infrastructure works during construction	200000	
		5.3 Engineering and Consultancy	300000	
		5.4 Operational cost during construction (office administration including establishment)	300000	
			Total Cost (INR)	12408000
			Total Cost (Euros @1euro=73INR))	169973

7.3.1.2 Option B – One Recovery Unit

The proposal for option B (as represented in Fig. 32, magnified Fig. A4) excludes two of the three recovery modules, but includes all other components including grid and island mode components. As seen in Table 5, the total cost estimate falls just below 100 lakhs. This option is an intermediate stage of implementation. After commissioning the remaining two modules will be ordered and retrofitted into the respective hydraulic lines.

Table 5, Project Estimates for Option B

Sr. No.	Category	Sub-category	Estimate (INR)	
1	Civil works	1.1 Intake pool	300003	3450000
		1.2 Penstock and Draft Tube	650000	
		1.3 Powerhouse	1400000	
		1.4 Tailrace canal	799997	
		1.5 Boundary wall	200000	
		1.6 Landscaping	200000	
2	Hydro-mechanical	2.1 Regulating gate on exit channel	200000	1630000
		2.2 Manually controlled valves	230000	
		2.3 Hydraulically operated deadweight valves	1200000	
3	Electromechanical and control system	3.1 Recovery unit	1022000	3285000
		3.2 Grid controller	876000	
		3.3 Island controller	1168000	
		3.4 E and M accessories	219000	
4	Power evacuation	4.1 Grid mode	240000	634000
		4.2 Island mode	394000	
5	Miscellaneous	5.1 Survey and investigation	100000	900000
		5.2 Infrastructure works during construction	200000	
		5.3 Engineering and Consultancy	300000	
		5.4 Operational cost during construction (office administration including establishment)	300000	
			Total Cost (INR)	9999000
			Total Cost (Euros @1euro=73INR))	136973

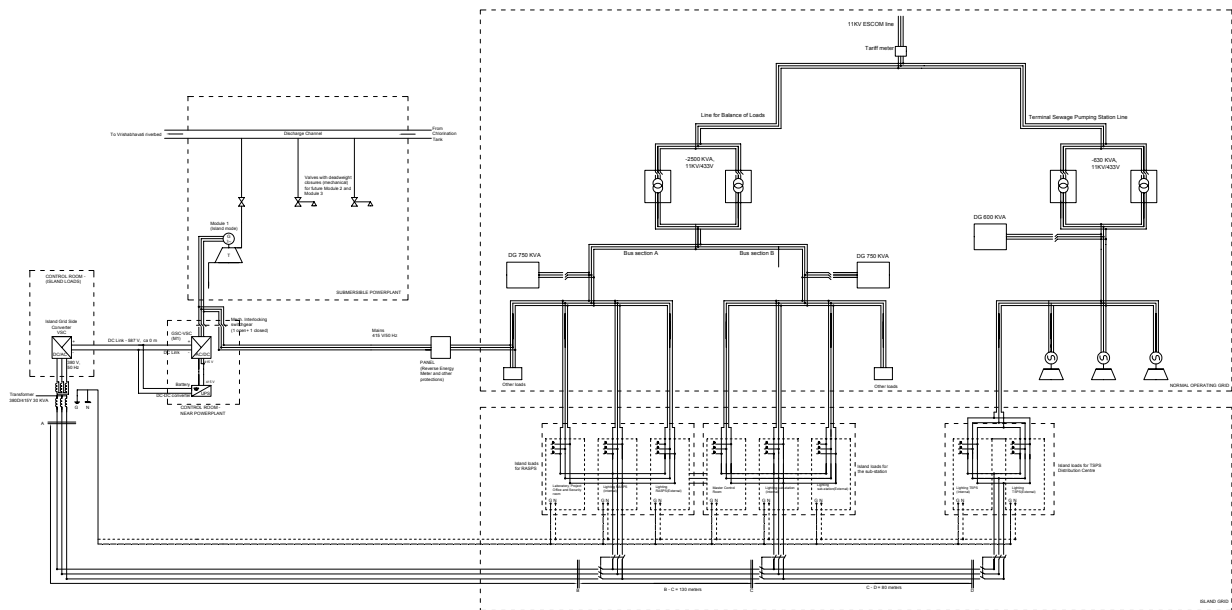


Fig. 32, Single line diagram for the implementation option B (single recovery unit with grid and island mode)

7.3.2 Dedicated Grid Mode

The system design that excludes the creation of island operation will be significant given the associated cost reductions, which will be analyzed in section 8. The two options with grid operation are discussed below.

7.3.2.1 Option C – Three Recovery Units

The plan for option C is shown in Fig. 33 (magnified Fig. A5), which looks much simplified without the complex island mode design. This implementation option will involve manual valves only and total project costs would be nearly 100 lakhs.

Table 6, Project Estimates for Option C

Sr. No.	Category	Sub-category	Estimate (INR)	
1	Civil works	1.1 Intake pool	300003	3550000
		1.2 Penstock and Draft Tube	650000	
		1.3 Powerhouse	1400000	
		1.4 Tailrace canal	799997	
		1.5 Boundary wall	200000	
		1.6 Landscaping	200000	
2	Hydro-mechanical	2.1 Regulating gate on exit channel	200000	890000
		2.2 Manually controlled valves	690000	
3	Electromechanical and control system	3.1 Recovery units	3066000	4526000
		3.2 Grid controller	1095000	
		3.3 E and M Accessories	365000	
4	Power evacuation	4.1 Grid mode	240000	240000
5	Miscellaneous	5.1 Survey and investigation	100000	900000
		5.2 Infrastructure works during construction	200000	
		5.3 Engineering and Consultancy	300000	
		5.4 Operational cost during construction (office administration including establishment)	300000	

Total Cost (INR) 10106000
Total Cost (Euros @1euro=73INR) 138438

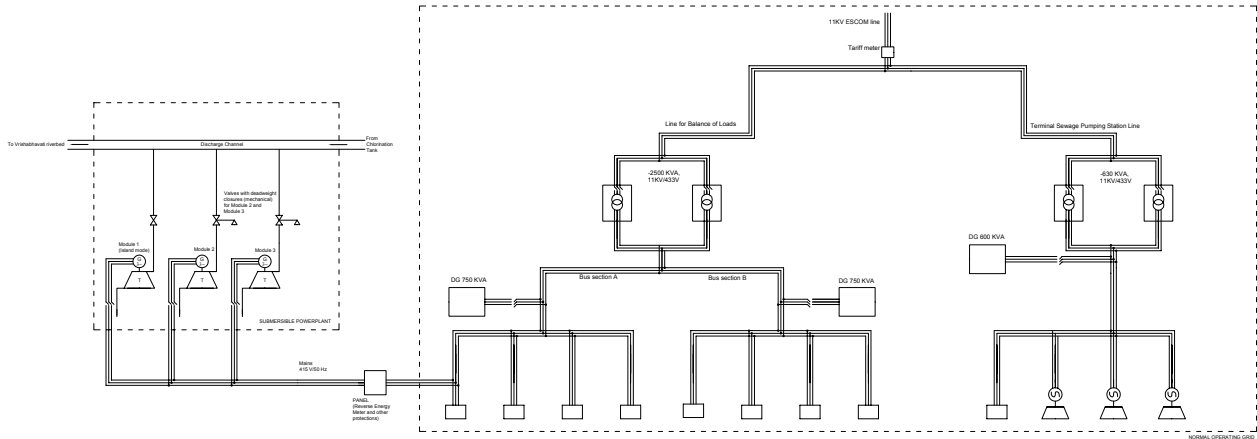


Fig. 33, Single line diagram for the implementation option C (three recovery units in grid mode only)

7.3.2.2 Option D – One Recovery Unit

This is the simplest and the most realistic implementation option for the promoters. The layout for option D (Fig. 34 and Fig. A6) comprising of one recovery unit connected to the grid, but includes infrastructure for 2 more units to be retrofitted at a later stage. The overall estimate is about 73 lakhs.

Table 7, Project estimates for option D

Sr. No.	Category	Sub-category	Estimate (INR)	
1	Civil works	1.1 Intake pool	300003	3550000
		1.2 Penstock and Draft Tube	650000	
		1.3 Powerhouse	1400000	
		1.4 Tailrace canal	799997	
		1.5 Boundary wall	200000	
		1.6 Landscaping	200000	
2	Hydro-mechanical	2.1 Regulating gate on exit channel	200000	430000
		2.2 Manually controlled valve	230000	
3	Electromechanical and control system	3.1 Recovery unit	1022000	2117000
		3.2 Grid controller	876000	
		3.3 E and M accessories	219000	
4	Power evacuation	4.1 Grid mode	240000	240000
5	Miscellaneous	5.1 Survey and investigation	100000	900000
		5.2 Infrastructure works during construction	200000	
		5.3 Engineering and Consultancy	300000	
		5.4 Operational cost during construction (office administration including establishment)	300000	

Total Cost (INR) 7237000
Total Cost (Euros @1euro=73INR) 99137

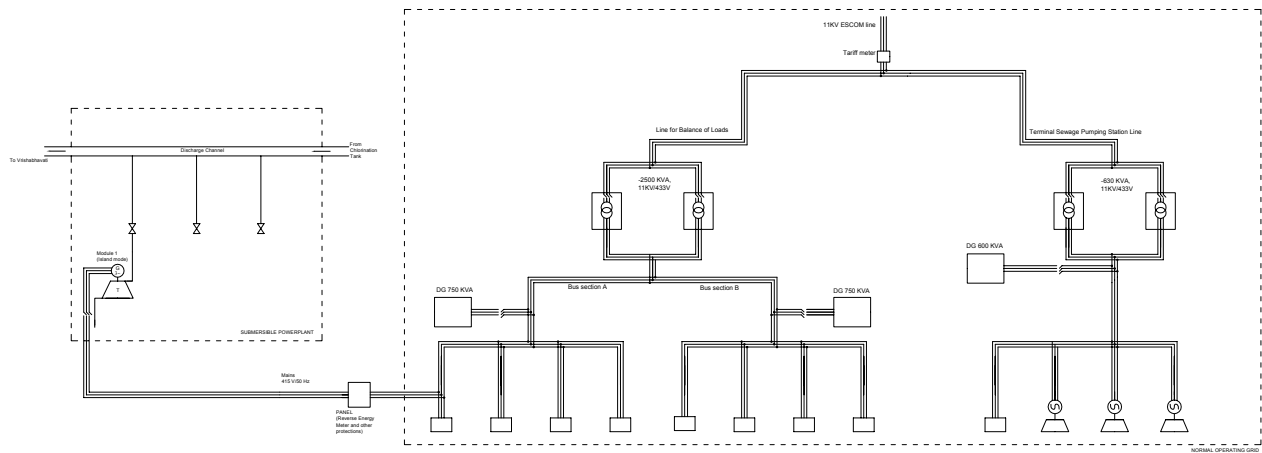


Fig. 34, Single line diagram for the implementation option D (single recovery unit in grid mode only)

7.4 Summary

The sharing proportions for the different options between the two promoters (KSB AG and IISc) are illustrated in Table 8. This gives an insight to the promoters to finalize on the implementation strategy for this energy recovery scheme.

Table 8, Summary of the project estimates and sharing pattern between partners

Sr. No.	Partners' contribution	Funding items	Estimates (in euros)			
			Option A	Option B	Option C	Option D
1	KSB AG	Civil works, Hydro-mechanical, power evacuation and miscellaneous	91973	91973	76438	70137
2	IISc	Electromechanical and Control system	78000	45000	62000	29000
Total (in euros)			169973	136933	138438	99137

Chapter 8 – Financial Studies

8.1 Revenue from Benefits

Since the recovered energy is utilized within the plant itself, there would be no direct revenue generation, but savings on the drawn electricity from the grid will be observed. However, in order to quantify these savings for carrying out financial studies, it is assumed that 1 kWh is equivalent to 8 INR (industrial rates based on energy utilization slabs). For 3 recovery units the daily energy generated is about 550 kWh/day (as discussed in section 5.2). In case of single recovery unit (for options B and D), an average of 12.5 kWe power capacity operating continuously with a plant load factor of 0.9 is assumed to deliver 270 kWh/day.

The financial studies for all the options that includes project costs, annual energy generation, generated revenue, annual costs (based on a discount rate and project life), present value and internal rate of return on the investments have been summarized Table 9.

Table 9, Financial assessment of implementation options for Mylasandra

Implementation Option	Total project cost	Annual energy generation	Revenue generated/cost savings	Discount rate	Life of project	Annual cost	Annual maintenance cost	Net annual cost	Income	Present value	Net present value
A	12408000	180675	1445400	5%	15	1195415	300000	1495415	-50015	-	-
B	9999000	98550	788400	5%	15	963327	300000	1263327	-474927	-	-
C	10106000	180675	1445400	5%	15	973635	300000	1273635	171765	1782861	-8323139
D	7237000	98550	788400	5%	15	697229	300000	997229	-208829	-	-

8.2 Cost-Benefit Analysis

The evaluation of the benefits of the projects in respect to the investment is carried out for both grid and island mode of operations. The island mode of operation is of particular interest since it involves more than 25% of the costs. In order to carry out different aspects of the economic analysis, a 5% discount rate and lifetime of 15 years is assumed.

Table 9, reveals that the hybrid mode of operation (grid and island mode) are less economical compared to the single mode of grid operation. Individual options will be subsequently analyzed.

8.2.1 Dedicated Grid Mode

From the two options having pure grid mode of operations, the option C seems to be favorable with an annual income of 1.8 lakhs, however even though the present value is positive, the net present value is negative. Further evaluations of economic parameter like internal rate of return cannot be determined.

8.2.2 Usefulness of Island Mode

The usefulness of the island mode has to be assessed from various angles. Firstly, the plant condition followed by the performance issues of the turbine-generator unit and then the system design aspects before looking at the economic perspective.

8.2.2.1 Plant conditions

The elaborate investigations carried out in section 2.3 where the active storage capacities for different tripping scenarios were studied, showed that even for the operation of a single recovery unit, the duration would not exceed 40 to 60 minutes delivering hardly between 9 and 14 kWh of electrical energy.

8.2.2.2 Performance of turbine-generator of the recovery unit

There is a unique case of shifting from grid mode to island mode as far as the turbine is concerned. It was seen from section 5.1.1, the operating speed of the turbine depends on stabilizing the load at 10 to 12 kWe in island mode. In case the load falls below the rated load, the flow through the turbine will increase drastically due to the operation of 4 – quadrant controller (5.2.2). The additional problem with part-load operation is that with increased flow, the duration of operation is going to be further reduced from the present range of 30 to 60 minutes. Therefore, the load on island side should be close to the nominal value to order to get some value from this feature.

8.2.2.3 Layout and system design

The system design with island mode becomes more complex with an advanced electronic controller, actuated valves (closing and opening) and planning an island grid load from the existing load with interlocking switchgears and additional protections. The costs of these additional components have already been dealt with, but the question is whether all this will add any operational value to the plant.

8.2.2.4 Economic assessment

It is clear that economically, the island mode is far too expensive and only value it can add is to supply 8 to 14 kWh of power when there is a grid failure for 40 to 60 minutes, but under some riders as mentioned above.

It may be better to plan another mode of energy backup for the critical loads instead of island arrangement.

Chapter 9 – Project Management and Schedule

9.1 Project Organization

The project is implemented through a mechanism as illustrated in Fig. 35. The promoters or funding bodies of the project namely, KSB AG and IISc, have given the responsibility of managing the complete project to Dr. Punit Singh Associates (Developer), who will be liable for every aspect of the project. This includes survey and investigations, publishing project reports, working with consultants and experts for the civil, electromechanical and power distribution of generated electricity.

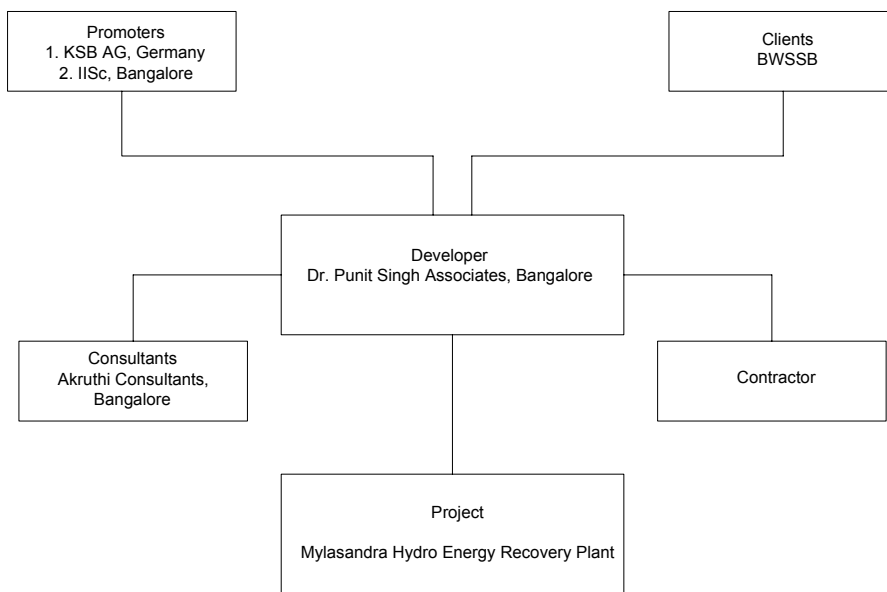


Fig. 35, Block diagram for the project management

The developer himself a scientist and designer of this project shall also be responsible for commissioning, trial running for a period of 3 months before handing over the plant to clients (BWSSB).

The developer with his team of consultants and contractors would work harmoniously with the promoters and clients during the construction phase of the project. Before, the commencement of the project he will get into an agreement with BWSSB on the modalities during construction, commissioning and handover.

The promoters shall provide finances to the developer for the completing the project as detailed out in this report after finalizing one of the proposed options. The developer should provide regular reports to the promoters and clients during construction.

The project should be completed not later than 8 months after the approval of implementation option (A, B, C or D) with a priority given to civil works. The electromechanical equipment that will be supplied from Germany would reach the site 4 months after the order of the equipment is placed. The milestones of the project is discussed in the subsequent section.

9.2 Project Schedule

Task	Details	Completion date
1	Submission of Detailed Project Report	25th July 2013
2	Review and decision on the implementation option by the promoters	31st July 2013
3	Placing the order for the electromechanical and control unit by IISc	10th Aug 2013
4	Qualification process for the contractor	25th Aug 2013
5	Release of the first installment for civil works from KSB	30th Aug 2013
6	Beginning of the civil works, hydromechanical and power evacuation works	1st Sep 2013
7	Completion of civil and associated site works	15th Jan 2014
8	Manufacture of the recovery unit and controller	30th Nov 2013

9	Testing and Optimization at Frankenthal	15th Dec 2013
10	Shipment of equipment from Germany	31st Dec 2013
11	Arrival of consignment at site	15th Feb 2014
13	Erection of electromechanical and control system	15th Mar 2014
14	Commissioning	1st April 2014
15	Trial phase	April-June 2014
16	Handover to clients	1st July 2014

Chapter 10 – Summary, Conclusions and Recommendations

The rationale behind this energy recovery plant in treatment plants is to demonstrate the scope and vast potential of hydro energy recovery in comparison with the more conventional methane gas based energy recovery that is becoming mandatory in all sewage treatment plants.

Recovering hydro energy in treatment plants is relatively challenging as it involves the study of behaviour of flowing water (treated or untreated) through different conduits of the plant (pipes or channels) that have substantial drop of head (1 meter and above) before they are delivered from source to sink.

The special case of Bangalore city's drinking water and wastewater is considered with respect to its valleys of which the Vrishabhavati valley is the focus of the study. This is because the source of drinking water from River Cauvery for Bangalore is brought back to same river as wastewater through the Vrishabhavathi River basin.

The treatment plant at Mylasandra presents an excellent case for hydro energy recovery, where a drop of nearly 7 meters is available at the exit of plant. In addition, the water available for recovery is treated without solids and turbidity, making the conceptualization of the recovery plant simpler.

The planning is done based on the flow characteristics of the treatment plant and the potential of recovery is determined. It is proposed to install 3 recovery units that will use the 48 MLD of flow to generate 555 kWh of electricity everyday. The energy will be integrated into the electrical distribution network of the plant, which will directly link up with energy savings.

The grid mode of energy recovery did not pose major design challenge compared to the island mode of operation required by the plant's operators during tripping of utility grid. The system design of island mode was comparatively challenging because it involved firstly, the study of available active storage volumes of the plant during tripping condition. This study revealed that a single recovery unit with a capacity of 12 kWe would operate only between 30 and 60 minutes before the water is emptied.

On the other hand to make an island mode operational, the system design incorporated actuators for valve closure, an advanced 4 quadrant variable speed controller and extensive wiring and switch gears for creating a dedicated island grid (of few selected critical loads). The cost-benefit analysis revealed that to generate energy of 8 to 14 kWh, project costs would have to be increased by at least 25%.

However, the dedicated grid mode (options C and D) presents a reasonable economic case. The full sized recovery plant (3 units) would generate a modest annual income of about 2 lakhs for an investment of 100 lakhs, even though economic parameters like net present value and internal rate of return paint a negative picture.

The developers who have carried out elaborate surveys and related investigations would strongly recommend the implementation of the dedicated grid mode first (either with option C or D) and bring in the island mode later after gaining sufficient experience and evaluating the usefulness of the hydro energy recovery plant with respect to the architecture of the treatment plant.

In cases of wastewater treatment plants, the developers would recommend that hydro energy recovery be made mandatory (wherever possible) in addition to energy recovery from methane gas.

To conclude the developers would recommend to undertake a feasibility of hydro energy recovery not only within the premises of treatment plants, but also along the valleys where it was found that nearly 35% of energy required for pumping drink water to Bangalore can be recovered in the return path along the Vrishabhavati and adjoining valleys.

Nomenclature

AC	Asbestos
DPR	Detailed Project Report
EL	Elevation
FSL	Full Supply Level
HDPE	High Density Polyethylene
HFL	High Flood Level
INR	Indian National Rupees
IRR	Internal Rate of Return
KPCL	Karnataka Power Corporation Limited
MIV	Main Inlet Valve
MSL	Mean Sea Level
NPV	Net Present Value
PLF	Plant Load Factor
RCC	Reinforced Cement Concrete
TMT	Thermo Mechanically Treated Steel
TWL	Tailrace Weir Level
UCR	Un-Coarse Masonry
UPS	Uninterrupted Power Supply
VSC	Variable Speed Controller
MLD	Million Liters per Day

References

- [1] Jiban Singh M, Somashekar R. K., Prakash K. L. and Shivanna K., 2010, 'Investigation of heavy metals in crystalline aquifer groundwater from different valleys of Bangalore, Karnataka', Journal of Geography and Regional Planning Vol. 3(10), pp. 262-270
- [2] Aline Choulot, Vincent Denis, and Petras Punys, 2012' Integration of Small Hydro Turbines into Existing Water Infrastructures', Hydropower – Practice and Application
- [3] Schedule of Rates for Hydro and Thermal Power Projects, Karnataka Power Corporation Ltd, 2012
- [4] KSB AG and Sub-Suppliers

Annexure

A1 Detailed Cost Estimates

A1.1 Civil Works and Hydro-Mechanical Costs

A1.1.1 Intake Pool

Item no.	Description	Unit	Quantity	Rate in Rs.	Amount in Rs. Lakhs
1	Excavation for seating the intake pool and appurtenant works including placing neatly or disposing off the excavated stuff as directed etc., complete with initial lead upto 1km and all lifts.				
a	In all kinds of soil including boulders upto 0.15 cum	cum	54	110	0.06
2	Providing embankment with homogenous soil available from excavation in layers of 25 to 30 cm including cost of all materials, machinery, labour, all operations such as excavation, sorting, transportation, dozing to the required depth, breaking clods, sectioning, watering & compaction to the required density control not less than 97%, using sheep foot / pad foot roller as stipulated etc., complete with initial lead upto 1Km & all lifts.	cum	16	90	0.01
3	Providing and laying insitu vibrated cement concrete M10 using approved clean,hard,graded aggregates including cost of all materials,machinery labour,form work, centering, scaffolding, cleaning, batching, mixing,placing in position, levelling, vibrating, finishing,curing etc., completewith initial lead upto 1km and all lifts.				
a	Using 40mm and down coarse aggregates and 28 days cube compressive strength not less than 10N/mm ² (100kg/cm ²) cement content = 235kg/cum Foundation filling,back filling,base course for all flooring and similar works	Cum	3	3,800	0.12
4	Providing and laying insitu vibrated cement concrete M-25 using approved, clean, hard graded aggregates including cost of all materials, machinery, labour, form work, centering, scaffolding, cleaning, batching, mixing, placing in position, levelling, vibrating, finishing, curing etc., complete with initial lead upto 1km and all lifts.				
a	Using 40mm and down coarse aggregates and 28 days cube compressive strength not less than 20N/mm ² (200kg/cm ²) cement content = 340kg/cum. For Pool walls, columns,footings and similar works	Cum	22	5,500	1.23
5(a)	Fabricating and placing in position reinforcement steel for RCC works including cleaning, straightening, cutting, bending, hooking, lapping, welding, wherever required ,binding with 1.25mm diameter soft annealed steel wire, cost of all materials, machinery, labour(excluding the cost of reinforcement steel, but including wastage) etc., complete with initial lead upto 1km and all lifts.	Tonne	2	15000	0.26
5(b)	Supply of reinforcement steel	Tonne	2	50,000	0.86
6	Fabrication, Erection, Supply, transport, loading, unloading, stacking of steel plates of all thicknesses conforming to BIS: 2062, Grade B, including excise duty , taxes octroi, transit insurance & Providing epoxy painting in side of transition etc., complete	M.T	0.22	100000	0.22

	Sub Total	2.76
7	Add 4.36% for W.C.T.	0.12
8	Contingency and unforeseen item 2%	0.06
9	Miscellaneous & rounded off	0.07
	Total	3.00

A1.1.2 Penstock and Draft Tube

Sl.no.	Description of Item	Unit	Quantity	Rate	Amount in Rs lakhs
1	Excavation for Penstock civil works and appurtenant works including placing neatly or disposing off the excavated stuff as directed etc., complete with initial lead upto 1km and all lifts.				
	In all kinds of soil including boulders upto 0.15 cum in volume	cum	86	110	0.09
2	Providing embankment with homogenous soil available from excavation in layers of 25 to 30 cm including cost of all materials, machinery, labour, all operations such as excavation, sorting transportation, dozing to the required depth, breaking clods, sectioning, watering & compaction to the required density control not less than 97%, using sheep foot / pad foot roller as stipulated etc., complete with initial lead upto 1Km & all lifts.	cum	26	90	0.02
3	Providing and laying insitu vibrated cement concrete M10 using approved clean,hard,graded aggregates including cost of all materials,machinery labour,form work, centering, scaffolding, cleaning, batching, mixing,placing in position, levelling, vibrating, finishing,curing etc., completewith initial lead upto 1km and all lifts. Using 40mm and down coarse aggregates and 28 days cube compressive strength not less than 10N/mm2 (100kg/cm2) cement content = 235kg/cum Foundation filling,back filling,base course for all flooring and similar works	Cum	11	3,800	0.41
4	Providing and laying insitu vibrated cement concrete M25 using approved clean, hard, graded aggregates including cost of all materials,mechinery labour,form work, centering, scaffolding, cleaning, batching, mixing, placing in position, levelling, vibrating, finishing, curing etc., completewith initial lead upto 1km and all lifts. Using 40mm and down coarse aggregates and 28 days cube compressive strength not less than 20N/mm ² (200Kg/cm ²), cement content = 340kg/cum for Tail race piers,abutments,draft tube slabs,diaphragm walls and similar works.	Cu.m	20	5500	1.10
5	Fabricating and placing in position reinforcement steel for RCC works including cleaning, straightening, cutting, bending, hooking,lapping,welding, wherever required ,binding with 1.25mm diameter soft annealed steel wire,cost of all materials, machinery, labour etc., complete with initial lead upto 1km and all lifts.(excluding the cost of reinforcement steel,but including wastage)	Tonne	1.85	15000	0.28

6	Supply of reinforcement steel	Tonne	1.85	50000	0.92
7	Supply, transport, loading, unloading, stacking of HDPE pipe of 500mm dia including excise duty, taxes octroi, transit insurance etc., complete	Rmt	81	1500	1.22
8	Conducting necessary testing such as radiography hydraulic etc., as per standards and submission of reports including cost of water X ray films all ancillary operations etc., complete	Rmt	81	500	0.41
9	Fabrication of draft tubes of galvanized steel with wall thickness of 6.5 mm, with flange joints, expansion joints and pressure tappings	lot	3	50000	1.50
Sub Total					5.95
9	Add 4.36% for W.C.T.				0.26
10	Miscellaneous				0.29
Total					6.50

A1.1.3 Powerhouse

Sl.no.	Description of Item	Unit	Quantity	Rate	Amount in Rs lakhs
1	Excavation for foundation in hard rock of all toughness including boulders exceeding 1.0 cum. In volume for seating all power house and appurtenant structures including tail race channel minimising damage to rock beyond excavation line including placing neatly and/or disposing off the excavated stuff as directed etc., complete with initial lead upto 1km and all lifts.	Cu.m	252	250	0.63
2	Providing embankment with homogenous soil available from excavation in layers of 25 to 30 cm including cost of all materials, machinery, labour, all operations such as excavation, sorting transportation, dozing to the required depth, breaking clods, sectioning, watering & compaction to the required density control not less than 97%, using sheep foot / pad foot roller as stipulated etc., complete with initial lead upto 1Km & all lifts.	cum	76	90	0.07
3	Providing and laying insitu vibrated cement concrete M10 using approved clean, hard, graded aggregates including cost of all materials, machinery labour, form work, centering, scaffolding, cleaning, batching, mixing, placing in position, levelling, vibrating, finishing, curing etc., complete with initial lead upto 1km and all lifts. Using 40mm and down coarse aggregates and 28 days cube compressive strength not less than 10N/mm ² (100kg/cm ²) cement content = 235kg/cum				
	Foundation filling, back filling, base course for all flooring and similar works	Cum	17	3,800	0.64
4	Providing and laying insitu vibrated cement concrete M25 using approved clean, hard, graded aggregates including cost of all materials, machinery labour, form work, centering, scaffolding, cleaning, batching, mixing, placing in position, levelling, vibrating, finishing, curing etc., complete with initial lead upto 1km and all lifts.				

Using 20mm and down coarse aggregates and 28 days cube compressive strength not less than 20N/mm² (200Kg/cm²), cement content = 340kg/cum

	Machine hall substructures(1 stage) including forming galleries, adits, openings, sumps,hatches etc., and similar works.	Cu.m	32	5500	1.79
5	Grouting foundations, base plates, pockets and inaccessible locations using free flow non shrink grout mix including cost of all operations such as mixing required consistency, conveying, pouring, scaffolding, labour, curing etc., complete with initial lead upto 1km and all lifts.	Tonne	0.25	25000	0.06
6(a)	Fabricating and placing in position reinforcement steel for RCC works including cleaning, straightening, cutting, bending, hooking, lapping, welding, wherever required ,binding with 1.25mm diameter soft annealed steel wire, cost of all materials, machinery, labour etc., complete with initial lead upto 1km and all lifts.(excluding the cost of reinforcement steel, but including wastage)	Tonne	1.51	15000	0.23
6(b)	Supply of reinforcement steel	Tonne	1.51	50,000	0.75
7a	Fabricating,transporting to site,hoisting and erecting structural steel member fabricated from rolled steel sections like channels,angles,flats, I-sections, plates,rails etc., as per drawing including cost of all materials, machinery, labour, operations such as cutting, bending, grinding, welding, etc., and providing one coat of zinc chromate red oxide primer after scrapping and cleaning the surface,scaffolding etc.,complete with initial lead upto 1km and all lifts.(excluding the cost of steel but including wastage)	Tonne	1.81	20000	0.36
7b	Supply of structural steel	Tonne	1.81	80000	1.45
8	Providing and constructing rubble stone masonry (uncoursed) for basement using approved rubble in CM 1:6 with bond stones 2m apart in each course with joints not more than 25mm wide including deep pointing in CM 1:3 after raking the joints, nicely lining, curing etc. complete with initial lead upto 50m and initial lift upto 1.50m.	Cum	60.72	2500	1.52
9	Providing and constructing burnt brick masonry with all class bricks for superstructure including necessary scaffolding tc., complete with initial lead upto 50m and initial lift upto 4m. In C.M. 1:6 including curing	Cum	7	4500	0.33
10	Providing plastering to stone masonry/BB masonry/ laterite masonry including raking joints, smooth finishing, curing, scaffold-ing etc., complete with initial lead upto 50m and initial lift upto 4m. 1.2cm thick in CM 1:6 propon.	Sqm	66	130	0.09
11	Providing and painting with water proof cement paint (Mylac or equivalent) of approved colour including scraping the surface, necessary scaffolding etc., complete with all leads and initial lift upto 4m. Two coats over one coat of primer	Sqm	66	60	0.04
12	Providing and fixing push and pull type rolling shutters made out of 18G x 7.5cm mild steel latches of convex corrugations complete with guides and bottom rails with	Sqm	0.58	2700	0.02

interlocking arrangements for steel latches by means of alternate end clips, suspension shafts with high tension coil type springs, locking arrangements, pulling hooks, handles with all fittings, accessories including two coats of synthetic enamel painting of approved quality over a coat of zinc chromate red oxide primer, etc., complete with all leads and initial lift upto 4m. Without top cover. (Mode of measurement - Depth: C/L shaft to floor level and width: end to end of channel).

13	Providing and fixing 150mm diameter PVC rain water down Rmt. take pipes with the necessary bends, shoes, clamps, including cost of all materials, labour etc., complete with all leads and lifts.	21	300	0.06	
14	Fixing Asbestos sheets for roofing and ridge coping with necessary fixtures and fastenings such as 'J' bolts, bitumen washers, etc., complete with initial lead upto 50m and initial lift upto 4.5m.	Sqm	84	350	0.29
15	Electrification			0.50	
16	Water supply and sanitary			0.50	
17	Dewatering during constructing of surface construction site including supply installation and removal of pumping equipment from the site 10 horse power working 8 hours a day for 3 months	Kwhr	5299	15	0.79
18	Providing earth mat below Power house foundation	LS		2.50	
Sub Total				12.62	
19	Add 4.36% for W.C.T.			0.55	
20	Contingency and unforeseen item 2%			0.25	
21	Miscellaneous			0.58	
Total				14.00	

A1.1.4 Tailrace Canal

Item no.	Description	Unit	Quantity	Rate in Rs.	Amount in Rs. Lakhs
1	Excavation for seating the tail race and appurtenant works including placing neatly or disposing off the excavated stuff as directed etc., complete with initial lead upto 1km and all lifts.				
a	In all kinds of soil including boulders upto 0.15 cum	cum	378	110	0.42
2	Providing embankment with homogenous soil available from excavation in layers of 25 to 30 cm including cost of all materials, machinery, labour, all operations such as excavation, sorting, transportation, dozing to the required depth, breaking clods, sectioning, watering & compaction to the required density control not less than 97%, using sheep foot / pad foot roller as stipulated etc., complete with initial lead upto 1Km & all lifts.	cum	113	90	0.10
3	Providing and laying insitu vibrated cement concrete M10 using approved clean,hard,graded aggregates including cost of all materials,machinery labour,form work, centering, scaffolding, cleaning, batching, mixing,placing in position, levelling,				

	vibrating, finishing, curing etc., complete with initial lead upto 1km and all lifts.					
a	Using 40mm and down coarse aggregates and 28 days cube compressive strength not less than 10N/mm ² (100kg/cm ²) cement content = 235kg/cum Foundation filling, back filling, base course for all flooring and similar works	Cum	28	3,800	1.07	
4	Providing and laying insitu vibrated cement concrete M-25 using approved, clean, hard graded aggregates including cost of all materials, machinery, labour, form work, centering, scaffolding, cleaning, batching, mixing, placing in position, levelling, vibrating, finishing, curing etc., complete with initial lead upto 1km and all lifts.					
	Using 40mm and down coarse aggregates and 28 days cube compressive strength not less than 20N/mm ² (200kg/cm ²) cement content = 340kg/cum.					
a	For Pool walls, columns, footings and similar works	Cum	68	5,500	3.75	
5(a)	Fabricating and placing in position reinforcement steel for RCC works including cleaning, straightening, cutting, bending, hooking, lapping, welding, wherever required, binding with 1.25mm diameter soft annealed steel wire, cost of all materials, machinery, labour (excluding the cost of reinforcement steel, but including wastage) etc., complete with initial lead upto 1km and all lifts.	Tonne	3	15000	0.49	
5(b)	Supply of reinforcement steel	Tonne	3	50,000	1.63	
6	Providing and constructing rubble stone masonry (uncoursed) for basement using approved rubble in CM 1:6 with bond stones 2m apart in each course with joints not more than 25mm wide including deep pointing in CM 1:3 after raking the joints, nicely lining, curing etc. complete with initial lead upto 50m and initial lift upto 1.50m.	Cum	30	2500	0.75	
	Sub Total				7.45	
7	Add 4.36% for W.C.T.				0.32	
8	Miscellaneous & rounded off				0.23	
	Total				8.00	

A1.2 Hydro-mechanical Works

Sl.No	Description	Nos.	Unit	Qty	Rate Rs	Amount Rs. Lacs
1	Preliminary works			LS		0.25
2	Design, fabrication, supply, erection, testing and commissioning of gates and hoists of specified size, with guides, gate leaves, seals, sill beam etc., in accordance with approved design and drawings, specifications, instructions etc., with all necessary embedded parts including cost of all materials, machinery, labour, painting etc., complete as per technical specifications with all leads and lifts					
A	Exit Channel					

i)	Service gate	1	M.T	1.50	110000	1.65
	Sub Total (sl.no. 1 and 2)					1.90
	Contingency and unforeseen item 2%					0.06
	Miscellaneous & rounded off					0.04
	Total (service gate)					2.00
3	DN 500 – Double Eccentric Butterfly Valves – Manually operated with Gear Box	1	lot	1	230000	2.30
4	DN 500 – Double Eccentric Butterfly Valves – hydraulic brake and lift unit (quick closing valve)	1	lot	2	600000	12.00
TOTAL						16.30

A1.3 Electromechanical and Control System

Option	Particulars	Bill of Quantities	Cost (INR)		Cost (Euros)		
			Item cost	Total cost	Item cost	Total cost	
A	3 PATs in pure grid mode and 1 PAT in island mode	A.1	3 PAT+AG	3066000		42000	
		A.2	Grid interface controller	1095000	5694000	15000	78000
		A.3	Island controller	1168000		16000	
		A.4	Miscellaneous/unforeseen	365000		5000	
B	1 PAT is pure grid mode and island mode	C.1	1 PAT+AG	1022000			
		C.2	Grid interface controller	876000	3285000	12000	45000
		C.3	Island controller	1168000		16000	
		C.4	Miscellaneous/unforeseen	219000		3000	
C	3 PATs in pure grid mode only	B.1	3 PAT+AG	3066000			
		B.2	Grid interface controller	1095000	4526000	15000	
		B.3	Miscellaneous/unforeseen	365000		5000	
D	1 PAT in grid mode only	D.1	1 PAT+AG	1022000			14000
		D.2	Grid interface controller	876000	2117000	12000	29000
		D.3	Miscellaneous/unforeseen	219000		3000	

A1.4 Power Evacuation

A1.4.1 Grid Mode

Sr. No.	Particulars	Qty	Unit Cost	Total Cost (INR)	
1	Distribution lines	units	(INR)		
1.1	A three phase distribution configuration for 3 generator units of load carrying capacity of 37.5 KW from the powerhouse chamber to the nearest distribution bar of the utility center with copper cable of specification 4×15 mm ²	meters	300	550	165000
1.2	Excavation, laying of cables	meters	100	100	10000
1.3	Earthing at powerhouse	lot	1	25000	25000
1.4	Miscellaneous (installation costs of panel and others)	lot	1	40000	40000
Total					240000

A1.4.2 Island Mode

Sr. No.	Particulars	Qty units	Requirement	Unit (INR)	Cost Total Cost (INR)
2.1	A three phase distribution configuration from single meters generator unit for 3 different island load centers for a load carrying capacity of 12.5 KW with copper cable of specification 4×15 mm ²		500	550	275000
2.2	Excavation, laying of cables	meters	500	100	50000
2.3	Interlocking switch	pcs	3	8000	24000
2.4	Miscellaneous (installation costs and others)	lot	1	45000	45000
				Total	394000

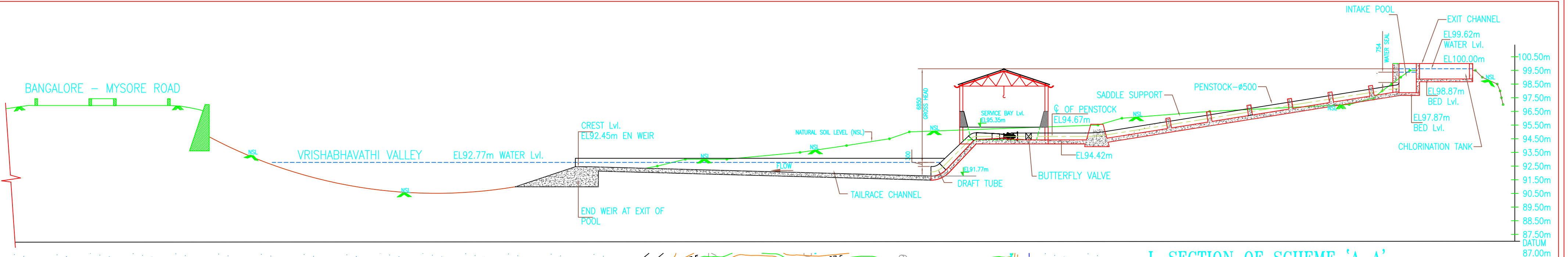
A2 Layouts

A2.1 Civil Layouts

Figure Number	Title
Fig. A1	General Layout, Plan and L-section
Fig. A2	Powerhouse and Intake pool, Plan and section

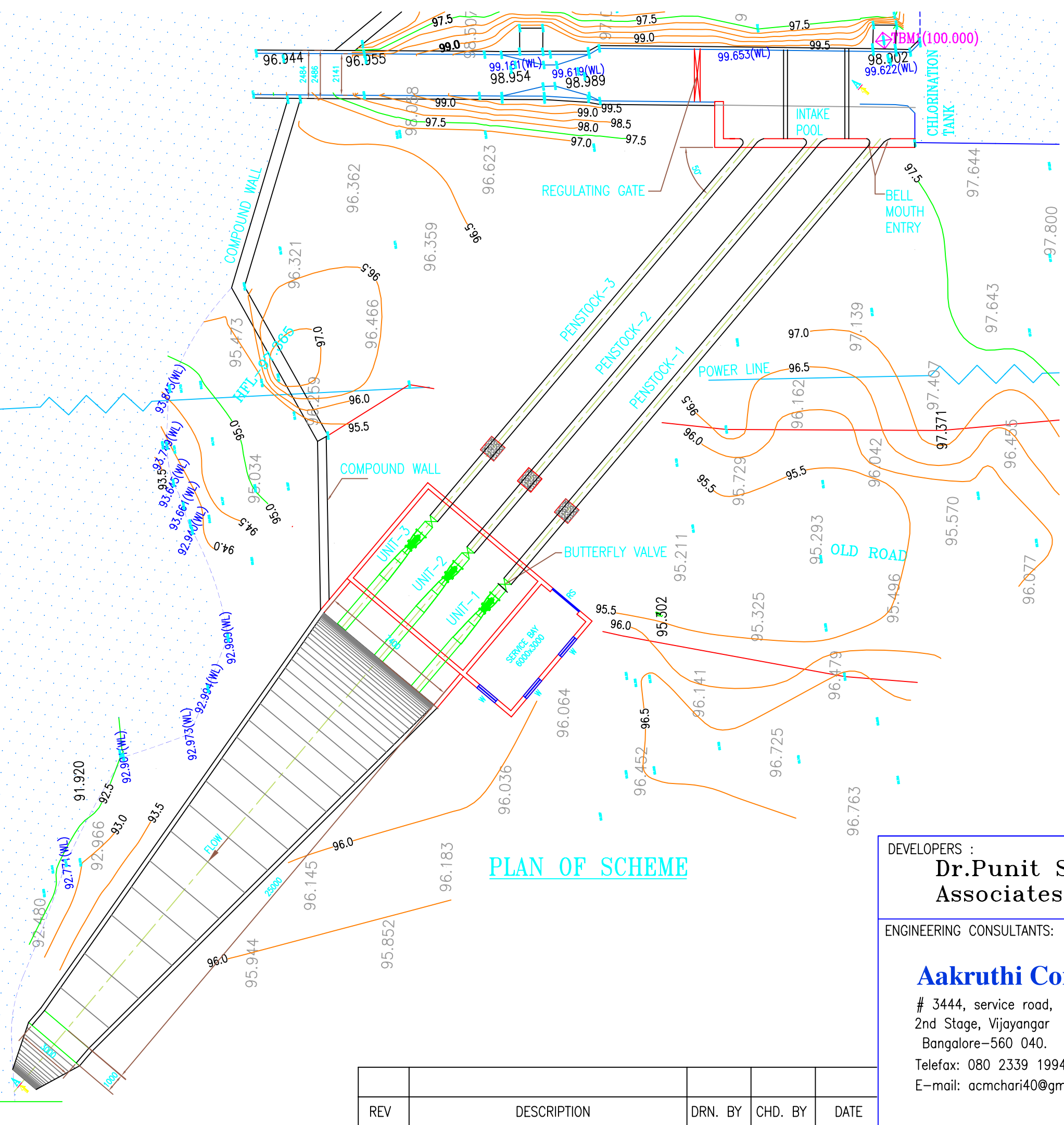
A2.2 Implementation Options

Figure Number	Title
Fig. A3	Single Line Diagram for Implementation Option A – Hybrid mode (grid and island mode) with three energy recovery units
Fig. A4	Single Line Diagram for Implementation Option B – Hybrid mode (grid and island mode) with a single energy recovery unit
Fig. A5	Single Line Diagram for Implementation Option C – Dedicated grid mode with three energy recovery units
Fig. A6	Single Line Diagram for Implementation Option D – Dedicated grid mode with single energy recovery unit



L-SECTION OF SCHEME 'A-A'

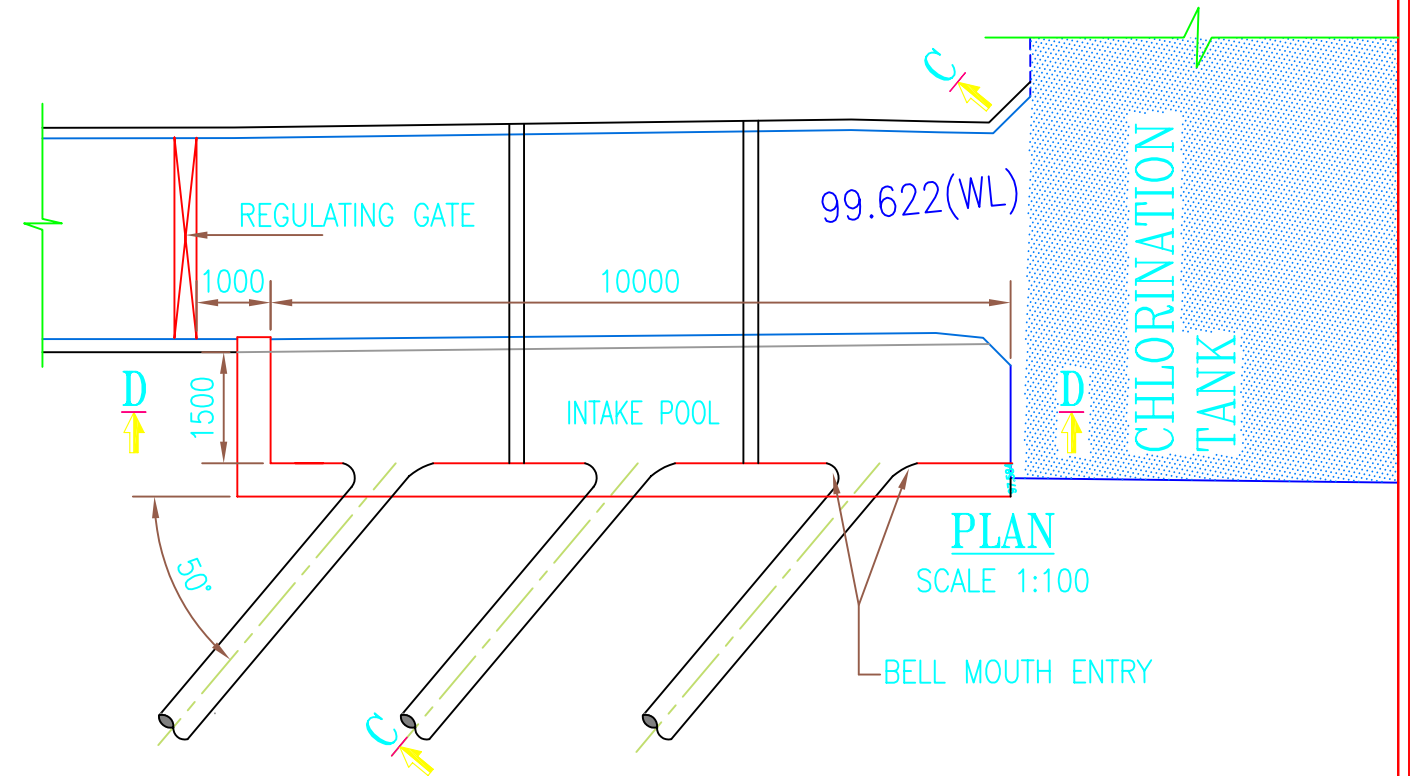
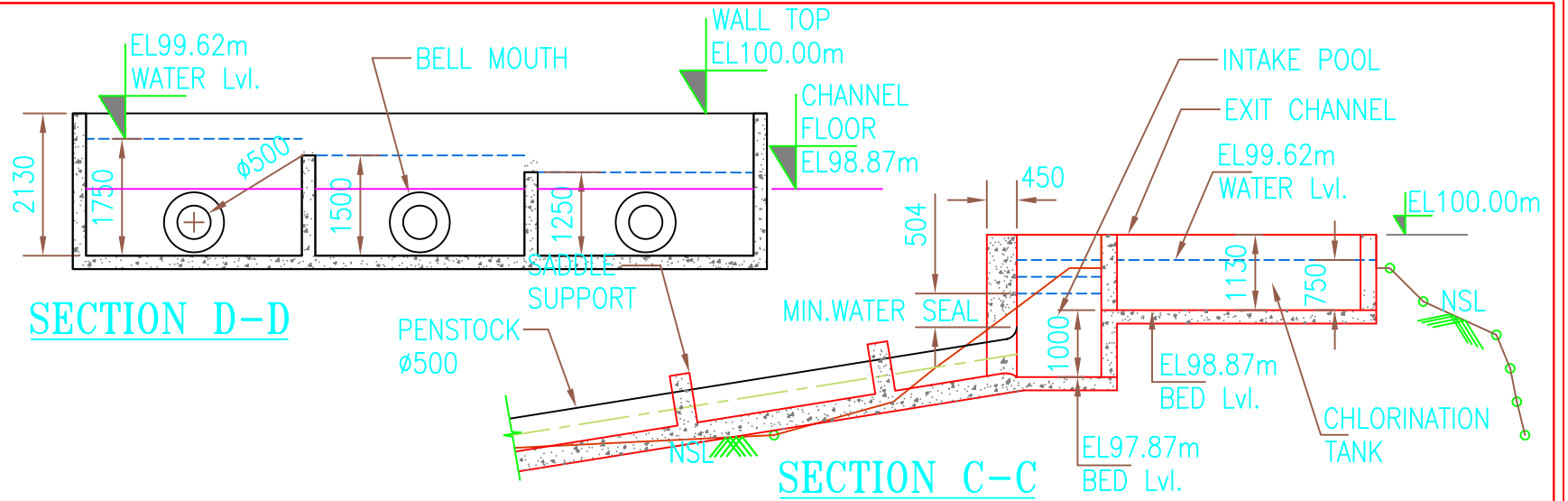
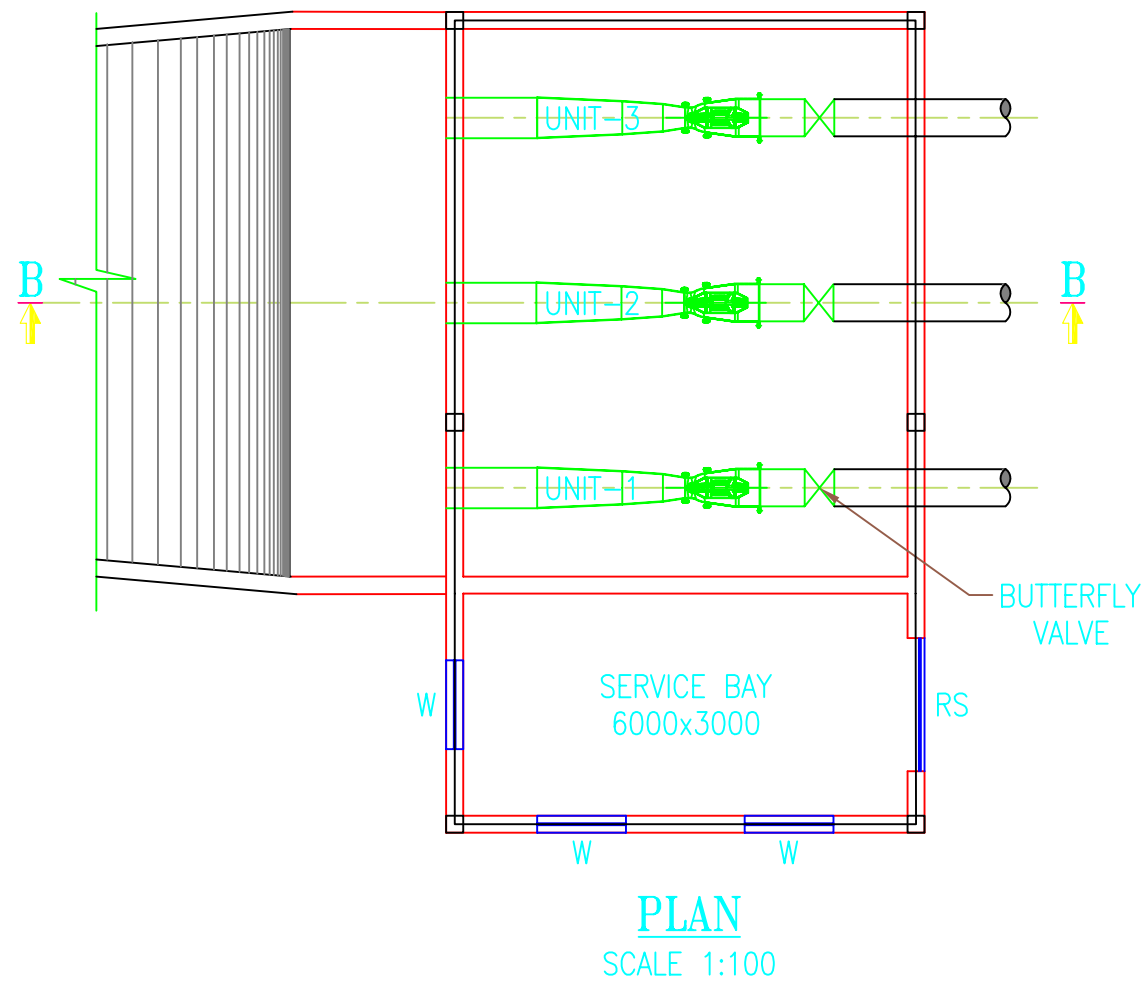
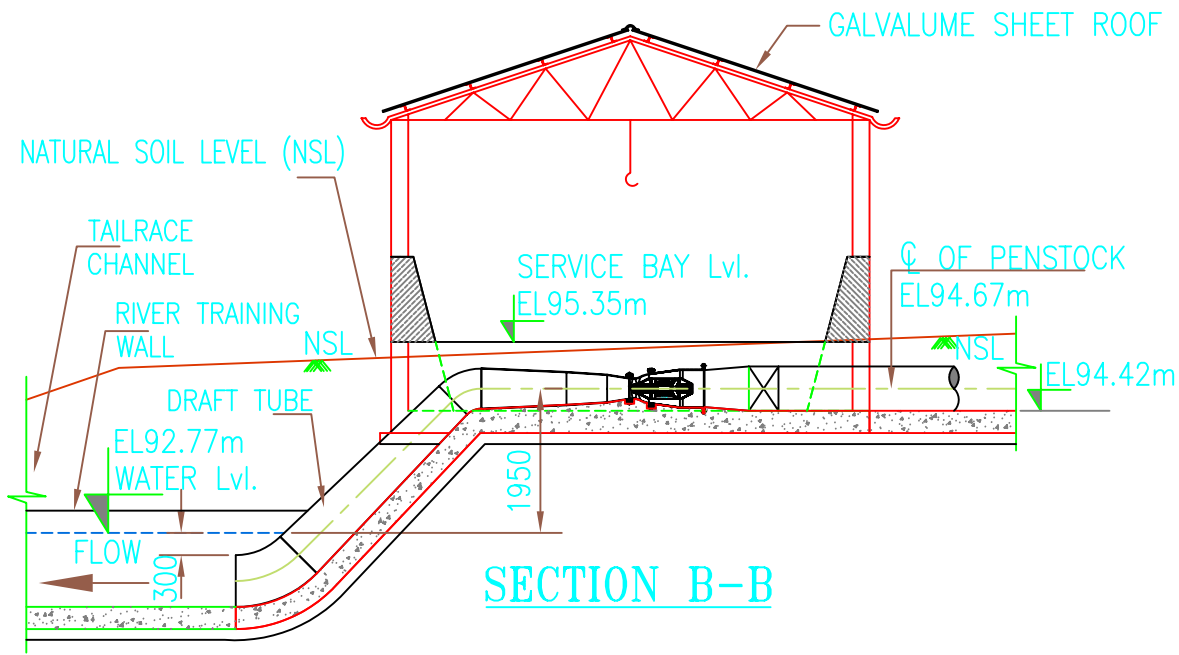
VRISHABHAVATHI RIVER



PLAN OF SCHEME

DEVELOPERS : Dr.Punit Singh Associates		MYLASANDRA HYDRO ENERGY RECOVERY PLANT ON VRISHABHAVATHI RIVER (3x12.5kW=37.5kW)	
ENGINEERING CONSULTANTS: Aakruthi Consultants. # 3444, service road, 2nd Stage, Vijayangar Bangalore-560 040. Telefax: 080 2339 1994 , 9448053550. E-mail: acmchari40@gmail.com		TITLE: GENERAL LAYOUT PLAN & L-SECTION	
DRG. No.-	AC-001-MLS-001	REV. No. △ RO	
SHEET No.-	SCALE- 1:200	APPD.	
DATE	DRN.	CHKD.	
06-07-13	S.N.K	A.C.M	

REV	DESCRIPTION	DRN. BY	CHD. BY	DATE



REV	DESCRIPTION	DRN. BY	CHD. BY	DATE

DEVELOPERS : Dr. Punit Singh Associates		MYLASANDRA HYDRO ENERGY RECOVERY PLANT ON VRISHABHAVATI RIVER (3x12.5kW=37.5kW)	
ENGINEERING CONSULTANTS: Aakruthi Consultants. # 3444, service road, 2nd Stage, Vijayangar Bangalore-560 040. Telefax: 080 2339 1994 , 9448053550. E-mail: acmchari40@gmail.com		TITLE: POWER HOUSE & INTAKE POOL PLAN & SECTION	
DRG. No.- AC-001-MLS-002		REV. No. RO	
SHEET No.-		SCALE- 1:100	
DATE 08-07-13	DRN. S.N.K	CHKD. A.C.M	APPD.

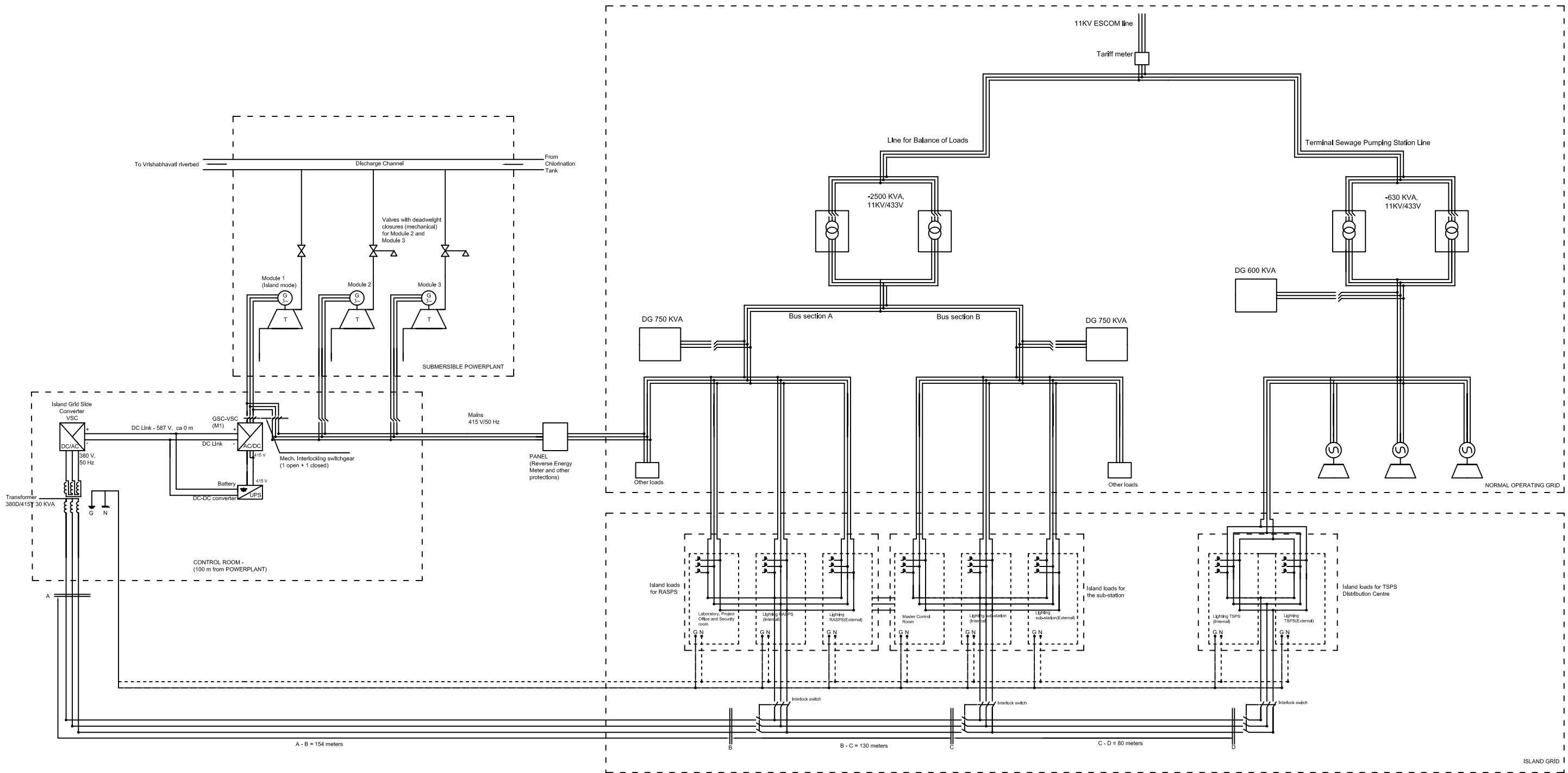


Fig. A.3, Single Line Diagram for Implementation Option A - Hybrid mode (grid and Island mode) with three energy recovery units

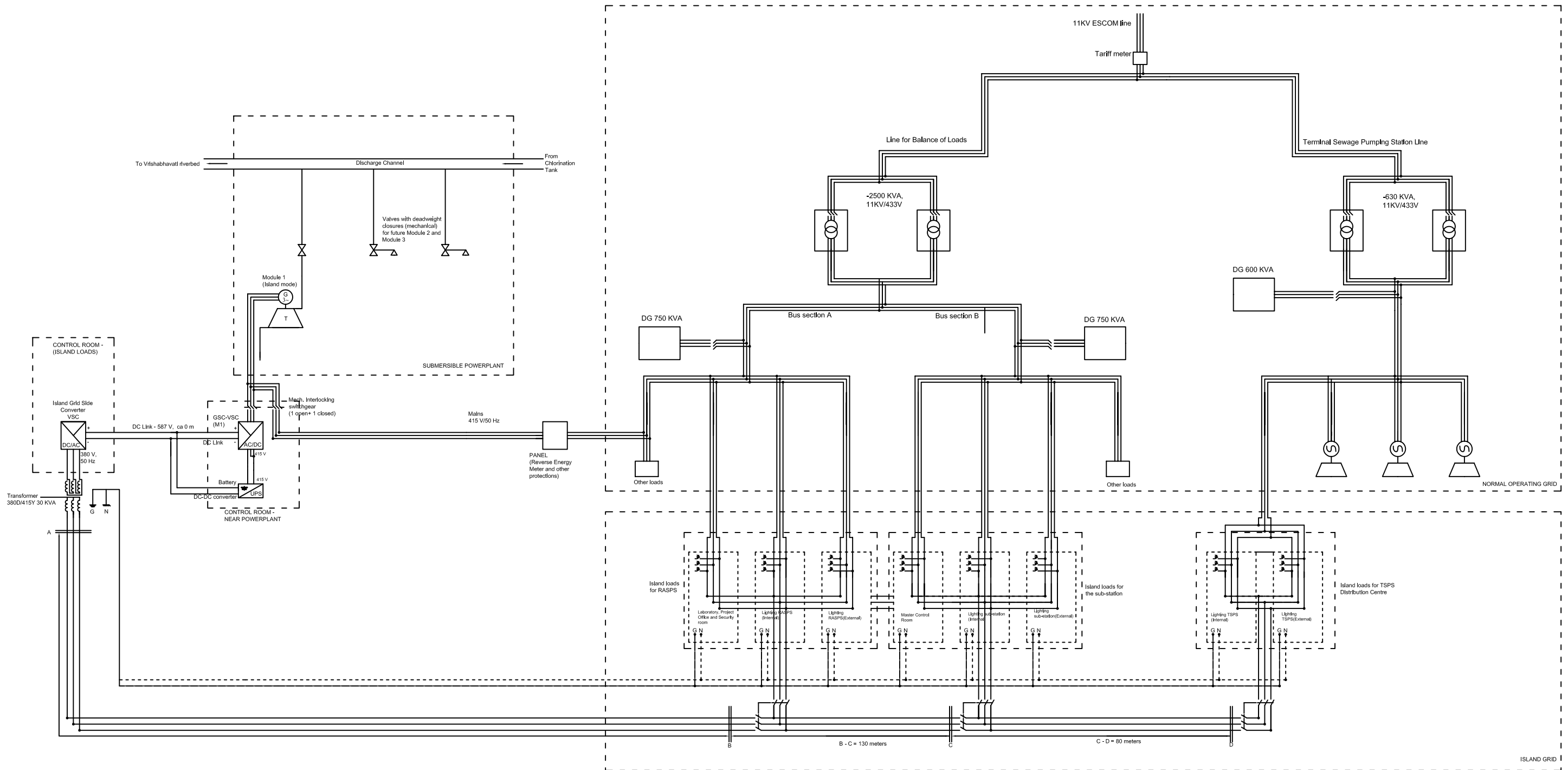


Fig. A.4, Single Line Diagram for Implementation Option B - Hybrid mode (grid and island mode) with single energy recovery unit

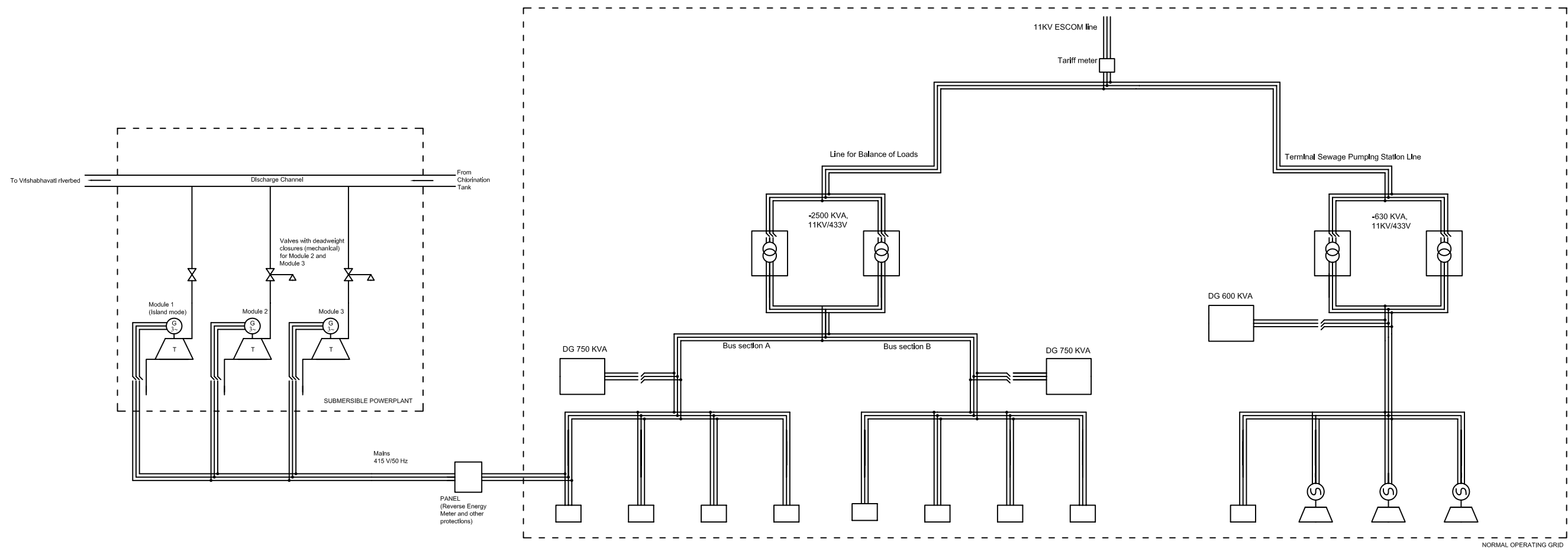


Fig. A.5, Single Line Diagram for Implementation Option C - Dedicated grid mode with three energy recovery units

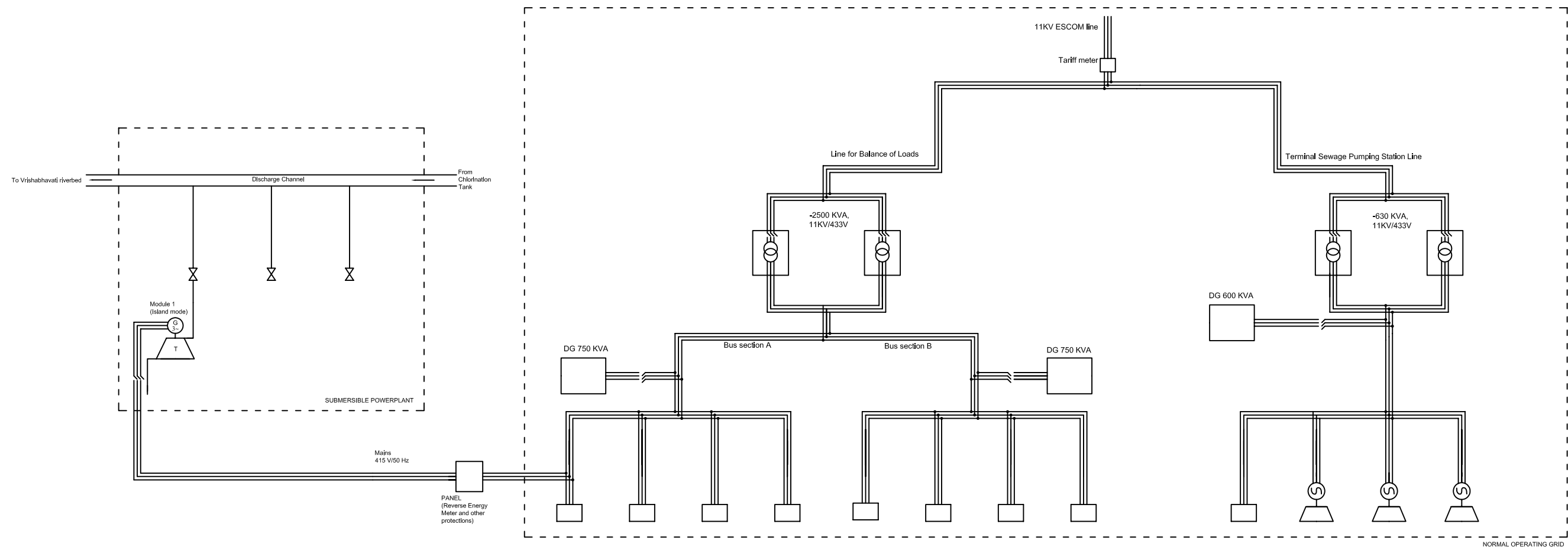


Fig. A.6, Single Line Diagram for Implementation Option D - Dedicated grid mode with single energy recovery unit